

**Exploring IPC Synthase:
A POTENTIAL ANTI-LEISHMANIAL
DRUG TARGET**



PhD Thesis
Durham University
Department of Chemistry

John G. M. Mina



Ustinov College

June 2010

Supervisors

Dr. Patrick G. Steel

Centre for Bioactive Chemistry, Chemistry Dept. Science labs,
Durham University, Durham, DH1 3LE, UK
p.g.steel@durham.ac.uk
+44 191 334 21 31

Dr. Paul W. Denny

Biophysical Sciences Institute, Chemistry Dept. Science labs,
Durham University, Durham, DH1 3LE, UK
p.w.denny@durham.ac.uk
+44 191 334 39 83

Examiners

Prof. Dr. David Parker

Centre for Bioactive Chemistry, Chemistry Dept. Science labs,
Durham University, Durham, DH1 3LE, UK
david.parker@durham.ac.uk
+44 191 33 42033

Dr. Terry Smith

Biomolecular Sciences Building, University of St Andrews
North Haugh, St Andrews, Fife, KY16 9ST, UK
tks1@st-andrews.ac.uk
+44 1334 46 34 12

ABSTRACT**Exploring IPC Synthase:
A POTENTIAL ANTI-LEISHMANIAL DRUG TARGET****John G. M. Mina**

Leishmaniasis is a widespread disease affecting 12 million people with about 2 million new cases recorded annually and 350 million people considered to be at risk worldwide. Consequently, it has been ranked category '1' by WHO-TDR in 2004. Currently available drugs are expensive and difficult to administer with toxic and/or teratogenic side effects. In addition, there are increasing levels of drug resistance. Therefore, there is a need for new effective drug treatments.

Earlier work in the group identified *Leishmania major* Inositol Phosphorylceramide Synthase (*Lmj*IPCS) as a functional orthologue of the fungal IPC synthase. This membrane bound enzyme has no mammalian equivalent therefore represents an attractive anti-Leishmanial drug target. The aim of this chemical biology project was to functionally characterise this enzyme and synthesise lead compounds for inhibitor design. The first aspect of the project focused on the establishment of a robust assay system that was used in the determination of the kinetic parameters of the enzyme. The established protocol was amenable to scaling-up processes and HTS. Validation of the assay was achieved using Aureobasidin A, a known fungal IPCS specific inhibitor, and two substrate mimics.

Phase two of the project involved the use of synthetic chemistry towards the enantioselective and diastereoselective synthesis of an array of substrate mimics to help identify the structural requirements for the substrate binding to the enzyme. The key reactions were asymmetric PT amino acid alkylation of benzophenone glycine imine and a stereospecific reduction of protected *N*-Boc-enones formed from the corresponding amino acid. The prepared alkenes were utilised in olefin cross metathesis reactions to yield a library of ceramide mimics variable in the sphingosine backbone. Deprotection-acylation sequence of the protected amino group resulted in variable *N*-acyl ceramide mimics. Screening of the substrate mimics library together with other putative inhibitors generated preliminary SAR data. Future work will involve using the SAR data generated in this study to design and synthesise new generations of inhibitors as well as substrate probes to help map the active site of the enzyme.



“ ... I can do all things through Christ who strengtheneth me.”

Philippians 4:13, KJV

TABLE OF CONTENT

Abstract	iii
Table of Content	v
Bibliography	xi
Acknowledgements.....	xii
Declaration.....	xiii
Copyright	xiii
Abbreviations.....	xiv
1 INTRODUCTION.....	2
1.1 Thesis Synopsis	2
1.2 Sphingolipids	3
1.2.1 Historical Perspective	3
1.2.2 Structure and Classification.....	4
1.2.3 Diversity between different species.....	8
1.2.4 Nomenclature.....	10
1.2.5 Metabolism	12
1.2.5.1 <i>De novo</i> Synthesis	12
1.2.5.2 Recycling, Salvage and Degradation.....	15
1.2.6 Biological Significance.....	16
1.2.6.1 Sphingolipids as Structural Components.....	16
1.2.6.2 Sphingolipid as Biological Signalling Agents.....	18
1.2.6.3 Defects in sphingolipids metabolism: the Sphingolipidoses	19
1.2.7 Sphingolipid Biosynthesis: An Attractive Drug Target	20
1.3 Kinetoplastidae: <i>Leishmania spp.</i> and <i>Trypanosoma brucei</i>	22
1.3.1 <i>Leishmania spp.</i> and the Leishmaniases.....	23
1.3.1.1 Introduction	23
1.3.1.2 Available treatment	24
1.3.2 <i>Trypanosoma brucei spp.</i> and HAT	26
1.3.2.1 Introduction	26
1.3.2.2 Available treatment	27
1.3.3 Putative Drug Targets against Leishmaniasis and HAT.....	28
1.4 The Kinetoplastid IPC Synthase(s): a Novel Drug Target	29
1.4.1 Identification and isolation	29
1.4.2 The Hypothetical Reaction Mechanism	30

1.4.3	The Biological Significance of IPC Synthases.....	31
1.4.4	<i>L. major</i> IPC Synthase.....	32
1.4.5	Topologies Studies	32
1.4.6	Sensitivity studies and drug target validation.....	33
1.5	Project Objectives and Work strategy	34
	References.....	35
2	CHARACTERISATION OF <i>Lmj</i>IPCS.....	39
2.1	Work Synopsis.....	39
2.1	Establishment of an <i>in-vitro</i> Activity Assay.....	40
2.1.1	Construction of the <i>Lmj</i> IPCS complemented Mutant Yeast Strain.....	40
2.1.2	Preparation of the Microsomal Membranes Fraction.....	41
2.1.2.1	Preparation of Crude microsomal membranes	41
2.1.2.2	Activity Assay of the Crude Microsomal Membranes.....	42
2.1.2.3	Preparation of Refined Microsomal Membranes	43
2.1.3	Establishment of <i>Lmj</i> IPCS Assay Conditions	45
2.1.3.1	Techniques of IPC Synthase Activity Assays	46
2.1.3.2	Activity vs. Variants of the Donor Substrate.....	47
2.1.3.3	Activity vs. Temperature.....	48
2.1.3.4	Activity vs. pH	49
2.1.3.5	Activity vs. Time & Protein Concentration.....	50
2.1.4	Validation of the Assay Protocol.....	52
2.1.4.1	Aureobasidin A Inhibition of <i>Lmj</i> IPCS	52
2.1.4.2	Substrate Analogues as Competitive Inhibitors of <i>Lmj</i> IPCS	53
2.2	Determination of the Kinetic Parameters	56
2.2.1	The Physical Aspects of the Assay Protocol	56
2.2.2	Initial Hypotheses for <i>Lmj</i> IPCS Kinetic Model	57
2.2.3	The Catalytic Cycle and the Reaction Rate Equation.....	59
2.2.4	V_{max} and K_m^{Cer} ($app.$) in terms of NBD-C ₆ -Ceramide	64
2.2.5	V_{max} and K_m^{PI} ($app.$) in terms of PI	64
2.2.6	Bi–Bi Substrate Kinetics and Surface Dilution Effect	67
2.3	Conclusion	70
	References.....	71
3	<i>Lmj</i>IPCS ORTHOLOGOUS ENZYMES.....	74
3.1	Work Synopsis.....	74
3.2	<i>Tb</i> SLS4 (<i>Tb</i> 09.211.1000)	74
3.2.1	Introduction	74

3.2.2	Construction of the <i>Tb</i> SLSs complemented Mutant Yeast Strain.....	75
3.2.3	<i>In vitro</i> assay of <i>Tb</i> SLS4 activity	76
3.2.3.1	Activity vs. Different Donor Substrates	77
3.2.3.2	Activity vs. Time.....	79
3.2.3.3	Aureobasidin A Inhibition.....	80
3.2.4	Reverse Activity	81
3.3	<i>At</i> IPCS 1, 2 & 3 (<i>At</i> 3g54020.1, <i>At</i> 2g37940.1 & <i>At</i> 2g29525.1).....	83
3.3.1	Introduction	83
3.3.2	Construction of the <i>At</i> IPCSs complemented Mutant Yeast Strain	83
3.3.3	Microsomes Preparation and <i>in vitro</i> Activity Assay.....	84
3.3.4	<i>At</i> IPCS1-3 are Functional IPC Synthases.....	84
3.3.4.1	Activity vs. Different Donor Substrates	84
3.3.4.2	Ab A inhibition.....	85
3.4	Conclusion	87
	References.....	88
4	SYNTHESIS OF SUBSTRATE ANALOGUES	90
4.1	Work Synopsis.....	90
4.2	The Rationale behind the Design of Potential Inhibitors	91
4.2.1	The Structural Features of Known Substrates and Inhibitors.....	91
4.2.2	The Template Structure for Potential Inhibitors.....	93
4.3	Synthesis of a Ceramide Analogues Library	94
4.3.1	Synthetic Routes to Sphingosine and ceramide.....	94
4.3.2	The Synthetic Strategy for the Parallel Synthesis	96
4.3.2.1	The Retro Synthetic Analysis for the Common Scaffold.....	96
4.3.2.2	The Proposed Synthetic Routes.....	97
4.3.3	Synthesis of Scaffold ‘1’: <i>N</i> -Boc-2-aminopent-4-ene-1,3-diol	97
4.3.4	Synthesis of the Scaffolds of 1-Deoxyceramide Analogues	100
4.3.4.1	Synthesis of Scaffold ‘2a’: <i>N</i> -Boc-2-aminopent-4-en-3-ol	100
4.3.4.2	Synthesis of Scaffold ‘2b’: <i>N</i> -Boc-2-aminohex-5-en-3-ol.....	101
4.3.5	Synthesis of Scaffolds ‘3’: <i>N</i> -Boc-2-aminopent-4-en-1-ol	102
4.3.5.1	Synthesis of the Benzophenone Glycine Imine.....	104
4.3.5.2	Synthesis of (2R) & (2S) <i>N</i> -Boc-2-aminopent-4-en-1-ol.....	105
4.3.6	Olefin Cross Metathesis (CM) of the Prepared Scaffolds	105
4.3.7	Deprotection and Acylation of CM Products	108
4.3.8	Synthesis of Ceramide-1-Phosphate Analogue	109
4.3.9	Synthesis of the 1-Phenyl-2-aminopropanol Series.....	109
4.4	Conclusions.....	111

References.....	112
5 SCREENING OF THE SUBSTRATE ANALOGUES.....	115
5.1 Work Synopsis.....	115
5.2 Preparation of the Screening Compounds.....	116
5.3 The Assay Protocol of the Inhibition Assays.....	116
5.4 Analysis of the Screening Results.....	117
5.4.1 The Ceramide Analogues Library.....	117
5.4.2 The Synthetic Intermediates.....	119
5.4.3 The Nor-Ephedrine (1-Phenyl-2-aminopropanol) Series.....	120
5.4.4 The β -blockers.....	120
5.4.5 Z-Prime Value of the Screening Assay.....	121
5.4.6 IC ₅₀ of the Representative Potent Compounds.....	123
5.4.7 Mass Spectrometry of the Representative Compounds.....	124
5.4.8 Pre-incubation with a Ceramide-1-phosphate Analogue (338).....	125
5.5 The SAR Analyses.....	126
5.5.1 Feature '1': 1-OH, H-Donor/H-Acceptor.....	126
5.5.2 Feature '2': 2S-NH-, H-Donor.....	127
5.5.3 Feature '3': 3R-OH, H-Donor/H-Acceptor.....	128
5.5.4 Feature '4': Position of the Double Bond.....	128
5.5.5 Feature '5': Sphingosine backbone Tail, Hydrophobic Surface.....	129
5.5.6 Feature '6': -CO-R, H-Acceptor.....	130
5.5.7 Feature '7': N-Acyl Hydrophobic Tail, Hydrophobic Surface.....	132
5.6 Conclusion.....	135
References.....	136
6 CONCLUSIONS AND FUTURE WORK.....	138
6.1 Conclusion.....	138
6.2 Proposed Future Work.....	139
6.2.1 Biological Approach.....	139
6.2.1.1 Enhancement of the Assay Protocol.....	139
6.2.1.2 Further Enzyme Activity Studies & Site directed mutagenesis of Arg262.....	139
6.2.1.3 Kinetics of PI Phosphorylation of LmjIPCS.....	140
6.2.2 Bioinformatics and <i>In Silico</i> Molecular Modelling.....	141
References.....	142
7 BIOLOGICAL MATERIALS AND METHODS.....	144

7.1	Materials	144
7.2	Instruments and Equipment	144
7.3	Solutions, Buffers and Media Compositions	145
7.4	Standard Protocols	146
7.4.1	Complementation of AUR1 mutant <i>S. cerevisiae</i>	146
7.4.2	AUR1 mutant <i>S. cerevisiae</i> culture	147
7.4.2.1	Agar Plates	147
7.4.2.2	Culture Scaling-up.....	148
7.4.3	Preparation of the Microsomal Membranes Fraction	148
7.4.3.1	Step 1: Preparation of Cell Extract.....	148
7.4.3.2	Step 2: Preparation of Crude Microsomal Membrane Fraction	148
7.4.3.3	Step 3: Preparation of CHAPS-washed Microsomal Membranes Fraction.....	149
7.4.3.4	Step 4: Determination of the Protein Content in Enzyme Units.....	149
7.4.4	NBD-C ₆ -Ceramide Fluorescence Assay.....	150
7.4.4.1	Protocol 'A': 96-well plate Assay	150
7.4.4.2	Protocol 'B': Thin Layer chromatography (TLC) Assay ⁵	150
7.4.4.3	Assay for Inhibitions Studies	151
7.4.5	Mass Spectrometry Analyses.....	151
	References.....	153
8	CHEMICAL SYNTHESIS EXPERIMENTAL DETAILS	155
8.1	General Procedures	155
8.1.1	IUPAC nomenclature	155
8.1.2	Solvents purification.....	155
8.1.3	Reaction Conditions, Monitoring and Purification	155
8.1.4	Column chromatography	155
8.1.5	Spectroscopic Data	156
8.1.6	Titration of Organometallic Reagents	156
8.2	Experimental Procedures	157
8.2.1	Commercially Available Starting Materials	157
8.2.2	Synthesis of Intermediate compounds.....	159
8.2.2.1	4E-1-deoxy ceramide analogues	159
8.2.2.2	5E-1-deoxy ceramide analogues	161
8.2.2.3	Ceramide analogues	163
8.2.2.4	4E-3-deoxy-ceramide analogues	168
8.2.3	General Procedure for Phase Transfer Catalysis ^{11, 15}	173
8.2.4	Olefin Cross Metathesis	177
8.2.4.1	4E-1-deoxy ceramide analogues	178
8.2.4.2	5E-1-deoxy ceramide analogues	179

TABLE OF CONTENT

8.2.4.3	Ceramide analogues	181
8.2.4.4	4E-3-deoxy ceramide analogues	185
8.2.5	Screening Compounds Library	187
8.2.5.1	4E-1-deoxy ceramide analogues	187
8.2.5.2	5E-1-deoxy ceramide analogues	193
8.2.5.3	Ceramide analogues	198
8.2.5.4	4E-3-deoxy ceramide analogues	204
8.2.5.5	3-phenyl-1-deoxy ceramide analogues.....	211
	References.....	214
APPENDIX 'A': EXPRESSION VECTOR P426MET25		216
APPENDIX 'B': MATRIX OF DILUTION EFFECT		218
APPENDIX 'C': SCREENING RESULTS TABLE		220
APPENDIX 'D': PUBLICATIONS		231

BIBLIOGRAPHY

John G. M. Mina

Egyptian

Born 6th Oct. 1977

June 2000,

B.Sc. (Honours) “Pharmacy and Pharmaceutical Sciences”

Faculty of Pharmacy, Cairo University - Egypt.

Jan. 2004,

Joined the Chemistry Department in Durham University, and that’s where my academic career began.

Nov. 2005

M.Sc. “**Stereocontrolled Synthesis of Highly Functionalized Heterocycles**”

Chemistry Department, Faculty of Sciences, Durham University - United Kingdom.

Supervisors: Prof. Dr. Judith A. K. Howard CBE FRS

Dr. Patrick G. Steel

Examiners: Dr. David R. W. Hodgson (Durham University)

Dr. Andrew Parsons (York University)

ACKNOWLEDGEMENTS

To
My parents,
All my teachers,
And my supervisors,

Prof. Judith A. K. Howard, FRS

&

Dr. Patrick G. Steel

&

Dr. Paul W. Denny

who taught me from A B C to Ph.D.

A massive thank you is due to my wife Aristeia for her endless and continuous support.

A big thank you to my dear friends Sam, Ahmed and Ali who always supported me.

Special thanks to Dr. Alan Kenwright, Dr. Andy Beeby, Dr AnnMarie O'Donoghue, Dr. David Hodgson, Dr. Maria Hinaje, Dr. Martin Cann, and all the NMR & MS service teamwork for their guidance and helpful discussions.

Thanks for all Wolfson Research Institute specially Simon Padbury and Diane Hart and CY001 colleagues, Dr. Kathryn Knight, Dr. Jonathan Sellars, Dr. Marie Landrum, Dr. Tom Woods, Michal Czyzewski, Peter Harrisson Dr. Matt Burton, Dr. Steve Bratt, Dr. Ahmed Ali, Nick Hughes, John Dunwell and Hazmi Tajuddin who always made the environment so joyful and encouraging.

DDECLARATION

The work in this report was carried out at the University of Durham as a conjunction work between the Department of Chemistry and Wolfson Research Institute between October 2006 and June 2010. It has not been submitted for any other degree and is the author's own work, except where acknowledged by reference.

CCOPYRIGHT

The copyright of this report rests with the author. This copy has been supplied on the understanding that it is copyright material and that no quotation from the report may be published without proper acknowledgement.

ABBREVIATIONS

1D	Unidimensional
2D	Bidimensional
Ac	Acetyl
aq.	Aqueous
Ar	Aromatic group
<i>At</i> IPCS	<i>Arabidopsis thaliana</i> IPC synthase
b	Broad (in IR spectroscopy)
b.p.	Boiling point
Bn	Benzyl
BSF	Blood stream form (for parasites)
Bu	Butyl
BuLi	Butyllithium
c.a.	<i>circa</i> , about
CHAPS	3-[(3- cholamidopropyl) dimethylammonio]-1-propanesulfonate
CHAPSO	3-[(3- cholamidopropyl) dimethylammonio]- 2-hydroxy-1-propanesulfonate
CM	Cross Metathesis
conc.	Concentrated
Cosy	^1H - ^1H correlation spectroscopy
Cpd	Compound
d	Doublet (in ^1H NMR spectroscopy)
D (#)	Domain (number) in protein sequence
Da	Dalton
DAG	Diacylglycerol
DCM	Dichloromethane (CH_2Cl_2)
dd	Doublet of doublet (in ^1H NMR spectroscopy)
ddd	Doublet of doublet of doublet (in ^1H NMR spectroscopy)
DIBAH	Diisobutylaluminium hydride
DMAP	4-(N,N-Dimethylamino)pyridine
DMF	N,N-dimethylformamide
DNA	Deoxyribonucleic acid
e.g.	For example
EDC	1-ethyl-3-(3-dimethylaminopropyl)carbodiimide
EDTA	Ethylene diamine tetracetic acid
eq.	Equivalents
ER	Endoplasmic Reticulum
ESMS	Electrospray Mass spectrometry
Et	Ethyl
g.	Gram
GC	Gas chromatography
GC / MS	Gas chromatography / Mass spectroscopy
GLS	Glycosphingolipid
GPCR	G-protein coupled receptor
h.	Hours
HAT	Human African Trypanosomiasis
HMBC	Heteronuclear shift correlation <i>via</i> multiple bond connectivities
HPTLC	High performance thin layer chromatography
HSQC	Heteronuclear single quantum correlation
i.e.	<i>In extensor</i>
IPC	Inositolphosphoryl ceramide
IPCase	IPC lyase
IR	Infrared
J / Hz	Coupling constant / Hertz (in NMR spectroscopy)
kDa	Kilo Dalton
kDNA	Kinetoplast DNA
k_m	Michaelis constant
L_α	Lamellar phase

ABBREVIATIONS

L _β	Gel phase
LDA	Lithium diisopropylamide
<i>Lmj</i> IPCS	<i>Leishmania major</i> IPC synthase
LPP	Lipid phosphate phosphatase
m	Multiplet (in ¹ H NMR spectroscopy)
m.p.	Melting point
Me	Methyl
mg.	Milligram
min	Minutes
MIPC	Mannose inositol phosphorylceramide
Ms	Mesyl (Methylsulfonyl)
MS	Mass spectrometry
NBD-C ₆ -ceramide	N-[6-[(7-nitro-2-1,3-benzoxadiazol-4-yl)amino]hexanoyl]-D-erythro-sphingosine
NMM	N methyl morpholine
NMR	Nuclear magnetic resonance
nOe	Nuclear Overhauser effect
nOesy	Nuclear Overhauser effect spectroscopy
Nu	Nucleophile
PC	Phosphatidylcholine
PCF	Procyclic form (for parasite)
PE	Phosphatidyl ethanolamine
P-EtN	Ethanolamine phosphate
pH	– Log [Hydrogen ion concentration]
Ph	Phenyl
pI	Isoelectric point
PI	Phosphatidylinositol
pK _a	Acid ionisation constant
PSL	Phosphosphingolipid
R	Alkyl group
R _f	Distance travelled on TLC
R.T / r.t	Room temperature
s	Singlet (in ¹ H NMR spectroscopy)
S1P	Sphingosine-1-phosphate
SAR	Structure Activity Relationship
<i>Sc</i> IPCS	<i>Saccharomyces cerevisiae</i> inositol phosphorylceramide synthase
SK	Sphingosine Kinase
SM	Starting material (in chemical context)
SM	Sphingomyelin (in biological context)
SMase	Sphingomyelinase
SMS	Sphingomyelin synthase
SPT	Serine palmitoyl transferase
t	Triplet (in ¹ H NMR spectroscopy)
TBS	<i>tert</i> -Butyldimethylsilyl
<i>Tb</i> SLS	<i>Trypanosoma brucei</i> sphingolipid synthase
tDOC	Taurodeoxycholate
Tfa	Trifluoroacetate
THF	Tetrahydrofuran
TLC	Thin layer chromatography
TM (#)	Transmembrane domain (in protein sequence)
v ₀	Initial velocity (enzyme kinetics)
V _{max}	Maximum velocity (enzyme kinetics)
VSG	Variant Surface Glycoprotein

Latin Symbols

Δ	Heat
δ / ppm	Chemical shifts / parts per million

CHAPTER I

INTRODUCTION

1 INTRODUCTION

1.1 Thesis Synopsis

The aim of this work is to functionally characterise the recently identified enzyme, Inositol Phosphorylceramide Synthase from *Leishmania major* (*Lmj*IPCS). This enzyme represents a promising drug target against Leishmaniasis and therefore warrants further study. Chapter ‘I’ will present the background to the project; a brief description of sphingolipids in terms of structure and function in addition to the differences in metabolism between fungi, higher plants, Kinetoplastidae and the mammalian systems. These differences form a corner stone of the project. Furthermore, the last section will demonstrate the disease burden of Leishmaniasis and HAT, caused by the related trypanosome *Trypanosoma brucei*.

The project focused on a set of key objectives. These included the establishment of a high-throughput compatible activity assay protocol and the determination of the kinetic parameters of *Lmj*IPCS. The achievement of these two objectives is discussed in Chapter ‘II’. Moreover, application of these protocols in the preliminary characterisation of the closely related *T. brucei* Sphingolipid Synthase, *Tb*SLS4, and the divergent *Arabidopsis thaliana* Inositol phosphorylceramide synthases, *At*IPCS1-3, is the focus of Chapter ‘III’. The third and fourth objectives focused on the chemical synthesis of a library of substrate analogues and the screening of this library against *Lmj*IPCS. Details of the synthesis strategy and the screening results will be discussed in Chapter ‘IV’ and Chapter ‘V’ respectively while the project conclusions together with the future work will be presented in Chapter ‘VI’. Finally, the biological materials and methods and the experimental details of the chemical synthesis will be demonstrated in Chapters ‘VII’ and ‘VIII’ respectively.

1.2 Sphingolipids

1.2.1 Historical Perspective

Sphingolipids, a class of natural products, were first characterised by the German-born chemist and clinician Johann L. W. Thudichum in 1884 by fractional crystallisation from human brain tissue.¹ He isolated three related waxy lipids, sphingomyelin (1), cerebroside (2) and cerebrosulfatide (3), which upon hydrolysis gave a long chain aliphatic amine that he named sphingosine after the Greek mythological monster, Sphinx, due to its enigmatic nature. In the early 1900s, it was recognized as “dihydroxyamino-octadecene”.²⁻⁴ The correct relative orientations of the key functional moieties of sphingosine (4) (Figure 1-1) were determined by Carter and co-workers in 1947.⁵ Subsequently, the first racemic synthesis of sphingosine was reported by Shapiro and Segal in 1954.⁶

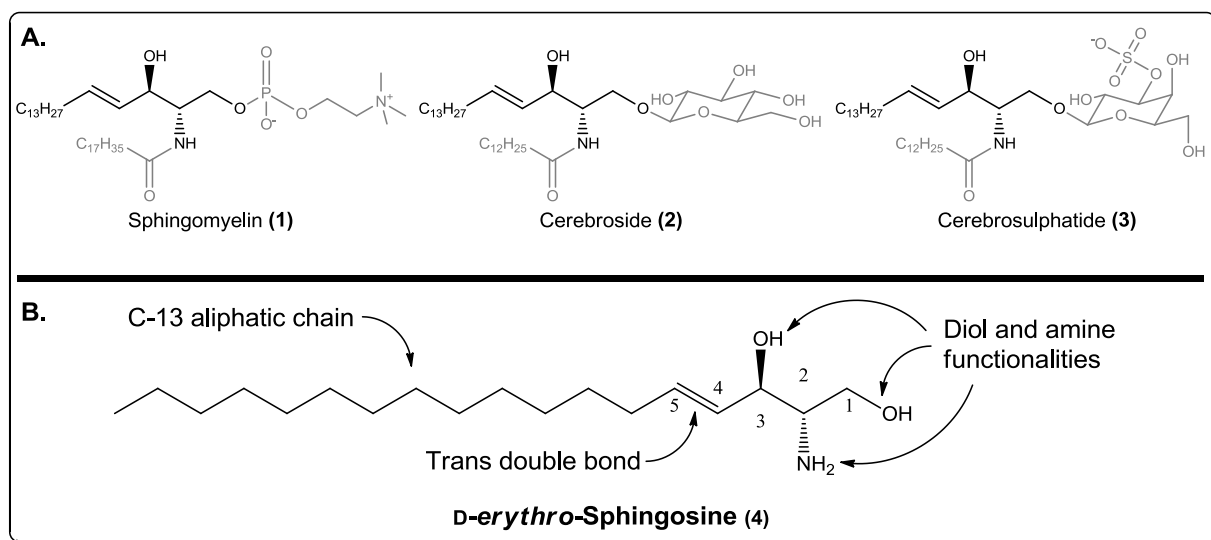
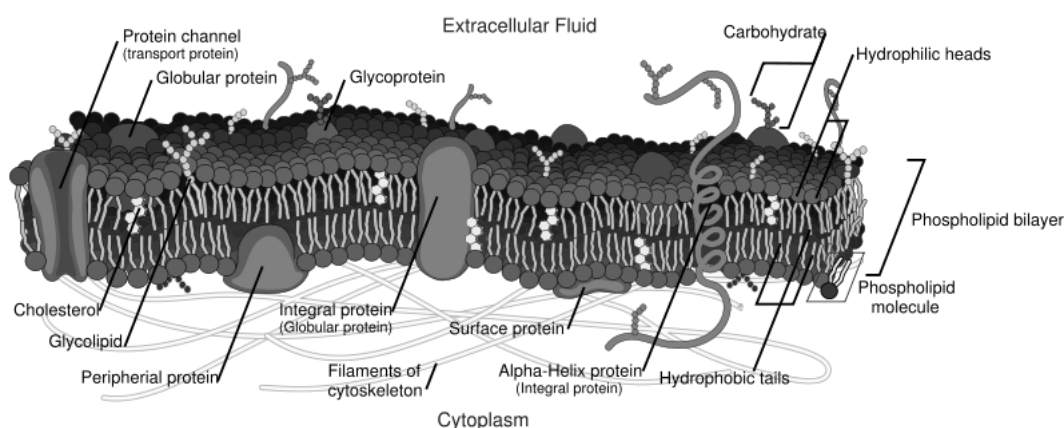


Figure 1-1: (A) The chemical structures of the lipids isolated by Thudichum (B) The key structural features of *D*-erythro-Sphingosine, (2*S*, 3*R*, *E*)-2-aminooctadec-4-ene-1,3-diol.

Over the last decade, there has been an exponentially growing interest in the study of sphingolipids; not only as structural components of the eukaryotic cell but also due to their interaction with a myriad of biological processes including signal transduction, cell growth, differentiation, apoptosis.⁷⁻¹¹ These are in addition to the relatively recent discovery of their role in the regulation of protein kinase C.¹²

1.2.2 Structure and Classification

Lipids are indispensable abundant structural components in eukaryotic plasma membranes (Figure 1-2) and intracellular organelles (25 % and 52 % of total lipid of mitochondrial membranes and chloroplasts respectively). In addition, lipids represent a major class of messenger and signal transduction bioactive molecules which modulate various cellular metabolic processes.¹³⁻¹⁴



<http://cellbiology.med.unsw.edu.au/units/science/lecture0803.htm>

Figure 1-2: Lipids are integral component of plasma membrane

On structural basis, lipids comprise a diverse range of naturally-occurring molecules and can be divided into eight categories. These are the fatty acyls, glycerolipids, glycerophospholipids, sphingolipids, sterol lipids, prenol lipids, saccharolipids, and polyketides (Figure 1-3).¹⁵ Three of these classes (Figure 1-3: b, c and d) consist of a long chain fatty acid backbone structure to which is attached a variety of charged, neutral, phosphorylated and or glycosylated moieties that results in both polar and non-polar regions which give them an amphipathic character, and accounts for their tendency to aggregate into membranous structures. The divergence encountered in their chemical structures allows them to play distinctive roles within cellular metabolism.¹³⁻¹⁴

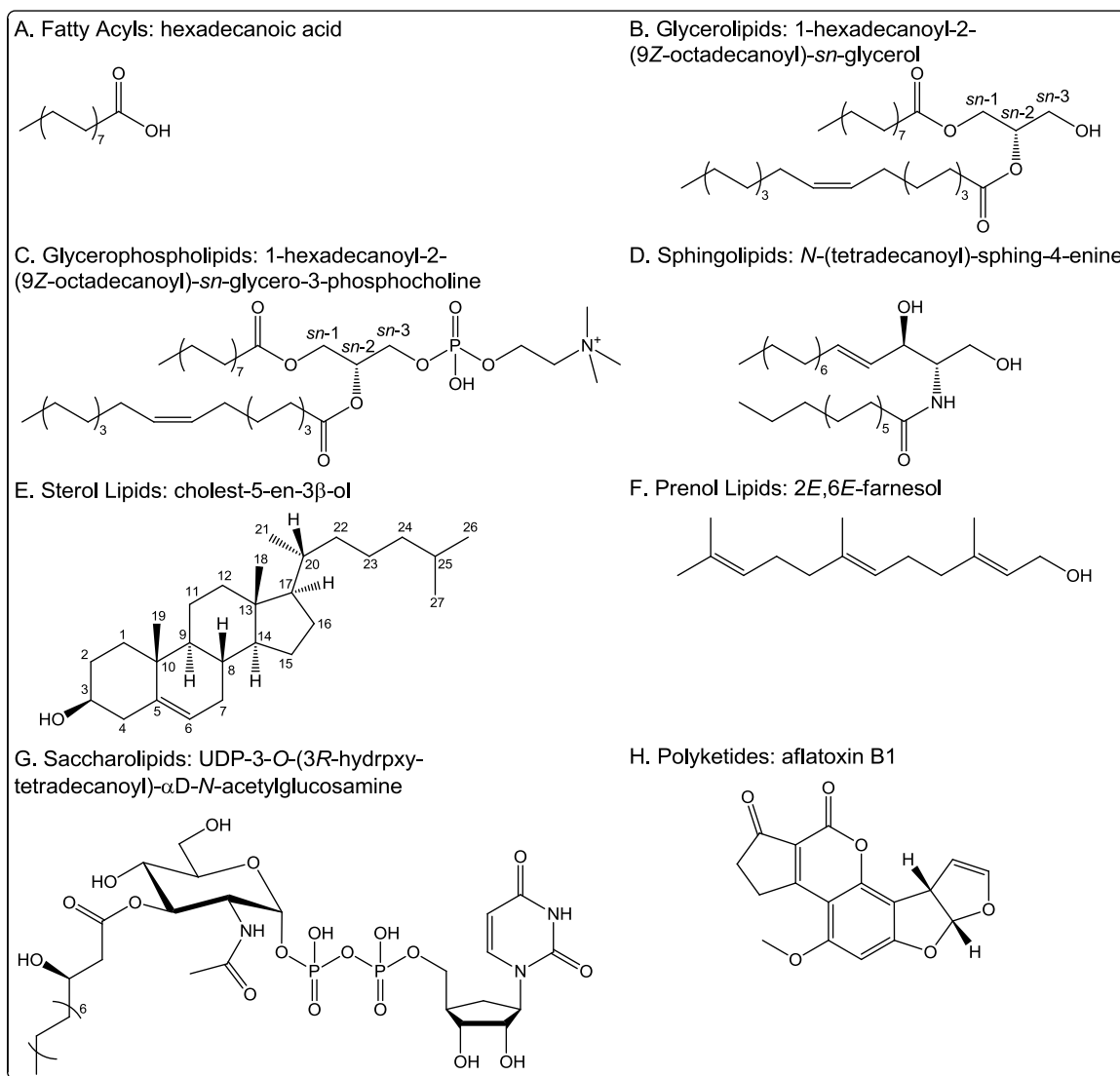


Figure 1-3: Representative examples of the primary categories of lipids

Importantly, whilst glycerolipids (b) and glycerophospholipids (c) are *mono-*, *bi-* or *tri-* acyl glycerol based, sphingolipids are distinguished by the presence of a structurally related family of backbones termed sphingoid bases (e.g. sphingosine) linked by an amide bond to an acyl group of a fatty acid to form *N*-acyl-sphingosines generically named “ceramides”. Relevant examples of sphingoid bases to the work presented in this thesis are illustrated in (Figure 1-4). There are considerable differences in the acyl chain between sphingolipids and the closely related, phospholipids. While phospholipids tend to have shorter acyl chains (16C-18C) with higher degrees of unsaturation, sphingolipids often have longer (20C-24C) saturated acyl chains.^{13, 16}

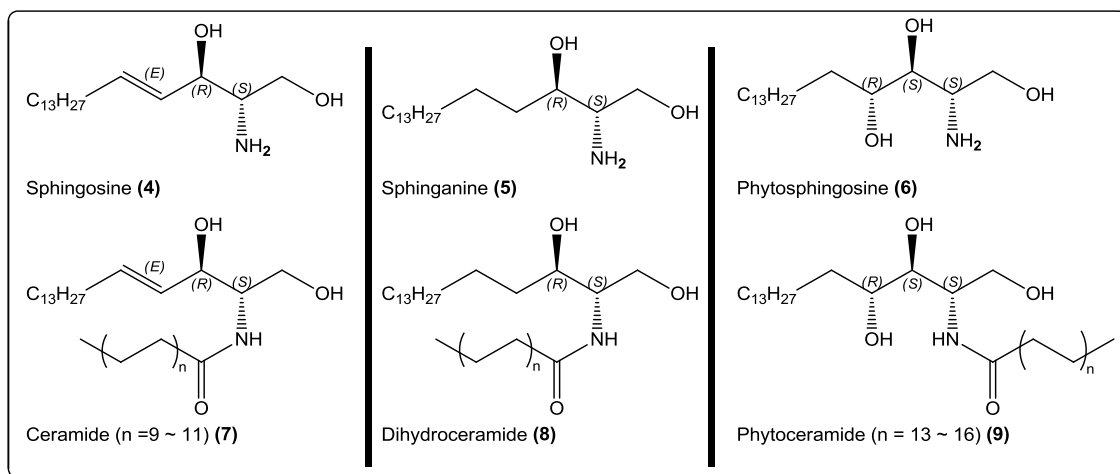


Figure 1-4: Sphingosine, sphinganine & phytosphingosine and the corresponding ceramides

However, in the so-called phosphosphingolipids, ceramides acquire a phosphate head group (e.g. ethanolamine phosphorylceramide and sphingomyelin) and exhibit structural features of both sphingolipids and phospholipids (Figure 1-5).

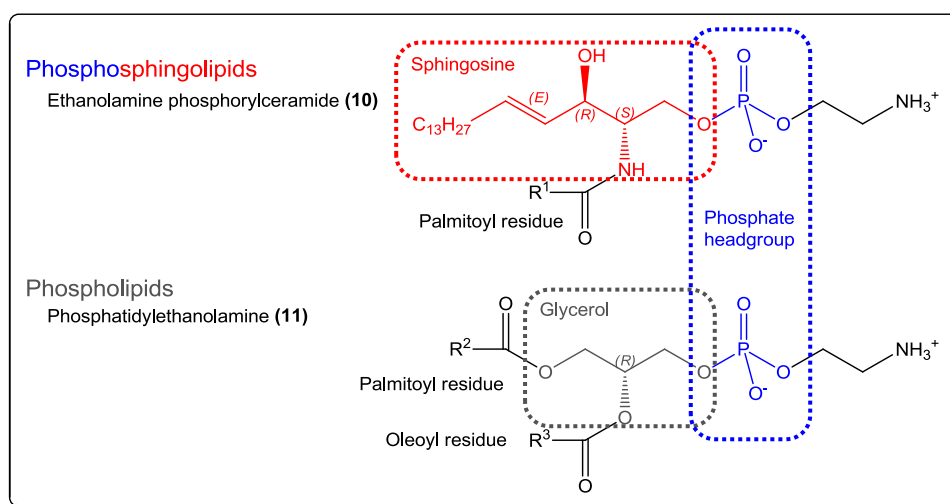
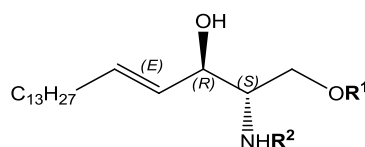


Figure 1-5: Phospholipids and Phosphosphingolipids

Excluding variation in the ceramide backbone, more than 300 different types of complex sphingolipids have been reported.¹⁷⁻¹⁹ These can be subdivided into seven classes²⁰ (Figure 1-6).^{15, 21} A fully comprehensive enumeration for all the structural variation of sphingolipids can be found online in continuously updated databases such as SphinGOMAP

(www.sphingomap.org), the Japanese Lipid Bank (<http://www.lipidbank.jp>) and the Lipid Maps Consortium (www.lipidmaps.org).



sphingolipid Class	Example	1-O- Head Group (R ₁)	(R ₂)
1. Sphingoid bases	Sphingosine-1-phosphate	PO ₃ ²⁻	H
2. Ceramides	Ceramide-1-phosphate	PO ₃ ²⁻	Fatty acyl group
3. Phosphosphingolipids	Sphingomyelin		Fatty acyl group
4. Cerebrosides Natural Glycosphingolipids	Glycosphingolipid Glcβ-Cer (d18:1/12:0)		Fatty acyl group
5. Gangliosides Natural Cerebrosides linked to Sialic	Glycosphingolipid (4'-Sialoyl) Glcβ-Cer (d18:1/12:0)		Fatty acyl group
6. Acidic Glycosphingolipids	Cerebrosulphatide (3'-sulfo) Galβ-Cer (d18:1/12:0)		Fatty acyl group
7. Sulfosphingolipids ²²	Sulfobacins ²³ Capnine ²⁴		

Figure 1-6: Representative Structures of sphingolipids classes (based on mammalian sphingosine)

1.2.3 Diversity between different species

With sphingolipids ubiquitous in nature, divergence is inevitable, and to-date, a vast array of sphingoid bases has been encountered. These include structural variations in terms of chain length, hydroxylation pattern (2, 3 or more OH groups), double bonds (number, position and conjugation) and branched side chains. Mammalian sphingoid bases are characterised by the predominance of C18 sphingosine. However, other chain lengths (C12 to C26) have been reported. In addition, variation in double bonds (e.g. Cpd 13), hydroxyl groups (e.g. Cpd 16, 18) and branched side chain sphingoid bases chains have been isolated (Figure 1-7). Additionally, *N*- and *O*-methyl-sphingoid bases, e.g. *N,N*-dimethylsphingosine have been found in small amounts.²⁰

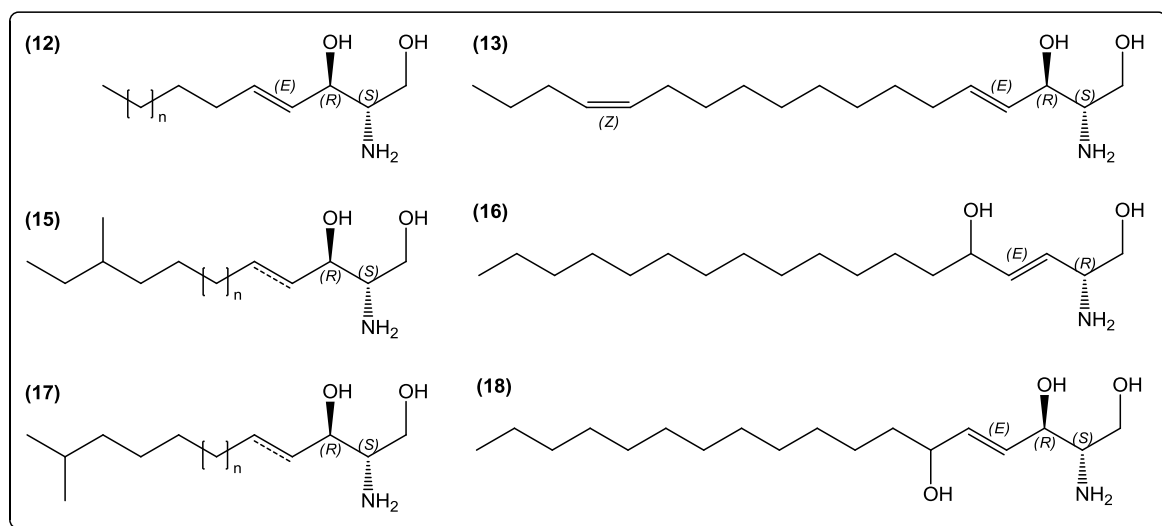


Figure 1-7: Variation in Mammalian sphingoid bases

In fungi and plants, sphingoid bases differ from those coming from mammalian species as they lack the C4-5 double bond, show a higher pattern of hydroxylation at C4 (Figure 1-4) and tend to have longer acyl chains (C28-C34).¹⁶

Sphingoid bases of sphingolipids from other species, including insects and aquatic organisms, extend the structural and compositional variation even further. For example,

uncommon C14 conjugated diene (Cpd 19) sphingoid base and a phytosphingosine with an odd number of carbon atoms C15 have been found. Furthermore, unique sphingoid bases with a cyclopropane ring in the alkyl side chain have been isolated from sponges (Cpd 20) (Figure 1-8).²⁰

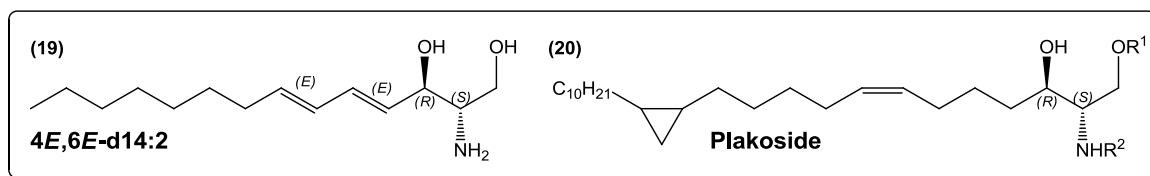


Figure 1-8: Variation in sphingoid bases from insects and sponges

The combination of these variations in the sphingoid base and the acylating fatty acid results in a massive structural divergence of the resulting ceramides. Enhanced variation is then encountered in further modifications to complex sphingolipids with a variety of head groups according to the host organism (Figure 1-9).

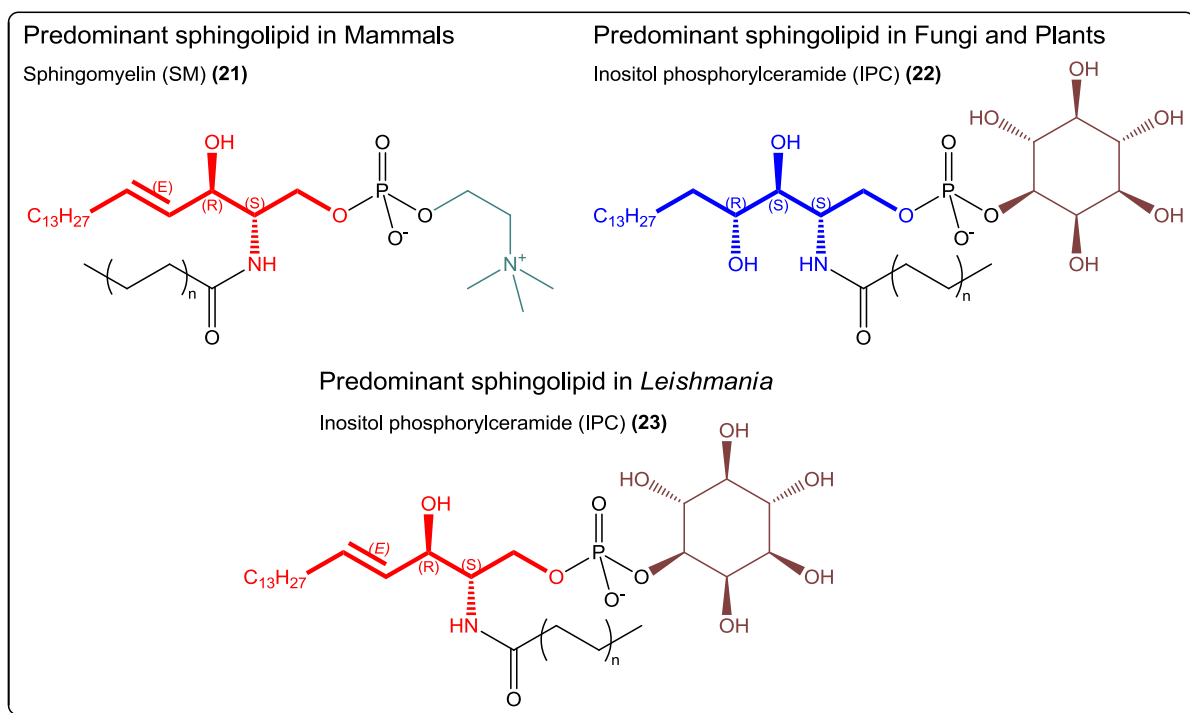


Figure 1-9: Host-based variation and partial similarities of complex sphingolipids

1.2.4 Nomenclature

Sphingolipids comprise an important class of compounds and are the focus for much contemporary research. Therefore, it has been necessary to establish a standard system for their nomenclature ensuring easier and effective communication to overcome the obsolete denotations that sometimes become confusing and misleading.

Some classes of sphingolipids had gained their own nomenclature system historically; e.g. ‘Svennerholm’ nomenclature²⁵ of gangliosides based on the number of sialic acid residues.^{13, 16} Many specialised and comprehensive reviews and online resources are continuously dealing with the problems regarding the development of a systematic protocol for the nomenclature of lipids in general.²⁶ This section will focus on the issues regarding nomenclature of sphingolipid subclasses relevant to this work following the recommendations of the Lipid Maps Consortium (www.lipidmaps.org).

Conventionally, the naturally occurring *D-erythro*-sphingosine diastereoisomer²⁶ (Figure 1-10, entry 1) has been agreed to be the standard form of sphingosine unless a different stereochemistry is indicated. The higher order sphingolipids, ceramides and sphingomyelin have been abbreviated to *Cer* and *SM* respectively, followed by parentheses defining the hydroxylation pattern, chain length and degree of unsaturation. Representative examples of sphingolipid classes to be encountered within this thesis are illustrated in Figure 1-10.¹⁵

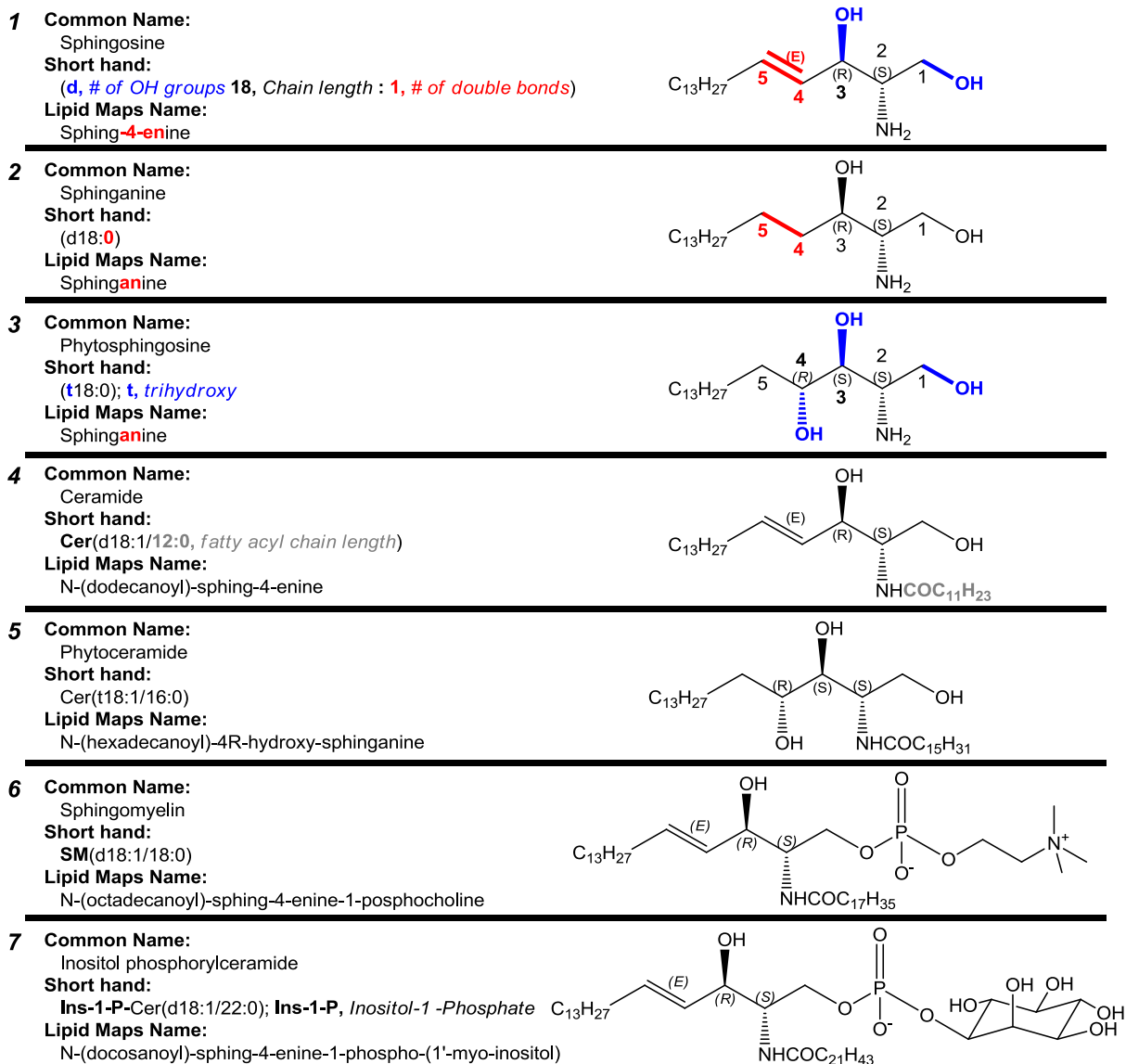


Figure 1-10: Common names and short hands of sphingolipid classes and their nomenclature according to Lipid Maps Consortium

1.2.5 Metabolism

Sphingolipid metabolism constitutes a highly complex network of interconnected pathways where ceramide (and dihydroceramide to a lesser degree) occupies a central position in biosynthesis and catabolism and thus, represents a metabolic hub.²⁷ In terms of ceramide, these pathways can be grouped into three clusters; *de novo* synthesis, recycling ‘salvage’ and degradation (Figure 1-11). To date, the mammalian sphingolipid metabolism has been extensively studied and many of the enzymes involved have been identified and characterised. Consequently, it will be used as the reference model in the following section.

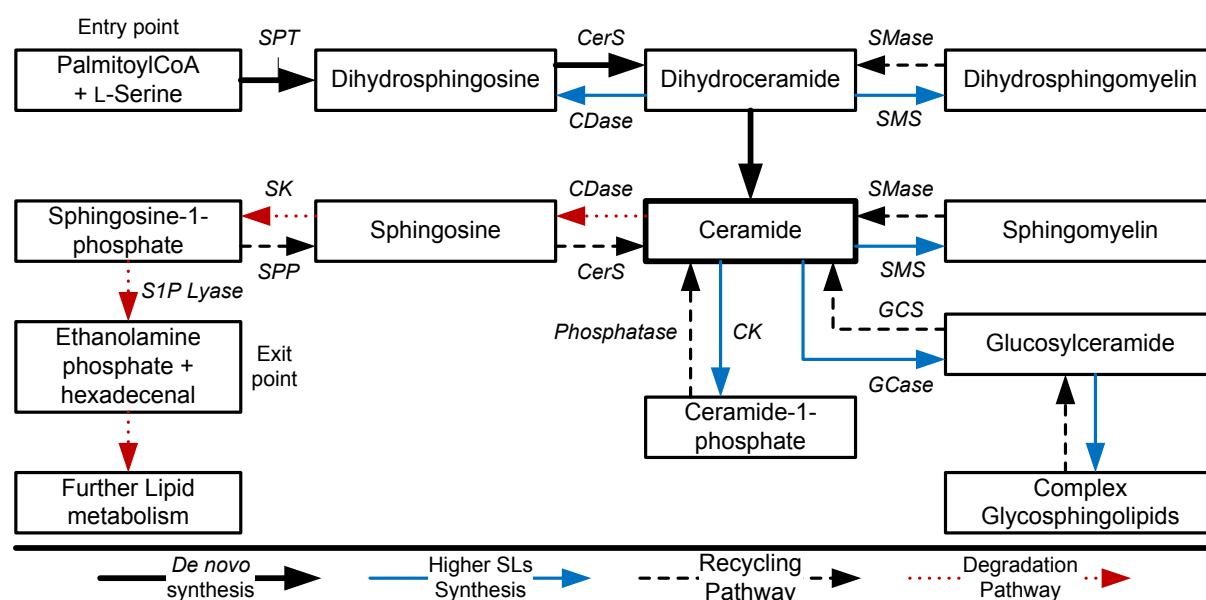


Figure 1-11: A simplified diagram of sphingolipids metabolism in mammalian cell. (Redrawn from ref. 27 with permission)

1.2.5.1 *De novo* Synthesis

De novo biosynthesis of sphingolipids takes place in the ER and Golgi apparatus.²⁸ It has a rate-limiting entry point, condensation of palmitoyl-CoA with L-serine catalysed by serine palmitoyl transferase (SPT) to produce 3-ketosphinganine in the ER. This is subsequently reduced to sphinganine. These two metabolic steps are largely conserved across all the Eukaryota (Figure 1-12).

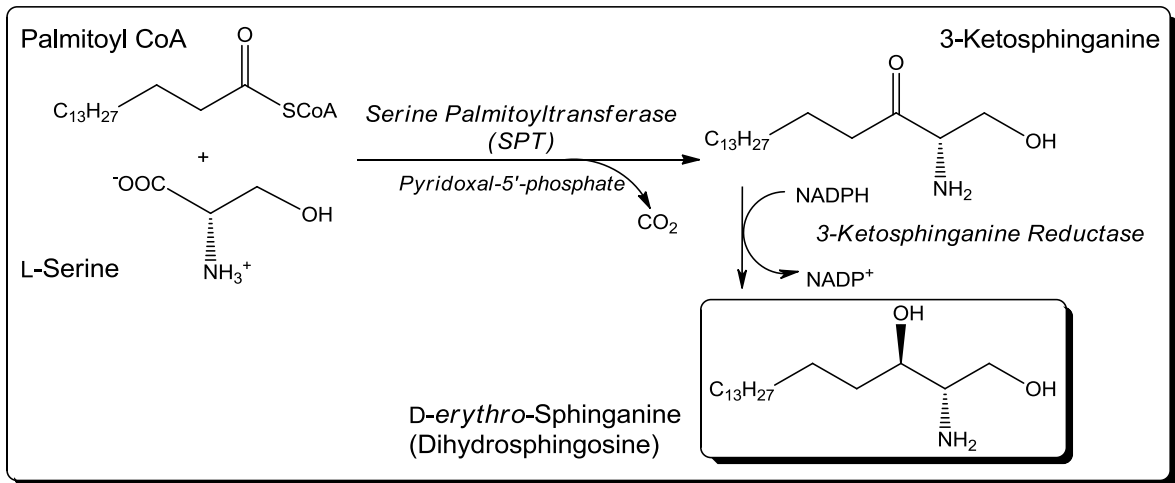


Figure 1-12: Mammalian biosynthesis of dihydrosphingosine

Following sphinganine formation, metabolic differences are encountered. While in fungi and higher plants sphinganine is hydroxylated to phytosphingosine then acylated to produce phytoceramide, in animal cells sphinganine is acylated to dihydroceramide which is later desaturated to form ceramide (Figure 1-13).²⁹

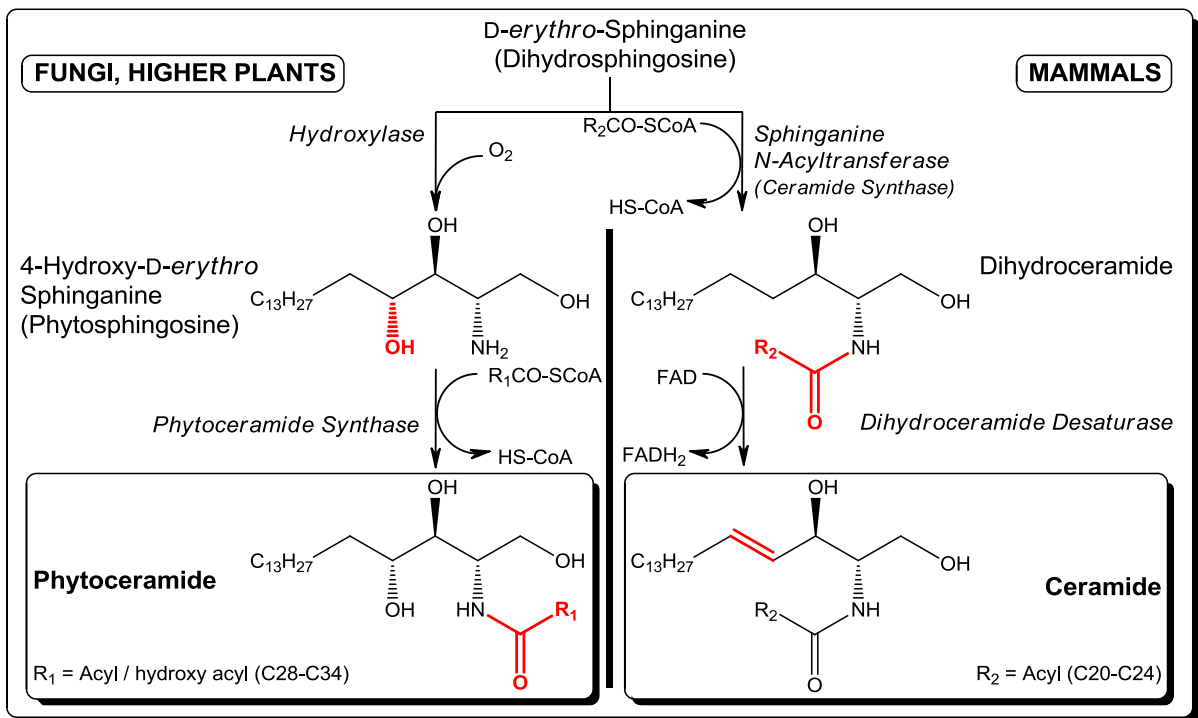


Figure 1-13: Sphinganine metabolism in different species

Ceramide (or phytoceramide), the simplest sphingolipid, is then transported from the ER to the Golgi apparatus where further synthesis of complex sphingolipids takes place.^{8, 30-32} Ceramide can be phosphorylated by ceramide kinase,³³ glycosylated by glucosyl or galactosyl ceramide synthases³⁴ or acquires a variety of neutral or charged head groups to form various complex sphingolipids depending on the host organism. For example, in animal cells¹⁶ ceramide is a substrate mainly for sphingomyelin synthase (SMS 1 & 2) to produce sphingomyelin. In contrast, fungi and higher plants utilise phytoceramide to produce inositol phosphorylceramide (IPC) as their principal complex sphingolipid, a reaction catalysed by IPC synthase. IPC is later used to produce more complex phosphosphingolipids (PSLs) (e.g. glycosylated PSLs in plants and mannose-IPC (MIPC) in yeast).^{29, 35-36} Finally, *Kinetoplastidae* represent a distinct third group³⁷ in which ceramide³⁸ acquires a phosphorylinositol head group to produce IPC (Figure 1-14).

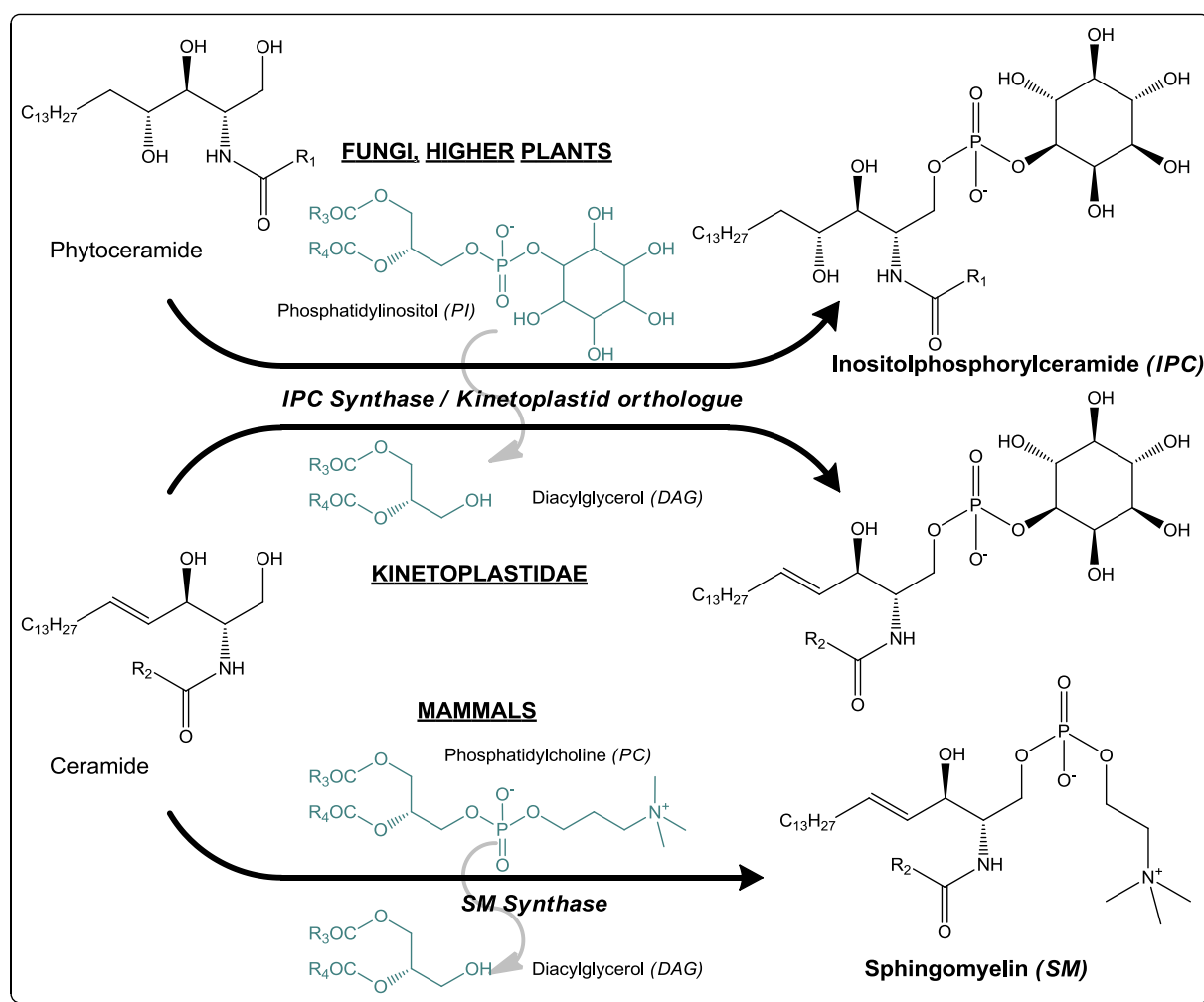


Figure 1-14: Divergence in the *post-ceramides* biosynthetic steps

It is noteworthy that although phosphoinositol-containing sphingolipids are completely absent from mammalian cells, the ceramide component of the *Kinetoplastidae* IPC shows more similarity to its mammalian counterpart, sphingomyelin.³⁹ Notably, it contains a sphingosine base and (C16-C18) fatty acid moieties⁴⁰⁻⁴² as opposed to the fungal IPC which has a phytosphingosine backbone attached to a very long chain (C26) fatty acid group (Figure 1-9).⁴³ These unique structural features indicate that the *Kinetoplastidae* IPC represents a stand-alone class of sphingolipids which is an intermediate between fungal and mammalian counterparts.

1.2.5.2 Recycling, Salvage and Degradation

In addition to the *de novo* synthesis, cellular levels of sphingolipids are modulated by the recycling/salvage and degradation pathways. These pathways operate in the direction of ceramide regeneration from complex sphingolipid reservoirs (GSLs and SMs) through the action of specific hydrolases. Based on the subcellular localisation, sphingolipid recycling can be categorised into two pathways: lysosomal and non-lysosomal degradation.

In lysosomal degradation, breakdown of GSLs occurs as sugar residues are cleaved leading to the formation of glucosylceramide and galactosylceramide. In turn, specific β -glucosidases and galactosidases hydrolyse these lipids to regenerate ceramide which is then deacylated by an acid ceramidase to form sphingosine.^{27, 44} In non-lysosomal degradation, breakdown of SM takes place. This is catalysed by acid, neutral or alkaline sphingomyelinases (SMases) according to the cellular localisation releasing ceramide. Additionally, SM can be degraded in extracellular membranes as in lipoproteins.³⁶ In all cases, the released ceramide can be either recycled into sphingolipid synthesis or degraded to sphingosine.^{27, 44}

The resultant sphingosine, produced from either pathway, is either recycled into sphingolipid biosynthesis or phosphorylated by a cytosolic sphingosine kinase (SK) yielding sphingosine-1-phosphate (S1P). S1P can itself be dephosphorylated back to sphingosine or irreversibly degraded by S1P lyase into non-sphingolipid molecules, ethanolamine phosphate (P-EtN) and hexadecenal, representing a unique exit point from the sphingolipid metabolic pathway (Figure 1-11).^{27, 44}

1.2.6 Biological Significance

Sphingolipids play two major interconnected roles within the cell. They are ubiquitous and essential structural components of eukaryotic membranes³⁷ as well as some prokaryotic organisms and viruses¹³. They are found predominantly in the outer leaflet of the plasma membrane,¹⁶ the lumen of intracellular organelles^{28,35} and lipoproteins.¹³ Additionally, sphingolipids are bioactive signalling molecules that control a plethora of cellular events. It is noteworthy that some sphingolipid metabolites can exhibit both structural and signalling functionalities. For example, glycosphingolipids have been reported to be involved in cellular recognition complexes (e.g. blood group antigens), cell adhesion and regulation of cell growth.¹⁶

1.2.6.1 Sphingolipids as Structural Components

The unique features of the molecular structure of sphingolipids comprising the free C3-hydroxyl group, the amide functionality (amine group in non-acylated sphingoid bases) and the C4-C5 *trans* double bond notably affect the biophysical properties of both simple sphingoid bases and complex sphingolipids. Comparative studies have reported how the interfacial regions of sphingomyelin (SM) and its phospholipid analogue, phosphatidylcholine (PC), differ significantly from each other.⁴⁵⁻⁴⁶ In SM the amide nitrogen and the C3-hydroxyl groups could act as hydrogen bond donors and acceptors whereas the amide carbonyl could act as hydrogen bond acceptor. However, in PC, the two ester carbonyls could only function as hydrogen bond acceptors (Figure 1-15).⁴⁷⁻⁴⁸

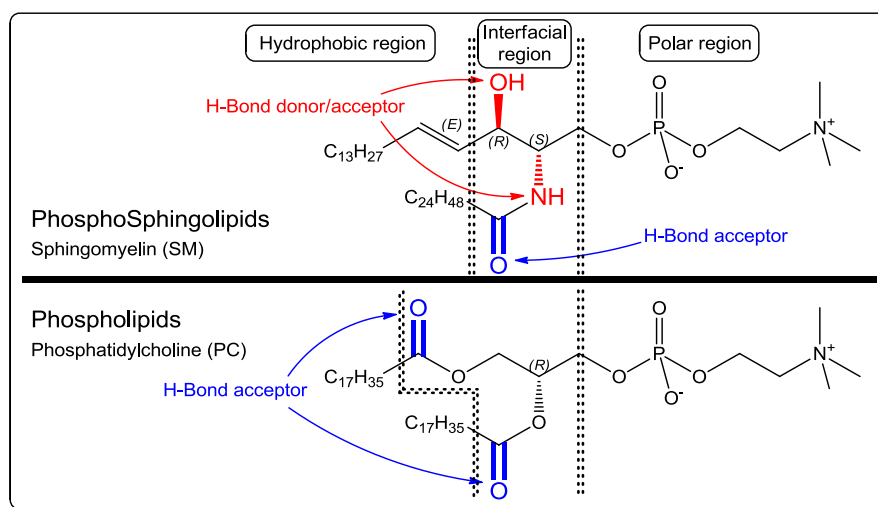


Figure 1-15: Molecular differences between SM and PC

These interfacial differences give SM the unique ability to form both *intra*- and *intermolecular* hydrogen bonding. SM spectroscopic studies have revealed a strong intramolecular hydrogen bond between the C3- hydroxyl and the bridging phosphate ester C1-oxygen. Such a hydrogen bond is unique for the naturally occurring diastereomer of SM.⁴⁹ Furthermore, the *trans* double bond seems to affect the strength of the hydrogen bonding interactions. For example, weaker intramolecular, but stronger intermolecular hydrogen bonds are formed in *dihydrosphingomyelin* assemblies compared to SM.⁴⁶

These molecular features explain the tendency of sphingolipids to cluster rather than behave like typical “fluid” membrane lipids. In general, naturally occurring sphingolipids undergo the L_{β} (gel phase) to L_{α} (lamellar phase) transition near the physiological temperature of 37 °C while this transition for naturally occurring phospholipids is near or below 0 °C. In addition, the long saturated alkyl chains of sphingolipids allow them to pack tightly with sterols.⁵⁰ Current knowledge suggests that the interaction between cholesterol and SM is stabilised by hydrogen bonding attributed to the amide functionality.⁴⁶ Analogous results have been reported with the SM fungal/plant counterpart, IPC, where it was shown that IPC was able to form sterol containing ordered domains in model systems.⁵⁰

These findings combined support the hypothesis regarding how sphingolipids interact with sterols to form laterally compact hydrophobic micro-domains known as ‘rafts’.⁵¹ These domains can readily segregate from the more disordered and expanded domains of unsaturated acyl chains of phospholipids.¹³ Membrane rafts have been proposed to function in a diverse array of processes from polarised trafficking of lipid modified proteins⁵² and the stabilisation of other types of biological structures such as lamellar bodies, to the assembly and activation of signal transduction complexes.^{13, 27, 53-55}

In a similar fashion, glycosphingolipids (GSLs) have the opportunity to form an extensive hydrogen-bonding network in the head group region. Therefore they form detergent-insoluble gel-phase domains⁴⁶ that have been implicated during the formation of ‘caveolae’.¹³

1.2.6.2 Sphingolipid as Biological Signalling Agents

Although sphingolipids are hydrophobic molecules and subject to subcellular localisation and a specialised transport system, their chemical structures provide the biophysical properties needed for their functions as bioactive signalling molecules. For example, the low pK_a (7 ~ 8) of sphingosine allows it to remain partially uncharged at physiological pH retaining the ability to move across membranes.¹³ Likewise, ceramide, a neutral species, is able to freely flip flop across membranes.²⁷

Sphingolipids represent an important group of bioactive molecules with a complex network of cell signalling effects. Sphingosine has been first identified to exert pleiotropic effects on protein kinases. Also, several sphingolipid metabolites have been reported to affect many cellular processes. For example, ceramide mediates many cell-stress responses, including the regulation of apoptosis,³⁵ whilst sphingosine-1-phosphate (S1P) has crucial roles in cell survival, cell migration and inflammation.²⁷

However, the investigation and deciphering of the functions of each specific sphingolipid remains challenging. This is due to the complexity in sphingolipid metabolic interconnection, their varied biophysical properties (neutral or charged), the hydrophobic nature of the involved enzymes and the presence of multiple pathways that can operate in parallel.²⁷ The interaction with other cellular metabolic pathways (e.g. phospholipid metabolism) introduces another layer of complexity.

Overall, the signalling effect of an individual sphingolipid could be defined as a three dimensional function in terms of subcellular localisation, regulation and mechanism of action. For example, phosphorylation of 1~3 % cytosolic sphingosine may double the levels of S1P that acts on G protein-coupled receptor (GPCR) to elicit a specific response.²⁷ Such signalling event can be described as a function of cytosolic S1P that is regulated by S1P Kinase and works through interaction of S1P with a GPCR. The description of such complex systems remains challenging and a comprehensive discussion of the issue is beyond the scope of this thesis.

1.2.6.3 Defects in sphingolipids metabolism: the Sphingolipidoses

The sphingolipidoses comprise a group of inherited metabolic disorders, e.g. hereditary sensory neuropathy type I, neurointestinal hyperplasia and colon tumorigenesis,^{13, 56} in which a mutation of one of the lipid hydrolases or activator proteins blocks sphingolipid degradation.⁵⁶ They are characterized by pathological accumulations of specific lipids in organs and tissues affecting primarily the central nervous system.⁵⁷ Most of these diseases are fatal in the first few years of life. However, there are two conditions (Gaucher's Type I and Fabry's diseases) which affects the systemic organs but not the central nervous system and result in longer life spans (Figure 1-16).⁵⁸

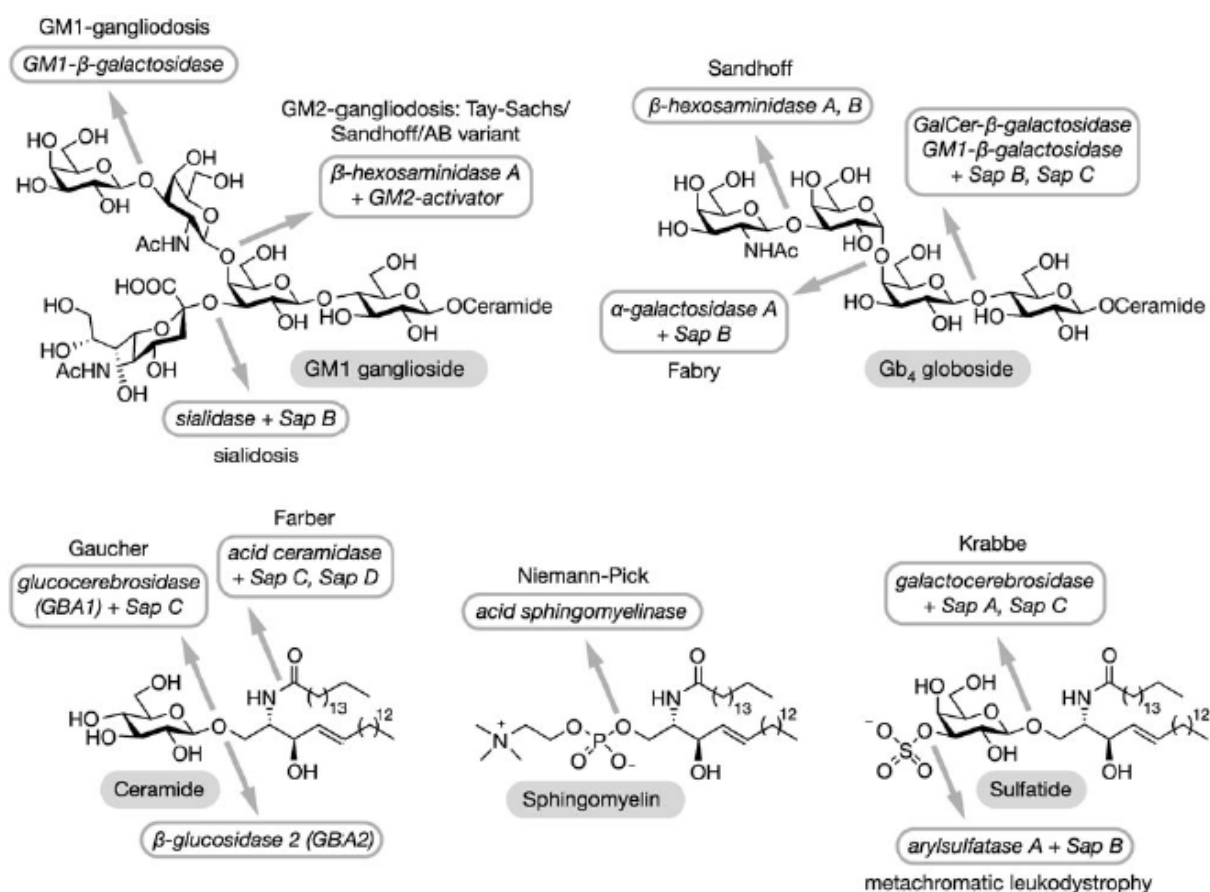


Figure 1-16: Overview of mammalian (glyco) sphingolipid catabolism. The enzyme/glycosidase and activator proteins responsible are indicated at the glycosidic linkage. The associated sphingolipidose that is manifested by an enzyme defect is also shown. (Reprinted from Ref. 59 with permissions)

1.2.7 Sphingolipid Biosynthesis: An Attractive Drug Target

The essential functions of sphingolipids coupled with the divergence in their biosynthetic pathways between mammals and pathogens have resulted in investigation of the biosynthetic enzymes as possible drug targets. Consequently, a list of inhibitors with enzyme targets spanning all the steps of sphingolipid biosynthesis has been described.^{13, 35}

The sphingolipid biosynthetic pathway is almost conserved until the synthesis of ceramide. Therefore, all the inhibitors that target the fungal enzymes before the ceramide step failed in drug development because of potential host toxicity as absolute selectivity has not been attainable (e.g. Fumonisin which inhibits phytoceramide synthase causes toxic effects in animals).³⁵ In contrast, the *post*-ceramide divergence represented by the absence of inositol-based sphingolipids from mammalian cells and the fact that IPC synthase has no mammalian equivalent highlights the therapeutic potential of putative inhibitors targeting the fungal IPC synthase(s). Such inhibitors could result in selective anti-fungal drugs with minimised host toxicity. Additionally, the recent identification and isolation of the functional orthologues of the fungal IPC synthase in the *TriTryp* genome (*Leishmania major*, *Trypanosoma brucei* and *Trypanosoma cruzi*) carried out by Denny *et al.*³⁷ has expanded the clinical prospects of IPC synthase(s) as potential anti-parasitic drug targets (*vide infra* 1.5 Project Objectives and Work Strategy).

To date, only three molecules, aureobasidin A,⁶⁰⁻⁶² khafrefungin⁶³ and rustmicin⁶⁴⁻⁶⁵ (Figure 1-17), have been reported as potent inhibitors against the fungal IPC synthase.^{13, 35, 66} Further extensions of their inhibitory effect to include the *Kinetoplastidae* orthologues have been shown.^{37, 67-68} Unfortunately, further development of all the three known inhibitors of IPC synthase have stalled either due to lack of physical properties required for an acceptable pharmacokinetic profile (e.g. aureobasidin A is very sparingly soluble in water)^{35, 66} or their highly complex chemical structures that render chemical synthesis challenging. Moreover, the few synthetic efforts reported that aimed to modify or synthesise analogues resulted in compounds with either reduced or no activity.^{66, 69}

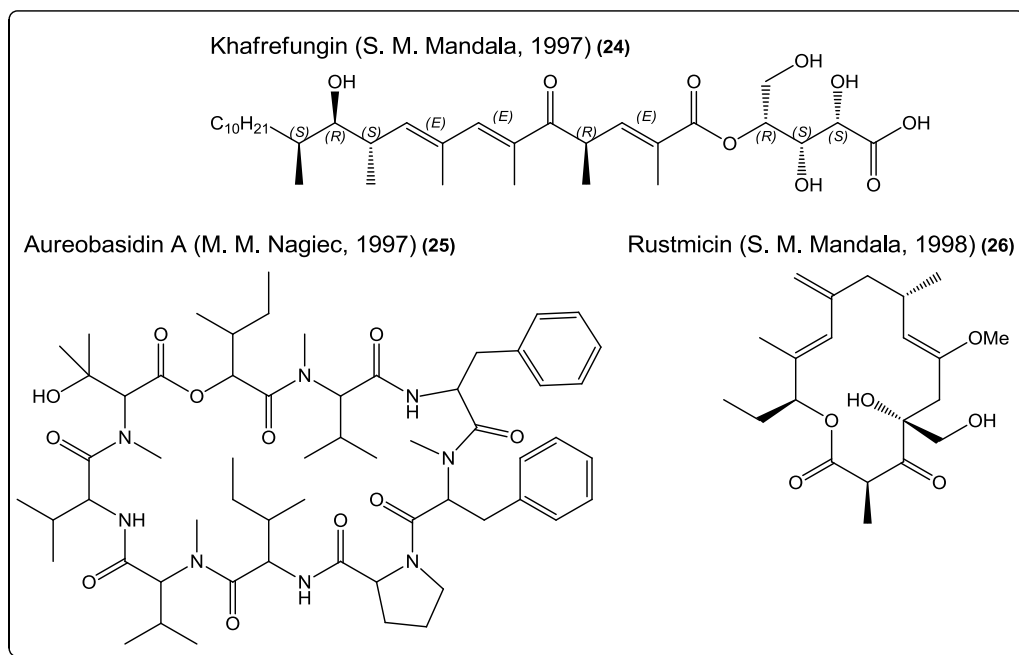


Figure 1-17: Inositol phosphorylceramide synthase inhibitors

1.3 Kinetoplastidae: *Leishmania* spp. and *Trypanosoma brucei*

Kinetoplastids are an important group of protozoan parasites. They are characterised by the presence of an internal structure containing an extensive mitochondrial DNA, termed the kinetoplast. *Trypanosomatids*, a subgroup of *Kinetoplastids*, have characteristic elongated to very slender single-flagellated cells.

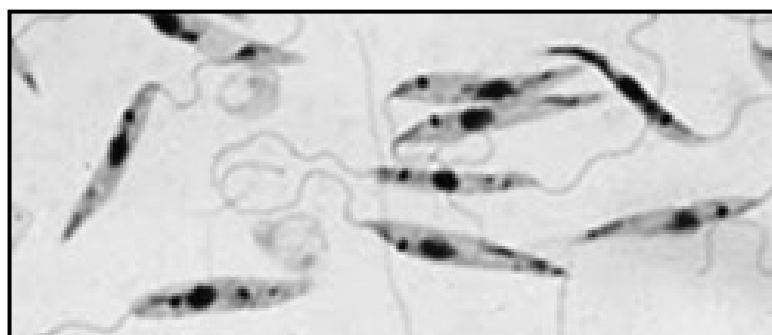


Figure 1-18: *Leishmania* parasite. (<http://www.google.com/> > image > *Leishmania*)

Leishmania spp. (causative agent of Leishmaniases) and *T. brucei* (causative agent of Human African Trypanosomiasis, HAT) belong to the family *Trypanosomatidae* (Figure 1-19). They are widespread vector-borne parasites causing a combined disease burden over 3.5 million Disability Adjusted Life Years. Conversely, the prevention measures (e.g. residual spraying of insecticides) proved effective against Chagas' disease caused by the closely related *T. cruzi* and the disease threat is retreating. In 2004, Leishmaniasis and HAT have been ranked Category '1' - Emerging and Uncontrolled Diseases - by the WHO (Table 1-1).⁷⁰

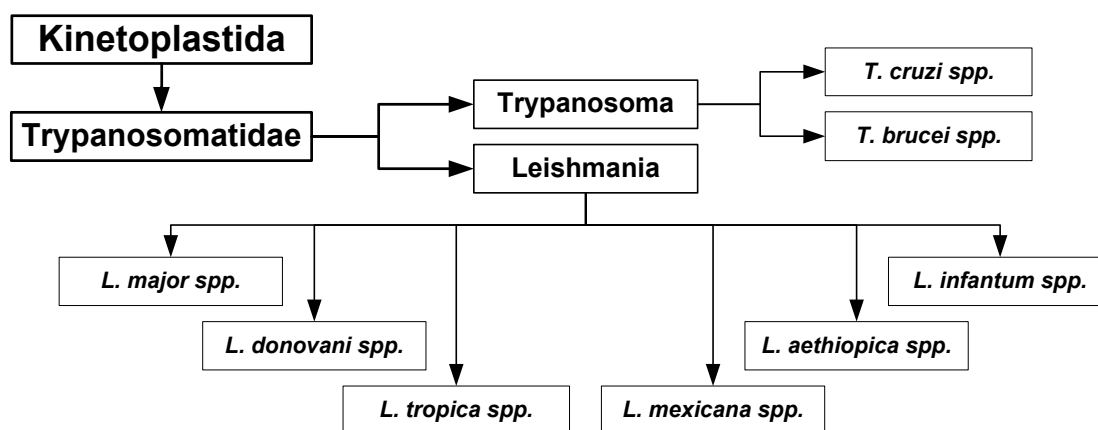


Figure 1-19: Taxonomy of Kinetoplastida

Table 1-1: Kinetoplastids Diseases Portfolio

	TDR disease category	Disease burden DALYs* (x1000)			Deaths (x1000)		
		Total	Male	Female	Total	Male	Female
<i>African trypanosomiasis</i>	1	1,525	996	559	48	31	17
<i>Leishmaniasis</i>	1	2,090	1,249	840	51	30	21
<i>Chagas disease</i>	3	667	343	324	14	8	7

* Disability Adjusted Life Years (the number of healthy years of life lost due to premature death and disability)

1.3.1 *Leishmania* spp. and the Leishmaniases

1.3.1.1 Introduction

Leishmania spp. comprise at least 16 widespread species and subspecies causing the Leishmaniasis complex in 88 countries over the five continents (Figure 1-20). It is one of the so-called ‘neglected’ diseases, i.e. low profile and status in public health priorities.⁷⁰ *Leishmania* is transmitted to mammals, including humans, by phlebotomine sandflies (Figure 1-21).⁷⁰⁻⁷¹ However, vertical (transplacental) transmission, venereal transmission, and even rare cases of direct horizontal transmission between dogs have been documented.⁷²

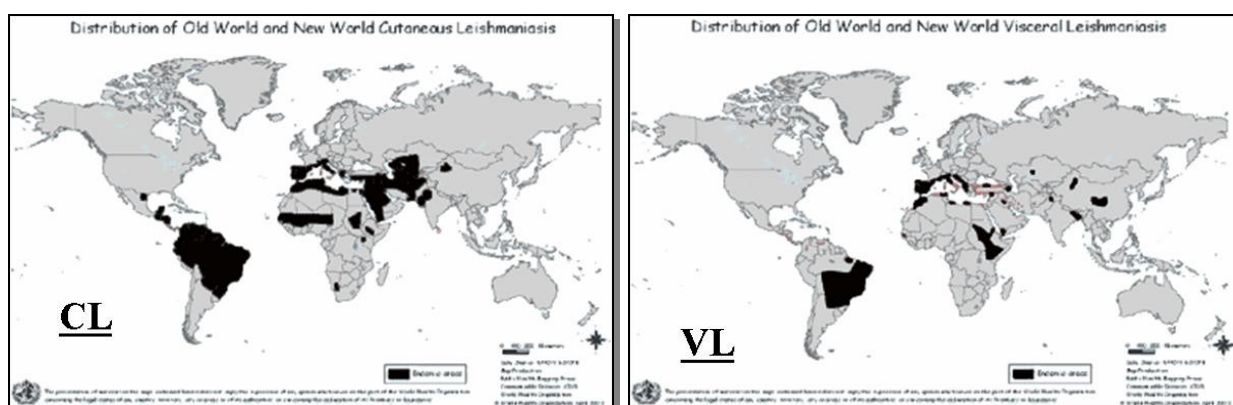


Figure 1-20: The Geographical distribution of Leishmaniasis worldwide. CL, Cutaneous Leishmaniasis; VL, Visceral Leishmaniasis. (www.who.org, 2007)

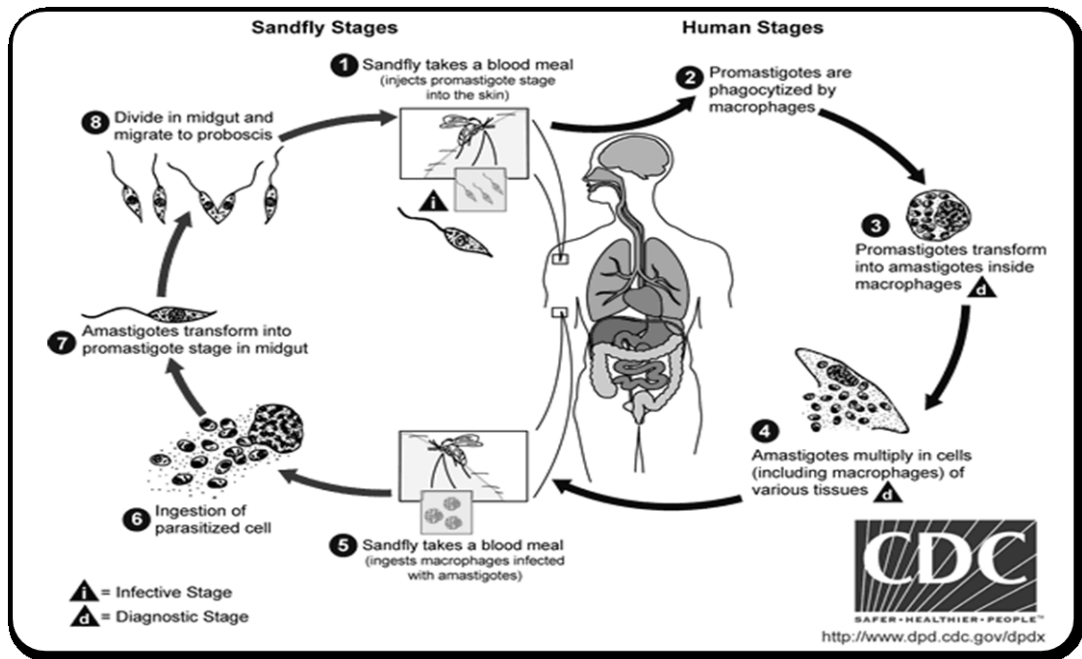


Figure 1-21: life Cycle of *L. major*

The Leishmaniasis are characterised by a spectrum of clinical manifestations: ulcerative skin lesions developing at the site of the sandfly bite (localised cutaneous leishmaniasis [LCL]); multiple non-ulcerative nodules (diffuse cutaneous leishmaniasis [DCL]); destructive mucosal inflammation (mucosal leishmaniasis ML); and disseminated visceral infection (visceral leishmaniasis VL). This last form is by far the most deadly reason which, if untreated, becomes lethal usually within several months.⁷⁰ Although most cases of CL heal spontaneously leaving the person immune to further infection, other forms of Leishmaniasis are extremely difficult to treat particularly in immune-compromised patients.

1.3.1.2 Available treatment

Whilst leishmania infections can be prevented by avoidance of sandflies bites through use of repellents or insecticides, vector and reservoir host control measures are expensive, requiring good infrastructure and maintenance and often give results which are short-lived.⁷⁰ Consequently, drugs represent a more viable solution.

There are a number of existing chemotherapies that have been used for decades. Treatment often requires a long course of intravenous pentavalent antimony drugs (e.g. Glucantime and

Pentostam), aminosidine or liposomal amphotericin B (Figure 1-22).^{70, 72-74} The most recent addition was in 2002 when Miltefosine,⁷⁵⁻⁷⁶ originally developed as anti-neoplastic agent, exhibited good efficacy against visceral Leishmaniasis *in vitro* and, with oral administration, in animals. Despite its teratogenic effects,⁷⁶ due to the lack of effective medications, it has been registered and is now used in India, Colombia, Guatemala and Germany.⁷⁷

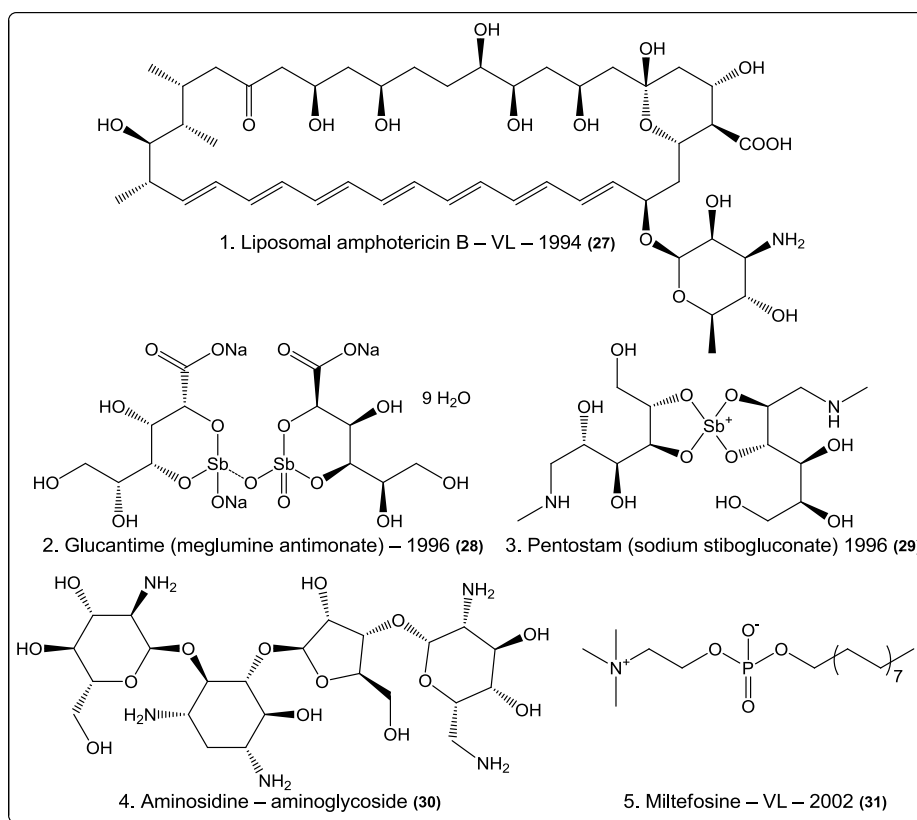


Figure 1-22: The commonly used anti-leishmanial therapeutic agents

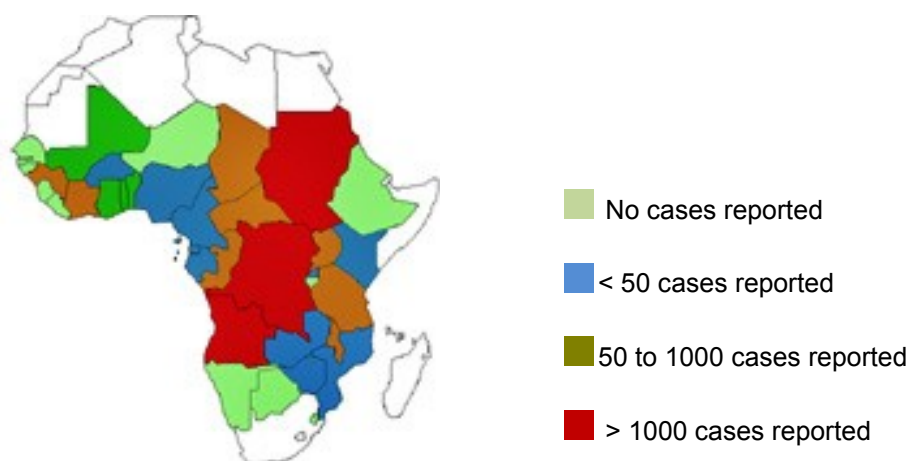
Other regimens of treatment include pentamidine⁷⁸, paromomycin, allopurinol, dapsone, fluconazole, itraconazole and ketoconazole. However, to-date all available chemotherapeutic agents suffer from being toxic⁷⁹ or inaccessible, both geographically and financially, in endemic areas where public health is under-resourced, poor and underdeveloped.

Overall, the lack of effective vaccines⁸⁰ and the alarming emergence of resistance⁸¹ to these drugs demand an intensive search for alternative anti-leishmanials to enable effective treatment and control. Therefore, the discovery of the *Lmj*IPCS by Denny *et al.*, represents a promising lead for drug targets against Leishmaniasis.

1.3.2 *Trypanosoma brucei* spp. and HAT

1.3.2.1 Introduction

T. brucei spp. are the causative agent of HAT, commonly known as African sleeping sickness. Like the leishmaniasis, it is a vector-borne parasitic disease transmitted to humans by the tsetse fly (*Glossina* Genus) bites. It can also be transmitted transplacentally, by mechanical transmission and via contaminated needles. In 2000 WHO estimated HAT to threaten 50 to 60 million people in 36 countries of sub-Saharan Africa (Figure 1-23), mainly in rural areas where health systems are weak or non-existent. By 2007, WHO surveillance policies had been reinforced and the number of reported new cases per year fell to 10,000.



Source: http://www.who.int/trypanosomiasis_african/disease/en/index.html, accessed 6th Feb 2010

Figure 1-23: Annual number of cases reported to WHO, 2000–2007

HAT takes two forms, depending on the parasite involved; *Trypanosoma brucei gambiense* (*T.b.g.*) is prevalent in west and central Africa (> 90% of reported cases); the disease is chronic, generally lasting several years. *Trypanosoma brucei rhodesiense* (*T.b.r.*) is found in eastern and southern Africa (< 10% of reported cases); the disease is acute, lasting from a few weeks to several months. However, in both cases without proper diagnosis and treatment the outcome is death without any major signs or symptoms.

HAT has two stages; the first stage (haemolympathic phase) entails bouts of fever, headaches, joint pains and itching while the second stage (neurological phase) begins once parasite crosses the blood-brain barrier and invades the central nervous system causing disturbed sleep patterns, coma and eventual death..

1.3.2.2 Available treatment

Generally, treatment depends on the stage of the disease. In the first stage, the drugs used are less toxic, easier to administer and more effective. Treatment in the second stage requires a drug that can cross the blood-brain barrier. Such drugs are considerably toxic and complicated to administer. Currently, four drugs are registered for HAT treatment and are provided free of charge to endemic countries through a WHO private partnership with Sanofi-Aventis (pentamidine, melarsoprol and eflornithine) and Bayer AG (suramin) (Figure 1-24).

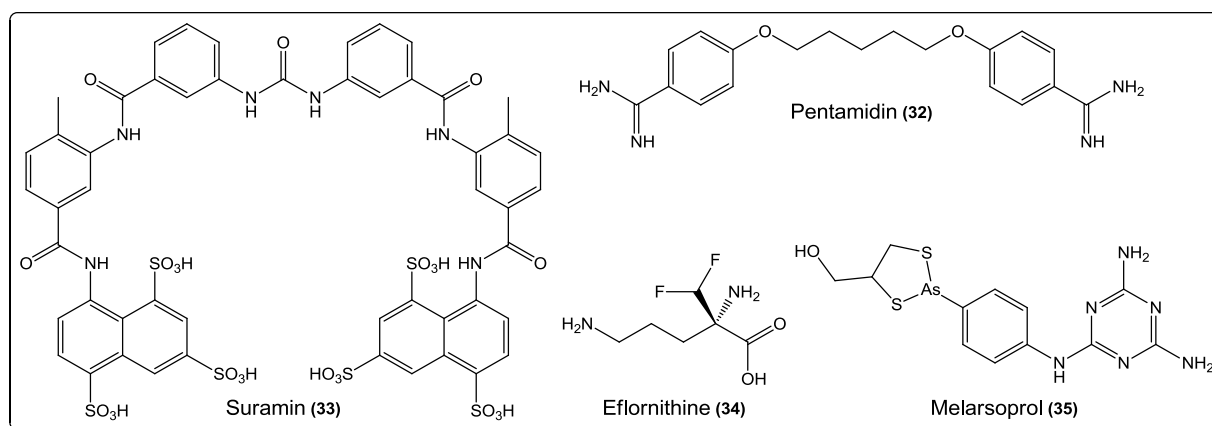


Figure 1-24: The commonly used anti-HAT therapeutic agents

Unfortunately, they all exhibit a broad range of adverse side-effects including death. Moreover, treatment regimens are usually highly restrictive particularly in the 2nd stage of the disease requiring hospital based I.V. treatment with continuous monitoring. Additionally, emerging drug resistance is an alarming problem.

1.3.3 Putative Drug Targets against Leishmaniasis and HAT

The current treatments for Leishmaniasis and HAT were developed many decades ago, and are often ineffective against resistant strains and/or possess toxic side effects.⁸² Thus, there has been an increasing demand for the identification of exploitable macromolecular targets for therapeutic development. Reflecting this, numerous pathways have attracted the attention as possible drug targets such as phosphorylation in kinase pathways and lipidation (e.g. farnesyltransferase and *N*-myristoltransferase).⁸³ Other proposed drug targets include tubulin, DNA topoisomerases, glucose and purine transporters and pyrimidine pathway in *Leishmania*, sterol biosynthesis (e.g. squalene synthase, SQS), histone deacetylases, glycolconjugates (e.g. Variant Surface Glycoprotein, VSG, in *T. brucei*) and kinetoplast DNA (kDNA) in general.⁸⁴ However, none of these researches have paid off yet.

1.4 The Kinetoplastid IPC Synthase(s): a Novel Drug Target

1.4.1 Identification and isolation

Precedent research reported that while *L. major*, *T. cruzi* parasites produce IPC as their principal complex sphingolipid, *T. brucei* parasite produces both IPC and SM.⁸⁵⁻⁸⁶ However, the enzymes responsible for such enigmatic functionality had not been isolated. In an attempt to identify this group of enzymes, Denny³⁷ screened the genome sequence databases of *L. major* (Sanger GeneDB) using a conserved motif shared by the lipid phosphate phosphatase (LPP) family, fungal AUR1p proteins, and animal sphingolipid synthases. The screen resulted in the identification of eight candidates, one of which (*Lmj*IPCS, *Lmj*F35.4990) encoded a putative transmembrane protein of unknown function with no orthologue in mammalian cells.

Additionally, orthologues of *Lmj*IPCS were found through a BLAST search of the *T. brucei* (4 sequences provisionally designated *Tb*SLS1–4) and *T. cruzi* (2 sequences provisionally designated *Tc*IPCS1 and *Tc*IPCS2) databases suggesting that the IPC synthase is a ubiquitous feature of this group of flagellated parasites. The *Tc*IPCS1 & 2 exhibited 52–53 % sequence identity and 69–70 % similarity with *Lmj*IPCS while *Tb*SLS1–4 exhibited 43–44 % identity and 61–63 % similarity with *Lmj*IPCS. Subsequent phylogenetic analyses of the kinetoplastid AUR1p orthologues identified them as a new separate class of eukaryotic phosphosphingolipid synthases (Figure 1-25).³⁷

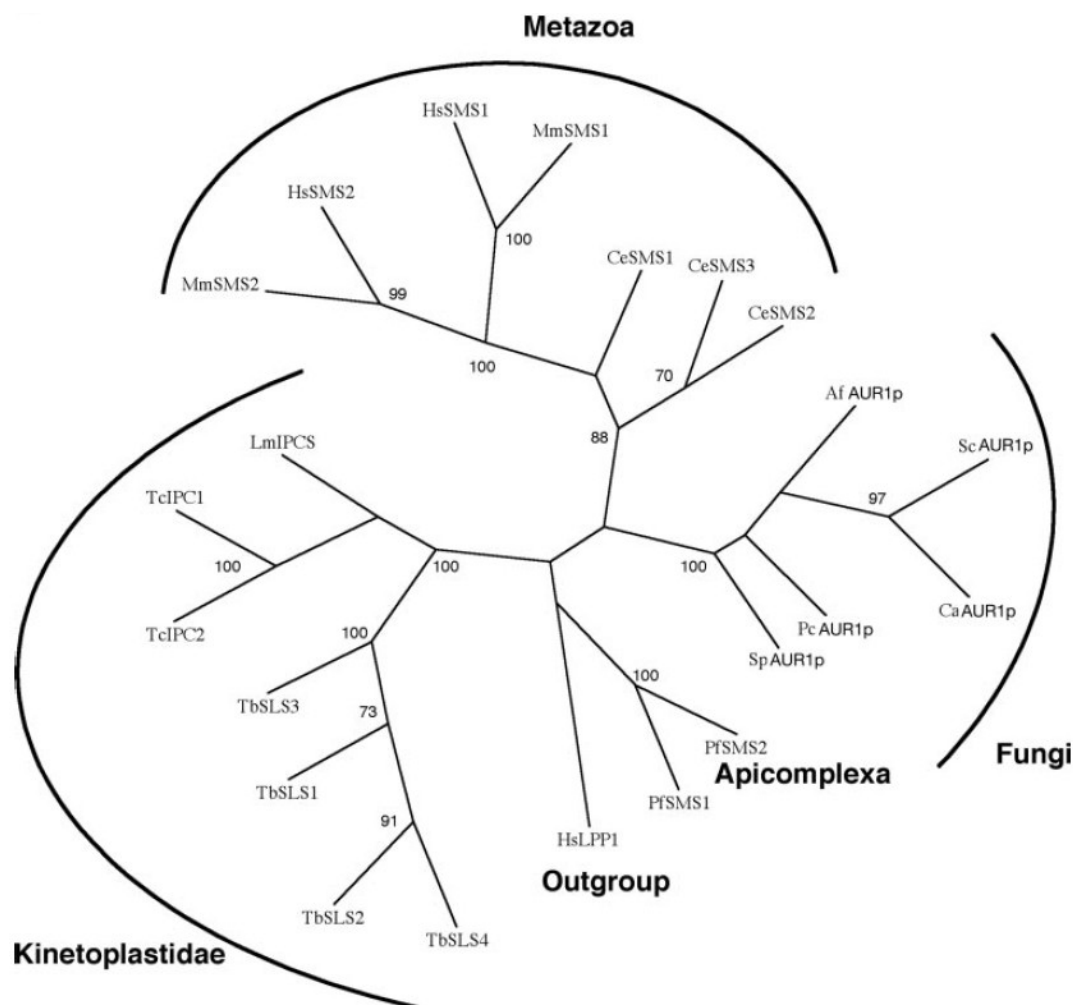


Figure 1-25: Phylogenetic Analysis of the Protozoan SpHINGOLIPID SYNTHASES

1.4.2 The Hypothetical Reaction Mechanism

All the identified kinetoplastid AUR1p orthologues demonstrated two conserved regions (CGDX₃SGHT & HYTXDVX₃YX₆FX₂YH) with respect to the animal SM synthases and LPP.⁸⁷ Similar observations were found for the fungal orthologue AUR1p.⁸⁸ These regions contain the so-called the catalytic triad (two Histidines and one Aspartate residues) that mediates nucleophilic attack on lipid phosphate ester during the transferase/hydrolase activity (Figure 1-26). Additionally, mutagenesis of this triad has been shown to deactivate the fungal IPC synthase and mammalian SMS activity.⁸⁹ However, the exact mechanisms of the catalytic action of these enzymes whether it is a sequential binding or a double displacement remain unknown.

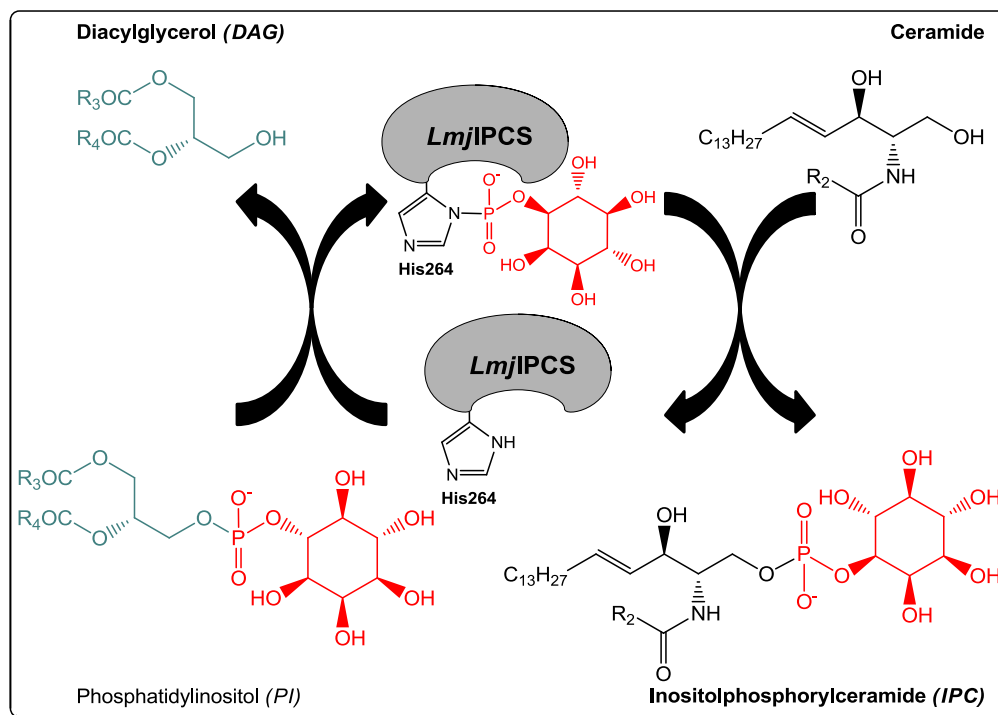


Figure 1-26: The hypothetical catalysis mechanism of *LmjIPCS* as an intersection between phospholipid and sphingolipid metabolism

1.4.3 The Biological Significance of IPC Synthases

In this biosynthetic step, the IPC synthase(s) (*LmjIPCS* in *L. major* and *TbSLSs* in *T. brucei*) catalyse(s) the analogous reaction mediated by SM synthase in mammalian cells. These evolutionarily divergent enzymes are both central in controlling a delicate balance of an intersection point between phosphoglycerolipids (PI in and DAG out) on one hand and phosphosphingolipids (PSLs) (ceramide in and IPC/SM out) on the other hand. Such control has significance as a regulator of the pro-apoptotic marker, ceramide and the mitogenic factor, DAG, a second messenger signalling molecule.⁹⁰ Accumulation of ceramide has been shown to induce programmed-cell death, apoptosis; an effect observed in the fungicidal activity of IPC synthase inhibitors³⁵ which is an analogous effect to the apoptotic ceramide role in mammalian cells. In addition to the mitogenic function, DAG has been attributed to play a role in several enzymatic activation and regulatory functions.¹³⁻¹⁴

1.4.4 *L. major* IPC Synthase

*Lmj*IPCS is encoded by a single-copy gene in *L. major*³⁷ and consists of 338 amino acids with MW of approximately 38 kDa (Figure 1-27). The active residues of the ‘Catalytic Triad’ have been identified by homology alignment and were proposed to be His264, Asp268 and His220. His264 is assumed to attack the electrophilic phosphorus in PI while the Asp268 is believed to act as a proton shuttle to facilitate such attack.⁹¹ However, the definite function of His220 remains unclear.

```

1  MTSHTAHDV  GGNEDIGTDH  VPWKQPLPL  CTQVMRFILL  LLLTVMFLGV  AILVANARMP
61  DPEKVRPLPD  LLESIPKVA  LLENGTNVII  FLLNATTVVV  GFKVFLLERH  MNGLPRVTFL
121  VGVPKIGSFL  NRMAFGVLD  GRRPFPLKNV  FPIMAIRFLT  SYAVVMVFRA  FVIMGTSYPA
181  TDNHCQNPQV  IEHPVLNVIL  TLVTLGSGAI  HCGDLMFSGH  TMILSLAFIL  AWDYSPFLHP
241  WAVRVWVSVL  LPISYYCILA  SRSHYTDDIL  VAMYVMIATY  KVIDHAETGA  PWQMQLLIRW
301  MPWPGANTIE  KWTAEDEVVV  VQTPAEDSTD  ASAALPEH

```

Figure 1-27: The Protein Sequence of *Lmj*IPCS. The Catalytic Triad is underlined

1.4.5 Topologies Studies

The first proposed structure of *Lmj*IPCS was introduced by *Denny et al.* and assumed that it consists of seven TMDs with the catalytic site facing the lumen of the Golgi apparatus. However, *Denny's* model lacked D2 motif present in orthologous enzymes in mammals (Figure 1-28: Panel A). A recent study by *Bangs' group*,⁹² introduced a different model. The early model was based on single sequence analysis of *Lmj*IPCS resulting in an extra helix (TMx, ~11 residues) between TM3 and TM4 and inversion of the upstream TM1–3 orientation to preserve the luminal positioning of the active-site in TM4 and TM6 while the recent model was produced using comparative alignment of single orthologous sequences from three kinetoplastid species, *Bang* discounted the TMx and claimed the presence of the conserved SM synthase D2 motif located in TM3 (Figure 1-28: Panel B).^{87, 89} However, to-date, experimental evidence to support either model is still lacking.

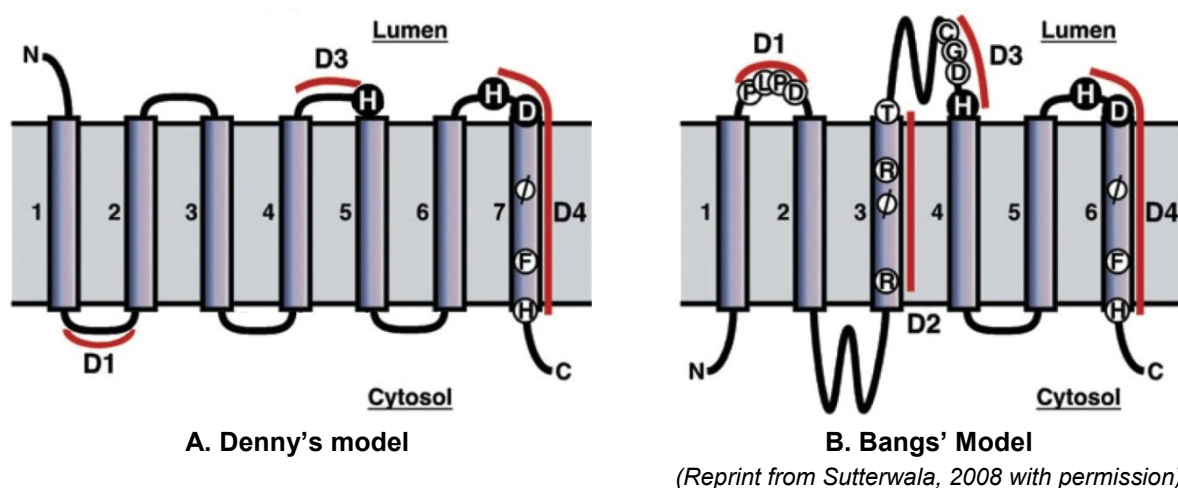


Figure 1-28: The proposed models for the AUR1p Kinetoplastid orthologues; (A) Denny's model assuming seven TMDs and lack of domain D2. (B) Bang's model of six TMDs illustrating the different domain according to Huitema et al. (2004) for human SMS2.

1.4.6 Sensitivity studies and drug target validation

Previous work within the group³⁷ involved the expression of the functional protozoan orthologue (*Lmj*IPCS) in a mutant yeast strain. Although the *Lmj*IPCS complemented yeast strain remained as sensitive to cycloheximide and myriocin as wild type yeast, it was resistant to aureobasidin A at 25 μ M (AbA MIC against *S. cerevisiae* is approximately 0.1 ~ 0.4 μ g/ml).^{66, 93} However, at AbA concentration equal to 100 μ M, inhibition of *Lmj*IPCS was apparent. Similarly, recent results have been reported by Tanaka et al.⁶⁷ confirmed the inhibitory effect of aureobasidin A on other leishmania species (e.g. *L. L. amazonensis*).

1.5 Project Objectives and Work strategy

With the AUR1p *kinetoplastid* orthologues, *Lmj*IPCS and *Tb*SLS4 have been isolated and identified, the next step was to characterise such enzymes so that their potential as putative drug targets can be further explored. The project primarily focuses on the characterisation of the *Lmj*IPCS with consideration of the possibility of expanding the techniques developed to the closely related *Tb*SLSs with an ultimate objective of exploiting their potential as a valid anti-protozoan drug targets. This project followed a logical set of objectives. Starting from the establishment of an *in vitro* activity assay protocol to the implementation of the assay in the determination of the kinetic parameters of *Lmj*IPCS and finally screening of a library of substrate mimics and custom drug-like molecules to generate a preliminary SAR data. The SAR data would provide a rationale for future work involving the synthesis of second generation library of inhibitors with a long-term objective for identifying drug-like inhibitor that can be upgraded to drug candidates suitable for clinical trials (Figure 1-29).

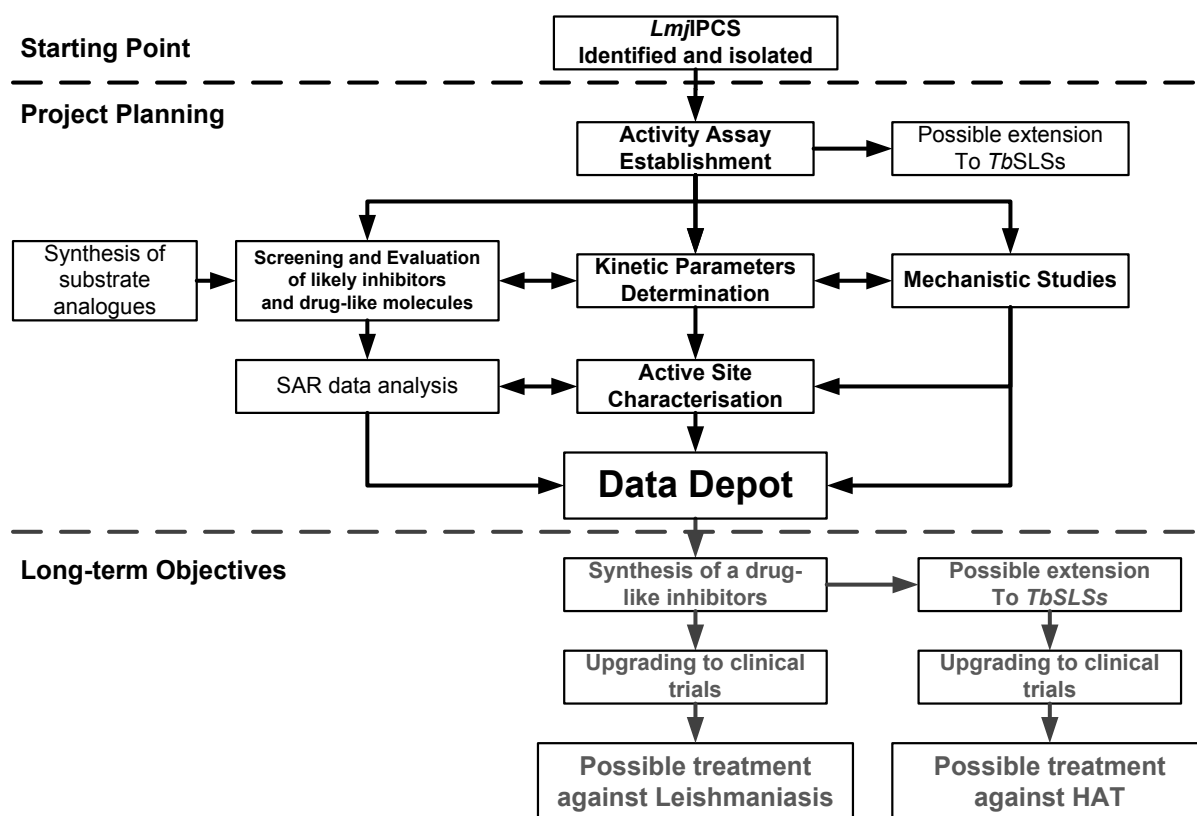


Figure 1-29 Project Objectives and Work Strategy

REFERENCES

1. J. L. W. Thudichum, *A Treatise on the Chemical Constitution of Brain*, London, 1884.
2. P. A. Levene and W. A. Jacobs, *J. Biol. Chem.*, 1912, **11**, 547-554.
3. P. A. Levene and C. J. West, *J. Biol. Chem.*, 1914, **16**, 549-553.
4. P. A. Levene and C. J. West, *J. Biol. Chem.*, 1914, **18**, 481-484.
5. H. E. Carter, F. J. Glick, W. P. Norris and G. E. Phillips, *J. Biol. Chem.*, 1947, **170**, 285-294.
6. D. Shapiro and K. Segal, *J. Am. Chem. Soc.*, 1954, **76**, 5894-5895.
7. A. Huwiler, T. Kolter, J. Pfeilschifter and K. Sandhoff, *Biochimica et Biophysica Acta (BBA) - Molecular and Cell Biology of Lipids*, 2000, **1485**, 63-99.
8. J. Ohanian and V. Ohanian, *Cell. Mol. Life Sci.*, 2001, **58**, 2053-2068.
9. O. Cu villier, *Biochimica et Biophysica Acta (BBA) - Molecular and Cell Biology of Lipids*, 2002, **1585**, 153-162.
10. B. J. Pettus, C. E. Chalfant and Y. A. Hannun, *Biochimica et Biophysica Acta (BBA) - Molecular and Cell Biology of Lipids*, 2002, **1585**, 114-125.
11. R. Buccoliero and A. H. Futerman, *Pharmacol. Res.*, 2003, **47**, 409-419.
12. Y. A. Hannun, C. R. Loomis, A. H. Merrill and R. M. Bell, *J. Biol. Chem.*, 1986, **261**, 2604-2609.
13. D. E. Vance and J. E. Vance, *Biochemistry of Lipids, Lipoproteins and Membranes*, 4th Edition edn., Elsevier Science, 2002.
14. D. E. Metzler, *Biochemistry; The Chemical Reactions of Living Cells*, 2nd edn., Elsevier Academic Press, 2003.
15. E. Fahy, S. Subramaniam, H. A. Brown, C. K. Glass, A. H. Merrill, Jr., R. C. Murphy, C. R. H. Raetz, D. W. Russell, Y. Seyama, W. Shaw, T. Shimizu, F. Spener, G. van Meer, M. S. VanNieuwenhze, S. H. White, J. L. Witztum and E. A. Dennis, *J. Lipid Res.*, 2005, **46**, 839-862.
16. M. I. Gurr, J. L. Harwood and K. N. Frayn, *Lipid Biochemistry: An Introduction*, 5 th edn., Blackwell Science Ltd., 2002.
17. R. M. Bell, A. H. Merrill, Jr. and Y. A. Hannun, *Advances in Lipid Research; Sphingolipids, Part A: Functions and breakdown products*, 1993, xiv+339p.
18. R. M. Bell, A. H. Merrill, Jr. and Y. A. Hannun, *Advances in Lipid Research; Sphingolipids, Part B: Regulation and function of metabolism*, 1993, xiv+384p.
19. A. H. Merrill, E. M. Schmelz, D. L. Dillehay, S. Spiegel, J. A. Shayman, J. J. Schroeder, R. T. Riley, K. A. Voss and E. Wang, *Toxicol. Appl. Pharmacol.*, 1997, **142**, 208-225.
20. S. T. Pruett, A. Bushnev, K. Hagedorn, M. Adiga, C. A. Haynes, M. C. Sullards, D. C. Liotta and A. H. Merrill, *J. Lipid Res.*, 2008, **49**, 1621-1639.
21. E. Fahy, S. Subramaniam, R. C. Murphy, M. Nishijima, C. R. H. Raetz, T. Shimizu, F. Spener, G. van Meer, M. J. O. Wakelam and E. A. Dennis, *J. Lipid Res.*, 2009, **50**, S9-14.
22. R. Anderson, M. Kates and B. E. Volcani, *Biochim. Biophys. Acta*, 1978, **528**, 89-106.
23. J. i. Kohayashi, S. Mikami, H. Shigemori, T. Takao, Y. Shimonishi, S. Izuta and S. Yoshida, *Tetrahedron*, 1995, **51**, 10487-10490.
24. W. Godchaux and E. R. Leadbetter, *J. Bacteriol.*, 1980, **144**, 592-602.
25. *Eur. J. Biochem.*, 1998, **257**, 293-298.
26. C. o. B. N. Iupac-Iub, *Chem. Phys. Lipids*, 1978, **21**, 159-173.
27. Y. A. Hannun and L. M. Obeid, *Nat. Rev. Mol. Cell Biol.*, 2008, **9**, 139-150.
28. G. Van Meer and Q. Lisman, *J. Biol. Chem.*, 2002, **277**, 25855-25858.
29. Y. Sugimoto, H. Sakoh and K. Yamada, *Curr. Drug Target - Infect. Disord.*, 2004, **4**, 311-322.
30. P. E. Bromley, Y. N. O. Li, S. M. Murphy, C. M. Sumner and D. V. Lynch, *Arch. Biochem. Biophys.*, 2003, **417**, 219-226.
31. M. O. Pata, Y. A. Hannun and C. K.-Y. Ng, *New Phytol.*, 2010, **185**, 611-630.
32. N. Bartke and Y. A. Hannun, *J. Lipid Res.*, 2009, **50**, S91-S96.
33. P. Rovina, A. Schanzer, C. Graf, D. Mechtcheriakova, M. Jaritz and F. Bornancin, *Biochimica Et Biophysica Acta-Molecular and Cell Biology of Lipids*, 2009, **1791**, 1023-1030.
34. A. Raas-Rothschild, I. Pankova-Kholmyansky, Y. Kacher and A. H. Futerman, *Glycoconjugate J.*, 2004, **21**, 295-304.
35. N. H. Georgopadakou, *Expert Opin. Invest. Drugs*, 2000, **9**, 1787-1796.
36. A. H. Merrill and K. Sandhoff, in *Biochemistry of Lipids, Lipoproteins and Membranes*, eds. D. E. Vance and J. E. Vance, Elsevier Science, Amsterdam, Editon edn., 2002, pp. 373-407

37. P. W. Denny, H. Shams-Eldin, H. P. Price, D. F. Smith and R. T. Schwarz, *J. Biol. Chem.*, 2006, **281**, 28200-28209.
38. K. Zhang, F.-F. Hsu, D. A. Scott, R. Docampo, J. Turk and S. M. Beverley, *Mol. Microbiol.*, 2005, **55**, 1566-1578.
39. G. Liebisch, B. Lieser, J. Rathenberg, W. Drobnik and G. Schmitz, *Biochim. Biophys. Acta*, 2004, 108-117.
40. R. Zufferey, S. Allen, T. Barron, D. R. Sullivan, P. W. Denny, I. C. Almeida, D. F. Smith, S. J. Turco, M. A. Ferguson and S. M. Beverley, *J. Bio. Chem.*, 2003, **278**, 44708-44718.
41. E. S. Kaneshiro, K. Jayasimhulu and R. L. Lester, *J. Lipid Res.*, 1986, **27**, 2171-2178.
42. B. N. Singh, C. E. Costello, D. H. Beach and G. G. Holz, *Biochem. Biophys. Res. Commun.*, 1988, **157**, 1239-1246.
43. R. C. Dickson and R. L. Lester, *Biochim. Biophys. Acta*, 1999, 347-357.
44. T. Kolter and K. Sandhoff, *Angewandte Chemie-International Edition*, 1999, **38**, 1532-1568.
45. C. M. Talbott, I. Vorobyov, D. Borchman, K. G. Taylor, D. B. DuPré and M. C. Yappert, *Biochimica et Biophysica Acta (BBA) - Biomembranes*, 2000, **1467**, 326-337.
46. B. Ramstedt and J. P. Slotte, *FEBS Lett.*, 2002, **531**, 33-37.
47. J. M. Boggs, *Biochim. Biophys. Acta*, 1987, **906**, 353-404.
48. J. M. Boggs, *Can J Biochem*, 1980, **58**, 755-770.
49. K. S. Bruzik, *Biochimica et Biophysica Acta (BBA) - Biomembranes*, 1988, **939**, 315-326.
50. A. Björkbom, H. Ohvo-Rekilä, P. Kankaanpää, T. K. M. Nyholm, B. Westerlund and J. P. Slotte, *Biochimica et Biophysica Acta (BBA) - Biomembranes*, **In Press, Corrected Proof**.
51. A. H. Futerman and Y. A. Hannun, *EMBO Reports*, 2004, **5**, 777-782.
52. D. A. Brown and E. London, *Annu. Rev. Cell Dev. Biol.*, 1998, **14**, 111-136.
53. T. Magee, N. Prinen, J. Alder, S. N. Pagakis and I. Parmryd, *Biol. Res.*, 2002, **35**, 127-131.
54. S. K. Pierce, *Nat. Rev. Immunol.*, 2002, **2**, 96-105.
55. D. A. Brown and E. London, *J. Biol. Chem.*, 2000, **275**, 17221-17224.
56. C.-S. Chen, M. C. Patterson, C. L. Wheatley, J. F. O'Brien and R. E. Pagano, *The Lancet*, 1999, **354**, 901-905.
57. F. M. Yatsu, *California Medicine*, 1971, **114**, 1-&.
58. R. O. Brady, *Annu. Rev. Biochem.*, 1978, **47**, 687-713.
59. T. Wennekes, R. van den Berg, R. G. Boot, G. A. van der Marel, H. S. Overkleeft and J. Aerts, *Angewandte Chemie-International Edition*, 2009, **48**, 8848-8869.
60. M. M. Nagiec, E. E. Nagiec, J. A. Baltisberger, G. B. Wells, R. L. Lester and R. C. Dickson, *J. Biol. Chem.*, 1997, **272**, 9809-9817.
61. N. Awazu, K. Ikai, J. Yamamoto, K. Nishimura, S. Mizutani, K. Takesako and I. Kato, *J Antibiot (Tokyo)*. 1995, **48**, 525-527.
62. K. Ikai, K. Takesako, K. Shiomi, M. Moriguchi, Y. Umeda, J. Yamamoto, I. Kato and H. Naganawa, *J Antibiot (Tokyo)*. 1991, **44**, 925-933.
63. S. M. Mandala, R. A. Thornton, M. Rosenbach, J. Milligan, M. Garcia-Calvo, H. G. Bull and M. B. Kurtz, *J. Biol. Chem.*, 1997, **272**, 32709-32714.
64. S. M. Mandala, R. A. Thornton, J. Milligan, M. Rosenbach, M. Garcia-Calvo, H. G. Bull, G. Harris, G. K. Abruzzo, A. M. Flattery, C. J. Gill, K. Bartizal, S. Dreikorn and M. B. Kurtz, *J. Biol. Chem.*, 1998, **273**, 14942-14949.
65. G. H. Harris, A. Shafiee, M. A. Cabello, J. E. Curotto, O. Genilloud, K. E. Goklen, M. B. Kurtz, M. Rosenbach, P. M. Salmon, R. A. Thornton, D. L. Zink and S. M. Mandala, *J Antibiot (Tokyo)*. 1998, **51**, 837-844.
66. Y. Sugimoto, H. Sakoh and K. Yamada, *Current Drug Targets - Infectious Disorders*, 2004, **4**, 311-322.
67. A. K. Tanaka, V. B. Valero, H. K. Takahashi and A. H. Straus, *J. Antimicrob. Chemother.*, 2007, **59**, 487-492.
68. K. Zhang, F. F. Hsu, D. A. Scott, R. Docampo, J. Turk and S. M. Beverley, *Mol. Microbiol.*, 2005, **55**, 1566-1578.
69. P. A. Aeed, C. L. Young, M. M. Nagiec and A. P. Elhammer, *Antimicrob. Agents Chemother.*, 2009, **53**, 496-504.
70. WHO. *The world health report 2004. Changing history*, <http://www.who.int/whr/2004/en/index.html>, (accessed June 12, 2007).
71. R. Reithinger, J. C. Dujardin, H. Louzir, C. Pirmez, B. Alexander and S. Brooker, *Lancet Infectious Diseases*, 2007, **7**, 581-596.
72. C. o. V. M. Center for Food Security and Public Health and A. Iowa State University, Iowa 50011, *Leishmaniasis (cutaneous and visceral)*, cfsph@iastate.edu, <http://www.cfsph.iastate.edu>.

73. L. Kedzierski, A. Sakthianandeswaren, J. M. Curtis, P. C. Andrews, P. C. Junk and K. Kedzierska, *Curr. Med. Chem.*, 2009, **16**, 599-614.
74. S. L. Croft and G. H. Coombs, *Trends Parasitol*, 2003, **19**, 502-508.
75. N. K. Verma and C. S. Dey, *Antimicrob. Agents Chemother.*, 2004, **48**, 3010-3015.
76. S. Sunder, T. K. Jha, C. P. Thakur, J. Engel, H. Sindermann, C. Fischer, K. Jungle, A. Bryceson and J. Berman, *N. Engl. J. Med.*, 2002, **347**, 1739-1746.
77. J. Soto and J. Berman, *Trans R Soc Trop Med Hyg*, 2006, **100**, S34-S40.
78. P. G. Bray, M. P. Barrett, S. A. Ward and H. P. de Koning, *Trends Parasitol*, 2003, **19**, 232-239.
79. F. Chappuis, S. Sundar, A. Hailu, H. Ghalib, S. Rijal, R. W. Peeling, J. Alvar and M. Boelaert, *Nat. Rev. Microbiol.*, 2007, **5**, 873-882.
80. C. I. de Oliveira, I. P. Nascimento, A. Barral, M. Soto and M. Barral-Netto, *Parasitol Int*, 2009, **58**, 319-324.
81. S. L. Croft, S. Sundar and A. H. Fairlamb, *Clin Microbiol Rev*, 2006, **19**, 111-126.
82. A. R. Renslo and J. H. McKerrow, *Nat. Chem. Biol.*, 2006, **2**, 701-710.
83. P. W. Bowyer, E. W. Tate, R. J. Leatherbarrow, A. A. Holder, D. F. Smith and K. A. Brown, *ChemMedChem*, 2008, **3**, 402-408.
84. H. K. Majumder, *Adv. Exp. Med. Biol.*, 2008, **625**, vii-viii.
85. M. L. S. Guthrie, S. Lee, L. Tetley, A. Acosta-Serrano and M. A. J. Ferguson, *Mol. Biol. Cell*, 2006, **17**, 5265-5274.
86. P. K. Patnaik, M. C. Field, A. K. Menon, G. A. M. Cross, M. C. Yee and P. Butikofer, *Mol. Biochem. Parasitol.*, 1993, **58**, 97-105.
87. K. Huitema, J. van den Dikkenberg, J. Brouwers and J. C. M. Holthuis, *EMBO J.*, 2004, **23**, 33-44.
88. S. A. Heidler and J. A. Radding, *Biochim. Biophys. Acta-Mol. Basis Dis.*, 2000, **1500**, 147-152.
89. T. P. Levine, C. A. R. Wiggins and S. Munro, *Mol. Biol. Cell*, 2000, **11**, 2267-2281.
90. J. C. M. Holthuis, F. G. Tafesse and P. Ternes, *J. Biol. Chem.*, 2006, **281**, 29421-29425.
91. Y. J. Sigal, M. I. McDermott and A. J. Morris, *Biochem. J.*, 2005, **387**, 281-293.
92. S. S. Sutterwala, F. F. Hsu, E. S. Sevova, K. J. Schwartz, K. Zhang, P. Key, J. Turk, S. M. Beverley and J. D. Bangs, *Mol. Microbiol.*, 2008, **70**, 281-296.
93. M. Endo, K. Takesako, I. Kato and H. Yamaguchi, *Antimicrob. Agents Chemother.*, 1997, **41**, 672-676.

CHAPTER II

CHARACTERISATION OF *Lmj*IPCS

2 CHARACTERISATION OF *Lmj*IPCS

2.1 Work Synopsis

This chapter describes work towards two major objectives of this project (Figure 2-30). The first objective focused on the establishment of an activity assay protocol for the *Lmj*IPCS. The requirements of the assay protocol included ease of accessibility, cost efficiency and providing a robust platform valid for high-throughput screening and amenable to scale-up and automation. The second objective comprised the determination of the kinetic parameters of *Lmj*IPCS using the established assay protocol. Once these objectives had been accomplished, a further objective was the application of these techniques established to other orthologous enzymes. This aspect will be further elaborated in Chapters III.

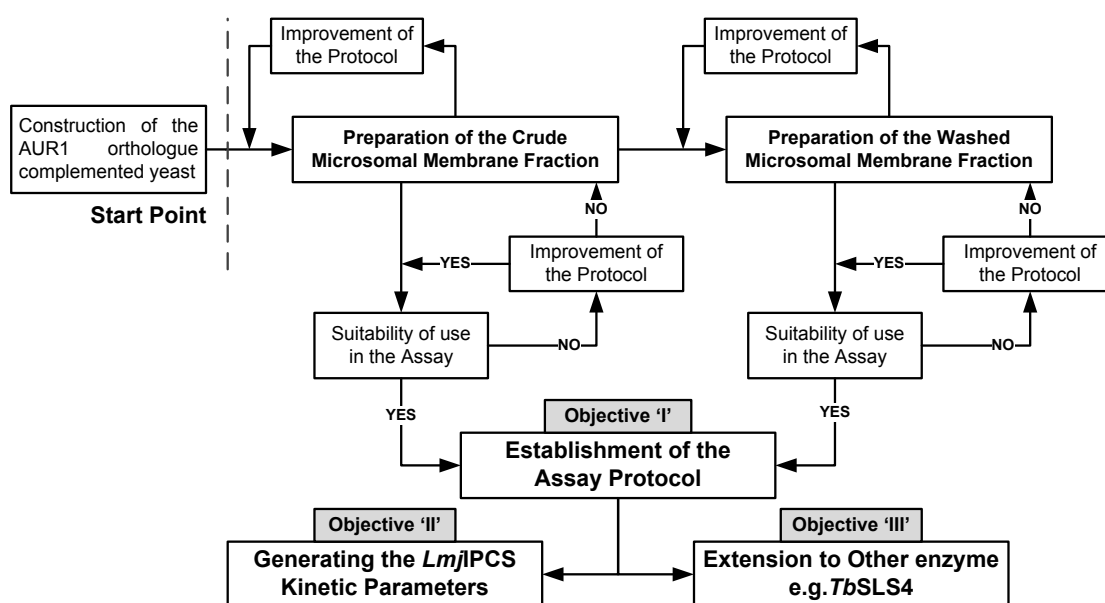


Figure 2-30: Work Strategy towards the set objectives

2.1 Establishment of an *in-vitro* Activity Assay

2.1.1 Construction of the *Lmj*IPCS complemented Mutant Yeast Strain

Given the objective of developing an *in-vitro* assay, an efficient method to produce the *Lmj*IPCS protein was required. This was simply achieved by construction of a mutant yeast strain as described in Denny *et al.*¹ Briefly, an auxotrophic *YPH499-HIS-GAL-AUR1 S. cerevisiae* strain was constructed in *YPH499* (*Mat a; ura3-52; lys2-801amber; ade2-101ochre; trp1-63; his3-200; leu2-1*) by bringing the expression of the native yeast *AUR1* gene under the control of the stringently regulated *GAL1* promoter that is repressed in the presence of glucose. The *AUR1* promoter in the yeast genome was exchanged by a selection marker/promoter *HIS/GAL1* cassette. Subsequent transformation into the haploid *YPH499* strain, selection on minimal medium lacking histidine but containing galactose, and confirmation of the insertion of the *HIS-GAL* fragment were performed. Additionally, the *Leishmania* candidate coding sequence (*Lmj*F35.4990) and the *AUR1* sequence were amplified from genomic DNA and cloned into the yeast expression vectors p426MET25 (*see* Appendix A) creating p426MET25-*Lmj*IPCS and p426MET25-*Sc*IPCS (*AUR1*) respectively.

The auxotrophic *YPH499-HIS-GAL-AUR1 S. cerevisiae* strain and the vectors p426MET25, p426MET25-*Lmj*IPCS and p426MET25-*Sc*IPCS (*AUR1*) were obtained from Dr. Denny. These were used in the transformation of the *YPH499-HIS-GAL-AUR1 S. cerevisiae* strain. Functionally complemented transformants were selected on non-permissive SD medium (0.17 % Bacto yeast nitrogen base, 0.5 % ammonium sulphate, and 2 % dextrose) containing the nutritional supplements necessary to allow selection of transformants (Figure 2-31).

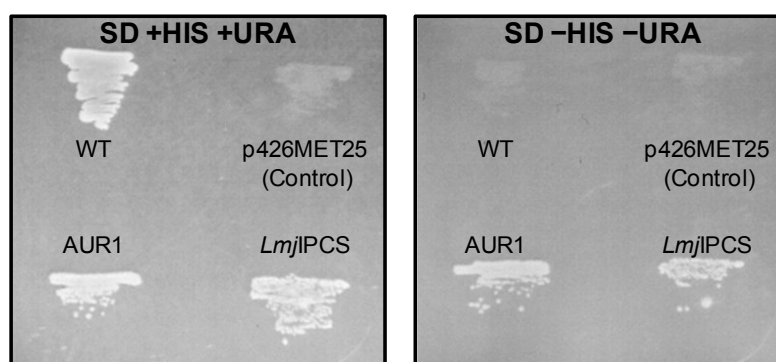


Figure 2-31: Transformation of *YPH499-HIS-GAL-AUR1 S. cerevisiae* with p426MET25 (Control), p426MET25-*Lmj*IPCS and p426MET25-*Sc*IPCS (*AUR1*). WT: *YPH499*

2.1.2 Preparation of the Microsomal Membranes Fraction

2.1.2.1 Preparation of Crude microsomal membranes

Having generated a complemented yeast strain, the next objective was the preparation of a microsomal membrane fraction enriched in *Lmj*IPCS suitable to conduct the proposed mechanistic studies and compound screening. Following a standard protocol reported by *Fischl et al.*² for the preparation of IPC synthase from *S. cerevisiae*, the isolated yield of crude *Lmj*IPCS microsomal membranes was considerably low, approximately 0.12 % of wet cell mass (WCM) compared to a yield of approximately 1.13 % of WCM (*S. cerevisiae* WT) reported previously.

In spite of the different nature of the two strains and the fact that the *Lmj*IPCS complemented yeast grows slower than wild type or *ScAURI* complemented yeast cells, a 100 fold reduced yield indicated a defect in the preparation protocol. This was likely attributed to the efficacy of the disruption/extraction step which was believed to have a critical effect on the yield of isolated microsomal membranes. Three variables were considered; the amount of glass beads, the volume of STE buffer and the number of vortex disruption cycles.

To test the effect of such variables on enhancing the isolated yield of microsomal membranes, the disruption/extraction process was modified. It was split into two steps, In step '1', the number of vortex mixing cycles was increased to 20 cycles (each included 1 minute vortex mixing and 1 minute rest on ice) using a larger volume of extraction buffer (approximately 1½ WCM ml) and (approximately 1½ WCM gm) of glass beads. This was followed by centrifugation (1500 × g, 4 °C and 10 min) and decantation of supernatant. In step '2', fresh STE buffer (approximately ½ WCM ml) was added followed by vortex mixing for additional 10 cycles, centrifugation and decantation of supernatant. The combined supernatants were further treated exactly as the literature protocol. The modified protocol resulted in an approximately 100 fold enhancement of the yield of crude *Lmj*IPCS microsomal membranes fraction.

2.1.2.2 Activity Assay of the Crude Microsomal Membranes

With an efficient preparation of the crude microsomal membranes achieved, the focus then moved to test and to quantify its content in terms of the *Lmj*IPCS transferase activity. Preliminary activity assays following *Figueiredo et al.*³ using the crude microsomal membranes exhibited high level of endogenous activity (> 25 % in terms of the donor substrate, PI, Figure 2-32). This was expected as it had been previously reported that PI accounts for approximately 20% of the phospholipid content in *S. cerevisiae* Golgi membranes.⁴

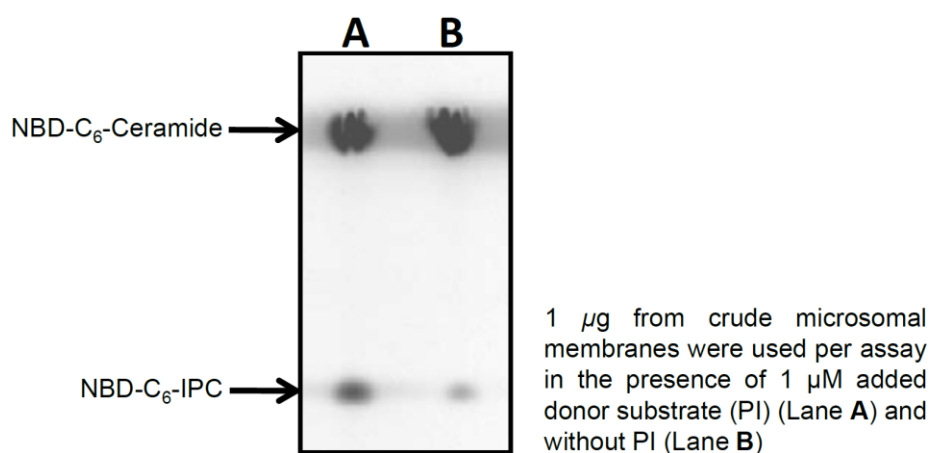


Figure 2-32: Endogenous activity in crude *Lmj*IPCS microsomal membranes

Although Figueiredo has reported the use of a crude microsomal fraction in the activity assay of the closely related enzyme *T. cruzi* IPC synthase, the protocol required the use of very high concentrations of added substrates to minimise background interference. Additional control experiments were needed to account for the endogenous activity. This procedure cannot overcome the limited dependence of the assay on the added (exogenous) PI particularly at low concentrations rendering the assay reproducibility problematic.

Similar observations regarding the background interference due to the endogenous activity were reported by *Aeed et al.*⁴ for microsomal membranes prepared from *C. albicans*. Aeed reported the necessity of using detergents to deplete the microsomal membranes of endogenous

PI so that accurate kinetic measurements would be possible. After the investigating the effect of 26 different membrane-perturbing agents on the activity and phase distribution of *C. albicans* IPC synthase activity in crude membranes, Aeed concluded that while non-ionic detergents (e.g. Triton X-100), the conventional zwitterionic detergents (e.g. Empigen BB), lysophospholipids and the sterol-containing agent, digitonin, caused drastic if not complete loss of enzyme activity while the zwitterionic sterol-based detergents such CHAPS, CHAPSO and taurodeoxycholate (tDOC) could efficiently solubilise the enzyme with minimal deterioration of activity. They stated that washing the membranes with 2.5 % CHAPS, approximately 50 % of the protein and 80 % of the phospholipids content were solubilised with no detectable loss of enzyme activity. Additionally, whilst subjecting the membranes to a second CHAPS-wash had a limited enhancement of the specific activity, a third wash had no value-add in the washing efficacy but resulted in noticeable loss in specific activity. Using such refined (washed) microsomal membranes, Aeed was able to demonstrate a considerable improvement in the assay reproducibility by reducing the background noise due to the endogenous activity rendering the assay to be 100 % dependent on added acceptor substrate analogue (NBD-C₆-Ceramide) and greater than 95 % dependent on added donor substrate (PI). Based on this precedent work, the crude *Lmj*IPCS microsomal membranes were considered unsuitable for mechanistic studies and that further purification was needed. Consequently, their use was limited to preliminary and qualitative experiments.

2.1.2.3 Preparation of Refined Microsomal Membranes

Following the protocol developed by Aeed *et al.*,⁴ the *Lmj*IPCS crude microsomal membranes were washed with 2.5 % CHAPS (1:1 detergent : protein). The CHAPS washed membranes maintained enzyme activity and exhibited more than a two fold increase in specific activity with minimised background noise. Comparison between crude and washed membranes in preliminary assays indicated that using washed membranes rendered the assay to be 100 % dependent on added NBD-C₆-ceramide and ≥ 90 % dependent on added PI (Figure 33).

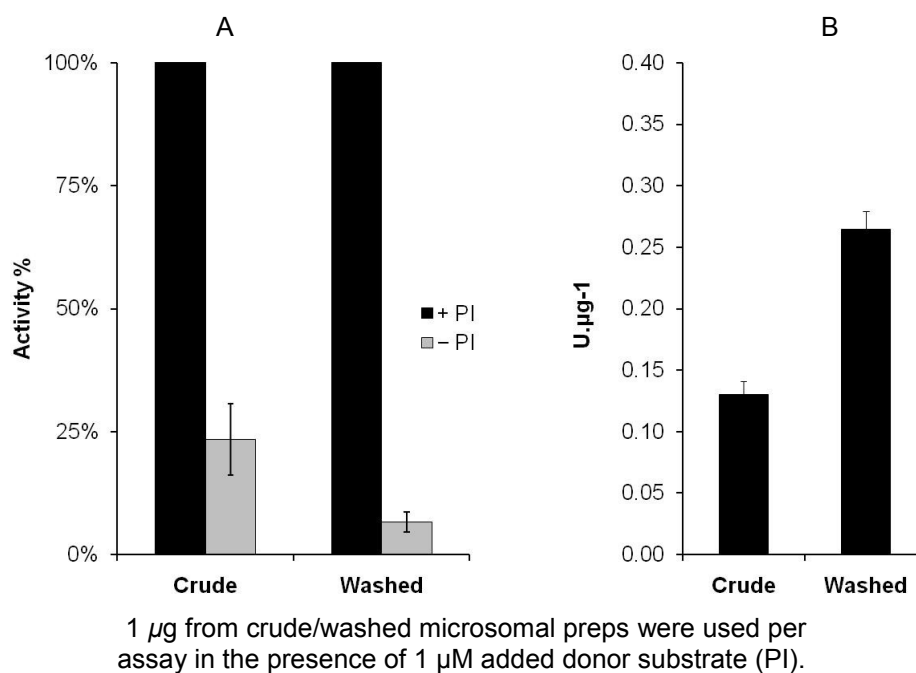


Figure 33: (A) Background noise in crude and CHAPS-washed membranes (B) Specific Activity of crude and CHAPS-washed membranes

This enhancement of the membranes performance can be attributed to the removal of most of the native PI content of the membranes along with low molecular weight and/or peripheral proteins. However, in contrast to Aeed's observations with *C. albicans* IPCS microsomal membranes, a second wash of the *Lmj*IPCS membranes resulted in drastic loss of protein content (> 90 %) in sedimentable pellet and complete deactivation of the enzyme. Consequently, further mechanistic and screening experiments were conducted using simply CHAPS-washed membranes.

Although, the CHAPS-washing enhanced the quality of the prepared membranes, the refined microsomal membranes exhibited considerable variation between different batches with the reduction in total protein content ranging from 86 % to 98 %. This subsequently caused fluctuation in the specific activity of the refined microsomal membranes. The inconsistent efficacy of the washing step could be attributed to several possible factors. For example, the uneven chemical composition of the crude microsomal membrane fractions arising from inevitable differences in the growth phase of the mutant yeast when harvested.⁵ Also, experimental errors in the protein quantification prior to CHAPS-washing could have crucial effect on the critical ratio of protein:CHAPS that would affect the washing efficacy and reproducibility. Such errors could also arise due to the presence of interfering compounds (e.g. storage buffer, STE buffer, protease inhibitors and the endogenous phospholipid content) and the

trans-membrane nature of the *Lmj*IPCS. Additionally, this could be due differences in the molar fraction of *Lmj*IPCS in the sedimented membranes pellet or that *Lmj*IPCS could exist in a deactivated form as a result of excessive de-lipidation during CHAPS-washing.

This variation in the specific activity of the refined membranes rendered the expression of *Lmj*IPCS content in terms of a definitive mg/ml concentration to be subjective and preparation dependent. Moreover, direct correlation between results generated using different batches of microsomal membranes would not be possible. The kinetic parameters presented in this work were produced using two different preparations of *Lmj*IPCS microsomal membranes (4.26 mg/ml, specific activity = 2.33 *picokat*/ml and 3.1 mg/ml, specific activity = 3.11 *picokat*/ml). Subsequently, to standardise the assay material, samples were normalized with respect to active enzyme content thereby removing variability in sample preparation and ensuring consistency across experiments.

Although the standardised unit for enzymatic activity is the katal⁶ where 1 kat = 1 mol(product).s⁻¹, the use of the enzyme unit (U)^{2, 5} is more conventional. Consequently, for the range of substrates concentrations used in the work presented here, a more practical value was the enzyme unit (U) where, “*One unit is the amount of enzyme that catalyses the formation of 1 picoMol of product per minute under specified conditions*” where 1 U corresponds to 16.67 *femtokats*.⁷ Subsequently, for every batch of prepared refined membranes, acetone pre-precipitated protein content was determined according to *Bradford*⁸ followed by generating an activity vs. protein concentration curve to determine the specific activity for such batch as U.mg⁻¹. Batch concentration was calculated as U/ μ l and aliquots were stored at -80 °C until use. Additionally, the reaction rate v and V_{max} were expressed in terms of pMol.min⁻¹.U⁻¹.

2.1.3 Establishment of *Lmj*IPCS Assay Conditions

Having prepared the *Lmj*IPCS microsomal membranes in a refined form suitable for accurate and reproducible results, attention turned to the establishment of the conditions of the activity assay in terms of temperature, time, pH and protein concentration. To accomplish the task, a review for previously described IPC synthases activity assays was performed prior to selection of compatible protocols that would fulfil the set requirements.

2.1.3.1 Techniques of IPC Synthase Activity Assays

Several activity assays for IPC synthase had been previously reported. In general, those assays can be grouped into two categories, radioactive⁹⁻¹² and fluorometric^{1, 4, 13-14} assays. These assays quantify the turnover of a radioactive substrate ($[^3\text{H}]$ ceramide/PI) or a fluorescent substrate analogue (NBD- C_6 -Ceramide or BODIPY[®] FL- C_5 -Ceramide) to the corresponding product, IPC. In all cases, the product IPC, needs isolation and this has been achieved using a variety of different techniques such as solvent-phase separation,¹⁵ HPTLC,¹⁻³ HPLC,¹³ affinity chromatography¹⁶ and anion exchange chromatography.⁴ A recent assay technique has been reported wherein a FRET-pair based quantification of the product that does not require product isolation has been employed.¹⁷

Within this work, two protocols were used. The Tris/HCl/BSA/EDTA system reported by *Figueiredo et al.*³ was mainly employed for preliminary, small scale and qualitative assays while the $\text{K}_2\text{HPO}_4/\text{KH}_2\text{PO}_4/\text{CHAPS}$ system reported by *Aeed et al.*,⁴ was used in mechanistic and screening experiments due to the potential of it to be used in 96-wellplate format. The former would be referred to as ‘*Protocol B*’ while the later would be referred to as ‘*Protocol A*’. These protocols rely on the quantification of the turnover of the commercially available fluorescent substrate analogue, NBD- C_6 -ceramide, into NBD- C_6 -IPC (Figure 34).

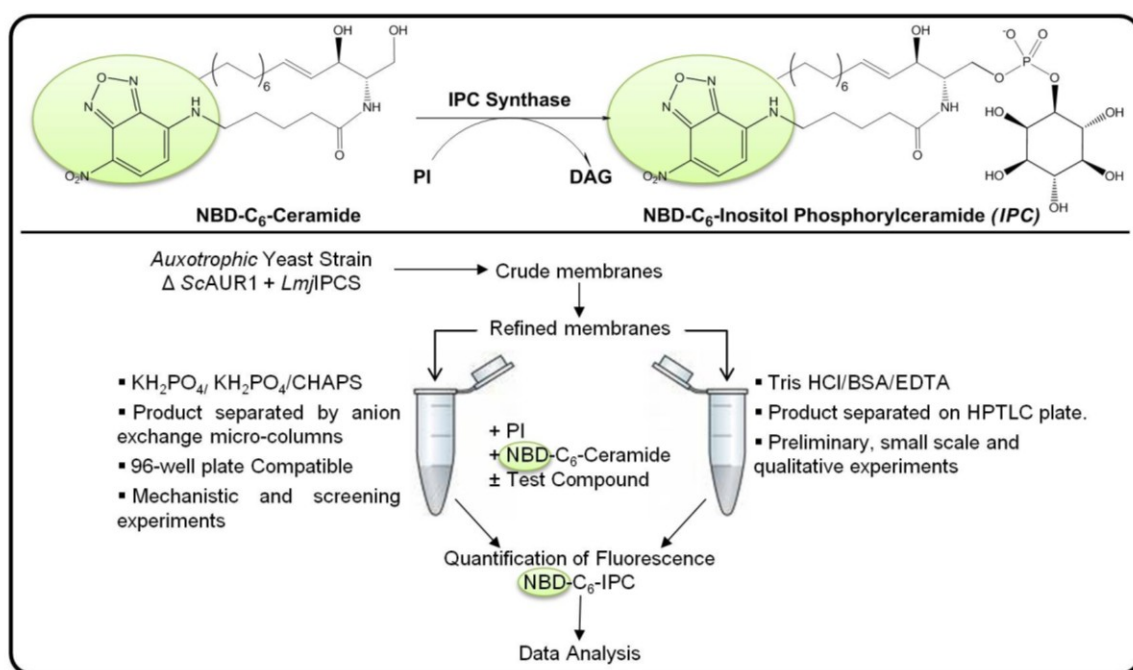


Figure 34: The two *Lmj*IPCS assay protocols utilised in this work

2.1.3.2 Activity vs. Variants of the Donor Substrate

While NBD-C₆-ceramide has been previously shown to act as an acceptor substrate for *Lmj*IPCS,¹ there was still a need for the selection of a donor substrate variant (mammalian PI or soybean PI). In precedent work by Figueiredo, soybean PI has been used in the activity assays of the closely related *Tc*IPCS.¹⁴ Therefore, following the same protocol, *Lmj*IPCS activity was measured against different variants of PI (main species: mammalian PI (18:0/20:4), soybean PI (16:0/18:2) and synthetic PI (16:0/16:0)). While mammalian PI and plant PI were shown to act almost as equally as donor substrates, synthetic PI resulted in a marginal increase of activity relative to the blank (no exogenous PI added) (Figure 35). Consequently, further experiments were performed using the mammalian variant of PI.

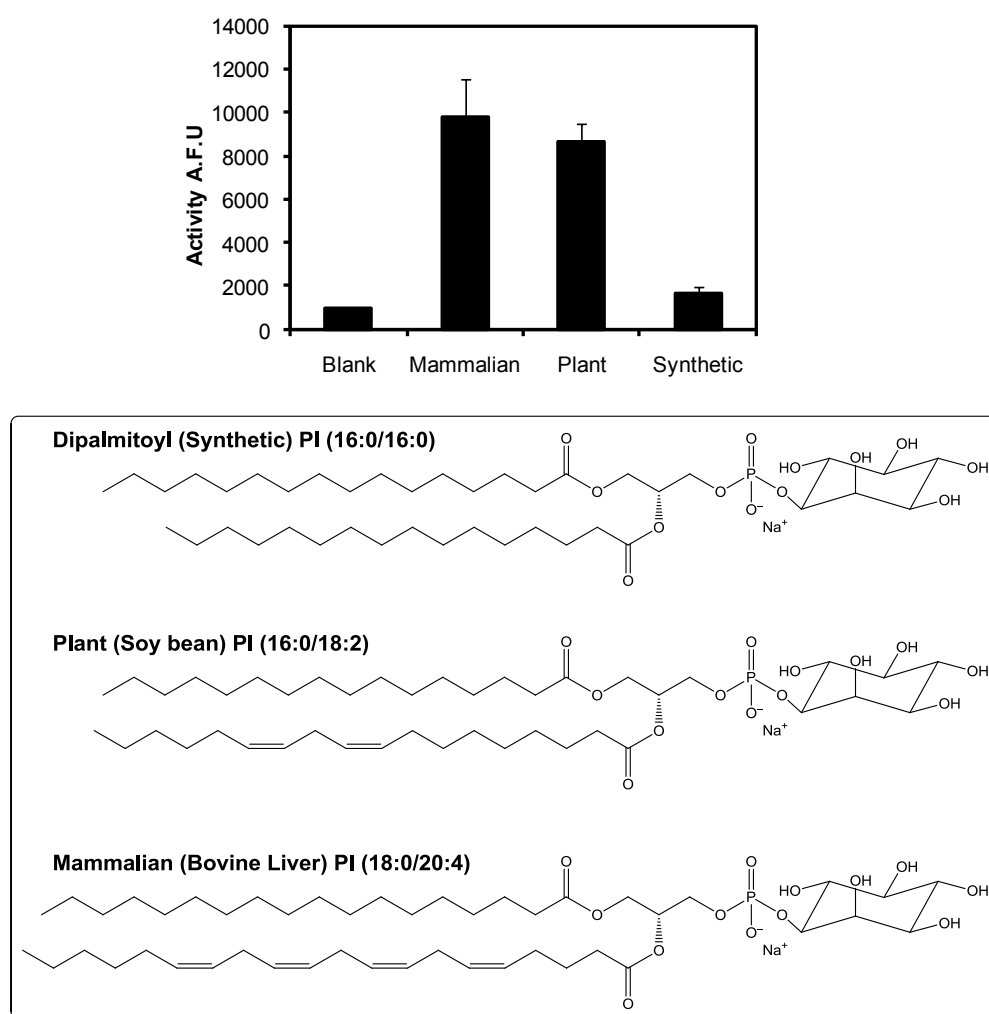


Figure 35: *Lmj*IPCS activity vs. PI variants.

2.1.3.3 Activity vs. Temperature

*Lmj*IPCS activity was measured at different temperatures between 4 °C up to 37 °C. *Lmj*IPCS exhibited the capacity to remain active over a broad range of temperatures, even at considerably low temperature (20 % activity at 4 °C). The optimum temperature was determined to be approximately 30 °C (Figure 36: A) with a sharp decline (~ 35 %) in activity from 30 °C to 33 °C. Given this and the fact that sand flies temperature would be close to their environment (tropical and subtropical region, 22~28 °C) and that mammalian host skin temperature would be in the range of 31~35 °C, the temperature profile of *Lmj*IPCS exhibiting highest activity in the range 26~33 °C with a maximal activity at 30 °C is a reasonable observation.

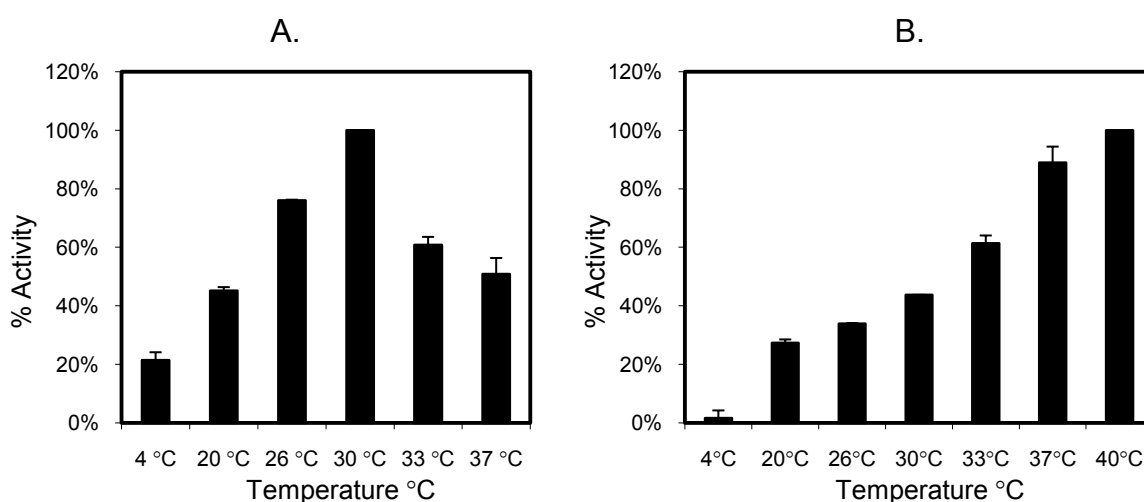


Figure 36: Activity vs. temperature Profile of (A) *Lmj*IPCS and (B) *Tb*SLS4

This is different from the temperature profile of the closely related *Tb*SLS4 (*T. brucei* Sphingolipid Synthase) where the activity was maximal at 40 °C and decreased with a lowering of temperature till diminished activity at 4 °C (*Pan-ssu Ying*, MSc 2008, Durham University, Figure 36: B). Such differences can be explained by the fact that while *T. brucei* is a bloodstream⁴ protozoan that causes fever in infected patients, *L. major* protozoan spans its life cycle^{4, 18} between the midgut of the invertebrate host (sandfly) and skin lesions in the mammalian host.

2.1.3.4 Activity vs. pH

To determine the optimum functional pH for *Lmj*IPCS, a series of reactions were conducted using Tris/HCl buffer over a pH range from 4.1 up to 9.0. The pH profile of *Lmj*IPCS revealed maximal activity at pH = 6 with asymmetric decline slopes at both sides of the maxima (Figure 37). While moving towards more acidic pH induced a slow decrease in activity, moving towards more alkaline pH resulted in a sharp reduction of the enzymatic activity. Similar observations have been previously reported with *Tc*IPCS³ which also exhibited maximal activity at approx. pH = 6.

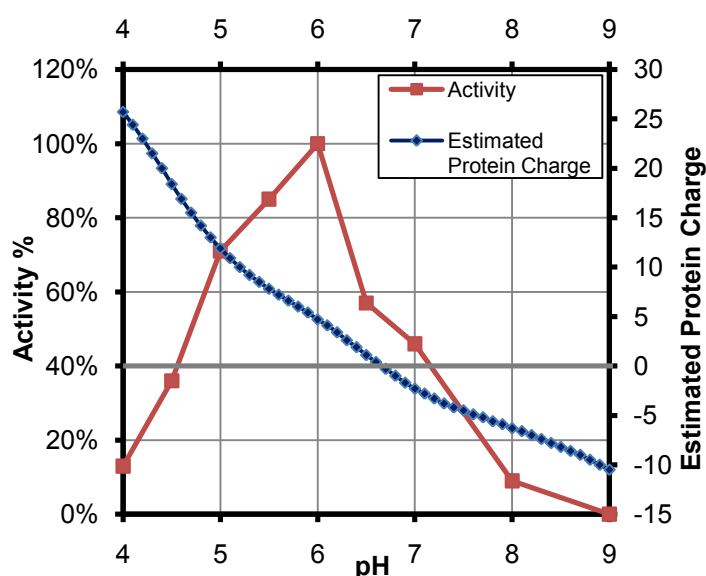


Figure 37: Activity vs. pH Profile and the estimated protein charge as predicted by Protein Calculator (<http://www.scripps.edu/~cdputnam/protcalc.html>)

Such observations can be explained in the light of cellular physiology of the host organism. Although leishmania parasites alternate between the neutral-alkaline HCO_3^- rich medium of the sandfly's midgut and the acidic environment of the mammalian macrophage lysosome,¹⁹ the intracellular pH (pH_i) of the parasites remains constant throughout their life cycle.¹⁸ The pH_i is estimated to be approximately 6.72 but subject to slight changes in response to environmental factors.¹⁸⁻²¹ An important factor to consider is the electrostatic nature of the enzyme. Although there is a lack of empirical data, submitting the protein sequence to Protein Calculator v3.3 (<http://www.scripps.edu/~cdputnam/protcalc.html>) predicted the $\text{pI} = 6.65$ and the total protein charge as presented in Figure 37. Clearly, there could be a correlation between the total protein

charge which will affect the ionisation constant of the catalytic triad and consequently the catalytic rate of the transferase activity.

Although the optimum pH was determined at approximately pH 6.0, further experiments were carried out at neutral pH 7.0 to facilitate product separation using the anion exchange micro-columns and to minimise any un-predicted ionisation of test compounds during the inhibitors screening process.

2.1.3.5 Activity vs. Time & Protein Concentration

With the optimum temperature and pH determined, the next goal was to determine the linear range of activity in terms of time and protein concentration. Consequently, *Lmj*IPCS activity was monitored over time up to 60 minutes following the typical assay reaction conditions. This revealed that *Lmj*IPCS activity was linear up to approximately 30 minutes of reaction time before it starts to taper off in a non-linear pattern (Figure 38). Consequently, all subsequent assays were conducted within the linear range of the graph with reaction times not exceeding 15 minutes. Additionally, when the assay was carried out without pre-incubating the membranes with PI, the reaction rate was reduced to approximately 60 %. However, no lag time could be detected under the assay conditions in contrast to that observed with *C. albicans*.⁴ The presence or absence of a lag time has important implications on the reaction kinetic scheme. This will be further elaborated in section 2.3.

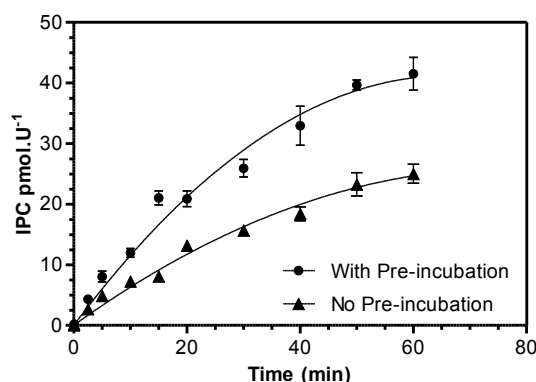


Figure 38: Activity vs. Time Profile

Although the rate of the reaction started to decrease after 30 minutes, only $\leq 12\%$ of the added donor substrate was consumed after 1 hour of the reaction time. The decrease in the rate of product formation could be attributed to product inhibition by either NBD- C_6 -IPC and/or DAG rather than exhaustion of the substrates. Alternatively, the products could remain associated with the microsomal membrane and in some way affect a change in the surface diffusion of the substrates to the active site. Unfortunately, in this respect, these hypotheses could not be tested in terms of IPC because of the unavailability of needed chemicals. However, measuring *Lmj*IPCS activity against an increasing concentration of DAG resulted in an $IC_{50} = 8.4 \pm 1.2 \mu\text{M}$ (Figure 39). In spite of the determined IC_{50} which indicates that a bulk concentration of DAG should be about twice that of NBD- C_6 -ceramide to elicit a considerable inhibition, the DAG produced by the enzyme might have a more profound inhibitory effect on the reaction rate due to its high localised surface concentration in the microsomes. This observation supported the initial hypothesis of possible (by) product feedback inhibition.

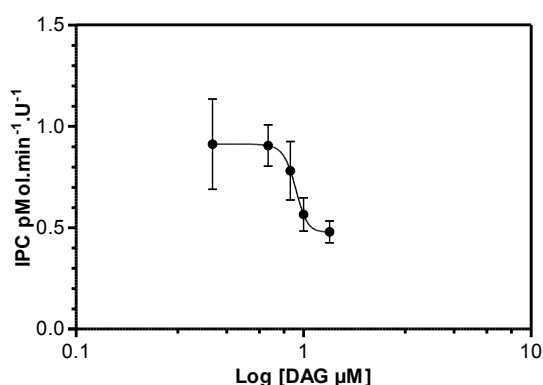


Figure 39: The inhibitory effect of DAG on *Lmj*IPCS activity

The final variable of the assay conditions to be determined was the linear range of activity in terms of enzyme concentration. Measuring the activity against an increasing enzyme concentration up to 3.5 U/assay (final concentration 87.5 U/ml), identified the linear range below 1 mU/assay (15 $\mu\text{U}/\mu\text{l}$) (Figure 40) under typical assay conditions. Above this concentration, the activity curve started to taper-off exhibiting non-linear behaviour. This deviation could be due to possible aggregation of the hydrophobic microsomal membranes at higher concentrations resulting in a change in the available enzyme surface that would affect accessibility to the active site.

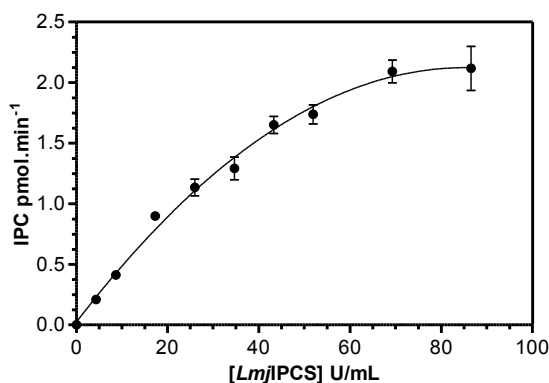


Figure 40: Activity vs. Enzyme Concentration

2.1.4 Validation of the Assay Protocol

Having established all the assay conditions, it was then necessary to confirm its validity for experimental investigation. As the ultimate application of the established assay was in screening of potential inhibitors against *Lmj*IPCS, the ideal validation experiment should test the inhibitory effect of a known IPC synthase inhibitor. Out of the three known fungal IPC synthase inhibitors, khafrefungin,²² rustmicin²³ and aureobasidin A,¹³ only the latest is commercially available.

2.1.4.1 Aureobasidin A Inhibition of *Lmj*IPCS

Although the inhibitory effect of aureobasidin A on *Leishmania spp.* remains a matter of debate,^{1, 11, 24-25} aureobasidin A could be still considered as a likely inhibitor against *Lmj*IPCS. Consequently, the activity of refined *Lmj*IPCS microsomal membranes was measured against an increasing concentration of aureobasidin A using both assay protocols previously described. The inhibition assays were carried out using microsomal preparation of *Sc*IPCS as a positive control and the results were visualised on HPTLC (Figure 41). Using ‘Protocol B’, aureobasidin A exhibited an apparent IC₅₀ between 10 ~ 50 μM in terms of *Lmj*IPCS. However, under the ‘Protocol A’ conditions, aureobasidin A inhibited only *Sc*IPCS with no inhibition of *Lmj*IPCS could be detected. These differences could be attributed to the combined effect of the different solubilising agent of the two protocols (BSA & CHAPS) with the very poor aqueous solubility of aureobasidin A (<http://bio.takara.co.jp>) that would render the effective concentration far below the added molar concentration. The yet observed inhibition of *Sc*IPCS in both cases is due to its very high sensitivity to aureobasidin A¹³ (Lit. IC₅₀ = 0.2 nM).²⁶

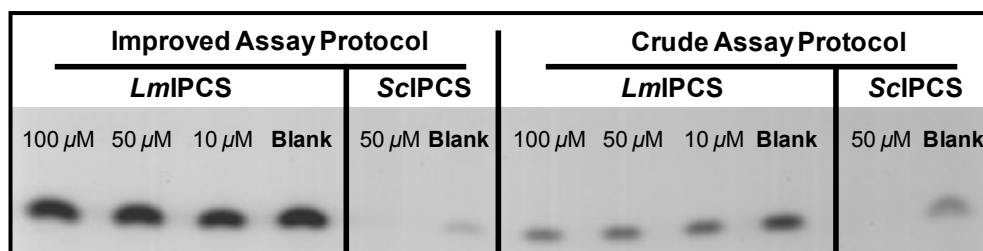


Figure 41: The inhibitory effect of Aureobasidin A on *Lmj*IPCS. *ScIPCS* was used as a control

Further investigation of the inhibitory profile of aureobasidin A on *Lmj*IPCS identified an $IC_{50} > 100 \mu\text{M}$ (Figure 42: A). Additionally, aureobasidin A was found to be a non-competitive inhibitor in terms of both substrates, NBD- C_6 -ceramide and PI (Figure 42: B, C) similar to recent observations in respect of an orthologous IPC synthase from *S. cerevisiae*.²⁷

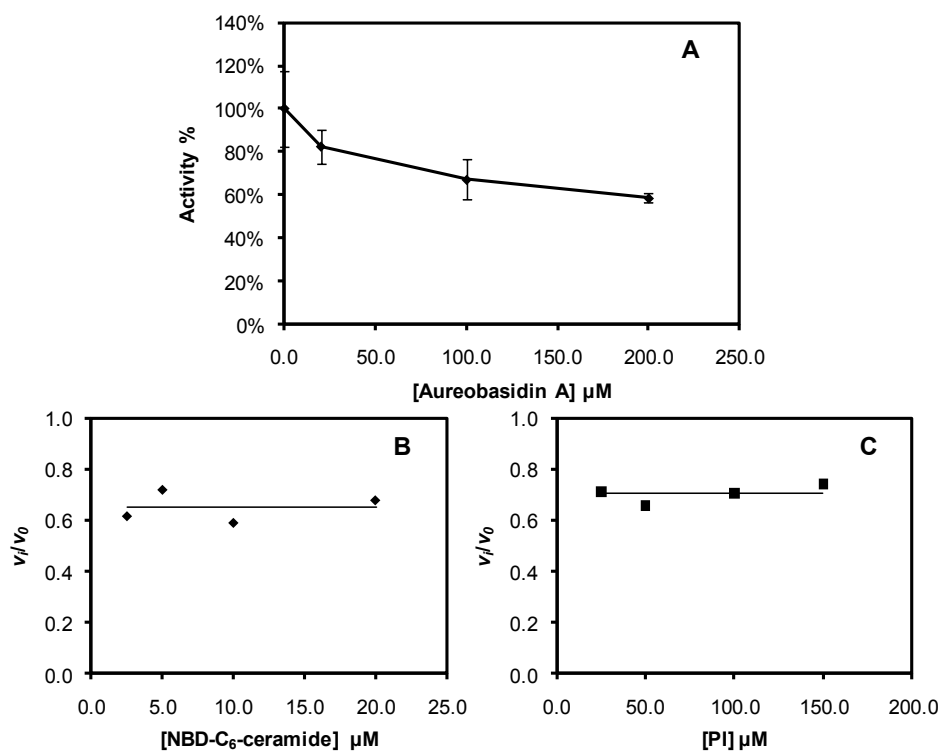


Figure 42: (A) Aureobasidin A inhibition of *Lmj*IPCS ($IC_{50} > 100 \mu\text{M}$). Determination of aureobasidin A mode of inhibition in terms of substrates, (B) Non-competitive in terms of NBD- C_6 -ceramide ([Ab A] = 0, 50 μM). (C) Non-competitive in terms of PI ([Ab A] = 0, 50 μM).

2.1.4.2 Substrate Analogues as Competitive Inhibitors of *Lmj*IPCS

Having validated the assay protocols in terms of a well-established fungal IPCS inhibitor, further validation in terms of potential inhibitory effect of substrate analogues was necessary.

Three compounds were chosen for this basic inhibition study; *D-erythro*-sphingosine (d18:1), *N*-acetyl-*D-erythro*-sphingosine (d18:1/2:0) and *N*-stearoyl-*D-erythro*-sphingosine (d18:1/18:0, natural mammalian ceramide). The inhibitory effect of these compounds was measured in terms of their ability to compete with the fluorescent NBD- C_6 -ceramide with variation in the quantity of the fluorescent product (NBD- C_6 -IPC) reflecting the effect of the substrate competitors on enzyme turnover.

Analyses of the synthetic analogues *D-erythro*-sphingosine and *N*-acetyl-*D-erythro*-sphingosine, using Protocol 'A' in the 96-well plate based assay demonstrated that they are, as expected, competitive with IC_{50} values of 52 μ M and 16 μ M respectively (Figure 43: A and B). However, unlike *D-erythro*-sphingosine and *N*-acetyl-*D-erythro*-sphingosine, *N*-stearoyl-*D-erythro*-sphingosine was insufficiently soluble in the phosphate-based buffer employed for the microtitre plate assay, curtailing analysis. This problem could be circumvented by using Protocol 'B' which contained defatted-BSA. In this buffer *N*-stearoyl-*D-erythro*-sphingosine was soluble and the results indicated that NBD- C_6 -ceramide exhibited an equivalent affinity for *Lmj*IPCS as the natural substrate (Figure 43: C).

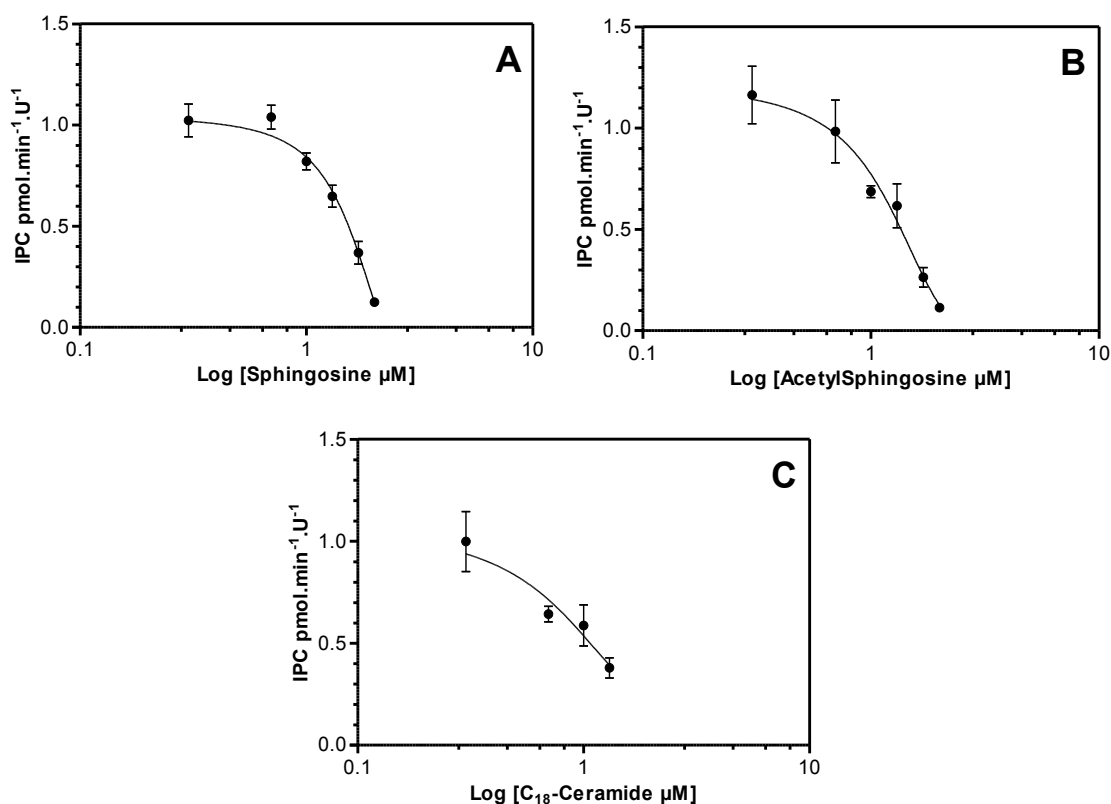


Figure 43: The inhibitory profile of NBD- C_6 -ceramide analogues. (A) *D-erythro*-sphingosine (d18:1). (B) *N*-acetyl-*D-erythro*-sphingosine (d18:1/2:0). (C) *N*-stearoyl-*D-erythro*-sphingosine (d18:1/18:0, natural mammalian ceramide).

Subsequent MS-ES⁺/ES⁻ analyses of the reaction product profiles (Figure 44) revealed the presence of a mass of 582.3 corresponding to IP-*N*-acetyl-*D*-erythro-sphingosine confirming that *N*-acetyl-*D*-erythro-sphingosine had been turned over by *Lmj*IPCS. This was expected as this ceramide analogue has previously been shown to act as a substrate for the yeast enzyme.¹⁵ Conversely, no IP-*D*-erythro-sphingosine could be detected in the MS spectra either in positive or negative ion mode, which indicated that *D*-erythro-sphingosine is not a substrate for *Lmj*IPCS; rather it is acting as a true inhibitor. This basic inhibition study of ceramide analogues demonstrated the validity of the established assay protocols to serve in the accomplishing the objective to be used in the screening of chemical libraries of potential inhibitors.

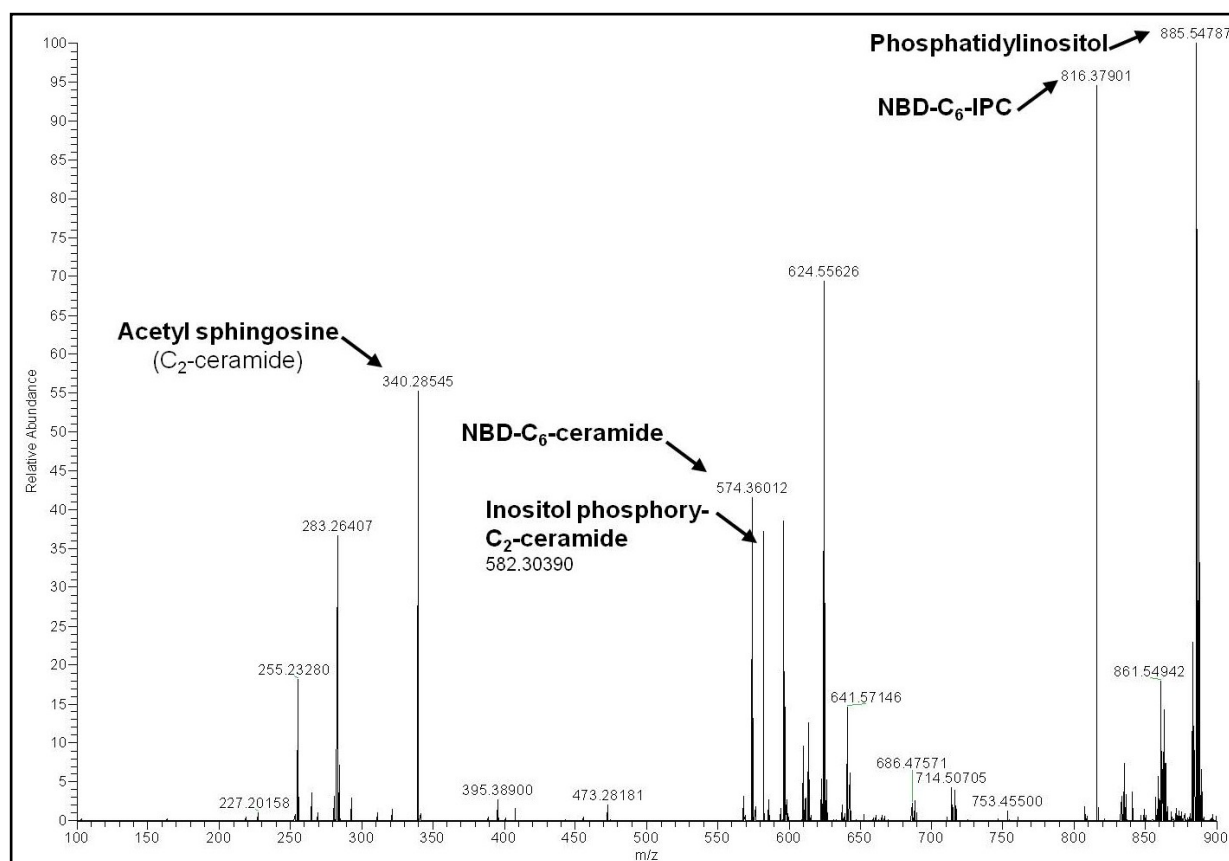


Figure 44: The Mass spectrum (ES⁻) of a standard *Lmj*IPCS activity assay in presence of *N*-acetyl-*D*-erythro-sphingosine. Highlighted peaks assign substrates and products.

2.2 Determination of the Kinetic Parameters

With the standard assay protocols defined and validated, the next objective was the determination of the kinetic parameters of *Lmj*IPCS. This required a closer investigation of the physical aspects of the assay system which are believed to have a critical effect on the enzyme interaction with the substrates and hence its activity. Only these physical aspects are defined, can initial hypotheses regarding the reaction kinetic model be made and an appropriate experimental layout be designed.

2.2.1 The Physical Aspects of the Assay Protocol

Due to the hydrophobic nature of both donor and acceptor substrates, PI and ceramide respectively, a common feature of IPC synthase activity assays is the presence of a solubilising agent⁵ (e.g. BSA, CHAPS or a cosolvent, EtOH). These disperse the sparingly water-soluble lipid substrates and products and bring the reaction mixture close to homogeneity. The work presented in this thesis was carried out using two assay protocols that differ in the solubilising agent and the buffer ingredient (Figure 34).

The assay reactions generally started with pre-drying PI in Eppendorf tubes. The pre-dried PI was presumed to be reconstituted into the solution by sonication and to exist in the form of vesicle at such low concentration²⁸ excluding the effect of the solubilising agent. In the presence of BSA (typically 4.5 nMol/assay), there is a lack of data about the possible patterns of interaction with PI but it could be postulated that PI will partition between pure PI vesicles and the hydrophobic grooves on the BSA surface.²⁹⁻³² A similar hypothesis was also assumed valid for the interaction between BSA and NBD-C₆-ceramide. Under these conditions, BSA would behave as a controlled release reservoir for NBD-C₆-Ceramide and to a lesser extent for PI.

However, the effect of CHAPS is more complex as a ‘Surface Dilution’ effect would be expected.³³ It is well established that an activity assay which is dependent on the concentration of a hydrophobic substrate shows a considerable deviation from classic Michaelis-Menten behaviour in the presence of a detergent.³⁴⁻³⁷ This is mainly because of the so-called “Surface Dilution Phenomenon”. In such assay, the substrate would exist in detergent mixed micelles and

the activity would depend on its respective surface concentration of the substrate in the micelles rather than its molar concentration.

2.2.2 Initial Hypotheses for *Lmj*IPCS Kinetic Model

Combined, the transferase activity of *Lmj*IPCS, the hydrophobic nature of substrates and the presence of CHAPS in the reaction mixture, made it difficult to predict which kinetic model would provide the best fit for the enzyme mechanism. A literature survey revealed that several transferases have been reported to follow Bi–Bi substrate kinetic model.³⁸⁻⁴⁴ This can follow either sequential-binding³⁹ (ordered or random) or double displacement kinetics³⁸ (Figure 45). While in the former, both substrates, **A** and **B**, must bind to the enzyme surface at the same time before the catalytic event takes place, in the latter; the enzyme binds the first substrate, **A**, and forms a substituted enzyme intermediate, **F**, releasing the first product, **P**. Then, the substituted enzyme would bind to the second substrate, **B**, and dissociate releasing the final product, **Q**, and regenerating the enzyme, **E**. Both mechanisms can be differentiated by the respective Lineweaver-Burk plot. While in sequential binding, it yields intersecting lines, parallel lines pattern is obtained in case of double displacement.

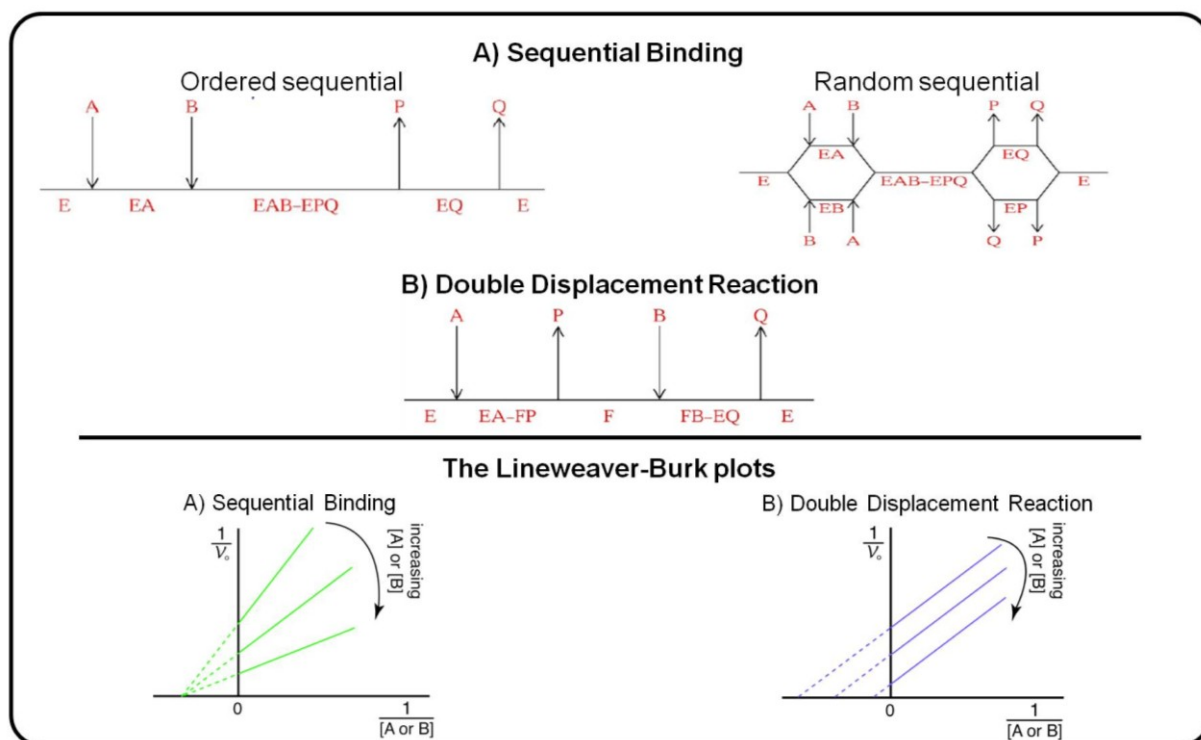


Figure 45: Bi-Bi Substrate Kinetic Models and the respective Lineweaver-Burk plots

Initially, on this basis a double displacement kinetic model⁴⁵ was hypothesised. However, ‘Surface Dilution’ kinetic effects remained to be considered.⁴⁶ Such kinetic dilemma dictated a better understanding of the possible interaction between NBD-C₆-ceramide, PI, CHAPS and *Lmj*IPCS microsomal membranes and this is discussed below.

While there is a lack of data about the nature of CHAPS/NBD-C₆-ceramide/PI mixed micelles under the established assay conditions, it was possible to build initial assumptions based on previously reported findings in precedent analogous systems. In a study investigating CHAPS micelles, Schürholz²⁸ has shown that both the critical concentration of free detergent $[D_w]^c$ which is necessary for lipid vesicle solubilisation and the critical micellar detergent : lipid ratio $R^c(M)$ strongly depend on the lipid composition. His results showed that CHAPS could solubilise PI vesicles at very low concentration $[D_w]^c = 0.27$ mM far below the CMC (4 ~ 10mM). Additionally CHAPS/PI mixed micelles had a detergent/lipid ratio of $R^c(M) = 0.17$. Based on these results, the $[D_w]^c$ for CHAPS under the assay conditions could be calculated from equation (2.1). Therefore, in a typical assay reaction ($[PI] = 100$ μ M), $[D_w]^c = 583$ μ M and at highest concentration of PI used ($[PI] = 250$ μ M), $[D_w]^c = 557$ μ M. In both cases $[D_w]^c$ is far below the CMC.

$$[D_T]^c = [D_w]^c + R^c(M) \times [L_T] \quad (2.1)$$

Where, $[D_T]^c$ = Total CHAPS concentration,
 $[L_T]$ = Total lipid concentration

At this point, it could be assumed that at $[D_T]^c = 600$ μ M, detergent concentration in assay mixture, CHAPS would essentially exist in a monomeric form with low contribution to the formed PI micelles (*c.a.* 15%). Thus the surface dilution effect due to CHAPS in the micelles would be minimal. Additionally, it was reasonable to suggest that the minor lipid component, NBD-C₆-ceramide, would partition between the PI micelles and the bulk CHAPS monomers. As a result, the concentrations of both substrates are interdependent *i.e.* changing the concentration of one would inevitably change the concentration of the other. These facts combined with the unravelled interaction of the substrates with the enzyme microsomal membranes suggested that a logical start point to address this issue would be to generate a basic set of kinetic data which would guide further experimental work.

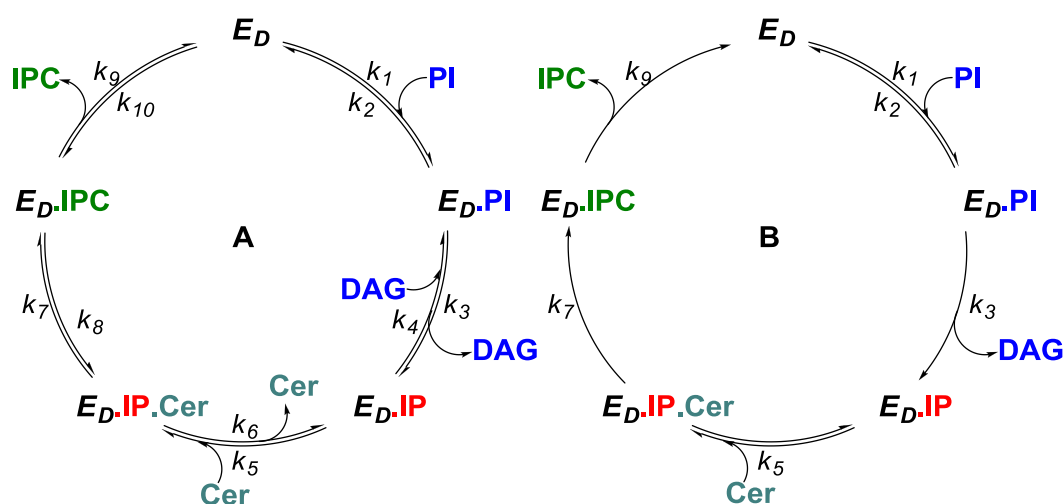
Given the concentrations present in the assay system, whilst changes in PI concentration would lead to large and significant variation in NBD-C₆-ceramide concentration, the reverse is

not the case. Consequently, a large ‘steady state’ PI concentration and a variable NBD-C₆-ceramide concentration were initially chosen to investigate the kinetic model. It is noteworthy that at such relatively low NBD-C₆-ceramide concentration in the assay, the reaction rate would be dependent on both its molar and surface concentrations.⁴⁷ All kinetic assays were carried out in triplicates; results were analysed using the software program Prism[®] 5.0 (GraphPad) and Excel[®] Solver Add-in (Microsoft).

2.2.3 The Catalytic Cycle and the Reaction Rate Equation

Assuming a double displacement model, the catalytic cycle could be divided into two sequential partial reactions in which the first product is DAG while the second is IPC. The kinetic equation was derived under the steady state approach conditions assuming that the overall catalytic reaction is reversible at all intermediate stages and the system is in equilibrium (Figure 46: A). However, assuming the initial rate assumptions, the concentrations of product, [IPC], and by-product, [DAG], were set to zero (Figure 46: B). Finally, the overall rate could be given by equation (2.2).

$$v = k_9[E_D \cdot IPC] \quad (2.2)$$



E_D : *Lmj*IPCS membranes associated with the detergent, CHAPS; **PI**: Phosphatidylinositol; $E_D \cdot PI$: *Lmj*IPCS-PI complex; **DAG**: Diacylglycerol; $E_D \cdot IP$: Intermediate substituted *Lmj*IPCS with phosphorylinositol group; **Cer**: Ceramide; $E_D \cdot IP \cdot Cer$: *Lmj*IPCS-IP-Ceramide complex; $E_D \cdot IPC$: *Lmj*IPCS-IPC complex; **IPC**: Inositol phosphorylceramide.

Figure 46: The hypothetical catalytic reaction scheme. (A) Assuming steady state approach. (B) Assuming initial rate conditions.

The derivation of the rate equation started with enumeration of the steady state equations of different forms of the enzyme in the catalytic cycle in terms of $[E_D \cdot IPC]$. Applying the mass conservation law in terms of total enzyme concentration $[E_T]$, the overall rate equation (2.7) could be derived as mentioned below.

■ Steady state at $E_D \cdot IPC$

$$k_7[E_D \cdot IP \cdot Cer] + k_{10}[E_D][IPC] = (k_9 + k_8)[E_D \cdot IPC]$$

$$\therefore [E_D \cdot IP \cdot Cer] = \frac{(k_9 + k_8)}{k_7}[E_D \cdot IPC] - \frac{k_{10}}{k_7}[E_D][IPC] \quad (2.3)$$

■ Steady state at $E_D \cdot IP \cdot Cer$

$$k_5[E_D \cdot IP][Cer] + k_8[E_D \cdot IPC] = (k_6 + k_7)[E_D \cdot IP \cdot Cer]$$

$$\therefore [E_D \cdot IP] = \frac{(k_6 + k_7)(k_9 + k_8)}{k_5 k_7 [Cer]} [E_D \cdot IPC] - \frac{k_{10}(k_6 + k_7)}{k_5 k_7 [Cer]} [E_D][IPC] - \frac{k_8}{k_5 [Cer]} [E_D \cdot IPC] \quad (2.4)$$

■ Steady state at $E_D \cdot IP$

$$k_3[E_D \cdot PI] + k_6[E_D \cdot IP \cdot Cer] = (k_5 [Cer] + k_4 [DAG])[E_D \cdot IP]$$

$$\begin{aligned} \therefore [E_D \cdot PI] = & \frac{(k_6 + k_7)(k_9 + k_8)}{k_3 k_7} [E_D \cdot IPC] + \frac{k_4 (k_6 + k_7)(k_9 + k_8) [DAG]}{k_3 k_5 k_7 [Cer]} [E_D \cdot IPC] \\ & - \frac{k_8}{k_3} [E_D \cdot IPC] - \frac{k_8 k_4 [DAG]}{k_3 k_5 [Cer]} [E_D \cdot IPC] - \frac{k_6 (k_9 + k_8)}{k_3 k_7} [E_D \cdot IPC] \\ & + \frac{k_6 k_{10}}{k_3 k_7} [E_D][IPC] - \frac{k_{10}(k_6 + k_7)}{k_3 k_7} [E_D][IPC] - \frac{k_4 k_{10}(k_6 + k_7) [DAG]}{k_3 k_5 k_7 [Cer]} [E_D][IPC] \end{aligned} \quad (2.5)$$

■ Steady state at E_D

$$k_1[E_D][PI] = k_2[E_D \cdot PI] + k_9[E_D \cdot IPC]$$

$$\therefore [E_D] = \frac{k_2}{k_1[\text{PI}]} [E_D \cdot \text{PI}] + \frac{k_9}{k_1[\text{PI}]} [E_D \cdot \text{IPC}] \quad (2.6)$$

■ According to the mass conservation law in terms of $[E_T]$

$$[E_T] = [E_D] + [E_D \cdot \text{PI}] + [E_D \cdot \text{IP}] + [E_D \cdot \text{IP} \cdot \text{Cer}] + [E_D \cdot \text{IPC}]$$

$$\begin{aligned} \therefore [E_T] = & \frac{v}{k_9} \left(1 + \frac{(k_6 + k_7)(k_9 + k_8)}{k_3 k_7} - \frac{k_8}{k_3} - \frac{k_6(k_9 + k_8)}{k_3 k_7} + \frac{(k_9 + k_8)}{k_7} \right) \\ & + \frac{v}{k_9} \left(\frac{k_9}{k_1} + \frac{k_2(k_6 + k_7)(k_9 + k_8)}{k_1 k_3 k_7} - \frac{k_2 k_8}{k_1 k_3} - \frac{k_2 k_6(k_9 + k_8)}{k_1 k_3 k_7} \right) \frac{1}{[\text{PI}]} \\ & + \frac{v}{k_9} \left(\frac{k_4(k_6 + k_7)(k_9 + k_8)[\text{DAG}]}{k_3 k_5 k_7} - \frac{k_8 k_4 [\text{DAG}]}{k_3 k_5} + \frac{(k_6 + k_7)(k_9 + k_8)}{k_5 k_7} \right. \\ & \left. - \frac{k_8}{k_5} \right) \frac{1}{[\text{Cer}]} + \frac{v}{k_9} \left(\frac{k_2 k_4(k_6 + k_7)(k_9 + k_8)[\text{DAG}]}{k_1 k_3 k_5 k_7} - \frac{k_2 k_8 k_4 [\text{DAG}]}{k_1 k_3 k_5} \right) \frac{1}{[\text{PI}]} \frac{1}{[\text{Cer}]} \\ & + [\text{IPC}] [E_D] \left(\frac{k_6 k_{10}}{k_3 k_7} - \frac{k_{10}}{k_7} - \frac{k_{10}(k_6 + k_7)}{k_3 k_7} + \frac{k_2 k_6 k_{10}}{k_1 k_3 k_7 [\text{PI}]} - \frac{k_2 k_{10}(k_6 + k_7)}{k_1 k_3 k_7 [\text{PI}]} \right. \\ & \left. - \frac{k_4 k_{10}(k_6 + k_7)[\text{DAG}]}{k_3 k_5 k_7 [\text{Cer}]} - \frac{k_{10}(k_6 + k_7)}{k_5 k_7 [\text{Cer}]} - \frac{k_2 k_4 k_{10}(k_6 + k_7)[\text{DAG}]}{k_1 k_3 k_5 k_7 [\text{PI}] [\text{Cer}]} \right) \end{aligned} \quad (2.7)$$

Additionally, the initial rate conditions were applied to equation (2.7) in two stages. First stage set the factors of the second reverse partial reaction to zero (k_{10} , k_8 and IPC concentration = 0). This reduced equation (2.7) to equation (2.8). in and the and DAG concentrations to zero. Finally, reduced forms of the rate equation at saturating concentrations of the substrates were deduced. In the second stage, the first reverse partial reaction was set to zero (k_4 and DAG concentration = 0). This reduced equation (2.8) to equation (2.9)

■ Setting the second reverse partial reaction to zero (k_{10} , k_8 and $[\text{IPC}] = 0$)

$$\begin{aligned} \frac{[E_T]}{v} = & \left(\frac{1}{k_9} + \frac{1}{k_7} + \frac{(k_6 + k_7)}{k_3 k_7} - \frac{k_6}{k_3 k_7} \right) + \left(\frac{1}{k_1} + \frac{k_2(k_6 + k_7)}{k_1 k_3 k_7} - \frac{k_2 k_6}{k_1 k_3 k_7} \right) \frac{1}{[\text{PI}]} \\ & + \left(\frac{k_4(k_6 + k_7)[\text{DAG}]}{k_3 k_5 k_7} + \frac{(k_6 + k_7)}{k_5 k_7} \right) \frac{1}{[\text{Cer}]} \\ & + \left(\frac{k_2 k_4(k_6 + k_7)[\text{DAG}]}{k_1 k_3 k_5 k_7} - \frac{k_2 k_4 [\text{DAG}]}{k_1 k_3 k_5 k_9} \right) \frac{1}{[\text{PI}]} \frac{1}{[\text{Cer}]} \end{aligned} \quad (2.8)$$

■ Setting the first reverse partial reaction to zero (k_4 and $[DAG] = 0$)

$$\frac{[E_T]}{v} = \left(\frac{1}{k_9} + \frac{1}{k_7} + \frac{(k_6 + k_7)}{k_3 k_7} - \frac{k_6}{k_3 k_7} \right) + \left(\frac{1}{k_1} + \frac{k_2(k_6 + k_7)}{k_1 k_3 k_7} - \frac{k_2 k_6}{k_1 k_3 k_7} \right) \frac{1}{[PI]} + \left(\frac{(k_6 + k_7)}{k_5 k_7} \right) \frac{1}{[Cer]} \quad (2.9)$$

■ Finally, *the rate equation* can be written in the following simplified form,

$$\frac{[E_T]}{v} = \emptyset_0 + \emptyset_{PI} \frac{1}{[PI]} + \emptyset_{Cer} \frac{1}{[Cer]} \text{ where,} \quad (2.10)$$

$$\emptyset_0 = \left(\frac{1}{k_8} + \frac{1}{k_7} + \frac{(k_6 + k_7)}{k_3 k_7} - \frac{k_6}{k_3 k_7} \right), \quad \emptyset_{PI} = \left(\frac{1}{k_1} - \frac{k_6}{k_1 k_7} + \frac{k_2(k_6 + k_7)}{k_1 k_3 k_7} \right)$$

$$\emptyset_{Cer} = \left(\frac{(k_6 + k_7)}{k_5 k_7} + \frac{k_4(k_6 + k_7)[DAG]}{k_3 k_5 k_7} \right)$$

■ Special conditions derivation

■ If both $[PI]$ and $[Cer]$ are saturating, equation (2.10) can be reduced to,

$$\frac{[E_T]}{v} = \emptyset_0 \text{ where, } v = \frac{[E_T]}{\emptyset_0} = V_{max} \quad (2.11)$$

■ While if only $[PI]$ is saturating, the equation can be reduced to,

$$\frac{[E_T]}{v} = \emptyset_0 + \emptyset_{Cer} \frac{1}{[Cer]} \text{ where by rearrangement gives,}$$

$$v = \frac{[E_T][Cer]}{\emptyset_0 [Cer] + \emptyset_{Cer}} = \frac{V_{max} [Cer]}{[Cer] + \emptyset_{Cer}/\emptyset_0} \text{ with } k_m^{Cer} (app.) = \emptyset_{Cer}/\emptyset_0 \quad (2.12)$$

■ Similarly, if only $[Cer]$ is saturating, the equation can be reduced to,

$$\frac{[E_T]}{v} = \emptyset_0 + \emptyset_{PI} \frac{1}{[PI]} \text{ where by rearrangement gives,}$$

$$v = \frac{[E_T][PI]}{\emptyset_0 [PI] + \emptyset_{PI}} = \frac{V_{max} [PI]}{[PI] + \emptyset_{PI}/\emptyset_0} \text{ with } k_m^{PI} (app.) = \emptyset_{PI}/\emptyset_0 \quad (2.13)$$

In summary, equation (2.10) represents the simplest form of the rate equation at any given concentrations of ceramide and PI while equation (2.11) gives the theoretical V_{max} when both substrates are saturating. Also, when either [PI] or [Cer] is saturating, equation (2.9) could be reduced to a simpler form resembling Michaelis-Menten kinetics, equation (2.12) or (2.13) respectively. However, the measured $k_{m(app.)}^{PI}$ and $k_{m(app.)}^{Cer}$ should be cautiously interpreted in terms of enzyme affinity to either substrate. It is noteworthy that although under initial rate assumptions, [DAG] was set to zero, it is evident that \emptyset_{Cer} parameter is dependent on [DAG] according to equation (2.9) and affects $k_{m(app.)}^{Cer}$ in equation (2.12). This means that increasing [DAG], either produced as a by-product or exogenously added to the reaction mixture, would be expected to have an inhibitory effect on the reaction rate, a previously validated hypothesis (*see* section 2.2.3.4). In addition DAG would be expected to act as a competitive inhibitor in terms of ceramide leading to higher $k_{m(app.)}^{Cer}$ value.

2.2.4 V_{max} and k_m^{Cer} (app.) in terms of NBD-C₆-Ceramide

As described earlier, changing the NBD-C₆-ceramide concentration within the range 0 μM up to 20 μM relative to PI concentration range (12.5 – 250 μM) is very low (*c.a.* 8% in average). Thus, PI concentration would remain almost constant ($\Delta[\text{PI}] \leq 3.2\%$, *see* Appendix B) across experiments. Measuring *Lmj*IPCS activity against an increasing concentration of NBD-C₆-ceramide (at a fixed $[\text{PI}] = 100 \mu\text{M}$) yielded a curve that fitted Michaelis-Menten kinetic model (Figure 47) with V_{max} and k_m^{Cer} (app.) equal to 2.1 $\text{pmol}\cdot\text{min}^{-1}\cdot\text{U}^{-1}$ and 3.5 μM respectively. Determination of the Hill constant (Figure 47) revealed a Hill slope = 2.7 (> 1.0) which indicated a co-operative binding and that the observed fit to Michaelis-Menten kinetic model is an apparent behaviour due to the saturating concentration of PI in the experiment. This could be explained by equation (2.10). However, the measured k_m^{Cer} (app.) would be equal to the value of ϕ_{Cer}/ϕ_0 .

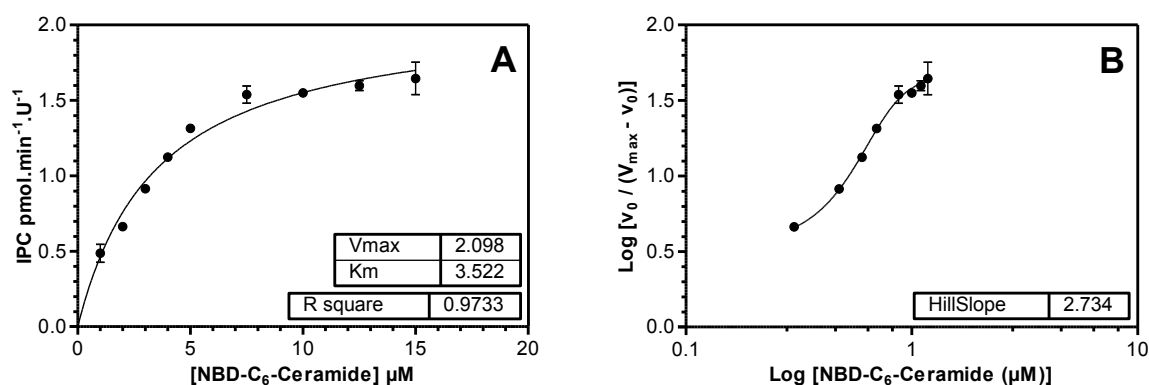


Figure 47: (A) *Lmj*IPCS Activity vs. NBD-C₆-ceramide [μM]. (B) Hill slope determination in terms of NBD-C₆-ceramide

2.2.5 V_{max} and k_m^{PI} (app.) in terms of PI

In contrast to NBD-C₆-ceramide, the determination of the (apparent) kinetic parameters of *Lmj*IPCS in terms of PI was not straightforward. Measuring *Lmj*IPCS activity against an increasing concentration of PI (at fixed $[\text{NBD-C}_6\text{-ceramide}] = 5 \mu\text{M}$) revealed an unexpected inhibitory effect of PI at high concentration with considerable deviation from apparent Michaelis-Menten kinetics (Figure 48: A). The observed inhibitory effect of PI at high

concentration has been previously reported by Aeed *et al*^A in terms of IPC synthase from *C. albicans*. Albeit, in Aeed's report, the concentration of PI was higher (400 μM) and the assay was performed at a saturating concentration of NBD- C_6 -ceramide. Aeed had justified the inhibition in terms of the relatively low affinity of PI for the IPC synthase which is consistent with the high levels of this substrate in the intact yeast Golgi membrane. Additionally, he identified an algorithm that incorporates a substrate inhibition parameter ' K_i ' to provide the best fit. Re-analysis of the data using this algorithm gave a better fit model (enhanced R^2 value from 0.79 to 0.85, *c.a.* 6%) (Figure 48: B) with V_{max} , k_m^{PI} and k_i^{PI} equal to 2.2 $\text{pMol}\cdot\text{min}^{-1}\cdot\text{U}^{-1}$, 54.4 μM and 220.3 μM respectively.

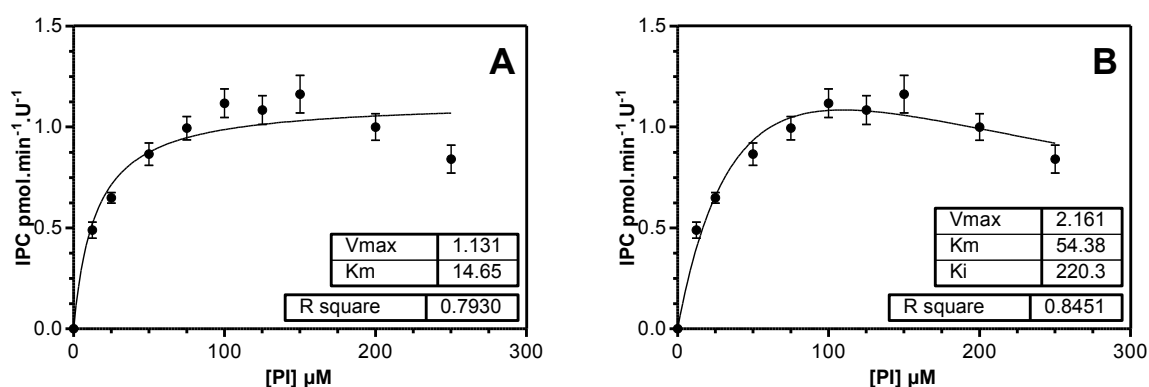


Figure 48: *Lmj*IPCS Activity vs. [PI] μM . (A) Using apparent Michaelis-Menten Kinetic model, [NBD- C_6 -ceramide] = 5 μM . (B) Using Substrate Inhibition Kinetic model, [NBD- C_6 -ceramide] = 5 μM

However, repeating the experiment at a higher concentration of NBD- C_6 -ceramide (20 μM), corresponding to $5.7 \times k_m^{Cer}$, resulted in no inhibitory effect of PI could be detected up to PI concentration = 250 μM (Figure 49: A). Interestingly, when the PI concentration was further increased at the same NBD- C_6 -ceramide concentration (20 μM) an inhibitory effect could be observed at PI concentration greater than 500 μM (Figure 49: B). These observations suggested an alternative explanation that under the specified assay conditions, the enzyme activity depends on the ratio of substrates concentrations rather than their molar concentrations. Consequently, a dilution effect should be considered.

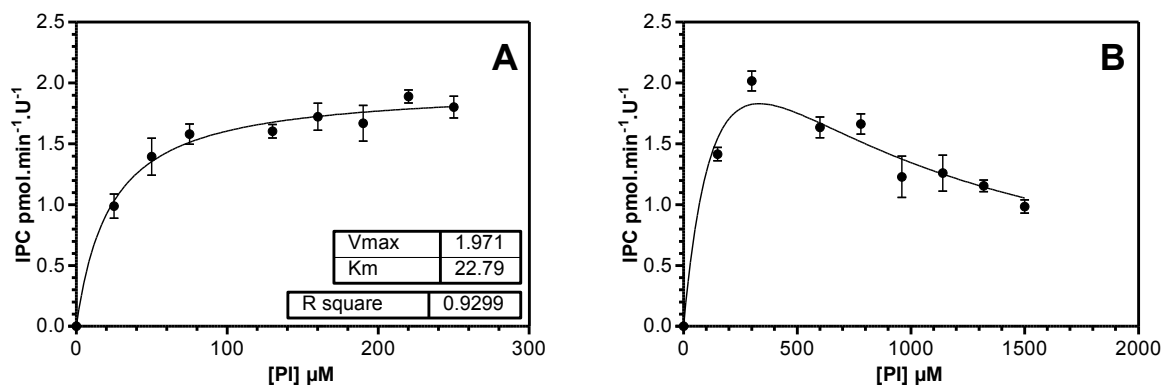


Figure 49: *Lmj*IPCS Activity vs. [PI] μM . (A) [PI] up to 250 μM exhibiting apparent Michaelis-Menten Kinetic model, [NBD- C_6 -ceramide] = 20 μM . (B) [PI] > 250 μM exhibiting Substrate Inhibition Kinetic model, [NBD- C_6 -ceramide] = 20 μM

Given the fact in this complex system the *Lmj*IPCS is a membrane enzyme activity acting on lipid substrates within mixed micelles, to facilitate further analyses a number of assumptions were made: PI micelles have a low molar % of CHAPS and can be considered as pure PI micelles; all lipids and detergent molecules have the same surface area; all lipids and detergent molecules have equal accessibility to the enzyme active site. All concentrations are expressed as molar fractions of total lipid plus detergent. Consequently, at [CHAPS] = 0.6 mM, increasing the molar concentration of PI from 0 – 250 μM would drop the molar fraction of NBD- C_6 -ceramide from 0.83% to 0.58% with a total reduction of 29% of the starting NBD- C_6 -ceramide concentration. This could explain the recurrent apparent inhibition at increasing PI concentrations at fixed concentration of NBD- C_6 -ceramide.

To verify this conclusion, the results of *Lmj*IPCS activity against substrate concentrations were re-analysed in terms of molar fractions. The molar fractions were calculated in terms of bulk concentrations of total lipids and detergent (Figure 50: A and C) and in terms of likely micellar concentrations of lipids and detergent (Figure 50: B and D). The re-plots of activity against NBD- C_6 -ceramide Mol% (Bulk and micellar) maintained an apparent good fit to Michaelis-Menten kinetic model. (Figure 50: A and B). This would be expected given that NBD- C_6 -ceramide is the minor lipid component in the assay. However, the re-plots in terms of PI Mol% maintained an apparent good fit to Michaelis-Menten equation only when expressed in bulk Mol% (Figure 50: C) but not in micellar Mol% (Figure 50: D). These observations

supported the dilution effect hypothesis and indicated that the activity is dependent on the bulk concentrations in terms of total lipids, PI and NBD- C_6 -ceramide, and detergent, CHAPS.

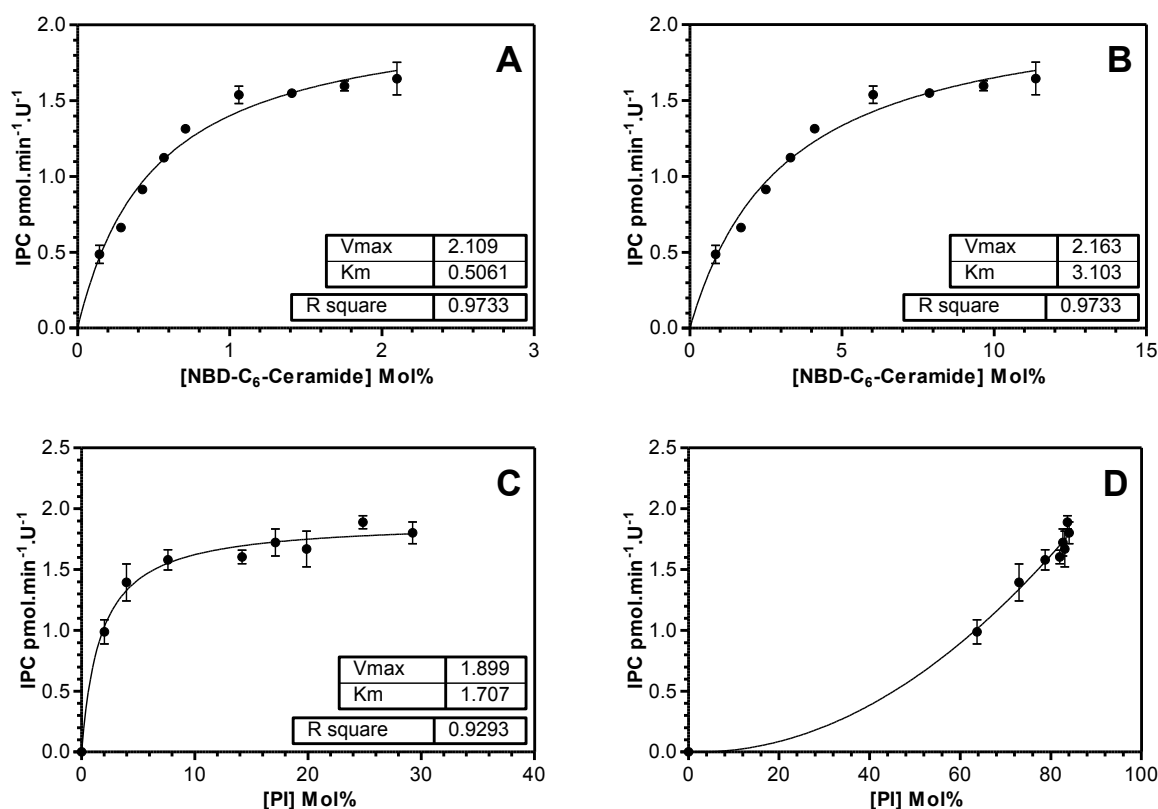


Figure 50: Activity vs. NBD- C_6 -ceramide, x -*abscissa* is expressed in Mol% relative to total lipids and CHAPS in reaction mixture (Graph A) & in Micelles (Graph B). Activity vs. PI, x -*abscissa* is expressed in Mol% relative to total lipids and CHAPS in reaction mixture (Graph C) & in Micelles (Graph D)

2.2.6 Bi-Bi Substrate Kinetics and Surface Dilution Effect

The presence of a dilution effect required further experimental data in order to determine the kinetic parameters of the kinetic equation and to confirm the initial hypothesis, a double displacement kinetic model. Towards this end, *Lmj*IPCS activity was measured against an increasing concentration of NBD- C_6 -ceramide at different fixed concentrations of PI (Figure 51: A). Generation of the Lineweaver-Burk plot of the data revealed an almost parallel pattern (Figure 51: B) that supported the initial hypothesis of double displacement kinetics.⁴⁵ A plot of the intercepts against the reciprocal of PI Mol% gave a linear relationship (Figure 51: C) as would be predicted from equation (2.10) with very low residual values (Figure 51: D).

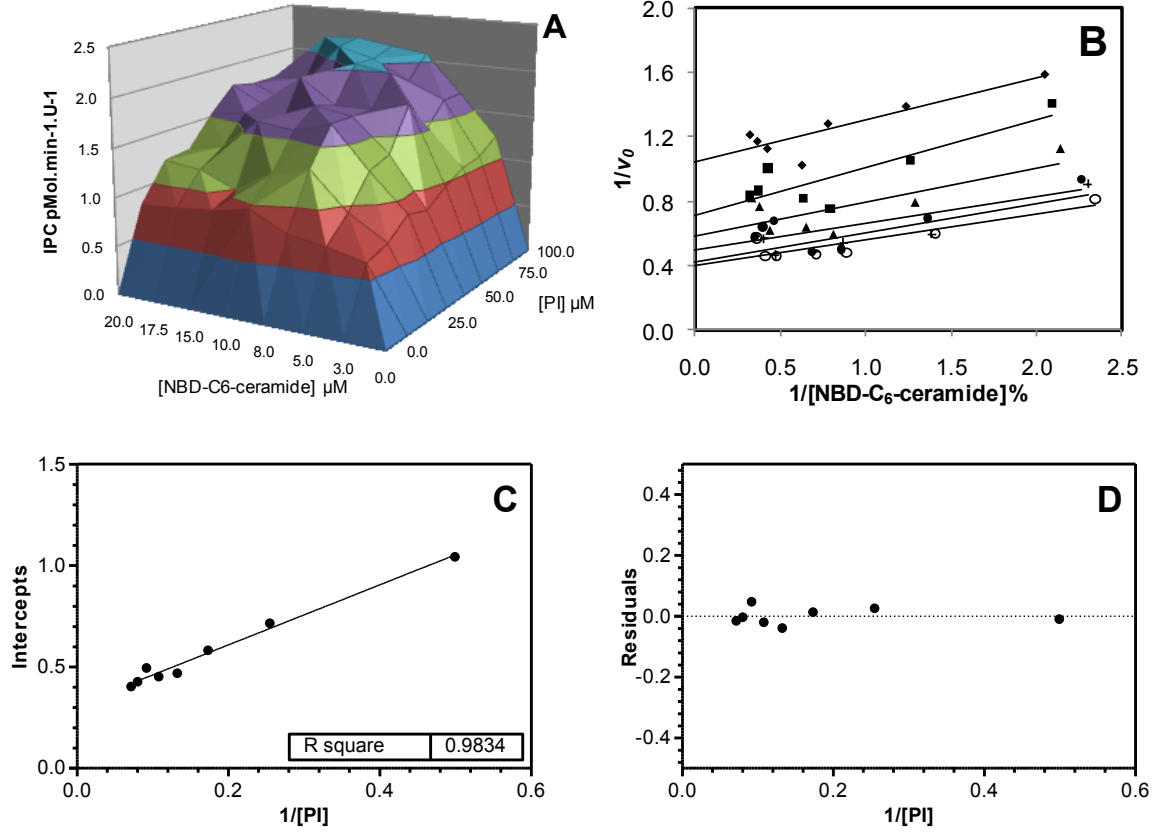


Figure 51: Top left: (A) *Lmj*IPCS Activity vs. an increasing [NBD-C₆-ceramide] (0 – 20 μM) at different fixed [PI] (12.5 – 100 μM). (B) The Lineweaver-Burk plot, error bars were removed for clarity. (C) A plot of the Intercepts of Graph ‘B’ against 1/[PI] and their the residual plot (D).

Subsequently, a global analysis of the data (56 points, mean values of 168 replicates) in terms of the surface dilution kinetic model developed by Deems⁴⁸ (equation 2.14, [PI] and [Cer] expressed as mol% in PI micelles) resulted in non convergent results. On contrary, when the generalised form of bi-bi substrate kinetic equation (equation 2.15) was used, a valid solution could be found. However, the global analysis resulted in a very low value for the parameter ϕ_{AB} (1.6×10^{-5}). This suggested the absence of the component $\frac{1}{[PI][Cer]}$ from the equation which reduces it to equation (2.10) and in turn supports the initial hypothesis of double displacement model. Nevertheless, it might be possible that $\frac{1}{[PI][Cer]}$ component is masked under the experimental conditions.

$$\frac{1}{v} = \frac{1}{V} + \left(\frac{k_s^{PI} k_m^{Cer}}{V[Cer]} \right) \frac{1}{[PI]} + \frac{k_m^{Cer}}{[Cer]} \quad (2.14)$$

$$\frac{[E_T]}{v} = \phi_0 + \phi_A \frac{1}{[PI]} + \phi_B \frac{1}{[Cer]} + \phi_{AB} \frac{1}{[PI][Cer]} \quad (2.15)$$

$$\frac{[E_T]}{v} = \varnothing_0 + \varnothing_{PI} \frac{1}{[PI]} + \varnothing_{Cer} \frac{1}{[Cer]} \quad (2.10)$$

Both the global analysis of the data and the graphical linear analysis yielded comparable results for the equation parameters (Table 2-1). The mean V_{max} and k_m^{Cer} values determined were $2.13 \text{ pMol} \cdot \text{min}^{-1} \cdot \text{U}^{-1}$ and $0.54 \text{ Mol}\%$ respectively and were comparable to the values determined using apparent Michaelis-Menten equation. However, k_m^{PI} ($4 \text{ Mol}\%$) was more than 2 fold the value determined using Michaelis-Menten kinetics. Cross validation of the results was achieved by plotting simulation curves by substituting equation 2.10 with the values determined. Comparable curves to the experimental data could be generated (Figure 52) with R^2 values greater than 0.90.

Table 2-1: The equation Parameters as determined by global analysis and linear analysis

	V_{max}	\varnothing_0	\varnothing_A	\varnothing_B	\varnothing_{AB}
Global Analysis (Solver – Excel)	2.31	0.26	0.82	0.14	1.0×10^{-5}
Graphical Linear Analysis	1.94	0.31	1.47	0.17	0.0

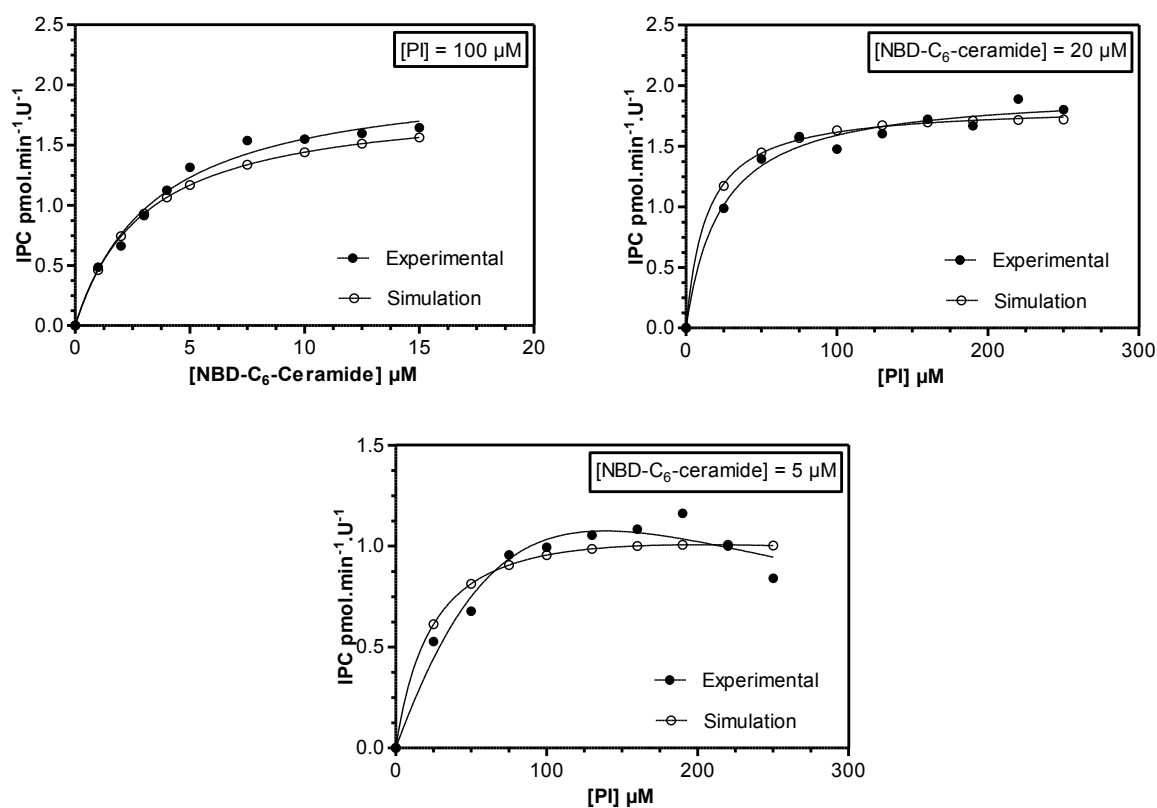


Figure 52: Simulation curves vs. Experimental curves

2.3 Conclusion

The work demonstrated in this chapter included the establishment of an assay protocol suitable for drug screening of potential inhibitors against *Lmj*IPCS. The typical assay concentrations are 10 μ g microsomal protein, 100 μ M PI, 5 μ M NBD-C₆-ceramide and 0.6 mM CHAPS in 40 μ L of 50 mM phosphate buffer. The established protocol has been validated in terms of aureobasidin A inhibition of *Lmj*IPCS. Determination of the kinetic parameters has shed light on the mechanistic aspects of *Lmj*IPCS in terms of relative affinities towards substrates and the kinetic model describing the enzyme mechanism of action. These findings will be further elaborated in Chapter VI regarding the rational design of inhibitors that target *Lmj*IPCS.

The previously described apparent inhibition of PI has now been demonstrated in terms of a dilution effect rather than an inhibitory effect of PI that confers a regulatory function of PI over IPC synthase activity.

To the best of the author's knowledge, no precedent kinetic analysis of a sphingolipid synthase (SM synthase or IPC synthase) has been demonstrated in terms of a double displacement kinetics employing dilution phenomenon in the kinetic analyses. The outcomes of this work have been recently accepted for publication (*see* Appendix D).

REFERENCES

1. P. W. Denny, H. Shams-Eldin, H. P. Price, D. F. Smith and R. T. Schwarz, *J. Biol. Chem.*, 2006, **281**, 28200-28209.
2. A. S. Fischl, Y. Liu, A. Browdy and A. E. Cremesti, *Methods Enzymol.*, 2000, **311**, 123-130.
3. J. M. Figueiredo, W. B. Dias, L. Mendonca-Previato, J. O. Previato and N. Heise, *Biochem. J.*, 2005 **387**, 519-529.
4. P. A. Aeed, A. E. Sperry, C. L. Young, M. M. Nagiec and Å. P. Elhammer, *Biochemistry*, 2004, **43**, 8483-8493.
5. J. Ko, S. Cheah and A. S. Fischl, *J. Bacteriol.*, 1994, **176**, 5181-5183.
6. *Eur J Biochem*, 1979, **97**, 319-320.
7. A. S. Fischl, Y. Liu, A. Browdy and A. E. Cremesti, *Methods Enzymol.*, 2000, **311**, 123-130.
8. M. Bradford, *Anal. Biochem.*, 1976, **72**, 248-254.
9. J. S. Ko, S. Cheah and A. S. Fischl, *J. Bacteriol.*, 1994, **176**, 5181-5183.
10. J. KO, S. CHEAH and A. S. FISCHL, *J Food Biochem*, 1995, **19**, 253-267.
11. M. M. Nagiec, E. E. Nagiec, J. A. Baltisberger, G. B. Wells, R. L. Lester and R. C. Dickson, *J. Biol. Chem.*, 1997, **272**, 9809-9817.
12. A. S. Fischl, Y. S. Liu, A. Browdy and A. E. Cremesti, *Sphingolipid Metabolism and Cell Signaling, Pt A*, 2000, **311**, 123-130.
13. W. Zhong, D. J. Murphy and N. H. Georgopapadakou, *FEBS Lett.*, 1999, **463**, 241-244.
14. J. M. Figueiredo, W. B. Dias, L. Mendonca-Previato, J. O. Previato and N. Heise, *Biochem. J.*, 2005, **387**, 519-529.
15. M. M. Nagiec, E. E. Nagiec, J. A. Baltisberger, G. B. Wells, R. L. Lester and R. C. Dickson, *J. Biol. Chem.*, 1997, **272**, 9809-9817.
16. , 2000.
17. *United States of America Pat.*, 2007.
18. D. Zilberstein and M. Shapira, *Annu. Rev. Microbiol.*, 1994, **48**, 449-471.
19. L. Vieira and Z. I. Cabantchik, *FEBS Letters*, 1995, **361**, 123-126.
20. L. Vieira, I. Slotki and Z. I. Cabantchik, *J. Biol. Chem.*, 1995, **270**, 5299-5304.
21. T. A. Glaser, J. E. Baatz, G. P. Kreishman and A. J. Mukkada, *Proc. Natl. Acad. Sci.*, 1988, **85**, 7602-7606.
22. S. M. Mandala, R. A. Thornton, M. Rosenbach, J. Milligan, M. Garcia-Calvo, H. G. Bull and M. B. Kurtz, *J. Biol. Chem.*, 1997, **272**, 32709-32714.
23. S. M. Mandala, R. A. Thornton, J. Milligan, M. Rosenbach, M. Garcia-Calvo, H. G. Bull, G. Harris, G. K. Abruzzo, A. M. Flattery, C. J. Gill, K. Bartizal, S. Dreikorn and M. B. Kurtz, *J. Biol. Chem.*, 1998, **273**, 14942-14949.
24. K. Zhang and S. M. Beverley, *Mol Biochem Parasitol*, 2010, **170**, 55-64.
25. K. Zhang, F.-F. Hsu, D. A. Scott, R. Docampo, J. Turk and S. M. Beverley, *Mol. Microbiol.*, 2005, **55**, 1566-1578.
26. R. C. Dickson, *Annu. Rev. Biochem.*, 1998, **67**, 27-48.
27. P. A. Aeed, C. L. Young, M. M. Nagiec and A. P. Elhammer, *Antimicrob. Agents Chemother.*, 2009, **53**, 496-504.
28. T. Schürholz, *Biophys. Chem.*, 1996, **58**, 87-96.
29. Y. Yong, Y. Pei Qing and J. Gang, *Chin. Chem. Lett.*, 2004, **15**, 1465-1468.
30. P. Ying, G. Jin and Z. Tao, *Colloids and Surfaces B: Biointerfaces*, 2004, **33**, 259-263.
31. P. Zunszain, J. Ghuman, T. Komatsu, E. Tsuchida and S. Curry, *BMC Struct Biol*, 2003, **3**, 6.
32. S. Sugio, A. Kashima, S. Mochizuki, M. Noda and K. Kobayashi, *Protein Eng.*, 1999, **12**, 439-446.
33. G. M. Carman, R. A. Deems and E. A. Dennis, *J. Biol. Chem.*, 1995, **270**, 18711-18714.
34. R. J. Buxeda, J. T. Nickels, C. J. Belunis and G. M. Carman, *J. Biol. Chem.*, 1991, **266**, 13859-13865.
35. T. G. Warner and E. A. Dennis, *J. Biol. Chem.*, 1975, **250**, 8004-8009.
36. J. T. Nickels, R. J. Buxeda and G. M. Carman, *J. Biol. Chem.*, 1992, **267**, 16297-16304.
37. Y. P. Lin and G. M. Carman, *J. Biol. Chem.*, 1990, **265**, 166-170.
38. J. Yao and G. D. Dotson, *Biochim. Biophys. Acta*, 2009, **1794**.
39. L. Luukkanen, J. Taskinen, M. Kurkela, R. Kostiaainen, J. Hirvonen and M. Finel, *Drug Metab. Dispos.*, 2005, **33**, 1017-1026.
40. D. M. Goodenough-Lashua and G. A. Garcia, *Bioorg. Chem.*, 2003, **31**, 331-344.
41. D. C. Prasher, M. C. Carr, D. H. Ives, T. C. Tsai and P. A. Frey, *J. Biol. Chem.*, 1982, **257**, 4931-4939.
42. D. H. Ives, D. C. Prasher and M. C. Carr, *Fed Proc*, 1980, **39**, 2031-2031.
43. L. J. Wong and P. A. Frey, *Fed Proc*, 1974, **33**, 1243-1243.

44. R. J. Moffet and W. A. Bridger, *J. Biol. Chem.*, 1970, **245**, 2758-2762.
45. C. P. Engel, *Enzyme Kinetics: The Steady-state Approach*, 1 st edn., John Wiley & Sons, 1977.
46. R. A. Deems, B. R. Eaton and E. A. Dennis, *J. Biol. Chem.*, 1975, **250**, 9013-9020.
47. E. Maréchal, M. A. Block, J. Joyard and R. Douce, *J. Biol. Chem.*, 1994, **269**, 5788-5798.
48. R. A. Demms, B. R. Eaton and E. A. Dennis, *J. Biol. Chem.*, 1975, **250**, 9013-9020.

CHAPTER III

*Lmj*IPCS
ORTHOLOGOUS
ENZYMES
*Tb*SLS4 & *At*IPCSs

3 *Lmj*IPCS ORTHOLOGOUS ENZYMES

3.1 Work Synopsis

Having established the *Lmj*IPCS activity assay and the determination of its kinetic parameters, the established characterisation techniques were applied to *Lmj*IPCS orthologues. The candidates selected for this were the closely related *Tb*SLS4 from *T. brucei* and the identified orthologous Plantae enzymes *At*IPCS 1, 2 & 3. Successful application of those techniques helped to characterise the former as a potential drug target for African Trypanosomiasis and demonstrate the IPC synthase activity of the later cluster of enzymes which had remained unidentified in the genome databases. The outcomes of this work, performed in collaboration with laboratory colleagues, have been recently published¹⁻² (*see* Appendix D). This chapter will discuss the relevant previous work and focus on the author's contributions to this work with respect to *Tb*SLS4 and *At*IPCS 1, 2 & 3.

3.2 *Tb*SLS4 (*Tb*09.211.1000)

3.2.1 Introduction

The *Trypanosoma brucei* genome has four tandem gene sequences (*Tb*09211.1030, *Tb*09.211.1020, *Tb*09.211.1010 and *Tb*09.211.1000; here annotated *Tb*SLS1-4 to reflect their 5' to 3' order) that were previously identified in the *T. brucei* genome database (www.genedb.org) as sequence orthologues of the *Lmj*IPCS.³ Importantly, knockdown of *Tb*SLS1-4 expression using inhibition RNA (RNAi) in bloodstream form parasites demonstrated that the enzyme activity is essential for growth thus validating it as a target for the development of new anti-HAT therapies.^{2, 4-5}

Previous work within the Denny group using metabolic labelling of *Lmj*IPCS complemented yeast with NBD-C₆-ceramide and HPTLC chromatographic separation of the synthesised sphingolipid products, demonstrated the synthesis of one labelled sphingolipid species identified

to be NBD-C₆-IPC. However, using the same mutant line, labelled under the same conditions but complemented with *TbSLS4* or *TbSLS1*, two predominant sphingolipid species were synthesized. One of these co-migrated with NBD-C₆-IPC, the other with NBD-C₆-SM and was SMase sensitive. It is noteworthy that while the dominant species in case of *TbSLS4* was NBD-C₆-SM, *TbSLS1* predominantly synthesised NBD-C₆-IPC with trace amounts of NBD-C₆-SM. This indicated that *TbSLS4* was a bi-functional enzyme with the ability to catalyze the biosynthesis of both IPC and SM, thus reflecting the sphingolipid profile of the parasite (Figure 3-1).^{2,4} This unusual behaviour required further characterisation of these enzymes.

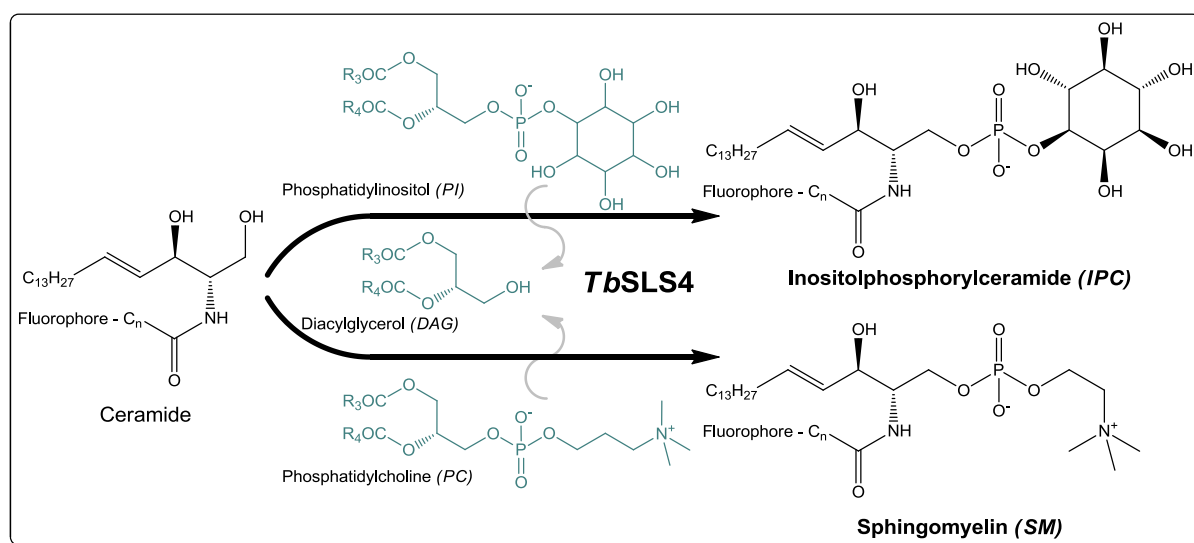


Figure 3-1: The catalytic transferase activity of *TbSLS4* as a bi-functional enzyme which can turn over both PC and PI into SM and IPC respectively.

3.2.2 Construction of the *TbSLS*s complemented Mutant Yeast Strain

The auxotrophic *YPH499-HIS-GAL-AUR1 S. cerevisiae* strains complemented with the vectors p426MET25, p426MET25-*TbSLS1*, p426MET25-*TbSLS4* and p426MET25-*ScIPCS* (AUR1) -obtained from Dr. Denny- were constructed as previously described under section 2.1.1. Similarly, Functionally complemented transformants were selected on non-permissive SD medium (0.17 % Bacto yeast nitrogen base, 0.5 % ammonium sulphate, and 2 % dextrose) containing the nutritional supplements necessary to allow selection of transformants (Figure 3-2).

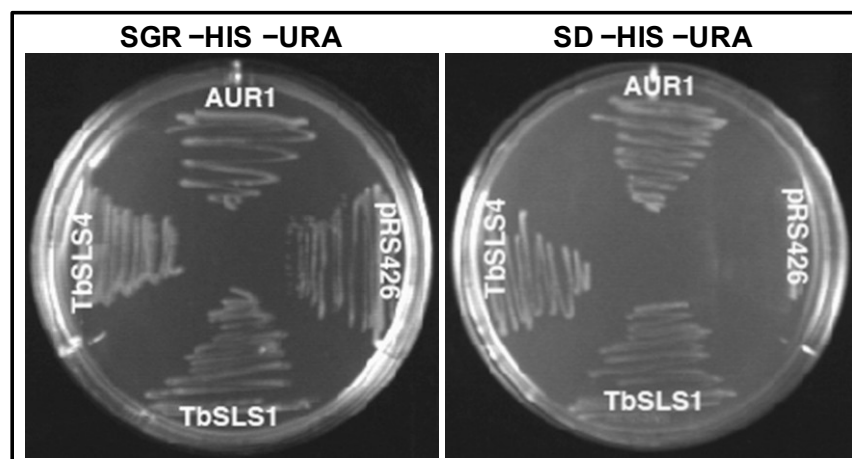


Figure 3-2: Transformation of *YPH499-HIS-GAL-AUR1 S. cerevisiae* with p426MET25 (Control), p426MET25-*TbSLS1*, p426MET25-*TbSLS4* and p426MET25-*ScIPCS* (AUR1).

3.2.3 *In vitro* assay of *TbSLS4* activity

To further analyse the observed activity of *TbSLS4*, microsomal membranes from exponentially growing *YPH499-HIS-GAL-AUR1 pRS426 TbSLS4* yeast were prepared as previously described⁶ and the isolated membrane fraction re-suspended in storage buffer (50 mM Tris-HCl pH 7.4, 20 % (v/v) glycerol, 5 mM MgCl₂) with Complete[®] EDTA-free Protease Inhibitor Cocktail at a protein concentration of 10 mg/ml. As for the *Lmj*IPCS material, the microsomal membranes were subsequently washed in 2.5 % CHAPS, isolated by ultracentrifugation, re-suspended in storage buffer at 10mg/ml and stored at -80 °C until use.

Initial activity assays were conducted using Protocol 'B' in which HPTLC analyses provide a qualitative assessment.⁷ Briefly, the assay mix contained 100 μM donor substrate (bovine liver PI, PC or PE), 10 μg of microsomes, 100 mM Tris-HCl, 10 mM EDTA, 6 mg/ml BSA and 5 μM NBD-C₆-ceramide. Following incubation at 30 °C for 60 minutes the reaction was quenched by the addition of 150 μl of chloroform:methanol:water (10:10:3). After biphasic separation the organic layer was removed, processed and analyzed using HPTLC plate separation. For inhibition experiments the reaction mix was pre-incubated for 30 minutes with appropriate quantities of aureobasidin A before the addition of the acceptor substrate NBD-C₆-ceramide.

3.2.3.1 Activity vs. Different Donor Substrates

Initial experiments focused on measuring the *Tb*SLS4 activity in terms of the potential donor substrates: mammalian PI, phosphatidylethanolamine (PE) and phosphatidylcholine (PC). These investigations required validation of the absence of background activity due to the endogenous yeast IPCS. Consequently, the activities of crude and washed *Sc*IPCS (*YPH499-HIS-GAL-AURI pRS426 AURI*) microsomes were first measured in terms of exogenous mammalian PI and PC (Figure 3-3). Whilst a detectable activity could be measured in case of the crude *Sc*IPCS microsomes (lanes 1), there was little enhancement of the turnover upon addition of PI (lanes 2) and no detectable effect on addition of PC (lanes 3). The CHAPS-washed *Sc*IPCS microsomes exhibited a similar profile to the crude microsomes but with a remarkably reduced turnover (lanes 4, 5 & 6). This drop in activity was attributed to the depletion of native yeast (polyhydroxylated) PI in the CHAPS-washed membranes combined with the inability of the *Sc*IPCS to turn over the exogenous PI (mammalian variant, predominant species is 16:0/20:4).⁸⁻⁹ Having confirmed the absence of background activity, it was possible to test *Tb*SLS4 activity profile in terms of the donor substrates (Figure 3-3).

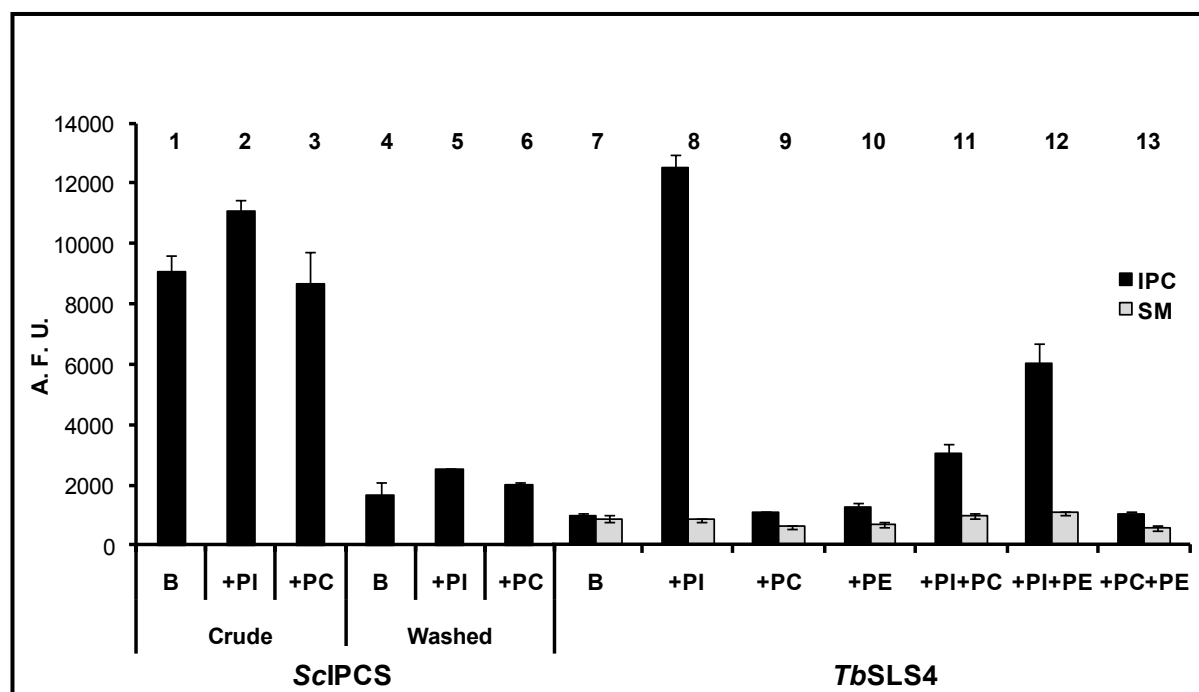


Figure 3-3: The activity profiles of *Sc*IPCS Control (using crude microsomes, lanes 1, 2 & 3, and CHAPS-washed microsomes, lanes 4, 5 & 6) and *Tb*SLS4 in terms of different donor substrates (using CHAPS-washed microsomes, individual donor substrates: lanes 7, 8, 9 & 10 and equimolar mixtures of donor substrates: lanes 11, 12 & 13. (B, Blank, no added exogenous donor substrate; PI, phosphatidylinositol; PC, phosphatidylcholine; PE, phosphatidylethanolamine).

Using CHAPS-washed microsomes of *TbSLS4*, a blank experiment (no added donor substrates) gave a trace amount of the products (NBD-C₆-IPC & NBD-C₆-SM) (lane 7). However, the addition of exogenous PI (mammalian) increased the formation of NBD-C₆-IPC more than 25 fold (lane 8). This demonstrated the ability of *TbSLS4* to catalyse the formation of IPC. In contrast to the activity profile observed in metabolic labelling experiments, the addition of exogenous PC (mammalian) did not reconstitute the activity of the enzyme as an SM synthase (lane 9). Furthermore, the addition of PE (mammalian) did not result in the formation of any other labelled species such as ethanolamine phosphoryl-NBD-C₆-ceramide (EPC) (lane 10). Subsequently, *TbSLS4* activity was measured upon the addition of equimolar mixtures of PI/PC, PI/PE and PC/PE (lanes 11, 12 & 13). In spite of the fact that no additional formation of either NBD-C₆-SM or ethanolaminephosphoryl-NBD-C₆-ceramide was detected, a significant reduction of NBD-C₆-IPC formation was observed. This indicated that although the added PC and PE could not be turned over by the enzyme, these lipid species may still be able to bind to the enzyme active site as one-site competitive inhibitors resulting in a reduced rate of NBD-C₆-IPC formation.

The failure to reconstitute the SM synthase activity was surprising. However, upon closer investigation of the literature it could be speculated that a possible reason for such observation was the PC variant used in those assays. While under the experimental conditions deployed, exogenous PC was from a mammalian source (predominant species 18:0/18:2), in other published work^{5,7} the plant variant of PC (16:0/18:2) which has a shorter (C16) 1-*sn*-acyl chain was utilised (Figure 3-4).

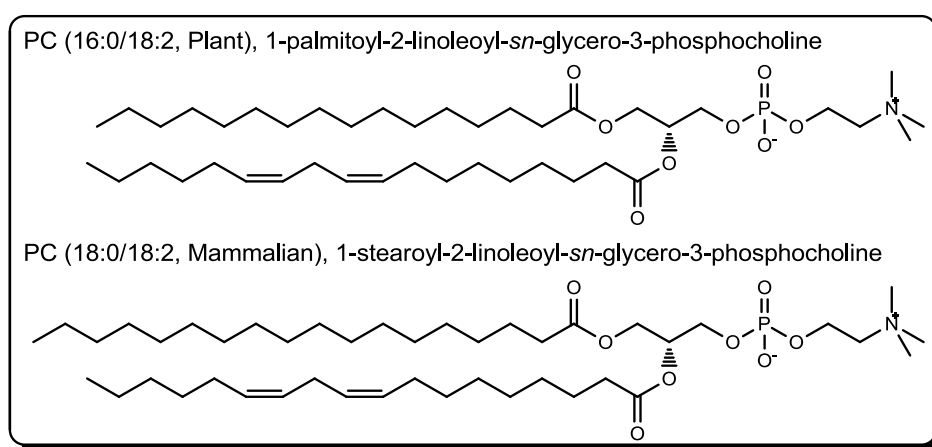


Figure 3-4: The chemical structure of mammalian and plant PC demonstrating the subtle structural difference due to the chain length of the 1-*sn*-acyl residue.

This assumption is consistent with the fact that *S. cerevisiae*, where both *TbSLS4* and *TbSLS1* function as SM synthases, predominantly possesses C32:2 (16:1/16:1) and C34:2 (16:1/18:1) PC variants.¹⁰ Additionally, in earlier work, *Richmond et al.*¹¹ has demonstrated that *T. brucei* procyclic and bloodstream forms harbour significant quantities of C36, C38 and C40 PC species in addition to minor quantities of the shorter C28 PC species.¹¹⁻¹² Also, Richmond has reported that a permeating feature of the *lyso*-PC molecules synthesized in *T. brucei* is that their acyl moiety (2-*sn*-acyl) is composed of a long and highly unsaturated chain of C22 (22:*x*; *x* = 4,5 & 6) in nearly 50 % of the metabolite population. Together these facts suggest the presence of a high PC population with the 1-*sn*-acyl shorter than C18 (C16 & C14) which is consistent with the hypothesis that only PC with a C16 or shorter 1-*sn*-acyl residue can be utilised by the SM synthase activity of *TbSLS4*. One way to validate this hypothesis is to measure the activity of *TbSLS4* against both PC variants under the same experimental conditions and within a pH range⁵ 5.5 ~7.5 as this also might have profound effect due to the anionic/cationic nature of the donor substrates.

3.2.3.2 Activity vs. Time

The *TbSLS4* activity profile was monitored, using protocol 'B', over time up to 50 minutes. The results showed only trace amounts of NBD-C₆-SM (most probably due to residual amounts of PC in CHAPS-washed microsomes) were formed over the time span of the experiment and were ignored in quantification. Consequently, using protocol 'A', *TbSLS4* activity was quantified in terms of NBD-C₆-IPC (Figure 3-5). In contrast to *Lmj*IPCS, the *TbSLS4* turnover rate reached a plateau after about 20 minutes of reaction time. The reasons behind such early decline in the turnover rate are unclear; however, this demonstrated the application of the 96-wellplate assay format in the study of *TbSLS4*.

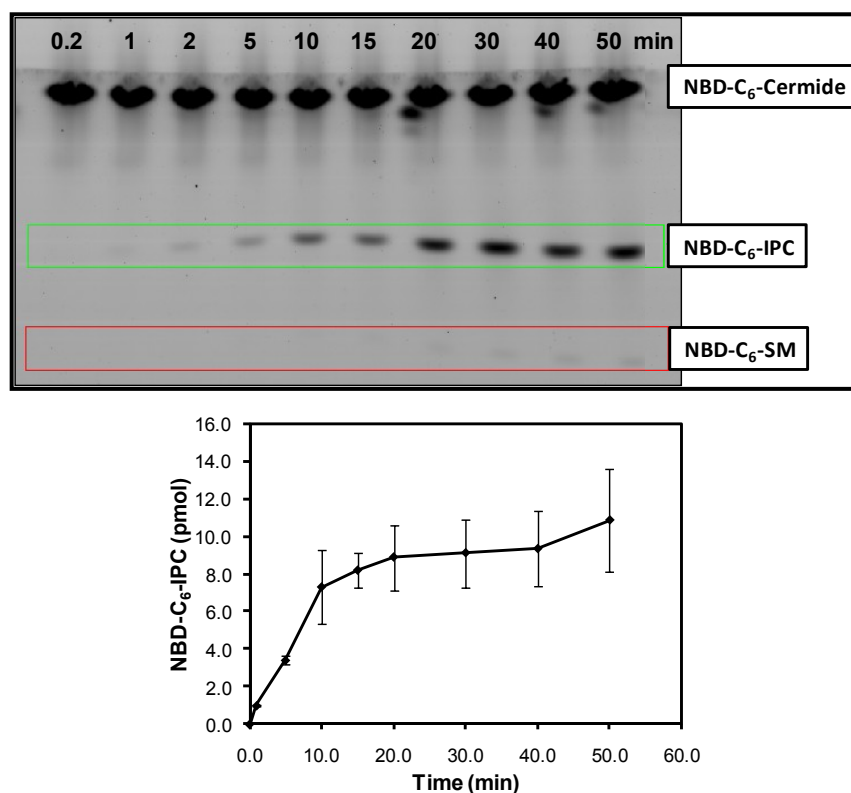


Figure 3-5: *TbSLS4* activity vs. Time. (Top) The visualisation of the measured *TbSLS4* activity over time using the HPTLC plate. (Bottom) Activity curve produced using the 96-wellplate format of protocol 'A' with detected fluorescence quantified in terms of NBD-C₆-IPC formation.

3.2.3.3 *Aureobasidin A* Inhibition

Previous work within the group identified that the fungal IPCS inhibitor aureobasidin A has a trypanocidal effect on the bloodstream form *T. brucei*.² Consequently, the activity of *TbSLS4* was measured against an increasing concentration of aureobasidin A (Figure 3-6). The inhibition profile revealed an $IC_{50} = 0.4$ nM (*c.f.* IC_{50} for *Lmj*IPCS > 100 μ M). Such potent effect is consistent with earlier work within the group and indicated that the trypanocidal effect of aureobasidin A is due to the inhibition of the essential enzyme *TbSLS4*. Additionally, this observation identifies *TbSLS4* to be different from the closely related orthologues *Lmj*IPCS and *Tc*IPCSs⁷ which are aureobasidin A insensitive. Although the reasons for this difference in aureobasidin A sensitivity are unclear, based on a recently proposed non-competitive inhibition

model,¹³ it might be attributed to the relative spatial organisation of the enzyme transmembrane helices.

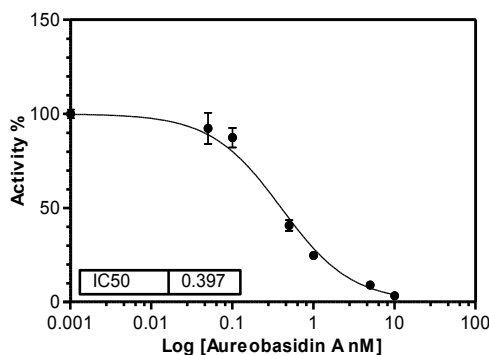


Figure 3-6: Aureobasidin A inhibition profile against *TbSLS4*.

3.2.4 Reverse Activity

Previous work has demonstrated developmental regulation of the predominant sphingolipid species in the lifecycle of the parasite.⁴ IPC was found to be predominant in the procyclic form (PCF) but undetectable in the blood stream form (BSF). This has been correlated with the developmental regulation of the different isoforms of the *TbSLSs*.¹⁴ However the fate of the accumulated IPC in the PCF remained unexplained. Towards this end, the ability of *TbSLS4* to catalyse the reverse activity (IPCase function) was investigated. Such activity would indicate a role in the remodelling of the parasite sphingolipids during the lifecycle.

Testing this hypothesis required NBD- C_6 -IPC which is not commercially available. Consequently, in a tenfold scaled-up experiment using *Lmj*IPCS microsomes, NBD- C_6 -ceramide was converted to NBD- C_6 -IPC which was subsequently purified using HPTLC. The resultant NBD- C_6 -IPC was kept at -80°C until use. Equivalent amounts (by protein concentration) of CHAPS-washed microsomal membranes containing *Lmj*IPCS or *TbSLS4* were added to NBD- C_6 -IPC in the presence or absence of DAG (acting as a potential acceptor substrate to form PI) (Figure 3-7). Under the experimental conditions *TbSLS4* exhibited the capacity to catalyse the reverse reaction in the presence of DAG whilst *Lmj*IPCS did not (Figure 3-7). Such activity suggests that *TbSLS4* might be involved in the recycling of the IPC during the lifecycle of the parasite.

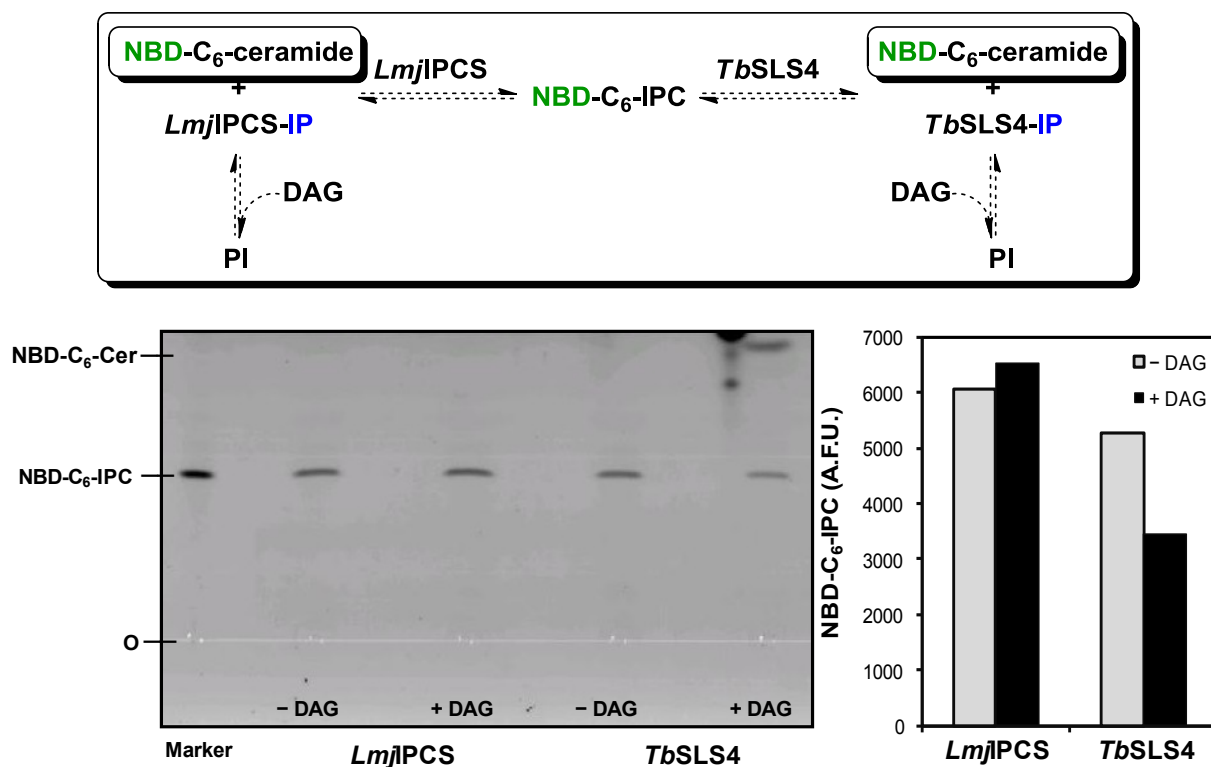


Figure 3-7: (Top) The hypothetical reaction scheme for the experiment design of the reverse activity of *Lmj*IPCS and *Tb*SLS4 with potential labelled products boxed. (Bottom) The visualisation of the NBD-C₆-IPC and the released NBD-C₆-ceramide using the HPTLC plate showing no reverse activity in case of *Lmj*IPCS and DAG-dependent reverse activity in case of *Tb*SLS4.

3.3 *At*IPCS 1, 2 & 3 (*At*3g54020.1, *At*2g37940.1 & *At*2g29525.1)

3.3.1 Introduction

Although the activity of an IPCS orthologue had been detected in bean microsomes,¹⁵ the plant enzyme remained unidentified. However, interrogation of the Arabidopsis genome database with the predicted protein sequence of *Lmj*IPCS³ identified opening reading frames encoding three highly related sequence orthologues –*At*IPCS1 (*At*3g54020.1), *At*IPCS2 (*At*2g37940.1) and *At*IPCS3 (*At*2g29525.1)– demonstrating 26, 29 and 31 % identity to the protozoan protein respectively. These newly identified putative plant IPC synthases form a new class of sphingolipid synthases¹ where the key motifs, D3 and D4 that contain the catalytic triad necessary for the transferase activity of the sphingolipid synthase family are conserved,¹⁶ but unlike their protozoan and mammalian counterparts, they lack a D1 domain¹⁷ and thus resembling the fungal IPC synthases. Despite the conservation of some of these motifs the plant sequences are divergent with respect to primary sequence.¹⁷⁻¹⁹

Previous work within the group demonstrated that the complementation of the AUR1 auxotrophic mutant *YPH499-HIS-GAL-AUR1* with *pRS426 At*IPCS1-3 restored the growth of the mutant yeast. These data indicated that *At*IPCS1, 2 and 3 are functional orthologues of fungal AUR1p.²⁰ Additionally, using a diffusion assay²⁰⁻²¹ the efficacy of two different classes of inhibitor were assayed against *YPH499-HIS-GAL-AUR1 pRS426 At*IPCS1, 2 and 3. The transgenic yeast strains were resistant to aureobasidin A at 100 μ M but remained sensitive to myriocin (SPT inhibitor). Further validation of the function of the isolated enzymes required an *in vitro* assay system suitable to test their hypothesised transferase activity.

3.3.2 Construction of the *At*IPCSs complemented Mutant Yeast Strain

As previously described under sections 2.1.1 and 3.2.2, the auxotrophic *YPH499-HIS-GAL-AUR1 S. cerevisiae* strains complemented with the vectors p426MET25, p426MET25-*At*IPCS1, p426MET25-*At*IPCS2, p426MET25-*At*IPCS3 and p426MET25-*Sc*IPCS (AUR1) -obtained from Dr. Denny- were constructed and functionally complemented transformants were selected on non-permissive SD medium (0.17 % Bacto yeast nitrogen base, 0.5 % ammonium sulphate, and

2 % dextrose) containing the nutritional supplements necessary to allow selection of transformants (Figure 3-8).

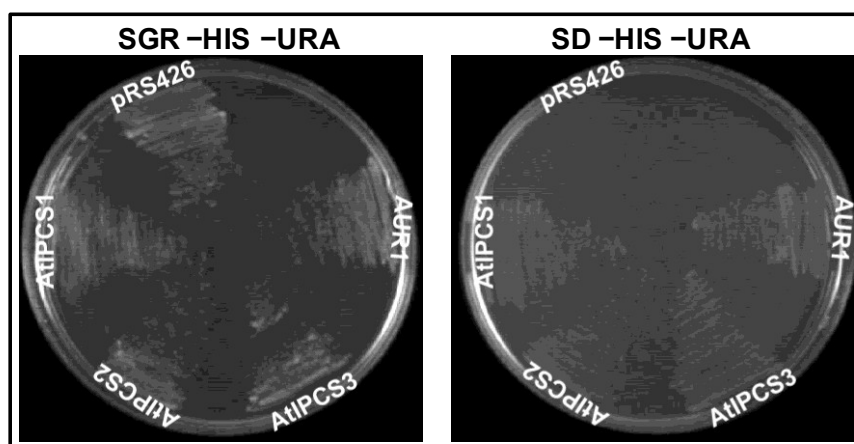


Figure 3-8: Transformation of *YPH499-HIS-GAL-AUR1 S. cerevisiae* with p426MET25 (Control), p426MET25-*AtIPCS1-4* and p426MET25-*ScIPCS* (*AUR1*).

3.3.3 Microsomes Preparation and *in vitro* Activity Assay

The *AtIPCS* microsomal membranes were prepared from *YPH499-HIS-GAL-AUR1 pRS246 AtIPCS1-3* and *YPH499-HIS-GAL-AUR1 pRS246 AUR1* and assayed as described previously. Assays were performed using protocol ‘B’. However, it was presumed that the most efficient donor substrate would have been the soybean PI (predominant species 16:0/18:2) (*c.f.* sections 2.1.3.2 & 3.2.2.1). This hypothesis was supported by experimental evidence as will be discussed below in section 3.3.3.1. It is noteworthy that CHAPS-washing the crude *AtIPCS* microsomes resulted in apparent inactivation of the enzyme *AtIPCS1* & 3. However, in the case of *AtIPCS2*, the enzyme remained active but with high background activity.

3.3.4 *AtIPCS1-3* are Functional IPC Synthases

3.3.4.1 Activity vs. Different Donor Substrates

Having established that *AtIPCS2* is the most highly expressed isoform, the most responsive isoform under the assay conditions and the only *AtIPCS* to give detectable activity after washing, CHAPS-washed *AtIPCS2* microsomes were prepared and tested against different donor substrate variants: mammalian, plant (soy) and synthetic (dipalmitoyl) PI. It has been found that while

*At*IPCS2 showed highest activity with the plant PI and considerable turnover with the mammalian variant, it could not utilise the synthetic variant (Figure 3-9). This could be attributed to the varying degrees of polyunsaturation between plant, mammalian and saturated dipalmitoyl PI which may confer conformational constraints that were not met by the active site of *At*IPCS2.

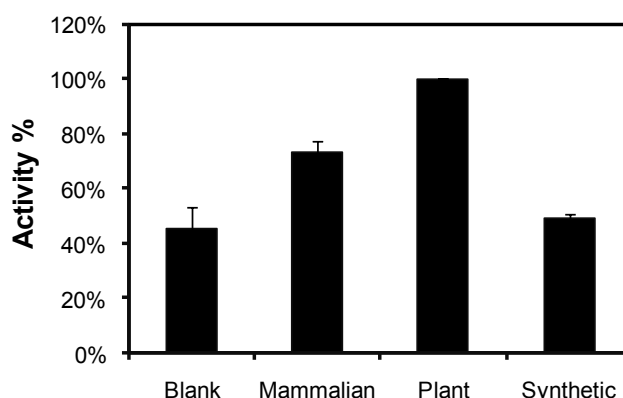


Figure 3-9: CHAPS-washed *At*IPCS2 activity vs. different variants of the donor substrates, PI.

3.3.4.2 *Ab A inhibition*

Using the established *in vitro* assay system, equal quantities (by protein concentration) of the microsomes prepared from *YPH499-HISGAL-AURI pRS426 At*IPCS1-3 were tested for IPC synthase activity in the presence of aureobasidin A (5.0 μ M) to suppress any possible background activity due to the yeast AUR1p. Although the turnover of *At*IPCS1-3 appeared low, the detectable activity was successfully quantified in terms of NBD-C₆-IPC (Figure 3-10). Similar observations of this low level of activity have been previously noted by Wang *et al.*¹⁶ Moreover, Wang has reported that the low level of activity was unaffected by the use of NBD-C₆-phytoceramide (plant variant) rather than NBD-C₆-ceramide as acceptor substrate.

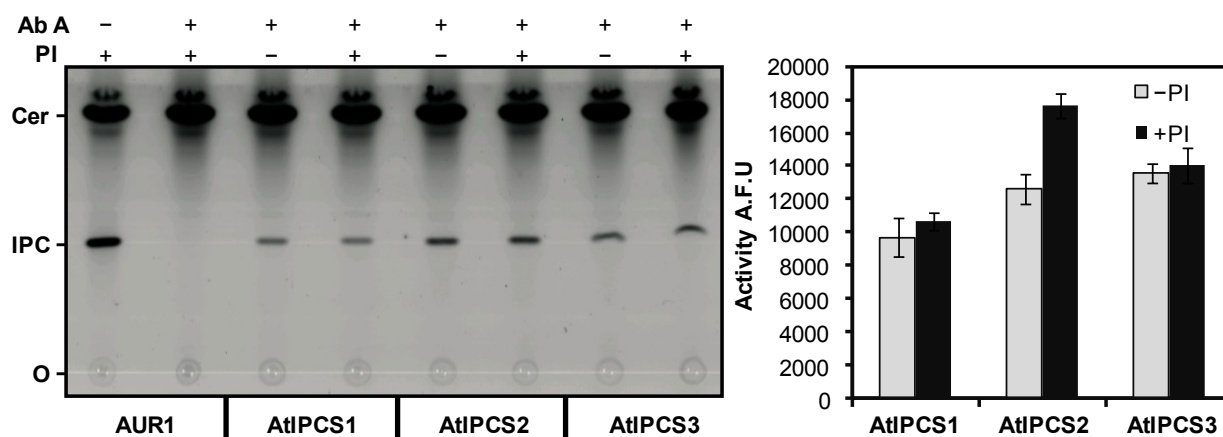


Figure 3-10: (Left) Assay in the presence of phosphatidylinositol (PI), with (+) or without (-) the specific fungal inhibitor aureobasidin A (AbA). In contrast to the *S. cerevisiae* IPC synthase (AUR1), the plant activity encoded by AtIPCS1-3 is insensitive to AbA at 5 μ M. (Right) Quantification of the produced NBD-C₆-IPC. Mean of 3 separate experiments, S.E. shown. A.F.U, Arbitrary Fluorescence Units.

The *in vitro* assay of AtIPCS1-3 has demonstrated that the three plant enzymes are active IPC synthases and confirmed that the Arabidopsis enzymes are aureobasidin A insensitive. This is in contrast to the IPCS activity assayed in Golden butter wax bean extracts that has been shown to be acutely sensitive to this inhibitor.¹⁵ The reasons for this difference in aureobasidin A sensitivity are unclear and no data are currently available for the bean sequence to help elucidate this discrepancy.

3.4 Conclusion

The work demonstrated in this chapter highlighted the successful application of the earlier established assay protocols to orthologous enzymes, both closely related (*TbSLS4*) and divergent (*AtIPCSs*). However, more work is required for further optimisation. Additionally, the inhibitory effect of aureobasidin A on *TbSLS4* has been established and a nanomolar IC_{50} value has been determined. Furthermore, the comparative capacity of *LmjIPCS* and *TbSLS4* to catalyse the reverse reaction has been investigated. To the best of the author's knowledge, *TbSLS4* represents the first IPC synthase with IPCase activity.

Using the established assay protocol, it was also possible to demonstrate the aureobasidin A insensitive IPC synthase turnover by all three identified sequence-divergent Arabidopsis isoforms. This evidence supports *AtIPCS1-3* as a new group of sphingolipid synthases within the wider enzyme family.¹ Moreover, in a concurrent work, it has been demonstrated that during a screen for factors involved in programmed cell death (PCD) defence mechanisms, an AUR1 functional orthologue was identified in Arabidopsis. However, the encoded protein demonstrated little homology to the yeast AUR1p, having most similarity to the more recently identified animal sphingomyelin synthases.¹⁶

REFERENCES

1. J. Mina, Y. Okada, N. Wansadhipathi-Kannangara, S. Pratt, H. Shams-Eldin, R. Schwarz, P. Steel, T. Fawcett and P. Denny, *Plant Mol. Biol.*, 2010, **73**, 399-407.
2. J. G. Mina, S. Y. Pan, N. K. Wansadhipathi, C. R. Bruce, H. Shams-Eldin, R. T. Schwarz, P. G. Steel and P. W. Denny, *Mol. Biochem. Parasitol.*, 2009, **168**, 16-23.
3. P. W. Denny, H. Shams-Eldin, H. P. Price, D. F. Smith and R. T. Schwarz, *J. Biol. Chem.*, 2006, **281**, 28200-28209.
4. S. S. Sutterwala, F. F. Hsu, E. S. Sevova, K. J. Schwartz, K. Zhang, P. Key, J. Turk, S. M. Beverley and J. D. Bangs, *Mol. Microbiol.*, 2008, **70**, 281-296.
5. E. S. Sevova, M. A. Goren, K. J. Schwartz, F.-F. Hsu, J. Turk, B. G. Fox and J. D. Bangs, *J. Biol. Chem.*, 2010, -.
6. A. S. Fischl, Y. S. Liu, A. Browdy and A. E. Cremesti, *Sphingolipid Metabolism and Cell Signaling, Pt A*, 2000, **311**, 123-130.
7. J. M. Figueiredo, W. B. Dias, L. Mendonca-Previato, J. O. Previato and N. Heise, *Biochem. J.*, 2005, **387**, 519-529.
8. M. R. W. Xue Li Guan, *Yeast*, 2006, **23**, 465-477.
9. T. I. Smirnova, T. G. Chadwick, R. MacArthur, O. Poluektov, L. Song, M. M. Ryan, G. Schaaf and V. A. Bankaitis, *J. Biol. Chem.*, 2006, **281**, 34897-34908.
10. H. A. Boumann, M. J. A. Damen, C. Versluis, A. J. R. Heck, B. de Kruijff and A. I. P. M. de Kroon, *Biochemistry*, 2003, **42**, 3054-3059.
11. G. S. Richmond and T. K. Smith, *Mol. Microbiol.*, 2007, **63**, 1078-1095.
12. P. K. Patnaik, M. C. Field, A. K. Menon, G. A. M. Cross, M. C. Yee and P. Butikofer, *Mol. Biochem. Parasitol.*, 1993, **58**, 97-105.
13. P. A. Aeed, C. L. Young, M. M. Nagiec and A. P. Elhammer, *Antimicrob. Agents Chemother.*, 2009, **53**, 496-504.
14. S. Kabani, K. Fenn, A. Ross, A. Ivens, T. Smith, P. Ghazal and K. Matthews, *BMC Genomics*, 2009, **10**, 427.
15. P. E. Bromley, Y. N. O. Li, S. M. Murphy, C. M. Sumner and D. V. Lynch, *Arch. Biochem. Biophys.*, 2003, **417**, 219-226.
16. W. M. Wang, X. H. Yang, S. Tangchaiburana, R. Ndeh, J. E. Markham, Y. Tsegaye, T. M. Dunn, G. L. Wang, M. Bellizzi, J. F. Parsons, D. Morrissey, J. E. Bravo, D. V. Lynch and S. Y. Xiao, *Plant Cell*, 2008, **20**, 3163-3179.
17. K. Huitema, J. van den Dikkenberg, J. Brouwers and J. C. M. Holthuis, *EMBO J.*, 2004, **23**, 33-44.
18. A. F. Neuwald, *Protein Sci.*, 1997, **6**, 1764-1767.
19. Y. J. Sigal, M. I. McDermott and A. J. Morris, *Biochem. J.*, 2005, **387**, 281-293.
20. M. M. Nagiec, E. E. Nagiec, J. A. Baltisberger, G. B. Wells, R. L. Lester and R. C. Dickson, *J. Biol. Chem.*, 1997, **272**, 9809-9817.
21. M. M. Nagiec, C. L. Young, P. G. Zaworski and S. D. Kobayashi, *Biochem. Biophys. Res. Commun.*, 2003, **307**, 369-374.

CHAPTER IV

SYNTHESIS OF
SUBSTRATE
ANALOGUES

4 SYNTHESIS OF SUBSTRATE ANALOGUES

4.1 Work Synopsis

This chapter describes the chemical synthesis of a first generation library of potential inhibitors. Screening of this library against *Lmj*IPCS using the assay protocol described in chapter II would generate basic SAR data which can be used to guide future synthesis of inhibitors and/or photolabelling probes with the ultimate objective of mapping the active site of *Lmj*IPCS (Figure 4-1). Results from the screening of this library together with the SAR data and recommendations for future design of inhibitors will be discussed in Chapter V.

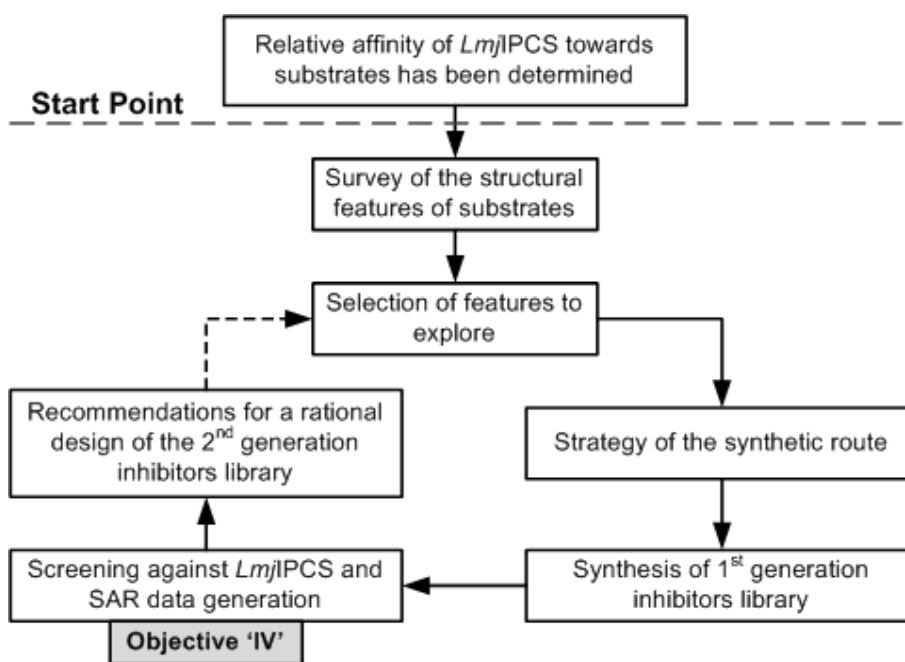


Figure 4-1: Work Strategy towards the set objectives

4.2 The Rationale behind the Design of Potential Inhibitors

4.2.1 The Structural Features of Known Substrates and Inhibitors

Having determined the kinetic parameters of *Lmj*IPCS, attention then turned towards the rational design of potential inhibitors against *Lmj*IPCS. The known fungal IPCS inhibitors (Figure 4-2) were excluded due to their complex structure and the fact that no modification to-date has resulted in more potent analogues. Additionally, the long studied khafrefungin, rustmicin and aureobasidin A exhibited a non-competitive¹ mode of inhibition which does not suggest usefulness in mapping the active site of *Lmj*IPCS (*see* section 1.2.7). However, a survey of the structural features of known donor and acceptor substrates (Figure 4-3) in addition to the previously described ceramide mimics (*see* section 2.2.4.2) represented a valid alternative for the rational design of substrate mimics that might result in potential inhibitors.

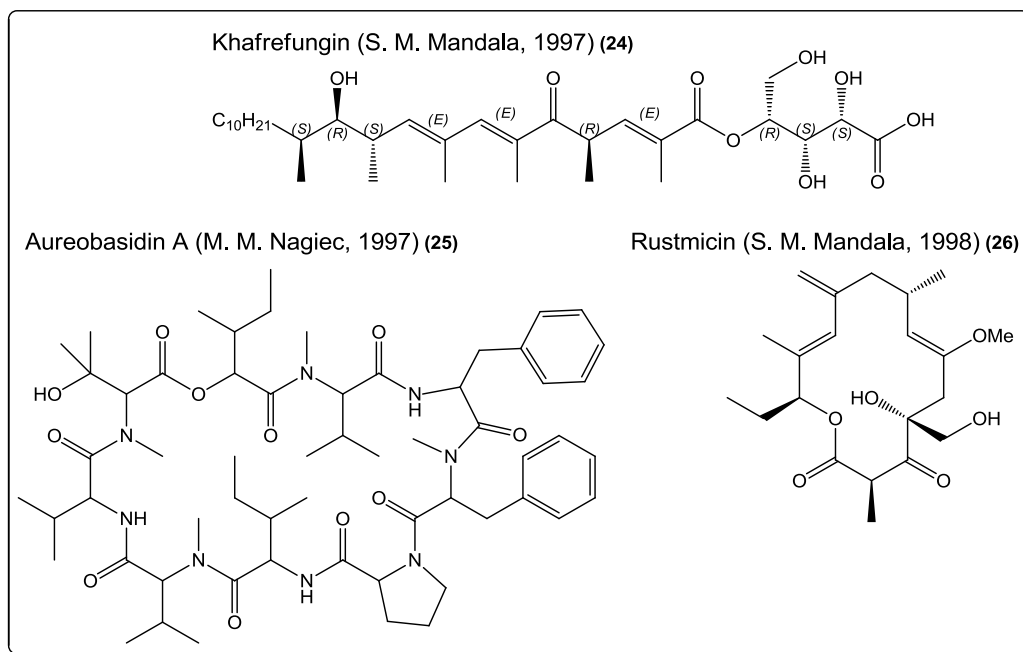


Figure 4-2: Inositol phosphorylceramide synthase inhibitors

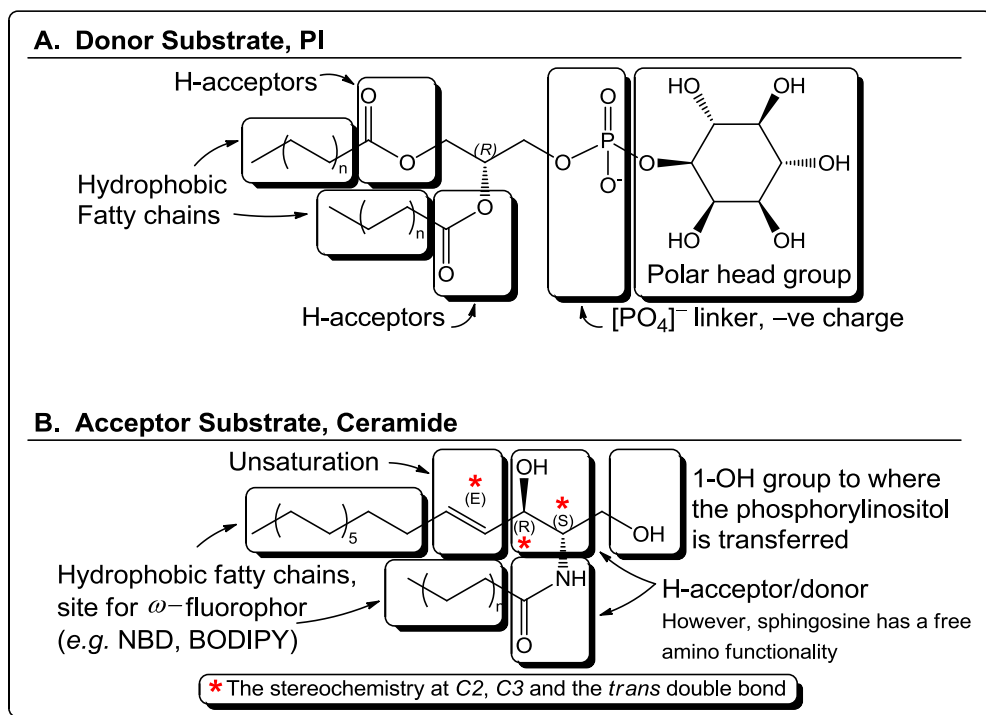


Figure 4-3: The structural features of known donor and acceptor substrates of *LmjIPCS*

It has been found that a common feature of all substrates was the presence of at least one long hydrophobic fatty chain which might be essential for binding into the hydrophobic pocket of this integral membrane protein. However, the requirement for a second hydrophobic fatty residue differs in the structural requirements of the donor and acceptor substrates, PI and ceramide respectively. It has been shown previously that reducing the length of the ceramide second fatty acid chain (*N*-acyl residue) to two carbons (*C*₂-ceramide), did not affect the capacity of *LmjIPCS* to turn it over to the respective product (*C*₂-IPC) (see section 2.2.4.2). This is consistent with earlier work in the literature that has reported the use of *C*₂-ceramide as a *C*₁₈-ceramide equivalent.²⁻⁶ Moreover, the commercially available ω-fluorescent *N*-acyl ceramide analogues (NBD-*C*₆/*C*₁₂-ceramide and BODIPY-FL-*C*₅-ceramide) that have variable *N*-acyl chain length have been widely used in studies of sphingolipid synthases.⁷⁻¹² In contrast, previous work with IPC synthase from *C. albicans*¹³ has shown that the lack of a second fatty acid residue (2-*sn*-acyl) in the donor substrate, i.e. *lyso*-PI, appeared to compete with the donor substrate, PI, and also resulted in a considerable deactivating solubilising effect on the microsomal membrane structure and subsequently the IPC synthase.

It is noteworthy, that the absence of an *N*-acyl moiety and the presence of an unmasked amino functionality as in sphingosine resulted in a true inhibitory effect on *Lmj*IPCS activity. This is consistent with precedent reports that had identified long chain 2-amino alcohols to exhibit many biological activities¹⁴ and in particular anti-leishmanial effects.¹⁵ This observation could be attributed to the fact that the amide functionality can act as both an H-donor and H-acceptor while the free, mostly protonated, NH₂ group would act as an H-donor only.

4.2.2 The Template Structure for Potential Inhibitors

At the onset, two possible approaches were considered for the inhibitor template structure. These are substrate-like (PI-like and/or ceramide-like) and product-like (IPC-like). The latter was excluded due to the complex chemical synthesis of phosphosphingolipids and based on the observation that *Lmj*IPCS does not catalyse the reverse activity, which render the enzyme affinity towards IPC uncertain. Although this might hold valid for *Lmj*IPCS, it can be further exploited in terms of inhibitors targeting *Tb*SLS4 which has demonstrated IPCase activity.

Apart from the exhausting and complex synthesis of phosphatidylinositol lipids,^{16, 17} it has been shown that *Lmj*IPCS shows relatively lower affinity towards PI (*c.f.* ceramide). Moreover, the presence of the enzyme in the form of microsomal membranes where there is always residual amounts of PI might suggest that the enzyme will be in the phosphorylated form which makes it less likely for a PI analogue to bind to the active site. In contrast, the kinetic analyses indicated a higher affinity of *Lmj*IPCS towards NBD-C₆-ceramide (comparable affinity as such towards natural C₁₈-ceramide) over PI. Also, considering the fact that C₂-ceramide has been shown to act as a substrate to the enzyme while sphingosine is not, suggests possible modulation of the enzyme activity using ceramide analogues which would range between one-site competitive binders to true inhibitors. Finally, the chemical synthesis literature has a wealth of knowledge of synthetic routes to sphingosines and ceramides that can be used in parallel synthesis of libraries of ceramide mimics. Therefore, the acceptor substrate, ceramide, was chosen to be the template for the inhibitor design in subsequent work.

4.3 Synthesis of a Ceramide Analogues Library

The library was designed to probe the structural features of ceramide (Figure 4-3). Even excluding the possibility of cyclic mimics, a large number of possible analogous compounds could be hypothesised. Six structural features were selected to probe their effect in terms of affinity towards *Lmj*IPCS and modulation of the enzyme activity. These included the presence or absence of the 1-hydroxy group, the presence or absence of the 3-hydroxy group, the position of the double bond, the nature/chain length of the sphingosine backbone, the presence or absence of the amide functionality and the nature/chain length of the *N*-acyl fatty acid residue (Figure 4-4).

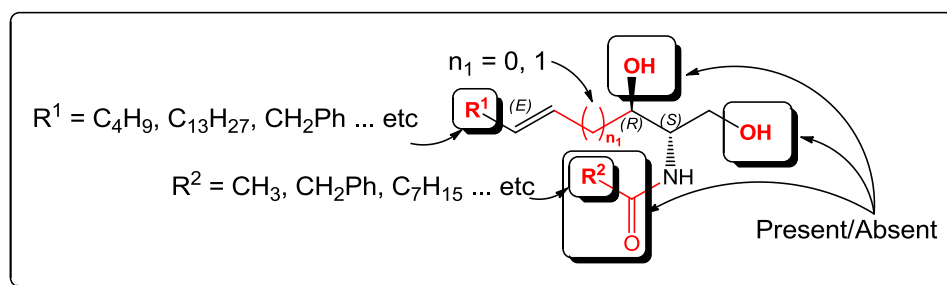


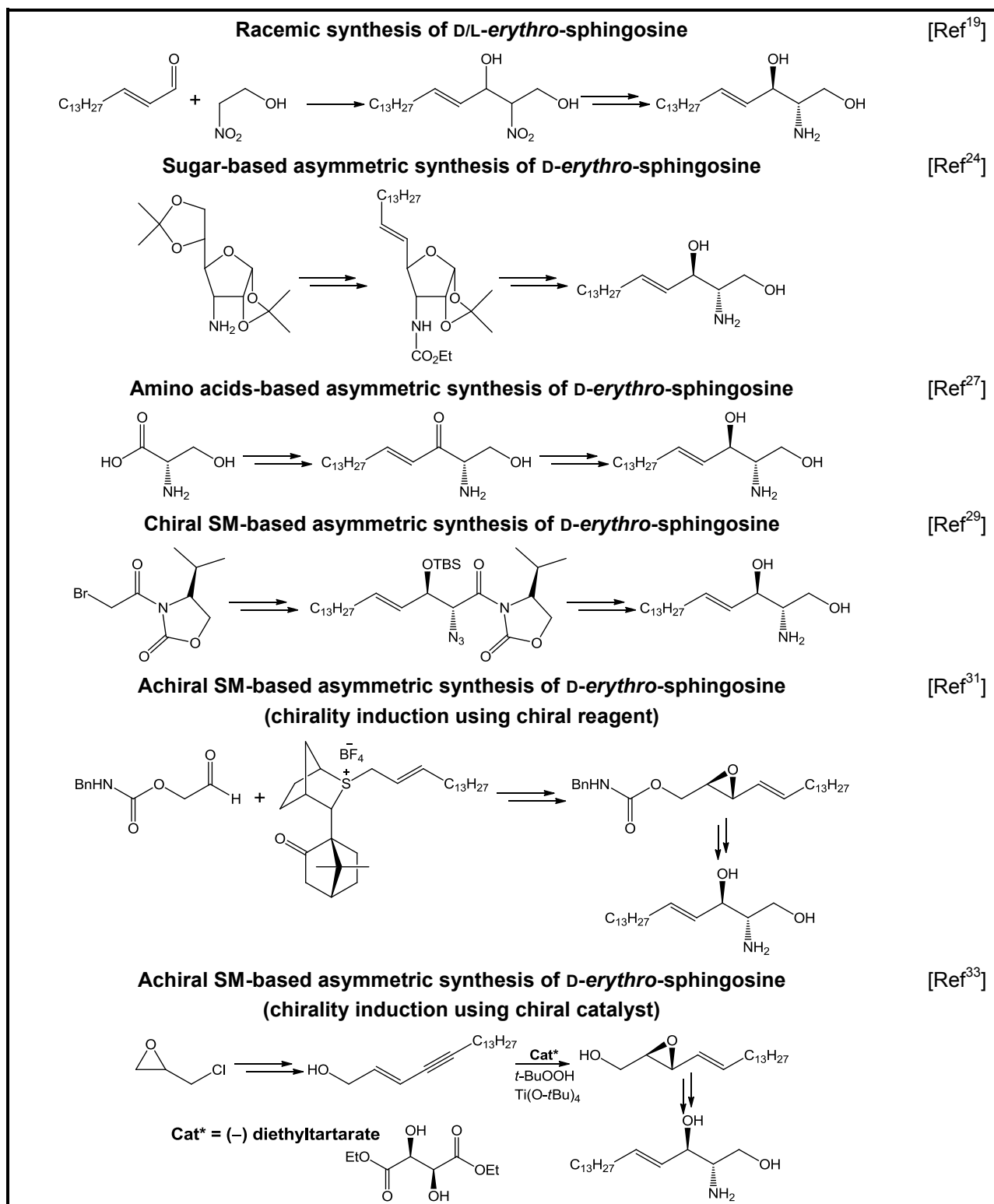
Figure 4-4: The structural features of the ceramide molecule with the selected features highlighted.

4.3.1 Synthetic Routes to Sphingosine and ceramide

Since the correct relative orientation of the functional moieties of sphingosine was presented by *Carter et al* in 1947,¹⁸ intensive synthetic efforts have been applied to its preparation. This is confirmed by the enormous number of reported chemical synthetic routes towards the preparation of sphingosine derivatives including ceramides. A comprehensive review of these synthetic routes is beyond the scope of this thesis. However, a brief summary will be presented to highlight the basis of the adopted synthetic strategy.

In stereochemical terms, sphingosine chemical syntheses can be simply categorised as racemic^{19, 20} or asymmetric syntheses. The latter can be subcategorised on the basis of the starting material as syntheses from chiral or achiral pool. While the chiral syntheses are based on sugar derivatives,²¹⁻²⁴ amino acids²⁵⁻²⁷ and their derivatives, Garner aldehydes²⁸ or other chiral

starting materials,^{29, 30} the latter introduce chirality using either chiral synthetic reagents or chiral catalysts (Scheme 4-1).³¹⁻³³

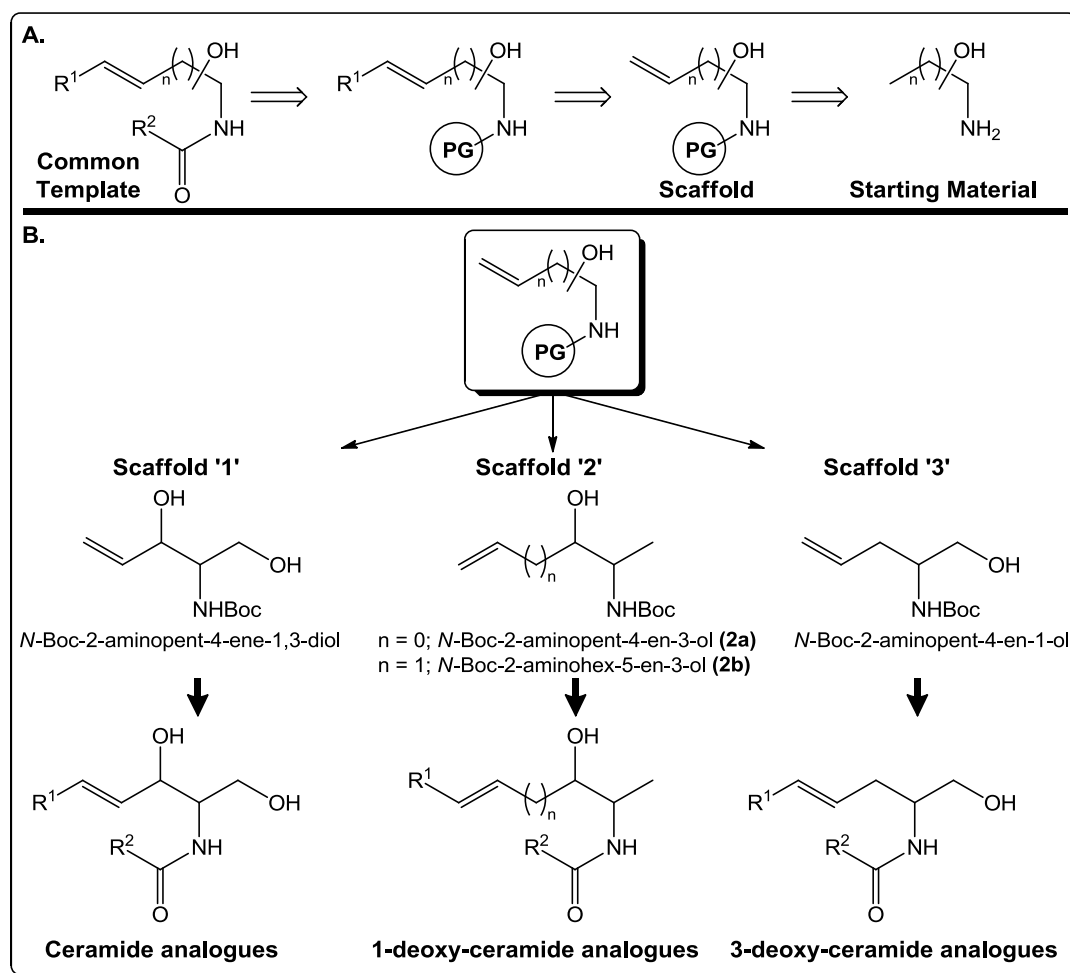


Scheme 4-1: Different Synthetic Routes to Sphingosine.

4.3.2 The Synthetic Strategy for the Parallel Synthesis

4.3.2.1 The Retro Synthetic Analysis for the Common Scaffold

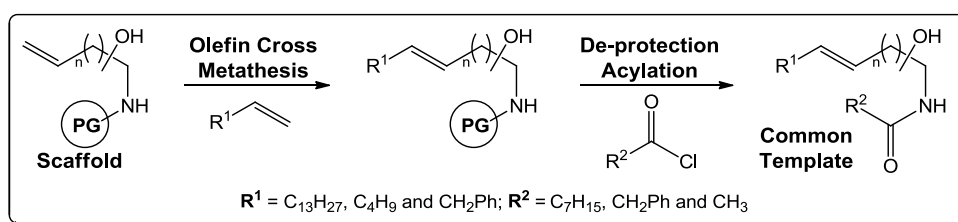
The starting material for the retro synthetic analysis was envisaged to be a set of hydroxylated amino alkene scaffolds from which ceramide analogues with different patterns of hydroxylation could be obtained. These scaffolds represent three series of analogues, ceramide, 1-deoxy-ceramide and 3-deoxy-ceramide analogues (Scheme 4-2). Screening of these series of analogues against *Lmj*IPCS would allow probing the selected set of the structural features of ceramide. Details of the proposed synthetic routes of these scaffolds will be discussed below.



Scheme 4-2: (A) The Retro Synthetic Analysis of the common scaffold for three series of analogues with different hydroxylation pattern. (B) The proposed three precursors for the synthesis of the analogues series. (PG, Protecting Group).

4.3.2.2 The Proposed Synthetic Routes

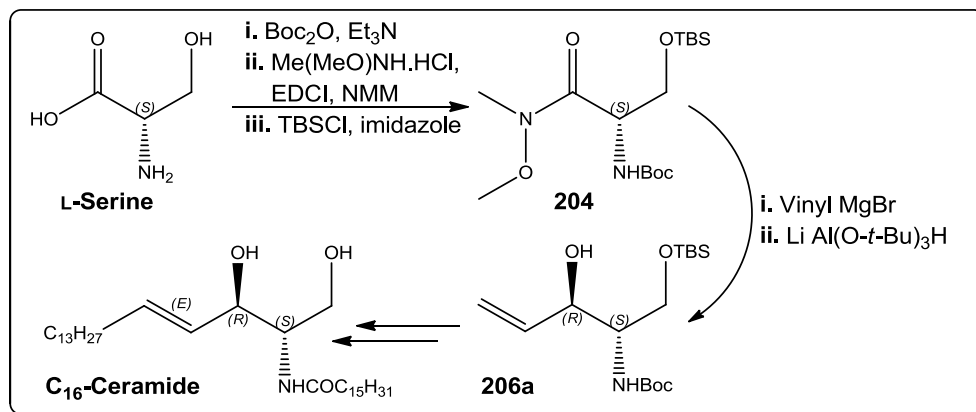
The main requirements of the synthetic routes were versatility (in terms of R^1 and R^2 , Scheme 4-3), atom efficiency and cost efficiency. In terms of versatility, the olefin cross metathesis can be utilised to form the sphingosine-like backbone chain (R^1). This methodology would allow the use of virtually any terminal alkene ($R^1\text{-CH=CH}_2$) and hence make the synthesis of an array of a large number of analogues possible. Furthermore, using a deprotection-acylation sequence, a variety of acyl chlorides can be used. This would result in a diverse range of the *N*-acyl residues (R^2) in the ceramide-like end product analogues (Scheme 4-3).



Scheme 4-3: Versatility of the proposed synthetic sequence.

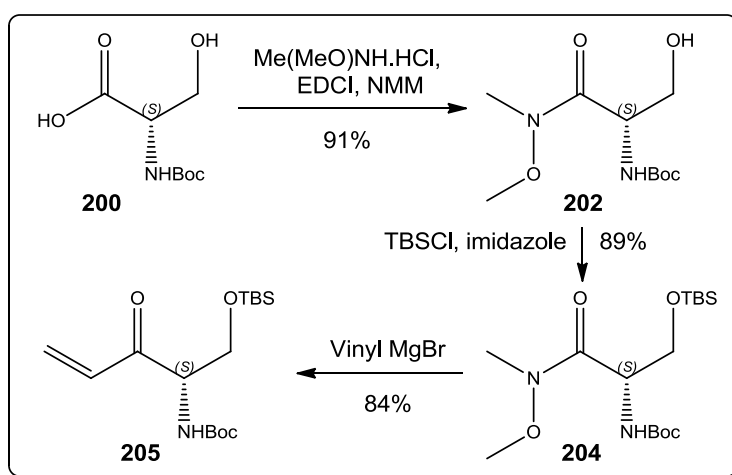
4.3.3 Synthesis of Scaffold '1': *N*-Boc-2-aminopent-4-ene-1,3-diol

Yamamoto *et al.*²⁶ had reported a versatile protocol for the synthesis of sphingosine and ceramide derivatives. Briefly, L-serine was Boc protected, converted to the Weinreb amide and then protected as the TBS ether followed by treatment with vinyl magnesium bromide to afford compound (206a) which was later used to prepare C_{16} -ceramide (Scheme 4-4).

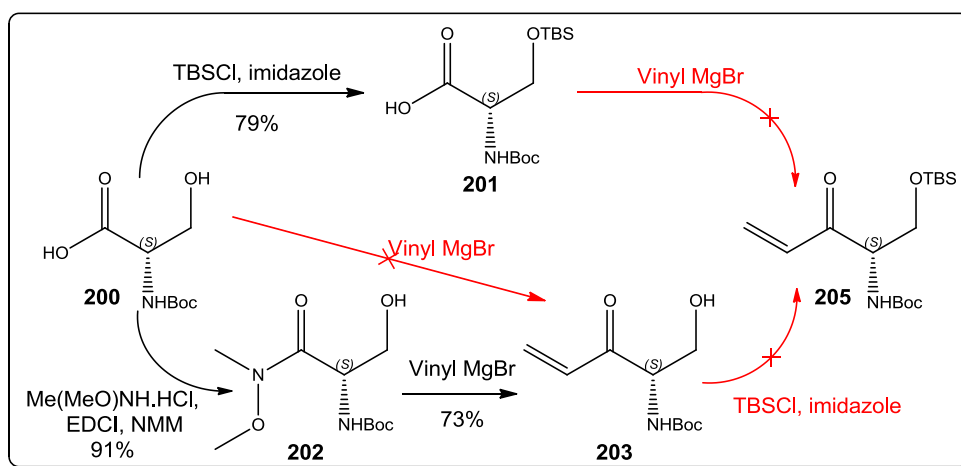


Scheme 4-4: Yamamoto's sequence for the synthesis of sphingosine and ceramide derivatives.

Consequently, *N*-Boc-L-serine was converted to the Weinreb amide (202) in a high yield (91%) using *N*-methylmorpholine (NMM), *N,O*-dimethylhydroxylamine hydrochloride and 1-ethyl-3-(3-dimethylaminopropyl)carbodiimide (EDC) hydrochloride as a coupling reagent (Scheme 4-5). Evidence for the formation of (202) was observed by the appearance of distinctive two sharp peaks at 3.78 ppm (OCH_3) and 3.24 ppm (NCH_3) in the ^1H NMR spectrum and confirmed by the upfield shift of the C1 175.0 to 170.9 ppm in the ^{13}C NMR spectrum and a peak at m/z 271.2 in the ESMS corresponding to $[\text{M}+\text{Na}]^+$. Subsequently, the primary hydroxyl group of (202) was protected as the TBS ether (204) in a high yield (89%). Evidence for the formation of (204) was observed by the loss of a broad OH peak above 3000 cm^{-1} in the IR spectrum and the appearance of the $2 \times \text{SiMe}$ and $\text{SiC}(\text{Me})_3$ peaks at 0.02, 0.01 ppm and 0.85 ppm respectively in the ^1H NMR spectrum coupled with a molecular ion at m/z 362.5 $[\text{M}+\text{H}]^+$ in the ESMS spectrum. Finally, the enone (205) was generated in very good yield (84%) upon treating (204) with an excess of vinyl magnesium bromide. Evidence for the formation of (205) was observed through the appearance of characteristic multiplets of the olefinic protons signal in the ^1H NMR spectrum at 6.55 ppm (4-*CH*), 6.34 ppm (5-*CH*_{trans}) and 5.83 ppm (5-*CH*_{cis}) and confirmed by a downfield shift of the C2 from 170.9 ppm to 196.8 ppm in the ^{13}C NMR spectrum. Spectral data of all intermediates up to (205) were identical to the previously reported syntheses.^{26, 34} It is noteworthy that attempts to modify Yamamoto's sequence resulted in failed reactions (Scheme 4-6).

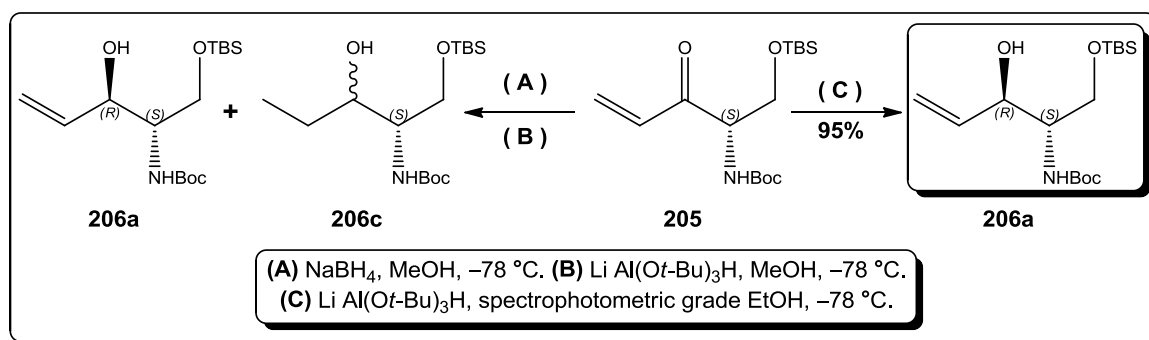


Scheme 4-5: Following the sequence of Yamamoto's synthesis (200 → 202 → 204 → 205).

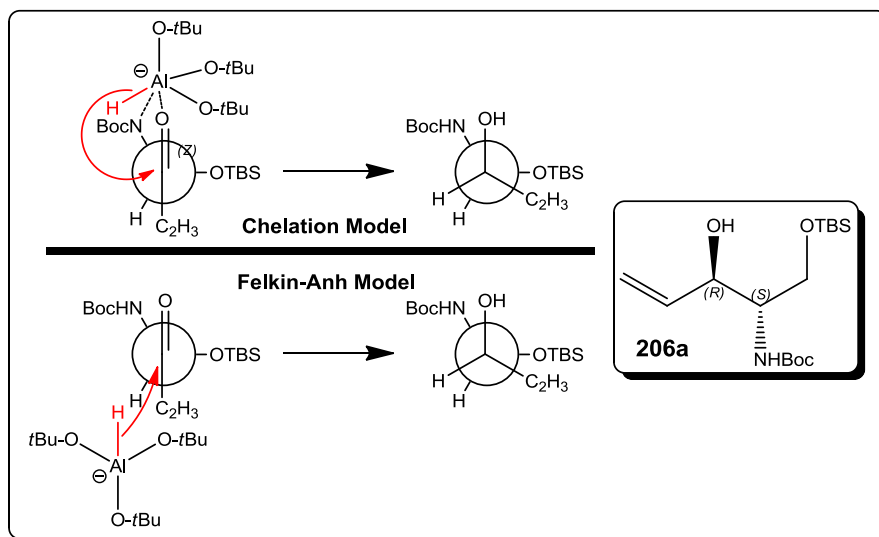


Scheme 4-6: Failed shortcut modifications of Yamamoto's synthesis.

With the enone (205) in hand, the next step was the stereospecific reduction to set the desired stereochemistry at C3. This reduction proved to be critically dependent on the solvent used and the reducing agent. Initial attempts to reduce the enone (205) using sodium borohydride at -78 °C in MeOH resulted in a complex mixture that consisted primarily of the fully reduced alcohol (206c) with a minor fraction of the desired alkene (206a) that could be detected in the ^1H NMR spectrum of the crude products. Recourse to lithium *tri-tert*-butoxy aluminium hydride in MeOH resulted in a mixture of the 1-4 Michael addition reduced product (206c) and the desired alkene (206a). However, the resultant mixture was inseparable using column chromatography. Finally the reduction was accomplished using lithium *tri-tert*-butoxy aluminium hydride in spectrophotometric grade ethanol (as in Yamamoto's report) to yield the desired product (206a) as a single diastereoisomer as ascertained by the ^1H NMR spectrum in high yield (95%) as viscous oil (Scheme 4-7). The stereochemical outcome of the reduction reaction which resulted in one single diastereoisomer can be explained using either Felkin-Anh assuming that the ($-\text{CH}_2\text{OTBS}$) to be the largest substituent on C2 model or the chelation model (Scheme 4-8).



Scheme 4-7: Synthesis of the Ceramide Analogues Precursor (206a).



Scheme 4-8: Stereochemistry of the reduction reaction in terms of Felkin-Anh model and chelation model.

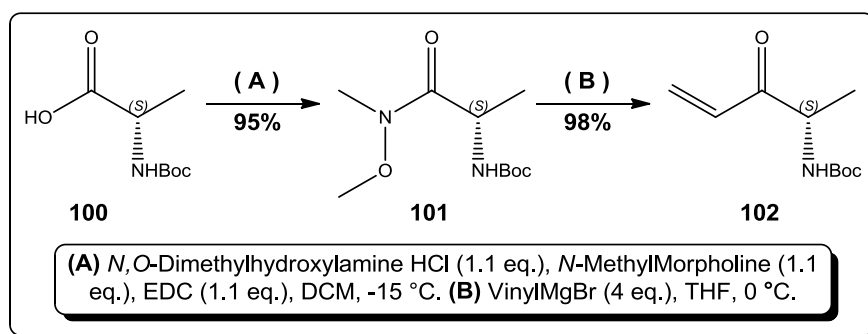
4.3.4 Synthesis of the Scaffolds of 1-Deoxyceramide Analogues

Having successfully synthesised the core for the ceramide analogues, attention then turned to the other series of analogues that lacked the primary (1-OH) hydroxyl group. Two different series of these analogues were synthesised which simply differed in the position of the double bond. The starting material for both was *N*-Boc-L-alanine.

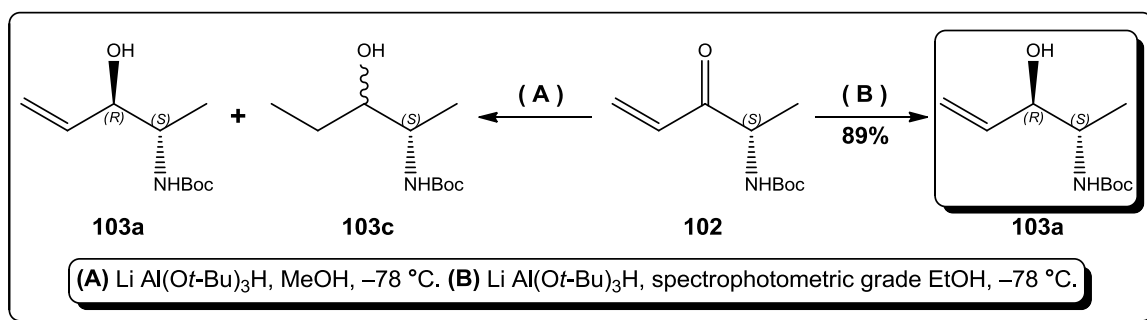
4.3.4.1 Synthesis of Scaffold '2a': *N*-Boc-2-aminopent-4-en-3-ol

Applying the same sequence previously described in the preparation of (206a), using *N*-Boc-L-alanine instead of *N*-Boc-L-serine as the starting material, an analogous precursor for 4*E*-1-deoxyceramide analogues could be prepared (Scheme 4-9). The data for all compounds was consistent with the proposed structures. Again, attempts to reduce the enone (102) using lithium *tri-tert*-butoxy aluminium hydride in MeOH resulted in an inseparable mixture of the fully reduced alcohol (103c) and the desired alkene (103a). Consequently, the desired product was successfully prepared using lithium *tri-tert*-butoxy aluminium hydride in spectrophotometric grade ethanol to yield (103a) in a high yield (89%) as a single diastereoisomer as ascertained by the ¹H NMR spectrum of the crude product. Evidence of the formation of (103a) was supported

by the appearance of a new multiplet peak at 4.22–4.16 (3-*H*) in ^1H NMR identical to the previously reported synthesis³⁵ of (103a) (Scheme 4-10).



Scheme 4-9: Synthesis of the enone (102) via a Weinreb amide intermediate.



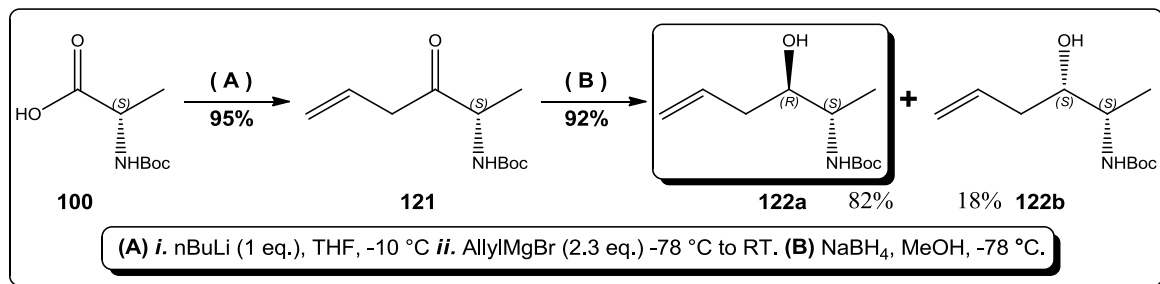
Scheme 4-10: Synthesis of the 4*E*-1-deoxyceramide Analogues Precursor (103a)

4.3.4.2 Synthesis of Scaffold '2b': *N*-Boc-2-aminohex-5-en-3-ol

An alternative route was explored to access analogues in which the position of the double bond is one methylene unit further. Based on a procedure initially reported by *Toumi et al.*,³⁶ *N*-Boc-L-alanine was first treated with an equimolar amount of *n*-BuLi followed by allylmagnesium bromide to afford the allyl ketone (121) as a crystalline white solid in high yield (95%). Evidence for the formation of (121) was observed in the IR spectrum by the absence of a broad hydroxyl peak above 3000 cm^{-1} and confirmed by the appearance of the olefinic protons peaks at 5.91 ppm (5-*H*) and 5.15 ppm (6-*H*₂) in the ^1H NMR spectrum, the downfield shift of the C3 to 207.6 ppm in the ^{13}C NMR spectrum. Subsequently, the allyl ketone (121) was then reduced using sodium borohydride at -78 °C to yield a mixture of diastereoisomers (122a) and

(122b) in a ratio of 82:18 respectively (as determined by the ^1H NMR spectrum of the crude products) and a total yield of 92 % (

Scheme 4-11).



Scheme 4-11: Synthesis of 5*E*-1-deoxyceramide Analogues Precursor (122a)

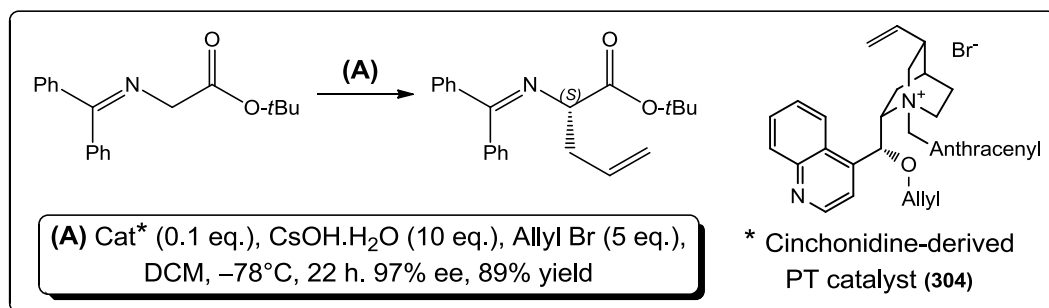
Although a complete separation of the two diastereoisomers was very difficult using column chromatography (R_f 122a \approx 0.30, R_f 122b \approx 0.32; EtOAc/pet. ether 25/75), a pure fraction of (122a) could be isolated. Evidence for the formation of (122a) was observed in the IR spectrum by the appearance of a hydroxyl peak at $3250\text{--}3350\text{ cm}^{-1}$ and the loss of the carbonyl band at 1726 cm^{-1} . Further confirmation was obtained through the appearance of a new signal at 3.71 ppm assigned to the carbinol (C-H) and the downfield shift of the C3 signal from 207.6 ppm to 73.4 ppm in the ^1H and ^{13}C NMR spectra respectively

4.3.5 Synthesis of Scaffolds '3': *N*-Boc-2-aminopent-4-en-1-ol

Having successfully established routes to the 3-hydroxylated core, the next objective was to establish a route for the 3-deoxy analogue. So far, the 3-oxygenated position was essential for the introduction of the long chain precursor (allyl or vinyl side chains); therefore, an alternative strategy was required.

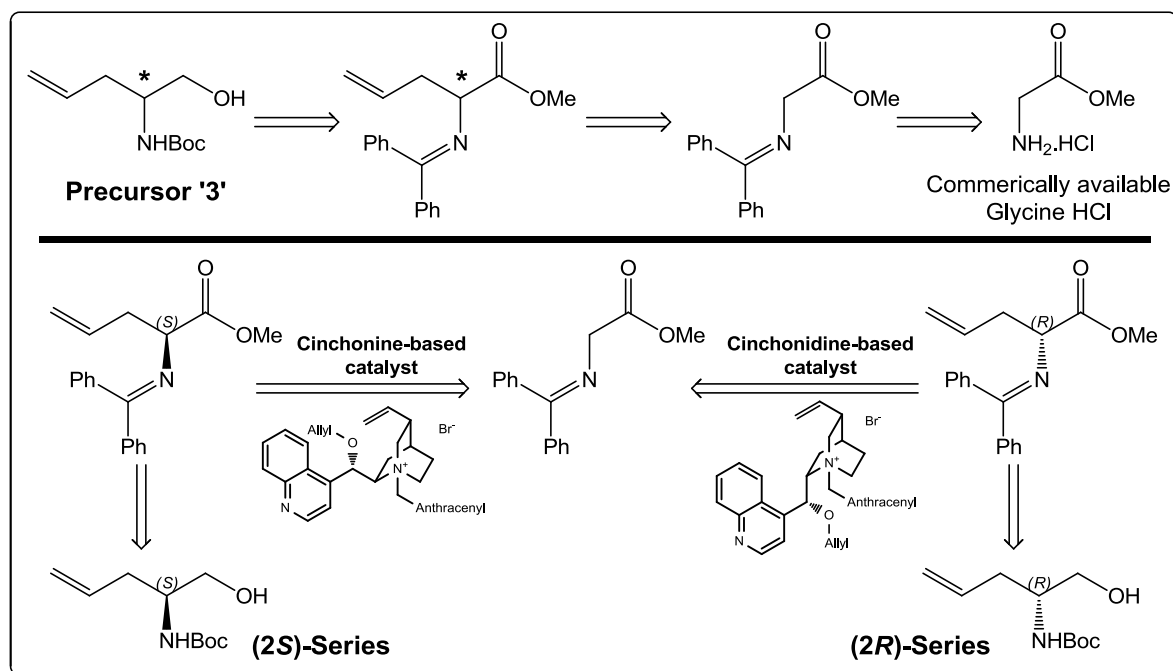
Since the early 1970s, phase-transfer catalysis (PTC) has been recognized as a versatile methodology for organic synthesis in both industrial and academic laboratories. This is because it features simple experimental operations, mild reaction conditions, inexpensive and environmentally benign reagents. In addition, it has become an increasingly expanding utility with applications in different asymmetric synthetic reactions.³⁷ Moreover, *O'Donnell* had

reported several studies³⁸⁻⁴¹ focused on the use of PTC in the asymmetric preparation of α -amino acids from the achiral glycine-derived Schiff base using cinchona alkaloids quaternary ammonium salts as active catalysts (Scheme 4-12).



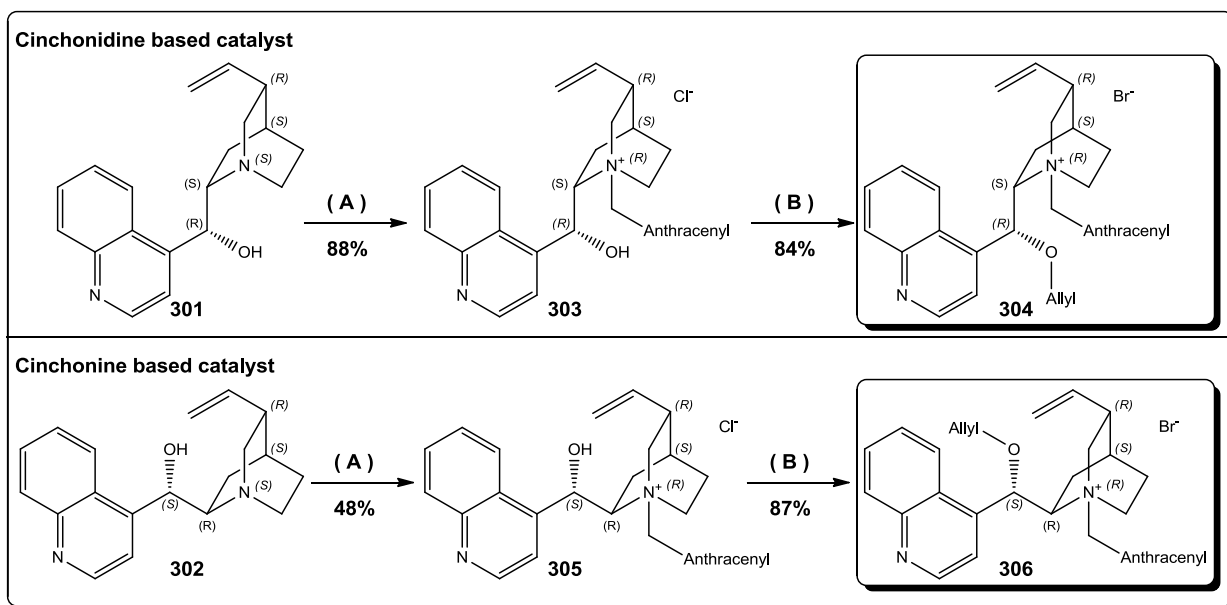
Scheme 4-12: An example of PTC in the enantioselective alkylation of a glycine Schiff base.

This strategy therefore seemed ideal for the goal of preparing precursor '3', *N*-Boc-2-aminopent-4-en-1-ol starting from the commercially available hydrochloride salt of glycine through asymmetric amino acid alkylation reaction. Additionally, using cinchona alkaloids (cinchonine and cinchonidine) derived PT catalysts, two series could be prepared from the glycine-derived Schiff base and the alkyl halide, allyl bromide. These two series would simply differ in the stereochemistry at C2 (Scheme 4-13).



Scheme 4-13: The retrosynthetic analysis of the precursor for the 3-deoxy ceramide analogues.

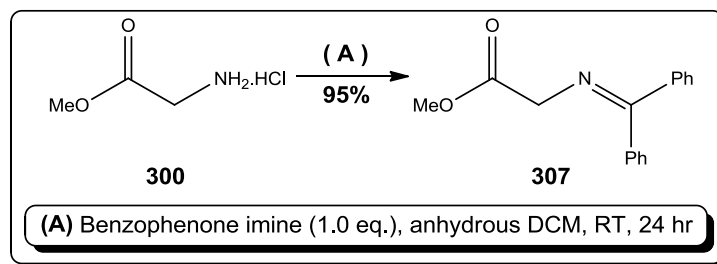
Towards this end, the cinchona alkaloids phase transfer catalysts were prepared in the active form, *O*-allyl.³⁸ Following previously reported procedures, the quaternary ammonium salts of cinchonidine (303)⁴² and cinchonine (305)⁴³ were prepared using 9-chloromethylantracene⁴² in refluxing toluene in 88% and 48% isolated yield respectively. Subsequently, the quaternary ammonium salts were converted to the allyl forms (304)⁴² and (306)⁴⁴ using allyl bromide and aq. KOH in Toluene/DCM at room temperature in 84% and 87% isolated yield respectively (Scheme 4-14). Spectral data of the synthesised catalysts were identical to literature reports.



Scheme 4-14: Synthesis of the phase-transfer active catalysts from the cinchona alkaloids.

4.3.5.1 Synthesis of the Benzophenone Glycine Imine

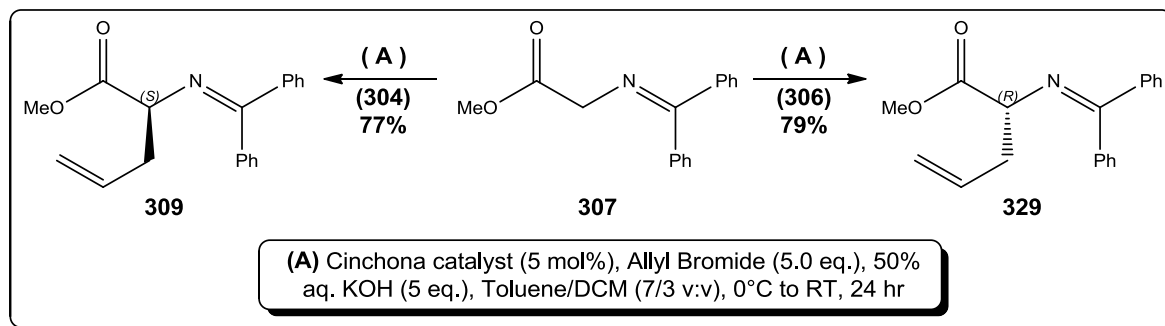
With the PT catalysts in hand, synthetic efforts were directed towards the synthesis of the glycine Schiff base. Consequently, following the procedure previously reported by O'Donnell,⁴⁰ the Schiff base (307) was successfully prepared from methyl glycine hydrochloride. Briefly, stirring of methyl glycine hydrochloride with an equimolar amount of benzophenone imine in anhydrous DCM afforded the desired product in very good isolated yield (80%) as white waxy solid. Evidence of the formation of (307) was observed in the IR spectrum by the absence of NH peaks above 3000 cm^{-1} and the upfield shift of the Ph_2C peak to 172.0 ppm (*cf.*, benzophenone imine 177 ppm) in the ^{13}C NMR spectrum and confirmed with the mass peak at m/z (ES^+) 254.4 $[\text{M}+\text{H}]^+$ (Scheme 4-15).



Scheme 4-15: Synthesis of the benzophenone glycine imine.

4.3.5.2 Synthesis of (2*R*) & (2*S*) *N*-Boc-2-aminopent-4-en-1-ol

With both the Schiff base (307) and the active catalysts (304) and (306) in hand, the preparation of the (2*R*)-4*E*-3-deoxyceramamide and the (2*S*)-4*E*-3-deoxyceramamide precursors was straightforward. The enantiomers (309) and (329) were prepared successfully in good yield (*c.a.* 78%, Scheme 4-16) using the general procedure for enantioselective phase-transfer amino acid alkylation^{42, 45} (*see* Chapter VIII). Unfortunately, due to technical difficulties, determination of the enantiomeric ratio of the precursors was not possible in the time available and the purified reaction products were assumed to be scalemic mixtures.

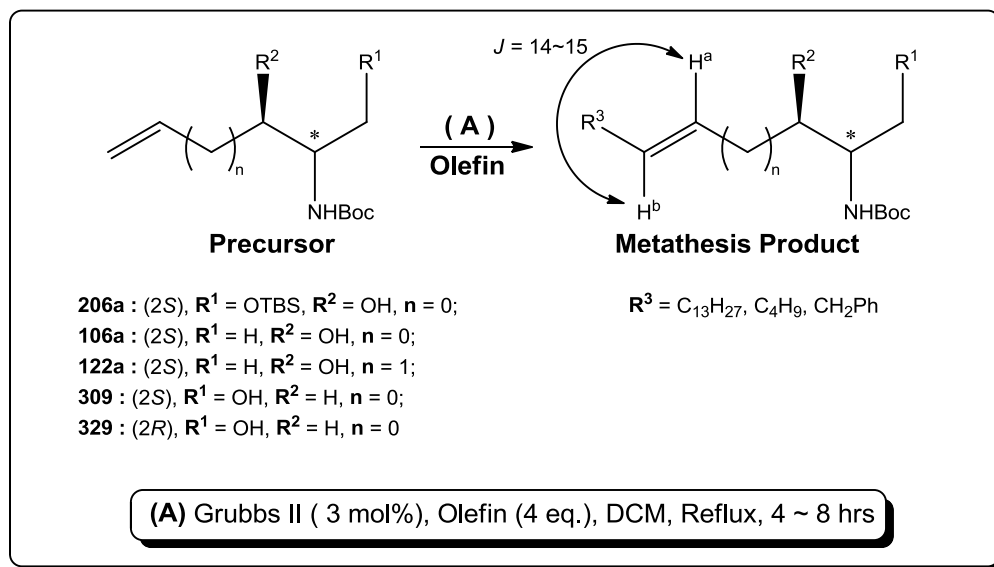


Scheme 4-16: The asymmetric alkylation of benzophenone glycine imine using phase-transfer catalysis.

4.3.6 Olefin Cross Metathesis (CM) of the Prepared Scaffolds

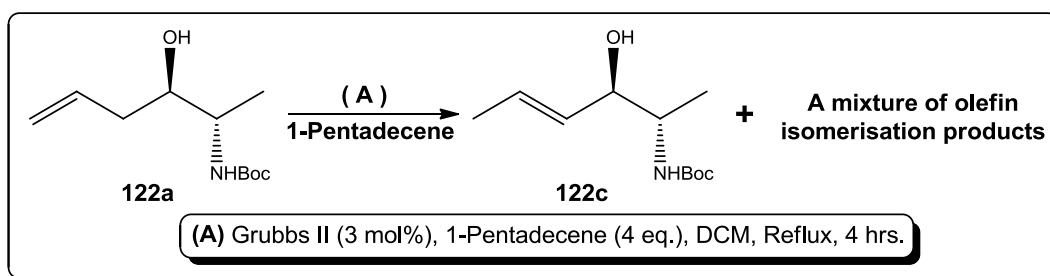
Having successfully prepared all the scaffolds (206a, 103a, 122a, 309 and 329) needed, these were subjected to olefin cross metathesis²⁶ conditions using 2nd generation Grubb's catalyst (0.3% mol) in refluxing DCM with four equivalents of the coupling olefins 1-pentadecene, 1-hexene and allyl benzene (Scheme 4-17). The double bond geometry in all purified products was

trans and this was confirmed by the coupling constant $J_{\text{Ha-Hb}} = 14\sim 15$ Hz in the ^1H NMR spectra. The *cis* diastereoisomer was not detected in the ^1H NMR spectra of the crude reaction mixtures or in the isolated fractions from column chromatography.



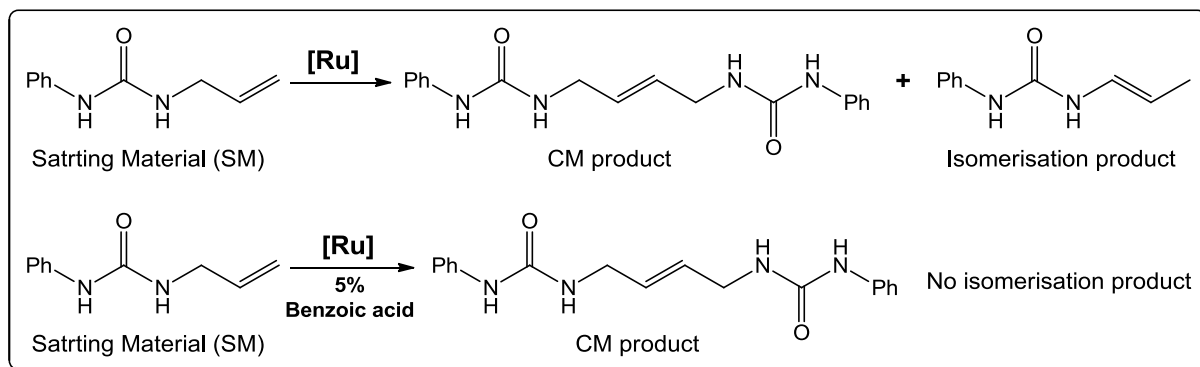
Scheme 4-17: The general scheme for the olefin cross metathesis reactions.

It is noteworthy that during the preparation of more material of the precursor (122a) few months after the first batch, repeating the same CM reactions resulted in a complex mixture of products. Separation of the crude products using column chromatography resulted in the isolation of (122c) (Scheme 4-18). Evidence for the formation of (122c) was supported by the appearance of a doublet at 1.71 ppm in the ^1H NMR spectrum corresponding to the methyl group ($\text{CH}_3\text{-CH=CH-}$) in the isomerised product and confirmed by the ^1H ^1H COSY 2D NMR spectrum. This suggested that the reaction course mainly followed an olefin isomerisation instead of the CM as suggested by trace peaks of the desired product in the ^1H NMR spectrum of the crude products (Scheme 4-18).

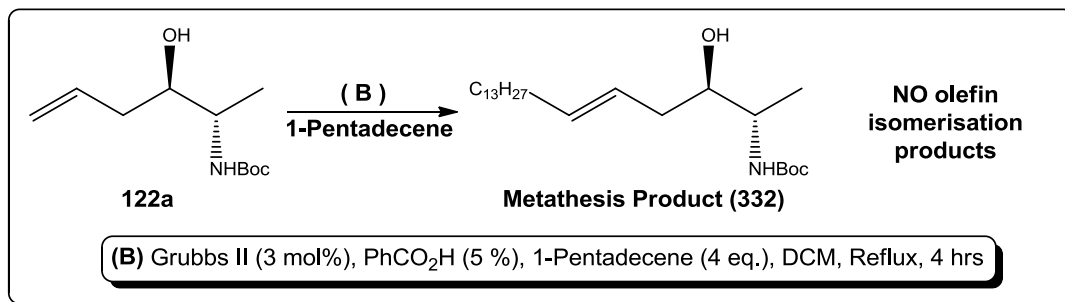


Scheme 4-18: Olefin Isomerisation in Olefin Cross Metathesis reactions.

Similar observations has been previously reported by *Gimeno et al.*⁴⁶ Gimeno recommended that the addition of a catalytic amount (5 %) of benzoic acid suppressed the olefin isomerisation and directed the reaction towards the metathesis product (Scheme 4-19). Following *Gimeno's* recommendations, conducting further CM reactions in the presence of 5% benzoic acid suppressed the isomerisation reaction and the reaction course was switched back towards the generation of the CM product (Scheme 4-20).



Scheme 4-19: Gimeno's observation of the olefin isomerisation and its suppression by the addition of 5% benzoic acid to the reaction mixture.



Scheme 4-20: Suppression of olefin isomerisation product in the CM reactions following Gimeno's recommendations.

While the precursors (103a), (122a), (309) and (329) afforded the corresponding crude products that were easily purified using column chromatography, the precursor (206a) resulted in highly non-polar crude products whose purification was difficult and time consuming. Consequently, (206a) was deprotected to afford the diol (207) in a high yield 92 % which was later subjected to olefin cross metathesis conditions to yield the corresponding products that were easy to purify (Scheme 4-21). All metathesis product yields are summarised in Table 4-1.

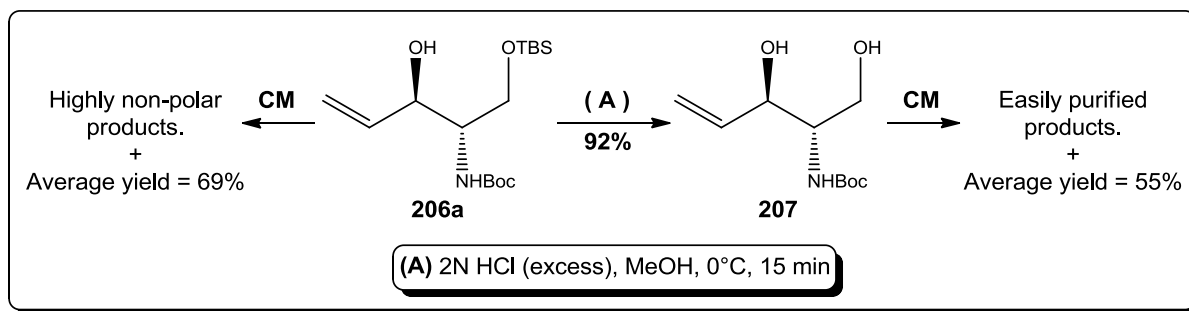
Scheme 4-21: (**206a**) vs. (**207**) as a convenient precursor for the olefin cross metathesis reaction.

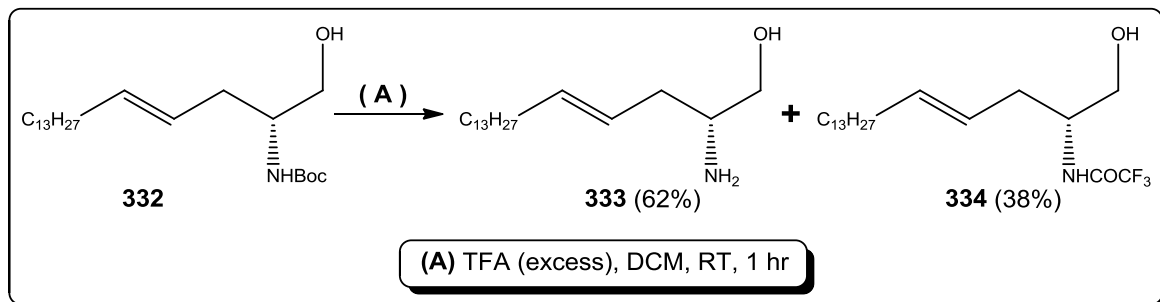
Table 4-1: Product yields of the Olefin Cross Metathesis reactions.

Precursor	Coupling Olefin	Yield %	Precursor	Coupling Olefin	Yield %
103a	1-pentadecene	52	206a	1-pentadecene	72
103a	1-hexen	67	206a	1-hexen	71
103a	allyl benzene	64	206a	allyl benzene	65
122a	1-pentadecene	53	207	1-pentadecene	44
122a	1-hexen	56	207	1-hexen	59
122a	allyl benzene	64	207	allyl benzene	62
309	1-pentadecene	53	329	1-pentadecene	62
309	1-hexen	71			
309	allyl benzene	50			

4.3.7 Deprotection and Acylation of CM Products

The CM products were later converted to the end products through a BOC deprotection-acylation sequence. Subjecting the Boc-protected compounds to acidic de-protection conditions using TFA, afforded the free amine compounds after workup. For each compound, a minor fraction was kept as the parent amine compound while the rest of the material was divided into three or four acylation reactions using different acyl chlorides (acetyl Cl, phenylacetyl Cl, benzoyl Cl and octanoyl Cl). Assessment of the crude product purity was based on crude ^1H NMR. Compounds that were $\geq 80\%$ pure were used as soon as they were produced. Others were purified by standard column chromatography. It is noteworthy that in the deprotection of (**332**), the crude product gave two major TLC spots (pet ether/EtOAc 3:1). A spot at the base line corresponding to the deprotected amine and a second spot ($R_f = 0.30$) almost co-eluting with the starting material. The fraction corresponding to the second spot was isolated and identified to be

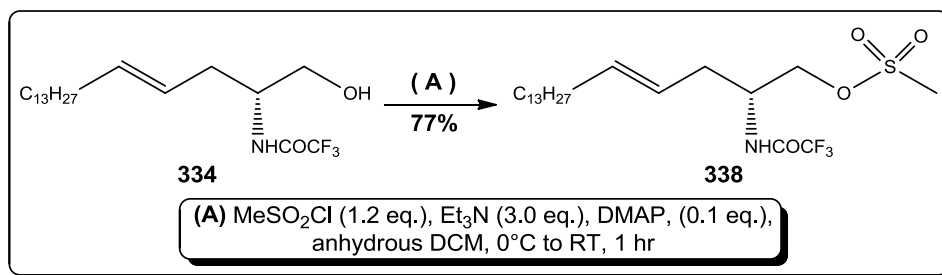
the trifluoroacetyl amide using ^{19}F NMR spectroscopy and ESMS (Scheme 4-22). This impurity has been observed in other reactions but in trace amounts and could not be isolated.



Scheme 4-22: Formation of the trifluoroacetyl amide in the TFA mediated deprotection of the Boc-protected compounds.

4.3.8 Synthesis of Ceramide-1-Phosphate Analogue

The compound (338) was prepared as a potential ceramide-1-phosphate analogue with the prospect that it might alkylate the active histidine residue in *Lmj*IPCS. However, the stability of this compound in the assay buffer was questionable. It was prepared from the surplus of the undesired product (334) in good yield, 77 % (Scheme 4-23).



Scheme 4-23: The synthesis of ceramide-1-phosphate analogue (338).

4.3.9 Synthesis of the 1-Phenyl-2-aminopropanol Series

The *N*-myristoyl derivatives of 1-phenyl-2-aminopropanol, *erythro*-MAPP, had been previously reported to mimic the action of ceramide. However, while the *D-erythro*-MAPP induced a concentration- and time-dependent growth suppression of HL-60 human

promyelocytic leukaemia cells, the *L-erythro*-MAPP enantiomer was without effect (Figure 4-5).⁴⁷

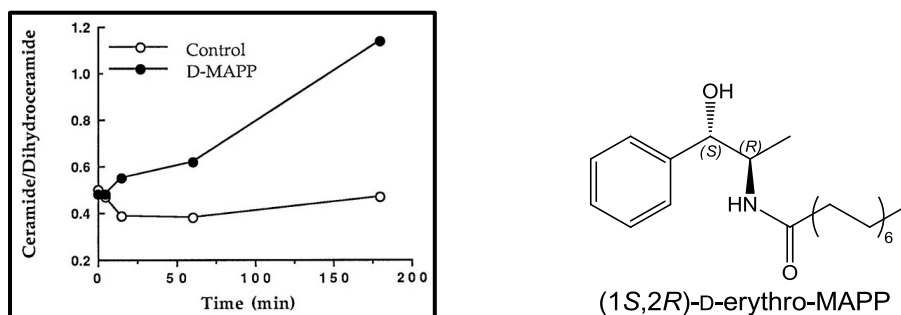
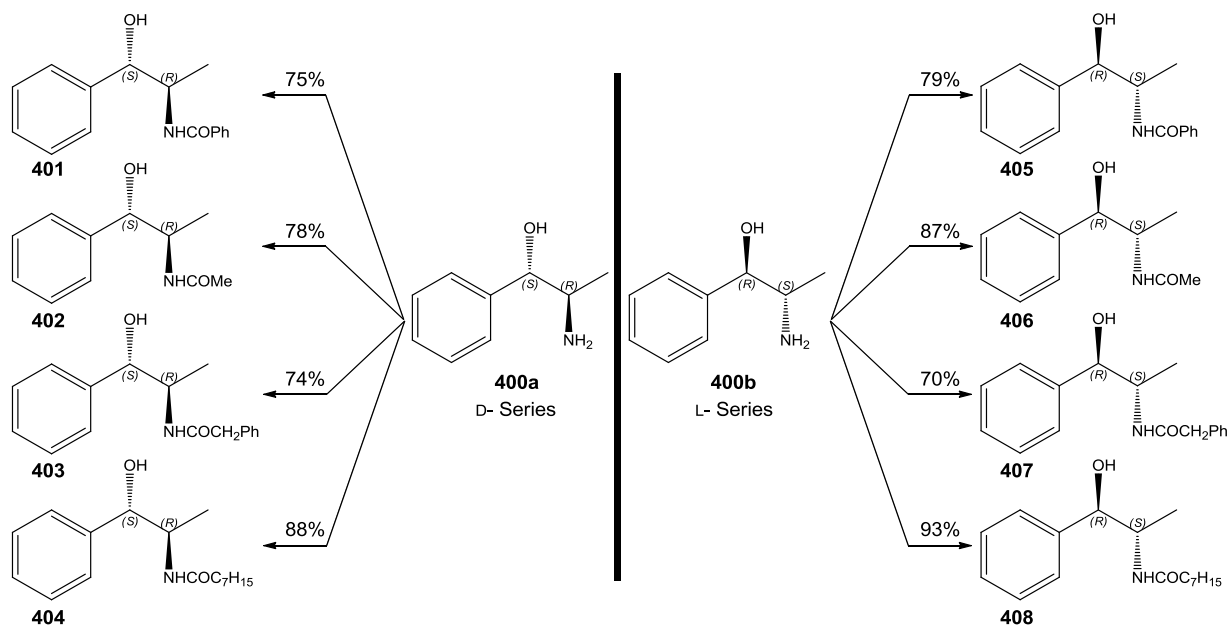


Figure 4-5: Effects of D- and L-e-MAPP on endogenous levels of ceramide. Reprint with permission "This figure was originally published in Journal of Biological Chemistry©. Bielawska et al. 1996; 271(21): 12646-12654.

With the starting material, 1-phenyl-2-aminopropanol, available in hand, analogues of *erythro*-MAPP were successfully prepared using acetyl chloride, phenylacetyl chloride, benzoyl chloride and octanoyl chloride to afford the corresponding products in good to high yields (Scheme 4-24).



Scheme 4-24: Synthesis of *erythro*-MAPP analogues.

4.4 Conclusions

The work presented in this chapter demonstrated the successful preparation of five series of ceramide mimics. These are ceramide, 1-deoxy-4*E*-ceramide, 1-deoxy-5*E*-ceramide, (2*R*)-3-deoxy-4*E*-ceramide and (2*S*)-3-deoxy-4*E*-ceramide analogues. In addition to the 1-Phenyl-2-aminopropanol derivatives and a potential ceramide-1-phosphate mimic. These analogues were prepared using well-established synthetic methodology.

The key reactions included a stereospecific reduction of an enone and asymmetric amino acid alkylation using PT catalysis. The key features of the synthetic routes included versatility in the sphingosine-backbone-mimic and the *N*-acyl residues which were introduced using olefin cross metathesis and deprotection-acylation sequence. The screening results of testing these analogues against LmjIPCS will be discussed in Chapter V.

REFERENCES

1. P. A. Aeed, C. L. Young, M. M. Nagiec and A. P. Elhammer, *Antimicrob. Agents Chemother.*, 2009, **53**, 496-504.
2. M. Y. Kim, C. Linardic, L. Obeid and Y. Hannun, *J. Biol. Chem.*, 1991, **266**, 484-489.
3. R. T. Dobrowsky and Y. A. Hannun, *J. Biol. Chem.*, 1992, **267**, 5048-5051.
4. J. Quintans, J. Kilkus, C. L. McShan, A. R. Gottschalk and G. Dawson, *Biochem. Biophys. Res. Commun.*, 1994, **202**, 710-714.
5. H.-q. Xie, *J. Neurochem.*, 1997, **69**, 1020-1030.
6. M. M. Nagiec, E. E. Nagiec, J. A. Baltisberger, G. B. Wells, R. L. Lester and R. C. Dickson, *J. Biol. Chem.*, 1997, **272**, 9809-9817.
7. S. S. Sutterwala, F. F. Hsu, E. S. Sevova, K. J. Schwartz, K. Zhang, P. Key, J. Turk, S. M. Beverley and J. D. Bangs, *Mol. Microbiol.*, 2008, **70**, 281-296.
8. P. W. Denny, H. Shams-Eldin, H. P. Price, D. F. Smith and R. T. Schwarz, *J. Biol. Chem.*, 2006, **281**, 28200-28209.
9. V. Gupta, G. A. Patwardhan, Q. J. Zhang, M. C. Cabot, S. M. Jazwinski and Y. Y. Liu, *J. Lipid Res.*, 2010, **51**, 866-874.
10. P. E. Bromley, Y. N. O. Li, S. M. Murphy, C. M. Sumner and D. V. Lynch, *Arch. Biochem. Biophys.*, 2003, **417**, 219-226.
11. R. M. Dean, A. Browdy, S. A. Heidler, J. A. Radding and A. S. Fischl, *FASEB J.*, 2001, **15**, A193-A193.
12. C. A. Redman, S. Kennington, T. Spathopoulou and J. R. Kusel, *Mol. Biochem. Parasitol.*, 1997, **90**, 145-153.
13. P. A. Aeed, A. E. Sperry, C. L. Young, M. M. Nagiec and A. P. Elhammer, *Biochemistry*, 2004, **43**, 8483-8493.
14. V. Constantinou-Kokotou, *Lett. Pept. Sci.*, 2002, **9**, 143-152.
15. E. del Olmo, M. Alves, J. L. López, A. Inchausti, G. Yaluff, A. Rojas de Arias and A. San Feliciano, *Bioorg. Med. Chem. Lett.*, 2002, **12**, 659-662.
16. S. J. Conway, J. Gardiner, S. J. A. Grove, M. K. Johns, Z. Y. Lim, G. F. Painter, D. Robinson, C. Schieber, J. W. Thuring, L. S. M. Wong, M. X. Yin, A. W. Burgess, B. Catimel, P. T. Hawkins, N. T. Ktistakis, L. R. Stephens and A. B. Holmes, *Org. Biomol. Chem.*, 2010, **8**, 66-76.
17. T. S. Elliott, J. Nemeth, S. A. Swain and S. J. Conway, *Tetrahedron: Asymmetry*, 2009, **20**, 2809-2813.
18. H. E. Carter, F. J. Glick, W. P. Norris and G. E. Phillips, *J. Biol. Chem.*, 1947, **170**, 285-294.
19. T. Hino, K. Nakakyama, M. Taniguchi and M. Nakagawa, *J. Chem. Soc.-Perkin Trans. 1*, 1986, 1687-1690.
20. J. A. Morales-Sema, Y. Diaz, M. I. Matheu and S. Castillon, *Synthesis-Stuttgart*, 2009, 710-712.
21. E. J. Reist and P. H. Christie, *J. Org. Chem.*, 1970, **35**, 3521-3524.
22. J. E. Milne, K. Jarowicki, P. J. Kocienski and J. Alonso, *Chem. Commun.*, 2002, 426-427.
23. H. P. Kokatla, R. Sagar and Y. D. Vankar, *Tetrahedron Lett.*, 2008, **49**, 4728-4730.
24. E. J. Reist and P. H. Christie, *J. Org. Chem.*, 1970, **35**, 4127-4130.
25. L. C. Dias, J. Fattori, C. C. Perez, V. M. de Oliveira and A. M. Aguilar, *Tetrahedron*, 2008, **64**, 5891-5903.
26. T. Yamamoto, H. Hasegawa, T. Hakogi and S. Katsumura, *Org. Lett.*, 2006, **8**, 5569-5572.
27. J. J. Park, J. H. Lee, Q. Li, K. Diaz, Y. T. Chang and S. K. Chung, *Bioorg. Chem.*, 2008, **36**, 220-228.
28. S. Grijalvo, X. Matabosch, A. Llebaria and A. Delgado, *Eur. J. Org. Chem.*, 2008, 150-155.
29. K. C. Nicolaou, T. Caulfield, H. Kataoka and T. Kumazawa, *J. Am. Chem. Soc.*, 1988, **110**, 7910-7912.
30. K. Kim, J. Kang, S. Kim, S. Choi, S. Lim, C. Im and C. Yim, *Arch. Pharmacol. Res.*, 2007, **30**, 570-580.
31. J. A. Morales-Serna, J. Llaveria, Y. Diaz, M. I. Matheu and S. Castillon, *Org. Biomol. Chem.*, 2008, **6**, 4502-4504.
32. D. Shapiro and K. Segal, *J. Am. Chem. Soc.*, 1954, **76**, 5894-5895.
33. H. Shibuya, K. Kawashima, M. Ikeda and I. Kitagawa, *Tetrahedron Lett.*, 1989, **30**, 7205-7208.
34. R. C. So, R. Ndonye, D. P. Izmirian, S. K. Richardson, R. L. Guerrero and A. R. Howell, *J. Org. Chem.*, 2004, **69**, 3233-3235.
35. T. Ibuka, H. Habashita, A. Otaka, N. Fujii, Y. Oguchi, T. Ueyhara and Y. Yamamoto, *J. Org. Chem.*, 1991, **56**, 4370-4382.
36. M. Toumi, F. Couty and G. Evano, *Angewandte Chemie-International Edition*, 2007, **46**, 572-575.
37. T. Hashimoto and K. Maruoka, *Chemical Reviews*, 2007, **107**, 5656-5682.
38. M. J. O'Donnell, *Aldrichimica Acta*, 2001, **34**, 3-15.
39. M. J. O'Donnell, W. D. Bennett and S. D. Wu, *J. Am. Chem. Soc.*, 1989, **111**, 2353-2355.

40. M. J. O'Donnell and R. L. Polt, *J. Org. Chem.*, 1982, **47**, 2663-2666.
41. M. J. O'Donnell, *Acc. Chem. Res.*, 2004, **37**, 506-517.
42. E. J. Corey, F. Xu and M. C. Noe, *J. Am. Chem. Soc.*, 1997, **119**, 12414-12415.
43. B. Lygo and P. G. Wainwright, *Tetrahedron*, 1999, **55**, 6289-6300.
44. J. Aires-de-Sousa, S. Prabhakar, A. M. Lobo, A. M. Rosa, M. J. S. Gomes, M. C. Corvo, D. J. Williams and A. J. P. White, *Tetrahedron-Asymmetry*, 2002, **12**, 3349-3365.
45. R. Chinchilla, C. Nájera and F. J. Ortega, *Tetrahedron-Asymmetry*, 2006, **17**, 3423-3429.
46. N. Gimeno, P. Formentín, J. H. G. Steinke and R. Vilar, *Eur. J. Org. Chem.*, 2007, **2007**, 918-924.
47. A. Bielawska, M. S. Greenberg, D. Perry, S. Jayadev, J. A. Shayman, C. McKay and Y. A. Hannun, *J. Biol. Chem.*, 1996, **271**, 12646-12654.

CHAPTER V

SCREENING OF THE
SUBSTRATE
ANALOGUES

5 SCREENING OF THE SUBSTRATE ANALOGUES

5.1 Work Synopsis

The work presented in this chapter demonstrates the achievement of the last objective of this chemical biology project in terms of generation of preliminary SAR data towards mapping the active site of *Lmj*IPCS (Figure 5-1). This chapter describes the screening of the library of ceramide analogues against *Lmj*IPCS, determination of the Z-prime value of the assay platform and finally demonstration of the proposed SAR hypotheses together with the recommended future work to test these hypotheses.

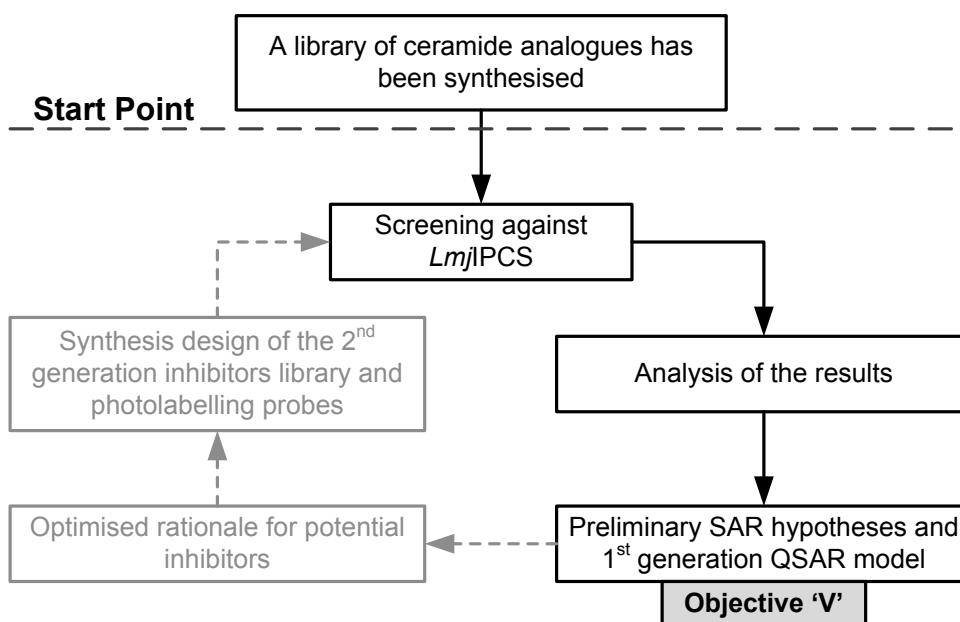


Figure 5-1: A flow chart of the process of screening of the substrate analogues against *Lmj*IPCS and the analysis of the results. Grey boxes and arrows represent future work.

5.2 Preparation of the Screening Compounds

All compounds were first dissolved in MeOH and 1.0 mM stock solutions were prepared in DMSO/MeOH (9:1 v/v) and 0.20 mM working solutions in DMSO/MeOH (98:2). All prepared solutions were stored at $-20\text{ }^{\circ}\text{C}$ until use. In addition to the final ceramide analogues the screening was expanded to include key synthetic intermediates that exhibit structural similarities to the ceramide scaffold and to act as controls to account for interference due to minor impurities that might have been carried over from previous reactions.

5.3 The Assay Protocol of the Inhibition Assays

The hydrophobic nature of most of the synthesised substrate analogues required special attention to ensure their solubility/dispersion in the reaction mixture. This required minor modifications to adapt the assay protocol for screening purposes. For each inhibition reaction, the donor substrate (PI) and test inhibitors were first dried into a reaction Eppendorf tube followed by addition of the reaction buffer, CHAPS and NBD- C_6 -ceramide followed by sonication for 3 minutes. The reaction was started by the addition of *Lmj*IPCS microsomes (Figure 5-2). This reverse of order of addition of reactants and conducting the reactions without pre-incubating of *Lmj*IPCS with PI allowed for the possibility that some screened compounds might act as competitive inhibitors in terms of PI in addition to maintaining the final DMSO concentration of 5 %. Final concentrations of the test compound, PI and NBD- C_6 -ceramide were 20 μM , 100 μM and 5 μM respectively. All reactions were done in triplicates with the inhibitory effect quantified by the change in the formation of the labelled product, NBD- C_6 -IPC.

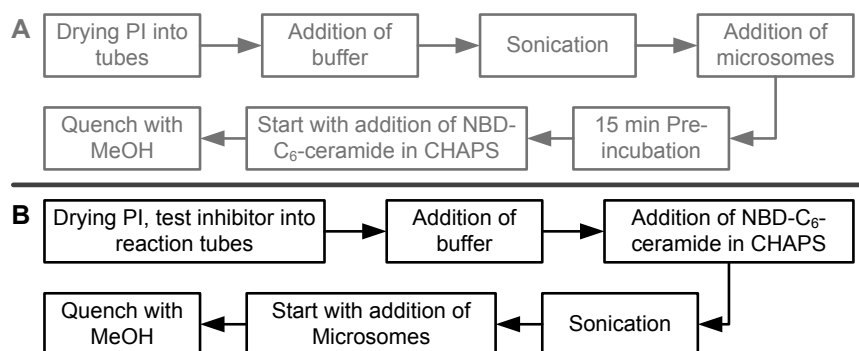


Figure 5-2: Comparison of the assay protocols. (A) Protocol used in determination of the kinetic parameters. (B) Protocol adapted for screening purposes.

5.4 Analysis of the Screening Results

Details of the results of all tested compounds are summarised in (Appendix C). The screening results of the ceramide analogues library and the key synthetic intermediates (that resembles ceramide) together with two classes of compounds, Nor-ephedrine derivatives and β -blockers, will be discussed below in separate graph for clarity reasons. This will be followed by the calculation of the Z -prime value for the inhibitions assays, the determination of the IC_{50} values of identified potent inhibitors and their mass spectrometric analyses.

5.4.1 The Ceramide Analogues Library

The screening of the ceramide analogues library identified 27 compounds with inhibitory effect greater than 40 % out of which 10 compounds showed inhibitory effect between 50~70 % and 3 compounds exhibited inhibition greater than 75 % against *Lmj*IPCS (Figure 5-3).

The top inhibitory compounds were compound (222) ($R^1 = C_{13}H_{27}$, $R^2 = \text{octanoyl}$) in Series 3 (ceramide analogues), compound (112) ($R^1 = C_{13}H_{27}$, $R^2 = \text{octanoyl}$) in Series 1 (1-deoxy-ceramide analogues) and compound (336) ($R^1 = C_{13}H_{27}$, $R^2 = \text{phenylacetyl}$) in Series 5 (2*R*-3-deoxy-ceramide analogues). These compounds exhibited 87 %, 79 % and 76 % inhibition of *Lmj*IPCS respectively.

In general, the results indicated a trend of a proportional increase in the inhibitory effect of the ceramide analogue based on their hydrophobicity. Changing the hydrophobic tail of the sphingosine backbone from CH_2Ph and C_4H_9 (less hydrophobic) to $C_{13}H_{27}$ (more hydrophobic) resulted in an almost regular trend of increasing the inhibition of *Lmj*IPCS. In contrast, although the change in the *N*-acyl residue appeared to be synergistic in terms of adding more hydrophobic character to the analogues, it showed a less regular pattern in terms of the inhibitory profile of the respective ceramide analogues on *Lmj*IPCS. Details of the preliminary SAR analysis will be further elaborated in section 5.5.

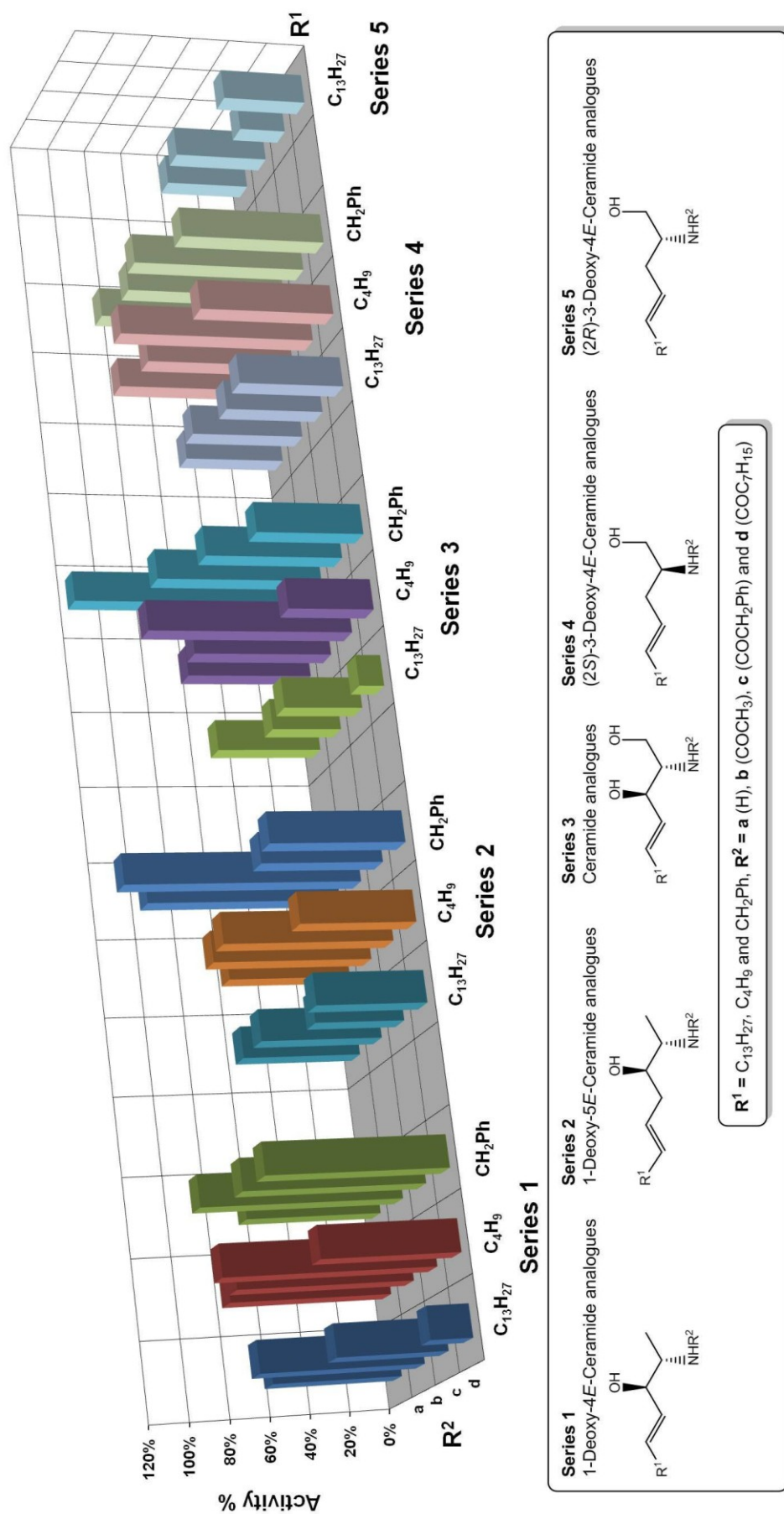


Figure 5-3: Screening Results of the ceramide analogues library

5.4.2 The Synthetic Intermediates

The set of synthetic intermediates consisted of the *N*-Boc protected CM products which comprised the starting materials for the Boc-deprotection acylation reactions (Figure 5-4). While the CM products that contained a short chain (C₄H₉) or an aromatic residue (CH₂Ph) in the sphingosine backbone showed poor or no ($\leq 17\%$) inhibition of *Lmj*IPCS, compounds with a long chain (C₁₃H₂₇) exhibited considerable inhibitory effect (29~59%) on the enzyme turnover. This could be attributed to the relative hydrophobicity of the analogues as it has been previously indicated.

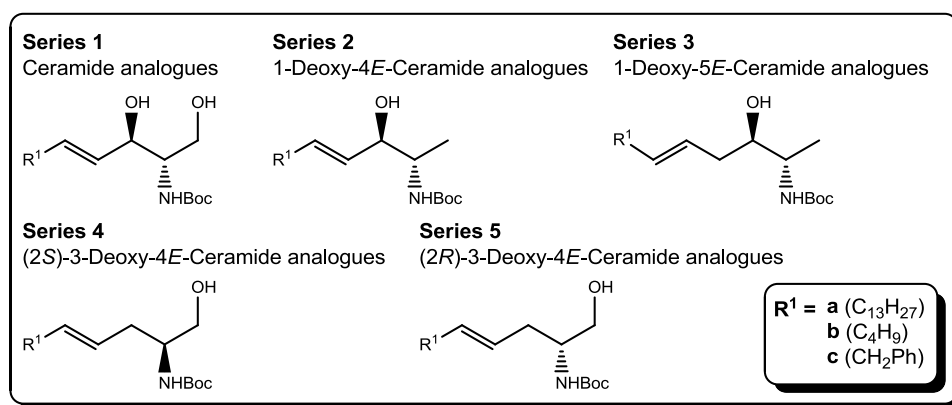
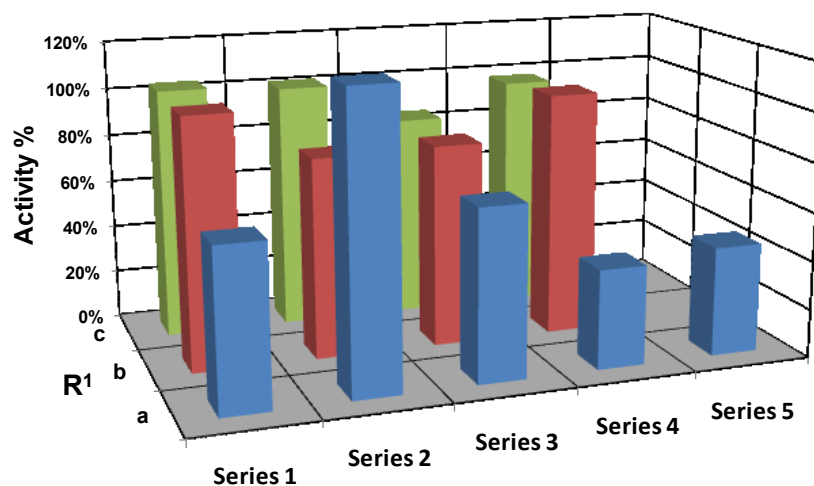


Figure 5-4: Screening results of the CM *N*-Boc protected compounds.

5.4.3 The Nor-Ephedrine (1-Phenyl-2-aminopropanol) Series

While all the derivatives of the (+)-(1*S*,2*R*)-1-Phenyl-2-aminopropanol exhibited poor or no inhibition (< 10 %), two derivatives from the (-)-(1*S*,2*R*)-1-Phenyl-2-aminopropanol, (405, R¹ = e) and (407), exhibited moderate inhibition 23 % and 33 % respectively against *Lmj*IPCS (Figure 5-5). These two small molecules (MW < 300 Da) could be further elaborated to as a design template with fewer rotatable bonds. Analogues derived from such template could lead to the generation of a pharmacophore model of the acceptor substrate of *Lmj*IPCS.

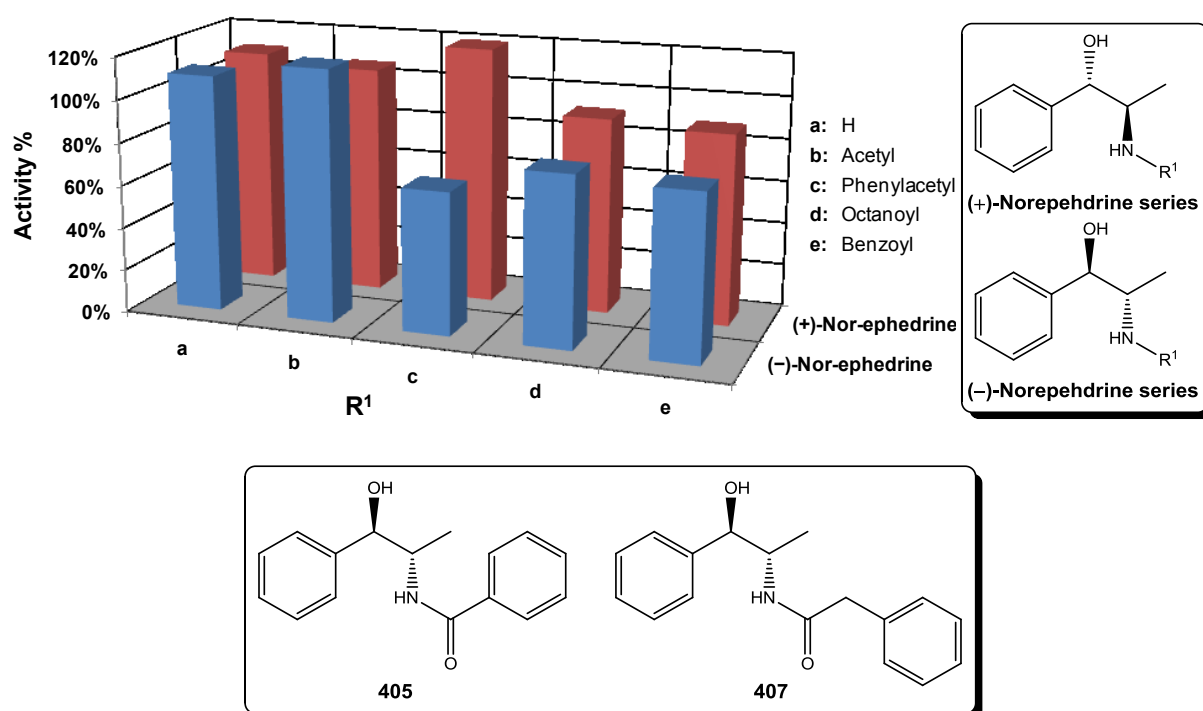


Figure 5-5: Screening results of the (+)-Nor-ephedrine series and the (-)-Nor-ephedrine series.

5.4.4 The β -blockers

It has been suggested that integral membrane lipid phosphate phosphatases (LPPs) and phosphotransferases function via a similar mechanism of action.¹ Additionally, several studies have reported that propranolol, a β -blocker, to exhibit inhibitory effect on lipid phosphate phosphatases.²⁻⁵ Moreover, the scaffold of the β -blockers exhibit structural similarities to that of

ceramide. Consequently, (\pm)-propranolol, (+)-propranolol, (-)-propranolol, betaxolol and ICI 118,551 were screened against *Lmj*IPCS and resulted in 48 %, 39 %, 50 %, 48 % and 54 % inhibition respectively (Figure 5-6). The slightly more potent effect of (+)-propranolol compared to (-)-propranolol might indicate a preferential stereochemistry of the secondary hydroxyl group. Importantly, the observed capacity of the β -blockers to inhibit *Lmj*IPCS could be further elaborated in the design of specific *Lmj*IPCS inhibitors that exploit the benefit of the pharmacokinetic profile of this class of drugs that had made it already to the pharmaceutical market.

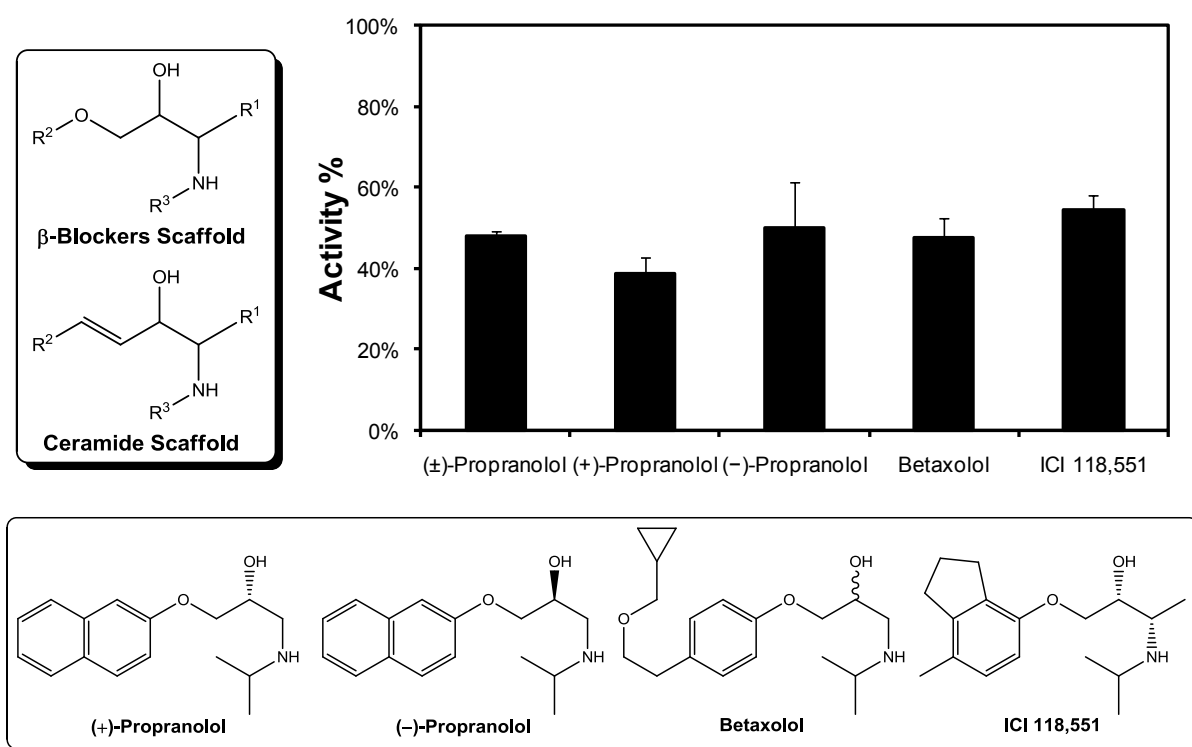


Figure 5-6: The selected β -blockers set and their screening results against *Lmj*IPCS.

5.4.5 Z-Prime Value of the Screening Assay

The established assay protocol was designed to be HTS-compatible. Therefore, statistical validation of the assay platform was required. This was accomplished using the Z-prime value, a dimensionless statistical parameter, which is commonly used to assess the quality of a high-throughput assay.⁶ It compares the mean value of the maximum signal control to the mean value of the minimum signal control according to equation 4.1. Z-prime will have a higher value when

(i) there is a wide separation band between the maximum and minimum controls and (ii) the standard deviations are low. For a good assay, Z -prime values for each plate should be greater than or equal to 0.5 with the Z -prime value of a perfect assay approaching 1.0.

$$Z = 1 - \left(\frac{(3 \times SD_{max}) + (3 \times SD_{min})}{|\bar{x}_{max} - \bar{x}_{min}|} \right) \quad (4.1)$$

SD_{max} = SD of the Maximum Signal Control SD_{min} = SD of the Minimum Signal Control
 \bar{x}_{max} = Mean of the Maximum Signal Control \bar{x}_{min} = Mean of the Minimum Signal Control

Evaluation of each screening assay results yielded an average Z -prime value less than 0.5. This is due to the lack of a potent inhibitor in these assays. However, using the identified potent inhibitors (112) and (336) in addition to the moderately active (\pm)-propranolol, the Z -prime value of the screening assay was recalculated (Figure 5-7). These calculations resulted in Z -prime value of 0.58, 0.42 and -0.18 when the minimum control was compound 112, compound 336 and (\pm)-propranolol respectively. This demonstrated that including a minimum signal control wherein inhibition is about 80 % renders the assay statistically valid for HTS screening.

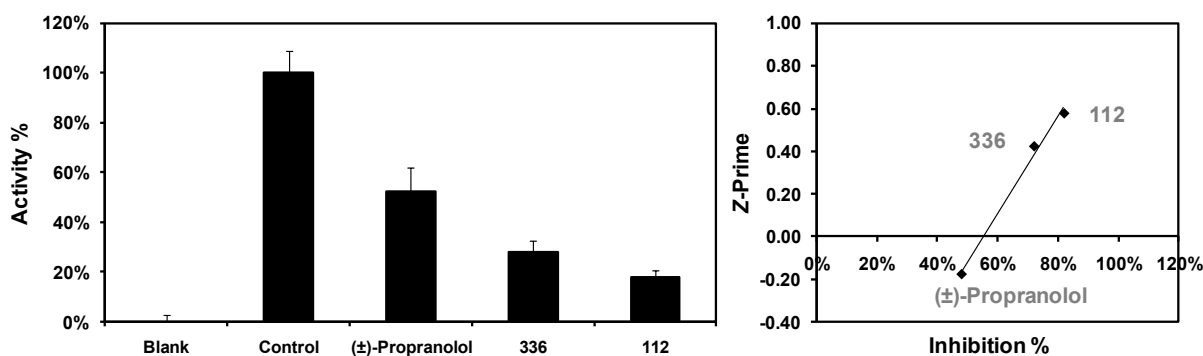


Figure 5-7: Left; Reference compounds and the respective measured activity of *Lmj*IPCS. Right; Correlation between the minimum signal control and the determined Z -Prime value.

5.4.6 IC₅₀ of the Representative Potent Compounds

To confirm the inhibitory effect of the lead compounds identified, dose-inhibition assays were performed and the respective IC₅₀ values were determined (Figure 5-8). The most potent inhibitor was compound (112) (IC₅₀ = 4.8 ± 1.17 μM). These dose-inhibition curves confirmed the potential hits identified. However, further analyses were required to determine whether these compounds act as true inhibitors or as competitive acceptor substrates that can be turned over by *Lmj*IPCS.

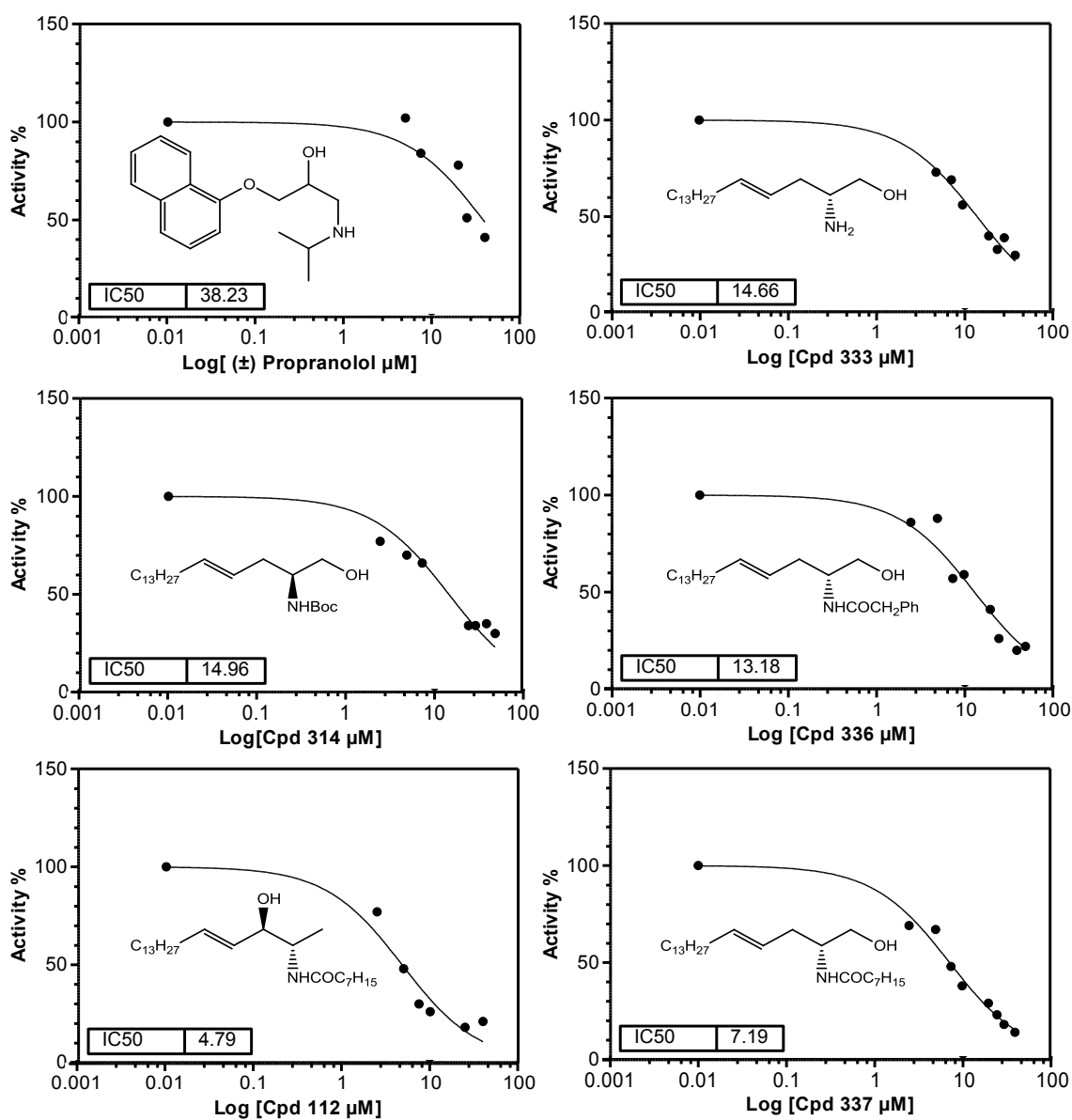
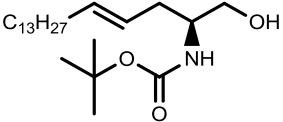
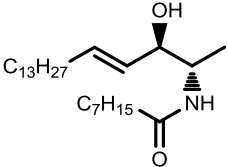
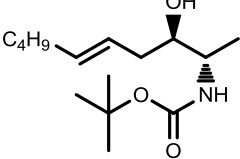
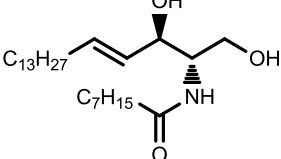
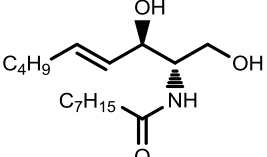
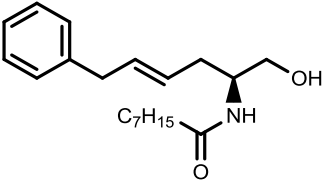
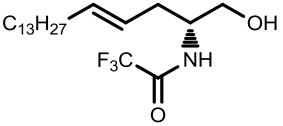
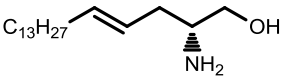
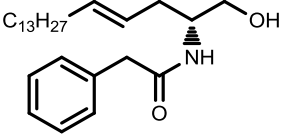
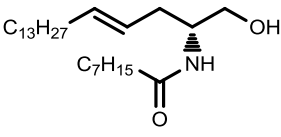
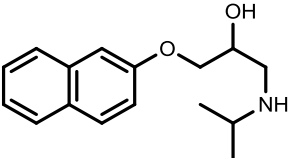


Figure 5-8: Inhibition curves and IC₅₀ values of select inhibitors.

5.4.7 Mass Spectrometry of the Representative Compounds

To distinguish between true inhibitors and competitive acceptor substrates, mass spectrometric analyses were required. Consequently, the organic extracts from the inhibition assays of representative compounds of different series of analogues were submitted for positive and negative ion mass spectrometry. The resultant MS spectra were searched for the mass peaks [M+IP] corresponding to the hypothetical products. Results of the analyses are summarised in Table 5-1.

Table 5-1: Mass spectrometric analysis of inhibition assays of select compounds demonstrating whether a turnover product was detected or not.

TEST COMPOUNDS	Product	TEST COMPOUNDS	Product
314 	Not Detected	112 	Not Detected
135 	Not Detected	222 	Detected
218 	Not Detected	328 	Not Detected
334 	Detected	333 	Not Detected
336 	Not Detected	337 	Detected
(±)-Propranolol 	Not Detected		

The results highlighted the possible structural features of a true acceptor substrate in terms of the importance of the long chain length of the sphingosine backbone (218 vs. 222), the electronic nature of the amide/amine functionality and the bulkiness/hydrophobicity of the *N*-acyl residue (333, 336 vs. 337). Additionally, the results showed that the presence of the 3-OH group is not essential for the turnover of *Lmj*IPCS (334, 337). Details of the SAR conclusions will be discussed in section 5.5.

5.4.8 Pre-incubation with a Ceramide-1-phosphate Analogue (338)

Initially, analogue (334) was speculated to act as a ceramide analogue whilst analogue (338) was expected to act as a PI analogue that might result in mesylation of the active His264 residue. The screening experiments have shown that analogues (334) and (338) resulted in 65 % and 18% inhibition of *Lmj*IPCS respectively. Moreover, the hypothetical product of analogue (334) has been detected in the MS analyses. This partially supported the initial hypothesis. Consequently, the activity of *Lmj*IPCS was measured with and without pre-incubation with PI in the presence or absence of analogue (338) (Figure 5-9). As expected, pre-incubation with PI resulted in enhanced activity. However, pre-incubation with PI in presence of analogue (338) diminished such enhancement. Surprisingly, pre-incubation with analogue (338) only, resulted in about 18 % enhancement of activity. These facts combined indicated an obscure effect of analogue (338). Delineation of such effect requires more detailed study with this class of potential ceramide-based alkylating agents.

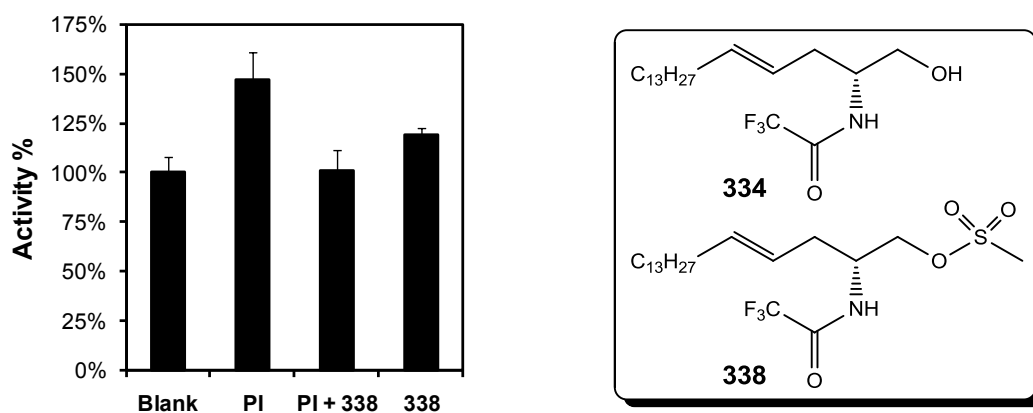


Figure 5-9: *Lmj*IPCS activity measured without (blank) pre-incubation or with pre-incubation with the donor substrate PI \pm analogue 338 (structure shown).

5.5 The SAR Analyses

The following analyses were aimed at the identification of the structural features of the acceptor substrate, ceramide, required for binding and turn over by *Lmj*IPCS. The derived SAR conclusions relied on the comparative analyses of the cumulative experimental observations. These conclusions are illustrated together with the recommended further work.

In addition to the lack of a crystal structure for *Lmj*IPCS or a closely related enzyme, the large number of rotatable bonds in the ceramide molecule and the difficulty in simulating its interaction with an integral membrane protein *in silico* rendered a robust pharmacophore search challenging. However, based on the experimental data, conclusions regarding the key structural features of ceramide could be elucidated. The seven pharmacophore features of ceramide (Figure 5-10) could be divided into two categories based on their necessity for binding and/or turnover by the enzyme.

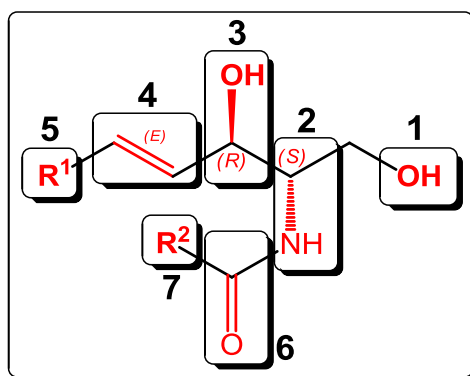


Figure 5-10: The structural features of the ceramide molecule.

5.5.1 Feature ‘1’: 1-OH, H-Donor/H-Acceptor

Although the primary 1-OH group is obviously essential for substrate turnover by *Lmj*IPCS (analogue 222), the experimental results indicates that it was not essential for binding e.g. analogue (112). Future work to probe this hypothesis could include the substitution of the 1-OH by other bioisosteres e.g. NH₂, F (Figure 5-11).⁷

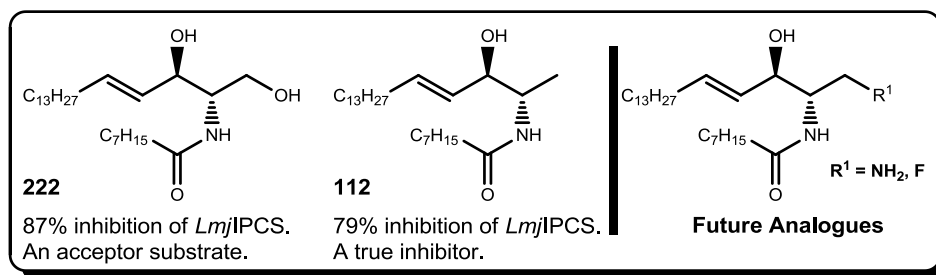


Figure 5-11: The primary 1-OH group as a structural feature of ceramide and possible future analogues with other bioisosteres.

5.5.2 Feature '2': 2S-NH-, H-Donor

The tangible enhancement (excluding 319 vs. 336) in the inhibitory effect of Series 5 relative to Series 4 (Figure 5-12) suggest that although there might be preferential affinity towards the C2 stereochemistry analogous to that of ceramide, it might not be essential for binding and turnover by the enzyme. However, these analogues lacked the 3-OH group where the cumulative effect of relative orientations at C2 and C3 might have a different effect.

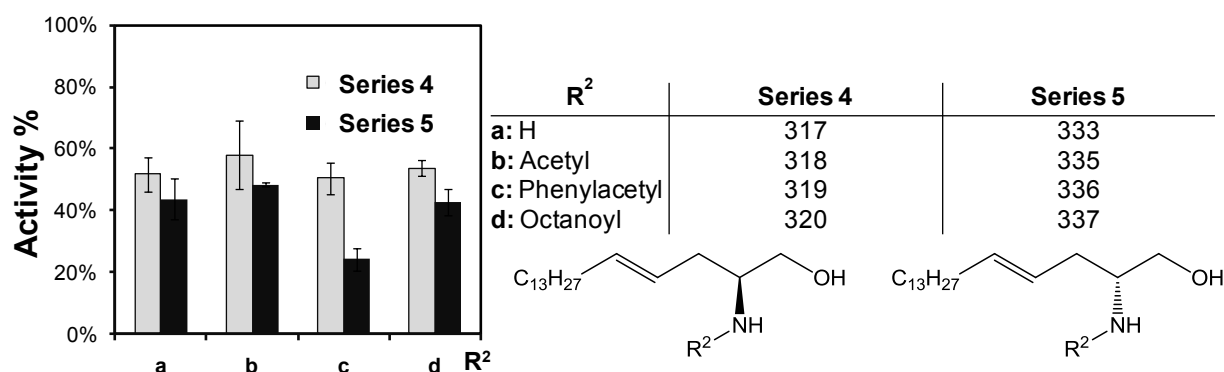


Figure 5-12: Comparative inhibitions by Series 4 vs. Series 5.

This hypothesis could be tested by changing the relative stereochemistries at C2 and C3 (Figure 5-13). Moreover, the importance of 2-NH₂ group can be probed by substitution by other bioisosteres e.g. OH, F. Also, it is noteworthy that changing the -NHCOR functionality to -NHR would switch this pharmacophore feature from H-donor to H-acceptor (*c.f.* Propranolol). This will be elaborated in section 5.5.1.6.

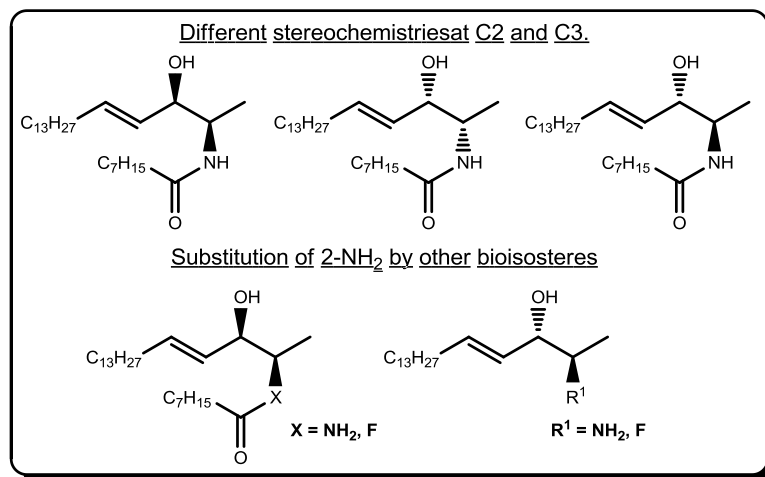


Figure 5-13: The proposed future analogues to probe the importance of the 2-NH₂ group in terms of relative stereochemistries at C2 and C3 and by using other bioisosteres.

5.5.3 Feature '3': 3R-OH, H-Donor/H-Acceptor

Based on the results of the MS analyses, it can be suggested that the 3R-OH is not essential for substrate turnover by *Lmj*IPCS. However, it does affect the binding affinity reflected by the comparative inhibition of *Lmj*IPCS by (222), (112) vs. (337), 87 % and 57 % inhibition respectively (Figure 5-14). This hypothesis could be probed by substitution with other bioisosteres e.g. NH₂, F. Additionally, the C3 relative stereochemistry to C2 could also be probed as (*see above* 5.5.1.2).

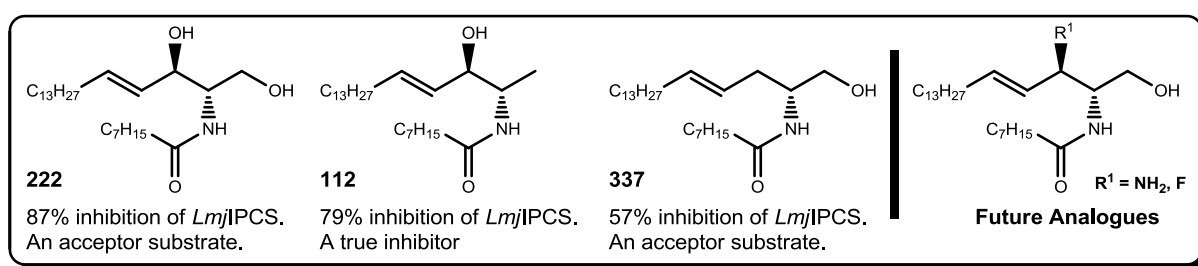


Figure 5-14: Comparative inhibition by 222 vs. 337

5.5.4 Feature '4': Position of the Double Bond

The comparison between the inhibition profiles of Series 1 (1-deoxy-4*E*-ceramide analogues) and Series 2 (1-deoxy-5*E*-ceramide analogues) shows that when the position of the double bond was analogous to natural sphingosine (Series 1), the inhibition was modulated by the added

hydrophobicity due to the *N*-acyl residue. In contrast, displacing the double bond one methylene unit further (Series 2) resulted in a different inhibition profile which appeared almost insensitive to the nature of the *N*-acyl residue (Figure 5-15: top). This is best demonstrated by the difference in the inhibition of *Lmj*IPCS by analogues (112) and (144).

Previous work by *Ramstedt*⁸ reported that the *trans* double bond has a considerable effect on the hydrogen bonding interactions of the 3-OH group in ceramide. Therefore, the encountered differences in the inhibitory profiles can be attributed to the different hydrogen bonding interactions of these analogues with the active site of *Lmj*IPCS. Additionally, the *trans* configuration of the double bond that might function as a structural constraint to control the orientation of the long hydrophobic tail required for binding. This hypothesis can be tested by the comparative screening of (112), 1-deoxy-5*E*-C₁₈-ceramide, dihydro-1-deoxy-C₁₈-ceramide and the *cis* diastereoisomer (Figure 5-15: bottom).

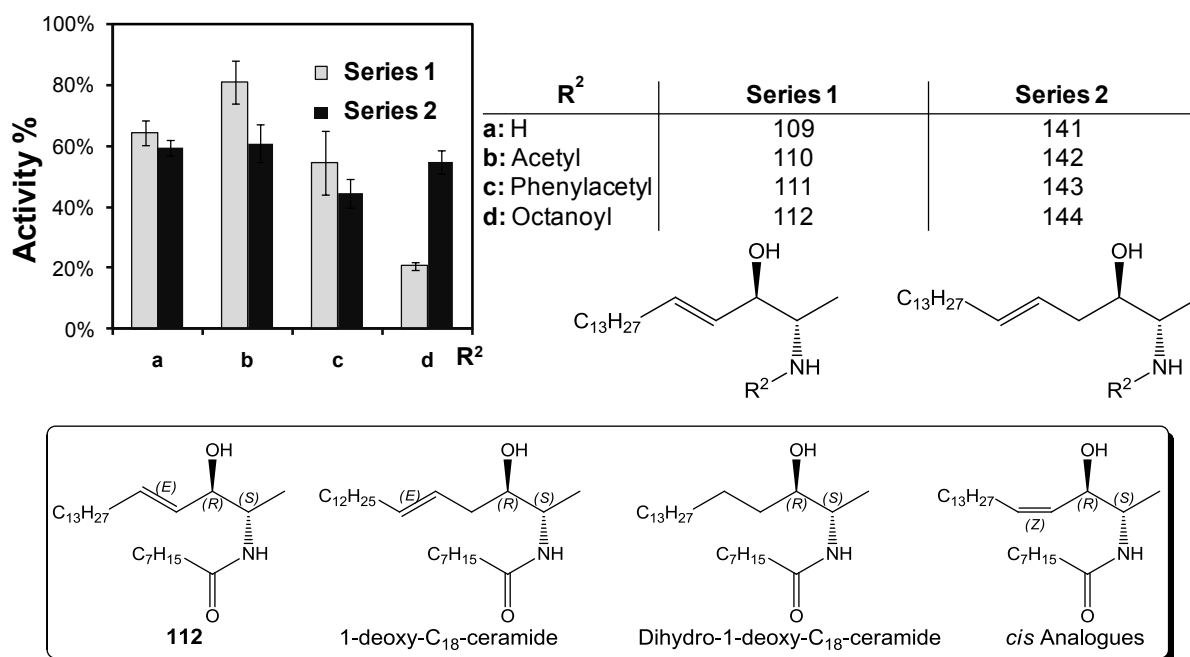


Figure 5-15: Top: Comparative inhibitions by Series 1 vs. Series 2. Bottom: The proposed future analogues with different backbone chain lengths and/or *cis* configuration.

5.5.5 Feature '5': Sphingosine backbone Tail, Hydrophobic Surface

The screening results of the ceramide analogues revealed that apart from three compounds (Figure 5-16) all analogues that exhibited greater than 40 % inhibition contained the long C₁₃H₂₇ hydrophobic tail in their backbones. This observation strongly suggests that the chain length of

the sphingosine backbone is crucial for binding to the enzyme. This is expected given the hydrophobic nature of *Lmj*IPCS as an integral membrane enzyme.

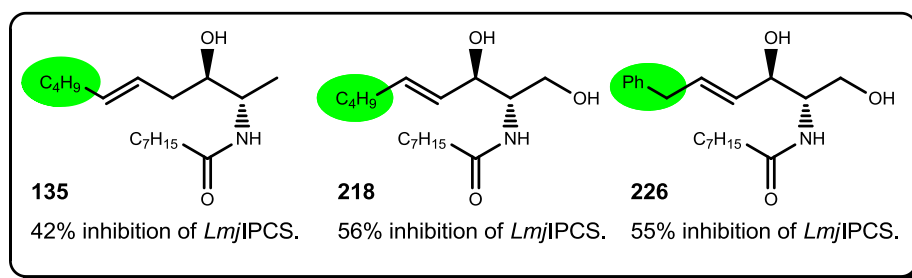


Figure 5-16: Inhibitors lacking the long chain C₁₃H₂₇.

However, the situation is clearly different in terms of the inhibition exhibited by the β -blockers. Therefore, the β -blockers might provide a different scaffold with no linear hydrophobic tail. However, the mode of action of the tested β -blockers on *Lmj*IPCS needs to be further verified. These hypotheses could be further tested by the synthesis of a medium length hydrophobic tail (C₈H₁₇) as previously described in 5.5.1.4 and/or substitution by a hydrophobic moiety analogous to propranolol or betaxolol (Figure 5-17).

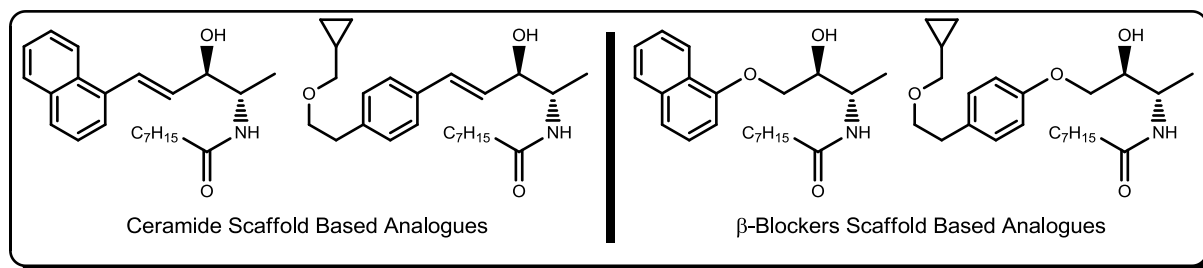


Figure 5-17: The proposed future analogues with different backbones as a hybrid of both the ceramide and β -blockers scaffolds.

5.5.6 Feature '6': -CO-R, H-Acceptor

Early work described in Chapter II has demonstrated that whilst acetyl sphingosine was an acceptor substrate, sphingosine was not. Additionally, the MS analyses described in section 5.4.7 had shown that while analogue (337) was turned over by the enzyme, analogue (333) was not

(Figure 5-18). Taken together, these results suggest that the (possibly protonated) free-amino group of sphingosine interferes electrostatically with the active site of the enzyme.

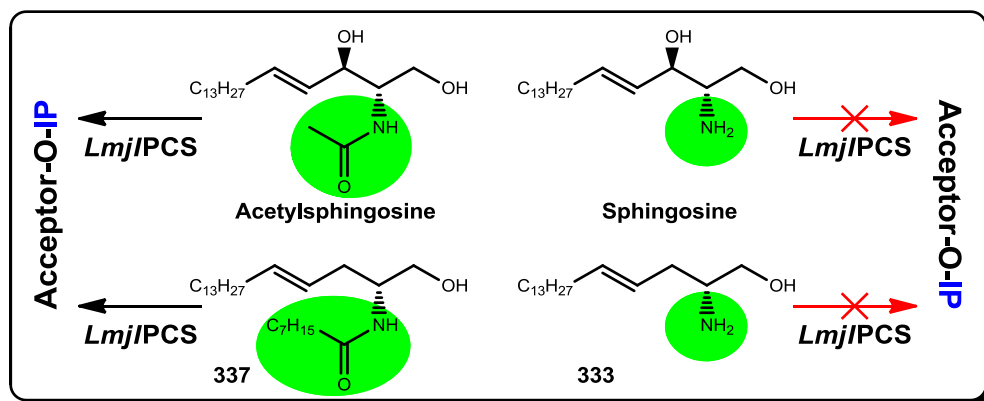


Figure 5-18: Both acetyl sphingosine and analogue (337) are acceptor substrates while sphingosine and analogue (333) are true inhibitors.

Similar observations have been previously reported e.g. the inhibitory effect of sphingosine analogues on the *S. cerevisiae* phosphatidate phosphatase,⁹ a member of the LPP enzyme superfamily believed to share a mechanism of action with the sphingolipid synthases.¹⁰ In addition, Sigal *et al.*¹ have proposed a generalised hypothetical mechanism of action for the phosphoryl transferases. This mechanism, in addition to the catalytic triad, involves two arginine and one lysine residues. These three residues are presumed to be in the protonated state and therefore can stabilise the transition state during the phosphate group transfer (Figure 5-19: A). Moreover, Sigal had demonstrated that one of the involved arginine residues is conserved across different families of enzymes and organisms. This residue is located close (5 amino acids away) to the active nucleophilic histidine residue of the active site. Investigation of the *LmjIPCS* sequence identified Arg262 as a conserved residue in all the identified orthologous IPC synthases in the *TriTryp* genome (Figure 5-19: sequence).¹¹ Consequently, Arg262 can be presumed a potential candidate residue involved in the stabilisation of the transition state during the phosphorylinositol group transfer by *LmjIPCS* (Figure 5-19: B). This speculation is consistent with the hypothesis that the protonated amino group of sphingosine electrostatically interferes with the protonated Arg262 which results in inhibition of the catalytic transfer mechanism.

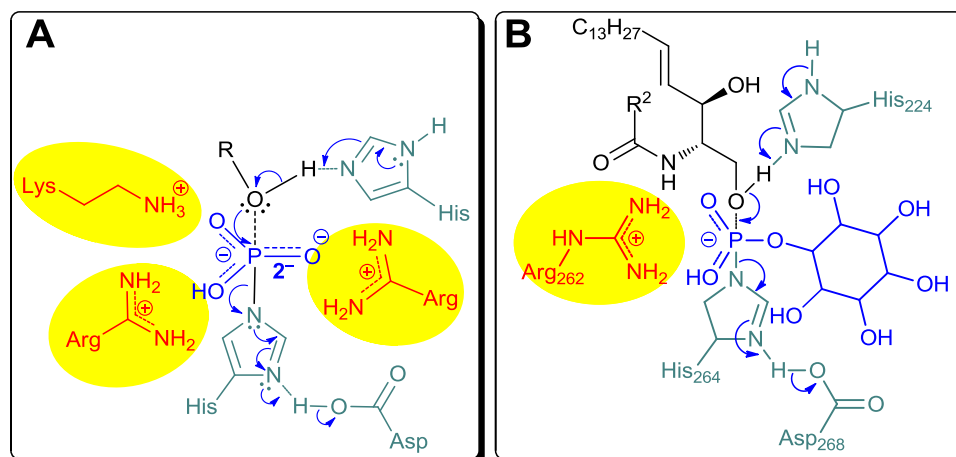


Figure 5-19: Top: The relative position of the proposed Arg262 residue to the His264 and the Asp268 in the *LmjIPCS* sequence. A. Sigal's proposed mechanism of action of phosphoryl transferases. B. The proposed mechanism of *LmjIPCS* based on Sigal's model.

The function of Arg262 could be verified by site-directed mutagenesis. Additionally, the electrostatic nature of the amino/amide group can be tested by the screening of the reduced (*N*-alkyl) form of a known acceptor substrate against *LmjIPCS* followed by MS of the organic extracts to check for product formation (Figure 5-18).

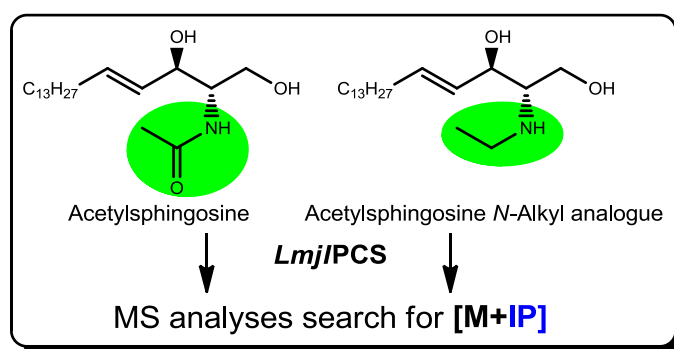


Figure 5-20: Proposed future work to test the difference in mode of action between *N*-acyl-sphingosines and reduced *N*-alkyl-sphingosine analogues.

5.5.7 Feature '7': *N*-Acyl Hydrophobic Tail, Hydrophobic Surface

It has been previously demonstrated that the chain length of the *N*-acyl group is not essential for the turnover of the acceptor substrate by the *LmjIPCS* e.g. acetyl sphingosine. However, a

comparison of the competitive inhibition of *Lmj*IPCS by analogue (222), C₈-ceramide, and analogue (220), C₂-ceramide suggests that the more hydrophobic the *N*-acyl residue, the higher the affinity to the active site. This hypothesis can be tested by the screening of a C₅-ceramide which would be expected to exhibit an intermediate affinity/inhibition between C₈-ceramide and C₂-ceramide.

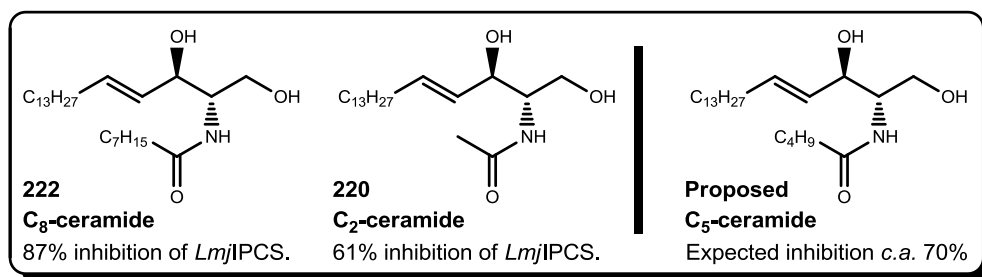


Figure 5-21: Competitive inhibition of C₈-ceramide vs. C₂-ceramide and the hypothetical of *Lmj*IPCS by C₅-ceramide.

Additionally, the screening results indicated that the bulkiness of the *N*-acyl residue might affect the ability of the enzyme to turn over the acceptor substrate analogues. MS analyses had shown that while NBD-C₆-ceramide and analogues (334) and (337) are acceptor substrates whilst analogue (336) is not (Figure 5-22).

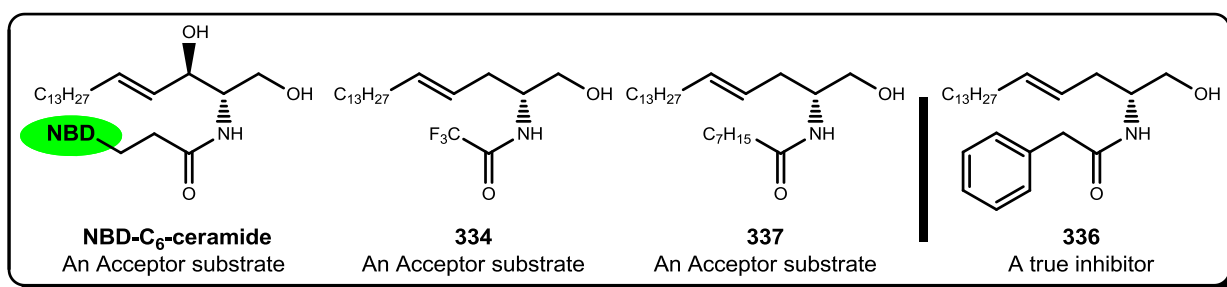


Figure 5-22: Comparison between the bulkiness of the *N*-acyl residues in acceptor substrates and the true inhibitor, analogue 336.

These observations suggest that presence of bulky substituent e.g. a phenyl group close to the amide functionality (1 methylene unit apart) could lead to a possible distortion of the active site resulting in a less than optimum conformation that whilst hindering the catalytic transfer

mechanism however, does not abolish the affinity to the active site. Similar ceramide analogues have been recently reported and proposed as chemotherapeutic agents for breast cancer (Figure 5-23: A).¹² Such hypothesis can be further studied and elaborated in the design of future inhibitors which maintain the affinity to the active site but cannot be turned over by the enzyme (Figure 5-23: B). It is noteworthy, that *Lmj*IPCS complemented an auxotrophic yeast strain where the acceptor substrate comes from a phytoceramide pool. Consequently, synthesis and screening of C2-hydroxylated *N*-acyl analogues might reveal interesting structural features of the active site of *Lmj*IPCS which resemble the fungal orthologue.

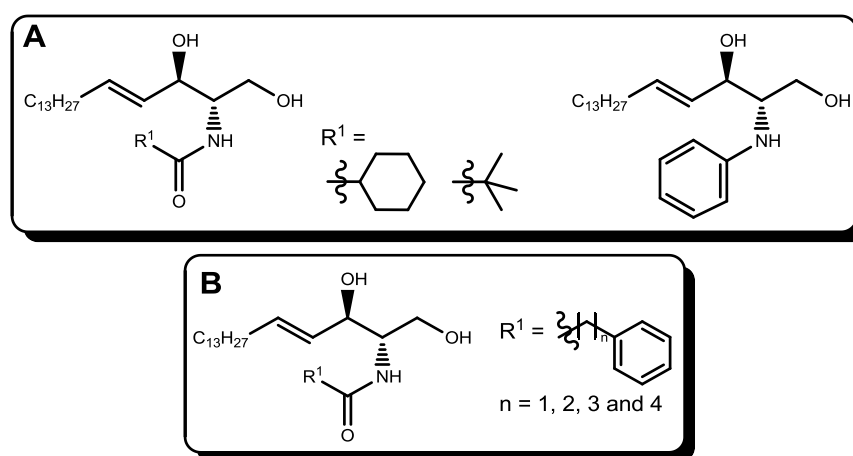


Figure 5-23: (A) The recently reported ceramide analogues with bulky *N*-acyl residues. (B) The proposed ceramide analogues for the determination of the optimum position of the bulky substituent in the *N*-acyl residue that maintains both the enzyme affinity and the true inhibition mode of action.

5.6 Conclusion

The screening of the library of ceramide mimics against *Lmj*IPCS using the assay protocol combined with the MS analyses has enabled the categorisation of the key structural features of ceramide, the acceptor substrate, in terms of binding affinity and turnover by the enzyme. These preliminary SAR conclusions will guide the optimisation process of the design of future inhibitors.

Additionally, two different classes of compounds, Norephedrine derivatives and β -blockers, have been screened against *Lmj*IPCS. Two (-)-norephedrine-derived compounds (405 and 407) have been identified as small molecules that could be further elaborated as a more constrained scaffold for future inhibitors. Moreover, the β -blockers tested against *Lmj*IPCS resulted in an average inhibition greater than 50%. Whilst the determination of their mode of action requires further studies, this class of compounds provides a new scaffold for *Lmj*IPCS inhibitors. Finally, the assay platform has been statistically validated for HTS with a *Z*-prime value greater than 0.5.

REFERENCES

1. Y. J. Sigal, M. I. McDermott and A. J. Morris, *Biochem. J.*, 2005, **387**, 281-293.
2. D. Albert, C. Pergola, A. Koeberle, G. Dodt, D. Steinhilber and O. Werz, *J. Leukocyte Biol.*, 2008, **83**, 1019-1027.
3. I. N. Fleming and S. J. Yeaman, *Biochem. J.*, 1995, **308**, 983-989.
4. S. Sozzani, D. E. Agwu, C. E. McCall, J. T. Oflaherty, J. D. Schmitt, J. D. Kent and L. C. McPhail, *J. Biol. Chem.*, 1992, **267**, 20481-20488.
5. H. Le Stunff, C. Peterson, R. Thornton, S. Milstien, S. M. Mandala and S. Spiegel, *J. Biol. Chem.*, 2002, **277**, 8920-8927.
6. J. H. Zhang, T. D. Y. Chung and K. R. Oldenburg, *J Biomol Screen*, 1999, **4**, 67-73.
7. L. M. A. Lima and E. J. Barreiro, *Curr. Med. Chem.*, 2005, **12**, 23-49.
8. B. Ramstedt and J. P. Slotte, *FEBS Lett.*, 2002, **531**, 33-37.
9. W. I. Wu, Y. P. Lin, E. Wang, A. H. Merrill, Jr. and G. M. Carman, *J Biol Chem*, 1993, **268**, 13830-13837.
10. K. Huitema, J. van den Dikkenberg, J. F. Brouwers and J. C. Holthuis, *Embo J*, 2004, **23**, 33-44.
11. P. W. Denny, H. Shams-Eldin, H. P. Price, D. F. Smith and R. T. Schwarz, *J. Biol. Chem.*, 2006, **281**, 28200-28209.
12. J. W. Antoon, J. W. Liu, A. P. Ponnappakkam, M. M. Gestaut, M. Foroozesh and B. S. Beckman, *Cancer Chemother Pharmacol*, 2010, **65**, 1191-1195.

CHAPTER VI

CONCLUSIONS AND
FUTURE **W**ORK

6 CONCLUSIONS AND FUTURE WORK

6.1 Conclusion

Using a chemical biology approach, the work presented in this thesis has characterised a potential drug target for the treatment of leishmaniasis, namely *Leishmania major* Inositol Phosphorylceramide Synthase (*Lmj*IPCS). A high-throughput compatible assay platform for *Lmj*IPCS was established. This platform enabled probing the enzyme affinity in terms of the donor substrate and determination of the linear assay conditions in terms of time, temperature, substrates and enzyme concentrations. Validation of the assay protocol was accomplished using the known fungal-IPCS inhibitor, aureobasidin A and two ceramide mimics, sphingosine and acetyl sphingosine.

Using the established protocol, the kinetic parameters of *Lmj*IPCS were determined in terms of both donor and acceptor substrates. The kinetic model applied surface-dilution considerations which is unprecedented with this class of enzymes. *Lmj*IPCS was found to obey the double displacement kinetic model with apparent $V_{max} = 2.31 \text{ pmol}\cdot\text{min}^{-1}\cdot\text{U}^{-1}$. The observed higher affinity of *Lmj*IPCS for NBD-C₆-ceramide relative to PI was in agreement with previous literature results.¹ Additionally, the techniques established with *Lmj*IPCS were successfully applied to the orthologous enzymes *Tb*SLS4 from *T. brucei* and *At*IPCS 1, 2 &3 from *A. thaliana*. The contribution of this work validated *Tb*SLS4 as a potential drug target against *T. brucei* and confirmed the IPC synthase activity of the identified *At*IPCS 1, 2 &3.

Furthermore, a first generation library of ceramide mimics has been synthesised. The library consisted of five series with different ceramide-based scaffolds. The key synthetic reactions included a stereospecific reduction of an enone and asymmetric amino acid alkylation using cinchona derived PT catalysts. Screening of the analogues library against *Lmj*IPCS enabled the categorisation of the key structural features of ceramide in terms of binding affinity and turnover by the enzyme. Based on the screening results a preliminary SAR conclusions could be drawn which will guide the optimisation process of the design of future inhibitors. Two different classed of compounds, Norephedrine derivatives and β -blockers, have been also identified as

potential scaffolds for future inhibitors targeting *Lmj*IPCS. Finally, the assay platform has been statistically validated for HTS with a *Z*-prime value greater than 0.5.²

To summarise, the work accomplished to-date sets a robust foundation upon which future work can be established with the ultimate objective of the development of new treatments for leishmaniasis and the closely related HAT and Chagas' disease.

6.2 Proposed Future Work

Building on the current data, future work can be divided into two categories: biological and *in silico* molecular modelling.

6.2.1 Biological Approach

6.2.1.1 Enhancement of the Assay Protocol

Possible enhancements could be made to the established protocols. These include improvement of the quality of the protein preparation and the assay protocol. The former would involve further purification³⁻⁴ of *Lmj*IPCS protein using affinity and size-exclusion chromatography to yield a high purity protein suitable for biophysical topological studies in synthetic lipid bilayers.⁵⁻⁶ On the other hand, development of the assay protocol could include the application of novel techniques such as FRET-pair-based direct quantification of the formation of NBD-IPC without the need for the laborious product isolation.⁷

6.2.1.2 Further Enzyme Activity Studies & Site directed mutagenesis of Arg262

Further studies of *Lmj*IPCS activity against variants of the acceptor substrate (e.g. dihydroceramide and the hydroxylated phytoceramide) and probing the metal dependency of *Lmj*IPCS would complete the kinetic profile of the enzyme and prove useful in molecular modelling of the active site. Also, comparative parallel screening of inhibitors that may target both SM and IPC synthases could prove invaluable in SAR analyses that would help the design of selective second generation inhibitors. Moreover, using site directed mutagenesis, it would be

possible to probe the proposed role of Arg262 in the catalytic transfer function of the *Lmj*IPCS and the orthologous Kinetoplastidae enzymes

6.2.1.3 Kinetics of PI Phosphorylation of *Lmj*IPCS

It has been shown that *Lmj*IPCS obeys the double displacement kinetic model. Consequently, investigation of the first partial reaction, phosphorylation of *Lmj*IPCS by PI, would provide evidence for four hypotheses (Figure 6-1). First, detection of [³H] labelled *Lmj*IPCS protein after incubation with the labelled phosphatidyl-[³H]inositol would provide a conclusive evidence for the substituted enzyme and consequently the double displacement mechanism. Such phosphorylated intermediate can be subjected to trypsin digest and MALDI spectrometric analysis to provide evidence for the active histidine residue. Additionally, the kinetic analysis of the enzyme phosphorylation reaction (K_m and V_{max}) would shed light about the physiological “ground state” of the enzyme which is believed to be in the phosphorylated form due to the abundance of PI in the Golgi membranes. Also, addition of NBD-DAG to the reaction mixture and investigation of the formation of NBD-Phosphatidyl-[³H]inositol will provide evidence whether the phosphorylation reaction is reversible or not.

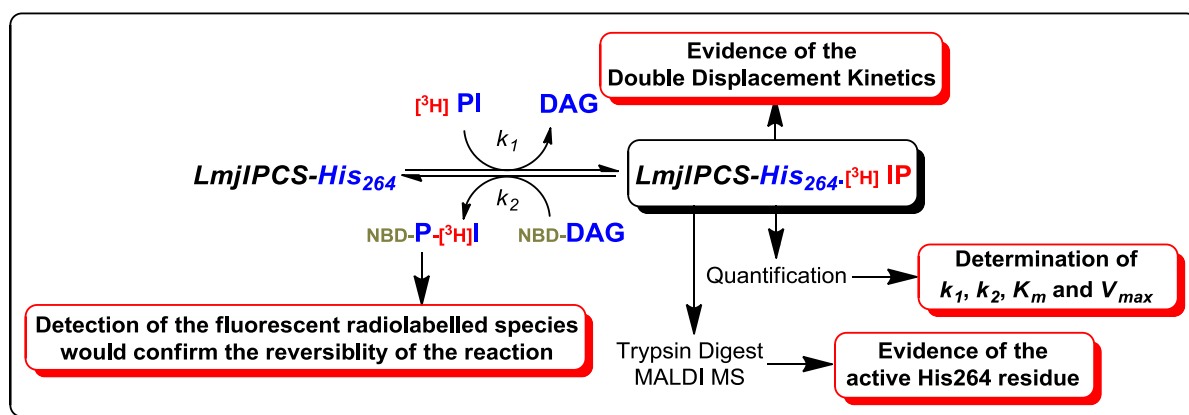


Figure 6-1: Investigation of the phosphorylation reaction of *Lmj*IPCS by PI would provide conclusive evidence for the double displacement kinetics and confirmation of the hypothesised active His264 residue. Additionally, the reversible nature and the kinetic parameters of the first partial reaction can be determined.

6.2.2 Bioinformatics and *In Silico* Molecular Modelling

In 1997, Neuwald¹⁰ had reported an unexpected structural relationship between integral membrane phosphatases and soluble haloperoxidases. He reported sequence motifs shared between type two phosphatidic acid phosphatase and soluble vanadium-dependent chloroperoxidase where these regions are also conserved in other soluble globular and membrane associated proteins. He suggested that a similar arrangement of catalytic residues of the active site within both soluble and membrane spanning domains. With the crystal structure of several chloroperoxidases available in PDB together with reiterative cycles of QSAR model enhancement, an initial model can be constructed and continuously optimised using and pharmacophore searches using conformationally constrained substrate analogues. Additionally, using molecular modelling software, a QSAR model can be generated based on the screening results of the library of ceramide mimics.

REFERENCES

1. P. A. Aeed, A. E. Sperry, C. L. Young, M. M. Nagiec and Å. P. Elhammer, *Biochemistry*, 2004, **43**, 8483-8493.
2. J. H. Zhang, T. D. Y. Chung and K. R. Oldenburg, *J Biomol Screen*, 1999, **4**, 67-73.
3. A. S. Fischl, Y. Liu and J. Ko, *FASEB J.*, 1998, **12**, L55.
4. A. S. Fischl, Y. S. Liu, A. Browdy and A. E. Cremesti, *Sphingolipid Metabolism and Cell Signaling, Pt A*, 2000, **311**, 123-130.
5. S. J. Singer, *Annual Review of Cell Biology*, 1990, **6**, 247-296.
6. T. Surrey and F. Jahng, *Proc. Natl. Acad. Sci. U. S. A.*, 1992, **89**, 7457-7461.
7. *United States of America Pat.*, 2007.
8. T. Mathew, M. Cavallari, A. Billich, F. Bornancin, P. Nussbaumer, G. De Libero and A. Vasella, *Chem. Biodiversity*, 2009, **6**, 1688-1715.
9. J. Cho, Y. M. Lee, D. Kim and S. Kim, *J. Org. Chem.*, 2009, **74**, 3900-3904.
10. A. F. Neuwald, *Protein Sci.*, 1997, **6**, 1764-1767.

CHAPTER VII

**BIOLOGICAL
MATERIALS AND
METHODS**

7 BIOLOGICAL MATERIALS AND METHODS

7.1 Materials

PI: L- α -phosphatidylinositol (Liver, Bovine, predominant species: 18:0/20:4, 1-*sn*-stearoyl-2-*sn*-arachidonoyl) and PI: L- α -phosphatidylinositol (Soybean, predominant species: 16:0/18:2, 1-*sn*-palmitoyl-2-*sn*-oleoyl) were from Avanti Polar Lipids. PI: L- α -phosphatidylinositol (synthetic, 1-*sn*,2-*sn*-dipalmitoyl), C₁₈-Ceramide (*N*-stearoyl-(2*S*,3*R*,*E*)-2-aminooctadec-4-ene-1,3-diol), CHAPS, Tris/HCl, sucrose, glucose (as monohydrate), ammonium sulphate, chloroform 99.8%, methanol 99.8%, formic acid, potassium formate, potassium monohydrogen phosphate, potassium dihydrogen phosphate and the β -blockers collection; (\pm) propranolol, (+) propranolol, (-) propranolol, betaxolol and ICI 118.551 were from Sigma Aldrich. D-erythro-sphingosine (d18:1) and *N*-acetyl-sphingosine (d18:1/2:0, C₂-Ceramide) were from TOCRIS BioScience. NBD-C₆-ceramide and yeast nitrogen base were from Invitrogen. DAG (1-*sn*-stearoyl-2-*sn*-arachidonoylglycerol) was from Enzo Life Sciences. AG4-X4 resin was from BioRad. Protease inhibitor, Complete[®] EDTA-free Protease Inhibitor Cocktail Tablets were from Roche Applied Science. 1.5 ml LoBind Tubes from Eppendorf were used for all assays reactions. Amino acids drop-out packages were from Clontech. Acid-washed glass beads (425-600 μ m, 30-40 U.S. sieve) were obtained from Sigma Aldrich. The protein assay kit was from BioRad using Coomassie[®] Brilliant Blue G-250. All reactions were carried out using high purity distilled deionised water. All other solvents used were of the highest purity available commercially.

7.2 Instruments and Equipment

All centrifugation steps were carried out using Beckman Coulter[®] centrifuges/ultracentrifuges. Eppendorf tubes were centrifuged using Boeco U-320. Disruption of yeast cells was performed using Vortex Mixer MT20 Chiltern[®]. Protein content was quantified using Boeco S-32 Spectrophotometer. The 96-well plate-based assays separation of products was done using a Millipore vacuum manifold system. The filtration steps were done using Millipore

MultiScreen[®] Solvinert 96-well filter plates; the filtrate was collected using OptiPlate-96 F (black plates) from Perkin Elmer. Fluorescence quantification was done using Fusion[®] α plate reader from Packard Bioscience. HPTLC plates were from Merck. Quantification of the TLC spots was carried out using Fuji FLA-3000 plate reader and AIDA Image Analyser[®] software (version 3.52). Mass Spectrometry analyses were performed on an LTQFT from ThermoFinnigan Corp.

7.3 Solutions, Buffers and Media Compositions

Details of the solutions, buffers and media compositions used are given below in Table 7-1 and Table 7-2.

Table 7-1: Solutions and Buffers Ingredients.

Buffers	Final Conc.	Vol./ weight	Stock solution
STE Buffer (50 ml)	25 mM	1.25 ml	Tris/HCl (1 M)
	250 mM	12.5	Sucrose (1 M)
	1 mM	100 μ L	EDTA (0.5 M)
		1 tab ad 50 ml	Complete [®] Protease Inhibitor Cocktail Water
Storage Buffer (50 ml)	50 mM	2.5 ml	Tris/HCl (1 M)
	10% w/v	6.25 ml	Glycerol (80% w/v)
	5 mM	0.25 ml	MgCl ₂ (1 M)
		1 tab ad 50 ml	Complete [®] Protease Inhibitor Cocktail Water
Tris/EDTA/BSA buffer (50 ml)	250 mM	12.5 ml	Tris/HCl (1 M)
	25 mM	2.5 ml	EDTA (0.5 M)
	15 mg/ml	750 mg ad 50 ml	Free-fatty-acid BSA Water
Phosphate Buffer (1 L)	71.4 mM	4.167 gm	KH ₂ PO ₄ ·H ₂ O
		11.0427 gm	K ₂ HPO ₄ ·7H ₂ O
		ad 1 L	Water
AG4-X4 Resin Suspension (20 ml)		4 gm	AG4-X4 Resin
		ad 20 ml	EtOH
TE Buffer (10 \times) (1 L)		100 ml	1 M Tris-HCl (pH 7.5)
		20 ml	500 mM EDTA (pH 8.0)
		ad 880 ml	Ultrapure Water
PEG 3350 (50%) (200 ml)		100 gm	PEG 3350
		ad 200 ml	Ultrapure Water

Buffers	Final Conc.	Vol./ weight	Stock solution
TE/Li Acetate (50 ml, 10×)		5 ml	1 M Li Acetate
		5 ml	10× TE Buffer500 mM EDTA (pH 8.0)
		ad 50 ml	Ultrapure Water
PEG/Li Acetate (50 ml, 10×)		5 ml	1 M Li Acetate
		5 ml	10× TE Buffer500 mM EDTA (pH 8.0)
		ad 50 ml	50% PEG 3350

Table 7-2: Growth Media Ingredients.

Growth Media		Vol./ weight	Stock solution
SD –HIS –URA (1 L)		20 gm	Glucose
		± 5 gm	Agar (Added for solid media preparation)
		1.7 gm	Yeast Nitrogen Base
		5 gm	Ammonium Sulphate
		0.7 gm	AAcids Drop-Out Supplement –HIS –URA –TRP
		2 ml	Tryptophane (10 mg/ml)
		ad 1000 ml	Water
YPGR (1 L)	Sol I	10 gm	Yeast Extract
		20 gm	Pepton
		ad 800 ml	Water 'autoclaved separately'
	Sol II	40 gm	Galactose
		20 gm	Raffinose
		ad 200 ml	Water 'autoclaved separately'
YPD (1 L)	Sol I	10 gm	Yeast Extract
		20 gm	Pepton
		ad 800 ml	Water 'autoclaved separately'
	Sol II	20 gm	Glucose
		ad 200 ml	Water 'autoclaved separately'

7.4 Standard Protocols

7.4.1 Complementation of AUR1 mutant *S. cerevisiae*

Previously in Denny's group, the auxotrophic *YPH499-HIS-GAL-AUR1 S. cerevisiae* strain was constructed by bringing the expression of the yeast AUR1 gene under the control of the stringently regulated GAL1 promoter that is repressed in the presence of glucose. The AUR1 promoter in the yeast genome was exchanged by a selection marker/promoter HIS/GAL1 cassette. This yeast strain was used in all complementation experiments. Briefly, 1 ml of YPGR

media was inoculated with *YPH499-HIS-GAL-AUR1* mutant yeast. The media was vortexed vigorously to disperse any clumps. The cells were then transferred to a flask containing 30 ml of YPGR and incubated at 30 °C overnight with shaking to stationary phase ($OD_{600} > 1.5$). The overnight culture was diluted into enough volume of YPGR media to produce an $OD_{600} = 0.2-0.3$. Following the dilution, the yeast culture was incubated at 30 °C with shaking till $OD_{600} = 0.5 \pm 0.1$. The cells were then placed into 50-ml tubes and centrifuge at $1,000 \times g$ for 5 min at room temperature. The supernatant was discarded and the cells were re-suspended in 5 ml sterile water. The cells were re-centrifuged at $1,000 \times g$ for 5 min at room temperature and the supernatant was discarded by decantation. The cell pellet was then re-suspended in 1 ml of freshly prepared, sterile $1 \times$ TE/Li Acetate buffer to form the yeast competent cells.

Consequently, 0.1 μ g of the control vector pRS246 or the complemented vector (pRS246-IPC synthase) was added to 10 μ L of Herring testes carrier DNA in an Eppendorf tube followed by the addition of 0.1 ml of the yeast competent cells and mixed by vortexing. This was followed by the addition of 0.6 ml of a freshly prepared sterile PEG/ Li Acetate solution and the mixture was vortexed at high speed followed by incubation at 30 °C for 30 minutes with shaking. After the incubation period, 70 μ L of DMSO were added and mixed by gentle inversion and swirling. Subsequently, the cells were subjected to a heat shock for 15 minutes in a 42 °C water bath. After the heat shock, the cells were chilled on ice for 1–2 min, centrifuged for 5 seconds at room temperature at 14,000 rpm. The supernatant was removed and the cells were re-suspended in 0.5 ml 1X TE buffer and plated onto agar plates of permissive (SGR –HIS –URA) and non-permissive media (SD –HIS –URA).

7.4.2 *AUR1* mutant *S. cerevisiae* culture

7.4.2.1 *Agar Plates*

Stocks of the complemented yeast were frozen at –80 °C in 10 % glycerol and cultures were maintained in SD –HIS –URA agar medium. For a typical procedure, the agar plates were inoculated with enough inoculum (from frozen stock, –80 °C) of the *AUR1*-mutant complemented yeast strain. The plates were incubated at 30 °C till convenient growth was noticed (approximately 4 days). The fully grown plate cultures were kept at 4 °C until use.

7.4.2.2 Culture Scaling-up

Cultures were propagated in liquid SD –HIS –URA media. Briefly, 5 ml liquid media were inoculated to approximately $OD_0 = 0.2$ and incubated at 30 °C till $OD \geq 0.8 \sim 1.0$ (late exponential or early stationary phase, approximately 24 hours). Fresh media (500 ml) were added and incubated at 30 °C till $OD \geq 0.8 \sim 1.0$ (approximately 48 hours). The culture was then scaled up by diluting into fresh media (5 L) and incubated at 30 °C till $OD \geq 0.6$ (mid to late exponential phase, approximately 24 hours).

7.4.3 Preparation of the Microsomal Membranes Fraction

7.4.3.1 Step 1: Preparation of Cell Extract

Crude membranes from the mutant *S. cerevisiae* were prepared essentially as described by *Fischl et al.*¹ The complemented yeast cells were propagated in liquid SD –HIS –URA media until $OD \geq 0.6$. Cells were harvested by centrifugation ($1500 \times g$, 4 °C, 10 min) and washed (twice) with cold PBS buffer. A 5 litre culture would typically result in 8.0 ~ 8.5 gm of wet cell mass (WCM). The pellet was re-suspended in STE buffer and the yeast cells were disrupted with pre-chilled glass beads, using a vortex mixer. Disruption step involved 10 cycles of 1 min vortex mixing followed with a 1 min rest on ice between each cycle. Glass beads, unbroken cells and cell-wall debris were removed by centrifugation (approximately $1500 \times g$, 4 °C, 15 min) to obtain the cell extract (supernatant).

7.4.3.2 Step 2: Preparation of Crude Microsomal Membrane Fraction

The microsomal membrane fraction – enriched in IPC Synthase – was isolated from the cell extract by differential centrifugation. A large granular fraction – including mitochondria and large cellular organelles – was initially removed by centrifugation ($27000 \times g$, 4 °C and 30 min). The supernatant was re-centrifuged ($150000 \times g$, 4 °C and 90 min) to obtain a pellet of the small granular fraction enriched in microsomal membranes. The pellet was suspended in storage buffer containing protease inhibitor and the protein content determined according to *Bradford*.² The concentration was adjusted to 20 mg/ml and 100 μ L aliquots were stored at –80 °C until use.

7.4.3.3 Step 3: Preparation of CHAPS-washed Microsomal Membranes Fraction

The crude microsomal membranes were adjusted to a concentration of 10 mg/ml using STE buffer and a 5 % CHAPS stock solution was diluted with STE buffer to 2.5 % concentration. Equal volume of the microsomal membranes and 2.5 % CHAPS were mixed together and kept on ice for 60 min without shaking. The mixture was centrifuged ($150000 \times g$, 4 °C and 90 min) and the sediment was re-suspended in storage buffer, protein content was quantified and kept at -80 °C until use. A second wash inactivated the enzyme.

7.4.3.4 Step 4: Determination of the Protein Content in Enzyme Units

The typical procedure of protein quantification included an ‘Acetone Precipitation’ as an initial step to remove interfering buffers and the phospholipids. The typical precipitation step included mixing 10 μ L of the microsomal membranes with 100 μ L of ice-cold acetone in 1.5 ml Eppendorf tube. The mixture was kept at 0 °C for 30 min and centrifuged (14000 rpm, 4 °C and 30 min). The supernatant was removed and the protein pellet was re-suspended in distilled water and quantified according to *Bradford*.²

To standardise the assay material, samples were normalized with respect to active enzyme content thereby removing variability in sample preparation and ensuring consistency across experiments. Although the standardised unit for enzymatic activity is the katal where 1 kat = 1 mol(product).s⁻¹,³ for the range of substrates concentrations used in the work presented here a more practical value is enzyme unit (U). One unit (U) of enzyme is defined as that which converts 1 pmol of substrate per minute under the conditions described (1 U = 1 pmol(product).min⁻¹) where 1 U corresponds to 16.67 *femtokats*.¹ The conversion of the fluorescent acceptor substrate NBD-C₆-ceramide to the product NBD-C₆-IPC was measured and quantified with respect to known concentrations of NBD-C₆-ceramide, activity calculated as U/ μ l and the samples were stored at -80 °C until use. Enzyme turnover was calculated per milligram of total protein in the sample (U.mg⁻¹).

7.4.4 NBD-C₆-Ceramide Fluorescence Assay

7.4.4.1 Protocol 'A': 96-well plate Assay

CHAPS-washed membranes⁴ were used in a reaction mix containing 100 μ M (or appropriate) PI, 50 mM KH₂PO₄ (pH 7.0) and 5 μ M (or appropriate) NBD-C₆-ceramide. Briefly, 4 μ L of 1 mM PI was dried into each reaction tube in a rotavapor (Eppendorf Concentrator 5301). To the dried PI, 28 μ L of 71.4 mM KH₂PO₄ buffer were added. The solution was sonicated for 2 min then rested on ice before the addition of 2 μ L of the microsomal membranes. Following pre-incubation at 30 °C for 30 minutes, the reaction was initiated by the addition of the NBD-C₆-ceramide and 2.4 mM CHAPS. The reaction was incubated for the specified period of time and subsequently quenched by the addition of 200 μ l of methanol 99.8 %.

Separation of the reaction product, NBD-C₆-IPC, from the substrate NBD-C₆-ceramide was achieved by applying the reaction mix to 100 μ l (sedimented gel volume) of AG4-X4 resin, formate form, in 96-well filter plates using a vacuum manifold. The resin was washed 5 \times 200 μ L methanol, the product was eluted into black OptiPlate® 96-F plates, to minimize background emission, (Perkin Elmer) using 4 \times 50 μ L of 1 M potassium formate in methanol and quantified using a fluorescence plate reader (Fusion™ α , Packard Bioscience) - excitation λ = 466 nm; emission λ = 536 nm. Typically, assays used were carried out in triplicate and results analysed using Prism 5.0 software (GraphPad).

7.4.4.2 Protocol 'B': Thin Layer chromatography (TLC) Assay⁵

1 μ L of 50 mM PI was dried into each reaction tube in a rotavapor (Eppendorf Concentrator 5301). To the dried PI, 20 μ L Tris/EDTA/BSA buffer were added, the solution was sonicated for 2 min, rested on ice for 1 min followed by addition of 2 μ L of the microsomal membranes and the volume was adjusted to 48 μ L with distilled water. After pre-incubation at 30 °C for 30 minutes, the reaction was started by addition of 2 μ L of 5 mM NBD-C₆-Ceramide. The final volume was 50 μ L and final concentrations of the reaction components were 1 mM PI, 100 mM Tris/HCl buffer (pH 7.4) and 200 μ M NBD-C₆-Ceramide. The reaction mixture was incubated at

30 °C for the required time before quenching with 150 μ L of Chloroform:Methanol:Water (10:10:3).

The resultant mixture was centrifuged to separate phases and the organic layer removed. The aqueous phase was then re-extracted with 50 μ L of chloroform. The combined organic extracts were dried in a rotavapor (Eppendorf Concentrator 5301) and re-suspended in 20 μ L of Chloroform:Methanol:Water 10:10:3. Reaction products were fractioned on HPTLC plates (silica gel 60 F₂₅₄) after equilibration or carried out in triplicates using the eluent system Chloroform:Methanol:aq. 0.25 % KCl (55:45:10). The R_f values for the excess NBD-C₆-Ceramide and the product NBD-C₆-IPC were 0.96, 0.57 respectively. Product quantification was carried out using a TLC plate reader (Fujifilm, FLA3000) and AIDA Image Analyzer software (version 3.52).

7.4.4.3 Assay for Inhibitions Studies

In the preliminary inhibition studies using an *N*-acetyl-sphingosine and D-erythro-sphingosine, substrate analogues were added with the fluorescent substrate NBD-C₆-ceramide in the quantities required.

In the screening of the synthesised substrate analogues library, the substrate analogues were dried into reaction tubes with PI followed by the addition of 50 mM KH₂PO₄ buffer (pH 7.0) and 5 μ M NBD-C₆-ceramide. The solution was sonicated for 2 min then rested on ice before pre-incubation at 30 °C for 15 minutes. The reaction was initiated by the addition of 2 μ L of the microsomal membranes. The reaction was then incubated at 30 °C for 15 min and subsequently quenched by the addition of 200 μ l of methanol. Separation and quantification were carried out as previously described.

7.4.5 Mass Spectrometry Analyses

Analyses were performed on an LTQFT (ThermoFinnigan Corp); an FTICR MS instrument equipped with a 7.0 T magnet. The assay protocol 'B' was deployed to minimise CHAPS content using washed membranes. The organic extracts were dried and re-suspended in chloroform and

introduced into the electrospray ion source by direct infusion from a syringe at a flow rate 3 $\mu\text{l}/\text{min}$. Positive ion measurements were made with the source voltage at 4.0 kV and negative ion measurements were made with the source voltage at 3.5 kV. The tube lens was kept at 100 V and the source temperature at 275 $^{\circ}\text{C}$ for all experiments.

REFERENCES

1. A. S. Fischl, Y. Liu, A. Browdy and A. E. Cremesti, *Methods Enzymol.*, 2000, **311**, 123-130.
2. M. Bradford, *Anal. Biochem.*, 1976, **72**, 248-254.
3. *Eur. J. Biochem.*, 1979, **97**, 319-320.
4. P. A. Aeed, A. E. Sperry, C. L. Young, M. M. Nagiec and Å. P. Elhammer, *Biochemistry*, 2004, **43**, 8483-8493.
5. J. M. Figueiredo, W. B. Dias, L. Mendonca-Previato, J. O. Previato and N. Heise, *Biochem. J.*, 2005 **387**, 519-529.

CHAPTER VIII

CHEMICAL
SYNTHESIS
EXPERIMENTAL
DETAILS

8 CHEMICAL SYNTHESIS EXPERIMENTAL DETAILS

8.1 General Procedures

8.1.1 IUPAC nomenclature

The IUPAC names were generated using ChemBioDraw (v12.0); CambridgeSoft.

8.1.2 Solvents purification

All solvents were dried and distilled by standard procedures¹ and stored under nitrogen before use,

- Petroleum ether (Petrol) was distilled and collected fractions correspond to a boiling point of 40-60°C
- THF and ether were distilled over sodium / benzophenone
- Dichloromethane over calcium hydride
- Toluene over sodium.

8.1.3 Reaction Conditions, Monitoring and Purification

- All sensitive reactions were performed under an inert atmosphere and done in dried glassware.
- All reactions were followed by thin layer chromatography (TLC) using normal phase silica plates which were revealed by UV (254 nm) for components with active chromophores or visualised by stains (phosphomolybdic acid in ethanol) and revealed by heating.
- Purification of the products was performed by flash column chromatography with normal phase silica gel (Kieselgur 40-60 µm silica) using an appropriate choice of eluent (or solvent system).

8.1.4 Column chromatography

- Purification of products by column chromatography were performed using an automatic flash chromatography system, CombiFlash[®] R_f; Teledyne-ISCO.

8.1.5 Spectroscopic Data

- Infrared spectra were recorded using a golden gate (ATR) on a Perkin-Elmer FT-IR 1600 spectrometer and reported in the following format ν_{max} frequency (*s*, *strong*; *br*, *broad* and *w*, *weak*) cm^{-1} .
- ^1H and ^{13}C NMR spectra were acquired in CDCl_3 or CD_3OD unless otherwise stated on a Varian VXR-400 (^1H at 400 MHz, ^{13}C at 101 MHz) and reported as follows:
- Chemical shift was reported in the following format; δ (ppm) (number of protons, multiplicity, coupling constant J (Hz), assignment).
- The residual protic solvent was used as internal reference:
 - CHCl_3 $\delta_{\text{H}} = 7.26$ ppm; CDCl_3 $\delta_{\text{C}} = 77.16$ ppm
 - CHD_2OD $\delta_{\text{H}} = 3.31$ ppm, 1.09 ppm; CD_3OD $\delta_{\text{C}} = 49.0$ ppm
- Assignment of stereochemistry was carried out with help of COSY, HSQC, HMBC and NOESY experiments.
- Low Resolution Mass Spectra were obtained on Waters Micromass LCT Mass spectrometer. Gas-Chromatography Mass Spectra (GC-MS) were taken using a Thermo-Finnigan Trace. High-resolution mass spectra (HRMS) were performed on a Thermo-Finnigan LTQ FT Mass Spectrometer by Durham University Mass Spectroscopy service

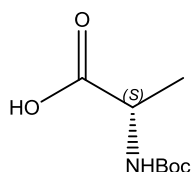
8.1.6 Titration of Organometallic Reagents

- Organolithium (RLi), Grignard reagents (RMgX), and LDA were titrated following a No-D NMR spectroscopy technique reported by Hoye et al.² using cyclooctene (COE) and 1,5-cyclooctadiene (COD) as an internal reference.

8.2 Experimental Procedures

8.2.1 Commercially Available Starting Materials

Boc-L-Ala-OH (100)



Commercially available from Novabiochem

Synonym: *N*-(*tert*-Butoxycarbonyl)-L-alanine, Boc-L-alanine

Molecular Formula: C₈H₁₅NO₄

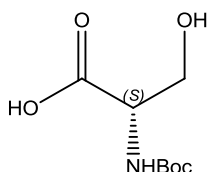
Molecular Weight: 189.21

CAS Number: 15761-38-3

Optical activity: $[\alpha]_D^{23} = -23^\circ$, *c* = 2 in acetic acid

mp: 79-83 °C (lit.)

Boc-L-Ser-OH (200)



Commercially available from Novabiochem

Synonym: *N*-(*tert*-Butoxycarbonyl)-L-Serine, Boc-L-serine

Molecular Formula: C₈H₁₅NO₅

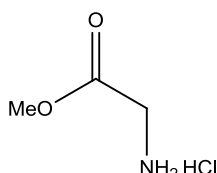
Molecular Weight: 205.21

CAS Number: 3262-72-4

Optical activity: $[\alpha]_D^{23} = -3^\circ$, *c* = 2 in acetic acid

mp: 91 °C (lit.)

NH₂-Gly-OMe HCl (300)



Commercially available from Novabiochem

Synonym: L-Glycine methyl ester hydrochloride

Molecular Formula: C₃H₇NO₂.HCl

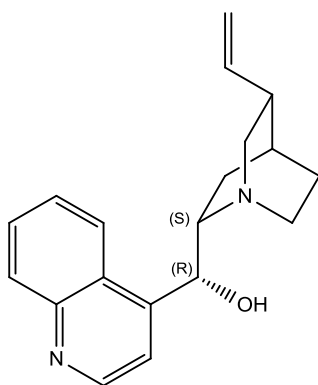
Molecular Weight: 125.55

CAS Number: 5680-79-5

Optical activity: $[\alpha]_D^{23} = -3^\circ$, *c* = 2 in acetic acid

mp: 175 °C (lit.)

(-)-Cinchonidine (301)



Commercially available from Sigma Aldrich

Molecular Formula: C₁₉H₂₂N₂O

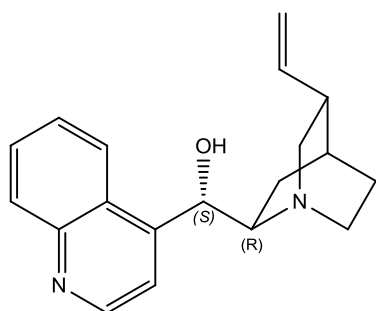
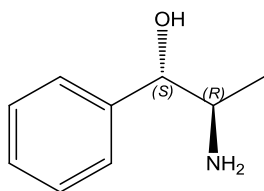
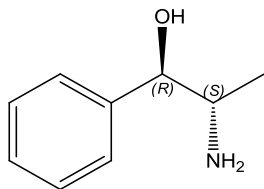
Molecular Weight: 294.39

CAS Number: 485-71-2

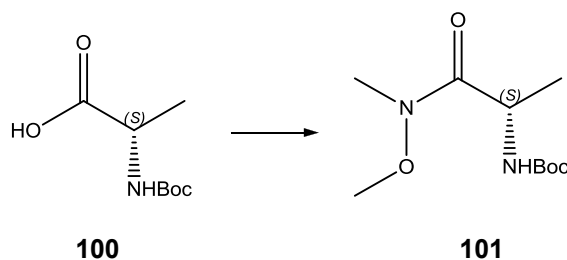
Assay: 96%

Optical activity: $[\alpha]_D^{23} = -106 \pm 4^\circ$, *c* = 1% in ethanol

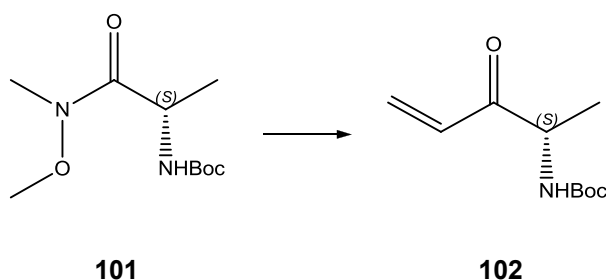
mp: 204-206 °C (lit.)

(+)-Cinchonine (302)**Commercially available from Sigma Aldrich****Molecular Formula:** C₁₉H₂₂N₂O**Molecular Weight:** 294.39**CAS Number:** 118-10-5**Assay:** 85% (15% dihydrocinchonine)**Optical activity:** $[\alpha]_{\text{D}}^{23} = +228^{\circ}$, c = 0.5% in ethanol**mp:** 258-260 °C (lit.)**(1*S*,2*R*)-(+)-Norephedrine (400a)****Commercially available from Sigma Aldrich****Synonym:** (1*S*,2*R*)-2-Amino-1-phenyl-1-propanol**Molecular Formula:** C₉H₁₃NO**Molecular Weight:** 151.21**CAS Number:** 37577-28-9**Optical activity:** $[\alpha]_{\text{D}}^{23} = +40^{\circ}$, c = 7 in 1 M HCl**mp:** 51-54 °C(lit.)**(1*R*,2*S*)-(-)-Norephedrine (400b)****Commercially available from Sigma Aldrich****Synonym:** (1*R*,2*S*)-2-Amino-1-phenyl-1-propanol**Molecular Formula:** C₉H₁₃NO**Molecular Weight:** 151.21**CAS Number:** 37577-28-9**Optical activity:** $[\alpha]_{\text{D}}^{23} = -41^{\circ}$, c = 7 in 1 M HCl**mp:** 51-53 °C(lit.)

8.2.2 Synthesis of Intermediate compounds

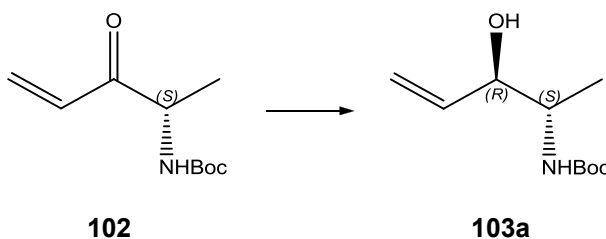
8.2.2.1 4*E*-1-deoxy ceramide analogues**(*S*)-tert-Butyl (1-(methoxy(methyl)amino)-1-oxopropan-2-yl)carbamate (101)³**

Procedure:⁴ To a solution of *N*-(*tert*-butoxycarbonyl)-L-alanine 100 (1.513 g, 8.0 mmol) in anhydrous CH₂Cl₂ (50 ml) was added *N*-methylmorpholine (0.967 ml, 8.8 mmol, 1.1 eq.) and *N*,*O*-dimethylhydroxylamine hydrochloride (0.859 g, 8.8 mmol, 1.1 eq.) at -15 °C. To the reaction mixture was added 1-ethyl-3-(3-dimethylaminopropyl) carbodiimide hydrochloride (1.53 g, 8.8 mmol, 1.1 eq.) over 30 min at the same temperature. The reaction mixture was stirred for 4 hrs then poured into ice and 1N HCl. The resulting mixture was extracted with CH₂Cl₂. The organic layers were combined, and washed with brine, dried over MgSO₄, filtered, and concentrated *in vacuo* to give the crude Weinreb amide as a white solid. Column chromatography on silica gel (from 25 % to 50 % EtOAc in pet. ether) gave 101 (1.69 g, 98 %) as a white solid. ν_{max} (ATR) 3293 (s), 2976, 1703, 1658, 1537, 1293, 1173, 1066, 981 cm⁻¹; δ_H (700 MHz, CDCl₃) 5.24 (1H, m, NH), 4.68 (1H, m, 2-*H*), 3.77 (3H, s, OCH₃), 3.20 (3H, s, NCH₃), 1.44 (9H, s, C(CH₃)₃), 1.31 (3H, d, *J* 6.9, 3-*H*₃); δ_C (176 MHz, CDCl₃) 173.8 C1, 155.3 NHCOO, 79.7 C(CH₃)₃, 61.8 OCH₃, 46.7 C2, 32.3 NCH₃, 28.5 C(CH₃)₃, 18.9 C3; *m/z* (ES⁺) 232.9 [M]⁺ C₁₀H₂₀O₄N₂²³ (Expected: 232.1), 255.1 [M+Na]⁺ C₁₀H₂₀O₄N₂²³Na (Expected: 255.1).

(*S*)-tert-Butyl (3-oxopent-4-en-2-yl)carbamate (102)⁵

Procedure:⁴ Vinyl magnesium bromide (12 ml of 0.6M solution in THF, 7.2 mmol, 4 eq.) was added dropwise at 0 °C to a solution of 101 (400 mg, 1.8 mmol) in anhydrous THF (10 ml). The reaction mixture was allowed to warm up to room temperature. After the reaction mixture was stirred for 1 hr at the same temperature, the reaction mixture was poured into ice cooled 2N HCl. The resulting mixture was extracted with ethyl acetate. The organic layers were combined, washed with brine, dried over MgSO₄, filtered, and concentrated *in vacuo* to give the crude products. Column chromatography on silica gel (from 10 % to 50 % EtOAc in pet. ether) gave 102 (335 mg, 98 %) as a white solid ($R_f \approx 0.37$; EtOAc/pet. ether 25/75). ν_{max} (ATR) 3382 (s), 2975, 2931, 1710, 1694, 1612, 1518, 1282, 1246, 1162, 1003 cm⁻¹; δ_H (700 MHz, CDCl₃) 6.45 (1H, dd, J 17.4, 10.5, 4-*H*), 6.37 (1H, dd, J 17.4, 1.3, 5-*H*_{trans}), 5.88 (1H, d, J 10.5, 1.3, 5-*H*_{cis}), 5.36 (1H, m, *NH*), 4.61 (1H, p, J 7.2, 2-*H*), 1.43 (9H, s, C(CH₃)₃), 1.33 (3H, d, J 7.2, 1-*H*₃); δ_C (176 MHz, CDCl₃) 198.8 C3, 155.3 NHCOO, 132.9 C4, 130.3 C5, 79.8 C(CH₃)₃, 53.2 C2, 28.5 C(CH₃)₃, 18.6 C1; m/z (ES⁺) 222.2 [M+Na]⁺ C₁₀H₁₇O₃N²³Na (Expected: 222.1).

***tert*-Butyl ((2*S*,3*R*)-3-hydroxypent-4-en-2-yl)carbamate (103a)⁶**

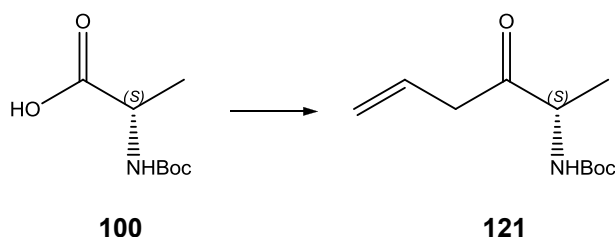


Procedure:⁴ To a solution of 102 (500 mg, 2.5 mmol) in spectrophotometric grade ethanol (31 ml) was added lithium *tri-tert*-butoxy aluminium hydride (1.40 g, 5.5 mmol, 2.2 eq.) at -78 °C. After the reaction mixture was stirred at the same temperature for 2 hrs, 0.1N HCl (15 ml) was added followed by Celite and EtOAc (15 ml). The resulting slurry was filtered through Celite and the filtering bed was washed with EtOAc (15ml). The two phases were separated and the aqueous phase was re-extracted with EtOAc. The organic extracts were combined, washed with NaHCO₃ and brine, dried over MgSO₄, filtered, and concentrated *in vacuo* to give the product as a single diastereoisomer 103a as ascertained by crude ¹H NMR. Column chromatography on silica gel (from 25 % to 50 % ethyl acetate in pet. ether) gave 103a (450 mg, 89 %) as a white solid ($R_f \approx 0.3$; EtOAc/pet. ether 25/75). ν_{max} (ATR) 3351 (br, s), 2986, 2937, 1679, 1529, 1280, 1161, 1021 cm⁻¹; δ_H (700 MHz, CDCl₃) 5.85 (1H, ddd, J 17.2, 10.6, 5.5, 4-*H*), 5.33 (1H, dt, J 17.2, 1.5, 5-*H*_{trans}), 5.23 (1H, dd, J 10.6, 1.5, 5-*H*_{cis}), 4.65 (1H, m, *NH*), 4.22–4.16

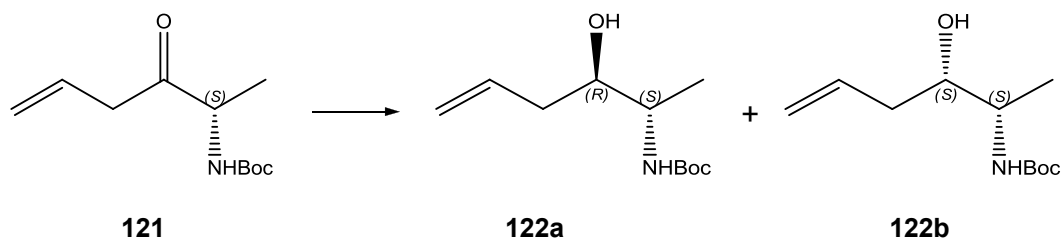
(1H, m, 3-*H*), 3.84 (1H, m, 2-*H*), 1.44 (9H, s, C(CH₃)₃), 1.09 (3H, d, *J* 6.9, 1-*H*₃); δ_C (176 MHz, CDCl₃) 156.5 NHCOO, 137.0 C₄, 116.7 C₅, 79.9 C(CH₃)₃, 75.9 C₃, 50.9 C₂, 28.5 C(CH₃)₃, 15.5 C₁; *m/z* (ES⁺) 224.3 [M+Na]⁺ C₁₀H₁₉O₃N²³Na (Expected: 224.1).

8.2.2.2 5*E*-1-deoxy ceramide analogues

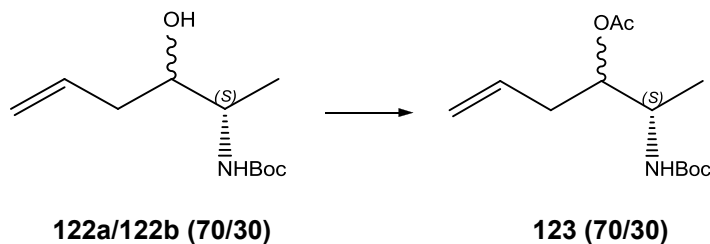
(*S*)-*tert*-Butyl (3-oxohex-5-en-2-yl)carbamate (**121**)⁷⁻⁸



Procedure:⁸ A solution of *n*-BuLi (1.4 M solution in hexanes, 7.2 ml, 10 mmol, 1.0 eq.) was added dropwise at $-10\text{ }^{\circ}\text{C}$ to a solution of *N*-(*tert*-butoxycarbonyl)-L-alanine **100** (1.89 g, 10 mmol) in anhydrous THF (100 ml). The resulting thick gelatinous suspension was stirred at $-10\text{ }^{\circ}\text{C}$ for 30 minutes, cooled to $-78\text{ }^{\circ}\text{C}$ and treated with a solution of allylmagnesium bromide (1.0 M solution in ether, 23.0 ml, 23 mmol, 2.3 eq.). The resultant light grey slurry was stirred for 1 hour at $-78\text{ }^{\circ}\text{C}$, warmed to room temperature over 1 hour, stirred at this temperature for an additional 30 minutes and then poured into a mixture of sat. aq. NH₄Cl solution, ice and ether. The organic layer was separated and the aqueous layer was extracted with ether. The combined organic layers were washed with brine, dried over MgSO₄, filtered and concentrated under *vacuo* to yield the desired product **121** as a crystalline white solid (2.03 g, 9.5 mmol, 95 %). The product was used without further purification (*R_f* \approx 0.80; EtOAc/pet. ether 67/33). ν_{max} (ATR) 3386, 2975, 2932, 1726, 1694, 1642, 1516, 1166 cm⁻¹; δ_H (500 MHz, CDCl₃) 5.91 (1 H, ddt, *J* 17.1, 10.2, 6.9, 5-*H*), 5.15 (3H, m, NH and 6-*H*₂), 4.41–4.31 (1H, m, 2-*H*), 3.34–3.21 (2H, m, 4-*H*₂), 1.43 (9H, s, C(CH₃)₃), 1.33 (3H, d, *J* 7.1, 1-*H*₃); δ_C (126 MHz, CDCl₃) 207.6 C₃, 155.3 NHCOO, 129.9 C₅, 119.5 C₄, 79.9 C(CH₃)₃, 54.9 C₂, 44.2 C₃, 28.5 C(CH₃)₃, 17.8 C₁; *m/z* (ES⁻) 212.1 [M-H]⁻; (ES⁺) 236.2 [M+Na]⁺; HRMS (ES⁺) found [M+Na]⁺ 236.1257, C₁₁H₁₉O₃N²³Na requires *M*⁺ 236.1257.

***tert*-Butyl (2*S*,3*R*)-3-hydroxyhex-5-en-2-ylcarbamate (122a)⁸**

Procedure:⁸ A solution of 121 (2 g, 9.4 mmol) in anhydrous methanol (60 ml) was treated with sodium borohydride (0.72 g, 18.5 mmol, 1.97 eq.) at -78 °C. The resulting mixture was stirred for 90 minutes, carefully quenched by addition of a sat. aq. NH_4Cl solution at -78 °C, warmed to room temperature, and diluted with 1M NaOH solution (24 ml) and ether (60 ml). The organic layer was separated and the aqueous layer was extracted with ether (2×20 ml). The combined organic extracts were washed with brine, dried over MgSO_4 , filtered and concentrated under vacuum to yield the crude product as a white solid consists of a mixture of 122a and 122b. The diastereoisomeric ratio was determined by analysis of the ^1H NMR spectra of the crude product and was found to be 82:18 of 122a:122b. The crude mixture was purified by chromatography (25 % ethyl acetate in pet. ether) to yield 0.73 g of a 70/30 mixture of 122a and 122b followed by 1.14 g of pure 122a with total yield 92 % (1.87 g, 8.7 mmol) (R_f 122a \approx 0.30, R_f 122b \approx 0.32; EtOAc/pet. ether 25/75). 122a; ν_{max} (ATR) 3358 (br, s), 2979, 2940, 1681 (s), 1526 (s), 1174 (s), 1024 (s) cm^{-1} ; δ_{H} (500 MHz, CDCl_3) 5.84 (1H, ddt, J 7.3, 10.3, 14.4, 5-*H*), 5.19–5.09 (2H, m, 6-*H*), 4.75 (1H, br s, *NH*), 3.71 (2H, m, 2-*H* and 3-*H*), 2.38–2.11 (3H, m, *OH*, 4-*H*), 1.44 (9H, s, $\text{C}(\text{CH}_3)_3$), 1.12 (3H, d, J 6.8, 1-*H*); δ_{C} (101 MHz, CDCl_3) 156.0 NHCOO , 134.8 C_5 , 118.2 C_6 , 79.6 $\text{C}(\text{CH}_3)_3$, 73.4 C_3 , 50.4 C_2 , 38.5 C_4 , 28.5 $\text{C}(\text{CH}_3)_3$, 14.7 C_1 ; m/z (ES^+) 238.2 $[\text{M}+\text{Na}]^+$; HRMS (ES^+) found $[\text{M}+\text{Na}]^+$ 238.1414, $\text{C}_{11}\text{H}_{21}\text{O}_3\text{N}^{23}\text{Na}$ requires M^+ 238.1414.

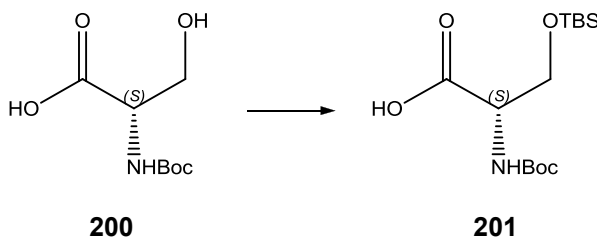
(2*S*)-2-(*tert*-Butoxycarbonylamino)hex-5-en-3-yl acetate (123)

Procedure: To a solution of a (70/30) mixture of the diastereoisomers 122a and 122b (0.7 g, 3.25 mmol) in anhydrous CH_2Cl_2 (40 ml) were added Et_3N (0.91 ml, 6.5 mmol, 2.0 eq.) and a

catalytic amount of DMAP (0.081 g, 0.65 mmol, 0.2 eq.). The reaction mixture was stirred for 5 min followed by dropwise addition of acetic anhydride (0.46 ml, 4.88 mmol, 1.5 eq.). The reaction mixture was stirred overnight at room temperature. Upon completion, the reaction mixture was transferred to an ice bath; 10 ml of 1M HCl were added to the reaction mixture and the two phases were allowed to separate. The aqueous phase was re-extracted with EtOAc (2 × 5 ml). The combined organic extracts were washed with sat. aq. NaHCO₃, brine and dried over MgSO₄ and filtered. The solvent was removed *in vacuo* yielding the crude product as viscous yellow oil. The crude product was purified by chromatography (from 5 % to 25 % ethyl acetate in pet. ether) to give 123 as a (70/30) mixture of two diastereoisomers (0.725 g, 2.82 mmol, 86%) ($R_f \approx 0.40, 0.55$; EtOAc/pet. ether 85/15). ν_{max} (ATR) 3346 (w), 2978, 1710 (s), 1691 (s), 1522, 1455, 1366, 1234 (s), 1173 (s), 1024 cm⁻¹; δ_H (700 MHz, CDCl₃) 5.72 (1H, ddt, J 17.1, 10.1, 7.1, 5-*H*), 5.07 (1H, d, J 17.1, 6-*H*_{trans}), 5.04 (1H, d, J 10.1, 6-*H*_{cis}), 4.90 (0.7H, ddd, J 8.0, 5.5, 4.3, 3-*H*), 4.87–4.83 (0.3H, m, *minor* 3-*H*), 4.65–4.54 (1H, m, NH), 3.91–3.80 (1H, m, 2-*H*), 2.35–2.22 (2H, m, 4-*H*₂), 2.06–1.99 (3H, m, OCOCH₃), 1.48–1.37 (9H, m, C(CH₃)₃), 1.12–1.05 (3H, m, 1-*H*₃); δ_C (176 MHz, CDCl₃) 170.81 (*minor* 170.59), 155.47 (*minor* 155.20), 133.45 (*minor* 133.22), 118.31 (*minor* 118.00), 79.50 (*minor* 79.44), 75.79 (*minor* 75.48), 48.12 (*minor* 48.07), 36.28 (*minor* 35.69), 28.48, 21.17 (*minor* 18.75), 15.51 (*minor* 14.30); m/z (ES⁺) 280.1 [M+Na]⁺; HRMS (ES⁺) found [M+Na]⁺ 280.1519, C₁₃H₂₃O₄N²³Na requires M^+ 280.1519.

8.2.2.3 Ceramide analogues

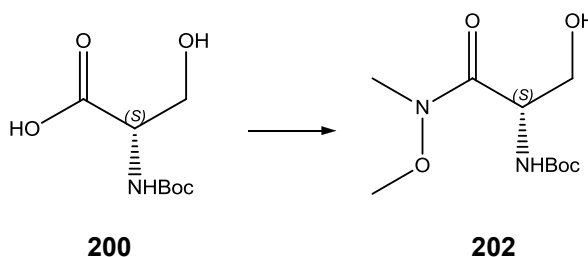
(*S*)-2-((*tert*-Butoxycarbonyl)amino)-3-((*tert*-butyldimethylsilyl)oxy)propanoic acid (**201**)^{4,8}



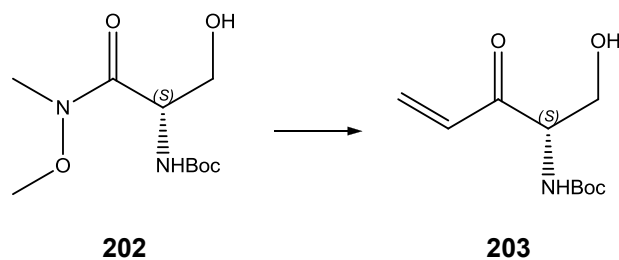
Procedure:⁸ To a solution of *N*-(*tert*-butoxycarbonyl)-L-serine **200** (512 mg, 2.5 mmol) in anhydrous DMF (12 mL), imidazole (509 mg, 7.5 mmol, 3 eq.) was added and the reaction mixture was cooled to 0 °C followed by addition of TBSCl (490 mg, 3.25 mmol, 1.3 eq.). The resulting mixture was slowly warmed to room temperature and stirred overnight and followed by TLC. Upon total consumption of the starting material (monitored by TLC), the reaction mixture

was poured into a mixture of ice cooled 1N HCl (5 mL) and ether (20 mL) to hydrolyze the silyl ester. The organic layer was separated and the aqueous layer was extracted with ether (2 × 20 ml). The combined organic extracts were washed with brine, dried over MgSO₄, filtered and concentrated under vacuum to yield the desired product as pale yellow sticky oil (630 mg, 1.97 mmol, 79 %). ν_{max} (ATR) 3380-3492 (br), 3451 (s), 2952, 2569, 1724, 1691, 1505 cm⁻¹; δ_H (200 MHz, CDCl₃) 8.49 (1H, br s, acidic OH), 5.35 (1H, br d, J 8.2, NH), 4.36 (1H, m, 2-*H*), 4.09 (1H, A of ABX syst., m, 3-*HH*), 3.83 (1H, B of ABX syst., dd, J 10.1, 3.5, 3-*HH*), 1.44 (9H, s, OC(CH₃)₃), 0.86 (9H, s, SiC(CH₃)₃), 0.03, 0.2 (2 × 3H, s, SiCH₃); δ_C (75 MHz, CDCl₃) 175.3 COOH, 155.5 NHCOO, 80.1 OC(CH₃)₃, 63.7 C3, 55.6 C2, 28.2 OC(CH₃)₃, 25.7 SiC(CH₃)₃, 18.4 SiC(CH₃)₃, -5.5 SiCH₃, -5.6 SiCH₃; m/z (ES⁺) 320.3 [M+H]⁺ C₁₄H₃₀O₅N (Expected: 320.2).

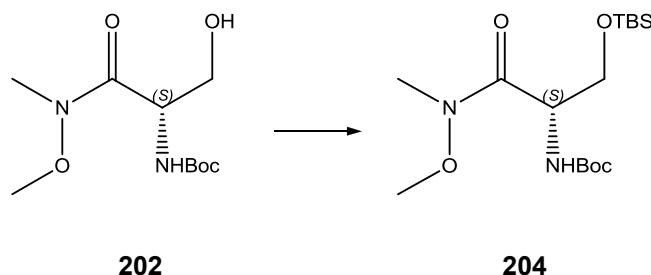
(*S*)-*tert*-Butyl (3-hydroxy-1-(methoxy(methyl)amino)-1-oxopropan-2-yl)carbamate (202)^{4,9}



Procedure:⁴ To a solution of *N*-(*tert*-butoxycarbonyl)-L-serine 200 (3.075 g, 15 mmol) in anhydrous CH₂Cl₂ (100 ml) was added *N*-methylmorpholine (1.812 ml, 16.5 mmol, 1.1 eq.) and *N,O*-dimethylhydroxylamine hydrochloride (1.610 g, 16.5 mmol, 1.1 eq.) at -15 °C. To the reaction mixture was added 1-ethyl-3-(3-dimethylaminopropyl)carbodiimide hydrochloride (2.874 g, 16.5 mmol, 1.1 eq.) over 30 min at the same temperature. The reaction mixture was stirred for 4 hrs then poured into ice and 1N HCl. The resulting mixture was extracted with CH₂Cl₂. The organic layers were combined, and washed with brine, dried over MgSO₄, filtered, and concentrated *in vacuo* to give the crude Weinreb amide 202 (3.400 gm, 91%) as a colourless solid. The crude product was at high purity and was used directly without further purification. ν_{max} (ATR) 3329, 2935, 1715, 1665, 1498, 1173 cm⁻¹; δ_H (500 MHz, CDCl₃) 5.57 (1H, br s, NH), 4.89–4.74 (1H, m, 2-*H*), 3.86–3.79 (2H, m, 3-*H*₂), 3.78 (3H, s, OCH₃), 3.24 (3H, s, NCH₃), 2.49 (1H, br s, OH), 1.45 (9H, s, C(CH₃)₃); δ_C (126 MHz, CDCl₃) 170.9 C1, 156.0 NHCOO, 80.3 C(CH₃)₃, 64.1 C3, 61.8 OCH₃, 52.5 C2, 31.1 NCH₃, 28.5 C(CH₃)₃; m/z (ES⁺) 271.2 [M+Na]⁺ C₁₀H₂₀O₅N₂²³Na (Expected: 271.1).

(*S*)-tert-Butyl (1-hydroxy-3-oxopent-4-en-2-yl)carbamate (203)¹⁰

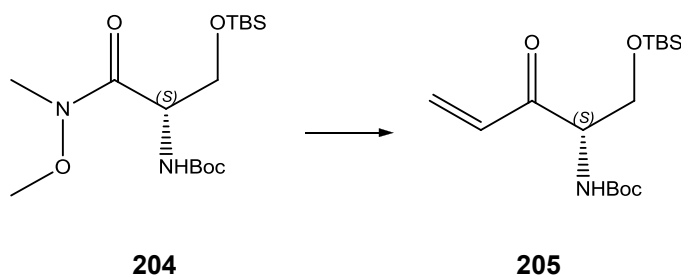
Procedure:⁴ A (0.6 M) solution of vinyl magnesium bromide (*c.a.* 22 ml, 12.9 mmol, 4 eq.) in THF was added dropwise at 0 °C to a solution of 202 (800 mg, 3.23 mmol) in anhydrous THF (30 ml). The reaction mixture was allowed to warm up to room temperature. After the reaction mixture was stirred for 1 hr at the same temperature, the reaction mixture was poured into ice cooled 2N HCl. The resulting mixture was extracted with ethyl acetate. The organic layers were combined, washed with brine, dried over MgSO₄, filtered, and concentrated in vacuo to give the crude products. Column chromatography on silica gel (from 40% to 80% EtOAc in pet. ether) gave 203 (510 mg, 73%) as a sticky oil (*R_f* ≈ 0.30; EtOAc/pet. ether 67/33). ν_{max} (ATR) 3384, 2978, 1681, 1501, 1366, 1162 cm⁻¹; δ_H (400 MHz, CDCl₃) 6.57 (1H, dd, *J* 17.4, 10.5, 4-*H*), 6.43 (1H, dd, *J* 17.4, 1.1, 5-*H_{trans}*), 5.92 (1H, dd, *J* 10.5, 1.1, 5-*H_{cis}*), 5.72 (1H, br s, NH), 4.66 (1H, s, 2-*H*), 4.00–3.80 (2H, m, 1-*H₂*), 2.91 (1H, br s, OH), 1.44 (9H, s, C(CH₃)₃); δ_C (101 MHz, CDCl₃) 196.6, 156.2, 132.9, 130.8, 80.6, 63.8, 60.0, 28.4; *m/z* (ES⁺) 238.0 [M+Na]⁺ C₁₀H₁₇O₄N²³Na (Expected: 238.1).

(*S*)-tert-Butyl (3,8,8,9,9-pentamethyl-4-oxo-2,7-dioxa-3-aza-8-siladecan-5-yl)carbamate (204)⁴

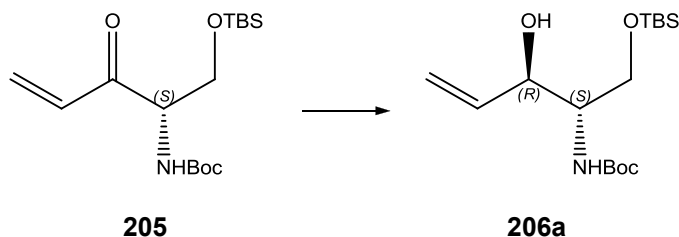
Procedure:⁹ To a solution of 202 (500 mg, 2.02 mmol) in anhydrous DMF (2.5 mL) were added imidazole (410 mg, 6.12 mmol, 3 eq.) and a catalytic amount of DMAP (25 mg, 0.2 mmol, 0.1 eq.) at 0 °C followed by addition of a solution of TBSCl (349 mg, 2.32 mmol, 1.15 eq.) in anhydrous DMF (2.5 ml). The resulting mixture was allowed to warm up to room

temperature, stirred overnight, and poured into sat. aq. NH_4Cl solution (5 ml) and extracted with CH_2Cl_2 (3×20 ml). The combined organic extracts were washed with brine, dried over MgSO_4 , filtered and concentrated under vacuum to yield the crude product as yellowish viscous oil. Column chromatography on silica gel (from 25% to 50% EtOAc in pet. ether) gave 204 (650 mg, 1.80 mmol, 89%) as a sticky oil ($R_f \approx 0.25$; EtOAc/pet. ether 25/75). ν_{max} (ATR) 2931, 2857, 2350, 1711, 1661, 1494, 1468, 1168, 1111, 837 cm^{-1} ; δ_{H} (700 MHz, CDCl_3) 5.35 (1H, br d, J 8.5, NH), 4.80–4.70 (1H, m, 5- H), 3.84 (1H, dd, J 9.4, 4.5, 6- HH), 3.78 (1H, dd, J 9.7, 4.5, 6- HH), 3.74 (3H, s, 1- H_3), 3.20 (3H, s, NCH_3), 1.43 (9H, s, $\text{C}(\text{CH}_3)_3$), 0.85 (9H, s, $\text{SiC}(\text{CH}_3)_3$), 0.02, 0.01 ($2 \times 3\text{H}$, s, SiCH_3); δ_{C} (176 MHz, CDCl_3) 170.9, 155.5, 79.7, 63.7, 61.6, 52.6, 32.3, 28.5, 25.9, -5.4, -5.4; m/z (ES^+) 385.2 $[\text{M}+\text{Na}]^+$ $\text{C}_{16}\text{H}_{34}\text{O}_5\text{N}_2^{28}\text{Si}^{23}\text{Na}$ (Expected: 385.1).

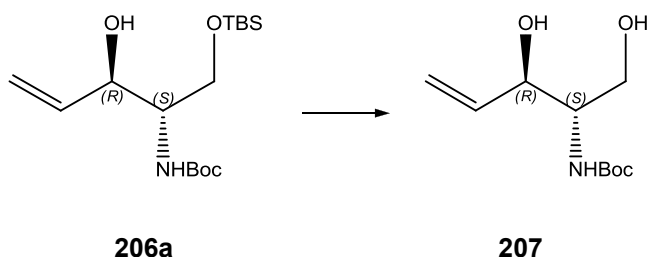
(*S*)-*tert*-Butyl (1-((*tert*-butyldimethylsilyl)oxy)-3-oxopent-4-en-2-yl)carbamate (205)⁴



Procedure:⁴ A (0.6 M) solution of vinyl magnesium bromide (*c.a.* 11 ml, 6.64 mmol, 4 eq.) in THF was added dropwise at 0 °C to a solution of 204 (600 mg, 1.66 mmol) in anhydrous THF (10 ml). The reaction mixture was allowed to warm up to room temperature. After the reaction mixture was stirred for 1 hour at the same temperature, the reaction mixture was poured into ice cooled 2N HCl. The resulting mixture was extracted with ethyl acetate. The organic layers were combined, washed with brine, dried over MgSO_4 , filtered, and concentrated in vacuo to give the crude products. Column chromatography on silica gel (from 5% to 20% EtOAc in pet. ether) gave 205 (920 mg, 84%) as a viscous oil ($R_f \approx 0.78$; EtOAc/pet. ether 25/75). ν_{max} (ATR) 3460, 2865, 1695, 1489, 1359, 1173 cm^{-1} ; δ_{H} (700 MHz, CDCl_3) 6.55 (1H, dd, J 17.5, 10.7, 4- CH), 6.34 (1H, dd, J 17.5, 1.0, 5- CH_{trans}), 5.83 (1H, d, J 10.7, 1.0, 5- CH_{cis}), 5.52 (1H, br d, J 6.8, NH), 4.63–4.56 (1H, m, 2- CH), 4.00 (1H, dd, J 10.2, 3.1, 1- CHH), 3.85 (1H, dd, J 10.2, 4.4, 1- CHH), 2.04 (1H, s, OH), 1.44 (9H, s, $\text{C}(\text{CH}_3)_3$), 0.83 (9H, s, $\text{SiC}(\text{CH}_3)_3$), 0.02, 0.01 ($2 \times 3\text{H}$, s, SiCH_3); δ_{C} (176 MHz, CDCl_3) 196.8, 155.3, 133.1, 129.3, 79.7, 63.4, 59.5, 28.3, 25.7, 18.2, -5.6; m/z (ES^+) 330.5 $[\text{M}+\text{H}]^+$ $\text{C}_{16}\text{H}_{32}\text{O}_4\text{N}_1^{28}\text{Si}$ (Expected: 330.2).

***tert*-Butyl ((2*S*,3*R*)-1-((*tert*-butyldimethylsilyl)oxy)-3-hydroxypent-4-en-2-yl)carbamate (206a)⁴**

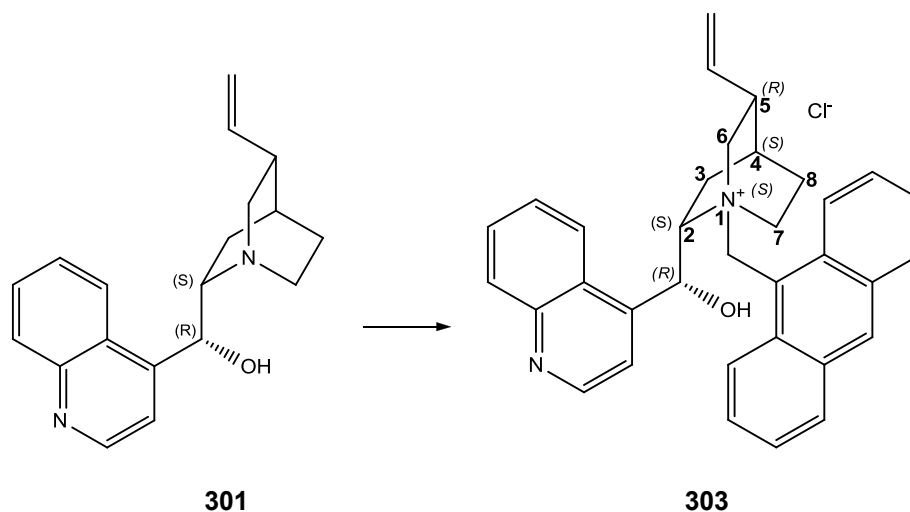
Procedure:⁴ To a solution of the enone 205 (910 mg, 2.77 mmol) in spectrophotometric grade ethanol (35 ml) was added lithium *tri-tert*-butoxy aluminium hydride (1.546 g, 6.1 mmol, 2.2 eq.) at -78 °C. After the reaction mixture was stirred at the same temperature for 2 hrs, 0.1N HCl (16.5 ml) was added followed by Celite and EtOAc (16.5 ml). The resulting slurry was filtered through Celite and the residue was washed with EtOAc (16.5ml). The two phases were separated and the aqueous phase re-extracted with EtOAc. The organic extracts were combined, washed with NaHCO_3 and brine, dried over MgSO_4 , filtered, and concentrated *in vacuo* to give the crude product as a single diastereomer (206a) as indicated by the ^1H NMR analysis. Column chromatography on silica gel (from 20% to 50% ethyl acetate in pet. ether) gave 206a (870 mg, 95%) as a viscous oil ($R_f \approx 0.40$; EtOAc/pet. ether 25/75). ν_{max} (ATR) 3445, 2940, 1699, 1494, 1168, 840 cm^{-1} ; δ_{H} (500 MHz, CDCl_3) 5.91 (1H, ddd, J 17.1, 10.6, 4.9, 4-*H*), 5.37 (1H, dd, J 17.1, 1.6, 5-*H*_{trans}), 5.27 (1H, br d, J 7.9, *NH*), 5.23 (1H, dd, J 10.6, 1.6, 5-*H*_{cis}), 4.29–4.22 (1H, m, 3-*H*), 3.91 (1H, dd, J 10.4, 2.9, 1-*HH*), 3.74 (1H, dd, J 8.3, 2.9 1-*HH*), 3.65–3.58 (1H, br s, *OH*), 3.47 (1H, m, 2-*H*), 1.44 (9H, s, $\text{OC}(\text{CH}_3)_3$), 0.88 (9H, s, $\text{SiC}(\text{CH}_3)_3$), 0.05, 0.04 ($2 \times 3\text{H}$, s, SiCH_3); δ_{C} (126 MHz, CDCl_3) 155.9, 138.0, 115.9, 79.7, 74.9, 63.6, 54.2, 28.5, 28.5, 25.9, 25.9, 18.2, -5.52, -5.54; m/z (ES^+) 332.4 $[\text{M}+\text{H}]^+$ $\text{C}_{16}\text{H}_{33}\text{O}_4\text{N}_1\text{Si}_1$ (Expected: 332.2), 354.4 $[\text{M}+\text{Na}]^+$ $\text{C}_{16}\text{H}_{33}\text{O}_4\text{N}_1^{28}\text{Si}^{23}\text{Na}$ (Expected: 354.2).

***tert*-Butyl ((2*S*,3*R*)-1,3-dihydroxypent-4-en-2-yl)carbamate (207)⁴**

Procedure: A solution of 206a (100 mg, 0.3 mmol) in methanol (1.5 ml) was treated with 2N HCl (150 μ l) dropwise at -0 $^{\circ}$ C. The resulting mixture was stirred for 15 minutes at the same temperature and monitored by TLC. Upon complete consumption of the starting material, the reaction was quenched by addition of a brine solution (5 ml) and extracted with EtOAc (2×10 ml). The combined organic layers were washed with brine, dried over $MgSO_4$, filtered and concentrated under vacuum to yield the crude product. Column chromatography on silica gel (from 25% to 50% ethyl acetate in pet. ether and elution with MeOH) gave 207 (60 mg, 2.76 mmol, 92 %) as viscous oil ($R_f \approx 0.13$; EtOAc/pet. ether 50/50). ν_{max} (ATR) 3456, 2931, 1705, 1510, 1177, 842 cm^{-1} ; δ_H (700 MHz, $CDCl_3$) 5.94 (1H, ddd, J 16.9, 10.6, 5.3, 4-*H*), 5.40 (1H, d, J 16.9, 5-*H*_{trans}), 5.35 (1H, br s, NH), 5.27 (1H, d, J 10.6, 5-*H*_{cis}), 4.39 (1H, br s, 3-*H*), 3.93 (1H, dd, J 11.2, 3.5, 1-*HH*), 3.74–3.68 (1H, m, 1-*HH*), 3.68–3.61 (1H, m, 2-*H*), 2.85 (1H, app d, J 4.5, 3-*OH*), 2.57 (1 H, br s, 1-*OH*), 1.45 (9H, s, $C(CH_3)_3$); δ_C (176 MHz, $CDCl_3$) 156.3, 137.6, 116.7, 80.1, 75.1, 62.7, 55.1, 28.5; m/z (ES^+) 240.4 $[M+Na]^+$ $C_{10}H_{19}O_4N^{23}Na$ (Expected: 240.1).

8.2.2.4 4*E*-3-deoxy-ceramide analogues

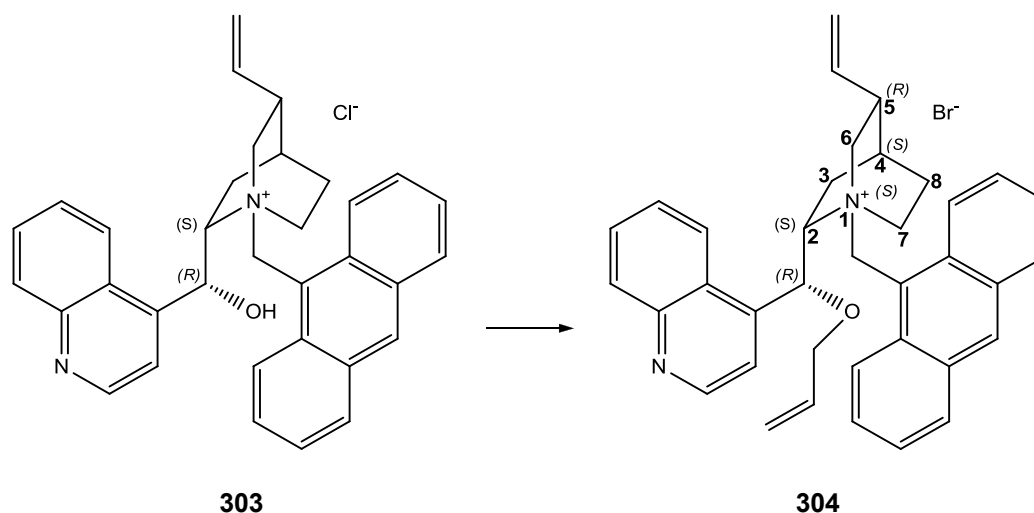
(1*S*,2*S*,4*S*,5*R*)-1-(Anthracen-9-ylmethyl)-2-((*R*)-hydroxy(quinolin-4-yl)methyl)-5-vinyl-1-azoniabicyclo[2.2.2]octane chloride (303)¹¹



Procedure:¹¹ To a suspension of cinchonidine 301 (294 mg, 1.0 mmol) in toluene (4 ml) was added 9-(chloromethyl)anthracene (237 mg, 1.05 mmol, 1.05 eq.), and the mixture was stirred at reflux 110 $^{\circ}$ C for 3 hrs. The mixture was cooled to room temperature, poured into 20 ml of ether. The solid residue was collected by centrifugation and decantation of the liquid phase. The

residue was washed by ether (2 × 20 ml) and collected by centrifugation. The mother liquor was concentrated *in vacuo* and the residue was dissolved in CH₂Cl₂/ether and kept at -20 °C to precipitate another fraction of the product. The combined solid residue was recrystallized from CH₂Cl₂/ether and kept at -20 °C to afford 303 (460 mg, 0.88 mmol, 88%) as light yellow solid (*R_f* ≈ 0.30; CH₂Cl₂/MeOH 93/7). δ_{H} (400 MHz, CDCl₃, 20 mg/ml)¹² 8.97 (1H, d, *J* 8.4), 8.86 (1H, d, *J* 4.3), 8.79 (2H, d, *J* 8.9), 8.17 (1H, d, *J* 4.9), 8.06–8.01 (2H, m, *J* 4.7), 7.71 (1H, d, *J* 8.2), 7.68–7.64 (1H, m), 7.61 (1H, d, *J* 7.8), 7.47–7.40 (1H, m), 7.29–7.21 (4H, m), 7.19–7.09 (1H, m), 7.09–7.04 (1H, m), 6.74 (2H, s), 5.42 (1H, ddd, *J* 16.8, 10.5, 6.1), 5.21 (1H, d, *J* 16.8), 4.90 (1H, dd, *J* 10.5, 1.4), 4.85–4.73 (1H, m), 4.72–4.58 (1H, m), 3.97 (1H, d, *J* 13.0), 2.58 (1H, dd, *J* 12.9, 10.6), 2.47 (1H, app. t, *J* 12.6), 2.18–2.06 (1H, m), 1.95–1.77 (2H, m), 1.77–1.56 (1H, m), 1.22–1.11 (1 H, m), 1.11–0.95 (1H, m); δ_{C} (176 MHz, CDCl₃) 149.01, 136.52, 133.38, 132.76, 131.21, 130.45, 130.39, 128.98, 128.86, 128.38, 127.76, 127.46, 127.23, 125.98, 125.73, 124.93, 124.91, 124.38, 124.06, 120.26, 118.26, 117.86, 67.22, 67.18, 61.58, 54.98, 50.66, 38.64, 25.99, 25.81, 23.50; *m/z* (ES⁺) 485.5 [M]⁺ C₃₄H₃₃ON₂ (Expected: 485.3).

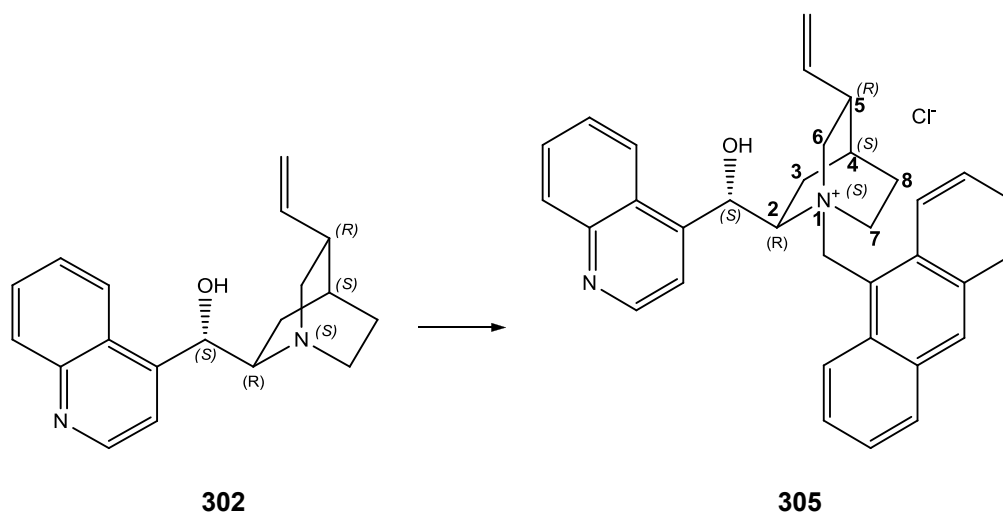
(1*S*,2*S*,4*S*,5*R*)-2-((*R*)-Allyloxy(quinolin-4-yl)methyl)-1-(anthracen-9-ylmethyl)-5-vinyl-1-azoniabicyclo[2.2.2]octane bromide (304)¹¹



Procedure:¹¹ To a suspension of 303 (200 mg, 0.39 mmol) in CH₂Cl₂ (5 ml) was added allyl bromide (100 μ l, 1.17 mmol, 3.05 eq.) and 50% aq. KOH solution (200 μ l, 1.9 mmol, 5 eq.). The resulting mixture was stirred vigorously at room temperature for 4 hrs. The mixture was diluted with water (6.25 ml) and extracted with CH₂Cl₂ (3 × 5 ml). The combined organic extracts were dried over MgSO₄, filtered and concentrated *in vacuo*. Recrystallization of the residue from MeOH/ether at -20 °C afforded the desired product 304 (190 mg, 0.32 mmol, 84%) as an orange

solid. δ_{H} (700 MHz, CD_3OD , 25 mg/ml)¹² 9.07 (1H, d, J 4.4), 8.93 (1H, s), 8.77 (1H, d, J 9.0), 8.63–8.56 (1H, m), 8.48 (1H, d, J 9.1), 8.31–8.26 (2H, m), 8.25 (1H, d, J 8.3), 8.01–7.93 (3H, m, J 15.0, 7.2), 7.83 (1H, dd), 7.79 (1H, dd, J 8.5, 7.2), 7.68 (2H, dd, J 14.4, 6.3), 6.98 (1H, s), 6.44 (2H, ddd, J 15.9, 11.0, 5.6), 5.92 (1H, d, J 13.9), 5.76–5.67 (2H, m), 5.58 (1H, d, J 10.4), 5.06–4.98 (2H, m, J 13.2), 4.59–4.52 (2H, m, J 13.0, 6.0), 4.51–4.42 (2H, m), 3.80 (1H, d, J 13.0), 3.30–3.24 (1H, m), 2.94 (1H, td, J 11.6, 5.1), 2.54–2.42 (2H, m, J 23.5, 13.6), 2.21 (1H, s), 2.00 (1H, s), 1.70–1.58 (2H, m); δ_{C} (176 MHz, CD_3OD) 151.05, 149.38, 142.94, 138.50, 134.80, 134.67, 134.61, 133.94, 133.10, 133.04, 131.52, 131.31, 131.18, 130.66, 129.41, 129.26, 127.08, 126.66, 126.57, 125.28, 124.88, 121.65, 119.12, 117.80, 71.44, 70.12, 63.55, 57.42, 53.69, 49.53, 39.48, 27.30, 26.26, 23.31; m/z (ES^+) 525.5 [$\text{M}]^+$ $\text{C}_{37}\text{H}_{37}\text{ON}_2$ (Expected: 525.3).

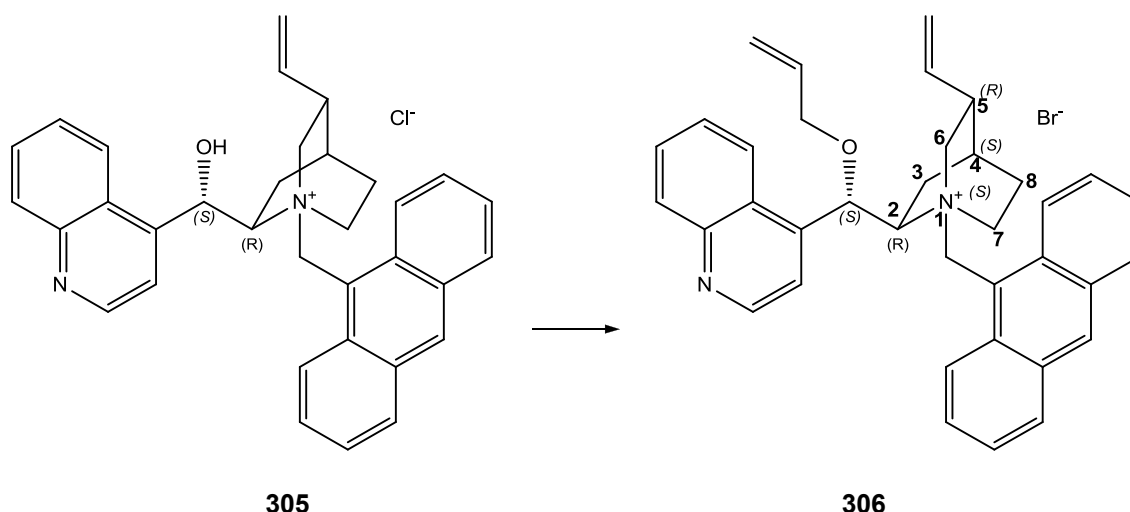
(1*S*,2*R*,4*S*,5*R*)-1-(Anthracen-9-ylmethyl)-2-((*S*)-hydroxy(quinolin-4-yl)methyl)-5-vinyl-1-azoniabicyclo[2.2.2]octane chloride (305)¹²



Procedure:¹² To a suspension of cinchonine 302 (294 mg, 1.0 mmol) in toluene (4 ml) was added 9-(chloromethyl)anthracene (237 mg, 1.05 mmol, 1.05 eq.), and the mixture was stirred at reflux 110 °C for 4 days. The mixture was cooled to room temperature, poured into 20 ml of ether. The solid residue was collected by centrifugation and decantation of the liquid phase. The residue was washed by ether (2 × 20 ml) and collected by centrifugation. The mother liquor was concentrated *in vacuo* and the residue was dissolved in CH_2Cl_2 /ether and kept at –20 °C to precipitate another fraction of the product. The combined solid residue was recrystallized from CH_2Cl_2 /ether and kept at –20 °C to afford 305 (250 mg, 0.48 mmol, 48%) as light yellow solid ($R_f \approx 0.30$; $\text{CH}_2\text{Cl}_2/\text{MeOH}$ 93/7). δ_{H} (700 MHz, CDCl_3 , 25 mg/ml)¹² 9.24 (1H, d, J 8.6), 8.92 (1H, d, J 6.7), 8.81 (1H, s), 8.41 (1H, d, J 8.7), 8.20 (1H, s), 8.02 (1H, d, J 3.7), 7.85 (1H, s),

7.55 (1H, d, J 8.1), 7.53 (1H, d, J 8.3), 7.45 (1H, d, J 8.2), 7.27–7.23 (1H, m), 7.21–7.16 (2H, m), 7.11–7.06 (1H, m, J 6.7), 7.06–7.02 (1H, m, J 7.2), 6.98–6.89 (3H, m), 6.46 (1H, d, J 13.7), 5.56 (1H, ddd, J 17.2, 10.5, 6.6), 5.00 (1H, d, J 10.5), 4.84 (1H, d, J 17.3), 4.75–4.68 (1H, m), 4.44–4.36 (1H, m), 4.24 (1H, t, J 11.5), 2.45 (2H, t, J 12.0), 2.30 (1H, dd, J 20.5, 10.7), 1.92 (1H, t, J 12.6), 1.73–1.64 (2H, m, J 23.5, 10.1), 1.49 (1H, s), 1.34 (1H, t, J 11.1), 0.65 – 0.57 (1H, m); δ_{H} (176 MHz, CDCl_3) 149.4, 147.0, 145.6, 135.6, 133.1, 132.8, 130.9, 130.4, 130.1, 129.0, 128.5, 128.2, 127.6, 127.3, 126.9, 124.9, 124.9, 124.61, 120.1, 118.1, 117.5, 67.8, 66.8, 57.6, , 54.3, 54.0, 38.1, 26.4, 24.1, 22.7; m/z (ES^+) 485.8 [M] $^+$ $\text{C}_{34}\text{H}_{33}\text{ON}_2$ (Expected: 485.3).

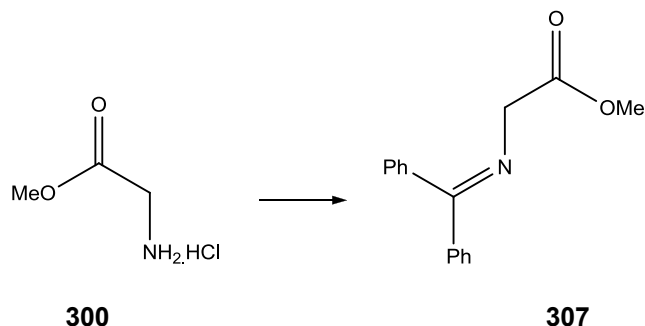
(1*S*,2*R*,4*S*,5*R*)-2-((*S*)-Allyloxy(quinolin-4-yl)methyl)-1-(anthracen-9-ylmethyl)-5-vinyl-1-azoniabicyclo[2.2.2]octane bromide (306)¹³



Procedure:¹¹ To a suspension of 305 (272 mg, 0.52 mmol) in CH_2Cl_2 (7 ml) was added allyl bromide (141 μl , 1.63 mmol, 3.05 eq.) and 50% aq. KOH solution (286 μl , 2.6 mmol, 5 eq.). The resulting mixture was stirred vigorously at room temperature for 4 hrs. The mixture was diluted with water (9 ml) and extracted with CH_2Cl_2 (3×7 ml). The combined organic extracts were dried over MgSO_4 , filtered and concentrated *in vacuo*. Recrystallization of the residue from MeOH/ether at -20 °C afforded the desired product 306 (275 mg, 0.45 mmol, 87%) as orange solid. δ_{H} (700 MHz, CD_3OD , 18 mg/ml)¹² 9.04 (1H, d, J 4.0), 9.01 (1H, d, J 9.0), 8.77 (2H, m), 8.27 (1H, d, J 8.7), 8.20–8.14 (3H, m), 8.00 (1H, s), 7.94–7.90 (2H, m), 7.84–7.79 (1H, m), 7.70–7.66 (1H, m), 7.62 – 7.57 (2H, m, J 10.4, 5.4), 6.90 (1H, s), 6.46–6.38 (1H, m), 6.13–5.99 (2H, m), 5.93 (1H, ddd, J 17.2, 10.6, 6.9), 5.72 (1H, d, J 17.2), 5.63 (1H, d, J 10.6), 5.19 (1H, d, J 10.5), 5.04 (1H, d, J 17.3), 4.58 (1H, m), 4.55 (1H, dd, J 12.8, 6.0), 4.41–4.34 (3H, m), 3.11 (1H, app. t, J 11.5), 2.77 (1H, m), 2.55–2.50 (1H, m), 2.25–2.14 (1H, m), 1.85–1.78 (2H, m),

1.64–1.55 (1H, m), 1.20–1.12 (1H, m), 0.70 (0.45H, t, J 7.4); m/z (ES^+) 525.7 [M] $^+$ $C_{37}H_{37}ON_2$ (Expected: 525.3).

Methyl 2-((diphenylmethylene)amino)acetate (307)¹⁴



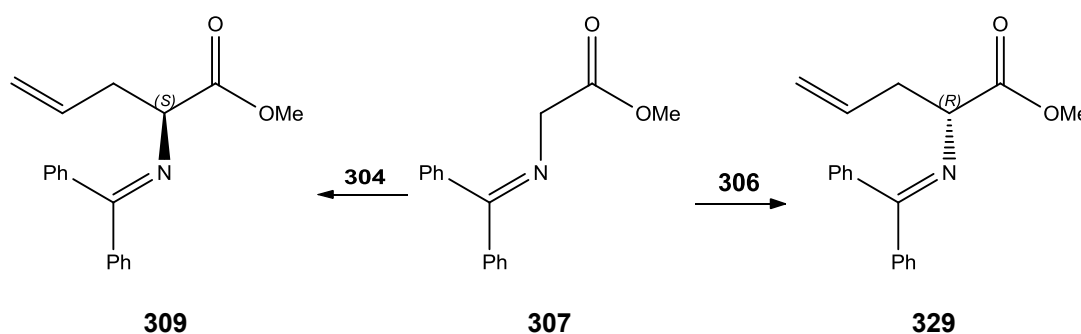
Procedure:¹⁴ To a suspension of methyl glycine hydrochloride 300 (753 mg, 6 mmol) in anhydrous CH_2Cl_2 (20 ml), an equimolar amount of benzophenone imine (1 ml, 6 mmol) was added and the reaction mixture was stirred at room temperature for 24 hr. The reaction mixture was filtered to remove NH_4Cl and evaporated to dryness on a rotary evaporator. The residue was dissolved in 20 mL of ether, filtered, washed with 20 mL of water, and dried over $MgSO_4$ to yield the crude product. Column chromatography on silica gel (from 10% to 50% ethyl acetate in pet. ether) gave 307 (1.221 g, 4.8 mmol, 80 %) as white waxy solid ($R_f \approx 0.33$; EtOAc/pet. ether 33/67). ν_{max} (ATR) 2948, 2890, 2361, 1970, 1752, 1622, 1573, 1384, 1195, 682 cm^{-1} ; δ_H (700 MHz, $CDCl_3$) 7.66 (2H, m, ArH), 7.49–7.42 (3H, m, ArH), 7.40 (1H, m, Ar'H), 7.33 (2H, m, Ar'H), 7.18 (2H, m, Ar'H), 4.22 (2H, s 2- H_2), 3.74 (3H, s, OCH₃); δ_C (176 MHz, $CDCl_3$) 172.0, 171.2, 139.3, 136.0, 130.6, 128.9, 128.9, 128.8, 128.2, 127.8, 55.7, 52.1; m/z (ES^+) 254.4 [$M+H$] $^+$ $C_{16}H_{16}O_2N$ (Expected: 254.1).

8.2.3 General Procedure for Phase Transfer Catalysis^{11, 15}

To an ice cooled solution of the Schiff base 307 in Toluene/CH₂Cl₂ (7:3 v/v), the cinchona catalyst 304 or 306 was added (5 mol%) followed by dropwise addition of allyl bromide (5.0 eq.) at 0 °C. The reaction mixture was stirred for 5 min before the dropwise addition of 50% aq. KOH (5 eq.). The reaction was stirred vigorously overnight from 0°C to room temperature. The reaction was monitored by TLC and upon completion; the reaction mixture was diluted with water (10 ml) and extracted with EtOAc (3 × 5 ml). The organics were dried over MgSO₄, filtered, and evaporated in vacuo, affording the crude products.

(*S*)-Methyl 2-((diphenylmethylene)amino)pent-4-enoate (309)¹¹

(*R*)-Methyl 2-((diphenylmethylene)amino)pent-4-enoate (329)



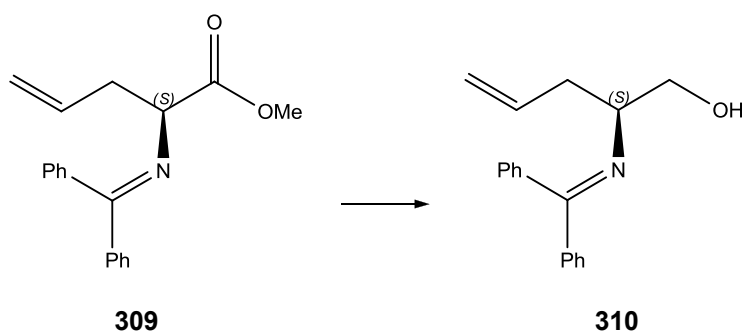
The asymmetric syntheses of 309 and 329 were carried out according to the general procedure mentioned above. However, the racemic mixture preparation was accomplished following the protocol described below.

Procedure:¹⁶⁻¹⁷ To a solution of the Schiff base 307 (80 mg, 0.32 mmol) in anhydrous THF (3 ml) was added a (1.8 M) solution of LDA (200 μ l, 0.35 mmol, 1.1 eq.) in THF at -78 °C. The reaction mixture was stirred for 30 min at the same temperature followed by addition of the allyl bromide (30 μ l, 0.33 mmol, 1.05 eq.). The reaction mixture was stirred for 60 min at -78 °C after which it was allowed to warm up to room temperature. The reaction was poured into ice water and extracted with EtOAc (3 × 5 ml). The organics were dried over MgSO₄, filtered, and evaporated in vacuo, affording the crude product (50 mg, 0.17 mmol, 57%). ν_{max} (ATR) 2954, 2385, 1704, 1491, 1168, 840 cm^{-1} ; δ_H (400 MHz, CDCl₃) 7.65–7.61 (2H, m, ArH), 7.47–7.42 (3H, m, ArH), 7.40–7.36 (1H, m, ArH), 7.35–7.30 (2H, m, ArH), 7.19–7.14 (2H, m, ArH), 5.67 (1H, ddt, J 17.1, 10.1, 7.2, 4-H), 5.07 (1H, dd, J 17.1, 2.0, 5-HH), 5.02 (1H, dd, J 10.1, 2.0, 5-

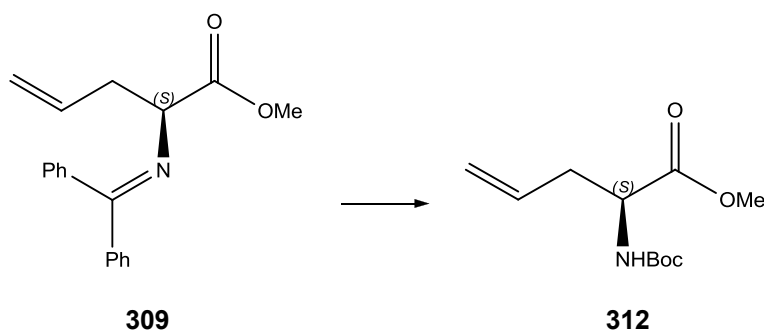
HH), 4.16 (1H, dd, *J* 7.8, 5.3, 2-*H*), 3.72 (3H, s, OCH₃), 2.75–2.56 (2H, m, 3-*H*₂); δ_C (101 MHz, CDCl₃) 172.4 (COOCH₃), 170.8 (Ph₂CN), 139.6 (Ar), 136.4 (Ar), 134.4 (Ar), 130.5 (C4), 128.94 (Ar), 128.78 (Ar), 128.61 (Ar), 128.14 (Ar), 128.03 (Ar), 117.8 (C5), 65.4 (C2), 52.1 (OCH₃), 38.3 (C3).

(S)-2-((Diphenylmethylene)amino)pent-4-en-1-ol (310)

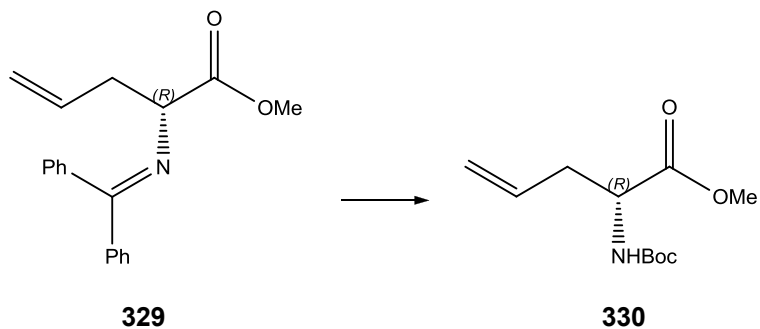
(It was prepared to test the synthetic route)



Procedure: A solution of 309 (50 mg, 0.18 mmol) in anhydrous ether (2 ml) was added dropwise to a stirred suspension of LiAlH₄ (15 mg, 0.39 mmol, 2.2 eq.) in anhydrous ether (2 ml) at -0 °C. The reaction mixture was allowed to warm up to room temperature, was stirred for additional 1 hour and followed by TLC. Upon completion, the reaction was carefully quenched with dropwise addition of water (150 μ l) followed by addition of 15% aq. NaOH (150 μ l), water (450 μ l), Celite and EtOAc (4 ml). The resulting slurry was filtered through Celite and the filtering bed was washed with EtOAc (2 \times 2 ml). The two phases were separated and the organic layer was washed with brine, dried over MgSO₄, filtered and evaporated *in vacuo* to afford the crude product 310 (36 mg, 0.16 mmol, 76%) as a pale yellow oil ($R_f \approx 0.45$; EtOAc/pet. ether 33/67). The product was pure enough and was used without further purification. δ_H (200 MHz, CDCl₃) 7.50–7.12 (10H, m, ArH), 5.86–5.58 (1H, m, 4-*H*), 5.13 (1H, d, *J* 3.7, 5-*H*_{cis}), 5.04 (1H, d, *J* 10.0, 5-*H*_{trans}), 3.61 (1H, dd, *J* 10.8, 4.1, 1-*HH*), 3.35 (1H, dd, *J* 10.8, 6.1, 1-*HH*), 2.74 (1H, qd, *J* 6.1, 4.1, 2-*H*), 2.37–2.17 (2H, m, 3-*H*₂);

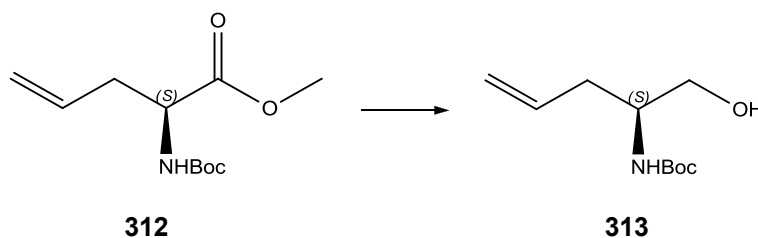
(S)-Methyl 2-((*tert*-butoxycarbonyl)amino)pent-4-enoate (312)¹⁸⁻¹⁹

Procedure:¹⁶ A mixture of the starting material 309 (735 mg, 2.51 mmol) and 4N HCl (3.1 ml, excess) in MeOH (10 ml) was refluxed for 1 hr. The reaction mixture was allowed to cool down to room temperature. The reaction mixture was extracted by ether (2 × 5 ml). The ether layer was discarded and the aqueous layer was basified by NaHCO₃ to pH 8 followed by addition of Boc₂O (Boc anhydride) (824 mg, 3.77 mmol, 1.5 eq.) and the reaction was stirred for 2 hrs at room temperature and monitored by TLC. The reaction volume was reduced under vacuum and extracted with EtOAc (3 × 10 ml). The combined organic extracts were washed with brine, dried over MgSO₄, filtered and evaporated in vacuo to afford the crude product. Column chromatography on silica gel (from 20% to 50% ethyl acetate in pet. ether) gave 312 (442 g, 1.9 mmol, 76%) as viscous liquid (*R*_f ≈ 0.42; EtOAc/pet. ether 33/67). ν_{max} (ATR) 3375, 2971, 2879, 1716, 1491, 1173, 840 cm⁻¹; δ_H (400 MHz, CDCl₃) 5.68 (1H, ddt, *J* 17.0, 9.7, 7.2, 4-*H*), 5.17–5.08 (2H, m, 5-*H*₂), 5.03 (1H, br d, *J* 6.2, NH), 4.37 (1H, dd, *J* 13.3, 6.2, 2-*H*), 3.72 (3H, s, OCH₃), 2.61 – 2.39 (2H, m, 3-*H*₂), 1.42 (9H, s, C(CH₃)₃); δ_C (126 MHz, CDCl₃) 171.2, 155.3, 132.4, 119.1, 79.9, 52.3, 36.9, 28.4; *m/z* (ES⁺) 253.0 [M+Na]⁺ C₁₁H₁₉O₂N₁²³Na₁ (Expected: 253.1).

(R)-Methyl 2-((*tert*-butoxycarbonyl)amino)pent-4-enoate (330)¹⁸⁻¹⁹

Procedure:¹⁶ A mixture of the starting material 329 (690 mg, 2.35 mmol) and 4N HCl (3.0 ml, excess) in MeOH (10 ml) was refluxed for 1 hr. The reaction mixture was allowed to cool down to room temperature. The reaction mixture was extracted by ether (2 × 5 ml). The ether layer was discarded and the aqueous layer was basified by NaHCO₃ to pH 8 followed by addition of Boc₂O (Boc anhydride) (775 mg, 3.53 mmol, 1.5 eq.) and the reaction was stirred for 2 hrs at room temperature and monitored by TLC. The reaction volume was reduced under vacuum and extracted with EtOAc (3 × 10 ml). The combined organic extracts were washed with brine, dried over MgSO₄, filtered and evaporated *in vacuo* to afford the crude product. Column chromatography on silica gel (from 20% to 50% ethyl acetate in pet. ether) gave 330 (408 g, 1.78 mmol, 75%) as viscous liquid ($R_f \approx 0.42$; EtOAc/pet. ether 33/67). ν_{max} (ATR) 3375, 2971, 2879, 1716, 1491, 1173, 840 cm⁻¹; δ_H (400 MHz, CDCl₃) 5.68 (1H, ddt, J 17.0, 9.7, 7.2, 4- H), 5.17–5.08 (2H, m, 5- H_2), 5.03 (1H, br d, J 6.2, NH), 4.37 (1H, dd, J 13.3, 6.2, 2- H), 3.72 (3H, s, OCH₃), 2.61–2.39 (2H, m, 3- H_2), 1.42 (9H, s, C(CH₃)₃); δ_C (126 MHz, CDCl₃) 171.2, 155.3, 132.4, 119.1, 79.9, 52.3, 36.9, 28.4; m/z (ES⁺) 253.1 [M+Na]⁺ C₁₁H₁₉O₂N₁²³Na₁ (Expected: 253.1).

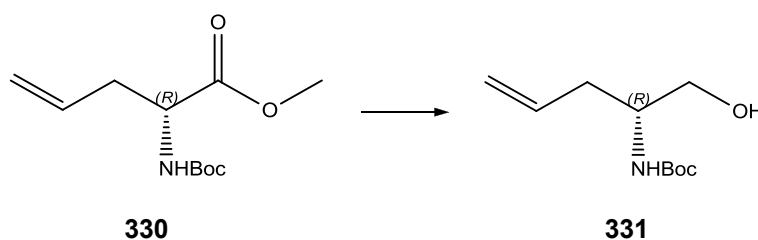
(*S*)-tert-Butyl (1-hydroxypent-4-en-2-yl)carbamate (313)²⁰



Procedure: A solution of 312 (332 mg, 1.45 mmol) in anhydrous ether (5 ml) was added dropwise to a stirred suspension of LiAlH₄ (100 mg, 3.19 mmol, 2.2 eq.) in anhydrous ether (5 ml) at -0 °C. The reaction mixture was allowed to warm up to room temperature, was stirred for additional 1 hr and followed by TLC. Upon completion, the reaction was carefully quenched with dropwise addition of water (1 ml) followed by addition of 15% aq. NaOH (1 ml), water (3 ml), Celite and EtOAc (10 ml). The resulting slurry was filtered through Celite and the filtering bed was washed with EtOAc (2 × 5 ml). The two phases were separated and the organic layer was washed with brine, dried over MgSO₄, filtered and evaporated *in vacuo* to afford the crude product 313 (265 mg, 1.32 mmol, 91%) as a pale yellow oil ($R_f \approx 0.25$; EtOAc/pet. ether 33/67). The product was pure enough and was used without further purification. ν_{max} (ATR) 3375, 2971,

2879, 1716, 1491, 1173, 840 cm^{-1} ; δ_{H} (700 MHz, CDCl_3) 5.78 (1H, ddt, J 17.2, 10.2, 7.1, 4- H), 5.11 (2H, m, 5- H_2), 4.72 (1H, br s, NH), 3.74–3.58 (3H, m, 1- CH_2 and 2- H), 2.67 (1H, br s, OH), 2.31 (1H, m, 3- HH), 2.23 (1H, m, 3- HH), 1.43 (9H, s, $\text{C}(\text{CH}_3)_3$); δ_{C} (101 MHz, CDCl_3) 156.56, 134.28, 118.23, 79.89, 65.54, 52.30, 36.10, 28.49; m/z (ES^+) 224.0 $[\text{M}+\text{Na}]^+$ $\text{C}_{10}\text{H}_{19}\text{O}_3\text{N}_1^{23}\text{Na}_1$ (Expected: 224.1).

(*R*)-tert-Butyl (1-hydroxypent-4-en-2-yl)carbamate (331)²⁰



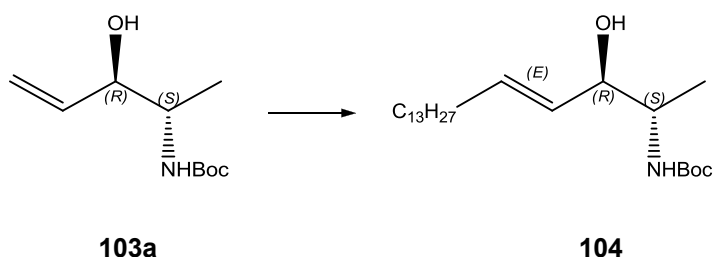
Procedure: A solution of 330 (388 mg, 1.69 mmol) in anhydrous ether (6 ml) was added dropwise to a stirred suspension of LiAlH_4 (102 mg, 3.72 mmol, 2.2 eq.) in anhydrous ether (6 ml) at -0°C . The reaction mixture was allowed to warm up to room temperature, was stirred for additional 1 hr and followed by TLC. Upon completion, the reaction was carefully quenched with dropwise addition of water (1 ml) followed by addition of 15% aq. NaOH (1 ml), water (3 ml), Celite and EtOAc (12 ml). The resulting slurry was filtered through Celite and the filtering bed was washed with EtOAc (2×5 ml). The two phases were separated and the organic layer was washed with brine, dried over MgSO_4 , filtered and evaporated *in vacuo* to afford the crude product 331 (270 mg, 1.34 mmol, 79%) as a pale yellow oil ($R_f \approx 0.25$; $\text{EtOAc}/\text{pet. ether}$ 33/67). The product was pure enough and was used without further purification. ν_{max} (ATR) 3375, 2971, 2879, 1716, 1491, 1173, 840 cm^{-1} ; δ_{H} (700 MHz, CDCl_3) 5.78 (1H, ddt, J 17.2, 10.2, 7.1, 4- H), 5.11 (2H, m, 5- H_2), 4.72 (1H, br s, NH), 3.74–3.58 (3H, m, 1- H_2 and 2- H), 2.67 (1H, br s, OH), 2.31 (1H, m, 3- HH), 2.23 (1H, m, 3- HH), 1.43 (9H, s, $\text{C}(\text{CH}_3)_3$); δ_{C} (101 MHz, CDCl_3) 156.56 (NHCOO), 134.28, 118.23, 79.89, 65.54, 52.30, 36.10, 28.49; m/z (ES^+) 224.0 $[\text{M}+\text{Na}]^+$ $\text{C}_{10}\text{H}_{19}\text{O}_3\text{N}_1^{23}\text{Na}_1$ (Expected: 224.1).

8.2.4 Olefin Cross Metathesis

To a solution of Grubbs II (0.3% mol) in CH_2Cl_2 , the starting material was added as a solution in CH_2Cl_2 followed by the addition of the coupling olefin in excess (5 eq.). The reaction mixture was refluxed, typically for 4~8 hrs. The reaction was followed by TLC and quenched by addition of potassium 2-isocyanoacetate (1.32% mol, 4.4 eq. to Grubbs catalyst).²¹ The reaction was stirred for 15 min at room temperature then evaporated *in vacuo* to yield the crude mixture which was purified by column chromatography on silica.⁴

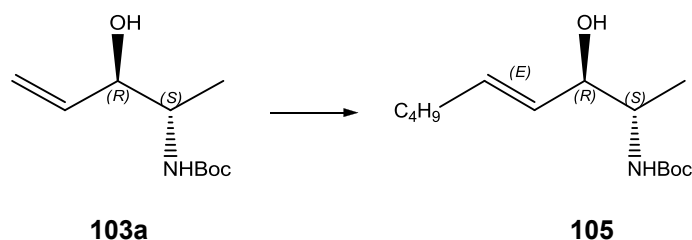
8.2.4.1 4E-1-deoxy ceramide analogues

tert-Butyl ((2*S*,3*R*,*E*)-3-hydroxyoctadec-4-en-2-yl)carbamate (104)



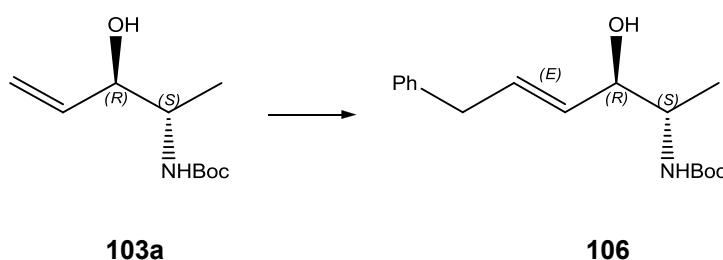
Yield (52%); ν_{max} (ATR) 3375, 2971, 2879, 1716, 1491, 1173, 840 cm^{-1} ; δ_{H} (700 MHz, CDCl_3) 5.75–5.66 (1H, m, 5-*H*), 5.43 (1H, dd, J 15.5, 6.6, 4-*H*), 4.68–4.60 (1H, m, *NH*), 4.14–4.06 (1H, m, 3-*H*), 3.83–3.75 (1H, m, 2-*H*), 2.07–2.01 (2H, m, 6- H_2), 1.44 (9H, s, $\text{C}(\text{CH}_3)_3$), 1.39–1.22 (22H, m, 7- H_2 to 17- H_2), 1.07 (3H, d, J 6.4, 1- H_3), 0.88 (3H, t, J 6.9, 18- H_3); δ_{C} (101 MHz, CDCl_3) 156.3 (NHCOO), 134.2, 128.5, 79.8, 75.9, 32.5, 32.1, 29.9, 29.8, 29.8, 29.7, 29.6, 29.5, 29.3, 28.5, 22.8, 15.6, 14.3; m/z (ES^+) 406.5 [$\text{M}+\text{Na}$]⁺; HRMS (ES^+) found [$\text{M}+\text{H}$]⁺ 384.3474, $\text{C}_{23}\text{H}_{46}\text{O}_3\text{N}_1$ requires M^+ 384.3472.

tert-Butyl ((2*S*,3*R*,*E*)-3-hydroxynon-4-en-2-yl)carbamate (105)



Yield (67%); ν_{max} (ATR) 3375, 2971, 2879, 1716, 1491, 1173, 840 cm^{-1} ; δ_{H} (400 MHz, CDCl_3) 5.76–5.65 (1H, m, 5-*H*), 5.42 (1H, ddt, J 15.4, 6.6, 1.4, 4-*H*), 4.74–4.61 (1H, m, NH), 4.13–4.05 (1H, m, 3-*H*), 3.84–3.72 (1H, m, 2-*H*), 2.01–2.07 (2H, m, 6-*H*₂), 1.43 (9H, s, $\text{C}(\text{CH}_3)_3$), 1.40–1.25 (4H, m, 7-*H*₂ and 8-*H*₂), 1.07 (3H, d, J 6.9, 1-*H*₃), 0.88 (3H, t, J 7.1, 9-*H*₃); δ_{C} (101 MHz, CDCl_3) 156.4, 134.1, 128.6, 79.7, 75.9, 51.2, 32.1, 31.5, 28.5, 22.3, 15.7, 14.0; m/z (ES^+) 280.0 $[\text{M}+\text{Na}]^+$; $\text{C}_{14}\text{H}_{27}\text{O}_3\text{N}_1\text{Na}_1$; HRMS (ES^+) found $[\text{M}+\text{H}]^+$ 258.2064, $\text{C}_{14}\text{H}_{28}\text{O}_3\text{N}_1$ requires M^+ 258.2064, $[\text{M}+\text{Na}]^+$ 280.1884, $\text{C}_{14}\text{H}_{27}\text{O}_3\text{N}_1^{23}\text{Na}_1$ requires M^+ 280.1883.

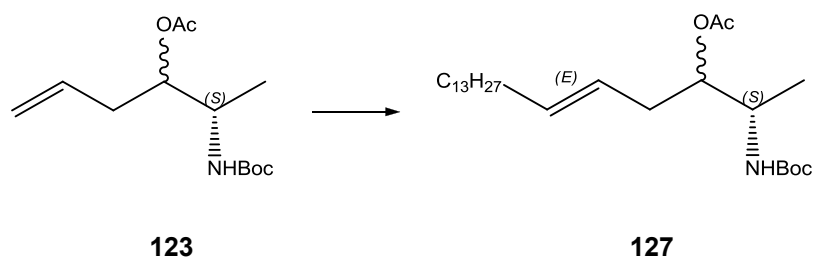
tert-Butyl ((2*S*,3*R*,*E*)-3-hydroxy-6-phenylhex-4-en-2-yl)carbamate (**106**)



Yield (64%) as viscous oil; ν_{max} (ATR) 3375, 2971, 2879, 1716, 1491, 1173, 840 cm^{-1} ; δ_{H} (400 MHz, CDCl_3) 7.32–7.24 (2H, m, Ar*H*), 7.23–7.14 (3H, m, Ar*H*), 5.93–5.83 (1H, m, 5-*H*), 5.53 (1H, ddt, J 15.3, 6.3, 1.4, 4-*H*), 4.74–4.66 (1H, m, NH), 4.19–4.13 (1H, m, 3-*H*), 3.86–3.73 (1H, m, 2-*H*), 3.40 (2H, d, J 6.8, 6-*H*₂), 1.44 (9H, s, $\text{C}(\text{CH}_3)_3$), 1.08 (3H, d, J 6.9, 1-*H*₃); δ_{C} (101 MHz, CDCl_3) 156.4, 140.1, 132.2, 130.2, 128.6, 128.9, 126.3, 79.8, 75.6, 51.2, 38.9, 28.5, 15.6; m/z (ES^+) 314.3 $[\text{M}+\text{Na}]^+$; $\text{C}_{17}\text{H}_{25}\text{O}_3\text{N}_1\text{Na}_1$; HRMS (ES^+) found $[\text{M}+\text{H}]^+$ 292.1908, $\text{C}_{17}\text{H}_{26}\text{O}_3\text{N}_1$ requires M^+ 292.1907.

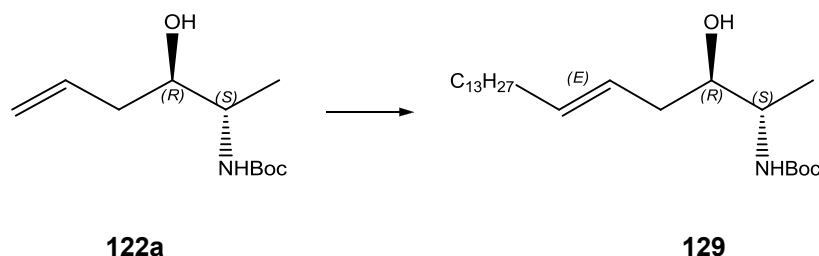
8.2.4.2 5*E*-1-deoxy ceramide analogues

(2*S*,*E*)-2-((*tert*-Butoxycarbonyl)amino)nonadec-5-en-3-yl acetate (**127**)



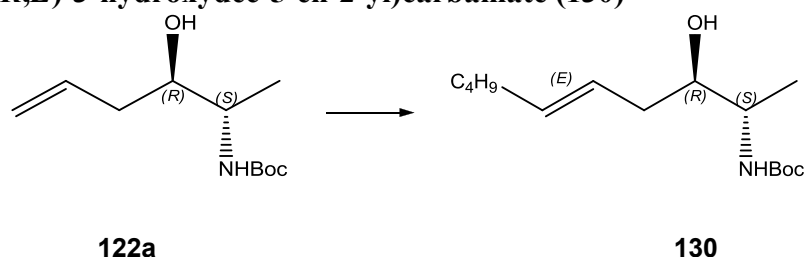
Yield (49%); ν_{max} (ATR) 3449, 2928, 1715, 1497, 1173, 839 cm^{-1} ; δ_{H} (700 MHz, CDCl_3) 5.52–5.44 (1H, m, 5-*H*), 5.34–5.27 (1H, m, 6-*H*), 4.87 (1H, ddd, J 7.9, 5.8, 4.0, 3-*H*), 4.64–4.55 (1H, m, *NH*), 3.91–3.80 (1H, m, 2-*H*), 2.30–2.16 (2H, m, 4-*H*₂), 2.07–1.99 (4H, m, 7-*HH* and OCOCH_3), 1.95 (1H, dd, J 14.2, 7.1, 7-*HH*), 1.43 (9H, s, $\text{C}(\text{CH}_3)_3$), 1.36–1.19 (22H, m, 8-*H*₂ to 18-*H*₂), 1.09 (3H, d, J 7.1, 1-*H*₃), 0.87 (3H, t, J 7.1, 19-*H*₃); δ_{C} (176 MHz, CDCl_3) 170.84, 155.21, 134.42, 124.44, 79.47, 75.96, 48.15, 34.54, 32.71, 32.05, 29.81, 29.79, 29.76, 29.69, 29.65, 29.54, 29.49, 29.31, 28.52, 22.82, 21.23, 15.50, 14.24; m/z (ES^+) 462.4 $[\text{M}+\text{Na}]^+$ $\text{C}_{26}\text{H}_{49}\text{O}_4\text{N}_1^{23}\text{Na}_1$; HRMS (ES^+) found $[\text{M}+\text{Na}]^+$ 462.3577, $\text{C}_{26}\text{H}_{49}\text{O}_4\text{N}_1^{23}\text{Na}_1$ requires M^+ 462.3559.

***tert*-Butyl ((2*S*,3*R*,*E*)-3-hydroxynonadec-5-en-2-yl)carbamate (129)**



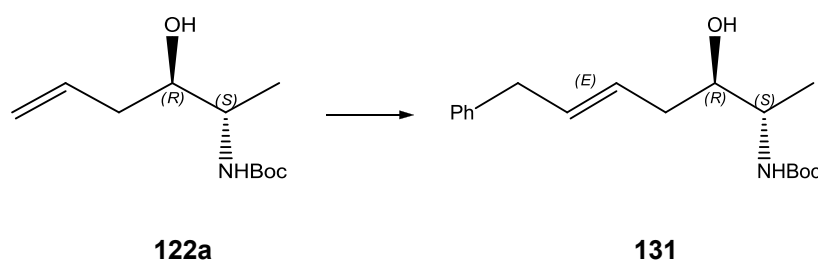
Yield (53%); ν_{max} (ATR) 3375, 2971, 2879, 1716, 1491, 1173, 840 cm^{-1} ; δ_{H} (700 MHz, CDCl_3) 5.55 (1H, dt, J 12.8, 6.7, 6-*H*), 5.43–5.36 (1H, m, 5-*H*), 4.83–4.68 (1H, m, *NH*), 3.73–3.58 (2H, m, 3-*H* and 2-*H*), 3.48 (1H, d, J 7.8, *OH*), 2.27–2.15 (4H, m, 4-*H*₂ and 7-*H*₂), 2.14–1.98 (2H, m, 7-*H*₂), 1.44 (9H, s, $\text{C}(\text{CH}_3)_3$), 1.38–1.22 (94 H, m, 8-*H*₂ to 18-*H*₂ and 1-*H*₃), 0.88 (3H, t, J 7.1, 19-*H*₃); δ_{C} (126 MHz, CDCl_3) 156.24, 135.03, 125.50, 79.56, 73.69, 50.35, 37.46, 32.88, 32.15, 29.90, 29.88, 29.85, 29.73, 29.66, 29.58, 29.45, 29.44, 28.63, 22.92, 14.35; m/z (ES^+) 398.5 $[\text{M}+\text{H}]^+$; HRMS (ES^+) found $[\text{M}+\text{H}]^+$ 398.3627, $\text{C}_{24}\text{H}_{48}\text{O}_3\text{N}_1$ requires M^+ 398.3629; $[\text{M}+\text{Na}]^+$ 420.3446, $\text{C}_{24}\text{H}_{47}\text{O}_3\text{N}_1^{23}\text{Na}_1$ requires M^+ 420.3448.

***tert*-Butyl ((2*S*,3*R*,*E*)-3-hydroxydec-5-en-2-yl)carbamate (130)**



Yield (56%); waxy solid; ν_{max} (ATR) 3449, 2928, 1715, 1497, 1173, 839 cm^{-1} ; δ_{H} (400 MHz, CDCl_3) 5.55 (1H, dt, J 13.2, 6.6, 6-*CH*), 5.43–5.34 (1H, m, 5-*H*), 4.83–4.70 (1H, m, *NH*), 3.74–3.58 (2H, m, 2-*H* and 3-*H*), 2.23–1.96 (4H, m, 4-*H*₂ and 7-*H*₂), 1.44 (9H, s, $\text{C}(\text{CH}_3)_3$), 1.39–1.23 (4H, m, 8-*H*₂ and 9-*H*₂), 1.15–1.02 (3H, d, J 6.8, 1-*H*₃), 0.89 (3H, t, J 7.1, 10-*H*₃); δ_{C} (101 MHz, CDCl_3) 156.0, 134.8, 125.6, 79.6, 73.5, 50.4, 37.2, 32.3, 31.6, 28.4, 22.2, 13.9; m/z (ES^+) 294.3 $[\text{M}+\text{Na}]^+$; HRMS (ES^+) found $[\text{M}+\text{H}]^+$ 272.2220, $\text{C}_{15}\text{H}_{30}\text{O}_3\text{N}_1$ requires M^+ 272.2220; $[\text{M}+\text{Na}]^+$ 294.2040, $\text{C}_{15}\text{H}_{29}\text{O}_3\text{N}_1^{23}\text{Na}_1$ requires M^+ 294.2040.

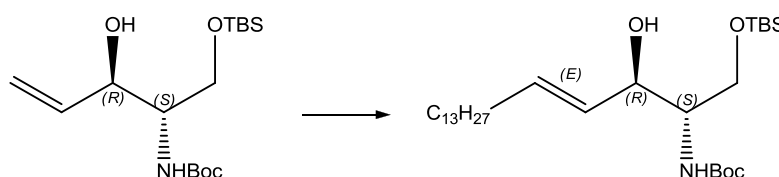
tert-Butyl ((2*S*,3*R*,*E*)-3-hydroxy-7-phenylhept-5-en-2-yl)carbamate (**131**)



Yield (64%) as viscous oil; ν_{max} (ATR) 3375, 2971, 2879, 1716, 1491, 1173, 840 cm^{-1} ; δ_{H} (700 MHz, CDCl_3) 7.30–7.27 (2H, m, *ArH*), 7.21–7.15 (3H, m, *ArH*), 5.71 (1H, dtd, J 15.2, 11.8, 6.6, 6-*H*), 5.53 (1H, dd, J 15.2, 6.3, 5-*H*), 4.80 (1H, br s, *NH*), 3.75–3.62 (2H, m, 3-*H* and 2-*H*), 3.36 (2H, d, J 6.6, 7-*H*₂), 2.24–2.05 (2H, m, 4-*H*₂), 1.44 (9H, s, $\text{C}(\text{CH}_3)_3$), 1.10 (3H, d, J 6.8, 1-*H*₃); δ_{C} (176 MHz, CDCl_3) 155.88, 140.56, 135.89, 133.24, 128.57, 127.42, 126.16, 79.58, 73.75, 50.37, 39.23, 39.22, 37.17, 28.55, 14.72; m/z (ES^+) 328.3 $[\text{M}+\text{Na}]^+$; HRMS (ES^+) found $[\text{M}+\text{H}]^+$ 306.2063, $\text{C}_{18}\text{H}_{28}\text{O}_3\text{N}_1$ requires M^+ 306.2064; $[\text{M}+\text{Na}]^+$ 328.1883, $\text{C}_{18}\text{H}_{27}\text{O}_3\text{N}_1^{23}\text{Na}_1$ requires M^+ 328.1883.

8.2.4.3 Ceramide analogues

tert-Butyl ((2*S*,3*R*,*E*)-1-((*tert*-butyldimethylsilyloxy)-3-hydroxyoctadec-4-en-2-yl)carbamate (**208**)⁴

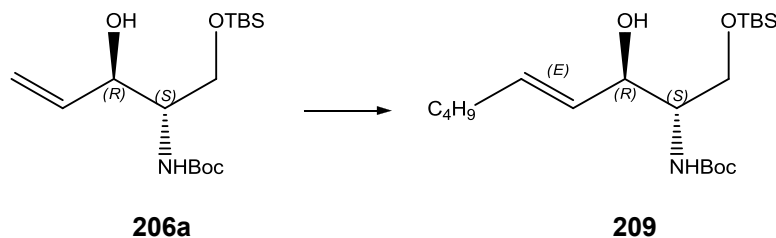


206a

208

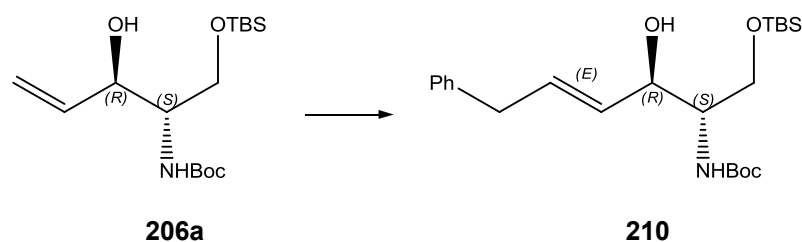
Yield (72%); ν_{max} (ATR) 3452, 2931, 1711, 1493, 1168, 835 cm^{-1} ; δ_{H} (400 MHz, CDCl_3) 5.74 (1H, dd, J 15.0, 7.0, 5- H), 5.49 (1H, dd, J 15.0, 5.9, 4- H), 5.29–5.16 (1H, m, NH), 4.23–4.13 (1H, m, 3- H), 3.93 (1H, dd, J 10.3, 3.0, 1- HH), 3.81–3.71 (1 H, m, 1- HH), 3.62–3.49 (1H, m, 2- H), 2.04 (2H, dd, J 14.2, 7.0, 6- H_2), 1.44 (9H, s, $\text{OC}(\text{CH}_3)_3$), 1.41–1.20 (22H, m, 7- H_2 to 17- H_2), 0.94 – 0.77 (12H, m, $\text{SiC}(\text{CH}_3)_3$ and 18- CH_3), 0.06 (6H, d, $2 \times \text{SiCH}_3$); δ_{H} (101 MHz, CDCl_3) 155.97, 133.24, 129.59, 79.57, 74.73, 63.59, 54.71, 32.45, 32.06, 29.83, 29.80, 29.65, 29.50, 29.35, 28.54, 25.96, 22.83, 18.28, 14.24, -5.46, -5.49; m/z (ES^+) 514.6 $[\text{M}+\text{H}]^+$; HRMS (ES^+) found $[\text{M}+\text{H}]^+$ 514.4277, $\text{C}_{29}\text{H}_{60}\text{O}_4\text{N}_1^{28}\text{Si}_1$ requires M^+ 514.4286, $[\text{M}+\text{Na}]^+$ 536.4096, $\text{C}_{29}\text{H}_{59}\text{O}_4\text{N}_1^{28}\text{Si}_1^{23}\text{Na}_1$ requires M^+ 536.4094.

***tert*-Butyl ((2*S*,3*R*,*E*)-1-((*tert*-butyldimethylsilyl)oxy)-3-hydroxynon-4-en-2-yl)carbamate (209)**



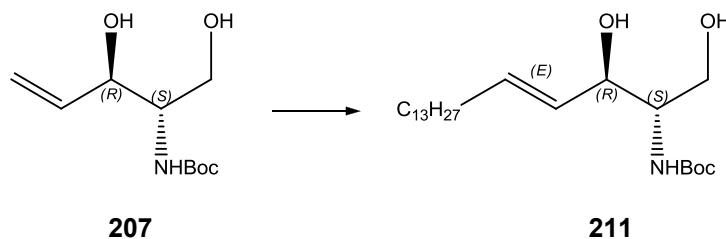
Yield (71%) as viscous oil; ν_{max} (ATR) 3375, 2971, 2879, 1716, 1491, 1173, 840 cm^{-1} ; δ_{H} (400 MHz, CDCl_3) 5.75 (1H, dt, J 15.1, 6.8, 1.3, 5- H), 5.50 (1H, dd, J 15.1, 5.9, 4- H), 5.29–5.14 (1H, m, NH), 4.23–4.13 (1H, m, 3- H), 3.97–3.88 (1H, m, 1- HH), 3.78–3.70 (1H, m, 1- HH), 3.63–3.46 (1H, m, 2- H), 2.12–1.96 (2H, m, 6- H), 1.44 (9H, s, $\text{OC}(\text{CH}_3)_3$), 1.39–1.20 (4H, m, 7- H_2 and 8- H_2), 0.95–0.79 (12H, m, $\text{SiC}(\text{CH}_3)_3$ and 9- CH_3), 0.06 (6H, d, $2 \times \text{SiCH}_3$); δ_{C} (101 MHz, CDCl_3) 154.44, 133.15, 129.64, 79.51, 74.81, 63.60, 32.11, 31.47, 28.54, 25.96, 22.33, 18.29, 14.04, -5.47, -5.50; m/z (ES^+) 388.5 $[\text{M}+\text{H}]^+$; HRMS (ES^+) found $[\text{M}+\text{H}]^+$ 388.2871, $\text{C}_{20}\text{H}_{42}\text{O}_4\text{N}_1^{28}\text{Si}_1$ requires M^+ 388.2878, $[\text{M}+\text{Na}]^+$ 410.2689, $\text{C}_{20}\text{H}_{42}\text{O}_4\text{N}_1^{28}\text{Si}_1^{23}\text{Na}_1$ requires M^+ 410.2697.

***tert*-Butyl ((2*S*,3*R*,*E*)-1-((*tert*-butyldimethylsilyl)oxy)-3-hydroxy-6-phenylhex-4-en-2-yl)carbamate (210)**



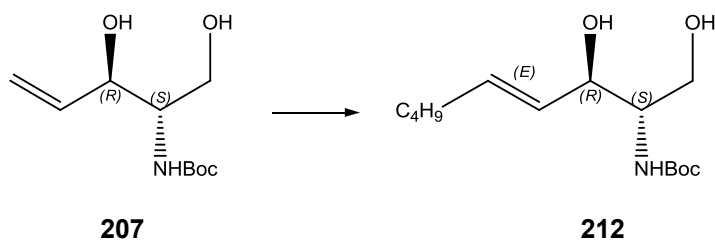
Yield (65%) as viscous oil; ν_{max} (ATR) 3375, 2971, 2879, 1716, 1491, 1173, 840 cm^{-1} ; δ_{H} (400 MHz, CDCl_3) 7.32–7.24 (2H, m, ArH), 7.24–7.11 (3H, m, ArH), 5.94 (1H, dt, J 15.2, 6.8, 1.4, 5-H), 5.64–5.54 (1H, m, 4-H), 5.28–5.20 (1H, m, NH), 4.30–4.20 (1H, m, 3-H), 3.92 (1H, dd, J 10.4, 3.0, 1-HH), 3.79–3.70 (1H, m, J 10.1, 3.0, 1-HH), 3.64–3.54 (1H, m, 2-H), 3.41 (2H, d, J 6.8, 6-H₂), 1.44 (9H, s, $\text{OC}(\text{CH}_3)_3$), 0.87 (9H, s, $\text{SiC}(\text{CH}_3)_3$), 0.04 (6H, d, $2 \times \text{SiCH}_3$); δ_{C} (101 MHz, CDCl_3) 155.89, 140.13, 138.05, 131.24, 128.66, 128.58, 126.24, 79.68, 74.52, 63.63, 54.72, 38.81, 28.53, 25.94, 18.26, -5.51, -5.54; m/z (ES^+) 422.5 $[\text{M}+\text{H}]^+$; HRMS (ES^+) found $[\text{M}+\text{H}]^+$ 422.2713, $\text{C}_{23}\text{H}_{40}\text{O}_4\text{N}_1^{28}\text{Si}_1$ requires M^+ 422.2721, $[\text{M}+\text{Na}]^+$ 444.2531, $\text{C}_{23}\text{H}_{39}\text{O}_4\text{N}_1^{28}\text{Si}_1^{23}\text{Na}_1$ requires M^+ 444.2541.

***tert*-Butyl ((2*S*,3*R*,*E*)-1,3-dihydroxyoctadec-4-en-2-yl)carbamate (211)⁴**



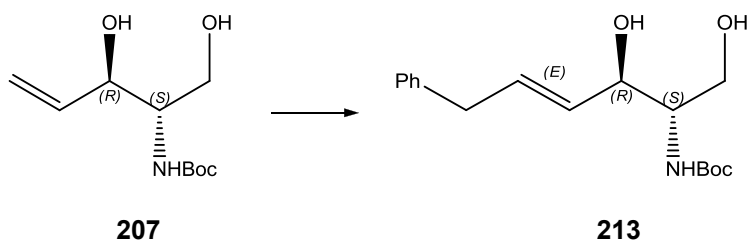
Yield (44%, 50%); ν_{max} (ATR) 3410, 2886, 2874, 1687, 1512, 1173 cm^{-1} ; δ_{H} (400 MHz, CDCl_3) 5.83–5.73 (1H, m, 5-H), 5.53 (1H, ddt, J 15.6, 6.5, 1.2, 4-H), 5.30 (1H, br d, J 6.4, NH), 4.38–4.28 (1H, m, 3-H), 3.94 (1H, app. d, J 10.0, 1-HH), 3.76–3.67 (1H, m, 1-HH), 3.63–3.54 (1H, m, 2-H), 2.50 (2H, br s, $2 \times \text{OH}$), 2.05 (2H, q, J 7.3, 6-H), 1.45 (9H, s, $\text{C}(\text{CH}_3)_3$), 1.42–1.18 (22H, m, 7-H₂ to 17-H₂), 0.88 (3H, t, J 6.9, 18-H₃); δ_{C} (101 MHz, CDCl_3) 158.1, 134.2, 128.9, 79.7, 74.9, 62.9, 56.0, 32.3, 31.9, 29.8, 29.6, 29.5, 29.3, 29.1, 29.1, 28.4, 22.6, 14.1; m/z (ES^+) 400.9 $[\text{M}+\text{H}]^+$; HRMS (ES^+) found $[\text{M}+\text{H}]^+$ 400.3419, $\text{C}_{23}\text{H}_{46}\text{O}_4\text{N}_1$ requires M^+ 400.3421, $[\text{M}+\text{Na}]^+$ 422.3238, $\text{C}_{23}\text{H}_{45}\text{O}_4\text{N}_1^{23}\text{Na}_1$ requires M^+ 422.3241.

***tert*-Butyl ((2*S*,3*R*,*E*)-1,3-dihydroxynon-4-en-2-yl)carbamate (212)**



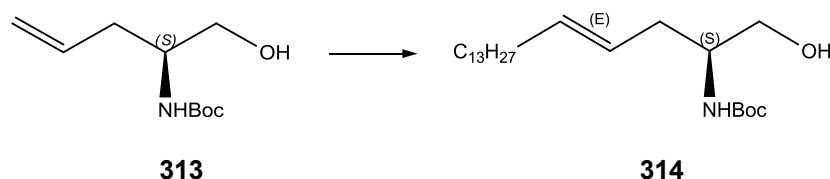
Yield (59%, 57%); ν_{max} (ATR) 3375, 2971, 2879, 1716, 1491, 1173, 840 cm^{-1} ; δ_{H} (400 MHz, CDCl_3) 5.76 (1H, dtd, J 15.4, 6.7, 1.1, 5- H), 5.51 (1H, dtd, J 15.4, 6.5, 1.3, 4- H), 5.32 (1H, br d, NH), 4.34–4.21 (1H, m, 3- H), 3.90 (1H, d, J 11.4, 1- HH), 3.68 (1H, d, J 11.0, 1- HH), 3.63–3.51 (1H, m, 2- H), 2.97 (2H, br s, $2 \times \text{OH}$), 2.05 (2H, dd, J 13.8, 6.7, 6- H_2), 1.44 (9H, s, $\text{C}(\text{CH}_3)_3$), 1.39–1.23 (4H, m, 7- H_2 and 8- H_2), 0.88 (3H, t, J 7.1, 9- H_3); δ_{C} (101 MHz, CDCl_3) 156.4, 134.2, 129.1, 79.9, 74.8, 62.8, 55.6, 32.1, 31.4, 28.5, 22.3, 14.0; m/z (ES^+) 274.6 $[\text{M}+\text{H}]^+$; HRMS (ES^+) found $[\text{M}+\text{H}]^+$ 274.2012, $\text{C}_{14}\text{H}_{28}\text{O}_4\text{N}_1$ requires M^+ 274.2013, $[\text{M}+\text{Na}]^+$ 296.1831, $\text{C}_{14}\text{H}_{27}\text{O}_4\text{N}_1^{23}\text{Na}_1$ requires M^+ 296.1832.

***tert*-Butyl ((2*S*,3*R*,*E*)-1,3-dihydroxy-6-phenylhex-4-en-2-yl)carbamate (213)**

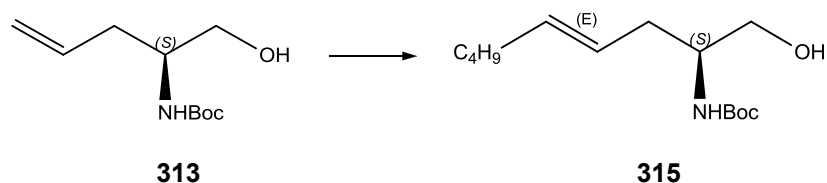


Yield (62%, 43%); ν_{max} (ATR) 3375, 2971, 2879, 1716, 1491, 1173, 840 cm^{-1} ; δ_{H} (400 MHz, CDCl_3) 7.32–7.26 (2H, m, Ar H), 7.23–7.19 (1H, m, Ar H), 7.18–7.14 (2H, m, Ar H), 6.00–5.90 (1H, m, 5- H), 5.61 (1H, dd, J 15.4, 6.2, 4- H), 5.30 (1H, br s, NH), 4.40–4.32 (1H, m, 3- H), 3.93 (1H, dd, J 11.2, 3.5, 1- HH), 3.71 (1H, dd, J 11.4, 3.5, 1- HH), 3.67–3.58 (1H, m, 2- H), 3.40 (2H, d, J 6.8, 6- H), 2.71–2.44 (2H, br m, $2 \times \text{OH}$), 1.45 (9H, s, $\text{C}(\text{CH}_3)_3$); δ_{C} (125 MHz, CDCl_3) 156.7, 139.3, 132.8, 130.7, 128.66, 128.62, 126.4, 80.7, 74.8, 62.8, 38.8, 28.5; m/z (ES^+) 329.9 $[\text{M}+\text{Na}]^+$; HRMS (ES^+) found $[\text{M}+\text{H}]^+$ 308.1855, $\text{C}_{17}\text{H}_{26}\text{O}_4\text{N}_1$ requires M^+ 308.1856, $[\text{M}+\text{Na}]^+$ 330.1673, $\text{C}_{17}\text{H}_{25}\text{O}_4\text{N}_1^{23}\text{Na}_1$ requires M^+ 330.1676.

8.2.4.4 4E-3-deoxy ceramide analogues

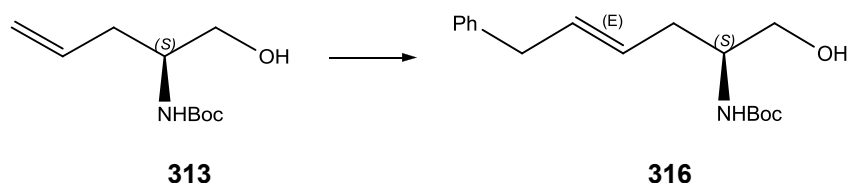
(S,E)-tert-Butyl (1-hydroxyoctadec-4-en-2-yl)carbamate (314)²²

Yield (53%); ν_{max} (ATR) 3375, 2971, 2879, 1716, 1491, 1173, 840 cm^{-1} ; δ_{H} (400 MHz, CDCl_3) 5.52 (1H, dt, J 13.4, 6.7, 5- H), 5.41–5.27 (1H, m, 4- H), 4.66 (1H, br s, NH), 3.73–3.48 (3H, m, 1- H_2 and 2- H), 2.57 (1H, br s, OH), 2.33–2.10 (2H, m, 3- H_2), 2.00 (2H, dt, J 14.0, 6.7, 6- H_2), 1.44 (9H, s, $\text{C}(\text{CH}_3)_3$), 1.39–1.14 (22H, m), 0.88 (3H, t, J 6.8, 18- H_3); δ_{C} (101 MHz, CDCl_3) 155.98, 134.82, 125.20, 79.85, 65.99, 52.74, 34.89, 32.73, 32.07, 29.84, 29.81, 29.78, 29.66, 29.54, 29.51, 29.32, 28.51, 22.84, 14.28; m/z (ES^+) 384.9 $[\text{M}+\text{H}]^+$; HRMS (ES^+) found $[\text{M}+\text{H}]^+$ 384.3470, $\text{C}_{23}\text{H}_{46}\text{O}_3\text{N}_1$ requires M^+ 384.2472, $[\text{M}+\text{Na}]^+$ 406.3288, $\text{C}_{23}\text{H}_{45}\text{O}_3\text{N}_1^{23}\text{Na}_1$ requires M^+ 406.3292.

(S,E)-tert-butyl (1-hydroxynon-4-en-2-yl)carbamate (315)

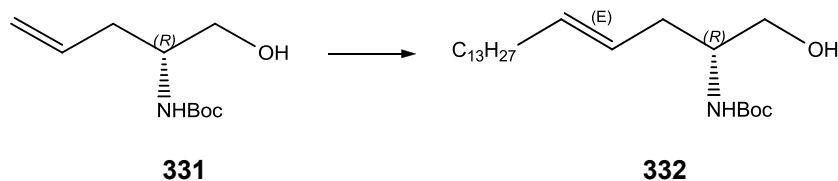
Yield (71%); ν_{max} (ATR) 3375, 2971, 2879, 1716, 1491, 1173, 840 cm^{-1} ; δ_{H} (400 MHz, CDCl_3) 5.58–5.46 (1H, m, 5- H), 5.41–5.29 (1H, m, 4- H), 4.67 (1H, br s, NH), 3.75–3.47 (3H, m, 1- H_2 and 2- H), 2.61 (1H, br s, OH), 2.32–2.10 (2H, m, 3- H_2), 2.02 (2H, dt, J 13.2, 4.1, 6- H_2), 1.44 (9H, s, $\text{C}(\text{CH}_3)_3$), 1.35–1.27 (4H, m, 7- H_2 and 8- H_2), 0.88 (3H, t, J 7.1, 9- H_3); δ_{C} (101 MHz, CDCl_3) 156.5, 134.5, 125.2, 79.7, 65.8, 52.6, 32.2, 31.5, 28.4, 22.1, 13.9; m/z (ES^+) 258.6 $[\text{M}+\text{H}]^+$ and 280.6 $[\text{M}+\text{Na}]^+$; HRMS (ES^+) found $[\text{M}+\text{H}]^+$ 258.2063, $\text{C}_{14}\text{H}_{28}\text{O}_3\text{N}_1$ requires M^+ 258.2064, $[\text{M}+\text{Na}]^+$ 280.1882, $\text{C}_{14}\text{H}_{27}\text{O}_3\text{N}_1^{23}\text{Na}_1$ requires M^+ 280.1883.

(S,E)-tert-Butyl (1-hydroxy-6-phenylhex-4-en-2-yl)carbamate (316)



Yield (50%); ν_{max} (ATR) 3375, 2971, 2879, 1716, 1491, 1173, 840 cm^{-1} ; δ_{H} (400 MHz, CDCl_3) 7.32–7.26 (2H, m, ArH), 7.22–7.14 (3H, m, ArH), 5.74–5.64 (1H, m, 5-H), 5.48 (1H, ddd, J 15.2, 7.1, 3.6, 4-H), 4.68 (1H, br s, NH), 3.77–3.50 (3H, m, 1- H_2 and 2- H), 3.35 (2H, d, J 6.7, 6- H_2), 2.53 (1H, br s, OH), 2.32–2.15 (2H, m, 3- H_2), 1.44 (9H, s, $\text{C}(\text{CH}_3)_3$); δ_{C} (176 MHz, CDCl_3) 156.03, 134.07, 130.06, 128.41, 128.40, 126.85, 126.04, 118.11, 78.80, 64.45, 55.63, 38.99, 29.67, 28.34; m/z (ES^+) 292.9.6 $[\text{M}+\text{H}]^+$ and 314.7 $[\text{M}+\text{Na}]^+$; HRMS (ES^+) found $[\text{M}+\text{H}]^+$ 292.1906, $\text{C}_{17}\text{H}_{26}\text{O}_3\text{N}_1$ requires M^+ 292.1907, $[\text{M}+\text{Na}]^+$ 314.1725, $\text{C}_{17}\text{H}_{25}\text{O}_3\text{N}_1^{23}\text{Na}_1$ requires M^+ 314.1727.

(*R,E*)-tert-Butyl (1-hydroxyoctadec-4-en-2-yl)carbamate (332)²²



Yield (62%); ν_{max} (ATR) 3375, 2971, 2879, 1716, 1491, 1173, 840 cm^{-1} ; δ_{H} (400 MHz, CDCl_3) 5.52 (1H, dtt, J 15.4, 6.6, 1.0, 5-H), 5.35 (1H, dtt, J 15.4, 7.1, 1.3, 4-H), 4.66 (1H, br s, NH), 3.70–3.53 (3H, m, 1- H_2 and 2- H), 2.57 (1H, br s, OH), 2.30–2.11 (2H, m, 3- H_2), 1.99 (2H, dd, J 13.7, 6.7, 6- H_2), 1.44 (9H, s, $\text{OC}(\text{CH}_3)_3$), 1.36–1.22 (22H, m, 7- H_2 to 17- H_2), 0.88 (3H, t, J 6.9, 18- H_3); δ_{C} (101 MHz, CDCl_3) 155.98, 134.82, 125.20, 79.85, 65.99, 52.74, 34.89, 32.73, 32.07, 29.84, 29.81, 29.78, 29.66, 29.54, 29.51, 29.32, 28.51, 22.84, 14.28; m/z (ES^+) 384.9 $[\text{M}+\text{H}]^+$; HRMS (ES^+) found $[\text{M}+\text{H}]^+$ 384.3470, $\text{C}_{23}\text{H}_{46}\text{O}_3\text{N}_1$ requires M^+ 384.2472, $[\text{M}+\text{Na}]^+$ 406.3288, $\text{C}_{23}\text{H}_{45}\text{O}_3\text{N}_1^{23}\text{Na}_1$ requires M^+ 406.3292.

8.2.5 Screening Compounds Library

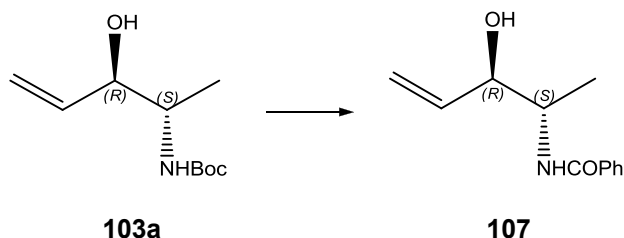
General procedure for BOC de-protection - Acylation Reactions

To a solution of the *N*-Boc protected starting material in CH₂Cl₂, TFA (excess) was added dropwise at room temperature and the reaction was monitored by TLC. Typically the reaction was complete in less than 1 hr. The reaction mixture was dried on the rotary evaporator to remove the excess TFA. The resulting residue (unprotected amine) was dissolved in CH₂Cl₂ (2 ml) and basified to pH 8 with aq. NaHCO₃ followed by the addition of the corresponding acid chloride (1.2 eq.). The reaction was monitored by TLC. Upon completion, the reaction was diluted with sat. aq. NH₄Cl. The phases were separated and the aqueous layer was extracted with twice CH₂Cl₂. The combined organic extracts were washed with brine, dried on anhydrous MgSO₄ and evaporated to yield the crude product. Assessment of the crude product purity was based on crude ¹H NMR. Compounds that were ≥80% pure were used as they soon as produced. Others were purified by standard column chromatography. All compounds used in the screening were characterised as an array (¹H NMR and Mass Spectrometry data).

8.2.5.1 4*E*-1-deoxy ceramide analogues

N-((2*S*,3*R*)-3-hydroxypent-4-en-2-yl)benzamide (107)

(It was prepared to test the synthetic route)

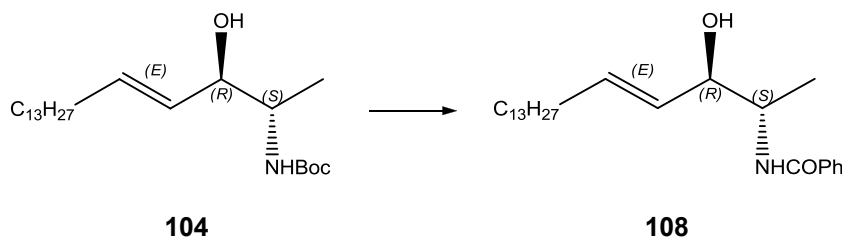


Yield (80%); δ_{H} (500 MHz, CDCl₃) 7.79–7.75 (2H, m, ArH), 7.51 (1H, m, ArH), 7.44 (2H, m, ArH), 6.30 (1H, br s, NH), 5.92 (1H, ddd, *J* 17.3, 10.6, 5.4, 4-*H*), 5.38 (1H, dt, *J* 17.3, 1.4, 5-*H*_{trans}), 5.27 (1H, d, *J* 10.6, 5-*H*_{cis}), 4.39–4.31 (2H, m, 3-*H* and 2-*H*), 2.17 (1H, s, OH), 1.23 (3H, d, *J* 6.9, 1-*H*₃); δ_{C} (126 MHz, CDCl₃) 168.1 CONH, 136.9 C4, 134.4 ArC1', 131.8 ArC4', 128.7

ArC3',5', 127.1 ArC2',6', 116.9 C5, 75.7 C3, 50.4 C2, 15.2 C1; m/z (ES⁺) 228.6 [M+Na]⁺, C₁₂H₁₅O₂N₁²³Na₁; HRMS (ES⁺) found [M+Na]⁺ 228.1008, C₁₂H₁₅O₂N₁²³Na₁ requires M^+ 228.1000.

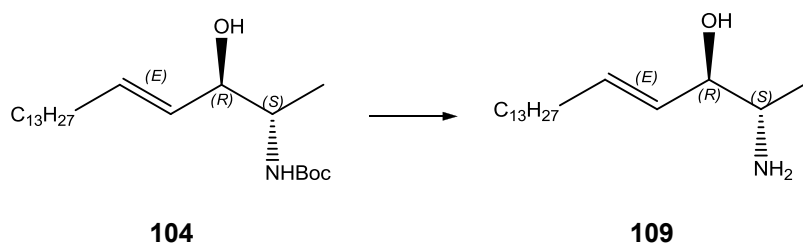
N-((2*S*,3*R*,*E*)-3-hydroxyoctadec-4-en-2-yl)benzamide (108)

(It was prepared to test the synthetic route)



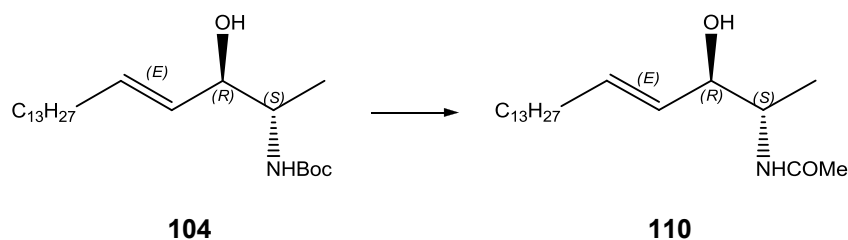
Yield (45%); δ_{H} (400 MHz, CDCl₃) 7.79–7.75 (2H, m, ArH), 7.53–7.47 (1H, m, ArH), 7.46–7.41 (2H, m, ArH), 6.34 (1H, br d, J 7.8, NH), 5.81–5.72 (1H, m, 5-*H*), 5.49 (1H, dd, J 15.4, 6.4, 4-*H*), 4.31 (1H, ddd, J 13.7, 6.9, 3.2, 3-*H*), 4.25 (1H, dd, J 6.4, 2.0, 2-*H*), 2.11–1.99 (2H, m, 6-*H*₂), 1.41–1.19 (25H, m, 7-*H*₂ to 17-*H*₂ and 1-*H*₃), 0.88 (3H, t, J 6.9, 18-*H*₃); m/z (ES⁺) 410.4 [M+Na]⁺ C₂₅H₄₁O₂N₁²³Na₁; HRMS (ES⁺) found [M+Na]⁺ 410.3047, C₂₅H₄₁O₂N₁²³Na₁ requires M^+ 410.3035.

(2*S*,3*R*,*E*)-2-aminooctadec-4-en-3-ol (109)



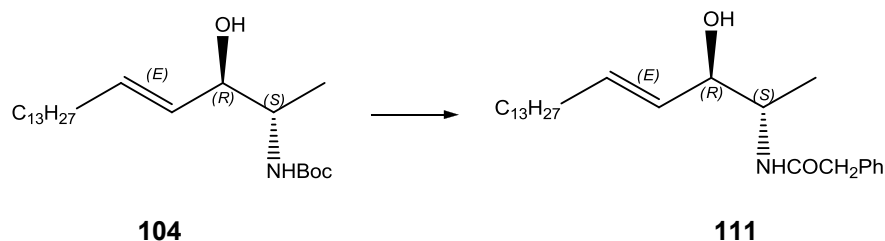
Yield (62%); δ_{H} (400 MHz, CDCl₃) 7.80 (2H, br s, NH₂), 5.77 (1H, dt, J 15.2, 6.4, 5-*H*), 5.37 (1H, dd, J 15.2, 6.1, 4-*H*), 4.41–4.24 (1H, m, 3-*H*), 3.40–3.28 (2H, m, 2-*H* and OH), 2.02 (2H, dd, J 13.7, 6.7, 6-*H*₂), 1.29–1.21 (25H, m, 7-*H*₂ to 17-*H*₂ and 1-*H*₃), 0.87 (3H, t, J 6.8, 18-*H*₃); m/z (ES⁺) 284.3 [M+H]⁺; HRMS (ES⁺) found [M+H]⁺ 284.2947, C₁₈H₃₈O₃N₁ requires M^+ 284.2948.

N-((2*S*,3*R*,*E*)-3-hydroxyoctadec-4-en-2-yl)acetamide (110)



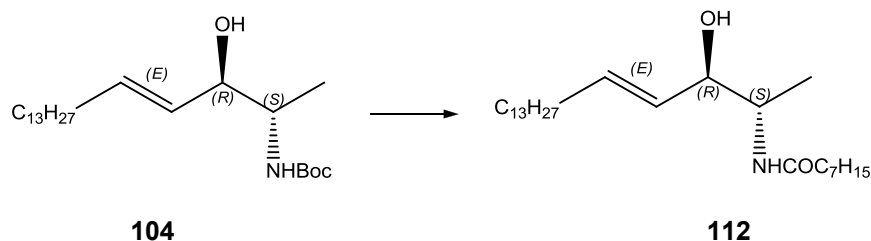
Yield (80%); δ_{H} (400 MHz, CDCl_3) 5.75–5.66 (1H, m, 5-*H*), 5.60 (1H, d, J 2.4, *NH*), 5.48–5.35 (1H, m, 4-*H*), 4.12 (1H, dd, J 6.7, 3.2, 3-*H*), 4.10–4.04 (1H, m, 2-*H*), 2.11–1.95 (5H, m, 6-*H*₂ and COCH_3), 1.40–1.11 (22H, m, 7-*H*₂ to 18-*H*₂), 1.08 (3H, d, J 6.9, 1-*H*₃), 0.87 (3H, t, J 6.8, 18-*H*₃); m/z (ES^+) 348.4 [$\text{M}+\text{Na}$]⁺; HRMS (ES^+) found [$\text{M}+\text{Na}$]⁺ 348.2871, $\text{C}_{20}\text{H}_{39}\text{O}_2\text{N}_1^{23}\text{Na}_1$ requires M^+ 348.2873.

N-((2*S*,3*R*,*E*)-3-hydroxyoctadec-4-en-2-yl)-2-phenylacetamide (111)



Yield (22%); δ_{H} (400 MHz, CDCl_3) 7.39–7.23 (5H, m, *ArH*), 5.64 (1H, dtd, J 15.0, 7.0, 0.9, 5-*H*), 5.51 (1H, br d, *NH*), 5.31 (1H, dd, J 15.0, 6.3, 4-*H*), 4.13–4.03 (2H, m, 3-*H* and 2-*H*), 3.58 (2H, s, PhCH_2), 1.98 (2H, dd, J 13.8, 7.0, 6-*H*₂), 1.39–1.18 (22H, m, 7-*H*₂ to 17-*H*₂), 1.01 (3H, d, J 6.8, 1-*H*₃), 0.88 (3H, t, J 6.9, 18-*H*₃); m/z (ES^+) 424.5 [$\text{M}+\text{Na}$]⁺; HRMS (ES^+) found [$\text{M}+\text{Na}$]⁺ 424.3182, $\text{C}_{26}\text{H}_{43}\text{O}_2\text{N}_1^{23}\text{Na}_1$ requires M^+ 424.3186.

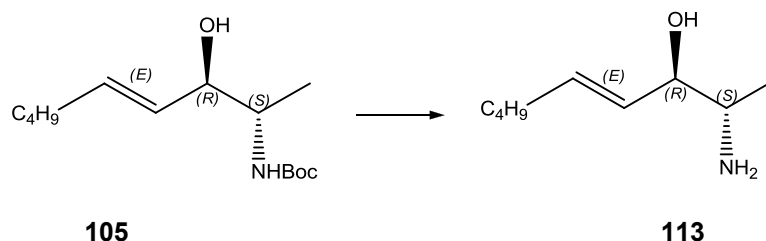
N-((2*S*,3*R*,*E*)-3-hydroxyoctadec-4-en-2-yl)octanamide (112)



Yield (41%); δ_{H} (400 MHz, CDCl_3) 5.71 (1H, dtd, J 14.9, 6.7, 1.1, 5-*H*), 5.43 (1H, dtd, J 15.4, 6.6, 1.4, 4-*H*), 4.64 (1H, br s, *NH*), 4.14–4.06 (1H, m, 3-*H*), 3.85–3.72 (1H, m, 2-*H*), 2.56 (1H, br s, *OH*), 2.04 (2H, dd, J 14.9, 7.0, 6-*H*₂), 1.40–1.20 (22 H, m, 7-*H*₂ to 17-*H*₂), 1.07 (3H, d,

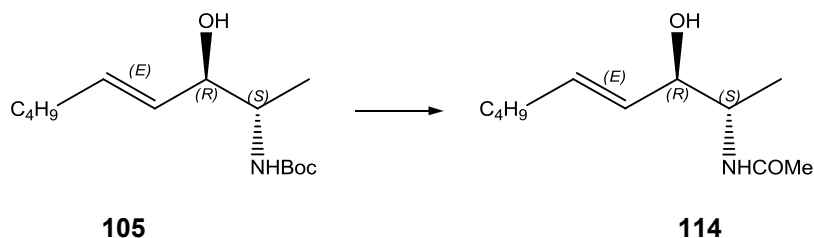
J 6.9, 1- H_3), 0.88 (3H, t, J 6.9, 18- H_3); m/z (ES^+) 432.6 [$M+Na$] $^+$; HRMS (ES^+) found [$M+Na$] $^+$ 432.3806, $C_{26}H_{51}O_2N_1^{23}Na_1$ requires M^+ 432.3812.

(2*S*,3*R*,*E*)-2-aminonon-4-en-3-ol (113)



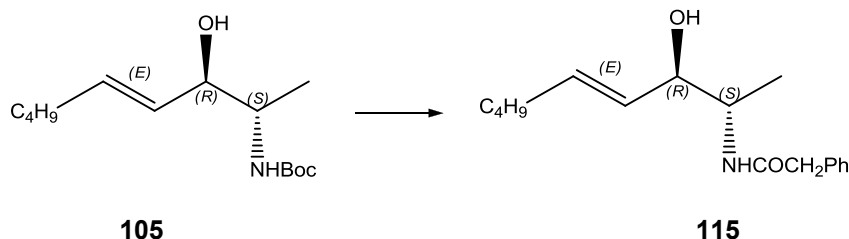
Yield (73%); δ_H (400 MHz, $CDCl_3$) 5.79–5.69 (1H, m, 5- H), 5.39 (1H, dd, J 14.9, 5.3, 4- H), 5.30 (2H, br s, NH_2), 4.32–4.24 (1H, m, 3- H), 3.33–3.21 (1H, m, 2- H), 2.03 (2H, dd, J 12.8, 5.2, 6- H_2), 1.41–1.26 (4H, m, 7- H_2 and 8- H_2), 1.15 (1H, d, J 6.5, 1- H_3), 0.88 (1H, t, J 6.9, 9- H_3); m/z (ES^+) 158.1 [$M+H$] $^+$; HRMS (ES^+) found [$M+Na$] $^+$ 158.1539, $C_9H_{19}O_1N_1^{23}Na_1$ requires M^+ 158.1539.

***N*-((2*S*,3*R*,*E*)-3-hydroxynon-4-en-2-yl)acetamide (114)**



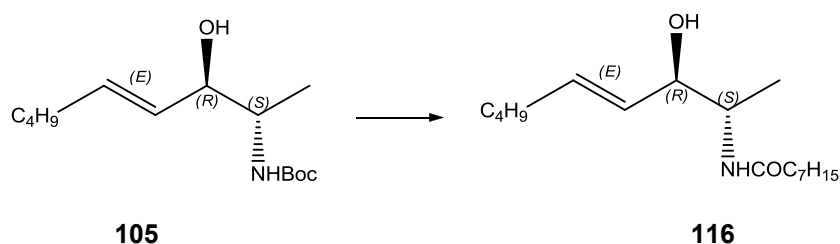
Yield (79%); δ_H (400 MHz, $CDCl_3$) 6.03 (1H, br s, NH), 5.74–5.62 (1H, m, 5- H), 5.41 (1H, dd, J 15.3, 6.4, 4- H), 4.16–4.00 (1H, m, 3- H and 2- H), 3.73 (1H, s, OH), 2.14–1.87 (5H, m, 6- H_2 and $COCH_3$), 1.44–1.25 (4H, m, 7- H_2 and 8- H_2), 1.06 (1H, d, J 6.8, 1- H_3), 0.88 (3H, t, J 6.8, 9- H_3); m/z (ES^+) 222.2 [$M+Na$] $^+$; HRMS (ES^+) found [$M+Na$] $^+$ 222.1463, $C_{11}H_{21}O_2N_1^{23}Na_1$ requires M^+ 222.1465.

***N*-((2*S*,3*R*,*E*)-3-hydroxynon-4-en-2-yl)-2-phenylacetamide (115)**



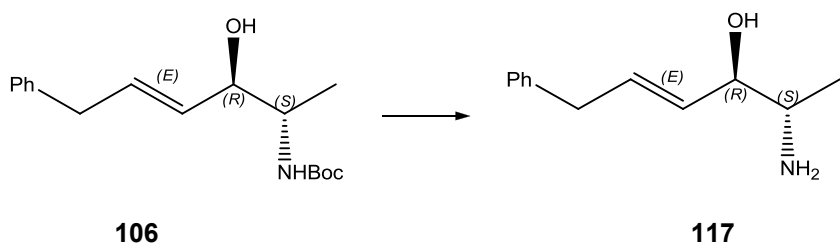
Yield (50%); δ_{H} (400 MHz, CDCl_3) 7.35–7.22 (5H, m, ArH), 5.69–5.59 (1H, m, 5-H), 5.32 (1H, dd, J 15.9, 6.3, 4-H), 4.19–3.98 (2H, m, 3-H and 2-H), 3.56 (2H, s, PhCH_2), 1.99 (2H, dd, J 13.3, 6.6, 6- H_2), 1.34–1.21 (2H, m, 7- H_2 and 8- H_2), 1.01 (1H, d, J 6.6, 1- H_3), 0.89 (1H, t, J 6.5, 9- H_3); m/z (ES^+) 298.3 $[\text{M}+\text{Na}]^+$; HRMS (ES^+) found $[\text{M}+\text{Na}]^+$ 298.1775, $\text{C}_{17}\text{H}_{25}\text{O}_2\text{N}_1^{23}\text{Na}_1$ requires M^+ 298.1778.

N-((2*S*,3*R*,*E*)-3-hydroxynon-4-en-2-yl)octanamide (116)



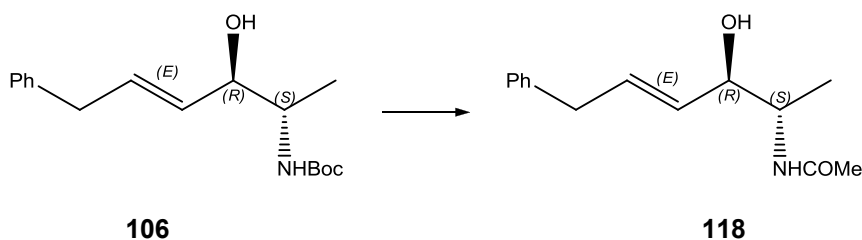
Yield (23%); δ_{H} (400 MHz, CDCl_3) 5.76–5.67 (1H, m, 5-H), 5.63 (1H, br d, J 7.7, NH), 5.41 (1H, dd, J 15.5, 6.3, 4-H), 4.11 (2H, m, 3-H and 2-H), 2.20–2.15 (2H, m, COCH_2), 2.10–2.02 (2H, m, 6- H_2), 1.66–1.58 (2H, m, COCH_2CH_2), 1.39–1.22 (12H, m, 7- H_2 , 8- H_2 and 4 \times octanoyl aliphatic CH_2), 1.09 (3H, d, J 6.8, 1- H_3), 0.92–0.85 (6H, m, 9- H_3 and octanoyl terminal CH_3); m/z (ES^+) 306.4 $[\text{M}+\text{Na}]^+$; HRMS (ES^+) found $[\text{M}+\text{Na}]^+$ 306.2402, $\text{C}_{17}\text{H}_{33}\text{O}_2\text{N}_1^{23}\text{Na}_1$ requires M^+ 306.2404.

(2*S*,3*R*,*E*)-2-amino-6-phenylhex-4-en-3-ol (117)



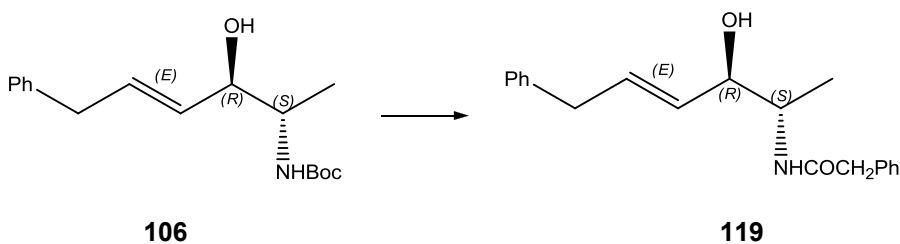
Yield (77%); δ_{H} (400 MHz, CDCl_3) 7.85 (2H, br s, NH_2), 7.29–7.23 (2H, m, ArH), 7.20–7.16 (1H, m, ArH), 7.14–7.11 (2H, m, ArH), 5.97–5.88 (1H, m, 5- H), 5.45 (1H, dd, J 15.5, 6.2, 4- H), 4.48–4.39 (1H, m, 3- H), 3.43–3.37 (1H, m, 2- H), 3.35 (2H, d, J 7.7, 6- H_2), 2.89 (1H, br s, OH), 1.19 (3H, d, J 6.5, 1- H_3); m/z (ES^+) 192.2 $[\text{M}+\text{H}]^+$; HRMS (ES^+) found $[\text{M}+\text{H}]^+$ 192.1383, $\text{C}_{12}\text{H}_{18}\text{O}_1\text{N}_1$ requires M^+ 192.1383.

***N*-((2*S*,3*R*,*E*)-3-hydroxy-6-phenylhex-4-en-2-yl)acetamide (118)**



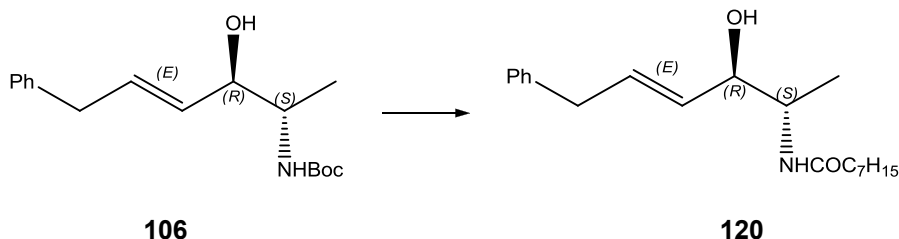
Yield (67%); δ_{H} (400 MHz, CDCl_3) 7.31–7.27 (2H, m, ArH), 7.22–7.14 (3H, m, ArH), 5.98 (1H, br s, NH), 5.93–5.82 (1H, m, 5- H), 5.50 (1H, dd, J 15.3, 6.2, 4- H), 4.21–4.13 (1H, m, 3- H), 4.06 (1H, dt, J 8.0, 4.0, 2- H), 3.38 (1H, d, J 6.7, 6- H_2), 2.85 (2H, br s, OH), 1.94 (3H, s, COCH_3), 1.08 (3H, d, J 6.9, 1- H_3); m/z (ES^+) 256.3 $[\text{M}+\text{Na}]^+$; HRMS (ES^+) found $[\text{M}+\text{Na}]^+$ 256.1307, $\text{C}_{14}\text{H}_{19}\text{O}_2\text{N}_1^{23}\text{Na}_1$ requires M^+ 256.1308.

***N*-((2*S*,3*R*,*E*)-3-hydroxy-6-phenylhex-4-en-2-yl)-2-phenylacetamide (119)**



Yield (87%); δ_{H} (400 MHz, CDCl_3) 7.35–7.10 (10H, m, ArH), 5.91 (1H, br s, NH), 5.86–5.77 (1H, m, 5- H), 5.40 (1H, dd, J 15.4, 6.0, 4- H), 4.18–3.96 (1H, m, 3- H), 3.60–3.49 (1H, m, 2- H), 3.42 (2H, s, COCH_2), 3.32 (2H, d, J 6.7, 6- H_2), 1.01 (3H, d, J 6.8, 1- H_3); m/z (ES^+) 332.3 $[\text{M}+\text{Na}]^+$; HRMS (ES^+) found $[\text{M}+\text{Na}]^+$ 332.1618, $\text{C}_{20}\text{H}_{23}\text{O}_2\text{N}_1^{23}\text{Na}_1$ requires M^+ 332.1621.

***N*-((2*S*,3*R*,*E*)-3-hydroxy-6-phenylhex-4-en-2-yl)octanamide (120)**

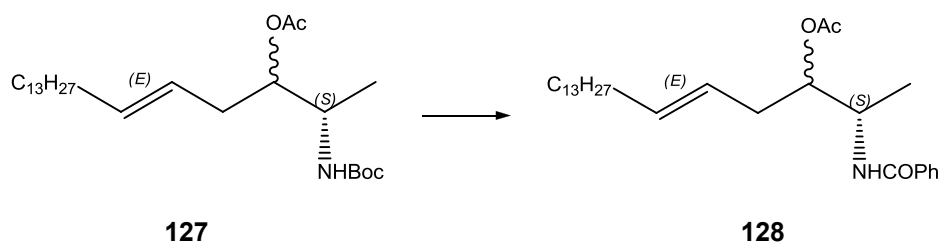


Yield (90%); δ_{H} (400 MHz, CDCl_3) 7.31–7.24 (2H, m, ArH), 7.22–7.12 (3H, m, ArH), 5.95–5.82 (2H, m, 5-H and NH), 5.50 (1H, dd, J 15.4, 6.2, 4-H), 4.20–4.03 (2H, m, 3-H and 2-H), 3.38 (1H, d, J 6.7, 6- H_2), 2.17–2.10 (2H, m, COCH_2), 1.66–1.51 (2H, m, COCH_2CH_2), 1.32–1.20 (8H, m, 4 \times CH_2), 1.08 (3H, d, J 6.8, 1- H_3), 0.87 (3H, t, J 6.8, octanoyl terminal CH_3); m/z (ES^+) 318.2 $[\text{M}+\text{H}]^+$, 340.4 $[\text{M}+\text{Na}]^+$; HRMS (ES^+) found $[\text{M}+\text{H}]^+$ 318.2431, $\text{C}_{20}\text{H}_{32}\text{O}_2\text{N}_1$ requires M^+ 318.2428.

8.2.5.2 5E-1-deoxy ceramide analogues

(2S,E)-2-benzamidononadec-5-en-3-yl acetate (128)

(It was prepared to test the synthetic route)

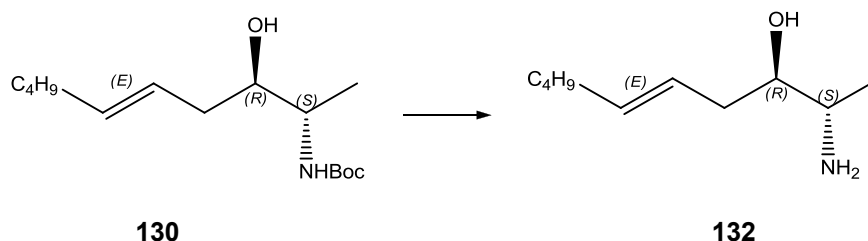


Characterised as a mixture of the two diastereoisomers (70:30) with the signals attributed to the minor diastereoisomers indicated where applicable;

Yield (85%); δ_{H} (700 MHz, CDCl_3) 7.81–7.70 (2H, m, ArH), 7.53–7.47 (1H, m, ArH), 7.47–7.38 (2H, m, ArH), 6.78–6.72 (1H, m, NH), 5.59–5.49 (1H, m, 6-H), 5.41–5.30 (1H, m, 5-H), 4.95 (1H, ddd, J 8.3, 5.7, 2.9, 3-H), 4.47–4.42 (0.3H, m, *minor* 2-H), 4.42–4.34 (0.7H, m, 2-H), 2.41–2.28 (2H, m, 4- H_2), 2.11 (3H, s, OCOCH_3), 1.98 (2H, dd, J 14.1, 6.9, 7- H_2), 1.39–1.18 (25H, m, 8- H_2 to 18- H_2 and 1- H_3), 0.88 (3H, t, J 7.1, 19- H_3); δ_{C} (176 MHz, CDCl_3) 171.87, 166.61, 134.86, 131.53, 128.68, 127.02, 126.99, 124.27, 76.36, 48.11, 35.11, 32.75, 32.06,

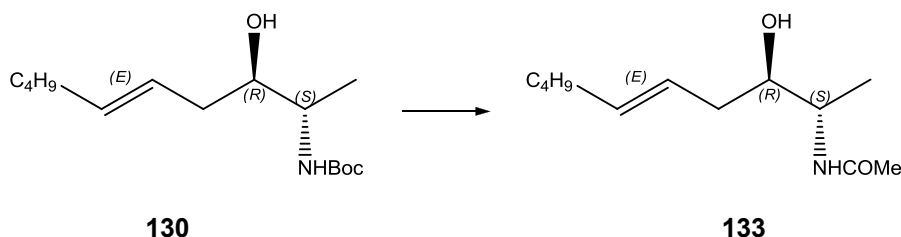
29.83, 29.82, 29.80, 29.77, 29.65, 29.51, 29.50, 29.33, 22.83, 21.23, 14.97, 14.26; m/z (ES^+) 444.5 $[M+H]^+$; HRMS (ES^+) found $[M+H]^+$ 444.3481, $C_{28}H_{46}O_3N_1$ requires M^+ 444.3472.

(2*S*,3*R*,*E*)-2-aminodec-5-en-3-ol (132)



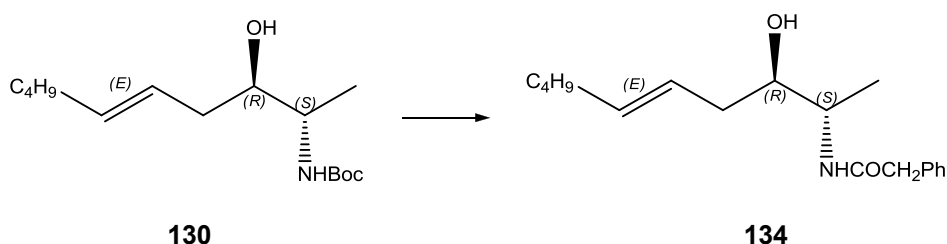
Yield (79%); δ_H (400 MHz, $CDCl_3$) 5.62–5.45 (1H, m, 6-*H*), 5.41–5.26 (1H, m, 5-*H*), 5.14 (1H, br s, NH_2), 3.83–3.71 (1H, m, 2-*H*), 3.31–3.13 (1H, m, 3-*H*), 2.27–1.93 (4H, m, 4-*H*₂ and 7-*H*₂), 1.33–1.29 (4H, m, 8-*H*₂ and 9-*H*₂), 1.16 (3H, d, J 6.1, 1-*H*₃), 0.87 (3H, t, J 7.0, 10-*H*₃); m/z (ES^+) 172.3 $[M+H]^+$, 194.3 $[M+Na]^+$; HRMS (ES^+) found $[M+H]^+$ 172.1696, $C_{10}H_{22}O_1N_1$ requires M^+ 172.1696.

***N*-((2*S*,3*R*,*E*)-3-hydroxydec-5-en-2-yl)acetamide (133)**



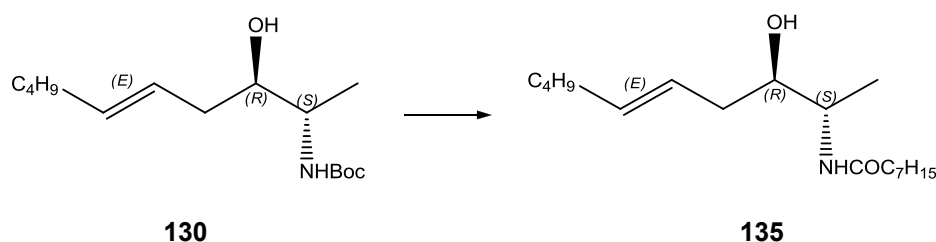
Yield (70%); δ_H (400 MHz, $CDCl_3$) 5.88 (1H, br s, NH), 5.55 (1H, dt, J 13.4, 6.6, 6-*H*), 5.44–5.34 (1H, m, 5-*H*), 4.01 (1H, ddd, J 8.5, 6.8, 3.0, 2-*H*), 3.64 (1H, ddt, J 8.5, 4.2, 3.1, 3-*H*), 2.11–1.99 (4H, m, 4-*H*₂ and 7-*H*₂), 1.98 (3H, s, $COCH_3$), 1.38–1.25 (4H, m, 8-*H*₂ and 9-*H*₂), 1.10 (3H, d, J 6.8, 1-*H*₃), 0.88 (3H, t, J 7.1, 10-*H*₃); m/z (ES^+) 236.3 $[M+Na]^+$; HRMS (ES^+) found $[M+Na]^+$ 236.1620, $C_{12}H_{23}O_2N_1^{23}Na_1$ requires M^+ 236.1621.

***N*-((2*S*,3*R*,*E*)-3-hydroxydec-5-en-2-yl)-2-phenylacetamide (134)**



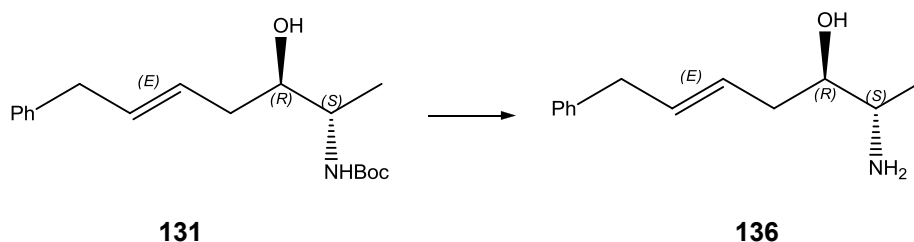
Yield (85%); δ_{H} (400 MHz, CDCl_3) 7.40–7.22 (5H, m, ArH), 5.73 (1H, br s, NH), 5.50 (1H, dt, J 15.2, 6.6, 6-H), 5.35 (1H, ddd, J 15.2, 7.7, 6.3, 5-H), 3.99 (1H, ddd, J 8.5, 6.9, 3.1, 2-H), 3.56 (1H, m, 3-H and PhCH_2), 2.22–2.08 (2H, m, 4- H_2), 2.06–1.92 (2H, m, 7- H_2), 1.34–1.28 (4H, m, 8- H_2 and 9- H_2), 1.04 (3H, d, J 6.9, 1- H_3), 0.88 (3H, t, J 7.1, 10- H_3); m/z (ES^+) 312.4 $[\text{M}+\text{Na}]^+$; HRMS (ES^+) found $[\text{M}+\text{Na}]^+$ 312.1935, $\text{C}_{18}\text{H}_{27}\text{O}_2\text{N}_1^{23}\text{Na}_1$ requires M^+ 312.1934.

***N*-(*(2S,3R,E)*-3-hydroxydec-5-en-2-yl)octanamide (135)**

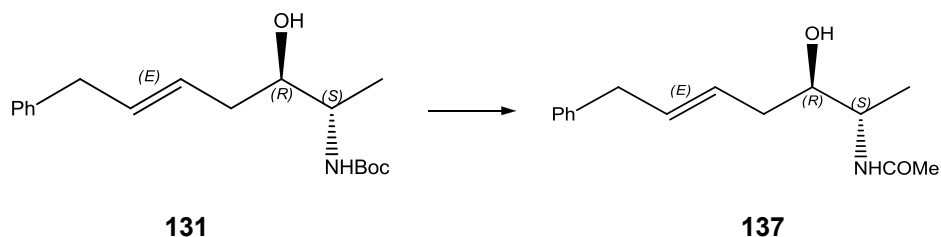


Yield (83%); δ_{H} (400 MHz, CDCl_3) 6.03–5.98 (1H, br s, NH), 5.54–5.43 (1H, m, 6-H), 5.35–5.25 (1H, m, 5-H), 4.23–4.11 (1H, m, 2-H), 4.05–3.98 (1H, m, 3-H), 2.35–2.27 (2H, m, COCH_2), 2.20–2.11 (2H, m, 4- H_2), 2.06–1.94 (2H, m, 7- H_2), 1.68–1.50 (2H, m, COCH_2CH_2), 1.39–1.19 (12H, m, 8- H_2 , 9- H_2 and $4 \times$ aliphatic CH_2), 1.14–1.05 (3H, d, J 6.9, 1- H_3), 0.86 (6H, 10- H_3 and octanoyl terminal CH_3); m/z (ES^+) 298.5 $[\text{M}+\text{H}]^+$, 320.5 $[\text{M}+\text{Na}]^+$; HRMS (ES^+) found $[\text{M}+\text{Na}]^+$ 320.2563, $\text{C}_{18}\text{H}_{35}\text{O}_2\text{N}_1^{23}\text{Na}_1$ requires M^+ 320.2560.

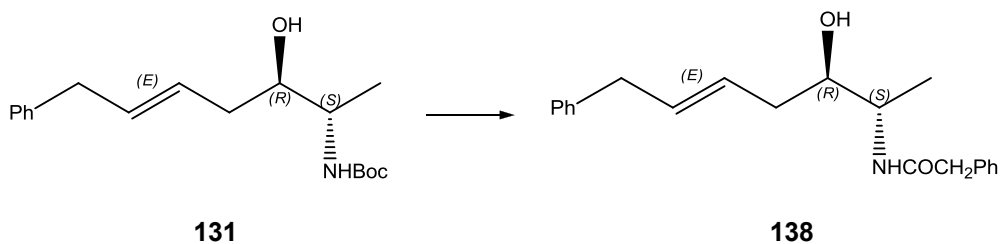
(*2S,3R,E*)-2-amino-7-phenylhept-5-en-3-ol (136)



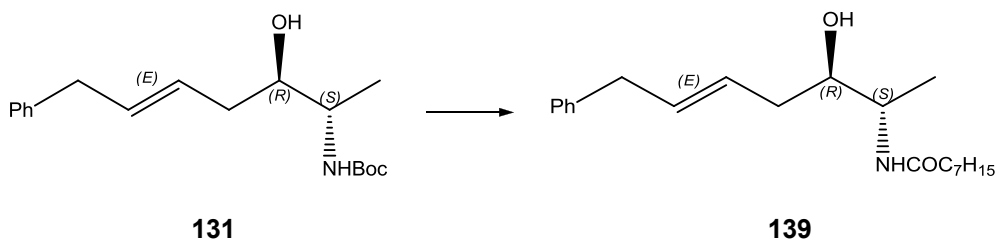
Yield (46%); δ_{H} (700 MHz, CDCl_3) 7.88 (2H, br s, NH_2), 7.20–7.11 (5H, m, ArH), 5.71–5.65 (1H, m, 6-H), 5.45–5.40 (1H, m, 5-H), 3.93–3.89 (1H, m, 3-H), 3.36 (1H, d, J 7.7, 2-H), 3.32 (2H, d, J 6.7, 7- H_2), 2.28–2.09 (2H, m, 4- H_2), 1.20 (3H, d, J 6.3, 1- H_3). m/z (ES^+) 206.3 $[\text{M}+\text{H}]^+$, 228.3 $[\text{M}+\text{Na}]^+$; HRMS (ES^+) found $[\text{M}+\text{H}]^+$ 206.1540, $\text{C}_{13}\text{H}_{20}\text{O}_1\text{N}_1$ requires M^+ 206.1539.

***N*-((2*S*,3*R*,*E*)-3-hydroxy-7-phenylhept-5-en-2-yl)acetamide (137)**

Yield (86%); δ_{H} (400 MHz, CDCl_3) 7.34–7.24 (2H, m, Ar*H*), 7.24–7.15 (3H, m, Ar*H*), 5.79 (1H, br s, NH), 5.73 (1H, ddd, J 15.2, 8.4, 4.3, 6-*H*), 5.52 (1H, ddd, J 15.2, 7.7, 6.4, 5-*H*), 4.03 (1H, dqd, J 13.8, 6.9, 3.0, 2-*H*), 3.72–3.65 (1H, m, 3-*H*), 3.37 (1H, d, J 6.7, 7-*H*₂), 2.30–2.04 (2H, m, 4-*H*₂), 1.98 (3H, s, COCH_3), 1.11 (3H, d, J 6.9, 1-*H*₃); m/z (ES^+) 248.4 $[\text{M}+\text{H}]^+$, 270.3 $[\text{M}+\text{Na}]^+$; HRMS (ES^+) found $[\text{M}+\text{Na}]^+$ 270.1464, $\text{C}_{15}\text{H}_{21}\text{O}_2\text{N}_1^{23}\text{Na}_1$ requires M^+ 270.1465.

***N*-((2*S*,3*R*,*E*)-3-hydroxy-7-phenylhept-5-en-2-yl)-2-phenylacetamide (138)**

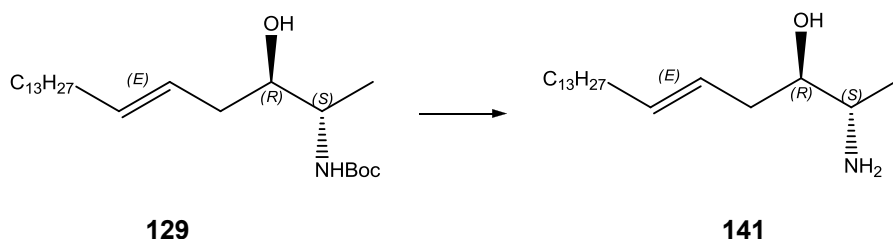
Yield (27%); δ_{H} (400 MHz, CDCl_3) 7.43–7.08 (10H, m, Ar*H*), 5.78–5.59 (1H, m, 6-*H*), 5.57–5.37 (1H, m, 5-*H*), 4.07–3.93 (1H, m, 2-*H*), 3.64–3.50 (3H, m, 2-*H* and PhCH_2), 3.34 (1H, d, J 6.7, 7-*H*₂), 2.25–1.93 (2H, m, 4-*H*₂), 1.03 (3H, d, J 6.8, 1-*H*₃); m/z (ES^+) 346.4 $[\text{M}+\text{Na}]^+$; HRMS (ES^+) found $[\text{M}+\text{Na}]^+$ 346.1779, $\text{C}_{21}\text{H}_{25}\text{O}_2\text{N}_1^{23}\text{Na}_1$ requires M^+ 346.1778.

***N*-((2*S*,3*R*,*E*)-3-hydroxy-7-phenylhept-5-en-2-yl)octanamide (139)**

Yield (70%); δ_{H} (400 MHz, CDCl_3) 7.31–7.27 (2H, m, Ar*H*), 7.23–7.15 (3H, m, Ar*H*), 5.87–5.65 (1H, m, NH and 6-*H*), 5.52 (1H, dt, J 14.2, 6.6, 5-*H*), 4.13–3.94 (1H, m, 2-*H*), 3.78–3.59

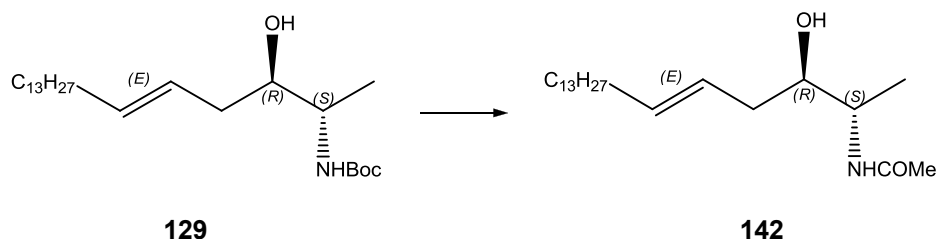
(1H, m, 3-*H*), 3.37(1H, d, *J* 6.6, 7-*H*₂), 2.32–2.04 (2H, m, COCH₂), 1.70–1.54 (2H, m, COCH₂CH₂), 1.37–1.21 (8H, m, 4 × aliphatic CH₂), 1.13 (3H, d, *J* 6.9, 1-*H*₃), 0.87 (3H, t, *J* 6.6, octanoyl terminal CH₃); *m/z* (ES⁺) 332.5 [M+H]⁺, 354.4 [M+Na]⁺; HRMS (ES⁺) found [M+Na]⁺ 354.2403, C₂₁H₃₃O₂N₁²³Na₁ requires *M*⁺ 354.2404.

(2*S*,3*R*,*E*)-2-aminononadec-5-en-3-ol (141)



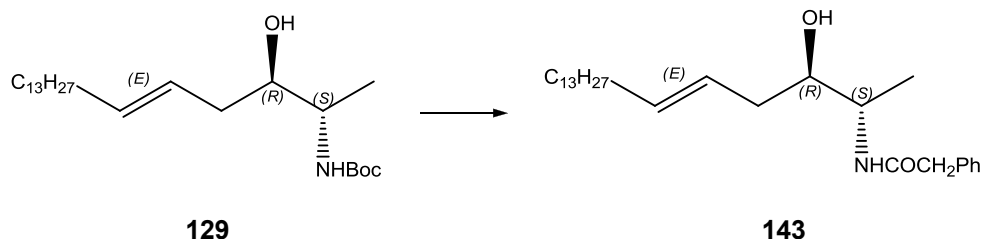
Yield (70%); δ_{H} (700 MHz, CDCl₃) 8.12 (2H, br s, NH₂), 5.56–5.48 (1H, m, 6-*H*), 5.38 (1H, dd, *J* 14.0, 6.7, 5-*H*), 3.73–3.67 (1H, m, 3-*H*), 3.65–3.60 (1H, m, 2-*H*), 2.15–2.07 (1H, m, 4-*HH*), 2.04–1.95 (3H, m, 4-*HH* and 7-*H*₂), 1.38–1.09 (26H, m, 8-*H*₂ to 18-*H*₂ and 1-*H*₃), 0.86 (3H, t, *J* 7.0, 19-*H*₃). *m/z* (ES⁺) 298.4 [M+H]⁺; HRMS (ES⁺) found [M+H]⁺ 298.3099, C₁₉H₄₀O₁N₁ requires *M*⁺ 298.3110.

***N*-((2*S*,3*R*,*E*)-3-hydroxynonadec-5-en-2-yl)acetamide (142)**



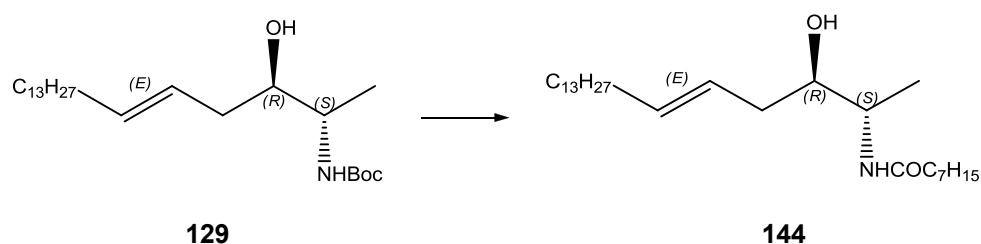
Yield (82%); δ_{H} (400 MHz, CDCl₃) 5.96 (1H, br d, *J* 6.0, NH), 5.54 (1H, dt, *J* 15.0, 6.6, 6-*H*), 5.45–5.34 (1H, m, 5-*H*), 4.00 (1 H, ddd, *J* 8.5, 6.9, 3.0, 3-*H*), 3.64 (1H, ddd, *J* 8.8, 4.4, 3.0, 2-*H*), 2.23–1.99 (4 H, m, 7-*H*₂ and 4-*H*₂), 1.97 (3H, s, COCH₃), 1.38–1.21 (22H, m, 8-*H*₂ to 18-*H*₂), 1.10 (3H, d, *J* 6.8, 1-*H*₃), 0.87 (3H, t, *J* 6.9, 19-*H*₃). *m/z* (ES⁻) 338.4 [M-H]⁻; (ES⁺) 362.4.3 [M+Na]⁺; HRMS (ES⁺) found [M+H]⁺ 340.3219, C₂₁H₄₂O₂N₁ requires *M*⁺ 340.3216.

***N*-((2*S*,3*R*,*E*)-3-hydroxynonadec-5-en-2-yl)-2-phenylacetamide (143)**



Yield (86%); δ_{H} (400 MHz, CDCl_3) 7.37–7.32 (2H, m, ArH), 7.31–7.24 (3H, m, ArH), 5.74 (1H, br d, J 8.3, NH), 5.50 (1H, dt, J 14.7, 6.6, 6-H), 5.34 (1H, ddd, J 15.2, 7.6, 6.4, 5-H), 3.99 (1H, ddd, J 8.4, 6.9, 3.1, 3-H), 3.73–3.64 (1H, m, 2-H), 3.55 (2H, s, PhCH_2), 2.15–2.08 (2H, m, 4- H_2), 2.06–1.94 (2H, m, 7- H_2), 1.36–1.22 (22H, m, 8- H_2 to 18- H_2), 1.04 (3H, d, J 6.8, 1- H_2), 0.88 (3H, t, J 6.9, 19- H_3). m/z (ES^-) 414.4 [$\text{M}-\text{H}$] $^-$; (ES^+) 438.4 [$\text{M}+\text{Na}$] $^+$; HRMS (ES^+) found [$\text{M}+\text{H}$] $^+$ 416.3533, $\text{C}_{27}\text{H}_{46}\text{O}_2\text{N}_1$ requires M^+ 416.3529.

N-((2*S*,3*R*,*E*)-3-hydroxynonadec-5-en-2-yl)octanamide (144)

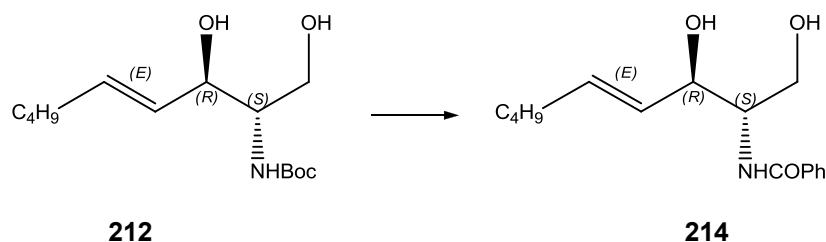


Yield (85%); δ_{H} (400 MHz, CDCl_3) 5.85 (1H, br d, J 8.4, NH), 5.55 (1H, dt, J 14.9, 6.6, 6-H), 5.39 (1H, ddd, J 15.0, 7.5, 6.4, 5-H), 4.03 (1H, ddd, J 8.7, 7.0, 3.0, 3-H), 3.64 (1H, ddd, J 8.8, 4.1, 3.0, 2-H), 2.33 (2H, t, J 7.5, COCH_2), 2.19–2.14 (2H, m, 4- H_2), 2.00 (2H, dd, J 13.7, 6.6, 7- H_2), 1.62 (2H, dd, J 13.3, 6.0, COCH_2CH_2), 1.34–1.22 (26H, m, 8- H_2 to 18- H_2 and 4 \times aliphatic CH_2), 1.10 (3H, d, J 6.8, 1- H_3), 0.87 (3H, t, J 6.7, 19- H_3). m/z (ES^-) 422. [$\text{M}-\text{H}$] $^-$; (ES^+) 446.4 [$\text{M}+\text{Na}$] $^+$; HRMS (ES^+) found [$\text{M}+\text{H}$] $^+$ 424.4174, $\text{C}_{27}\text{H}_{54}\text{O}_2\text{N}_1$ requires M^+ 424.4155.

8.2.5.3 Ceramide analogues

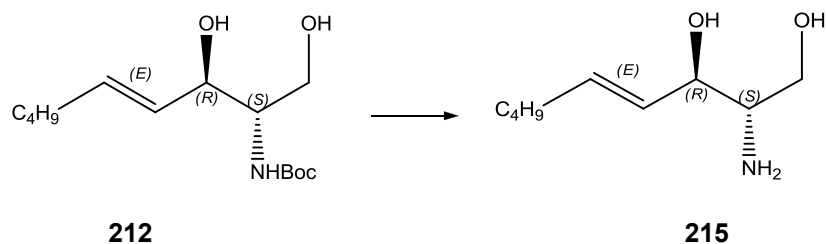
N-((2*S*,3*R*,*E*)-1,3-dihydroxynon-4-en-2-yl)benzamide (214)

(It was prepared to test the synthetic route)



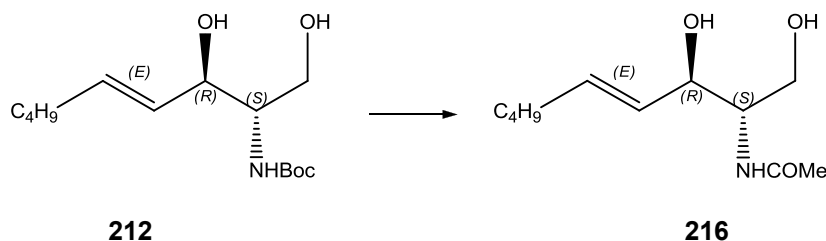
Yield (25%); δ_{H} (400 MHz, CDCl_3) 7.82–7.78 (2H, m, ArH), 7.51–7.46 (1H, m, ArH), 7.46–7.40 (2H, m, ArH), 7.03 (1H, br d, NH), 5.82 (1H, dt, J 16.0, 6.8, 5-*H*), 5.59 (1H, dd, J 16.0, 6.3, 4-*H*), 4.47–4.42 (1H, m, 3-*H*), 4.13–4.04 (2H, m, 2-*H* and 1-*HH*), 3.81 (1H, dd, J 11.3, 2.4, 1-*HH*), 2.36 (2H, br s, 2 \times OH), 2.07 (2H, dd, J 13.8, 6.8, 6-*H*₂), 1.38–1.21 (4H, m, 7-*H*₂ and 8-*H*₂), 0.87 (3H, t, J 7.0, 9-*H*₃); m/z (ES^-) 276.3 [M]⁻ $\text{C}_{16}\text{H}_{22}\text{O}_3\text{N}_1$; HRMS (ES^+) found [$\text{M}+\text{Na}$]⁺ 300.1588, $\text{C}_{16}\text{H}_{23}\text{O}_3\text{N}_1^{23}\text{Na}_1$ requires M^+ 300.1576.

(2S,3R,E)-2-aminonon-4-ene-1,3-diol (215)



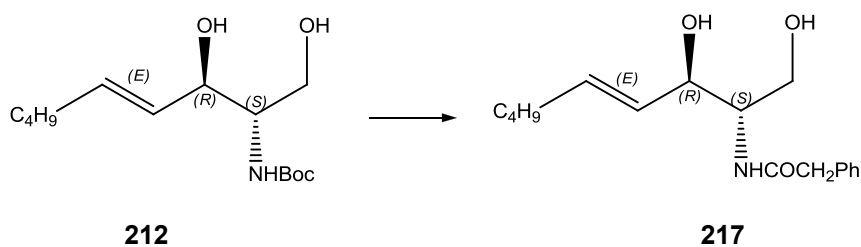
Yield (54%); δ_{H} (400 MHz, CDCl_3) 5.80–5.71 (1H, m, 5-*H*), 5.42 (1H, dd, J 15.2, 6.7, 4-*H*), 4.31 (4H, br s, NH_2 and 2 \times OH), 4.25–4.19 (1H, m, 3-*H*), 3.78–3.63 (2H, m, 2-*H* and 1-*HH*), 3.06 (1H, dd, J 8.7, 4.2, 1-*HH*), 2.04 (2H, dd, J 13.1, 6.5, 6-*H*₂), 1.39–1.26 (4H, m, 7-*H*₂ and 8-*H*₂), 0.88 (3H, t, J 7.0, 9-*H*₃); m/z (ES^+) 174.3 [$\text{M}+\text{H}$]⁺, 196.4 [$\text{M}+\text{Na}$]⁺; HRMS (ES^+) found [$\text{M}+\text{H}$]⁺ 174.1490, $\text{C}_9\text{H}_{20}\text{O}_2\text{N}_1$ requires M^+ 174.1489.

***N*-((2S,3R,E)-1,3-dihydroxynon-4-en-2-yl)acetamide (216)**



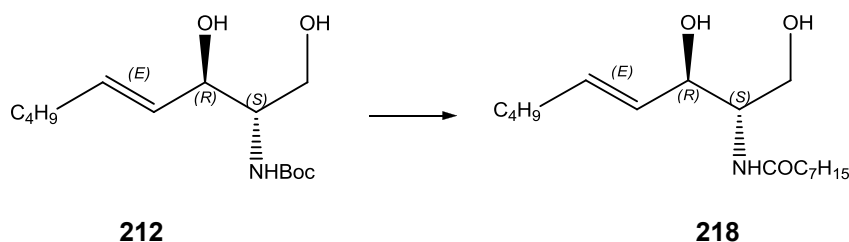
Yield (73%); δ_{H} (700 MHz, CDCl_3) 6.44 (1H, br d, J 13.7, NH), 5.82–5.76 (1H, m, 5-*H*), 5.41 (1H, dd, J 15.1, 5.7, 4-*H*), 4.47–4.39 (1H, m, 3-*H*), 3.87–3.77 (2H, m, 2-*H* and 1-*HH*), 3.35–3.29 (1H, m, 1-*HH*), 2.09–2.00 (5H, m, 6-*H*₂ and COCH_3), 1.41–1.23 (4H, m, 7-*H*₂ and 8-*H*₂), 0.88 (3H, t, J 7.3, 9-*H*₃). m/z (ES^+) 238.2 $[\text{M}+\text{Na}]^+$ $\text{C}_{11}\text{H}_{21}\text{O}_3\text{N}_1^{23}\text{Na}_1$; HRMS (ES^+) found $[\text{M}+\text{Na}]^+$ 238.1419, $\text{C}_{11}\text{H}_{21}\text{O}_3\text{N}_1^{23}\text{Na}_1$ requires M^+ 238.1419.

***N*-((2*S*,3*R*,*E*)-1,3-dihydroxynon-4-en-2-yl)-2-phenylacetamide (217)**

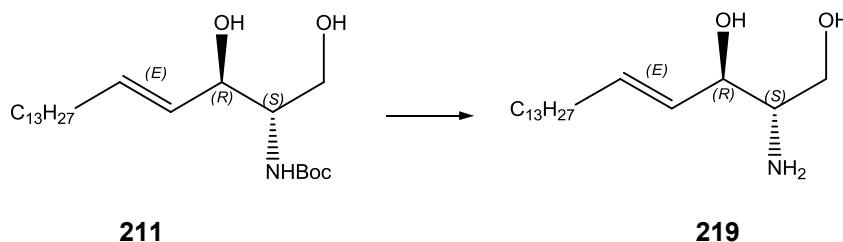


Yield (65%); δ_{H} (400 MHz, CDCl_3) 7.35–7.23 (5H, m, Ar*H*), 6.34 (1H, br d, J 6.6, NH), 5.66 (1H, dt, J 14.9, 6.7, 5-*H*), 5.40 (1H, dd, J 14.9, 6.5, 4-*H*), 4.23–4.16 (1H, m, 3-*H*), 3.88–3.79 (2H, m, 2-*H* and 1-*HH*), 3.61 (1H, dd, J 10.9, 2.7, 1-*HH*), 3.56 (2H, s, PhCH_2), 1.98 (1H, dd, J 13.5, 6.8, 6-*H*₂), 1.32–1.25 (4H, m, 7-*H*₂ and 8-*H*₂), 0.88 (3H, t, J 7.0, 9-*H*₃); m/z (ES^+) 292.2 $[\text{M}+\text{H}]^+$, 314.2 $[\text{M}+\text{Na}]^+$; HRMS (ES^+) found $[\text{M}+\text{H}]^+$ 292.1907, $\text{C}_{17}\text{H}_{26}\text{O}_3\text{N}_1$ requires M^+ 292.1913.

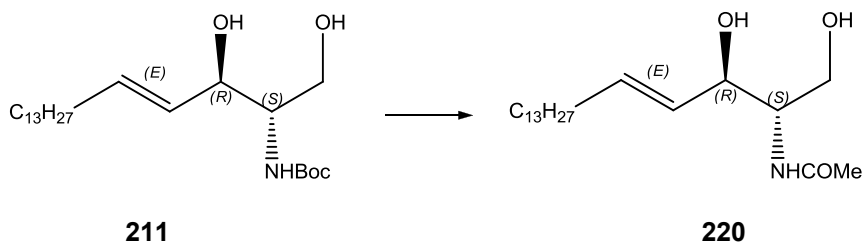
***N*-((2*S*,3*R*,*E*)-1,3-dihydroxynon-4-en-2-yl)octanamide (218)**



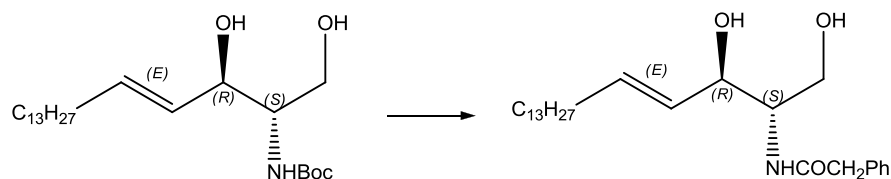
Yield (68%); δ_{H} (400 MHz, CDCl_3) 6.44 (1H, br s, NH), 5.74 (1H, dt, J 15.9, 6.7, 5-*H*), 5.49 (1H, dd, J 15.9, 6.0, 4-*H*), 4.30–4.21 (1H, m, 3-*H*), 3.94–3.84 (2H, m, 2-*H* and 1-*HH*), 3.71–3.63 (1H, m, 1-*HH*), 2.24–2.16 (2H, m, COCH_2), 2.04 (2H, dd, J 13.0, 6.7, 6-*H*₂), 1.64–1.55 (2H, m, COCH_2CH_2), 1.34–1.21 (4H, m, 7-*H*₂ and 8-*H*₂), 0.87, 0.86 ($2 \times 3\text{H}$, t, J 6.5, 9-*H*₃ and octanoyl terminal CH_3); m/z (ES^+) 300.3 $[\text{M}+\text{H}]^+$; HRMS (ES^+) found $[\text{M}+\text{H}]^+$ 300.2536, $\text{C}_{17}\text{H}_{34}\text{O}_3\text{N}_1$ requires M^+ 300.2539.

(2*S*,3*R*,*E*)-2-aminooctadec-4-ene-1,3-diol (219)⁴

Yield (64%); δ_{H} (400 MHz, CDCl_3) 5.87–5.79 (1H, m, 5-*H*), 5.53 (1H, dd, *J* 15.4, 6.5, 4-*H*), 4.78 (2H, br s, NH_2), 4.41–4.36 (1H, m, 3-*H*), 4.10 (1H, dd, *J* 11.5, 2.7, 1-*HH*), 3.93 (1H, m, 2-*H*), 3.73 (1H, dd, *J* 11.5, 3.5, 1-*HH*), 2.77 (2H, br s, 2 \times *OH*), 2.06 (2H, dd, *J* 14.0, 7.0, 6-*H*₂), 1.67 (1 H, dq, *J* 12.2, 6.0, 17-*H*₂), 1.48–1.22 (20H, m, 7-*H*₂ to 16-*H*₂), 0.89 (1H, t, *J* 7.5, 18-*H*₃); *m/z* (ES^+) 300.5 [$\text{M}+\text{H}$]⁺, 322.5 [$\text{M}+\text{Na}$]⁺; HRMS (ES^+) found [$\text{M}+\text{H}$]⁺ 300.2902, $\text{C}_{18}\text{H}_{38}\text{O}_2\text{N}_1$ requires M^+ 300.2897.

***N*-((2*S*,3*R*,*E*)-1,3-dihydroxyoctadec-4-en-2-yl)acetamide (220)**

Yield (71%); δ_{H} (400 MHz, CDCl_3) 5.81 (1H, dt, *J* 14.6, 7.1, 5-*H*), 5.51 (1H, dd, *J* 15.4, 6.4, 4-*H*), 5.39 (1H, br s, *NH*), 4.38–4.32 (1H, m, 3-*H*), 4.07 (1 H, dd, *J* 11.6, 2.7, 2-*H*), 3.83–3.78 (1H, m, 1-*HH*), 3.73 (1H, dd, *J* 11.6, 2.9, 1-*HH*), 2.09–1.98 (5H, m, 6-*H*₂ and COCH_3), 1.39–1.20 (22H, m, 7-*H*₂ to 17-*H*₂), 0.87 (1H, t, *J* 6.7, 18-*H*₃); *m/z* (ES^+) 364.4 [$\text{M}+\text{Na}$]⁺; HRMS (ES^+) found [$\text{M}+\text{Na}$]⁺ 364.2829, $\text{C}_{20}\text{H}_{39}\text{O}_3\text{N}_1^{23}\text{N}_1$ requires M^+ 364.2822.

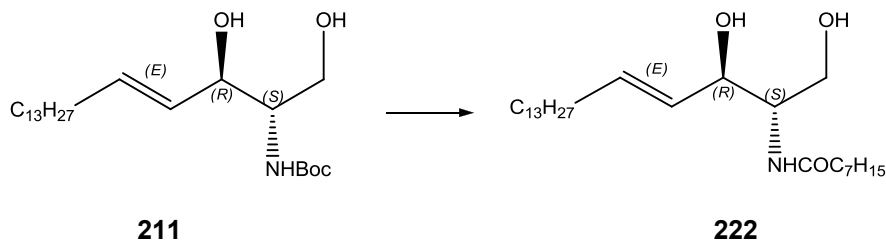
***N*-((2*S*,3*R*,*E*)-1,3-dihydroxyoctadec-4-en-2-yl)-2-phenylacetamide (221)**

211

221

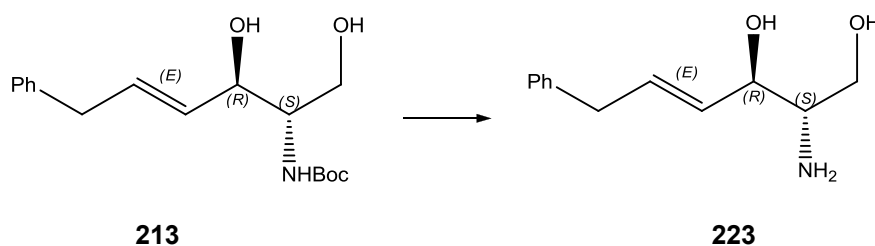
Yield (44%); δ_{H} (400 MHz, CDCl_3) 7.38–7.25 (5H, m, ArH), 6.21 (1H, br d, J 7.0, NH), 5.73–5.63 (1H, m, 5-*H*), 5.42 (1H, dd, J 15.4, 6.5, 4-*H*), 4.27–4.20 (1H, m, 3-*H*), 3.90–3.83 (2H, m, 2-*H* and 1-*HH*), 3.65 (1H, dd, J 11.8, 3.9, 1-*HH*), 3.60 (2H, s, PhCH_2), 2.97–2.64 (2H, m, 2 \times OH), 1.99 (2H, dd, J 13.8, 6.9, 6-*H*₂), 1.34–1.16 (22H, m, 7-*H*₂ to 17-*H*₂), 0.88 (1H, t, J 6.8, 18-*H*₃); m/z (ES^+) 440.5 [$\text{M}+\text{Na}$]⁺; HRMS (ES^+) found [$\text{M}+\text{H}$]⁺ 418.3324, $\text{C}_{26}\text{H}_{44}\text{O}_3\text{N}_1$ requires M^+ 418.3316.

***N*-((2*S*,3*R*,*E*)-1,3-dihydroxyoctadec-4-en-2-yl)octanamide (222)**



Yield (38%); δ_{H} (400 MHz, CDCl_3) 6.25 (1H, br d, J 7.8, NH), 5.84–5.74 (1H, m, 5-*H*), 5.53 (1H, dd, J 15.5, 6.5, 4-*H*), 4.36–4.30 (1H, m, 3-*H*), 3.96 (1H, dd, J 11.1, 3.7, 1-*HH*), 3.93–3.88 (1 H, m, 2-*H*), 3.70 (1H, dd, J 11.1, 2.9, 1-*HH*), 2.71 (2H, br s, 2 \times OH), 2.27–2.20 (2H, m, COCH_2), 2.06 (2H, dd, J 14.6, 7.4, 6-*H*₂), 1.71–1.57 (2H, m, COCH_2CH_2), 1.43–1.18 (28H, m, 7-*H*₂ to 17-*H*₂ and 4'-*H*₂ to 7'-*H*₂), 0.92–0.83 (6H, m, 18-*H*₃ and octanoyl terminal CH_3); m/z (ES^+) 426.4 [$\text{M}+\text{H}$]⁺; HRMS (ES^+) found [$\text{M}+\text{Na}$]⁺ 448.3761, $\text{C}_{26}\text{H}_{44}\text{O}_3\text{N}_1$ requires M^+ 448.3767.

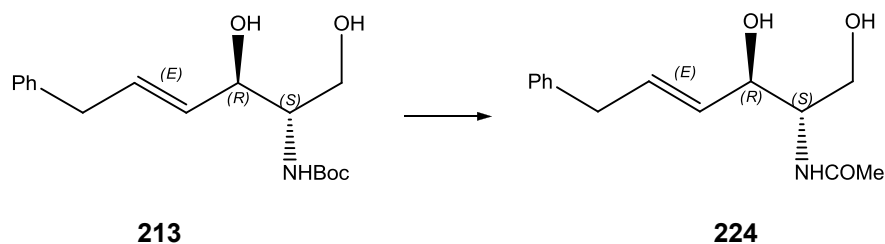
(2*S*,3*R*,*E*)-2-amino-6-phenylhex-4-ene-1,3-diol (223)



Yield (67%); δ_{H} (400 MHz, CDCl_3) 7.25–7.20 (2H, m, ArH), 7.16–7.07 (3H, m, ArH), 5.88 (1H, dt, J 15.0, 6.6, 5-*H*), 5.42 (1H, dd, J 15.0, 5.0, 4-*H*), 4.87 (2H, br s, NH_2), 4.40–4.29 (1H,

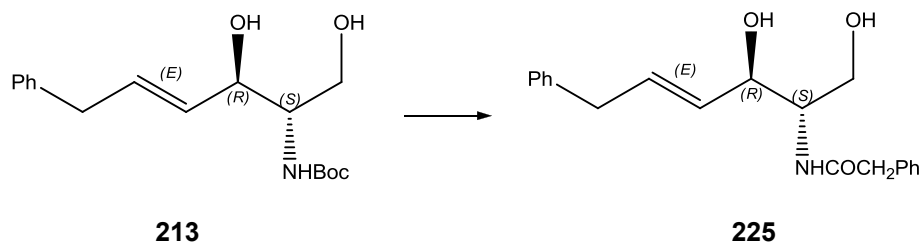
m, 3-*H*), 3.76–3.67 (2H, m, 3-*H* and 1-*HH*), 3.41–3.33 (1H, m, 1-*HH*), 3.30 (2H, d, *J* 6.6, 6-*H*₂), 3.21–3.14 (2H, br s, 2 × *OH*); *m/z* (ES⁺) 208.2 [M+H]⁺; HRMS (ES⁺) found [M+H]⁺ 208.1331, C₁₂H₁₈O₂N₁ requires *M*⁺ 208.1338.

***N*-((2*S*,3*R*,*E*)-1,3-dihydroxy-6-phenylhex-4-en-2-yl)acetamide (224)**



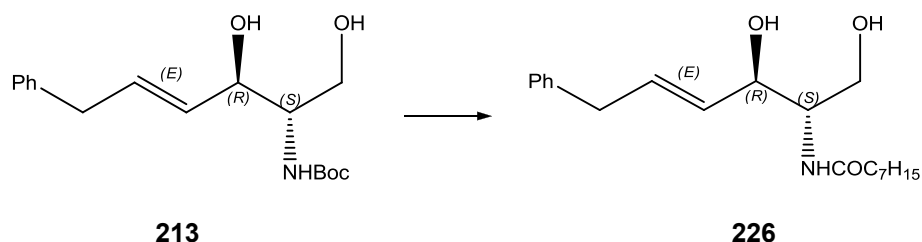
Yield (31%); δ_{H} (400 MHz, CDCl₃) 7.32–7.27 (2H, m, Ar*H*), 7.23–7.14 (3H, m, Ar*H*), 6.32 (1H, br d, *NH*), 5.96 (1H, dt, *J* 15.4, 6.7, 5-*H*), 5.61 (1H, dd, *J* 15.4, 6.0, 4-*H*), 4.38–4.32 (1H, m, 3-*H*), 3.99–3.88 (2H, m, 2-*H* and 1-*HH*), 3.70 (1H, dd, *J* 11.0, 2.8, 1-*HH*), 3.40 (1H, d, *J* 6.7, 6-*H*₂), 2.01 (3H, s, COCH₃); *m/z* (ES⁺) 250.1 [M+H]⁺, 272.1 [M+Na]⁺; HRMS (ES⁺) found [M+Na]⁺ 272.1248, C₁₄H₁₉O₃N₁²³Na₁ requires *M*⁺ 272.1263.

***N*-((2*S*,3*R*,*E*)-1,3-dihydroxy-6-phenylhex-4-en-2-yl)-2-phenylacetamide (225)**



Yield (85%); δ_{H} (400 MHz, CDCl₃) 7.34–7.25 (6H, m, Ar*H*), 7.22–7.11 (4H, m, Ar*H*), 6.32 (1H, br d, *J* 7.5, *NH*), 5.82 (1H, dt, *J* 15.0, 6.8, 5-*H*), 5.47 (1H, dd, *J* 15.0, 5.8, 4-*H*), 4.24–4.18 (1H, m, 3-*H*), 3.89–3.84 (1H, m, 2-*H*), 3.81 (1H, dd, *J* 11.1, 4.0, 1-*HH*), 3.59 (1H, dd, *J* 11.1, 3.2, 1-*HH*), 3.51 (2H, s, COCH₂), 3.31 (2H, d, *J* 6.8, 6-*H*₂), 2.25 (2H, br s, 2 × *OH*); *m/z* (ES⁺) 326.2 [M+H]⁺; HRMS (ES⁺) found [M+H]⁺ 326.1767, C₂₀H₂₄O₃N₁ requires *M*⁺ 326.1756.

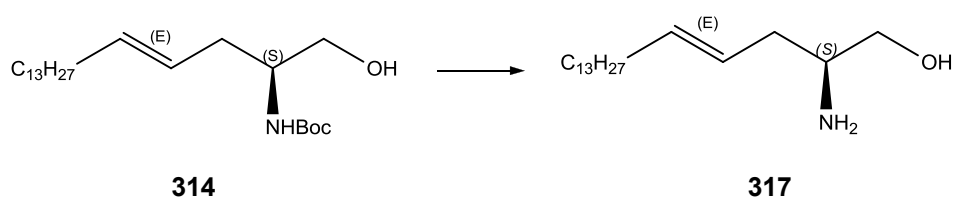
***N*-((2*S*,3*R*,*E*)-1,3-dihydroxy-6-phenylhex-4-en-2-yl)octanamide (226)**



Yield (82%); δ_{H} (400 MHz, CDCl_3) 7.31–7.23 (3H, m, ArH), 7.22–7.18 (1H, m, ArH), 7.17–7.11 (2H, m, ArH), 6.41 (1H, br d, J 6.6, NH), 5.92 (1H, dt, J 15.3, 6.8, 5-H), 5.58 (1H, dd, J 15.3, 6.1, 4-H), 4.33–4.27 (1H, m, 3-H), 3.89 (2H, m, 2-H and 1-HH), 3.66 (1H, dd, J 12.6, 4.7, 1-HH), 3.38 (2H, d, J 6.8, 6-H₂), 2.23–2.10 (2H, m, COCH_2), 1.63–1.53 (2H, m, COCH_2CH_2), 1.32–1.22 (8H, m, 4 \times aliphatic CH_2), 0.87 (3H, t, J 6.8, octanoyl terminal CH_3); m/z (ES^+) 334.2 $[\text{M}+\text{H}]^+$; HRMS (ES^+) found $[\text{M}+\text{Na}]^+$ 334.2393, $\text{C}_{20}\text{H}_{32}\text{O}_3\text{N}_1$ requires M^+ 334.2382.

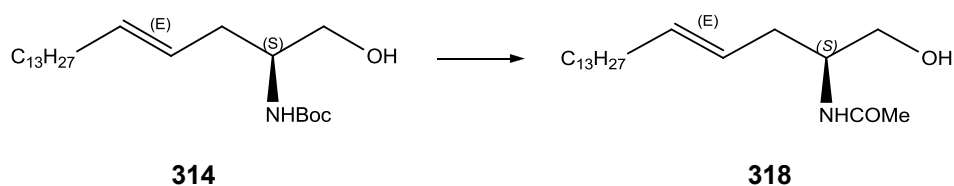
8.2.5.4 4E-3-deoxy ceramide analogues

(S,E)-2-aminooctadec-4-en-1-ol (317)



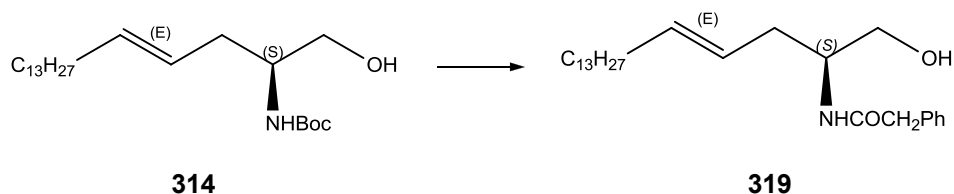
Yield (61%); δ_{H} (400 MHz, CDCl_3) 5.51 (1H, dt, J 13.9, 6.5, 5-H), 5.38–5.30 (1H, m, 4-H), 3.60 (1H, d, J 8.2, 1-HH), 3.33 (1H, dd, J 10.2, 8.2, 1-HH), 2.97–2.83 (1H, m, 2-H), 2.34 (3H, br s, NH_2 and OH), 2.20–2.10 (1H, m, 3-H₂), 1.99 (2H, dd, J 13.5, 6.6, 6-H₂), 1.37–1.20 (22H, m, 7-H₂ to 17-H₂), 0.87 (3H, t, J 6.5, 18-H₃); m/z (ES^+) 284.2 $[\text{M}+\text{H}]^+$; HRMS (ES^+) found $[\text{M}+\text{H}]^+$ 284.2947, $\text{C}_{18}\text{H}_{38}\text{O}_1\text{N}_1$ requires M^+ 284.2953.

(S,E)-N-(1-hydroxyoctadec-4-en-2-yl)acetamide (318)



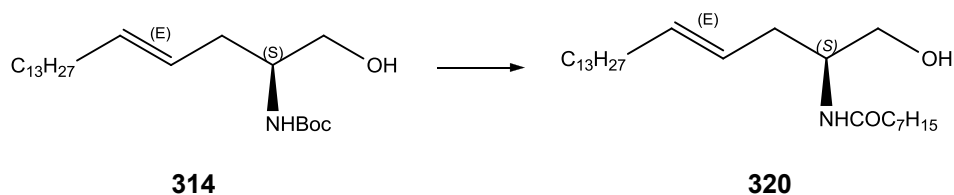
Yield (68%); δ_{H} (700 MHz, CDCl_3) 5.82 (1H, br d, J 14.8, NH), 5.51 (1H, dt, J 15.0, 6.7, 5- H), 5.34 (1H, dt, J 15.1, 7.1, 4- H), 3.91 (1H, tdd, J 11.1, 7.2, 3.6, 2- H), 3.65 (1H, dd, J 11.0, 3.3, 1- HH), 3.58 (1H, dd, J 11.1, 5.7, 1- HH), 3.25 (1H, br s, OH), 2.27–2.22 (1H, m, 3- HH), 2.17 (1H, dt, J 14.1, 7.1, 3- HH), 1.98 (5H, m, 6- H_2 and COCH_3), 1.35–1.30 (2H, m, 7- H_2), 1.30–1.22 (20H, m, 8- H_2 to 17- H_2), 0.87 (3H, t, J 7.1, 18- H_3); m/z (ES^-) 324.4 [$\text{M}-\text{H}$] $^-$; (ES^+) 326.4 [$\text{M}+\text{H}$] $^+$; HRMS (ES^+) found [$\text{M}+\text{H}$] $^+$ 326.3046, $\text{C}_{20}\text{H}_{40}\text{O}_2\text{N}_1$ requires M^+ 326.3035.

(*S,E*)-*N*-(1-hydroxyoctadec-4-en-2-yl)-2-phenylacetamide (319)



Yield (82%); δ_{H} (700 MHz, CDCl_3) 7.36–7.33 (1 H, m, Ar H), 7.30–7.28 (1 H, m, Ar H), 7.25–7.22 (1 H, m, Ar H), 5.58 (1H, br d, J 5.6, NH), 5.32 (1H, dt, J 14.7, 6.6, 5- H), 5.23–5.18 (1 H, m, 4- H), 3.88 (1H, dtd, J 13.2, 6.5, 3.8, 2- H), 3.61 (1H, dd, J 11.1, 3.5, 1- HH), 3.58 (2H, s, Ph CH_2), 3.54 (1H, dd, J 11.1, 6.2, 1- HH), 2.19–2.14 (1H, m, 3- HH), 2.09–2.04 (1H, m, 3- HH), 1.88 (2H, dd, J 13.2, 6.5, 6- H_2), 1.31–1.23 (22H, m, 7- H_2 to 17- H_2), 0.88 (3H, t, J 7.0, 18- H_3); m/z (ES^-) 400.5 [$\text{M}-\text{H}$] $^-$; (ES^+) 402.4 [$\text{M}+\text{H}$] $^+$; HRMS (ES^+) found [$\text{M}+\text{H}$] $^+$ 402.3356, $\text{C}_{26}\text{H}_{44}\text{O}_2\text{N}_1$ requires M^+ 402.3348.

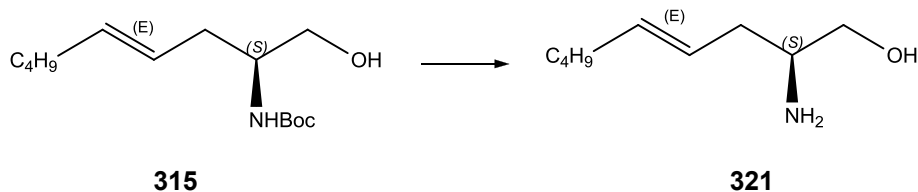
(*S,E*)-*N*-(1-hydroxyoctadec-4-en-2-yl)octanamide (320)



Yield (85%); δ_{H} (700 MHz, CDCl_3) 5.71 (1 H, br s, NH), 5.52 (1H, dt, J 14.8, 6.8, 5- H), 5.37–5.31 (1H, m, 4- H), 3.91 (1H, tdd, J 10.8, 6.9, 3.6, 2- H), 3.65 (1H, dd, J 10.9, 3.1, 1- HH), 3.58 (1H, dd, J 11.0, 6.0, 1- HH), 3.28 (1H, br s, OH), 2.26 (1H, dt, J 13.5, 6.6, 3- HH), 2.20–2.14 (3H, m, 3- HH and COCH_2), 1.99 (2H, dd, J 14.3, 7.1, 6- H_2), 1.60 (2H, dt, J 14.6, 7.4, COCH_2CH_2), 1.35–1.22 (30H, m, 7- H_2 to 17- H_2 and $4 \times$ aliphatic CH_2), 0.87 (6H, t, J 7.1, 18- H_3).

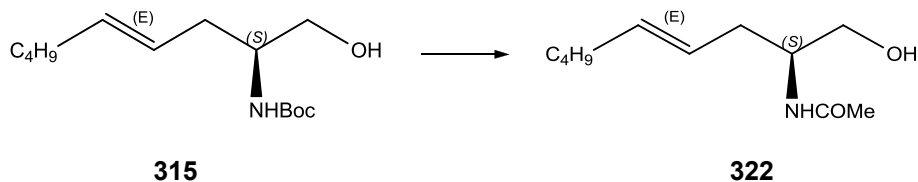
and terminal octanoyl CH_3); m/z (ES^-) 408.5 [$M-H$] $^-$; (ES^+) 410.5 [$M+Na$] $^+$; HRMS (ES^+) found [$M+H$] $^+$ 410.3999, $C_{26}H_{52}O_2N_1$ requires M^+ 410.3998.

(*S,E*)-2-aminonon-4-en-1-ol (321)



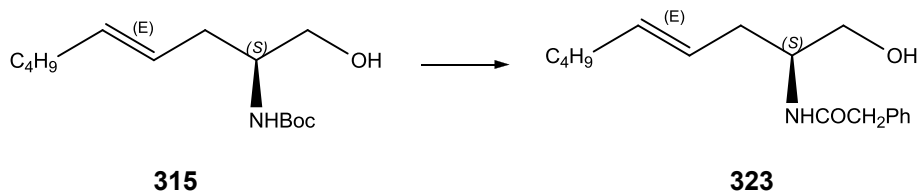
Yield (34%); δ_H (400 MHz, $CDCl_3$) 5.57–5.46 (1H, m, 5-*H*), 5.35 (1H, dd, J 13.9, 7.6, 4-*H*), 3.77–3.48 (2H, m, 2-*H* and 1-*HH*), 3.33 (1H, s, 1-*HH*), 2.91 (3H, br s, NH_2 and OH), 2.36–2.10 (2H, m, 3- H_2), 2.01 (2H, dd, J 13.4, 7.0, 6- H_2), 1.40–1.23 (4H, m, 7- H_2 and 8- H_2), 0.89 (3H, t, J 6.9, 9- H_3); m/z (ES^+) 158.2 [$M+H$] $^+$; HRMS (ES^+) found [$M+H$] $^+$ 158.1545, $C_9H_{20}O_1N_1$ requires M^+ 158.1545.

(*S,E*)-*N*-(1-hydroxynon-4-en-2-yl)acetamide (322)



Yield (82%); δ_H (400 MHz, $CDCl_3$) 5.66 (1H, br d, J 6.6, NH), 5.58–5.47 (1H, m, 5-*H*), 5.40–5.30 (1H, m, 4-*H*), 4.05–3.97 (1H, m, 2-*H*), 3.67 (1H, dd, J 11.1, 3.6, 1-*HH*), 3.59 (1H, dd, J 11.1, 6.3, 1-*HH*), 3.33 (1H, br s, OH), 2.37–2.13 (2H, m, 3- H_2), 2.10–1.95 (5H, m, 6- H_2 and $COCH_3$), 1.37–1.27 (4H, m, 7- H_2 and 8- H_2), 0.89 (3H, t, J 6.7, 9- H_3); m/z (ES^+) 222.2 [$M+Na$] $^+$; HRMS (ES^+) found [$M+Na$] $^+$ 222.1466, $C_{11}H_{21}O_2N_1^{23}Na_1$ requires M^+ 222.1470.

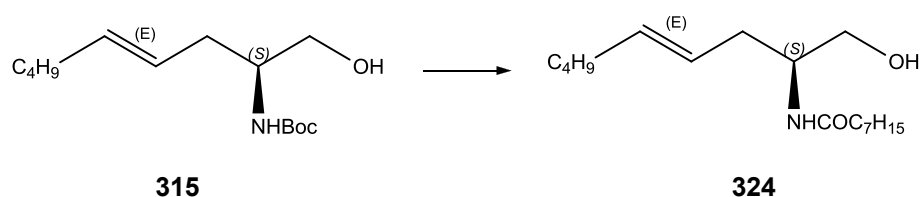
(*S,E*)-*N*-(1-hydroxynon-4-en-2-yl)-2-phenylacetamide (323)



Yield (31%); δ_H (400 MHz, $CDCl_3$) 7.36–7.26 (4H, m, ArH), 7.24–7.21 (1H, m, J 5.3, 3.1, ArH), 5.68 (1H, br d, J 7.0, NH), 5.30 (1H, dt, J 14.2, 6.6, 5-*H*), 5.19 (1H, dt, J 15.2, 7.1, 4-*H*),

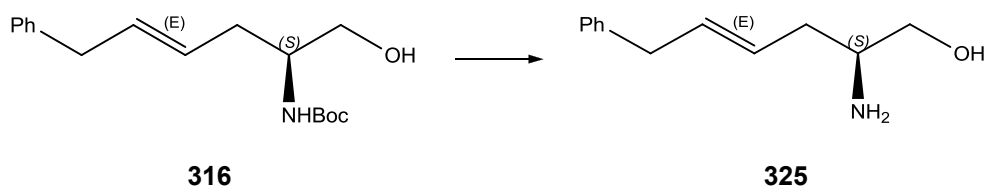
3.89 (1H, tdd, J 10.8, 7.0, 3.8, 2- H), 3.64 (2H, s, PhCH_2), 3.61 (1H, dd, J 11.2, 3.6, 1- HH), 3.53 (1H, dd, J 11.8, 5.2, 1- HH), 2.15 (1H, dt, J 13.5, 4.9, 3- HH), 2.05 (1H, dd, J 14.3, 7.3, 3- HH), 1.89 (2H, dd, J 13.7, 7.0, 6- H_2), 1.33–1.23 (4H, m, 7- H_2 and 8- H_2), 0.89 (4H, t, J 7.0, 9- H_3); m/z (ES^-) 274.3 [$\text{M}-\text{H}$] $^-$; (ES^+) 298.3 [$\text{M}+\text{Na}$] $^+$; HRMS (ES^+) found [$\text{M}+\text{H}$] $^+$ 276.1958, $\text{C}_{17}\text{H}_{26}\text{O}_2\text{N}_1$ requires M^+ 276.1964.

(*S,E*)-*N*-(1-hydroxynon-4-en-2-yl)octanamide (324)



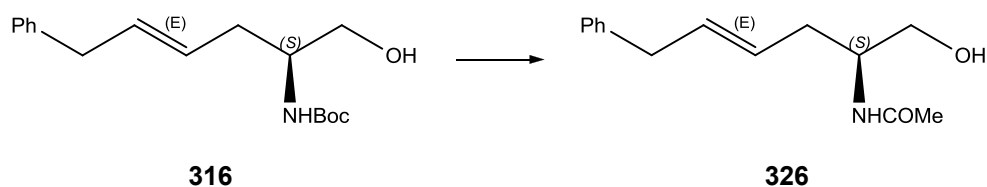
Yield (27%); δ_{H} (400 MHz, CDCl_3) 5.63 (1H, br d, J 6.2, NH), 5.53 (1H, dt, J 15.0, 6.7, 5- H), 5.39–5.30 (1 H, m, 4- H), 3.93 (1H, tdd, J 9.5, 6.4, 3.4, 2- H), 3.67 (1H, dd, J 11.0, 3.4, 1- HH), 3.59 (1H, dd, J 11.1, 6.2, 1- HH), 2.31–2.15 (4H, m, 3- H_2 and COCH_2), 2.01 (3H, dd, J 13.5, 6.6, 6- H_2), 1.61 (4H, dt, J 15.3, 7.7, COCH_2CH_2), 1.37–1.23 (12H, m, 7- H_2 , 8- H_2 and $4 \times$ aliphatic CH_2), 0.89 (3H, t, J 7.0, 9- H_3), 0.87 (9 H, td, J 7.0, terminal octanoyl CH_3); m/z (ES^-) 282.4 [$\text{M}-\text{H}$] $^-$; (ES^+) 306.4 [$\text{M}+\text{Na}$] $^+$; HRMS (ES^+) found [$\text{M}+\text{H}$] $^+$ 284.2581, $\text{C}_{17}\text{H}_{34}\text{O}_2\text{N}_1$ requires M^+ 284.2590.

(*S,E*)-2-amino-6-phenylhex-4-en-1-ol (325)



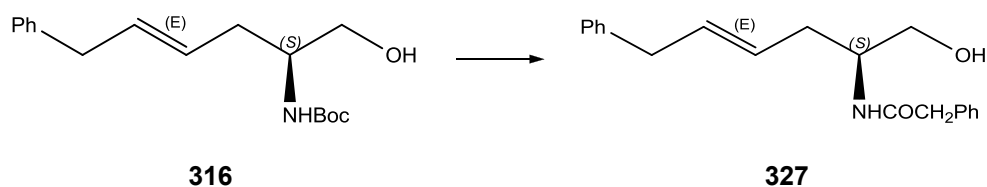
Yield (30%); δ_{H} (700 MHz, CDCl_3) 7.49–7.04 (5H, m, ArH), 5.75–5.67 (1H, m, 5- H), 5.47–5.42 (1H, m, 4- H), 3.71 (2H, m, 1- H_2), 3.34 (2H, d, J 6.7, 6- H_2), 2.41–2.33 (1H, m, 2- H), 2.27–2.18 (2H, m, 3- H_2); 1.90 (3H, br s, NH_2 and OH). m/z (ES^+) 192.2 [$\text{M}+\text{H}$] $^+$, $\text{C}_{12}\text{H}_{17}\text{O}_1\text{N}_1$. HRMS could not be obtained for this compound.

(*S,E*)-*N*-(1-hydroxy-6-phenylhex-4-en-2-yl)acetamide (326)



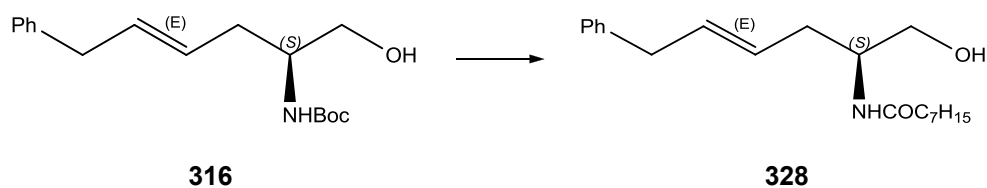
Yield (36%); δ_{H} (700 MHz, CDCl_3) 7.72–6.93 (5H, m, ArH), 5.71 (1H, dd, J 14.2, 6.5, 5-*H*), 5.62 (1H, br d, J 4.9, NH), 5.50–5.42 (1H, m, 4-*H*), 4.12–4.00 (1H, m, 2-*H*), 3.60 (1H, dd, J 11.0, 5.3, 1-*HH*), 3.40 (1H, dd, J 11.0, 6.8, 1-*HH*), 3.35 (2H, d, J 6.6, 6- H_2), 2.42–2.28 (2H, m, 3- H_2), 1.95 (1H, s, COCH_3). m/z (ES^+) 256.2 $[\text{M}+\text{Na}]^+$; HRMS (ES^+) found $[\text{M}+\text{Na}]^+$ 256.1320, $\text{C}_{14}\text{H}_{19}\text{O}_2\text{N}_1^{23}\text{Na}_1$ requires M^+ 256.1313.

(*S,E*)-*N*-(1-hydroxy-6-phenylhex-4-en-2-yl)-2-phenylacetamide (327)

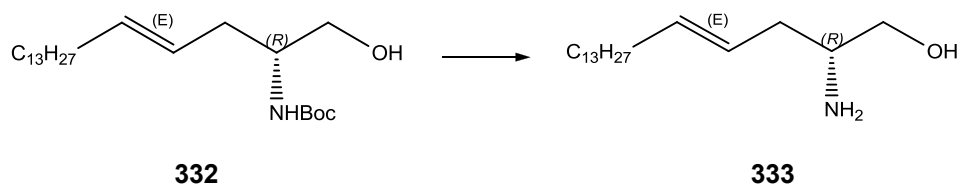


Yield (21%); δ_{H} (700 MHz, CDCl_3) 7.54–6.95 (10H, m, ArH and Ar'*H*), 5.66 (1H, br d, J 6.7, NH), 5.57–5.51 (1H, m, 5-*H*), 5.32 (1H, dd, J 15.6, 6.5, 4-*H*), 3.94–3.89 (1H, m, 2-*H*), 3.66–3.63 (1H, m, 1-*HH*), 3.62 (1H, d, J 5.4, PhCH_2CO), 3.57 (1H, d, J 5.1, 1-*HH*), 3.23 (1H, d, J 6.7, 6- H_2), 2.25–2.19 (1H, m, 3-*HH*), 2.10 (1H, m, 3-*HH*); m/z (ES^+) 332.3 $[\text{M}+\text{Na}]^+$; HRMS (ES^+) found $[\text{M}+\text{Na}]^+$ 332.1613, $\text{C}_{20}\text{H}_{23}\text{O}_2\text{N}_1^{23}\text{Na}_1$ requires M^+ 332.1626.

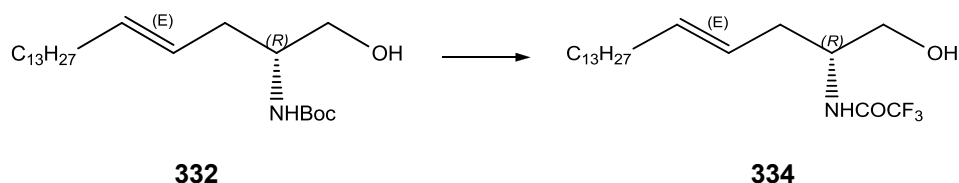
(*S,E*)-*N*-(1-hydroxy-6-phenylhex-4-en-2-yl)octanamide (328)



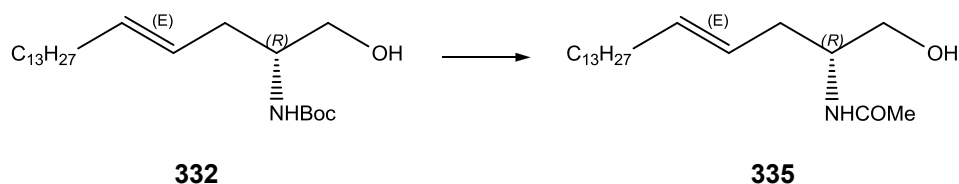
Yield (31%); δ_{H} (700 MHz, CDCl_3) 7.21–7.13 (5H, m, ArH), 5.82 (1H, br d, J 6.7, NH), 5.73–5.67 (1H, m, 5-*H*), 5.41 (1H, dd, J 15.7, 6.4, 4-*H*), 3.98–3.94 (1H, m, 2-*H*), 3.68 (1H, dd, J 11.1, 3.9, 1-*HH*), 3.62 (1H, dd, J 10.7, 5.9, 1-*HH*), 3.34 (2H, d, J 7.2, 6- H_2), 2.39–2.15 (5H, m, 3- H_2 and COCH_2), 1.62 (2H, dd, J 14.6, 7.2, COCH_2CH_2), 1.34–1.22 (12H, m, 7- H_2 , 8- H_2 and 4 \times aliphatic CH_2), 0.87 (3H, td, J 6.5, terminal octanoyl CH_3); m/z (ES^+) 318.3 $[\text{M}+\text{H}]^+$; (ES^+) 340.3 $[\text{M}+\text{Na}]^+$ HRMS (ES^+) found $[\text{M}+\text{Na}]^+$ 340.2246, $\text{C}_{20}\text{H}_{31}\text{O}_2\text{N}_1^{23}\text{Na}_1$ requires M^+ 340.2252.

(*R,E*)-2-aminooctadec-4-en-1-ol (333)

Yield (62%); δ_{H} (400 MHz, CDCl_3) 5.51 (1H, dt, J 13.9, 6.5, 5-*H*), 5.38–5.30 (1H, m, 4-*H*), 3.60 (1H, d, J 8.2, 1-*HH*), 3.33 (1H, dd, J 10.2, 8.2, 1-*HH*), 2.97–2.83 (1H, m, 2-*H*), 2.34 (3H, br s, NH_2 and OH), 2.20–2.10 (1H, m, 3-*H}_2*), 1.99 (2H, dd, J 13.5, 6.6, 6-*H}_2*), 1.37–1.20 (22H, m, 7-*H}_2* to 17-*H}_2*), 0.87 (3H, t, J 6.5, 18-*H}_3*); m/z (ES^+) 284.2 [$\text{M}+\text{H}$] $^+$; HRMS (ES^+) found [$\text{M}+\text{H}$] $^+$ 284.2947, $\text{C}_{18}\text{H}_{38}\text{O}_1\text{N}_1$ requires M^+ 284.2953.

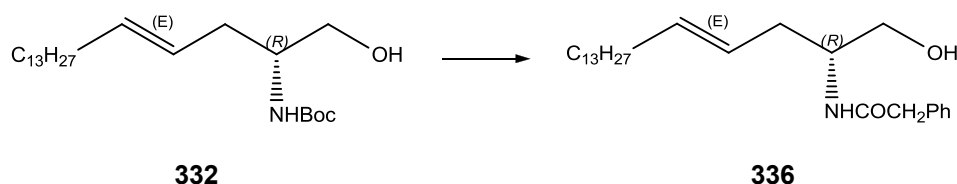
(*R,E*)-2,2,2-trifluoro-*N*-(1-hydroxyoctadec-4-en-2-yl)acetamide (334)

Yield (38%); δ_{H} (400 MHz, CDCl_3) 6.56 (1H, br d, J 7.0, NH), 5.56 (1H, dt, J 15.0, 6.8, 5-*H*), 5.35 (1H, dt, J 15.0, 7.2, 4-*H*), 4.05–3.97 (1H, m, 2-*H*), 3.73 (2H, app. d, J 3.8, 1-*H}_2*), 2.39–2.25 (2H, m, 3-*H}_2*), 2.00 (2H, dd, J 13.8, 6.9, 6-*H}_2*), 1.38–1.20 (22H, m, 7-*H}_2* to 17-*H}_2*), 0.88 (3H, t, J 6.9, 18-*H}_3*); δ_{F} (376 MHz, CDCl_3) -75.87 CF_3 ; m/z (ES^-) 378.4 [$\text{M}-\text{H}$] $^-$; (ES^+) 402.4 [$\text{M}+\text{Na}$] $^+$; HRMS (ES^+) found [$\text{M}+\text{Na}$] $^+$ 402.2603, $\text{C}_{20}\text{H}_{36}\text{O}_2\text{N}_1\text{F}_3$ $^{23}\text{Na}_1$ requires M^+ 402.2608.

(*R,E*)-*N*-(1-hydroxyoctadec-4-en-2-yl)acetamide (335)

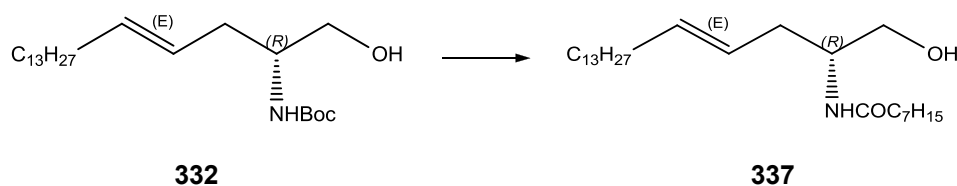
Yield (88%); δ_{H} (700 MHz, CDCl_3) 5.82 (1H, br d, J 14.8, NH), 5.51 (1H, dt, J 15.0, 6.7, 5- H), 5.34 (1H, dt, J 15.1, 7.1, 4- H), 3.91 (1H, tdd, J 11.1, 7.2, 3.6, 2- H), 3.65 (1H, dd, J 11.0, 3.3, 1- H), 3.58 (1H, dd, J 11.1, 5.7, 1- H), 3.25 (1H, br s, OH), 2.27–2.22 (1H, m, 3- H), 2.17 (1H, dt, J 14.1, 7.1, 3- H), 1.98 (5H, m, 6- H_2 and COCH_3), 1.35–1.30 (2H, m, 7- H_2), 1.30–1.22 (20H, m, 8- H_2 to 17- H_2), 0.87 (3H, t, J 7.1, 18- H_3); m/z (ES^-) 324.4 [$\text{M}-\text{H}$] $^-$; (ES^+) 326.4 [$\text{M}+\text{H}$] $^+$; HRMS (ES^+) found [$\text{M}+\text{H}$] $^+$ 326.3046, $\text{C}_{20}\text{H}_{40}\text{O}_2\text{N}_1$ requires M^+ 326.3035.

(*R,E*)-*N*-(1-hydroxyoctadec-4-en-2-yl)-2-phenylacetamide (336)



Yield (47%); δ_{H} (700 MHz, CDCl_3) 7.36–7.33 (2H, m, Ar H), 7.30–7.28 (1H, m, Ar H), 7.25–7.22 (2H, m, Ar H), 5.58 (1H, br d, J 5.6, NH), 5.32 (1H, dt, J 14.7, 6.6, 5- H), 5.23–5.18 (1H, m, 4- H), 3.88 (1H, dtd, J 13.2, 6.5, 3.8, 2- H), 3.61 (1H, dd, J 11.1, 3.5, 1- H), 3.58 (2H, s, PhCH_2), 3.54 (1H, dd, J 11.1, 6.2, 1- H), 2.19–2.14 (1H, m, 3- H), 2.09 – 2.04 (1H, m, 3- H), 1.88 (2H, dd, J 13.2, 6.5, 6- H_2), 1.31–1.23 (22H, m, 7- H_2 to 17- H_2), 0.88 (3H, t, J 7.0, 18- H_3); m/z (ES^-) 400.5 [$\text{M}-\text{H}$] $^-$; (ES^+) 402.4 [$\text{M}+\text{H}$] $^+$; HRMS (ES^+) found [$\text{M}+\text{H}$] $^+$ 402.3356, $\text{C}_{26}\text{H}_{44}\text{O}_2\text{N}_1$ requires M^+ 402.3348.

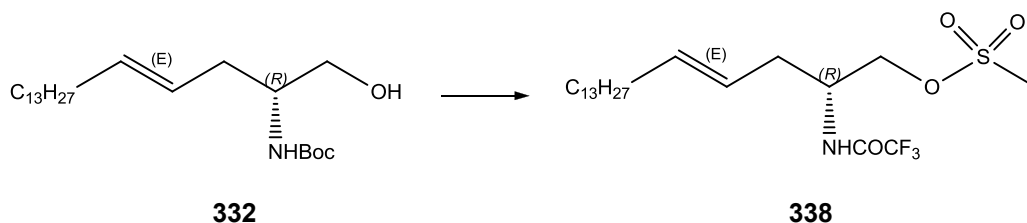
(*R,E*)-*N*-(1-hydroxyoctadec-4-en-2-yl)octanamide (337)



Yield (76%); δ_{H} (700 MHz, CDCl_3) 5.71 (1 H, br s, NH), 5.52 (1 H, dt, J 14.8, 6.8, 5- H), 5.37–5.31 (1H, m, 4- H), 3.91 (1H, tdd, J 10.8, 6.9, 3.6, 2- H), 3.65 (1H, dd, J 10.9, 3.1, 1- H), 3.58 (1H, dd, J 11.0, 6.0, 1- H), 3.28 (1H, br s, OH), 2.26 (1H, dt, J 13.5, 6.6, 3- H), 2.20–2.14 (3H, m, 3- H and COCH_2), 1.99 (2H, dd, J 14.3, 7.1, 6- H_2), 1.60 (2H, dt, J 14.6, 7.4, COCH_2CH_2), 1.35–1.22 (30H, m, 7- H_2 to 17- H_2 and 4 \times aliphatic CH_2), 0.87 (6H, t, J 7.1, 18- H_3)

and terminal octanoyl CH_3); m/z (ES^-) 408.5 [$M-H$] $^-$; (ES^+) 410.5 [$M+Na$] $^+$; HRMS (ES^+) found [$M+H$] $^+$ 410.3999, $C_{26}H_{52}O_2N_1$ requires M^+ 410.3998.

(*R,E*)-2-(2,2,2-trifluoroacetamido)octadec-4-en-1-yl methanesulfonate (338)

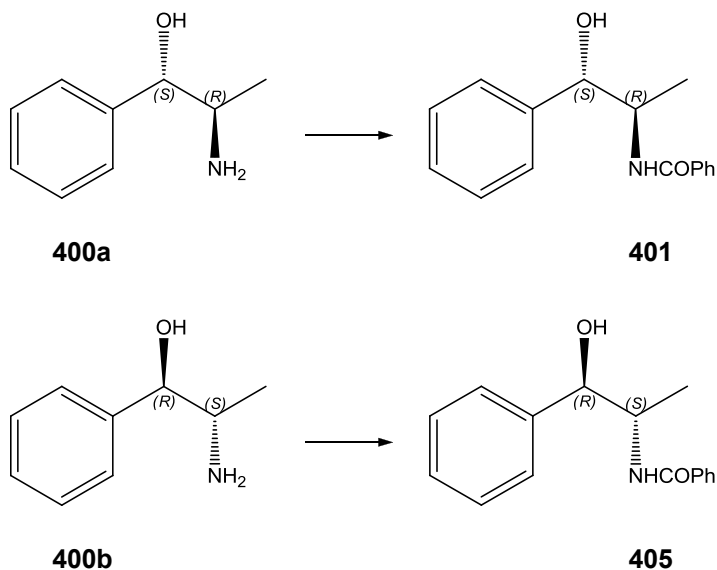


Yield (77%); δ_H (700 MHz, $CDCl_3$) 6.55 (1H, br d, J 7.5, NH), 5.61 (1H, dt, J 14.1, 6.8, 5- H), 5.32 (1H, dt, J 15.4, 7.5, 4- H), 4.36 (1H, dd, J 10.9, 3.6, 1- HH), 4.28 (1H, dd, J 10.8, 4.6, 1- HH), 4.21 (1H, dt, J 7.7, 5.7, 2- H), 3.05 (3H, s, SO_2CH_3), 2.37 (2H, dd, J 11.3, 6.9, 3- H_2), 2.01 (2H, dd, J 14.3, 7.2, 6- H_2), 1.37–1.21 (25H, m, 7- H_2 to 17- H_2), 0.88 (4H, t, J 7.0, 18- H_3); δ_F (658 MHz, $CDCl_3$) -75.98 ; m/z (ES^+) 458.2 [$M+H$] $^+$; HRMS (ES^+) found [$M+H$] $^+$ 458.2561, $C_{21}H_{39}O_4N_1F_3S_1$ requires M^+ 458.2552.

8.2.5.5 3-phenyl-1-deoxy ceramide analogues

***N*-((1*S*,2*R*)-1-hydroxy-1-phenylpropan-2-yl)benzamide (401)**

***N*-((1*R*,2*S*)-1-hydroxy-1-phenylpropan-2-yl)benzamide (405)**

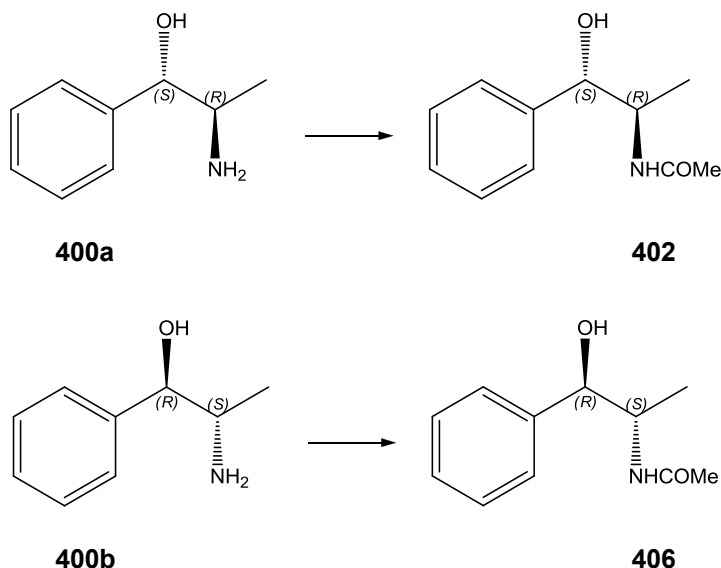


Yield (401, 75%; 405, 79%); δ_H (400 MHz, $CDCl_3$) 7.75 (2H, m, ArH), 7.54–7.48 (1H, m, ArH), 7.46–7.40 (2H, m, ArH), 7.40–7.33 (4H, m, $Ar'H$), 7.31–7.27 (1H, m, $Ar'H$), 6.29 (1H, m,

NH), 4.97 (1H, m, 1-*H*), 4.55 (1 H, dqd, *J* 13.8, 6.9, 2.8, 2-*H*), 3.56 (1H, d, *J* 3.9, *OH*), 1.12 (3H, d, *J* 6.9, 3-*H*₃); *m/z* (ES^+) 256.4 [$\text{M}+\text{H}$]⁺; HRMS (ES^+) found [$\text{M}+\text{H}$]⁺ 256.1332, $\text{C}_{16}\text{H}_{18}\text{O}_2\text{N}_1$ requires M^+ 256.1332.

***N*-((1*S*,2*R*)-1-hydroxy-1-phenylpropan-2-yl)acetamide (402)**

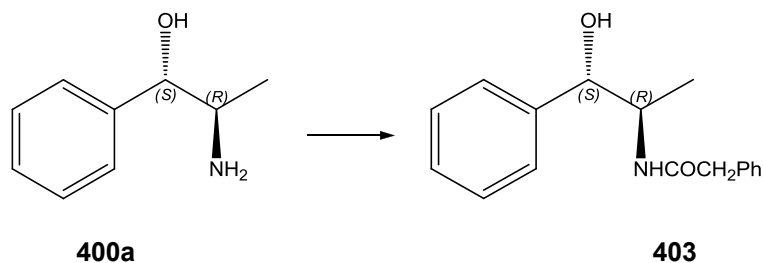
***N*-((1*R*,2*S*)-1-hydroxy-1-phenylpropan-2-yl)acetamide (406)**

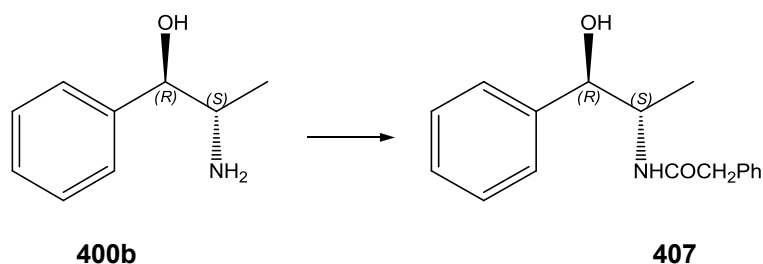


Yield (402, 78%; 406, 88%); δ_{H} (400 MHz, CDCl_3) 7.36–7.30 (4H, m, *ArH*), 7.30–7.25 (1H, m, *ArH*), 5.80 (1H, br s, *NH*), 4.85 (1H, d, *J* 2.7, 1-*H*), 4.41–4.19 (1H, m, 2-*H*), 3.79 (1H, br s, *OH*), 1.98 (3H, s, COCH_3), 0.99 (3H, d, *J* 7.0, 3-*H*₃); *m/z* (ES^+) 194.3 [$\text{M}+\text{H}$]⁺; HRMS (ES^+) found [$\text{M}+\text{H}$]⁺ 194.1175, $\text{C}_{11}\text{H}_{16}\text{O}_2\text{N}_1$ requires M^+ 194.1176.

***N*-((1*S*,2*R*)-1-hydroxy-1-phenylpropan-2-yl)-2-phenylacetamide (403)**

***N*-((1*R*,2*S*)-1-hydroxy-1-phenylpropan-2-yl)-2-phenylacetamide (407)**

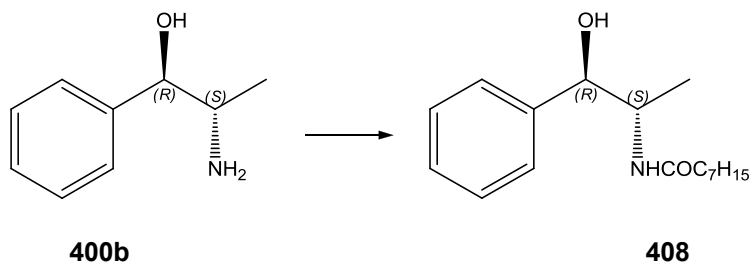
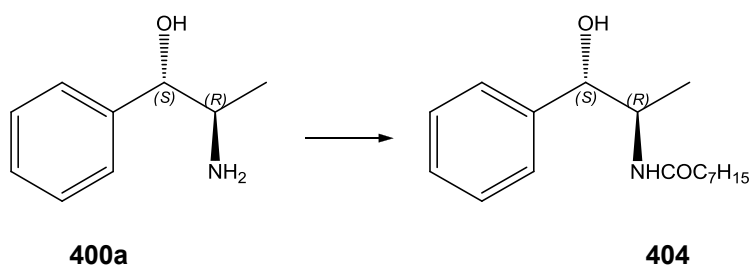




Yield (403, 74%; 407, 70%); δ_{H} (400 MHz, CDCl_3) 7.42–7.11 (10H, m, ArH and Ar'H), 5.56 (1H, br s, NH), 4.75 (1H, m, 1-H), 4.30 (1H, pd, J 7.0, 3.1, 2-H), 3.54 (2H, m, COCH_2), 0.93 (3H, d, J 7.0, 3- CH_3); m/z (ES^+) 270.4 $[\text{M}+\text{H}]^+$; HRMS (ES^+) found $[\text{M}+\text{H}]^+$ 270.1488, $\text{C}_{17}\text{H}_{20}\text{O}_2\text{N}_1$ requires M^+ 270.1489.

***N*-((1*S*,2*R*)-1-hydroxy-1-phenylpropan-2-yl)octanamide (404)**

***N*-((1*R*,2*S*)-1-hydroxy-1-phenylpropan-2-yl)octanamide (408)**



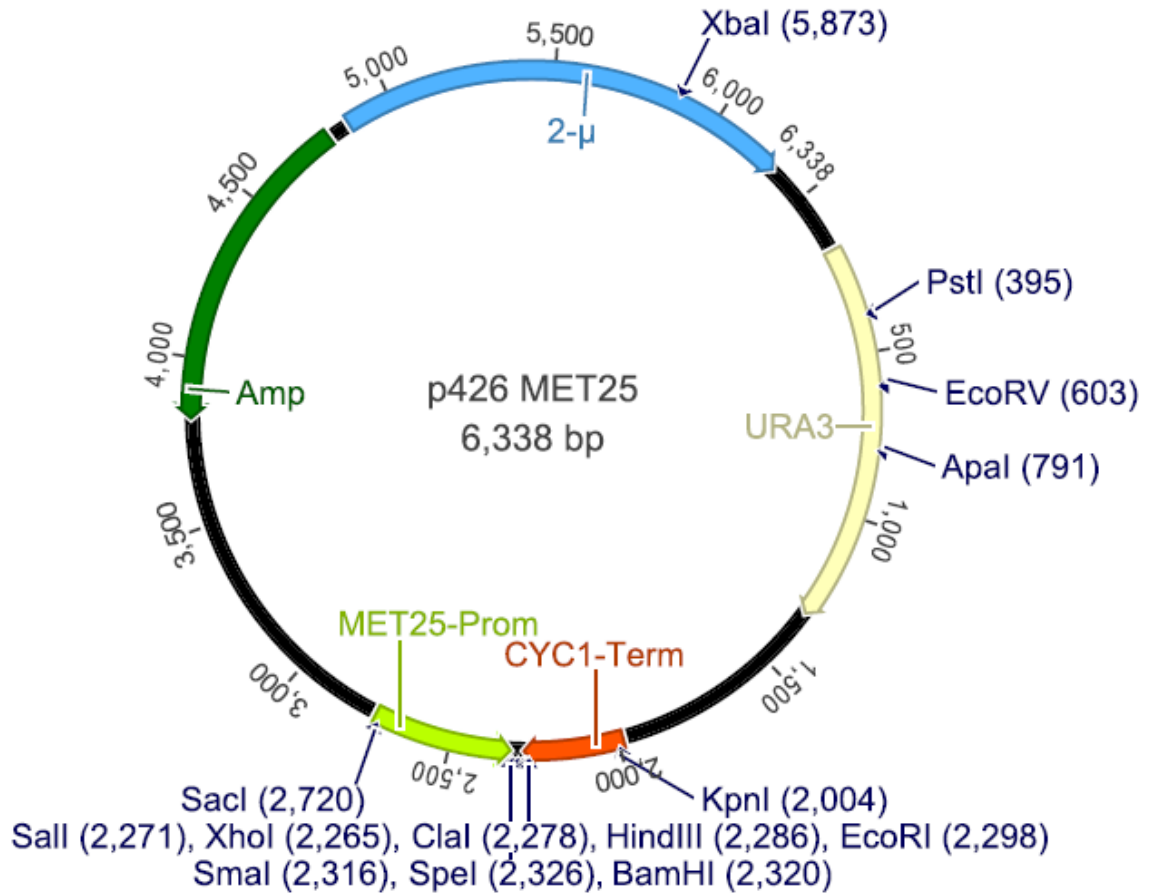
Yield (404, 88%; 408, 93%); δ_{H} (400 MHz, CDCl_3) 7.29–7.24 (4H, m, ArH), 7.23–7.18 (1H, m, ArH), 5.86 (1H, br s, NH), 4.75 (1H, d, J 2.8, 1-H), 4.23 (1H, ddd, J 8.1, 7.0, 2.8, 2-H), 2.14–2.03 (2H, m, COCH_2), 1.62–1.47 (2H, m, COCH_2CH_2), 1.22 (8H, m, 4 \times aliphatic CH_2), 0.93 (6H, d, J 6.9, 3- H_3), 0.83 (3H, t, J 6.8 aliphatic terminal CH_3); m/z (ES^+) 278.5 $[\text{M}+\text{H}]^+$; HRMS (ES^+) found $[\text{M}+\text{H}]^+$ 278.2114, $\text{C}_{17}\text{H}_{28}\text{O}_2\text{N}_1$ requires M^+ 278.2115.

REFERENCES

1. D. D. Perrin, W. L. F. Armarego and D. R. Perrin, *Purification of Laboratory Chemicals* 3rd edn., Butterworth-Heinemann Ltd, 1988.
2. T. R. Hoye, B. M. Eklov and M. Voloshin, *Org. Lett.*, 2004, **6**, 2567-2570.
3. L. Kosynkina, W. Wang and T. C. Liang, *Tetrahedron Lett.*, 1994, **35**, 5173-5176.
4. T. Yamamoto, H. Hasegawa, T. Hakogi and S. Katsumura, *Org. Lett.*, 2006, **8**, 5569-5572.
5. P. K. Chakravarty, W. J. Greenlee, W. H. Parsons, A. A. Patchett, P. Combs, A. Roth, R. D. Busch and T. N. Mellin, *J. Med. Chem.*, 1989, **32**, 1886-1890.
6. T. Ibuka, H. Habashita, A. Otaka, N. Fujii, Y. Oguchi, T. Uyehara and Y. Yamamoto, *J. Org. Chem.*, 1991, **56**, 4370-4382.
7. M. Toumi, F. Couty and G. Evano, *Tetrahedron Lett.*, 2008, **49**, 1175-1179.
8. M. Toumi, F. Couty and G. Evano, *Angewandte Chemie-International Edition*, 2007, **46**, 572-575.
9. R. C. So, R. Ndonge, D. P. Izmirian, S. K. Richardson, R. L. Guerrero and A. R. Howell, *J. Org. Chem.*, 2004, **69**, 3233-3235.
10. Japan Pat., 2006-206546 2006.
11. E. J. Corey, F. Xu and M. C. Noe, *J. Am. Chem. Soc.*, 1997, **119**, 12414-12415.
12. B. Lygo and P. G. Wainwright, *Tetrahedron*, 1999, **55**, 6289-6300.
13. J. Aires-de-Sousa, S. Prabhakar, A. M. Lobo, A. M. Rosa, M. J. S. Gomes, M. C. Corvo, D. J. Williams and A. J. P. White, *Tetrahedron-Asymmetry*, 2002, **12**, 3349-3365.
14. M. J. O'Donnell and R. L. Polt, *J. Org. Chem.*, 1982, **47**, 2663-2666.
15. R. Chinchilla, C. Nájera and F. J. Ortega, *Tetrahedron-Asymmetry*, 2006, **17**, 3423-3429.
16. S. M. Jones, J. E. Urch, M. Kaiser, R. Brun, J. L. Harwood, C. Berry and I. H. Gilbert, *J. Med. Chem.*, 2005, **48**, 5932-5941.
17. M. J. O'Donnell, J. M. Boniece and S. E. Earp, *Tetrahedron Lett.*, 1978, **19**, 2641-2644.
18. T. Ohshima, T. Shibuguchi, Y. Fukuta and M. Shibasaki, *Tetrahedron*, 2004, **60**, 7743-7754.
19. T. Ohshima, V. Gnanadesikan, T. Shibuguchi, Y. Fukuta, T. Nemoto and M. Shibasaki, *J. Am. Chem. Soc.*, 2003, **125**, 11206-11207.
20. H. Matsunaga, T. Ishizuka and T. Kunieda, *Tetrahedron*, 1997, **53**, 1275-1294.
21. B. R. Galan, K. P. Kalbarczyk, S. Szczepankiewicz, J. B. Keister and S. T. Diver, *Org. Lett.*, 2007, **9**, 1203-1206.
22. T. Kawate, N. Fukuta, A. Nishida and M. Nakagawa, *Chem. Pharm. Bull.*, 1997, **45**, 2116-2118.

APPENDICES

APPENDIX 'A': EXPRESSION VECTOR p426MET25



APPENDIX 'B': MATRIX OF DILUTION EFFECT

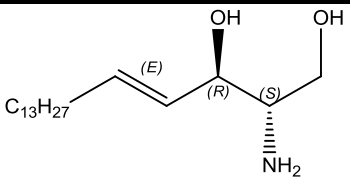
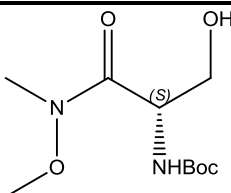
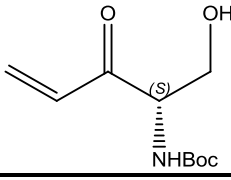
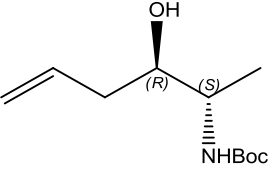
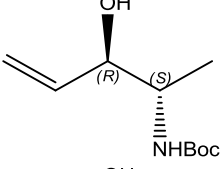
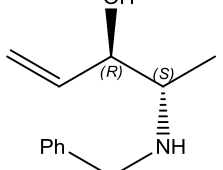
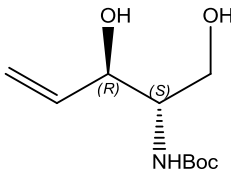
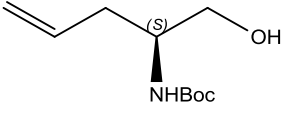
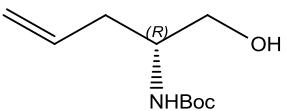
APPENDIX B: MATRIX OF DILUTION EFFECT

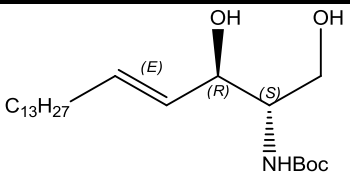
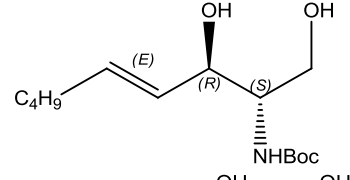
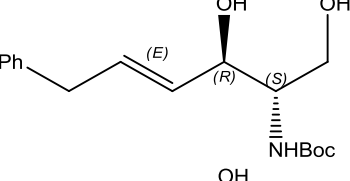
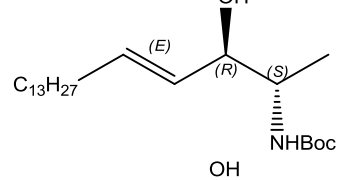
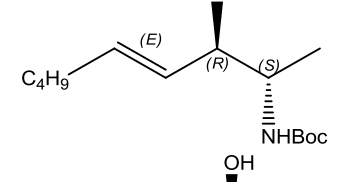
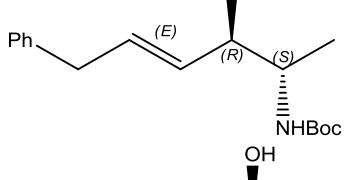
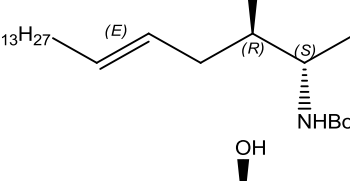
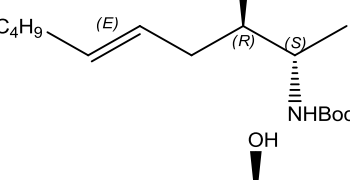
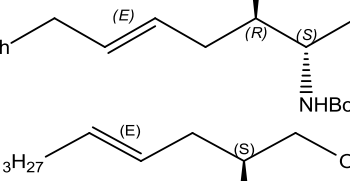

Total Lipid + CHAPS (µM)	PI %
Cer %	

Legend

CHAPS = 600		PI (µM)										Δ		
		0.0PI %	12.5PI %	25.0PI %	50.0PI %	75.0PI %	100.0PI %	125.0PI %	150.0PI %	200.0PI %	250.0PI %	250.0PI %	Δ	Δ/[Cer] %
Cer (µM)	0.0	600.0	612.5	625.0	650.0	675.0	700.0	725.0	750.0	800.0	850.0	850.0	29.4%	29.4%
Cer %	0.00%	0.00%	0.00%	0.00%	0.00%	0.00%	0.00%	0.00%	0.00%	0.00%	0.00%	0.00%	0.00%	0.00%
Cer	1.0	601.0	613.5	626.0	651.0	676.0	701.0	726.0	751.0	801.0	851.0	851.0	29.4%	29.4%
Cer %	0.17%	0.16%	0.16%	0.15%	0.15%	0.15%	0.14%	0.14%	0.13%	0.12%	0.12%	0.12%	0.05%	29.4%
Cer	2.0	602.0	614.5	627.0	652.0	677.0	702.0	727.0	752.0	802.0	852.0	852.0	29.3%	29.3%
Cer %	0.33%	0.33%	0.33%	0.32%	0.31%	0.30%	0.28%	0.28%	0.27%	0.25%	0.23%	0.23%	0.10%	29.3%
Cer	3.0	603.0	615.5	628.0	653.0	678.0	703.0	728.0	753.0	803.0	853.0	853.0	29.3%	29.3%
Cer %	0.50%	0.49%	0.49%	0.48%	0.46%	0.44%	0.43%	0.41%	0.40%	0.37%	0.35%	0.35%	0.15%	29.3%
Cer	4.0	604.0	616.5	629.0	654.0	679.0	704.0	729.0	754.0	804.0	854.0	854.0	29.3%	29.3%
Cer %	0.66%	0.65%	0.65%	0.64%	0.61%	0.59%	0.57%	0.55%	0.53%	0.50%	0.47%	0.47%	0.19%	29.3%
Cer	5.0	605.0	617.5	630.0	655.0	680.0	705.0	730.0	755.0	805.0	855.0	855.0	29.2%	29.2%
Cer %	0.83%	0.81%	0.81%	0.79%	0.76%	0.74%	0.71%	0.68%	0.66%	0.62%	0.58%	0.58%	0.24%	29.2%
Cer	7.5	607.5	620.0	632.5	657.5	682.5	707.5	732.5	757.5	807.5	857.5	857.5	29.2%	29.2%
Cer %	1.23%	1.21%	1.19%	1.14%	1.10%	1.06%	1.06%	1.02%	0.99%	0.93%	0.87%	0.87%	0.36%	29.2%
Cer	10.0	610.0	622.5	635.0	660.0	685.0	710.0	735.0	760.0	810.0	860.0	860.0	29.1%	29.1%
Cer %	1.64%	1.61%	1.57%	1.52%	1.46%	1.41%	1.41%	1.36%	1.32%	1.23%	1.16%	1.16%	0.48%	29.1%
Cer	12.5	612.5	625.0	637.5	662.5	687.5	712.5	737.5	762.5	812.5	862.5	862.5	29.0%	29.0%
Cer %	2.04%	2.00%	1.96%	1.89%	1.82%	1.75%	1.75%	1.69%	1.64%	1.54%	1.45%	1.45%	0.59%	29.0%
Cer	15.0	615.0	627.5	640.0	665.0	690.0	715.0	740.0	765.0	815.0	865.0	865.0	28.9%	28.9%
Cer %	2.44%	2.39%	2.34%	2.26%	2.17%	2.10%	2.10%	2.03%	1.96%	1.84%	1.73%	1.73%	0.70%	28.9%
Cer	12.5	612.5	625.0	637.5	662.5	687.5	712.5	737.5	762.5	812.5	862.5	862.5	29.0%	29.0%
Cer %	2.04%	2.00%	1.96%	1.89%	1.82%	1.75%	1.75%	1.69%	1.64%	1.54%	1.45%	1.45%	0.59%	29.0%
Cer	15.0	615.0	627.5	640.0	665.0	690.0	715.0	740.0	765.0	815.0	865.0	865.0	28.9%	28.9%
Cer %	2.44%	2.39%	2.34%	2.26%	2.17%	2.10%	2.10%	2.03%	1.96%	1.84%	1.73%	1.73%	0.70%	28.9%
Cer	17.5	617.5	630.0	642.5	667.5	692.5	717.5	742.5	767.5	817.5	867.5	867.5	28.8%	28.8%
Cer %	2.83%	2.78%	2.72%	2.62%	2.53%	2.44%	2.44%	2.36%	2.28%	2.14%	2.02%	2.02%	0.82%	28.8%
Cer	20.0	620.0	632.5	645.0	670.0	695.0	720.0	745.0	770.0	820.0	870.0	870.0	28.7%	28.7%
Cer %	3.23%	3.16%	3.10%	2.99%	2.88%	2.78%	2.78%	2.68%	2.60%	2.44%	2.30%	2.30%	0.93%	28.7%
Δ = 3.23%	0.0%	3.16%	0.1%	3.10%	0.1%	2.99%	0.3%	2.68%	0.5%	2.44%	0.6%	2.30%	0.93%	28.7%
Δ/[PI] %	0.0%	3.2%	3.1%	3.0%	2.9%	2.8%	2.7%	2.6%	2.5%	2.4%	2.3%	2.3%	0.7%	2.3%

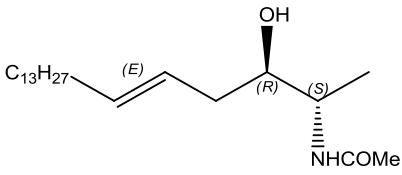
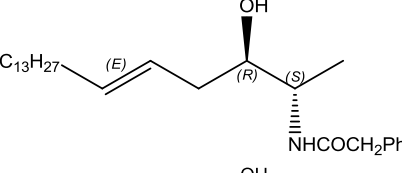
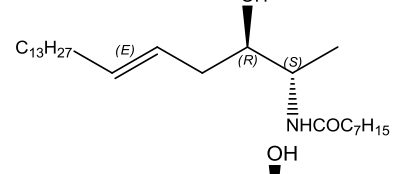
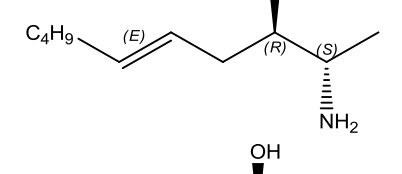
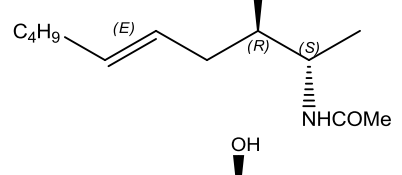
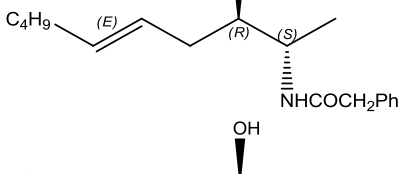
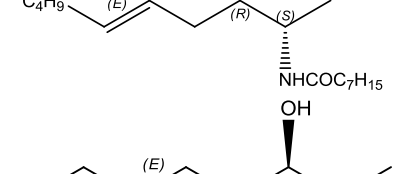
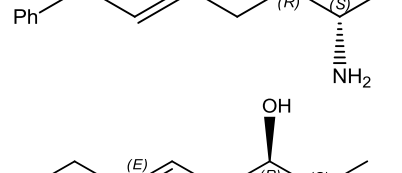
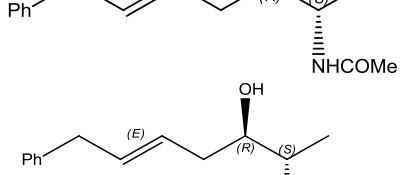
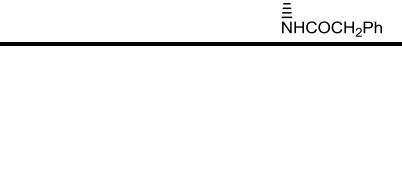
APPENDIX 'C': SCREENING RESULTS TABLE

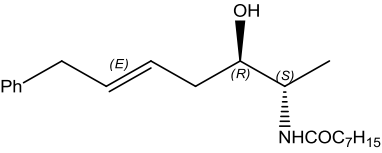
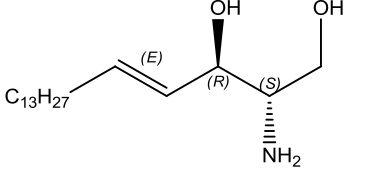
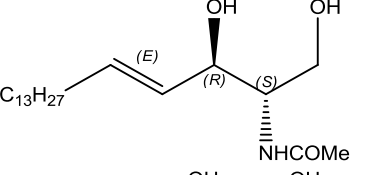
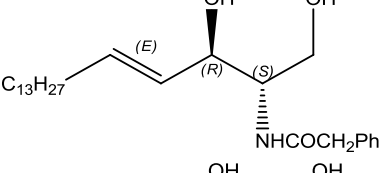
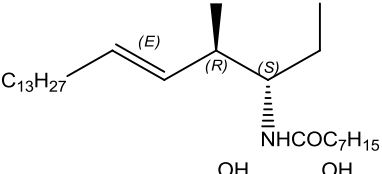
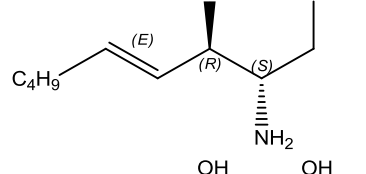
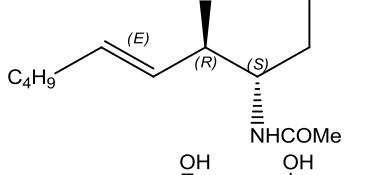
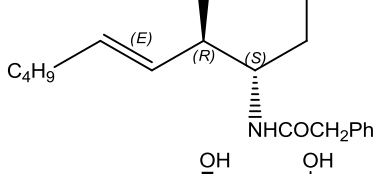
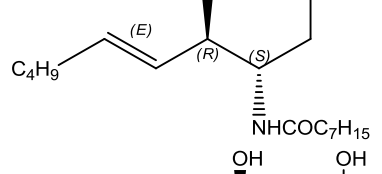
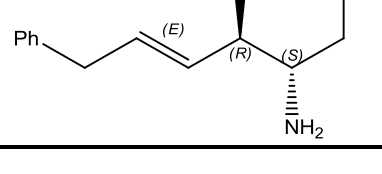
Cpd Class	#	Structure	Act%	SE
Ref compounds				
Sph			53%	1.8%
Synthetic intermediates				
Early intermediates				
202			112%	11.5%
203			81%	7.0%
Pre-CM				
122a			89%	19.0%
103a			75%	7.6%
107			104%	0.5%
207			91%	16.5%
313			76%	1.0%
331			114%	1.4%

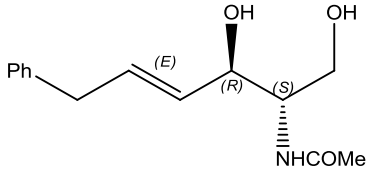
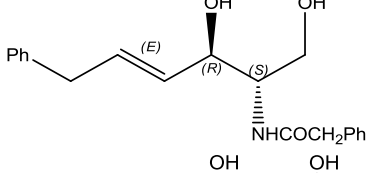
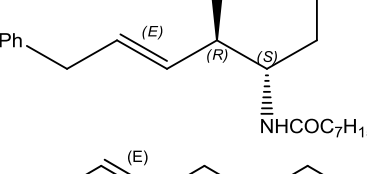
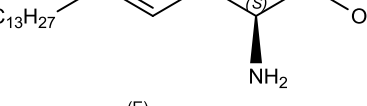
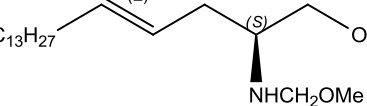
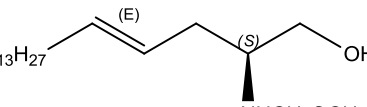
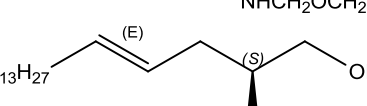
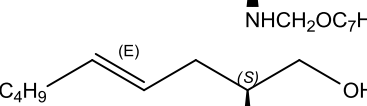
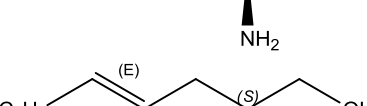
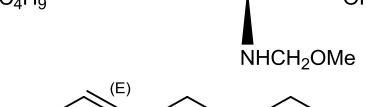
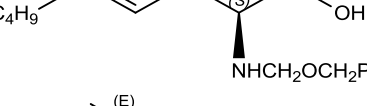
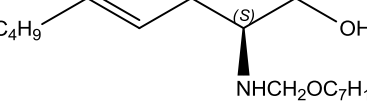
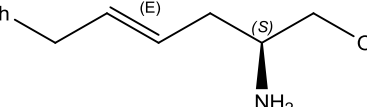
Cpd Class	#	Structure	Act%	SE
Boc-protected CM products				
	211		66%	8.0%
	212		103%	5.0%
	213		104%	12.4%
	104		139%	5.7%
	105		163%	3.2%
	106		102%	1.3%
	129		71%	2.8%
	130		84%	6.4%
	131		85%	8.5%
	314		41%	3.5%

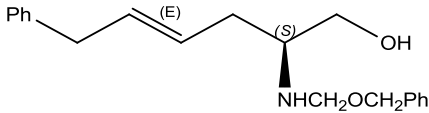
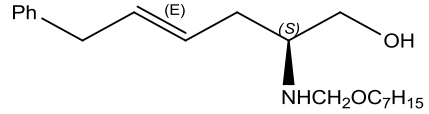
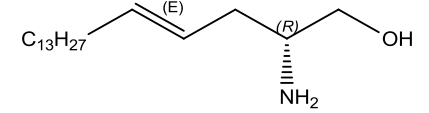
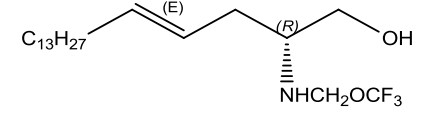
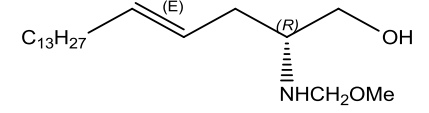
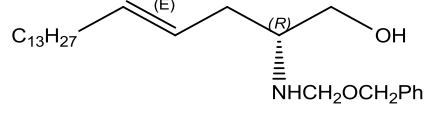
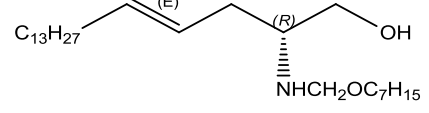
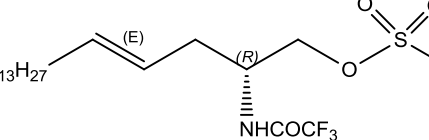
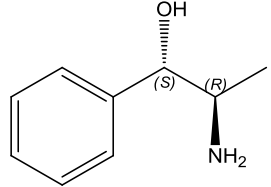
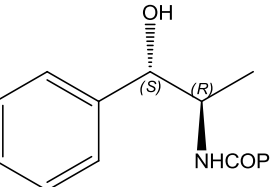
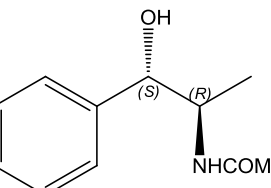
Cpd Class	#	Structure	Act%	SE
	315		101%	5.0%
	316		98%	6.2%
	332		45%	14.8%
Ac protected CM products				
	127		54%	4.2%
	128		54%	2.0%
	108		60%	2.2%
Library Compounds				
	109		64%	4.1%
	110		81%	7.0%
	111		55%	10.5%

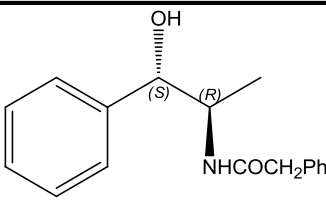
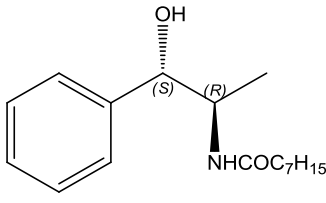
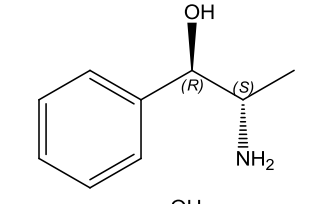
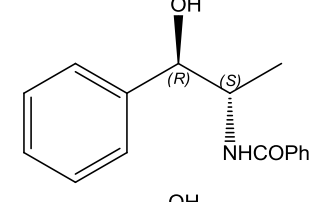
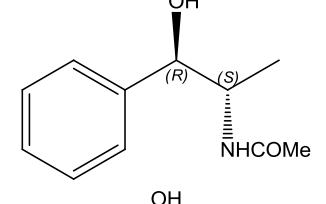
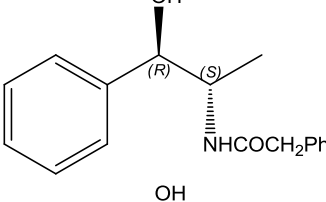
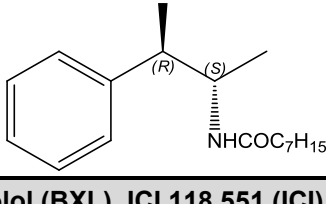
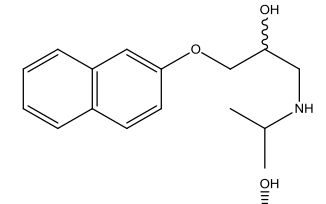
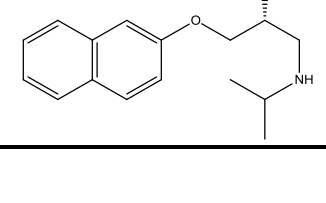
Cpd Class	#	Structure	Act%	SE
	112		21%	1.5%
	113		81%	8.0%
	114		87%	6.2%
	115		105%	1.5%
	116		68%	5.0%
	117		68%	8.0%
	118		101%	9.4%
	119		90%	8.1%
	120		90%	8.5%
	141		60%	2.4%

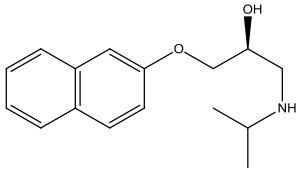
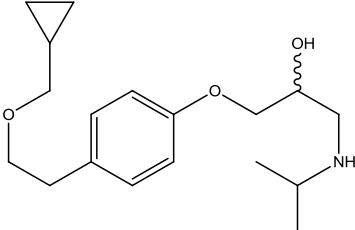
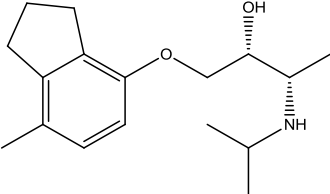
Cpd Class	#	Structure	Act%	SE
	142		61%	6.2%
	143		45%	4.8%
	144		55%	3.9%
	132		62%	0.0%
	133		80%	9.0%
	134		85%	6.0%
	135		58%	3.8%
	136		99%	6.0%
	137		129%	0.5%
	138		62%	16.5%

Cpd Class	#	Structure	Act%	SE
	139		68%	8.3%
	219		54%	9.5%
	220		36%	4.5%
	221		40%	1.0%
	222		13%	3.5%
	215		65%	2.5%
	216		71%	3.0%
	217		104%	3.0%
	218		44%	0.5%
	223		119%	10.0%

Cpd Class	#	Structure	Act%	SE
	224		86%	7.5%
	225		71%	1.5%
	226		55%	4.3%
	317		52%	5.5%
	318		58%	11.0%
	319		50%	5.2%
	320		54%	2.7%
	321		83%	17.5%
	322		77%	6.0%
	323		101%	7.5%
	324		69%	3.0%
	325		88%	6.1%
	326		83%	10.0%

Cpd Class	#	Structure	Act%	SE
	327		89%	2.0%
	328		74%	6.6%
	333		43%	6.6%
	334		35%	4.5%
	335		48%	0.6%
	336		24%	3.8%
	337		43%	4.4%
	338		82%	5.7%
1-Phenyl-2-aminopropanol (PAP) Derivatives				
	(+)PAP		111%	6.7%
	401		89%	11.6%
	402		107%	25.9%

Cpd Class	#	Structure	Act%	SE
	403		123%	11.8%
	404		92%	3.7%
(-)-PAP			111%	20.5%
	405		77%	11.0%
	406		118%	9.5%
	407		67%	9.5%
	408		80%	0.5%
Beta Blockers, Propranolol (PPL), Betaxolol (BXL), ICI 118,551 (ICI)				
(±)PPL			48%	1.3%
(+)PPL			39%	3.9%

Cpd Class	#	Structure	Act%	SE
(-)PPL			50%	11.5%
BXL			48%	5.1%
ICI			54%	4.0%

APPENDIX 'D': PUBLICATIONS



Contents lists available at ScienceDirect

The International Journal of Biochemistry & Cell Biology

journal homepage: www.elsevier.com/locate/biocel

A plate-based assay system for analyses and screening of the *Leishmania major* inositol phosphorylceramide synthase

John G. Mina^{a,b}, Jackie A. Mosely^a, Hayder Z. Ali^a, Hosam Shams-Eldin^c, Ralph T. Schwarz^{c,d}, Patrick G. Steel^{a,*}, Paul W. Denny^{a,b,*}

^a Biophysical Sciences Institute, Department of Chemistry and School of Biological and Biomedical Sciences, Durham University, Durham DH1 3LE, UK

^b School of Medicine and Health, Durham University, Queen's Campus, Stockton-on-Tees TS17 6BH, UK

^c Institut für Virologie, Zentrum für Hygiene und Infektionsbiologie, Philipps-Universität Marburg, Hans-Meerwein-Strasse, 35043 Marburg, Germany

^d Unité de Glycobiologie Structurale et Fonctionnelle, UMR CNRS/USTL n° 8576 - IFR 118, Université des Sciences et Technologies de Lille, 59655 Villeneuve D'Ascq Cedex, France

ARTICLE INFO

Article history:

Received 5 March 2010

Received in revised form 4 June 2010

Accepted 9 June 2010

Available online 16 June 2010

Keywords:

Inositol phosphorylceramide synthase

Leishmania species

Leishmaniasis

Kinetics

Inhibition

ABSTRACT

Sphingolipids are key components of eukaryotic membranes, particularly the plasma membrane. The biosynthetic pathway for the formation of these lipid species is largely conserved. However, in contrast to mammals, which produce sphingomyelin, organisms such as the pathogenic fungi and protozoa synthesize inositol phosphorylceramide (IPC) as the primary phosphosphingolipid. The key step involves the reaction of ceramide and phosphatidylinositol catalysed by IPC synthase, an essential enzyme with no mammalian equivalent encoded by the *AUR1* gene in yeast and recently identified functional orthologues in the pathogenic kinetoplastid protozoa. As such this enzyme represents a promising target for novel anti-fungal and anti-protozoal drugs. Given the paucity of effective treatments for kinetoplastid diseases such as leishmaniasis, there is a need to characterize the protozoan enzyme. To this end a fluorescent-based cell-free assay protocol in a 96-well plate format has been established for the *Leishmania major* IPC synthase. Using this system the kinetic parameters of the enzyme have been determined as obeying the double displacement model with apparent $V_{\max} = 2.31 \text{ pmol min}^{-1} \text{ U}^{-1}$. Furthermore, inhibitory substrate analogues have been identified. Importantly this assay is amenable to development for use in high-throughput screening applications for lead inhibitors and as such may prove to be a pivotal tool in drug discovery.

© 2010 Elsevier Ltd. All rights reserved.

1. Introduction

The insect vector borne protozoan parasites of the family Kinetoplastidae cause a range of human diseases, including the leishmaniasis and African Sleeping Sickness. These infections are of increasing prevalence, particularly in developing countries, and have been classified by the World Health Organisation as Category I emerging or uncontrolled diseases (Remme et al., 2002). For example, the *Leishmania* spp. (the causative agents of the leishma-

niases) infect more than 12 million people in five continents and are endemic in 88 nation states putting over 350 million people at risk, with instances of leishmaniasis not uncommon in certain regions of North America and southern Europe. Moreover, the spread and severity of disease is exacerbated by its status as an important co-infection in AIDS patients and the overlap in prevalence of HIV and *Leishmania* (Alvar et al., 2008). In the absence of effective vaccines, the treatment of kinetoplastid infections is difficult with the most serious visceral form of leishmaniasis often requiring a long, costly course of drug therapy. In addition, available drugs often exhibit serious side-effects and resistance is rapidly emerging (Remme et al., 2002). These facts make the discovery and validation of new therapeutic agents a priority.

The diverse, amphipathic sphingolipids consist of a sphingoside backbone with long-chain base and polar alcohol attachments. These essential lipid species are found in all eukaryotic cells, as well as in some prokaryotic organisms and viruses (Smith and Merrill, 2002). In eukaryotes, the unmodified sphingolipid, ceramide, is a precursor for the synthesis of complex sphingolipids in the Golgi apparatus. The resultant lipid species are subsequently concentrated in the outer leaflet of the plasma membrane. Here, together

Abbreviations: PI, phosphatidylinositol; PC, phosphatidylcholine; IPC, inositol phosphorylceramide; SM, sphingomyelin; PSL, phosphosphingolipid; NBD-C₆-ceramide, *N*-[6-[(7-nitro-2-1,3-benzoxadiazol-4-yl)amino]hexanoyl]-*D*-erythro-sphingosine; CHAPS, 3-[(3-cholamidopropyl) dimethylammonio]-1-propanesulfonate; *Lmj*IPCS, *Leishmania major* IPC synthase.

* Corresponding authors at: Biophysical Sciences Institute, Department of Chemistry, Durham University, Durham DH1 3LE, UK. Tel.: +44 191 334 3983.

E-mail addresses: p.g.steel@durham.ac.uk (P.G. Steel), p.w.denny@durham.ac.uk (P.W. Denny).

URL: <http://www.bsi.durham.ac.uk> (P.W. Denny).

¹ Tel.: +44 191 334 2131.

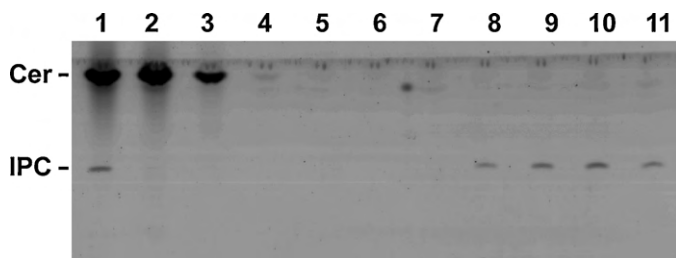


Fig. 1. Separation of NBD-C₆-IPC product from NBD-C₆-ceramide substrate by anion exchange chromatography. Thin layer chromatography analysis of fractions demonstrating the separation of NBD-C₆-IPC product from NBD-C₆-ceramide substrate. (1) Reaction product; (2) column flow through; (3–5) methanol wash; (6–9) elution Cer–NBD-C₆-ceramide; IPC–NBD-C₆-IPC.

with sterols, they form the microdomains known as lipid rafts (Futerman and Hannun, 2004). Such domains have been suggested to be central to a wide array of cellular processes, including the formation of signal transduction complexes (Magee et al., 2002; Pierce, 2002) and the polarized trafficking of lipid-modified proteins (Brown and London, 1998). Importantly, sphingolipid metabolites such as ceramide and phosphorylated sphingosine (sphingosine-1-phosphate), are also involved in the intracellular signal transduction processes that regulate cell growth, differentiation and programmed cell death (apoptosis) (Futerman and Hannun, 2004).

Sphingolipids demonstrate structural divergence in evolution. Whilst sphingomyelin (SM) is the predominant phosphosphingolipid (PSL) of mammalian cells, inositol phosphorylceramide (IPC) is found in the fungi, plants and some protozoa but not in mammals (Lester and Dickson, 1993; Sperling and Heinz, 2003). SM is formed by the transfer of the phosphorylcholine head group from the phospholipid phosphatidylcholine (PC) to ceramide, a reaction catalysed by SM synthase (Huitema et al., 2004). The related enzyme, IPC synthase, mediates the formation of IPC in fungi, plants and the pathogenic kinetoplastid protozoa (e.g. *Leishmania* spp.) by catalyzing the transfer of phosphorylinositol from phosphatidylinositol (PI) to ceramide or phytoceramide (Becker and Lester, 1980; Bromley et al., 2003; Denny et al., 2006). In the fungi this enzyme activity has been attributed to the AUR1p protein first identified in *Saccharomyces cerevisiae* and subsequently in several fungal pathogens (Heidler and Radding, 1995; Heidler and Radding, 2000). We have isolated a functional orthologue of this protein in the kinetoplastid, protozoan parasite *Leishmania major* (*Lmj*IPCS) (Denny et al., 2006). *Lmj*IPCS is encoded by a single gene (GeneDB, *Lmj*F35.4990), and closely related orthologues are found in the complete genome sequences of the related kinetoplastid pathogens, *Trypanosoma brucei* (the causative agent of African Sleeping Sickness) and *Trypanosoma cruzi* (Chagas Disease) (Denny et al., 2006). IPC synthase activity is evident in both the insect and mammalian stages of the *L. major* lifecycle, however in the intra-macrophage form the parasite is predicted to scavenge host cell ceramide for use as substrate by *Lmj*IPCS (Zhang et al., 2005, 2009).

As an essential activity with no mammalian equivalent the fungal IPC synthase has become a recognized and well studied drug target (Georgopapadakou, 2000; Nagiec et al., 1997a). The discovery of functional orthologues in the kinetoplastid pathogenic protozoa has led to its further consideration as an anti-protozoal target (Suzuki et al., 2008). It is known that *Lmj*IPCS activity is susceptible to the established fungal inhibitor aureobasidin A (Denny et al., 2006). In addition, this compound has been demonstrated to inhibit the growth and infectivity of *L. amazonensis* (Tanaka et al., 2007). Furthermore, recent work in our laboratory (Mina et al., 2009) and elsewhere (Sutterwala et al., 2008) has both genetically and pharmacologically validated the kinetoplastid enzyme as a tar-

get in *T. brucei*. Therefore, further study of the *Lmj*IPCS (and other kinetoplastid orthologues) is vital in moving towards the ultimate goal of identifying compounds with the potential for development into much needed, pharmacologically active anti-protozoals. Herein we report the establishment of a robust 96-well plate based assay system that uses easily obtainable, transgenic yeast-derived material, together with its application to detail the kinetic parameters of *Lmj*IPCS and demonstrate the inhibitory effects of several substrate analogues.

2. Materials and methods

2.1. Materials

Phosphatidylinositol (bovine liver PI; predominant species 1-stearoyl-2-arachidonoyl-*sn*-glycero-3-phospho-1-myoinositol sodium salt) was from Avanti Polar Lipids. *D-erythro*-Sphingosine (d18:1; sphing-4-enine, (2*S*,3*R*,*E*)-2-aminooctadec-4-ene-1,3-diol) and *N*-acetyl-*D-erythro*-sphingosine (d18:1/2:0; *N*-acetyl-sphing-4-enine, (2*S*,3*R*,4*E*)-*N*-acetyl-2-aminooctadec-4-ene-1,3-diol) were from TOCRIS BioScience. C₁₈-Ceramide (d18:1/18:0; *N*-stearoyl-*D-erythro*-sphingosine, (2*S*,3*R*,4*E*)-*N*-stearoyl-2-aminooctadec-4-ene-1,3-diol) and diacylglycerol (1-octadecanoyl-2-(5*Z*,8*Z*,11*Z*,14*Z*-eicosatetraenoyl)-*sn*-glycerol) were from Sigma-Aldrich. NBD-C₆-ceramide (*N*-[6-[(7-nitro-2-1,3-benzoxadiazol-4-yl)amino]hexanoyl]-*D-erythro*-sphingosine) was from Invitrogen.

2.2. Preparation of *Lmj*IPCS microsomal material

Auxotrophic AUR1 mutant *S. cerevisiae* was complemented by the expression of the *L. major* IPC synthase to create YPH499–HIS–GAL–AUR1 pRS246 *Lmj*IPCS (Denny et al., 2006). These cells were propagated in SD medium (0.17% Bacto yeast nitrogen base, 0.5% ammonium sulphate and 2% dextrose) containing the appropriate nutritional supplements, and microsomes prepared from an exponentially growing culture (Fischl et al., 2000). Briefly, approximately 8.0 g of wet cell mass was suspended in STE buffer (25 mM Tris–HCl pH 7.4, 250 mM sucrose and 1 mM EDTA) containing Complete[®] EDTA-free Protease Inhibitor Cocktail (Roche Applied Science) and the yeast disrupted by vortex mixing with pre-chilled acid-washed glass beads (425–600 μm, Sigma-Aldrich). After the removal of the glass beads, unbroken cells and cell-wall debris by centrifugation (1500 × g, 4 °C and 15 min), the microsomal membrane fraction was isolated by differential centrifugation. Subsequently the large granular fraction was removed (27,000 × g, 4 °C and 30 min) and the microsomal membrane fraction isolated (150,000 × g, 4 °C and 90 min). The microsomes were re-suspended at a concentration of 10 mg ml⁻¹ in storage buffer (50 mM Tris/HCl pH 7.4, 20% (v/v) glycerol, 5 mM MgCl₂) containing protease inhibitor. As required, the microsomal membranes were washed in 2.5% CHAPS (Sigma-Aldrich; 4 °C, 60 min), isolated by centrifugation (150,000 × g, 4 °C and 90 min), assayed for protein content (CBQCA, Invitrogen) and re-suspended in storage buffer. A second wash inactivated the enzyme.

Different preparations of microsomal membranes were utilized in this study and these varied in specific *Lmj*IPCS enzyme activity. Therefore, to standardise the assay material samples were normalized with respect to active enzyme content ensuring consistency across experiments. Although the standardised unit for enzymatic activity is the katal where 1 kat = 1 mol (product)⁻¹ s⁻¹ (International Union of Biochemistry, 1979), for the range of substrates concentrations used in the work presented here a more practical value is enzyme unit (U). One unit (U) of enzyme is defined as that which converts 1 pmol of substrate per minute under the conditions described (1 U = 1 pmol (product) min⁻¹), where 1 U cor-

responds to 16.67 femtokats (Fischl et al., 2000). The conversion of the fluorescent acceptor substrate NBD-C₆-ceramide to the product NBD-C₆-IPC was measured and quantified with respect to known concentrations of NBD-C₆-ceramide, activity calculated as U μl⁻¹ and the samples were stored at -80 °C until use. Enzyme turnover was calculated per milligrams of total protein in the sample (U mg⁻¹).

2.3. Thin layer chromatography (TLC) based *Lmj*IPCS synthase assay

Both unwashed and CHAPS-washed (1 μg) microsomal membranes were used in a 50 μl assay mix containing 1 mM PI, 100 mM Tris-HCl (pH 7.4) and 200 μM NBD-C₆-ceramide (Figueiredo et al., 2005). The reaction was pre-incubated before the addition of the NBD-C₆-ceramide at 30 °C (the established optimum temperature in the assay) for 30 min and subsequently for a further hour before quenching with 150 μl of chloroform:methanol:water (10:10:3). After biphasic separation the organic layer was removed, dried in a rotavapor (Eppendorf Concentrator 5301) and re-suspended in 20 μl of 10:10:3. The reaction products were fractionated using HPTLC silica plates (Merck) and the eluent system chloroform:methanol:aqueous 0.25% KCl (55:45:10). The *R_f* values for the substrate, NBD-C₆-ceramide, and the product, NBD-C₆-IPC were 0.96 and 0.57 respectively. Quantification was carried out using a FLA3000 scanner (Fujifilm) and AIDA Image Analyzer[®] software (version 3.52).

2.4. 96-well plate-based *Lmj*IPCS assay for kinetic analyses

CHAPS-washed membranes (Aeed et al., 2004), 0.6U or as described, were used in a reaction mix containing 100 μM (or as indicated) PI, 50 mM KH₂PO₄ (pH 7.0) and 5 μM (or as indicated) NBD-C₆-ceramide. Following pre-incubation at 30 °C for 30 min, the reaction was initiated by the addition of the NBD-C₆-ceramide (5 μM or as indicated) and 2.4 mM CHAPS. The reaction was incubated for the specified period of time and subsequently quenched by the addition of 200 μl of methanol. Separation of the reaction product, NBD-C₆-IPC, from the substrate NBD-C₆-ceramide was achieved by applying the reaction mix to 100 μl (sedimented gel volume) of AG4-X4 resin (BioRad), formate form, in 96-well Multiscreen[®] Solvint filter plates (Millipore) using a vacuum manifold (Millipore). The resin was washed 5 times with 200 μl methanol, the product was eluted into OptiPlate[™] 96-F plates (PerkinElmer) using 200 μl of 1 M potassium formate in methanol and quantified using a fluorescence plate reader (FLx800[™], BioTek)—excitation λ = 485 nm; emission λ = 528 nm. Assays used were carried out in triplicate and results analysed using Prism 5.0 software (GraphPad) and Excel[®] Solver Add-in (Microsoft Office). The separation protocol was validated by collecting fractions from a 5-fold scale up of the process and fractionating them by TLC as above (Fig. 1).

Substrate analogues were employed in inhibition studies and added with the fluorescent substrate NBD-C₆-ceramide in the quantities indicated.

The assay system was validated as excellent for screening purposes with a *Z'* value of 0.58 (Zhang et al., 1999). Calculation of this value utilized 2 bespoke inhibitors, (4*E*) *N*-(phenylacetyl)-1-deoxy sphing-4-enine and (2*R*,4*E*) *N*-phenylacetyl-2-amino-octadec-4-en-1-ol whose synthesis and screening will be subsequently reported.

2.5. Mass spectrometry

Analyses were performed on an LTQFT (ThermoFinnigan Corp.); an FTICR MS instrument equipped with a 7.0 T magnet. Chloroform

extracts were introduced into the electrospray ion source by direct infusion from a syringe at a flow rate of 3 μl min⁻¹. Positive ion measurements were made with the source voltage at 4.0 kV and negative ion measurements were made with the source voltage at 3.5 kV. The tube lens was kept at 100 V and the source temperature at 275 °C for all experiments.

2.6. Cytotoxicity screening

L. major (MHOM/IL/81/Friedlin) and *L. mexicana* (MNYC/BZ/62/M379) parasites were maintained at 26 °C in Schneider's *Drosophila* media (Sigma-Aldrich) supplemented with heat inactivated foetal bovine sera (15% for promastigotes and 20% for amastigotes; Biosera). *L. mexicana* promastigotes were transformed into axenic amastigotes by a pH and temperature shift as previously described (Bates, 1994). In 96-well plates (Nunc) parasites at 10⁵ ml⁻¹ were incubated with compounds in triplicate (including miltefosine (Cayman Chemical) as a positive control, and untreated parasites and media as negative controls) for 24 h before incubation with Alamar Blue (Invitrogen) for 4 h prior to assessing cell viability using a fluorescent plate reader (Biotek; 560EX nm/600EM nm). *ED*₅₀ was calculated after plotting cell viability (as percent of untreated control) against log compound concentration (μM).

3. Results and discussion

3.1. Assay of *Lmj*IPCS microsomal material

The high levels of endogenous PI present in yeast microsomes (Aeed et al., 2004) rendered establishing the kinetic parameters of *Lmj*IPCS with respect to this donor substrate problematic. Initial assay experiments using unrefined material derived from *Lmj*IPCS complemented HIS-GAL-AUR1 auxotrophic yeast IPCS mutants (Denny et al., 2006) demonstrated that endogenous, microsomal PI accounted for approximately 25% of the measured *Lmj*IPCS turnover (Fig. 2A), making accurate determination of the enzyme kinetic parameters impossible. A similar problem has previously been identified with the use of *T. cruzi* derived microsomes in an

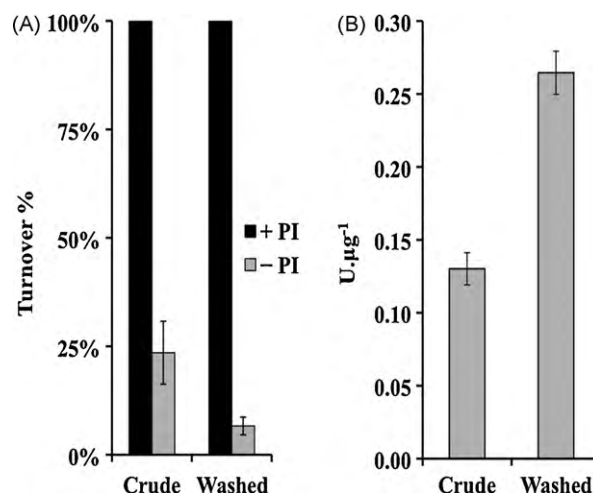


Fig. 2. Turnover of *Lmj*IPCS in CHAPS-washed and crude (unwashed) microsomal preparations. Measured by the incorporation of the fluorescent acceptor substrate, NBD-C₆-ceramide, into NBD-C₆-IPC product. Fluorescent IPC was quantified following fractionation by HPTLC as described. (A) Assay of *Lmj*IPCS activity in crude or washed microsomes with (black) or without (grey) the addition of the donor substrate, bovine phosphatidylinositol (PI). The background due to endogenous PI (grey) is reduced after washing the membraneous material. Results normalized with respect to +PI samples. (B) The specific activity of *Lmj*IPCS, as determined by the formation of IPC, is enhanced in the washed microsomes. Note 2-fold increase in specific activity (based on total protein content per assay).

assay of *Tc*IPCS turnover (Figueiredo et al., 2005). However, it has been demonstrated that washing microsomal membranes derived from the pathogenic yeast, *Candida albicans* with a zwitterionic detergent (CHAPS) removed endogenous substrate lipids without affecting IPCS activity (Aeed et al., 2004). Adopting this approach and employing microsomes from *Lmj*IPCS complemented HIS-GAL-AUR1 yeast, washed with CHAPS as described, the parasite enzyme assay proved to be dependent not only on the addition of the fluorescent acceptor substrate, NBD- C_6 -ceramide, but now also more than 90% dependent on the addition of the donor substrate (bovine liver PI; Fig. 2A). It has previously been demonstrated that the *S. cerevisiae* orthologous enzyme, AUR1p, is unable to utilise bovine liver PI (Mina et al., 2009). In the present assay system, the CHAPS-washed microsomes also demonstrated an approximately 2-fold higher level of enzyme turnover than equivalent quantities of crude material (Fig. 2B). This increase is most likely due to enrichment of the sample for *Lmj*IPCS as other proteins are washed away from the detergent insoluble material. However, the removal of microsomal proteins and lipids may also reduce the spatial volume of the washed material leading to more rapid diffusion of applied exogenous substrates into the membranes. Taken together these data indicate that washing the microsomes with CHAPS depletes them of PI, and perhaps (phyto)ceramide, thereby facilitating more accurate determination of the kinetics of *Lmj*IPCS. Moreover, the fact that *Lmj*IPCS remained highly active within a detergent resistant lipid environment suggests that the enzyme may reside within CHAPS-resistant lipid microdomains *in vivo* (Rouvinski et al., 2003).

3.2. Determination of *Lmj*IPCS assay parameters

Using the 96-well plate formatted system described, reproducible, quantitative kinetic data could be obtained for the enzyme from CHAPS-washed *Lmj*IPCS yeast microsomes. In the first instance the formation of product (IPC) over time was determined. The results demonstrated that the reaction rate is linear for 30 min before it decreases over time (Fig. 3A). As a consequence all subsequent assays were performed with a 15 min reaction time to ensure linearity under the specified conditions, turnover was assumed to be equivalent to initial velocity (v_0).

Since both substrates are in excess and only approximately 12% of the limiting acceptor substrate, NBD- C_6 -ceramide, is consumed after 1 h, the reasons for the decrease in reaction rate above 30 min are unclear. The IPC product may be localised around the enzyme affecting a change in the diffusion rate of the substrates to the active site. It is also possible that *Lmj*IPCS activity is modulated by inhibitory feedback from the synthesized NBD- C_6 -IPC or diacylglycerol (DAG) which is formed as a by-product of IPC synthase turnover (Denny et al., 2006). Analysis of the inhibitory affect of DAG indicated a $\log IC_{50}$ value of 0.92 ± 0.08 and an IC_{50} of $8.3 \mu M$ (Fig. 3B) supporting the latter hypothesis.

Product (NBD- C_6 -IPC) formation also increased in a linear manner with increasing enzyme concentration up to 0.8 U/assay (Fig. 3C). However, the linear relationship deviated beyond this point (data not shown). Notably, increasing the concentration of enzyme also leads to a change in the protein: lipid: detergent (CHAPS) ratio and hence modulates the substrate concentration at the active site of *Lmj*IPCS. Taking this observation into account 0.6 U of *Lmj*IPCS (within the linear range) was employed in all subsequent analyses.

3.3. Determination of *Lmj*IPCS kinetic parameters

Having established a standardized set of conditions that gave a linear response, and in which endogenous interfering substrate was minimized by detergent washing, the kinetic parameters of *Lmj*IPCS with respect to both the acceptor (NBD- C_6 -ceramide)

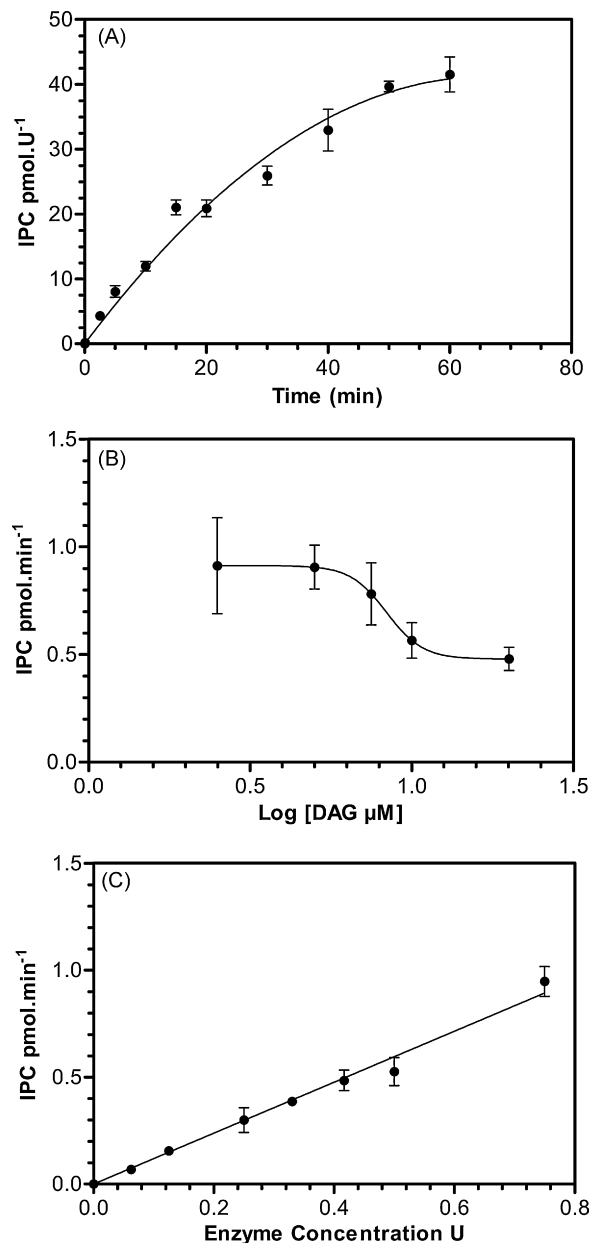


Fig. 3. *Lmj*IPCS turnover versus time, enzyme concentration and in presence of DAG. Determined using the 96-well plate formatted assay as described, with fluorescent NBD- C_6 -ceramide as acceptor substrate ($5 \mu M$), and bovine phosphatidylinositol (PI; $100 \mu M$) as the donor substrate. IPC quantified with respect to NBD- C_6 -ceramide standard curve. All points in triplicate, error bars shown. (A) *Lmj*IPCS turnover versus time. Turnover defined as pmol IPC produced per unit of enzyme (pmol U^{-1}) under the conditions employed. $R^2 = 0.95$. (B) *Lmj*IPCS turnover versus DAG concentration. Turnover is defined as pmol IPC produced per minute ($\text{pmol min}^{-1} \text{U}^{-1}$) under the conditions employed. $R^2 = 0.86$. (C) *Lmj*IPCS turnover versus enzyme concentration: linear range. Turnover is defined as pmol IPC produced per minute (pmol min^{-1}) under the conditions employed. $R^2 = 0.98$.

and donor (PI) substrates were determined. Initially, the data obtained were tested against the Michaelis–Menten model and with respect to increasing concentrations of NBD- C_6 -ceramide gave a curve of good fit ($R^2 = 0.97$; Fig. 4A). The apparent K_m for the acceptor substrate was $3.5 \pm 0.35 \mu M$ and the apparent V_{max} $2.1 \pm 0.07 \text{ pmol min}^{-1} \text{U}^{-1}$. However, determination of the Hill constant revealed a Hill slope of 2.7 that indicated co-operative binding of substrates was occurring (Hill, 1910).

In contrast, with [NBD- C_6 -ceramide] fixed at $5 \mu M$, the data with respect to the PI showed a poor fit to the Michaelis–Menten

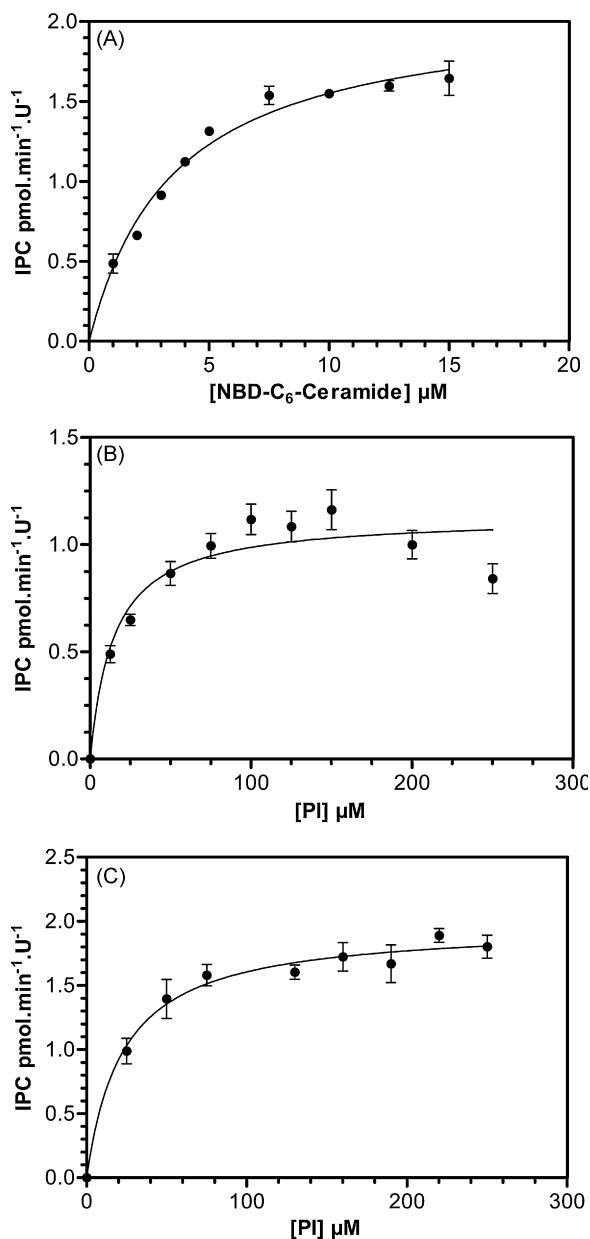


Fig. 4. *LmjIPCS* turnover versus acceptor substrate (NBD-C₆-ceramide) and donor substrate (phosphatidylinositol) concentrations. Determined using the 96-well plate formatted assay as described, with fluorescent NBD-C₆-ceramide as acceptor substrate, and bovine phosphatidylinositol (PI) as the donor substrate. IPC quantified with respect to NBD-C₆-ceramide standard curve. All points in triplicate, error bars shown. (A) *LmjIPCS* turnover (defined as pmol IPC min⁻¹ U⁻¹; v_0) demonstrated apparent Michaelis-Menten kinetics - $v_0 = V_{\max}[S]/(K_m + [S])$ - with respect to the acceptor substrate NBD-C₆-ceramide (S). Non-linear analysis calculated the apparent $K_m = 3.5 \pm 0.35 \mu\text{M}$; and the apparent $V_{\max} = 2.1 \pm 0.1 \text{ pmol min}^{-1} \text{ U}^{-1}$. $R^2 = 0.97$, indicating a good fit to the model. [PI] = 100 μM . (B) *LmjIPCS* turnover (v_0) with respect to the donor substrate (S), phosphatidylinositol (PI), did not fit the Michaelis-Menten model. $R^2 = 0.76$. [NBD-C₆-ceramide] = 5 μM . (C) However, *LmjIPCS* turnover (v_0) with respect to PI fits a Michaelis-Menten model at high NBD-C₆-ceramide concentration. $R^2 = 0.93$. Non-linear analysis calculated the apparent $K_m = 22.8 \pm 4.6 \mu\text{M}$ and the apparent $V_{\max} = 2.0 \pm 0.07 \text{ pmol min}^{-1} \text{ U}^{-1}$. [NBD-C₆-ceramide] = 20 μM .

equation ($R^2 = 0.82$; Fig. 4B), with considerable deviation at high concentrations of donor substrate. The enzyme orthologue from the pathogenic yeast *C. albicans* has previously been shown to behave in a similar manner, a phenomenon which was described as being caused by substrate inhibition (Aeed et al., 2004). However, at a higher, saturating concentration of the acceptor substrate, [NBD-

C₆-ceramide] = 20 μM ($>5 \times$ apparent K_m), no apparent inhibition at high [PI] could be detected (Fig. 4C). This strongly suggested that activity is dependent on the substrate molar ratio, with a dilution effect being observed with low NBD-C₆-ceramide (5 μM) and high PI ($>150 \mu\text{M}$). The mol% concentration of NBD-C₆-ceramide dropped 30% from 0.82% at 12.5 μM PI and 600 μM CHAPS to 0.58% 250 μM PI and 600 μM CHAPS. In contrast a change in concentration of the acceptor substrate has little effect on the mol% concentration of PI (14.3% at 1 μM NBD-C₆-ceramide and 600 μM CHAPS to 13.9% at 20 μM NBD-C₆-ceramide and 600 μM CHAPS) and CHAPS.

PI vesicles can be solubilised by 0.27 mM CHAPS, far below the CMC of this detergent ($[D_w]^c$: critical concentration of free detergent; Schürholz, 1996). Therefore under the experimental conditions employed (0.6 mM CHAPS) in the assay system PI/CHAPS mixed micelles are formed. The molar detergent to lipid ratio of these (R^c) is 0.17, meaning that CHAPS is a minor component, approximately 15% of the total molar concentration in micelles (Schürholz, 1996). Based on these data the $[D_w]^c$ in the assay system employed can be calculated using Eq. (1) (Schürholz, 1996).

$$\begin{aligned} [D_T]^c &= [D_w]^c + R^c(M) \times [L_T] \\ [D_T]^c &= \text{Total CHAPS concentration,} \\ [L_T] &= \text{Total lipid concentration} \end{aligned} \quad (1)$$

At $[D_T]^c = 600 \mu\text{M}$ in the reaction mix the $[D_w]^c$ (270 μM) is exceeded under all conditions employed in this study and CHAPS exists primarily in a monomeric form with a minor proportion associated with PI in micelles (2.8% at 100 μM PI).

Given the fact that in this complex system the *LmjIPCS* is a membrane enzyme acting on lipid substrates within mixed micelles the deviation from Michaelis-Menten kinetics observed is unsurprising. To facilitate further analyses a number of assumptions were made, namely: the kinetic parameters would be determined using the steady state approach; initial rate assumptions are applied; PI/CHAPS micelles have a low mol% of CHAPS (approximately 15%); all lipids and detergent molecules have the same surface area; all lipids and detergent molecules have equal accessibility to the enzyme active site. All concentrations are expressed as molar fractions of total lipid plus detergent.

Subsequently a series of assay reactions were carried out with varying acceptor substrate concentrations, [NBD-C₆-ceramide], at different fixed [PI] (12.5–100 μM). A global analysis of the data points (56 mean points of 168 replicates) employing the surface dilution kinetic model, which considers the surface concentration of lipids ([PI] and [Cer]) expressed as mol% in PI/CHAPS micelles; Demms et al., 1975), resulted in non-convergent results. However, given that *LmjIPCS* is an integral membrane protein within microsomal membranes the enzyme can fuse with PI/CHAPS micelles, or maintain its integrity and bounce between micelles whilst interacting with the bulk monomeric CHAPS/NBD-C₆-ceramide in the assay buffer. Both cases would confer bulk concentration dependence to the kinetics (Carman et al., 1995).

Lineweaver-Burk analyses of the data set gave a near parallel pattern (Fig. 5A), with a plot of the intercepts demonstrating a linear correlation to $1/[PI]$ mol% (Fig. 5B). A subsequent global analysis of these data in terms of a generalised form of a bi-bi substrate kinetic equation (Engel, 1977; Eq. (2)) provided a solution for the values of the equation parameters, where $\theta_0 = 0.26$, $\theta_A = 0.82$, $\theta_B = 0.14$, $\theta_{AB} = 1.0 \times 10^{-5}$. From these $V_{\max} = 2.31 \text{ pmol min}^{-1} \text{ U}^{-1}$, $K_m [PI] = 3.15 \text{ mol\%}$ and $K_m [\text{NBD-C}_6\text{-ceramide}] = 0.54 \text{ mol\%}$.

$$\frac{[E_T]}{v} = \theta_0 + \theta_A \frac{1}{[PI]} + \theta_B \frac{1}{[Cer]} + \theta_{AB} \frac{1}{[PI][Cer]} \quad (2)$$

Notably, the relatively high affinity of the acceptor substrate for *LmjIPCS* compared with that of the donor PI was consistent with the proposal that ceramide, a highly bioactive molecule, is

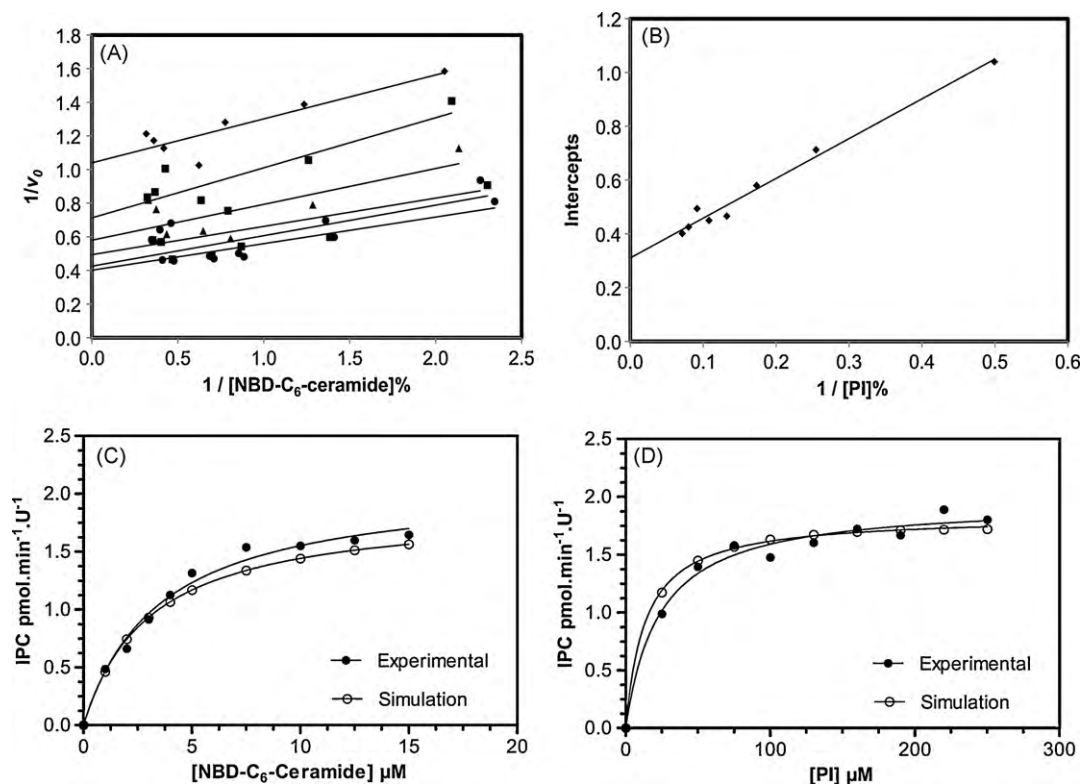


Fig. 5. *LmjIPCS* turnover with varying acceptor substrate (NBD-C₆-ceramide) and different fixed donor substrate (phosphatidylinositol) concentrations. Determined using the 96-well plate formatted assay as described, with fluorescent NBD-C₆-ceramide as acceptor substrate, and bovine phosphatidylinositol (PI) as the donor substrate. IPC quantified with respect to NBD-C₆-ceramide standard curve. All data points in triplicate, error bars omitted for clarity. Donor (PI) and acceptor (ceramide) substrate concentrations varied as indicated. (A) Plots of $1/v_0$ vs. $1/[S]$ %, where *S* is NBD-C₆-ceramide as a molar fraction. Initial velocities (v_0) were determined with six concentrations of PI (12.5, 25, 37.5, 62.5, 87.5 and 100 μ M). The data points were generated from three independent determinations of v_0 . (B) Plot of the intercepts of $1/v_0$ from A against $1/[S]$ %, where *S* is PI as a molar fraction. (C) Simulation and experimental data: [NBD-C₆-ceramide] = variable, [PI] = 100 μ M. (D) Simulation and experimental data: [NBD-C₆-ceramide] = 20 μ M, [PI] = variable.

the rate-limiting substrate in the *in situ* IPC synthase reaction. In contrast PI is a relatively abundant substrate in most membranous environments (Aeed et al., 2004; Dickson, 1998; Leber et al., 1995).

Based on these data the value \emptyset_{AB} was assumed to be zero thereby reducing Eq. (2) to that describing double displacement kinetics (Eq. (3)). Details of the factors of \emptyset_0 , \emptyset_A , \emptyset_B are in supplementary data (S1).

$$\frac{[E_T]}{v} = \emptyset_0 + \emptyset_A \frac{1}{[PI]} + \emptyset_B \frac{1}{[Cer]} \quad (3)$$

These analyses provide strong support for the notion that *LmjIPCS* functions via a double displacement model. This is further evidenced by the close correlation of experimental data with simulations derived from Eq. (3) (Fig. 5C and D).

With this in mind, the apparent fit to the Michaelis–Menton model with respect to ceramide initially observed was most likely due to pre-incubation with saturating levels of PI leaving the majority of the enzyme in an intermediate phosphorylated state. In this state it is predicted that *LmjIPCS* has mediated the transfer of the phosphorylinositol group of PI to the reactive histidine within the identified catalytic triad (Denny et al., 2006) with the concomitant release of DAG. Notably mutation of His-294 within the yeast AUR1p triad has been shown to result in non-viable haploid cells (Levine et al., 2000) and the equivalent mutation (His-264) in *LmjIPCS* rendered it unable to complement auxotrophic AUR1p mutant yeast (Mina and Denny, unpublished). The second step in the reaction is then initiated by the addition of acceptor substrate (ceramide) when the phosphorylated intermediate is subjected to nucleophilic attack by the oxygen of the ceramide hydroxyl group,

resulting in phosphoryl group transfer to the sphingoid base thus forming IPC.

3.4. Substrate analogues as competitive inhibitors

The delineation of the kinetic parameters of *LmjIPCS* also provided the opportunity to begin to further understand the mode of action of this enzyme and perhaps, via a rational approach, to design specific inhibitors. Given the high affinity of the acceptor substrate for *LmjIPCS*, the ability of natural ceramide (Cer; 18:1/18:0; *N*-stearoyl-*D*-erythro-sphingosine) and the ceramide analogues *D*-erythro-sphingosine and *N*-acetyl-*D*-erythro-sphingosine to compete with fluorescent NBD-C₆-ceramide was analysed, with variation in the quantity of the product (NBD-C₆-IPC) reflecting the effect of the substrate competitors on enzyme turnover.

Unlike *N*-acetyl-*D*-erythro-sphingosine and *D*-erythro-sphingosine, *N*-stearoyl-*D*-erythro-sphingosine was insufficiently soluble in the phosphate-based buffer employed for the microtitre plate assay, curtailing analysis. This problem could be circumvented by using a Tris-based buffer system containing defatted-BSA. Here *N*-stearoyl-*D*-erythro-sphingosine was soluble and the results indicated that NBD-C₆-ceramide exhibited an affinity for *LmjIPCS* equivalent to that of the natural substrate (data not shown). Analyses of the more soluble synthetic analogues, *N*-acetyl-*D*-erythro-sphingosine and *D*-erythro-sphingosine, using the phosphate-based buffer system in the 96-well plate based assay demonstrated that they are, as expected, competitive with respect to NBD-C₆-ceramide: IC_{50} values of 16 and 52 μ M respectively (Fig. 6A and B). Subsequent MS-ES⁺/ES⁻ analyses of

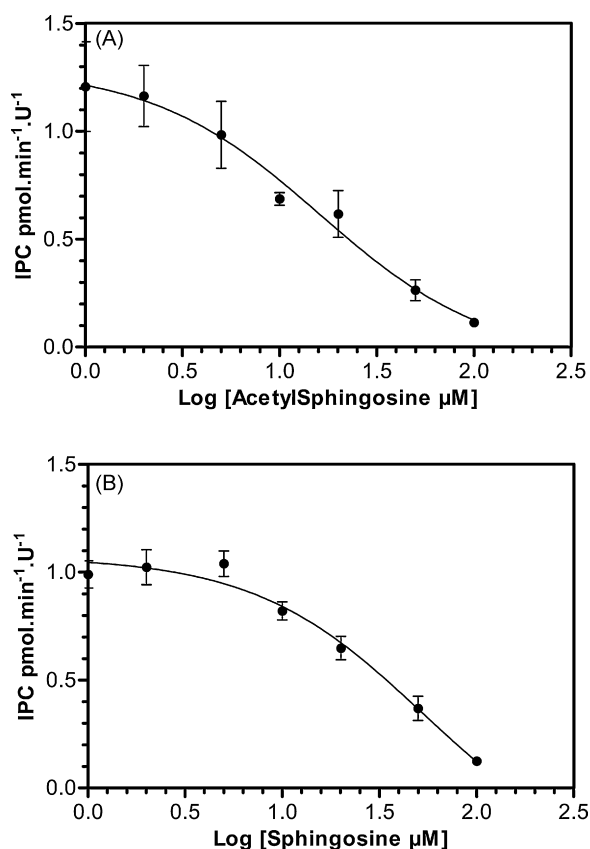


Fig. 6. Competitive inhibition of *LmjIPCS* activity. Determined using the 96-well plate formatted assay as described, with fluorescent NBD-C₆-ceramide as acceptor substrate, and bovine phosphatidylinositol (PI) as the donor substrate. IPC quantified with respect to NBD-C₆-ceramide standard curve. All points in triplicate, error bars shown. Donor substrate (PI) concentration at 100 μM, acceptor (NBD-C₆-ceramide) substrate at 5 μM. $\log IC_{50} = \log(10^{\log K_i}(1 + [\text{NBD-C}_6\text{-Cer}]/\text{NBD-C}_6\text{-Cer } K_m))$, [NBD-C₆-Cer] = 5.0 μM, $K_m = 3.5$ μM. (A) *N*-acetyl-D-erythro-sphingosine is a competitive inhibitor of *LmjIPCS*: $\log IC_{50} = 1.2 \pm 0.2$; $IC_{50} = 16$ μM; $R^2 = 0.83$. (B) *D*-erythro-Sphingosine is a competitive inhibitor of *LmjIPCS*: $\log IC_{50} = 1.7 \pm 0.2$; $IC_{50} = 53$ μM; $R^2 = 0.93$.

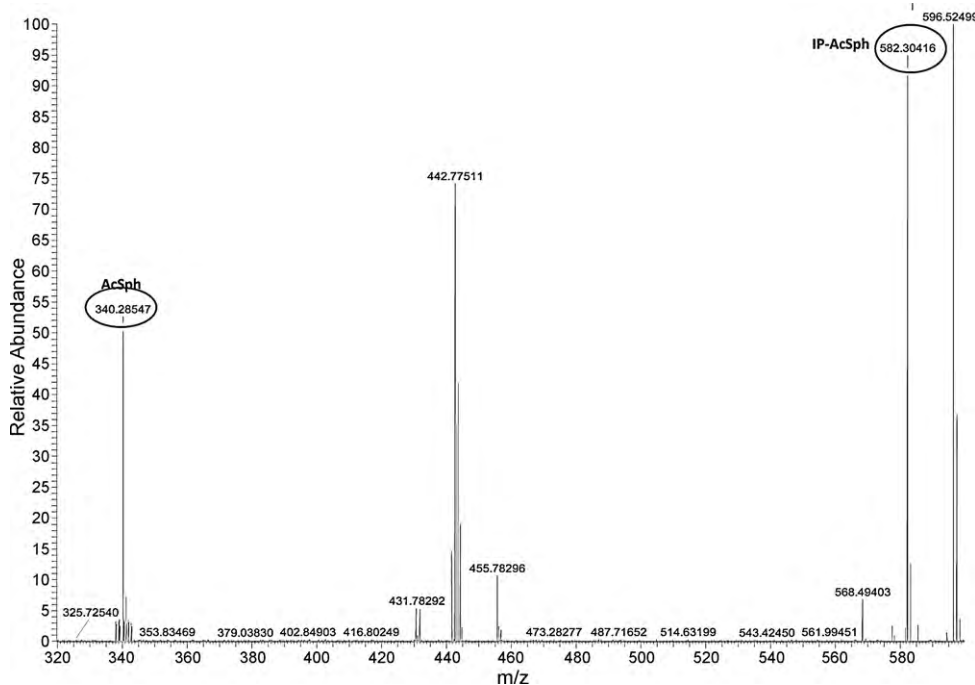


Fig. 7. Mass spectrometric analyses of reaction products from *N*-acetyl-D-erythro-sphingosine. Negative ion mass spectrum demonstrating that *N*-acetyl-D-erythro-sphingosine (AcSph, mass = 340.3) is a substrate for *LmjIPCS*, giving the product inositol phosphoryl acetyl-D-erythro-sphingosine (IP-AcSph, mass = 582.3).

Table 1

Efficacy of ceramide analogues against *L. major* and *L. mexicana*. Established using the Alamar Blue assay system.

	<i>L. major</i> promastigotes	<i>L. mexicana</i> promastigotes	<i>L. mexicana</i> amastigotes
Miltefosine			
log ED_{50}	0.20	0.15	1.10
SE log ED_{50}	0.06	0.06	0.03
ED_{50} μM	1.59	1.41	12.6
Sphingosine			
log ED_{50}	0.81	0.91	1.12
SE log ED_{50}	0.13	0.14	0.04
ED_{50} μM	6.49	8.18	13.3
Acetylceramide			
log ED_{50}	1.63	1.81	ND
SE log ED_{50}	0.14	0.18	ND
ED_{50} μM	43.0	64.5	ND

ND = not determined; ED_{50} = Effective dose, 50%; SE = standard error.

the reaction product profiles (Fig. 7) revealed the presence of a mass of 582.3 corresponding to IP-*N*-acetyl-D-erythro-sphingosine confirming that *N*-acetyl-D-erythro-sphingosine had been turned over by *LmjIPCS*. This was expected as this ceramide analogue has previously been shown to act as a substrate for the yeast enzyme (Nagiec et al., 1997b). Conversely, no IP-D-erythro-sphingosine could be detected in the MS spectra either in positive or negative ion mode, which indicated that D-erythro-sphingosine is not a substrate for *LmjIPCS*, rather it is acting as a true inhibitor (data not shown). Screening this inhibitor against *L. major* and *L. mexicana* promastigotes (insect stage) and *L. mexicana* amastigotes (mammalian stage) demonstrated its efficacy against both species and lifecycle stages (ED_{50} of 6.5, 8.2 and 13.3 μM respectively; Table 1). It should be noted that it is unclear whether this was a target specific effect, however the substrate analogue *N*-acetyl-sphingosine was considerably less cytotoxic such that it was not possible to determine its ED_{50} versus *L. mexicana* amastigotes (Table 1).

In structure-function terms these data indicated that the free-amino group present in D-erythro-sphingosine abolishes enzyme activity, whilst masking this group with even a minimal acyl moiety

(*N*-acetyl-*D*-erythro-sphingosine) restored it. Similarly, sphingosine analogues have demonstrated an inhibitory effect on the *S. cerevisiae* phosphatidate phosphatase (Wu et al., 1993), a member of the LPP enzyme superfamily which are believed to share a mechanism of action with the sphingolipid synthases (Huitema et al., 2004). Taken together it may be hypothesized that the protonated free-amino group of *D*-erythro-sphingosine electrostatically interferes with the active site of these enzymes, an observation which may potentially be exploited in the rational design of specific enzyme inhibitors.

4. Summary

Using the multi-well format assay established in this work we have deduced the kinetic parameters of *Lmj*IPCS with respect to both the donor (PI) and acceptor (NBD- C_6 -ceramide) substrates, and provided evidence that the enzyme functions through a bi-bi (ping-pong) substrate kinetic model. These data provide the first direct indication of the mechanism of action of the sphingolipid synthase family. Such analyses would not have been possible using a conventional assay system such as that previously employed for the *T. cruzi* orthologue (Figueiredo et al., 2005). However, by employing a complemented yeast system, large quantities of active *Lmj*IPCS could be isolated in a cost effective manner avoiding the handling of pathogenic material. Furthermore washing the microsomal starting material with CHAPS removed endogenous, contaminating donor substrate (PI) leaving an environment in which the enzyme exhibited not only a dependency on exogenous PI, but also a higher level of specific activity.

With a Z' value of 0.58 (Zhang et al., 1999), the assay system described lends itself to high-throughput screening for inhibitors of a protozoal enzyme activity that has been demonstrated to be essential for kinetoplastid pathogens (Mina et al., 2009; Sutterwala et al., 2008). The assay of ceramide analogues demonstrated this potential and provides the backbone for consideration of rationally designed enzyme inhibitors. In the longer term, it is hoped that it will assist in the discovery of new, much needed therapies for leishmaniasis and African Sleeping Sickness.

Supplementary data

S1 derivation of Eq. (3): The hypothetical catalytic reaction scheme assuming double displacement kinetics and initial rate conditions.

E_D : *Lmj*IPCS associated with the detergent, CHAPS; PI: phosphatidylinositol; E_D -PI: *Lmj*IPCS-PI complex; DAG: diacylglycerol; E_D -IP: phosphorylated intermediate *Lmj*IPCS with phosphorylinositol group; Cer: ceramide; E_D -IP-Cer: *Lmj*IPCS-IP-ceramide complex; E_D -IPC: *Lmj*IPCS-IPC complex; IPC: inositol phosphorylceramide.

Acknowledgements

This work was funded by Biotechnology and Biological Research Council (BB/D52396X/1) and Royal Society (2005/R1) grants to PWD and a British Council/Deutscher Akademischer Austausch Dienst Academic Research Collaboration Award to PWD and RTS. JGM is funded by an Overseas Research Studentship and a Wolfson Research Institute Award. JAM is an Engineering and Physical Sciences Research Council Academic Fellow. This work was also supported in part by Deutsche Forschungsgemeinschaft, Bonn and a Wolfson Research Institute Small Grants Award. We thank Drs. Ann-Marie O'Donoghue and David Hodgson (Department of Chemistry, Durham University) and Dr. Buddhapriya Chakrabarti

(Department of Mathematical Sciences, Durham University) for helpful discussions.

Appendix A. Supplementary data

Supplementary data associated with this article can be found, in the online version, at doi:10.1016/j.biocel.2010.06.008.

References

- Aeed PA, Sperry AE, Young CL, Nagiec MM, Elhammer AP. Effect of membrane perturbants on the activity and phase distribution of inositol phosphorylceramide synthase, development of a novel assay. *Biochemistry* 2004;43:8483–93.
- Alvar J, Aparicio P, Aseffa A, Den Boer M, Cañavate C, Dedet JP, et al. The relationship between leishmaniasis and AIDS: the second 10 years. *Clin Microbiol Rev* 2008;21:334–59.
- Bates PA. Complete developmental cycle of *Leishmania mexicana* in axenic culture. *Parasitology* 1994;108:1–9.
- Becker GW, Lester RL. Biosynthesis of phosphoinositol-containing sphingolipids from phosphatidylinositol by a membrane preparation from *Saccharomyces cerevisiae*. *J Bacteriol* 1980;142:747–54.
- Bromley PE, Li YO, Murphy SM, Sumner CM, Lynch DV. Complex sphingolipid synthesis in plants: characterization of inositolphosphorylceramide synthase activity in bean microsomes. *Arch Biochem Biophys* 2003;417:219–26.
- Brown DA, London E. Functions of lipid rafts in biological membranes. *Annu Rev Cell Dev Biol* 1998;14:111–36.
- Carman GM, Deems RA, Dennis EA. Lipid signaling enzymes and surface dilution kinetics. *J Biol Chem* 1995;270:18711–4.
- Demms RA, Eaton BR, Dennis EA. Kinetic analysis of phospholipase A-2 activity toward mixed micelles and its implications for the study of lipolytic enzymes. *J Biol Chem* 1975;250:9013–20.
- Denny PW, Shams-Eldin H, Price HP, Smith DF, Schwarz RT. The protozoan inositol phosphorylceramide synthase: a novel drug target which defines a new class of sphingolipid synthase. *J Biol Chem* 2006;281:28200–9.
- Dickson RC. Sphingolipid functions in *Saccharomyces cerevisiae*: comparison to mammals. *Annu Rev Biochem* 1998;67:27–48.
- Engel CP. *Enzyme kinetics: the steady-state approach*. 1st ed. John Wiley & Sons; 1977.
- Figueiredo JM, Dias WB, Mendonca-Previato L, Previanto J, Heise N. Characterization of the inositol phosphorylceramide synthase activity from *Trypanosoma cruzi*. *Biochem J* 2005;387:519–29.
- Fischl AS, Liu Y, Browdy A, Cremesti AE. Inositolphosphorylceramide synthase from yeast. *Methods Enzymol* 2000;311:123–30.
- Futerman AH, Hannun YA. The complex life of simple sphingolipids. *EMBO Reports* 2004;5:777–82.
- Georgopapadakou NH. Antifungals targeted to sphingolipid synthesis: focus on inositol phosphorylceramide synthase. *Expert Opin Investig Drugs* 2000;9:1787–96.
- Heidler SA, Radding JA. The AUR1 gene in *Saccharomyces cerevisiae* encodes dominant resistance to the antifungal agent aureobasidin A (LY295337). *Antimicrob Agents Chemother* 1995;39:2765–9.
- Heidler SA, Radding JA. Inositol phosphoryl transferases from human pathogenic fungi. *Biochim Biophys Acta* 2000;1500:147–52.
- Hill AV. The possible effects of the aggregation of the molecules of haemoglobin on its dissociation curves. *Proc Physiol Soc* 1910;40(Suppl.):4–7.
- Huitema K, van den Dikkenberg J, Brouwers JF, Holthuis JC. Identification of a family of animal sphingomyelin synthases. *EMBO J* 2004;23:33–44.
- International Union of Biochemistry. Units of enzyme activity. *Eur J Biochem* 1979;97:319–20.
- Leber A, Hrastnik C, Daum G. Phospholipid-synthesizing enzymes in Golgi membranes of the yeast, *Saccharomyces cerevisiae*. *FEBS Lett* 1995;377:271–4.
- Lester RL, Dickson RC. Sphingolipids with inositolphosphate-containing head groups. *Adv Lipid Res* 1993;26:253–74.
- Levine TP, Wiggins CA, Munro S. Inositol phosphorylceramide synthase is located in the Golgi apparatus of *Saccharomyces cerevisiae*. *Mol Biol Cell* 2000;11:2267–81.
- Magee T, Prinen N, Alder J, Pagakis SN, Parmryd I. Lipid rafts: cell surface platforms for T-cell signalling. *Biol Res* 2002;35:127–31.
- Mina JG, Pan SY, Wansadhipathi NK, Bruce CR, Shams-Eldin H, Schwarz RT, et al. The *Trypanosoma brucei* sphingolipid synthase, an essential enzyme and drug target. *Mol Biochem Parasitol* 2009;1688:16–23.
- Nagiec MM, Nagiec EE, Baltisberger JA, Wells GB, Lester RL, Dickson RC. Sphingolipid synthesis as a target for antifungal drugs. *J Biol Chem* 1997a;272:9809–17.
- Nagiec MM, Nagiec EE, Baltisberger JA, Wells GB, Lester RL, Dickson RC. Sphingolipid synthesis as a target for antifungal drugs. Complementation of the inositol phosphorylceramide synthase defect in a mutant strain of *Saccharomyces cerevisiae* by the AUR1 gene. *J Biol Chem* 1997b;272:9809–17.
- Pierce SK. Lipid rafts and B-cell activation. *Nature Rev Immunol* 2002;2:96–105.
- Remme JHF, Blas E, Chitsulo L, Desjeux PMP, Engers HD, Kanyok TP, et al. Strategic emphases for tropical diseases research: a TDR perspective. *Trends Parasitol* 2002;18:421–6.
- Rouviniski A, Gahali-Sass I, Stav I, Metzger E, Atlan H, Taraboulos A. Both raft- and non-raft proteins associate with CHAPS-insoluble complexes: some APP in large complexes. *Biochem Biophys Res Commun* 2003;308:750–8.

- Schürholz T. Critical dependence of the solubilization of lipid vesicles by the detergent CHAPS on the lipid composition. Functional reconstitution of the nicotinic acetylcholine receptor into preformed vesicles above the critical micellization concentration. *Biophys Chem* 1996;58:87–96.
- Smith WL, Merrill AH. Sphingolipid metabolism and signaling. *J Biol Chem* 2002;277:25841–2.
- Sperling P, Heinz E. Plant sphingolipids: structural diversity, biosynthesis, first genes and functions. *Biochim Biophys Acta* 2003;1632:1–15.
- Sutterwala SS, Hsu FF, Sevova ES, Schwartz KJ, Zhang K, Key P, et al. Developmentally regulated sphingolipid synthesis in African trypanosomes. *Mol Microbiol* 2008;70:281–96.
- Suzuki E, Tanaka AK, Toledo MS, Levery SB, Straus AH, Takahashi HK. Trypanosomatid and fungal glycolipids and sphingolipids as infectivity factors and potential targets for development of new therapeutic strategies. *Biochim Biophys Acta* 2008;1780:362–9.
- Tanaka AK, Valero VB, Takahashi HK, Straus AH. Inhibition of *Leishmania* (*Leishmania*) *amazonensis* growth and infectivity by aureobasidin A. *J Antimicrob Chemother* 2007;59:487–92.
- Wu WI, Lin YP, Wang E, Merrill Jr AH, Carman GM. Regulation of phosphatidate phosphatase activity from the yeast *Saccharomyces cerevisiae* by sphingoid bases. *J Biol Chem* 1993;268:13830–7.
- Zhang J-H, Chung TDY, Oldenburg KR. A simple statistical parameter for use in evaluation and validation of high throughput screening assays. *J Biomol Screen* 1999;4:67–73.
- Zhang K, Hsu F-F, Scott DA, Docampo R, Turk J, Beverley SM. *Leishmania* salvage and remodelling of host sphingolipids in amastigote survival and acidocalcisome biogenesis. *Mol Microbiol* 2005;55:1566–78.
- Zhang O, Wilson MC, Xu W, Hsu FF, Turk J, Kuhlmann FM, et al. Degradation of host sphingomyelin is essential for *Leishmania* virulence. *PLoS Pathog* 2009;5:e1000692.



The *Trypanosoma brucei* sphingolipid synthase, an essential enzyme and drug target[☆]

John G. Mina^{a,b,1}, Ssu-Ying Pan^{a,1}, Nilu K. Wansadhipathi^{a,b}, Catherine R. Bruce^{a,b}, Hosam Shams-Eldin^c, Ralph T. Schwarz^{c,d}, Patrick G. Steel^a, Paul W. Denny^{a,b,*}

^a Centre for Bioactive Chemistry, Department of Chemistry and School of Biological and Biomedical Sciences, Durham University, Durham DH1 3LE, UK

^b School of Medicine and Health, Durham University, Queen's Campus, Stockton-on-Tees, TS17 6BH, UK

^c Institut für Virologie, Zentrum für Hygiene und Infektionsbiologie, Philipps-Universität Marburg, Hans-Meerwein-Strasse, 35043 Marburg, Germany

^d Unité de Glycobiologie Structurale et Fonctionnelle, UMR CNRS/USTL n° 8576 - IFR 118, Université des Sciences et Technologies de Lille, 59655 Villeneuve D'Ascq cedex, France

ARTICLE INFO

Article history:

Received 26 August 2008

Received in revised form 10 June 2009

Accepted 11 June 2009

Available online 21 June 2009

Keywords:

Trypanosoma

Trypanosomiasis

Sphingolipid synthase

Drug target

ABSTRACT

Sphingolipids are important components of eukaryotic membranes, particularly the plasma membrane, and are involved in a diverse array of signal transduction processes. In the Eukaryota the biosynthetic pathway for the formation of these lipid species is largely conserved. However, in contrast to mammals which produce sphingomyelin (SM), several pathogenic fungi and protozoa synthesize inositol phosphorylceramide (IPC) as the primary phosphosphingolipid. This process is catalyzed by the enzyme IPC synthase, a recognized target for anti-fungals encoded by the *AUR1* gene in yeast. Recently, functional orthologues of the *AUR1p* have been identified in a group of insect vector-borne pathogenic protozoa, the Kinetoplastida, which are responsible for a range of so-called neglected diseases. Of these the *Trypanosoma brucei* species are the causative agents of human African trypanosomiasis in many of the most under-developed regions of Africa. The available treatments for these diseases are limited, of decreasing efficacy, and often demonstrate severe side-effects. Against this background the *T. brucei* sphingolipid synthase, an orthologue of the yeast *AUR1p*, may represent a promising target for novel anti-protozoals. Our studies identify an isoform of this protein as a novel bi-functional enzyme capable of catalyzing the synthesis of both IPC and SM, both known to be present in the parasite. Furthermore, the synthase is essential for parasite growth and can be inhibited by a known anti-fungal at low nanomolar levels *in vitro*. Most notably this drug demonstrates trypanocidal activity against cultured bloodstream form parasites. Thus, the *T. brucei* sphingolipid synthase represents a valid and promising drug target.

© 2009 Elsevier B.V. All rights reserved.

1. Introduction

Trypanosoma brucei species are protozoan parasites of the order Kinetoplastida and the etiological agents of both human African trypanosomiasis (HAT, sleeping sickness), and diseases of economically important animals (e.g. nagana in cattle) [1]. These diseases are endemic in much of sub-Saharan Africa, with HAT causing a burden of approximately 1.6 million disability adjusted life years

(<http://www.who.int/tdr/>). This distribution across some of the most under-developed regions of the world is coupled with a paucity of effective therapies, with those available being either too expensive (e.g. eflornithine) or exhibiting catastrophic side-effects (e.g. melarsoprol). Together with the leishmaniases (caused by the related *Leishmania* species) HAT has been described as an emerging or uncontrolled disease. Therefore, there is an urgent need for new, validated drug targets and anti-HAT compounds to combat a disease causing in excess of 50,000 deaths per annum [2].

Sphingolipids are a diverse group of amphipathic lipids that perform essential functions in eukaryotes. For example, the unmodified sphingolipid ceramide acts as a secondary signalling molecule [3] and more complex species are implicated in the formation and function of signal transduction complexes [4,5]. The primary phosphosphingolipid species in mammalian species, including humans, is sphingomyelin (SM). SM is formed by the transfer of the phosphorylcholine head group from phospholipid phosphatidylcholine (PC) to ceramide, a reaction catalyzed by SM synthase [6]. In contrast

[☆] Since the initial submission of this work to Molecular and Biochemical Parasitology a paper has been published in Molecular Microbiology identifying and characterising the same family of enzymes in *Trypanosoma brucei*: Sutterwala S.S., Hsu F.F., Sevova E.S., Schwartz K.J., Zhang K., Key P., Turk J., Beverley S.M., Bangs J.D. Developmentally regulated sphingolipid synthesis in African trypanosomes (2008) 70:281–296.

* Corresponding author at: Centre for Bioactive Chemistry, Department of Chemistry, Durham University, Durham, DH1 3LE, UK. Tel.: +44 0 191 334 3983.

E-mail address: p.w.denny@durham.ac.uk (P.W. Denny).

¹ These authors contributed equally to this work.

fungi, plants and at least some protozoa produce inositol phosphorylceramide (IPC) as their primary phosphosphingolipid [7]. In these organisms IPC synthase catalyzes the transfer of phosphorylinositol from phosphatidylinositol (PI) to ceramide [8–10]. IPC synthase has long been established and studied as a target for novel anti-fungals [11,12]. More recently this enzyme has come under scrutiny as a potential target for anti-protozoals [13]. With the recent identification and characterization of the *Leishmania* IPC synthase (LmIPCS; [10]) it has become possible both to validate this protozoan activity as a drug target and, furthermore, begin to investigate potential inhibitors, including those known to act against the fungal IPC synthase. Four closely related orthologues of LmIPCS are apparent in the *T. brucei* database [10], and mass spectrometry of isolated fractions has revealed that whilst the predominant phosphosphingolipid in pathogenic bloodstream form parasites is SM [14]; insect stage, procyclic *T. brucei* also contain IPC [15].

Here we describe the characterization of the African trypanosome, *T. brucei*, sphingolipid synthase 4 (TbSLS4) which demonstrates itself to be a novel bi-functional enzyme with the ability to catalyze the biosynthesis of both IPC and SM, thus reflecting the sphingolipid profile of the parasite. Importantly, the IPC synthase activity of TbSLS4 is acutely sensitive to the well characterized specific fungal inhibitor aureobasidin A [11,12] and pathogenic bloodstream form *T. brucei* are rapidly killed at sub-micromolar concentrations of this drug. Furthermore, down-regulation of TbSLS1–4 using inhibition RNA (RNAi) in bloodstream form parasites demonstrated that the enzyme activity is essential for growth thus validating it as a target for the development of new anti-HAT therapies.

2. Materials and methods

2.1. Functional identification of the *T. brucei* sphingolipid synthase

A common, conserved AUG start codon was predicted for all four TbSLS isoforms by examination of the genome sequence (www.genedb.org). Subsequently, TbSLS1 (Tb09211.1030) and TbSLS4 (Tb09211.1000) were amplified with *Pfu* polymerase (Promega) from *T. brucei* strain Lister 427 genomic DNA using primer pairs (homologous sequence underlined): TbSLS1–CCG-GAATTCATGATTAGTTACCCTTCTCTCTCCC and CCGCTCGAGTCATAC-CTCGTTAGTTGATAC; TbSLS4–CCGGAATTCATGATTAGTTACCCTTCTCTCTCCC and CCGCTCGAGTCACACATACGCCACATTTAAAC;

The PCR products were subsequently cloned into the yeast expression vector pRS426 MET [16] to give pRS426 TbSLS1 and pRS426 TbSLS4. These, together with pRS426 AUR1, pRS426 human sphingomyelin synthase 1 and 2 (HsSMS1 and 2) and empty vector (pRS426), were used to transform the YPH499-HIS-GAL-AUR1 *Saccharomyces cerevisiae* strain [10]. Transformants were selected on non-permissive SD medium (0.17% Bacto yeast nitrogen base, 0.5% ammonium sulphate and 2% dextrose) or permissive SGR medium (0.17% Bacto yeast nitrogen base, 0.5% ammonium sulphate, 4% galactose and 2% raffinose) containing the appropriate nutritional supplements at 30 °C.

2.2. Metabolic labelling and analyses

Yeast were grown to exponential phase in SD or SGR as indicated and 2.5 OD₆₀₀ units incubated in 1 ml of SD or SGR supplemented with 5 μM of NBD C₆-ceramide (Invitrogen) conjugated to fat-depleted bovine serum albumin (Sigma–Aldrich) for 120 min at 30 °C. Yeast were harvested by centrifugation and washed twice with phosphate buffered saline. Chloroform/methanol (0.4 ml; 1:1, v/v) was added and cells were disintegrated with glass beads. The pellet was re-extracted with chloroform/methanol/water (10:10:3) and the lipid fraction isolated by phase separation. After drying in a rotavapor (Eppendorf Concentrator 5301) reaction products

were re-suspended in 20 μl of 10:10:3 and cell mass equivalents fractionated using HPTLC silica plates (Merck) and the eluent system chloroform:methanol:aqueous 0.25% KCl (55:45:10). Imaging and quantification was carried out using a FLA3000 scanner (Fuji-film) and AIDA Image Analyzer[®] software (version 1.3). Vero cells were labelled and processed for use as controls and standards as previously described [10].

Sphingomyelinase (*Bacillus cereus*, Sigma–Aldrich) was used to identify sphingomyelin in the NBD C₆-ceramide lipids extracted from the complemented yeast as previously described [17]. Briefly, YPH499-HIS-GAL-AUR1 *S. cerevisiae* complemented with pRS426 TbSLS4 (in SD) or transformed with pRS426 HsSMS2 or empty vector (in permissive SGR, or for a limited period SD) were grown to exponential phase. After adjustment to an optical density of 0.5 OD₆₀₀ in 5 ml of either SD or SGR, cells were labelled for 16 h with 2 μM of NBD C₆-ceramide conjugated to fat-depleted bovine serum albumin as previously described [6]. Labelled lipid fractions from these were prepared and dried as above with 50 μg of sphingomyelin (Sigma–Aldrich), and re-suspended, with sonication in a water bath, in 600 μl of 20 mM Tris–HCl (pH 7.4), 10 mM MgCl₂ and 0.05% (w/v) Triton X-100. Subsequently, samples (300 μl) were incubated with or without 2 units of *B. cereus* sphingomyelinase (Sigma–Aldrich) at 37 °C for 120 min. Equivalent lipid extracts were fractionated and analyzed as above.

2.3. In vitro assay of TbSLS4 activity

Microsomal membranes from exponentially growing YPH499-HIS-GAL-AUR1 pRS426 TbSLS4, pRS426 LmIPCS or pRS426 AUR1 [10] were prepared as previously described [18] and the isolated membrane fraction re-suspended in storage buffer (50 mM Tris–HCl pH 7.4, 20% (v/v) glycerol, 5 mM MgCl₂) with Complete[®] EDTA-free Protease Inhibitor Cocktail (Roche Applied Science) at a protein concentration of 10 mg/ml. The microsomal membranes were subsequently washed in 2.5% CHAPS (w/v; Sigma–Aldrich; 4 °C, 60 min), isolated by centrifugation (150,000 × g, 4 °C and 90 min), re-suspended in storage buffer at 10 mg/ml and stored at –80 °C until use.

The assay mix contained 100 μM donor substrate (bovine liver PI, PC or PE, Avanti Polar Lipids), 10 μg of microsomes, 100 mM Tris–HCl, 10 mM EDTA, 6 mg/ml BSA and 5 μM NBD C₆-ceramide [19]. Following incubation at 30 °C for 60 min the reaction was quenched by the addition of 150 μl of chloroform:methanol:water (10:10:3). After biphasic separation the organic layer was removed, processed and analyzed as above.

For inhibition experiments the reaction mix was pre-incubated for 30 min with appropriate quantities of aureobasidin A (Takara) before the addition of NBD C₆-ceramide.

2.4. Parasite culture

Bloodstream form *T. brucei* strains Lister 427 and its engineered variant, Single Marker Bloodstream form (SMB, T7RNAP::TETR::NEO; [20]) were maintained *in vitro* at 37 °C with 5% CO₂ in HMI-9 medium supplemented with 10% FCS and, for SMB, 2.5 μg/ml G418.

2.5. Inhibition RNA (RNAi) of TbSLS

An 165 base pair sequence fragment common to all four TbSLS open reading frames was amplified from genomic DNA using *Pfu* polymerase and primer pair (homologous sequence underlined): CATAGATCTAGAGGTTCCATACACTGTG and CATAGATCTAGACGAGAGGCAACGATGC.

This PCR product was cloned into the RNAi vector p2T7 [21] and, following linearization, 10 μg transfected into SMB *T. brucei* and

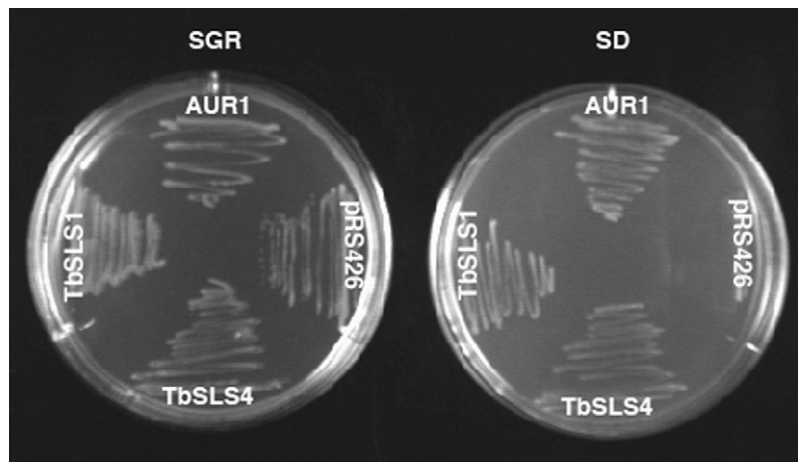


Fig. 1. Transformation with pRS426 TbSLS4 and pRS426 TbSLS1, as well as pRS426 AUR1 (the *S. cerevisiae* IPC synthase), rescues the auxotrophic mutant YPH499-HIS-GAL-AUR1 allowing it to grow in the presence of glucose (SD media). YPH499-HIS-GAL-AUR1 pRS426 (empty vector) does not grow in the presence of glucose (SD), however all lines are viable in the absence of glucose and the presence of galactose (SGR).

transformants selected using 2 μ g/ml phleomycin (Sigma–Aldrich). Following induction with 1 μ g/ml doxycycline cell growth was determined at 24 h intervals by light microscopy using an Improved Neubauer Haemocytometer.

48 h post-induction total RNA was isolated (RNeasy[®], Qiagen) and RT-PCR was performed (SuperScript II, Invitrogen) using the primer pairs:

TbSLS: AACTGTACCTTCTCACCG and CGAGAGGCAACGATGC;
Tb β tubulin: GGAGCGCATCAATGTGTAC and CAGGCAGCAGGT-GACGCCG.

2.6. *T. brucei* susceptibility to aureobasidin A

T. brucei Lister 427 were cultured in the presence of various concentrations of aureobasidin A. Growth was analyzed at 24 h intervals as above.

3. Results and discussion

3.1. Identification and characterization of the *T. brucei* sphingolipid synthase

Four tandem gene sequences (Tb09211.1030, Tb09.211.1020, Tb09.211.1010 and Tb09.211.1000; here annotated TbSLS1–4 to reflect their 5'–3' order) were previously identified in the *T. brucei* genome database (www.genedb.org) as sequence orthologues of the inositol phosphorylceramide synthase (LmIPCS) from the related kinetoplastid parasite, *Leishmania* [10]. The predicted open reading frames encode four closely related trans-membrane proteins with more than 90% identity and 94% similarity. Most variation occurs at the carboxy-termini, a region predicted to lie on the cytosolic side of the membrane away from the active site at the Golgi lumen, with another variable domain close to and within the second predicted trans-membrane domain [10]. One of the predicted *T. brucei* sphingolipid synthase isoforms (Tb09.211.1000; TbSLS4) was the focus of this study. In addition, the isoform most distant from TbSLS4 with respect to the internal variable domain (Tb09.211.1030; TbSLS1) was also subjected to preliminary analyses.

The auxotrophic mutant *S. cerevisiae* strain, YPH499-HIS-GAL-AUR1, has the essential AUR1 IPC synthase gene under the control of a galactose inducible promoter. Therefore it is unable to grow in the presence of the repressor glucose, a phenotype that is res-

cued by the ectopic expression of LmIPCS [10]. Similarly, TbSLS4 and TbSLS1 expression complemented the YPH499-HIS-GAL-AUR1 mutant yeast line indicating that they are also functional orthologues of the yeast AUR1 gene (Fig. 1). The yeast IPC synthase (AUR1) also complemented this mutant line. Significantly, neither HsSMS1 nor HsSMS2 complemented the YPH499-HIS-GAL-AUR1 yeast (data not shown) indicating that sphingomyelin synthase activity alone is not sufficient to rescue the mutant.

To understand the function of the *T. brucei* sphingolipid synthase, the auxotrophic YPH499-HIS-GAL-AUR1 yeast cells complemented with either TbSLS4, TbSLS1 or yeast AUR1 were metabolically labelled with fluorescent NBD C₆-ceramide, a substrate for sphingolipid synthases, including those from the kinetoplastids [10]. Under the conditions described, the AUR1 complemented *S. cerevisiae* auxotrophic mutant synthesized IPC as the only labelled product. In contrast, both TbSLS4 and TbSLS1 complemented mutant yeast were shown to synthesize two major labelled lipid species. One of these co-migrated with SM, the other with IPC. The latter at levels equivalent to those produced in the AUR1 complemented yeast (Fig. 2A). In addition, TbSLS4 complemented yeast synthesized a third species which co-migrated with an unknown lipid (X) produced by labelled mammalian cells (Vero). As a control YPH499-HIS-GAL-AUR1 cells harbouring an empty vector (pRS426) were cultured in both permissive (SGR) and non-permissive (SD) media. Both lines grew equivalently in both media for 16 h and for a further 8 h after dilution to an optical density 0.3 OD₆₀₀, and remained viable (by plating on permissive media, data not shown). Labelling of these dividing cells with NBD C₆-ceramide in their respective media under the same conditions as above demonstrated that in non-permissive SD no labelled IPC is produced, indicating the down-regulation of AUR1p (Fig. 2B).

TbSLS4 was chosen for further study due to the relative predominance of the SM-like species in the labelled complemented yeast. Unlike IPC, SM is known to be present in the pathogenic bloodstream form of the parasite [14]. The labelled SM-like species (and the unknown X) proved to be susceptible to sphingomyelinase (which breaks down SM into phosphorylcholine and ceramide) when lipid extracts were treated with this enzyme, thereby confirming its identity (Fig. 3A). In contrast the IPC produced was insensitive to this enzyme treatment. Extracts from the auxotrophic mutant expressing HsSMS2, which produce an equivalent quantity of labelled SM under permissive conditions (SGR), acted as a control for SMase activity.

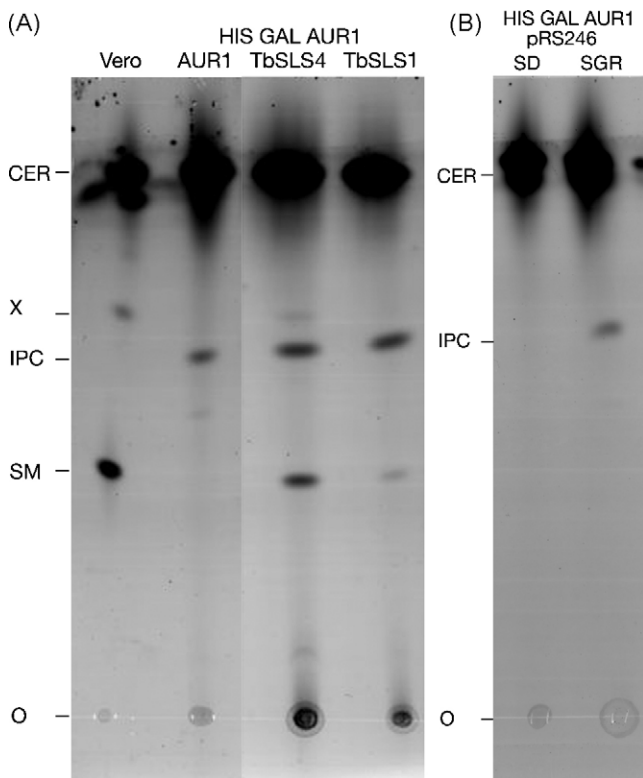


Fig. 2. (A) Metabolic labelling of yeast IPC synthase (AUR1) complemented YPH499-HIS-GAL-AUR1 with NBD C₆-ceramide in glucose-containing media (SD) showed that they synthesize only labelled IPC. In contrast the same mutant line, labelled under the same conditions, but complemented with TbSLS4 or TbSLS1 synthesized two predominant sphingolipid species, one of which co-migrated with IPC, the other with SM. In addition, in TbSLS4 complemented yeast a minor labelled species (X) was evident which co-migrated with an unknown detected in labelled mammalian cell (Vero) extracts, in which the predominant complex sphingolipid is SM. (B) The yeast IPC synthase (AUR1) is down-regulated in YPH499-HIS-GAL-AUR1 cells transformed with empty vector (pRS426) when incubated in non-permissive, glucose-containing media (SD). This is demonstrated by the lack of detectable IPC in yeast metabolically labelled with NBD C₆-ceramide in SD under the same conditions as above. In galactose-containing, glucose-free media (SGR) the synthesis of IPC is clearly evident. NBD C₆-ceramide labelled lipid extracts fractionated by HPTLC, representative of at least three independent experiments. O, origin; IPC, inositol phosphorylceramide; SM, sphingomyelin; Cer, ceramide (migrating at the front); X, unknown sphingolipid. All lipid extracts normalised with respect to cell mass.

Together these data suggest that TbSLS4 is a novel bi-functional enzyme acting as both a SM and an IPC synthase. This is consistent with previous analyses which demonstrated that the parasite harbours both SM [14] and IPC phosphosphingolipids [15].

3.2. *In vitro* analyses of TbSLS4 activity

To further investigate the function of TbSLS4, microsomal material was isolated from the TbSLS4 and AUR1 complemented yeast as described and used in an *in vitro* assay utilising the common acceptor substrate NBD C₆-ceramide and the candidate donor substrates bovine liver PI, PC and phosphatidylethanolamine (PE; a potential substrate for ethanolamine phosphorylceramide synthesis [22]). Notably, when assayed, the yeast AUR1 crude microsomal material showed significant IPC synthase turnover, but demonstrated little significant increase in this on the addition of the donor substrate PI. As expected, no detectable SM synthesis was observed with or without the addition of PC (Fig. 4A). In order to clearly assign enzyme function this assay was refined according to data obtained from the analysis of LmIPCS (Mina et al. in preparation). In brief, microsomal fractions were washed with ice-

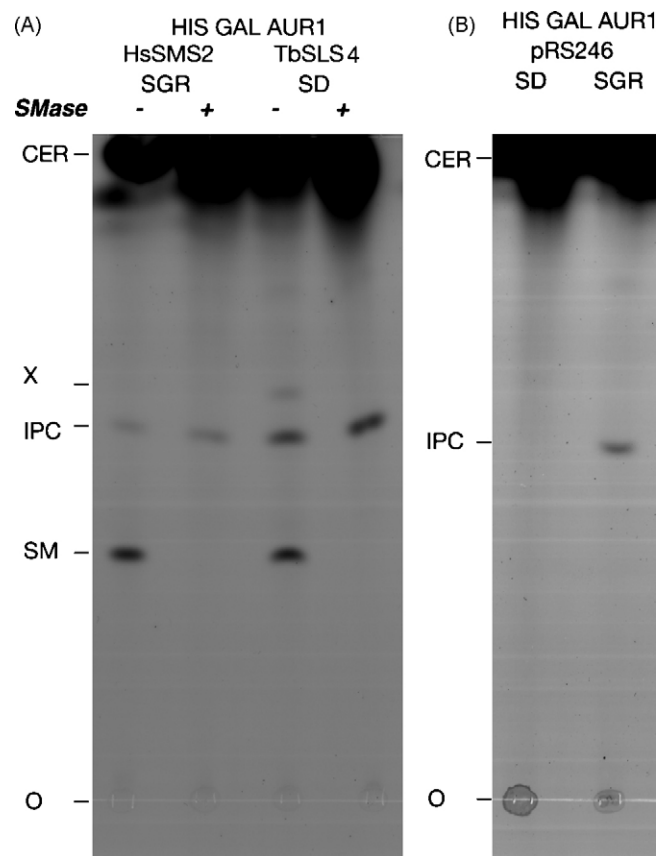


Fig. 3. (A) Sphingomyelinase (SMase) treatment of lipids extracted from YPH499-HIS-GAL-AUR1 complemented with TbSLS4, grown in glucose-containing media (SD) and labelled with NBD C₆-ceramide, demonstrated that the predicted sphingomyelin species is SMase sensitive, as is unknown X. In contrast the predicted IPC is insensitive. As a control, YPH499-HIS-GAL-AUR1 expressing human SM synthase 2 (HsSMS2, grown in permissive SGR media) was utilized as they produce equivalent quantities of labelled SM to the TbSLS4 line. (B) The yeast IPC synthase (AUR1) is down-regulated in YPH499-HIS-GAL-AUR1 cells transformed with empty vector (pRS426) incubated in non-permissive SD under the same conditions as the SMase treated samples. This is demonstrated by the lack of detectable IPC in yeast metabolically labelled with NBD C₆-ceramide in SD. In galactose-containing, glucose-free media (SGR) the synthesis of IPC is clearly evident. NBD C₆-ceramide labelled lipid extracts fractionated by HPTLC, representative of at least three independent experiments. O, origin; IPC, inositol phosphorylceramide; SM, sphingomyelin; Cer, ceramide (migrating at the front); X, unknown sphingolipid. All lipid extracts normalised with respect to cell mass.

cold 2.5% 3-[3-(cholamidopropyl) dimethylammonio]-1-propane sulfonate (CHAPS) to remove endogenous (i.e. yeast) substrates. This facilitated analyses of the effect of adding exogenous substrate to the reaction—in this case the candidate donor substrates (PI, PC or PE) plus the known acceptor substrate NBD C₆-ceramide. Without the addition of the donor substrate the CHAPS-washed AUR1 microsomes, compared to the crude unwashed sample, demonstrated a relatively low level of IPC synthase turnover and, as expected no evidence of SM synthase function (Fig. 4A, crude and washed). Importantly, the addition of PI or PC had no discernable effect on enzyme turnover in the washed sample indicating that the yeast IPC synthase is either substrate specific (and unable to utilize bovine PI) or that the detergent treatment had disrupted the protein (Fig. 4A, +PI and +PC washed). In contrast, assay of identically treated TbSLS4 microsomes showed that the addition of PI led to a large (more than 12-fold) increase in the formation of IPC (Fig. 4B, +PI). This demonstrated that TbSLS4 functions as an IPC synthase, an activity not attributable to background AUR1 expression.

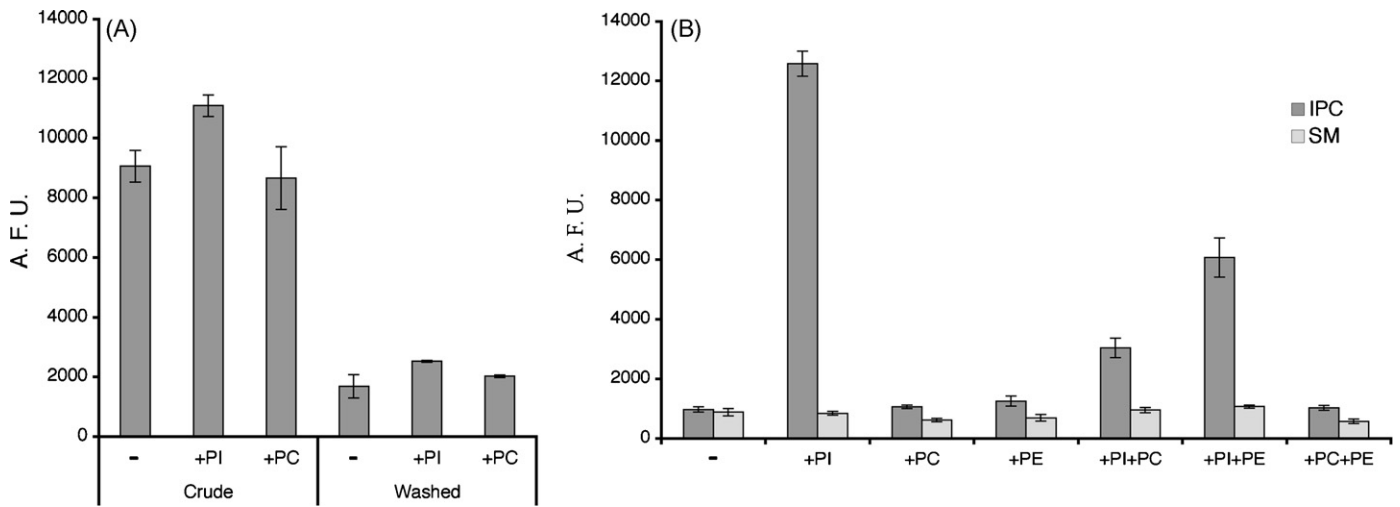


Fig. 4. Detergent-washed microsomes extracts from YPH499-HIS-GAL-AUR1 TbSLS4 yeast demonstrate IPC synthase enzyme turnover on the addition of the donor substrate PI and acceptor substrate NBD C₆-ceramide, but no further production of other sphingolipid species on the addition of alternative donors PC and PE. (A) The addition of bovine liver PI led to a marginal increase in IPC production in unwashed (crude) AUR1 microsomes when compared to the control (–). In CHAPS-treated microsomes (washed) IPC synthase (AUR1) turnover was minimal without donor substrate (–) and unchanged by the addition of either PI or PC as donors. This demonstrated that the yeast IPC synthase (AUR1) was unable to utilize these donor substrates under the experimental conditions. (B) In contrast, assay of TbSLS4 microsomes (CHAPS-treated, as the washed sample in A) demonstrated a greater than 12-fold increase in IPC over a sample without donor substrate (–) on the addition of PI. PC and PE had no demonstrable effect on enzyme turnover. However, both inhibited IPC synthesis when added together with PI at equivalent molar quantities: PC by approximately 4-fold and PE by approximately 2-fold. NBD C₆-ceramide labelled lipid extracts fractionated by HPTLC and quantified as described, standard deviation of three independent experiments shown. AFU, arbitrary fluorescence units; IPC, inositol phosphorylceramide; SM, sphingomyelin; –, no donor substrate added; PI, bovine liver phosphatidylinositol; PC, bovine liver phosphatidylcholine; PE, bovine liver phosphatidylethanolamine.

Surprisingly, given the identification of SM as a TbSLS4 product above (Fig. 3A), bovine PC – a potential donor substrate for a SM synthase – had no significant effect on enzyme activity (Fig. 4B, +PC). The addition of PE was similarly ineffectual (Fig. 4B, +PE). However, when PC or PE were added simultaneously as molar equivalents with PI to the assay system, the quantity of IPC produced decreased 4- and 2-fold respectively. This suggested that both PC and PE bind competitively with PI to the same region of the enzyme (Fig. 4B, +PI+PC and +PI+PE).

Taken together these results indicate that TbSLS4 functions as an IPC synthase but also binds PC (and PE) and can participate in the synthesis of SM. The lack of *in vitro* SM synthase activity in the presence of exogenous PC is surprising and may relate to substrate specificity (see yeast AUR1 and bovine PI, Fig. 4A, washed). One possibility is that TbSLS4, in this assay, is unable to utilize bovine liver PC. This donor substrate is a mixed natural product with predominantly C36:2 PC. In contrast, *S. cerevisiae*, where both TbSLS4 and TbSLS1 function as SM synthases, predominantly possesses C32:2 and C34:2 PC [23]. Perhaps TbSLS favours these relatively short acyl groups? However, *T. brucei* procyclic and bloodstream forms harbour significant quantities of C36, C38 and C40 PC species [14,24,25], indicating that any substrate selectivity is perhaps due more subtle structural differences. In support of this, although TbSLS4 can utilize bovine liver PI (predominantly C38:4) efficiently as a substrate for IPC synthesis, procyclic form parasites (known to synthesize IPC [15]) harbour only trace levels of the C38:4 PI [14].

3.3. Inhibition of TbSLS4 using a known anti-fungal agent

IPC synthase is a recognized target for anti-fungal drugs and the natural product aureobasidin A is a widely utilized and specific experimental inhibitor [26]. This drug also specifically inhibits the activity of *Leishmania* LmIPCS, a TbSLS orthologue, albeit at a concentration several orders of magnitude higher than those for the *S. cerevisiae* enzyme [10].

To establish the efficacy of aureobasidin A against the *T. brucei* enzyme the previously described *in vitro* assay was employed using CHAPS-washed TbSLS4 microsomes with NBD C₆-ceramide and bovine PI as receptor and donor substrates respectively. As a control identically prepared LmIPCS microsomes were assayed in the same manner. Given the inactivity of the yeast enzyme in this assay system it was not possible to include this as a further control. The synthesis of labelled IPC was used as a measure of IPC synthase turnover. From this assay it was evident that the *T. brucei* enzyme is acutely sensitive to the drug (Fig. 5A). Following reanalysis of the linear portion of the curve (0–0.5 nM aureobasidin A), the turnover was calculated to be 50% inhibited (IC₅₀) by 0.42 nM aureobasidin A. TbSLS4 turnover was undetectable at a concentration of 50 nM aureobasidin A. In contrast, the IC₅₀ for LmIPCS inhibition by aureobasidin A was more than 200,000 times higher, with precipitation of the drug at concentrations above 100 μM (Fig. 5B) preventing the determination of an absolute value.

3.4. Validation of TbSLS as a target of anti-protozoals

Using a sequence fragment common to all four TbSLS isoforms an RNAi construct was prepared in the p2T7 vector [21] and used to specifically inhibit TbSLS expression in cultured bloodstream form *T. brucei* (SMB). Non-induced TbSLS RNAi cells grew in a similar manner to control SMB parasites carrying empty vector with or without the doxycycline. In contrast, doxycycline induction of TbSLS RNAi saw the parasites cease division and led to some cell death as scored by light microscopy. RT-PCR, using β tubulin as a control, confirmed the specificity of the TbSLS mRNA inhibition (Fig. 6).

This genetic approach validated TbSLS as an essential enzyme for pathogenic bloodstream form parasite growth. Given the *in vitro* data shown above in which aureobasidin A was demonstrated to inhibit TbSLS4, the efficacy of this natural compound was tested against cultured bloodstream form *T. brucei* (Lister 427; Fig. 7). When the concentration of aureobasidin A was 1 μM cell growth

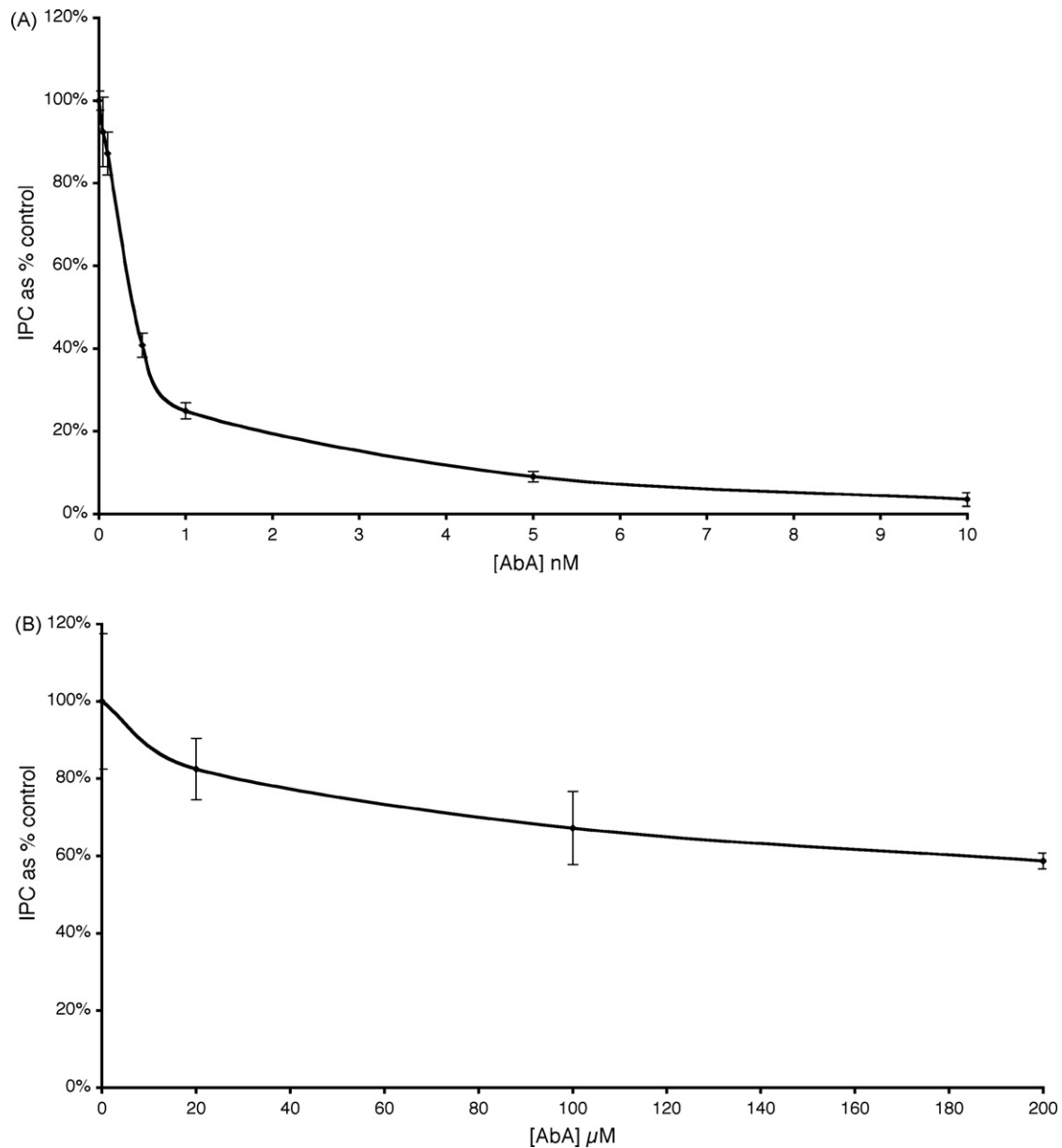


Fig. 5. The fungal IPC synthase inhibitor aureobasidin A is active against TbSLS activity. (A) TbSLS4 IPC synthase turnover determined using the described *in vitro* assay in the presence of aureobasidin A (AbA). The IC_{50} was calculated from the linear portion of the curve as being 0.42 nM. (B) *L. major* IPC synthase turnover was confirmed to be relatively refractory to AbA [10]. The IC_{50} was in excess of 100 μ M, more than 200,000 times greater than that for TbSLS4. Turnover, as determined by IPC production, was scored as 100% in the absence of the inhibitor.

was completely inhibited and the parasites were scored as dead by light microscopy after 24 h. The EC_{50} of aureobasidin A against the parasites was estimated from these data as being below 250 nM. However, it is the trypanocidal activity of this compound at higher concentrations that is of most significance.

3.5. Summary

Previous studies using pharmacological and genetic inhibition of the first step in sphingolipid biosynthesis, catalyzed by serine palmitoyltransferase, showed that this pathway is essential for the viability of both bloodstream and procyclic forms of *T. brucei* [17,27]. This is in contrast to the related protozoan parasite *Leishmania major* where this enzyme, though essential for sphingolipid biosynthesis, is non-essential for both viability and pathogenesis [28,29]. These studies indicate that sphingolipid biosynthesis could be a viable drug target in the African trypanosomes.

The sphingolipid biosynthetic pathway is largely conserved across the Eukaryota. However, whilst animal cells synthesize the phosphosphingolipid SM, yeast and plants, plus at least some protozoa, produce IPC [7]. The IPC synthase of pathogenic fungi has long been validated and studied as a drug target [11], and the recent identification of a functional orthologue in the protozoan Kinetoplastids, the causative agents of several so-called neglected diseases, has led to its consideration as a target for anti-protozoal agents [10]. In this study we confirm that two of the four closely related *T. brucei* orthologues (TbSLS4 and 1) of the *Leishmania* IPC synthase (LmIPCS) are also functional orthologues of the *S. cerevisiae* enzyme encoded by *AUR1*. However surprisingly, unlike the *Leishmania* enzyme (and *AUR1*) TbSLS4 and 1 are able to catalyze the synthesis of both IPC and SM, which reflects the known sphingolipid content of *T. brucei* cells [15]. In an *in vitro* assay system utilizing TbSLS4 complemented *AUR1* mutant yeast microsomes, it was demonstrated that the *T. brucei* enzyme was able to function as an IPC synthase. Although PC

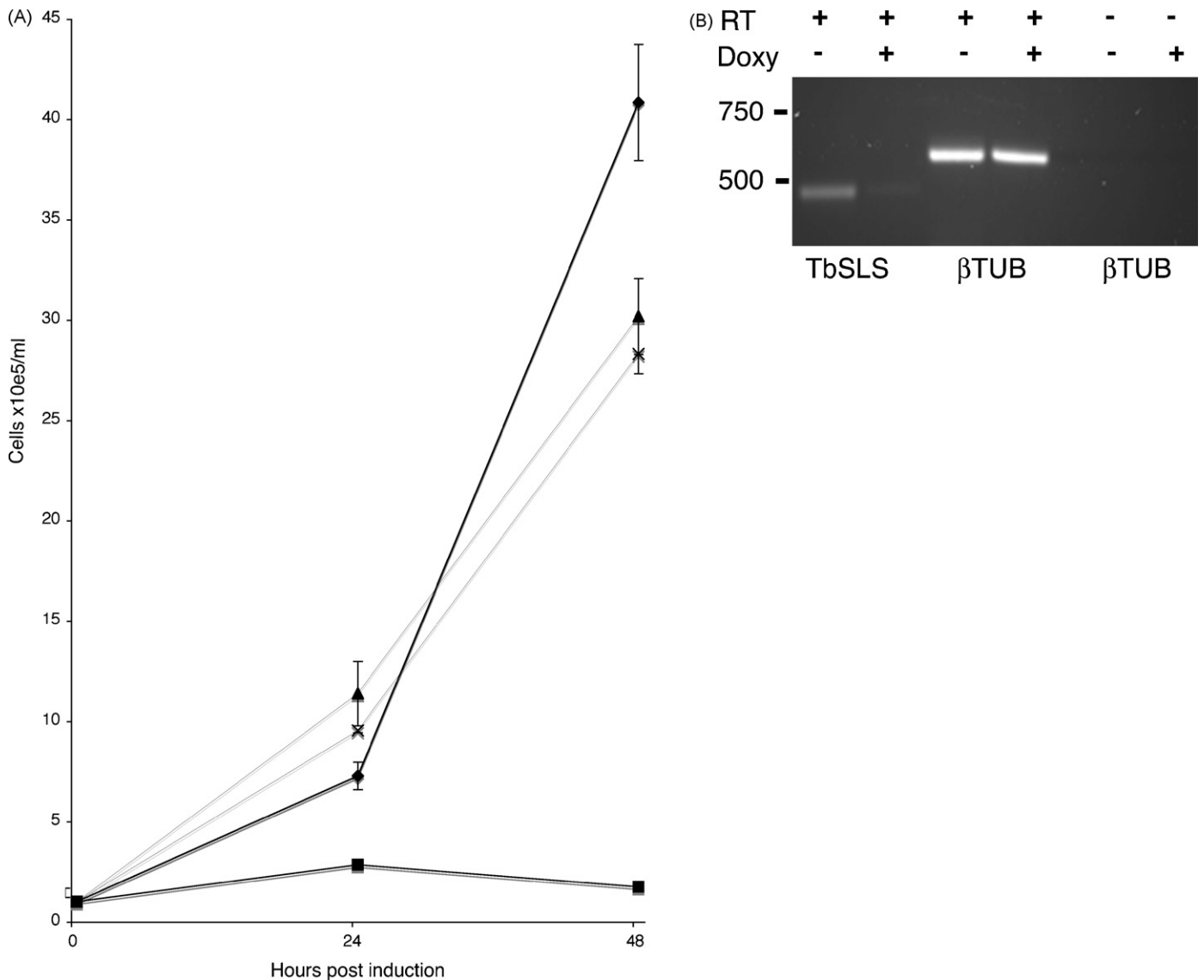


Fig. 6. TbSLS is an essential enzyme in bloodstream form *T. brucei*. (A) Inhibition RNA of TbSLS. Cell counts over a 48 h period: (▲) mock transfected cells non-induced; (×) mock transfected cells induced by 1 μ g/ml doxycycline; (◆) TbSLS RNAi cells non-induced; (■) TbSLS RNAi cells induced by 1 μ g/ml doxycycline. Error bars for standard deviation over three replicates are shown. (B) RT-PCR using total RNA isolated from TbSLS RNAi parasites with or without doxycycline induction (Doxy). RT, reverse transcriptase. β TUB, β tubulin control.

(and PE) was demonstrated to be a competitive binder with respect to PI, SM synthase activity could not be constituted possibly due to some level of specificity with respect to the donor substrate PC. Clearly, substrate specificity and the mechanism of action of TbSLS4 warrant further investigation to disentangle the detected IPC synthase function from the apparent SM synthase activity. Determination of the kinetic parameters of TbSLS4 would facilitate this, for example with respect to determining the binding constants for the apparent competitive IPC synthase inhibitors—PC and PE. In this respect it should be noted that the *T. brucei* enzyme is unlike its orthologues from the other kinetoplastid parasites where both the *Leishmania* (Fig. 5B) and *Trypanosoma cruzi* enzymes (Casbon and Denny, unpublished) demonstrate only IPC synthase activity in the *in vitro* system employed here. It is also clearly important to fully analyse the other three TbSLS isoforms to determine their function.

The known yeast and fungal IPC synthase inhibitor, aureobasidin A, has previously been shown to be active against the related kinetoplast, *Leishmania* species, inhibiting growth, but not affecting

viability, in culture [30]. However, it has been demonstrated that the *L. major* IPC synthase is refractory to aureobasidin A (Fig. 5B) and that its effect against this species in culture is non-specific [28]. A similar situation has been observed with respect to the causative agent of Chagas disease, *T. cruzi* [19]. In contrast, this study showed that aureobasidin A demonstrated a high level of efficacy against TbSLS4 turnover *in vitro*, with an IC_{50} of 0.42 nM. In light of these results demonstrating the ability of a known inhibitor to affect enzyme activity, it was important to validate TbSLS as a potential target of anti-trypanosome drugs. Simultaneous RNAi of all four closely related isoforms of TbSLS demonstrated that this enzyme is essential for growth and so represents a new, much needed anti-trypanosome target. Furthermore, aureobasidin A proved highly effective and trypanocidal against cultured bloodstream form *T. brucei*, with a sub-micromolar EC_{50} .

Together these data raise the possibility of the discovery of a new generation of lead inhibitors directed against TbSLS, ultimately leading to novel drugs for the treatment of human African trypanosomiasis.

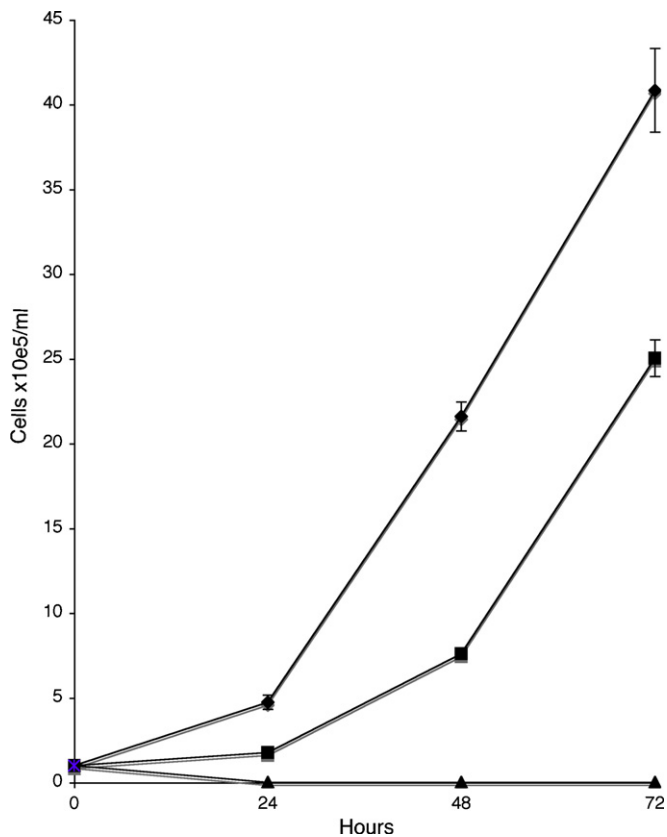


Fig. 7. Aureobasidin A is trypanocidal against bloodstream form *T. brucei*. Cell counts over 72 h with (▲); 1 μM aureobasidin A (AbA); (■) 250 nM AbA; (◆) control. Error bars for standard deviation over three replicates are shown.

Acknowledgements

This work was funded by Biotechnology and Biological Research Council (BB/D52396X/1) and Royal Society (2005/R1) grants to PWD and a British Council/Deutscher Akademischer Austausch Dienst Academic Research Collaboration Award to PWD and RTS. JGM and NKW are funded by the Overseas Research Student Award Scheme. This work was also supported in part by a Wolfson Research Institute Collaborative Small Grants Scheme and Deutsche Forschungsgemeinschaft, Bonn. We thank Dr. Joost Holhuis (Institute of Biomembranes, Utrecht University) for providing HsSMS1 and 2 cDNA clones and Dr. Paul Yeo (Durham University) for helpful discussions.

References

- [1] Barrett MP, Burchmore RJ, Stich A, et al. The trypanosomiasis. *Lancet* 2003;362:1469–80.
- [2] Remme JHF, Blas E, Chitsulo L, et al. Strategic emphases for tropical diseases research: a TDR perspective. *Trends Parasitol* 2002;18:421–6.
- [3] Futerman AH, Hannun YA. The complex life of simple sphingolipids. *EMBO Rep* 2004;5:777–82.
- [4] Magee T, Prinen N, Alder J, Pagakis SN, Parmryd I. Lipid rafts: cell surface platforms for T-cell signalling. *Biol Res* 2002;35:127–31.
- [5] Pierce SK. Lipid rafts and B-cell activation. *Nature Rev Immunol* 2002;2:96–105.

- [6] Huitema K, van den Dikkenberg J, Brouwers JF, Holthuis JC. Identification of a family of animal sphingomyelin synthases. *EMBO J* 2004;23:33–44.
- [7] Lester RL, Dickson RC. Sphingolipids with inositolphosphate-containing head groups. *Adv Lipid Res* 1993;26.
- [8] Becker GW, Lester RL. Biosynthesis of phosphoinositol-containing sphingolipids from phosphatidylinositol by a membrane preparation from *Saccharomyces cerevisiae*. *J Bacteriol* 1980;142:747–54.
- [9] Bromley PE, Li YO, Murphy SM, Sumner CM, Lynch DV. Complex sphingolipid synthesis in plants: characterization of inositolphosphorylceramide synthase activity in bean microsomes. *Arch Biochem Biophys* 2003;417:219–26.
- [10] Denny PW, Shams-Eldin H, Price HP, Smith DF, Schwarz RT. The protozoan inositol phosphorylceramide synthase: a novel drug target which defines a new class of sphingolipid synthase. *J Biol Chem* 2006;281:28200–9.
- [11] Georgopadakou NH. Antifungals targeted to sphingolipid synthesis: focus on inositol phosphorylceramide synthase. *Expert Opin Investig Drugs* 2000;9:1787–96.
- [12] Nagiec MM, Nagiec EE, Baltisberger JA, Wells GB, Lester RL, Dickson RC. Sphingolipid synthesis as a target for antifungal drugs. Complementation of the inositol phosphorylceramide synthase defect in a mutant strain of *Saccharomyces cerevisiae* by the AUR1 gene. *J Biol Chem* 1997;272:9809–17.
- [13] Suzuki E, Tanaka AK, Toledo MS, Levery SB, Straus AH, Takahashi HK. Trypanosomatid and fungal glycolipids and sphingolipids as infectivity factors and potential targets for development of new therapeutic strategies. *Biochim Biophys Acta* 2008;1780:362–9.
- [14] Patnaik PK, Field MC, Menon AK, Cross GA, Yee MC, Bfitikofer P. Molecular species analysis of phospholipids from *Trypanosoma brucei* bloodstream and procyclic forms. *Mol Biochem Parasitol* 1993;58:67–106.
- [15] Güther ML, Lee S, Tetley L, Acosta-Serrano A, Ferguson MA. GPI-anchored proteins and free GPI glycolipids of procyclic form *Trypanosoma brucei* are nonessential for growth, are required for colonization of the tsetse fly, and are not the only components of the surface coat. *Mol Biol Cell* 2006;17:5265–74.
- [16] Sikorski RS, Hieter P. A system of shuttle vectors and yeast host strains designed for efficient manipulation of DNA in *Saccharomyces cerevisiae*. *Genetics* 1989;122:19–27.
- [17] Sutterwala SS, Creswell CH, Sanyal S, Menon AK, Bangs JD. De novo sphingolipid synthesis is essential for viability, but not for transport of glycosylphosphatidylinositol-anchored proteins, in African trypanosomes. *Eukaryot Cell* 2007;6:454–64.
- [18] Fischl AS, Liu Y, Browdy A, Cremesti AE. Inositolphosphoryl ceramide synthase from Yeast. *Methods Enzymol* 2000;311:123–30.
- [19] Figueiredo JM, Dias WB, Mendonca-Previato L, Previato JO, Heise N. Characterization of the inositol phosphorylceramide synthase activity from *Trypanosoma cruzi*. *Biochem J* 2005;387:519–29.
- [20] Wirtz E, Leal S, Ochatt C, Cross GA. A tightly regulated inducible expression system for conditional gene knock-outs and dominant-negative genetics in *Trypanosoma brucei*. *Mol Biochem Parasitol* 1999;99:89–101.
- [21] LaCount DJ, Bruse S, Hill KL, Donelson JE. Double-stranded RNA interference in *Trypanosoma brucei* using head-to-head promoters. *Mol Biochem Parasitol* 2000;111:67–76.
- [22] Tafesse FG, Ternes P, Holhuis JCM. The multigenic sphingomyelin synthase family. *J Biol Chem* 2006;281:29421–5.
- [23] Boumann HA, Damen MJA, Versluis C, Heck AJR, de Kruijff B, de Kroo AIPM. The two biosynthetic routes leading to phosphatidylcholine in yeast produce different sets of molecular species. Evidence for lipid remodeling. *Biochemistry* 2003;42:3054–9.
- [24] Richmond GS, Smith TK. A novel phospholipase from *Trypanosoma brucei*. *Mol Microbiol* 2007;63:1078–95.
- [25] Richmond GS, Smith TK. The role and characterization of phospholipase A1 in mediating lysophosphatidylcholine synthesis in *Trypanosoma brucei*. *Biochem J* 2007;405:319–29.
- [26] Sugimoto Y, Sakoh H, Yamada K. IPC synthase as a useful target for antifungal drugs. *Curr Drug Targets Infect Disord* 2004;4:311–22.
- [27] Fridberg A, Olson CL, Nakayasu ES, Tyler KM, Almeida IC, Engman DM. Sphingolipid synthesis is necessary for kinetoplast segregation and cytokinesis in *Trypanosoma brucei*. *J Cell Sci* 2008;121:522–35.
- [28] Denny PW, Goulding D, Ferguson MA, Smith DF. Sphingolipid-free *Leishmania* are defective in membrane trafficking, differentiation and infectivity. *Mol Microbiol* 2004;52:313–27.
- [29] Zhang K, Showalter M, Revollo J, Hsu FF, Turk J, Beverley SM. Sphingolipids are essential for differentiation but not growth in *Leishmania*. *EMBO J* 2003;22:6016–26.
- [30] Tanaka AK, Valero VB, Takahashi HK, Straus AH. Inhibition of *Leishmania (Leishmania) amazonensis* growth and infectivity by aureobasidin A. *J Antimicrob Chemother* 2007;59:487–92.

Functional analyses of differentially expressed isoforms of the *Arabidopsis* inositol phosphorylceramide synthase

J. G. Mina · Y. Okada · N. K. Wansadhipathi-Kannangara ·
S. Pratt · H. Shams-Eldin · R. T. Schwarz ·
P. G. Steel · T. Fawcett · P. W. Denny

Received: 2 November 2009 / Accepted: 9 March 2010 / Published online: 23 March 2010
© Springer Science+Business Media B.V. 2010

Abstract Sphingolipids are key components of eukaryotic plasma membranes that are involved in many functions, including the formation signal transduction complexes. In addition, these lipid species and their catabolites function as secondary signalling molecules in, amongst other processes, apoptosis. The biosynthetic pathway for the formation of sphingolipid is largely conserved. However, unlike mammalian cells, fungi, protozoa and plants synthesize inositol phosphorylceramide (IPC) as their primary phosphosphingolipid. This key step involves the transfer of the phosphorylinositol group from phosphatidylinositol (PI) to

phytoceramide, a process catalysed by IPC synthase in plants and fungi. This enzyme activity is at least partly encoded by the *AURI* gene in the fungi, and recently the distantly related functional orthologue of this gene has been identified in the model plant *Arabidopsis*. Here we functionally analysed all three predicted *Arabidopsis* IPC synthases, confirming them as aureobasidin A resistant *AUR1p* orthologues. Expression profiling revealed that the genes encoding these orthologues are differentially expressed in various tissue types isolated from *Arabidopsis*.

Keywords *Arabidopsis* · *AUR1* · Expression · Inositol phosphorylceramide · IPC synthase · Sphingolipids

The authors J. G. Mina and Y. Okada contributed equally to this work.

J. G. Mina · N. K. Wansadhipathi-Kannangara · S. Pratt ·
P. G. Steel · P. W. Denny
Biophysical Sciences Institute, Department of Chemistry
and School of Biological and Biomedical Sciences, Durham
University, Durham, UK

J. G. Mina · N. K. Wansadhipathi-Kannangara · S. Pratt ·
P. W. Denny (✉)
School of Medicine and Health, Durham University,
Queen's Campus, Stockton-on-Tees, U.K.
e-mail: p.w.denny@durham.ac.uk

Y. Okada · T. Fawcett (✉)
School of Biological and Biomedical Sciences,
Durham University, Durham, UK
e-mail: tony.fawcett@durham.ac.uk

H. Shams-Eldin · R. T. Schwarz
Institute for Virology, Medical Center of Hygiene & Medical
Microbiology, Philipps-University Marburg, Marburg, Germany

R. T. Schwarz
Unité de Glycobiologie Structurale et Fonctionnelle,
Université des Sciences et Technologies de Lille, Lille, France

Abbreviations

AbA	Aureobasidin A
BSA	Bovine serum albumin
Cer	Ceramide
IPC	Inositol phosphorylceramide
NDB C ₆ -ceramide	6-((N-(7-nitrobenz-2-oxa-1,3-diazol-4-yl)amino) hexanoyl)sphingosine
PI	Phosphatidylinositol
SD	Synthetic minimal media with glucose
SGR	Synthetic minimal media with galactose
SM	Sphingomyelin

Introduction

The diverse, amphipathic sphingolipids consist of a long chain base backbone with long-chain fatty acid and polar

alcohol attachments. These lipid species are ubiquitous membrane components of eukaryotic cells, as well as being found in some prokaryotic organisms and viruses (Smith and Merrill 2002). Studies in mammals and yeast have shown that they are important structural components of membranes and also serve as bioactive molecules involved in cell signalling and regulation (Dickson et al. 2006; Fernandis and Wenk 2007; Hanada et al. 1992). The unmodified sphingolipid, ceramide, is an intermediate in complex sphingolipid biosynthesis in the Golgi apparatus. These complex species ultimately concentrate in the outer leaflet of the plasma membrane where, with sterols, they form lipid raft microdomains (Futerman and Hannun 2004). Rafts have been proposed to be central to a multitude of cellular processes, from the polarized trafficking of lipid-modified proteins (Brown and London 1998) to the formation of signal transduction complexes (Magee et al. 2002; Pierce 2002). Furthermore, sphingolipid metabolites such as ceramide and phosphorylated sphingosine (sphingosine-1-phosphate), are central to intracellular signal transduction processes that regulate cell growth, differentiation and apoptosis (programmed cell death—PCD; Futerman and Hannun 2004).

The biosynthesis of sphingolipids shows commonality between mammals, fungi and plants up to the formation of ceramide (phytoceramide in plants and fungi), but the predominant complex phosphosphingolipid species subsequently synthesized differs. Mammals produce sphingomyelin (SM; a ceramide unit with a phosphorylcholine moiety), whereas fungi and plants synthesize inositol phosphorylceramide (IPC) by the transfer of the phosphorylinositol group from phosphatidylinositol (PI) to phytoceramide, a reaction catalysed by IPC synthase. This enzyme was shown to be at least partly encoded by the *AURI* gene in yeast and other fungi (Nagiec et al. 1997), and recently an accessory protein involved in IPC synthase activity (KEI1p) in these organisms has been identified (Sato et al. 2009). However, the plant enzyme remained unidentified although the activity had been measured in bean microsomes (Bromley et al. 2003). Then, during a screen for factors involved in PCD defence mechanisms, an *AURI* functional orthologue was identified in Arabidopsis. However, the encoded protein demonstrated little homology to the yeast *AUR1p*, having most similarity to the more recently identified animal sphingomyelin synthases (Wang et al. 2008). This lack of similarity to the long known fungal enzyme (Nagiec et al. 1997) lay behind the previously fruitless search for the plant orthologue (Dunn et al. 2004).

Here we demonstrate that all three orthologues identifiable in the Arabidopsis genome database represent aureobasidin A resistant functional orthologues and that, through phylogenetic analyses, these represent a new group

of sphingolipid synthases within the wider enzyme family. Furthermore, we show the expression profile of all three isoforms in the tissues of Arabidopsis. This demonstrated that there is differential expression of IPC synthase, an enzyme central to the synthesis of plasma membrane sphingolipids (Dunn et al. 2004) and a regulator of PCD (Wang et al. 2008) in this plant species.

Materials and methods

Complementation of auxotrophic *AURI* mutant yeast with AtIPCS1-3

Arabidopsis IPC synthase 1, 2 and 3 (AtIPCS1–At3g54020.1, AtIPCS2–At2g37940.1 and AtIPCS3–At2g29525.1) were amplified from Arabidopsis cDNA using primers 5' AtIPCS1 EcoRI gaattcATGACGCTTTATATTCCGCCGCG and 3' AtIPCS1 SalI gtcgacGAGCAGAGATCTCATGTGCC; 5' AtIPCS2 EcoRI gaattcATGACACTTTATATTCC TCGTG and 3' AtIPCS2 SalI gtcgacTCACGCGCCATT CATTGTG; 5' AtIPCS3 EcoRI gaattcATGCCGGTTTAC GTTGATCGCG and 3' AtIPCS3 SalI gtcgacTCAATGAT CATCTGCTACATTG.

The products were subsequently cloned into the yeast vector pRS426MET25, creating pRS426 AtIPCS1-3. In the YPH499–HIS–GAL–*AUR1* *S. cerevisiae* strain expression of the essential *AURI* gene (Nagiec et al. 1997) is under the control of the *GALI* promoter and is repressed in the presence of glucose (Denny et al. 2006). YPH499–HIS–GAL–*AUR1* was transformed with pRS426 AtIPCS1-3 and pRS426 *AUR1* and functionally complemented transformants selected on non-permissive SD medium containing necessary nutritional supplements (Denny et al. 2006).

Diffusion assay of complemented auxotrophic *AURI* mutant yeast

YPH499–HIS–GAL–*AUR1* pRS246 AtIPCS1-3 and YPH499–HIS–GAL–*AUR1* pRS246 *AUR1* were assayed for susceptibility to aureobasidin A (Takara) and myriocin (Sigma) as previously described (Nagiec et al. 2003). Briefly, 2.4×10^7 logarithmically dividing cells were embedded in 15 ml of YPD-agarose (1% yeast extract, 2% peptone, 2% dextrose, 0.8% agarose) on 100 cm² square Petri dishes (Sarstedt). Inhibitors were applied in Me₂SO at the concentrations described below and the dishes incubated at 30°C.

Microsomal assay of AtIPCS

For in vitro assay microsomal membranes were prepared from YPH499–HIS–GAL–*AUR1* pRS246 AtIPCS1-3 and YPH499–HIS–GAL–*AUR1* pRS246 *AUR1* and assayed as

described (Mina et al. 2009). In brief, assays were performed in 50 μ l of 100 mM Tris HCl pH 7.4, 10 mM EDTA and 6 mg/ml defatted BSA, with or without 1 mM PI (soybean, Avanti Polar Lipids; predominant species C16:0-C18:2) and 5 μ M aureobasidin A, and with 2 μ l of microsomes (10 mg/ml protein) and 2 μ l of 5 mM NBD C₆-Ceramide (Molecular Probes) in DMSO. After incubation at 30°C for 60 min the reaction was stopped by the addition of 150 μ l of chloroform/methanol/water (10:10:3 v/v/v) and the lipid fraction isolated by phase separation. This process facilitated reproducible quantitative analyses of IPC formation. Following equilibration (Synergy HT, Bio-tek) samples were analysed by high performance thin-layer chromatography (Denny et al. 2001; Ralton and McConville 1998), imaged using a FLA3000 scanner (Fuji) and quantified using the Aida V3.11 software package.

Plant growth and harvesting of material

Arabidopsis thaliana (Col-0) plants were grown under long-day conditions (16 h day/8 h night) and the following tissues were harvested at specific development stages (Boyes et al. 2001). Rosette leaves were collected at stage 3.90, cauline leaves and stem were collected at stage 5.10, roots and flowers were collected at stage 6.50, siliques were collected at stage 8.00.

RNA isolation and RT

Plant tissue was harvested and immediately frozen in liquid nitrogen. Total RNA was isolated using an RNeasy Plant Mini Kit (Qiagen), including DNase I digestion, according to the manufacturers instructions.

RNA integrity was tested by electrophoresis on 1% agarose gels and was quantified by measuring the absorbance at 260 nm. The $A_{260\text{ nm}}/A_{280\text{ nm}}$ ratios of purified RNA samples were in the range of 2.0 to 2.1 and were determined to be free of genomic DNA by the absence of larger, intron containing, PCR products.

RT reactions were carried out on 1.0 μ g of total plant RNA using Superscript III reverse transcriptase (Invitrogen) and oligo dT primer according to the manufacturers instructions.

Real-time qRT-PCR conditions and analysis

Steady-state levels of RNA for each AtIPCS gene in plant material were analysed using SYBR green to monitor DNA synthesis with a Rotor-Gene RG-3000 (Corbett Research) instrument. Amplification was achieved with the following gene-specific primers; AtIPCS1-forward 5'-AGCCTCTTG ATTATTGCGTC-3' and AtIPCS1-reverse 5'-ACAACG GCATTGCTCCCT-3' to give a 145 bp product; AtIPCS2-

forward 5'-AGCCTCTTGATCATTGCCTC-3' and AtIPCS2-reverse 5'-GACTGCTGTGTTGCTCCCA-3' to produce a 145 bp product; AtIPCS3-forward 5'-TGGCTTAT GGCAGTAATACAG-3' and AtIPCS3-reverse 5'-GCCAG AAATGGCAGAACGTTCT-3' to produce a 141 bp product. To determine the highest specificity and sensitivity qPCR profile for each AtIPCS transcript, titration experiments were performed over a range of MgCl₂ concentrations (1.5 to 5 mM) and primer concentrations from (0.1 to 0.5 μ M). Concentrations were considered optimal at the lowest C_T value that reproducibly gave an amplicon of the correct size in the absence of primer dimers. Based on results of these optimization experiments, qPCR assays for the AtIPCS1 transcript contained 3 mM MgCl₂ and 0.5 μ M of each primer; the AtIPCS2 transcript 3 mM MgCl₂ and 0.4 μ M of each primer; and the AtIPCS3 transcript 4 mM MgCl₂, 0.4 μ M of the forward and 0.5 μ M of the reverse primer. The reactions (total volume 20 μ l) also contained 2 μ l of 10 \times PCR buffer, 10 pg of cDNA, 200 μ M dNTPs, SYBR Green I dye and 2 Units of Taq polymerase. Assays were carried out using the following conditions: 1 cycle of 10 min of 95°C, followed by 30 cycles of 10 s of 95°C, 15 s at 52°C and 20 s of 72°C. Amplicon dissociation curves were recorded at the end of the PCR cycles. External standard curves were constructed using the three AtIPCS cDNAs and relevant gene-specific primer pairs and used to determine the number of transcripts for each gene.

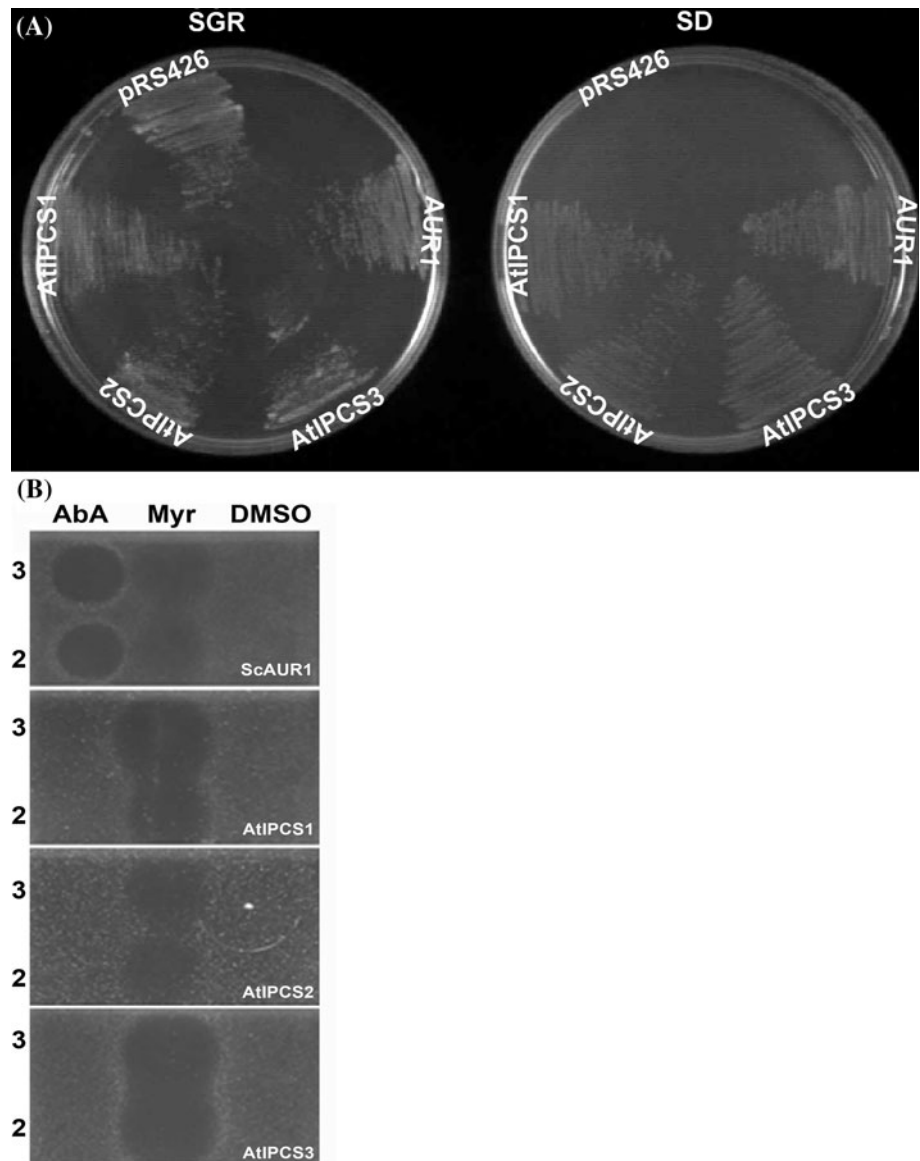
Results

AtIPCS1-3 complement an *AURI* auxotrophic mutant yeast and confer aureobasidin A resistance

Interrogation of the Arabidopsis genome database with the predicted protein sequence of the protozoan IPC synthase from *Leishmania major* (*LmIPCS*) (Denny et al. 2006) identified opening reading frames encoding three highly related sequence orthologues—Arabidopsis IPC synthase 1 (AtIPCS1–At3g54020.1), AtIPCS2 (At2g37940.1) and AtIPCS3 (At2g29525.1)—demonstrating 26, 29 and 31% identity to the protozoan protein. Subsequently, AtIPCS2 has been isolated, characterised and designated ERH1 (Wang et al. 2008). The open reading frames of AtIPCS1-3, when cloned into an URA3 selectable expression vector to create pRS426 AtIPCS1-3, restored the growth of the *AURI* auxotrophic mutant YPH499-HIS-GAL-AUR1, as did the ectopic expression of *S. cerevisiae* AUR1p (AUR1) (Fig. 1a). These data indicated that AtIPCS1, 2 and 3 are functional orthologues of fungal AUR1p, a protein that forms at least part of an IPC synthase (Nagiec et al. 1997).

By diffusion assay (Nagiec et al. 1997, 2003) the efficacy of two different classes of inhibitor were assayed

Fig. 1 AtIPCS1-3 complements a yeast *AUR1* auxotrophic mutant and confers aureobasidin A resistance. **a** YPH499-HIS-GAL-AUR1 auxotrophic yeast transformed with pRS246MET25 either empty or bearing *AUR1* or AtIPCS1-3 and grown under permissive (SGR) or non-permissive conditions (SD). **b** 100 μ M aureobasidin A (AbA) in DMSO, 1 mM myriocin (Myr) in DMSO and DMSO alone spotted in 2 and 3 μ l quantities onto YPH499-HIS-GAL-AUR1 complemented with *AUR1* or AtIPCS1-3 on non-permissive SD plates. pRS426—YPH499-HIS-GAL-AUR1 pRS426MET25; AUR—YPH499-HIS-GAL-AUR1 pRS426 ScAUR1; AtIPCS1-3—YPH499-HIS-GAL-AUR1 pRS426 AtIPCS1-3. Grown on either permissive (non-glucose containing) SGR -HIS -URA or non-permissive (glucose containing) SD-HIS-URA



against YPH499-HIS-GAL-AUR1 pRS426 AtIPCS1, 2 and 3. The transgenic yeast were resistant to aureobasidin A (AbA, a fungal IPC synthase inhibitor) at 100 μ M (Fig. 1b), a concentration shown to inhibit the growth of *LmIPCS* complemented yeast (Denny et al. 2006), but remained sensitive to myriocin (which inhibits the first step in sphingolipid biosynthesis—serine palmitoyltransferase, SPT). Indeed, yeast complemented with the plant enzymes appeared to be more sensitive to the SPT inhibitor than the *AUR1* control, a similar observation had previously been made with regard to the *LmIPCS* complemented yeast (Denny et al. 2006). The *in vitro* assay for AtIPCS1-3 described below (Fig. 2a) confirmed that the Arabidopsis enzymes are AbA insensitive. In contrast, the IPCS activity from Golden butterwax bean extracts has been shown to be acutely sensitive to this inhibitor (Bromley et al. 2003).

The reasons for this difference in AbA sensitivity are unclear and no data are currently available, for the bean sequence, to help elucidate this discrepancy.

AtIPCS1-3 are functional IPC synthases

In vitro assay of microsomes prepared from YPH499-HIS-GAL-AUR1 pRS426 AtIPCS1-3 demonstrated that the three plant enzymes are active IPC synthases (Fig. 2a). However, their turnover appeared low when compared to an *S. cerevisiae* *AUR1* control. This was also noted by Wang et al. (2008) and was unaffected by the use of NBD C₆-phytoceramide rather than C₆-ceramide as acceptor substrate. In support of the data shown above (Fig. 1b), AtIPCS1-3 activity was insensitive to the addition of AbA at a concentration (5 μ M) that completely inhibited the

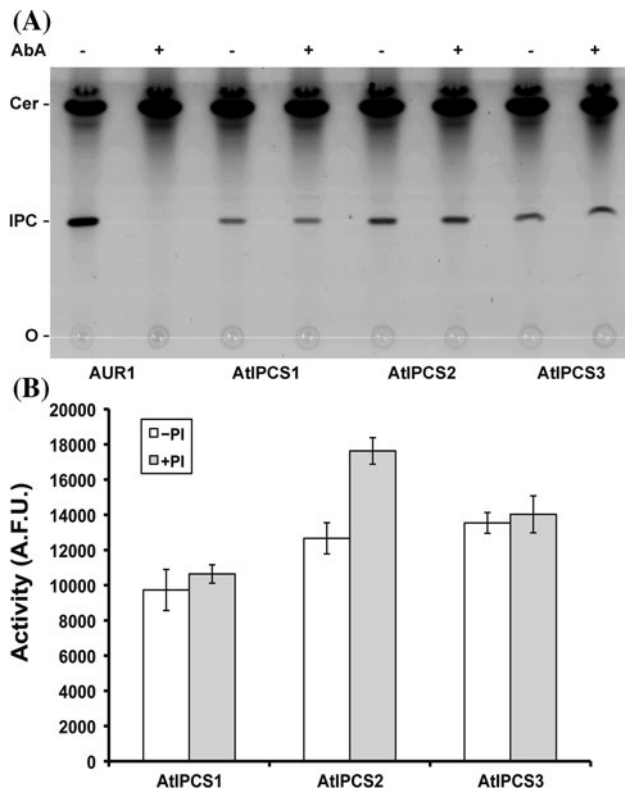


Fig. 2 AtIPCS1-3 encode functional IPC synthases. In vitro assay of microsomal extracts from YPH499-HIS-GAL-AUR1 pRS246 AtIPCS1-3 and YPH499-HIS-GAL-AUR1 pRS246 AUR1. Assay in the presence of phosphatidylinositol (PI) with (+) or without (-) the specific fungal inhibitor aureobasidin A (AbA). In contrast to the *S. cerevisiae* IPC synthase (AUR1), the plant activity encoded by AtIPCS1-3 is insensitive to AbA at 5 μ M. Markers of NDB C₆-ceramide and NBD C₆-IPC, and the origin (O) indicated. Assay with (+) or without (-) donor substrate PI in the presence of 5 μ M AbA. Enzyme turnover is only significantly enhanced by the addition PI in the case of AtIPCS2. Mean of 3 separate experiments, standard error shown. A.F.U.—Arbitrary Fluorescence Units

yeast enzyme (Fig. 2a). Thereafter this inhibitor was applied to the reaction mix for assay of AtIPCS1-3 at 5 μ M.

In the experiment (Fig. 2a) above the plant (and yeast) enzymes are assayed in the presence of exogenous soybean PI. To ascertain the effect of adding this exogenous donor substrate samples were assayed with and without PI in the reaction mix (Fig. 2b). All samples showed a similar level of activity in the absence of donor substrate but, surprisingly, only AtIPCS2 demonstrated any significant increase in turnover on the addition of PI. This indicated that the AtIPCS1 and 3 are unable to utilize substrate from this source effectively. Similar results were obtained utilizing bovine PI which has previously been demonstrated to be effectively utilized by the protozoan orthologues from both *L. major* and *Trypanosoma brucei* but not by *S. cerevisiae* AUR1p (Mina et al. 2009). Despite this, these data confirm

AtIPCS1-3 as functional orthologues of AUR1p, forming at least part of an IPC synthase.

The plant IPC synthases form a new class of sphingolipid synthase

The key motifs, D3 and D4, of the sphingolipid synthase family are conserved in the plant IPC synthases (Wang et al. 2008). However, unlike their protozoan and mammalian counterparts they lack a D1 domain (Huitema et al. 2004). In this they resemble the fungal IPC synthases and it may be hypothesized that D1 is involved in the binding of ceramide, a substrate for the protozoan and mammalian enzymes, whereas another unidentified region is involved in binding the phytoceramide substrate to the plant and fungal IPC synthases. Despite the conservation of some of these motifs the plant sequences are divergent with respect to primary sequence and so, until recently, remained cryptic within the genome databases (Wang et al. 2008). This divergence was illustrated by phylogenetic analysis of predicted SM and IPC synthase sequences which demonstrated that the plant enzymes, the three orthologues identified in the *Oryza sativa* (rice) database are included, form a new clade of sphingolipid synthases (Fig. 3).

Expression profiling of AtIPCS1-3

Estimates of the relative abundance of transcripts can be made from their representation within the EST databases. For the three AtIPCS genes described a similar number of AtIPCS1 and AtIPCS3 transcripts are present, whilst the largest number is for AtIPCS2 (Table 1; data derived from TAIR BLAST version 2.2.8). However, these data do not give any information regarding the tissue location of the transcripts and are therefore of limited use when investigating the expression of gene families. Tissue-specific transcript abundance data can be obtained from multiple microarray experiments using Genevestigator (Grennan 2006). Only AtIPCS2 is represented on the Affymetrix arrays that are used to derive these data and this shows that the gene is expressed in cauline leaves, roots and rosette leaves at similar levels and these are approximately twice the expression levels seen in stems, flowers and siliques (Table 2).

Given the limitations of these data sets, in order to establish a complete expression profile for each AtIPCS isoform, real time quantitative RT-PCR was performed on RNA isolated from various Arabidopsis tissues (Fig. 4). AtIPCS2 was the most highly expressed of the three isoforms in all tissues. In agreement with the Genevestigator data, the highest levels of AtIPCS2 transcript were seen in root, rosette leaves and cauline leaves and these were five to ten fold greater than the levels of transcripts in siliques,

Fig. 3 The plant IPC synthase defines a new class of sphingolipid synthases. Maximum parsimony analysis of Animalae, Fungi, Trypanosomatidae and Plantae sphingolipid synthase sequences. Bootstrap scores >60 indicated. *Homo sapiens* LPP1 (outgroup) accession number: O14494; *Arabidopsis thaliana* IPCS1-3 accession numbers: At3g54020.1, At2g37940.1, At2g29525.1; *Oryza sativa* IPCS1-3: NP_001044812, NP_001055712, NP_001055096; *T. brucei* SLS1-4: Tb09.211.1030, Tb09.211.1020, Tb09.211.1010, Tb09.211.1000; *T. cruzi* IPCS1&2: Tc00.1047053506885.124, Tc00.1047053510729.290; *L. major* IPCS: LmjF35.4990; *Aspergillus fumigatus* AUR1p: AAD22750; *Candida albicans* AUR1p: AAB67233; *Pneumocystis carinii* AUR1p: CAH17867; *Saccharomyces cerevisiae* AUR1p: NP_012922; *Schizosaccharomyces pombe* AUR1p: Q10142; *Caenorhabditis elegans* SMS1-3: Q9U3D4, AAA82341, AAK84597; *Homo sapiens* SMS1&2: AB154421, Q8NHU3; *Mus musculus* SMS1&2: Q8VCQ6, Q9D4B1

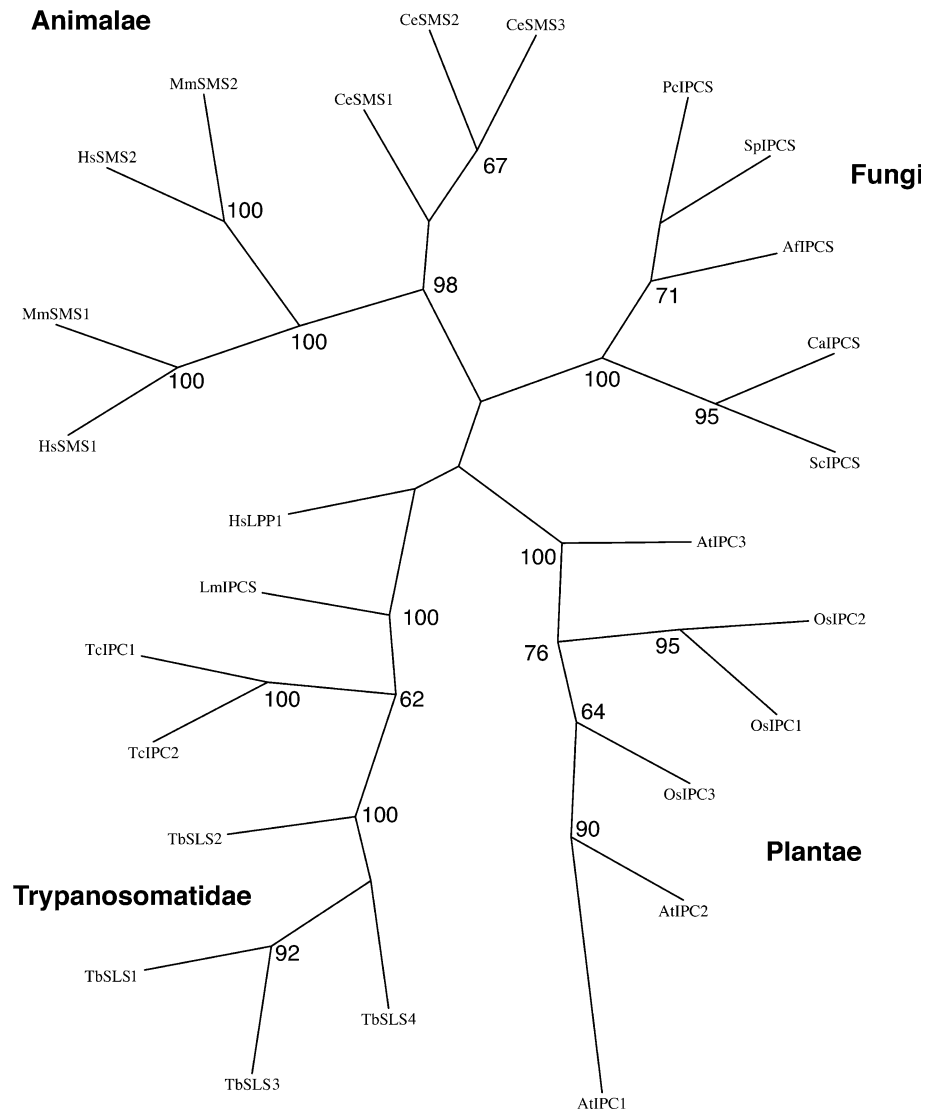


Table 1 EST numbers for AtIPCS genes derived from TAIR BLAST version 2.2.8

	EST
AtIPCS1	32
AtIPCS2	57
AtIPCS3	25

Table 2 Microarray data for AtIPCS2 in the genevestigator database

Root	Rosette leaf	Cauline leaf	Stem	Flower	Siliques
2383	2135	2509	1167	998	705

stems and flowers. The patterns of expression determined by these two methods are in general agreement but the relative levels differ, this may reflect differences in the plant material used in the each case. Genevestigator uses a

large number of microarray experiments to generate data and is therefore robust, however the data represents plant material grown under different conditions and which may have been harvested at different times within a developmental stage. The quantitative RT-PCR data presented here is determined from plants grown and harvested under identical conditions and therefore represents transcript levels at defined developmental stages in these tissues.

AtIPCS1 transcripts are expressed at low levels in all tissues, ranging from 0.05% of AtIPCS2 levels in rosette leaves to 2.8% of AtIPCS2 levels in stems. While AtIPCS3 transcripts are also present in low levels in cauline leaves, rosette leaves, roots and stems (ranging from 0.02 to 0.67% of AtIPCS2 transcripts) they are present at similar levels to AtIPCS2 transcripts in stem (84% of AtIPCS2 levels) and flower (74% of AtIPCS2 levels).

The data presented here adds to existing studies by providing tissue specific expression data for all the

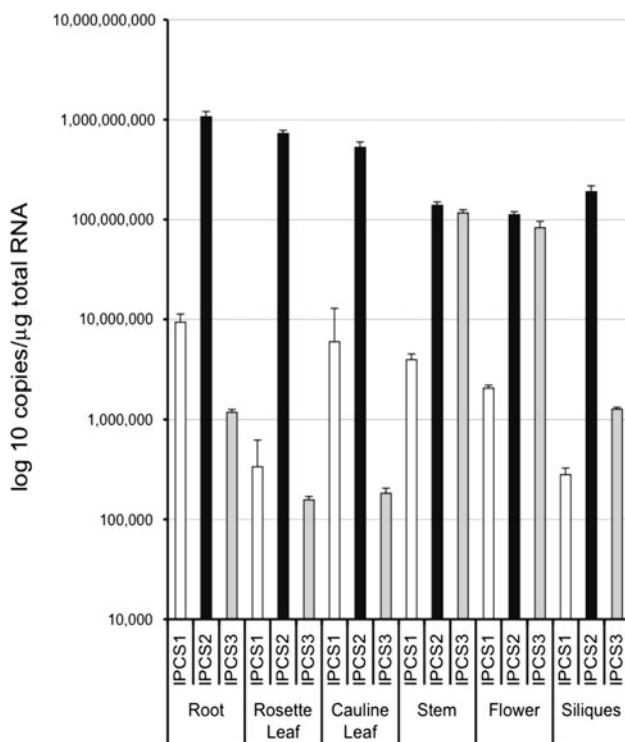


Fig. 4 Steady-state levels of AtIPCS isoform mRNAs in plant tissues. The numbers of AtIPCS1-3 transcripts were determined in total RNA from various tissues, by quantitative RT-PCR using a standard curve for each transcript. AtIPCS2 (At2g37940.1) is the most abundant form in roots, leaves and siliques, whereas stems and flowers have similar numbers of AtIPCS2 and AtIPCS3 (At2g29525.1) transcripts. AtIPCS1 (At3g54020.1) transcript is uniformly low in all tissues

isoforms of AtIPCS which may indicate a specific role for AtIPCS3 in stems and flowers.

Discussion

The data presented describe the analyses of all three orthologues of the recently identified Arabidopsis IPC synthase (Wang et al. 2008). They all represented functional orthologues of *S. cerevisiae* IPC synthase, AUR1p, and demonstrated activity in an in vitro assay. However, unlike the yeast activity the Arabidopsis enzyme is resistant to aureobasidin A, a non-competitive inhibitor of the fungal IPC synthase with an unknown mechanism of action (Zhong et al. 1999). Conversely, it has previously been shown that the IPCS activity in Golden butterwax bean extracts was acutely sensitive to this inhibitor (Bromley et al. 2003). The reasons for this discrepancy are unclear, however it is notable that similarly profound differences in aureobasidin A sensitivity have been observed within the kinetoplastid parasite IPCS orthologues. Whilst the *L. major* enzyme is relatively refractory to the drug, the

T. brucei sphingolipid synthase (TbSLS) is highly sensitive (Mina et al. 2009). No reason for this can be deduced from the primary sequence data and it may be envisaged that this diversity is due to subtle differences in 3-dimensional enzyme structure.

In the in vitro, microsome-based assay all three Arabidopsis isoforms demonstrated IPC synthase turnover. However, although the presence of PI (from soybean or bovine sources) led to a significant increase in turnover with AtIPCS2, AtIPCS1 and 3 were refractory to the addition of this donor substrate. This indicated that PI from these sources was utilized inefficiently by these Arabidopsis isoforms. Similarly, it has been noted that mammalian PI is not efficiently utilized by the *S. cerevisiae* IPC synthase activity (Mina et al. 2009). Notably, unlike the yeast phospholipids (Guan and Wenk 2006), plant and mammalian PIs exhibit varying degrees of polyunsaturation (Thompson and MacDonald 1975, 1976). It may be hypothesized this polyunsaturation may confer structural constraints and make it less acceptable to the *S. cerevisiae* enzyme. However, the lack of reactivity of AtIPCS1 and with plant derived PI (soybean, C16:0–C18:2) is less easy to explain. It is possible that the endogenous yeast PI has a higher affinity for these isoforms and outcompetes the exogenous substrate. Attempts to minimize the available quantity of endogenous PI to test this were made by detergent washing as previously (Mina et al. 2009). However, this led to apparent inactivation of the enzymes. Alternatively, significant differences may exist in the substrate requirements of these Arabidopsis isoforms. Notably, AtIPCS1 transcript level is low in all plant tissue and AtIPCS3 in many, including siliques, perhaps reflecting the level of acceptable donor PI in seeds (such as soybeans, the source of PI in these experiments).

Despite these variances, all the plant IPC synthase orthologues identified share the motifs predicted to form the catalytic triad that promotes nucleophilic attack on lipid phosphate ester bonds which, in the case of IPC synthase, is thought to lead to the transfer of an inositol phosphate group from PI to the 1-hydroxyl group of (phyto)ceramide releasing diacylglycerol as a by-product (Huitema et al. 2004; Neuwald 1997). Therefore it is likely that the eukaryotic sphingolipid synthases possess a common mechanism of action, indicating a single evolutionary origin. In contrast, the prokaryotic SM synthase lacks the catalytic triad (Luberto et al. 2003) and is likely to have evolved independently. Phylogenetic analyses show the plant proteins forming a distinct clade, thereby defining a new class of eukaryotic sphingolipid synthases.

It has been demonstrated, by RNAi of the first enzyme in the biosynthetic pathway—serine palmitoyltransferase, that sphingolipid biosynthesis per se is essential for the viability of Arabidopsis (Chen et al. 2006). Furthermore,

recent work has suggested that the plant IPC synthase is pivotal in pathogen-resistance associated PCD. By analyses of leaf tissue from an ERH1 (AtIPCS2) insertion mutant Wang et al. (2008) detected a significant increase in ceramide levels, an observation consistent with the fact that ceramide is a substrate for IPCS. Importantly, ceramide is a key regulator of PCD (Futerman and Hannun 2004) and the accumulation of this factor was co-incident with PCD at the site of powdery mildew infection in *Arabidopsis* (Wang et al. 2008). This work is further supported by similar observations in accelerated-cell-death (*acd11* and *acd5*) mutants of *Arabidopsis* in which a sphingosine transfer protein (ACD11) or a ceramide kinase (ACD5) are affected (Brodersen et al. 2002; Liang et al. 2003). Given the prominence of AtIPCS2 as a putative regular of PCD the differential expression levels of each of the three functional *Arabidopsis* orthologues may shed light on this key process in the whole plant.

Acknowledgments This work was funded by Biotechnology and Biological Research Council (BB/D52396X/1) and Royal Society (2005/R1) grants to PWD and a British Council/Deutscher Akademischer Austausch Dienst Academic Research Collaboration Award to PWD and RTS. JGM and NKW are funded by the Overseas Research Student Award Scheme. JGM is also funded by the Wolfson Research Institute. This work was also supported in part by the Wolfson Research Institute Collaborative Small Grants Scheme and Deutsche Forschungsgemeinschaft, Bonn.

References

- Boyes DC, Zayed AM, Ascenzi R, McCaskill AJ, Hoffman NE, Davis KR, Gortlach J (2001) Growth stage-based phenotypic analysis of *Arabidopsis*: a model for high throughput functional genomics in plants. *Plant Cell* 13:1499–1510
- Brodersen P, Petersen M, Pike HM, Olszak B, Skov S, Odum N, Jorgensen LB, Brown RE, Mundy J (2002) Knockout of *Arabidopsis* accelerated-cell-death11 encoding a sphingosine transfer protein causes activation of programmed cell death and defense. *Genes Dev* 16:490–502
- Bromley PE, Li YNO, Murphy SM, Sumner CM, Lynch DV (2003) Complex sphingolipid synthesis in plants: characterization of inositolphosphorylceramide synthase activity in bean microsomes. *Arch Biochem Biophys* 417:219–226
- Brown DA, London E (1998) Functions of lipid rafts in biological membranes. *Annu Rev Cell Dev Biol* 14:111–136
- Chen M, Han G, Dietrich CR, Dunn TM, Cahoon EB (2006) The essential nature of sphingolipids in plants as revealed by the functional identification and characterization of the *Arabidopsis* LCB1 subunit of serine palmitoyltransferase. *Plant Cell* 18:3576–3593
- Denny PW, Field MC, Smith DF (2001) GPI-anchored proteins and glycoconjugates segregate into lipid rafts in *Kinetoplastida*. *FEBS Lett* 491:148–153
- Denny PW, Shams-Eldin H, Price HP, Smith DF, Schwarz RT (2006) The protozoan inositol phosphorylceramide synthase: a novel drug target which defines a new class of sphingolipid synthase. *J Biol Chem* 281:28200–28209
- Dickson RC, Sumanasekera C, Lester RL (2006) Functions and metabolism of sphingolipids in *Saccharomyces cerevisiae*. *Prog Lipid Res* 45:447–465
- Dunn TM, Lynch DL, Michaelson LV, Napier JA (2004) A post-genomic approach to understanding sphingolipid metabolism in *Arabidopsis thaliana*. *Ann Bot* 93:483–497
- Fernandis AZ, Wenk MR (2007) Membrane lipids as signaling molecules. *Curr Opin Lipidol* 18:121–128
- Futerman AH, Hannun YA (2004) The complex life of simple sphingolipids. *EMBO reports* 5:777–782
- Grennan AK (2006) Genevestigator. Facilitating web-based gene-expression analysis. *Plant Physiol* 141:1164–1166
- Guan XL, Wenk MR (2006) Mass spectrometry-based profiling of phospholipids and sphingolipids in extracts from *Saccharomyces cerevisiae*. *Yeast* 23:465–477
- Hanada K, Nishijima M, Kiso M, Hasegawa A, Fujita S, Ogawa T, Akamatsu Y (1992) Sphingolipids are essential for the growth of Chinese hamster ovary cells. Restoration of the growth of a mutant defective in sphingoid base biosynthesis by exogenous sphingolipids. *J Biol Chem* 267:23527–23533
- Huitema K, van den Dikkenberg J, Brouwers JF, Holthuis JC (2004) Identification of a family of animal sphingomyelin synthases. *EMBO J* 23:33–44
- Liang H, Yao N, Song JT, Luo S, Lu H, Greenberg JT (2003) Ceramides modulate programmed cell death in plants. *Genes Dev* 17:2636–2641
- Luberto C, Stonehouse MJ, Collins EA, Marchesini N, El-Bawab S, Vasil AI, Vasil ML, Hannun YA (2003) Purification, characterization, and identification of a sphingomyelin synthase from *Pseudomonas aeruginosa*. PlcH is a multifunctional enzyme. *J Biol Chem* 278:32733–32743
- Magee T, Prinen N, Alder J, Pagakis SN, Parmryd I (2002) Lipid rafts: cell surface platforms for T-cell signalling. *Biol Res* 35:127–131
- Mina JG, Pan SY, Wansadhipathi NK, Bruce CR, Shams-Eldin H, Schwarz RT, Steel PG, Denny PW (2009) The *Trypanosoma brucei* sphingolipid synthase, an essential enzyme and drug target. *Mol Biochem Parasitol* 168:16–23
- Nagiec MM, Nagiec EE, Baltisberger JA, Wells GB, Lester RL, Dickson RC (1997) Sphingolipid synthesis as a target for antifungal drugs. Complementation of the inositol phosphorylceramide synthase defect in a mutant strain of *Saccharomyces cerevisiae* by the AUR1 gene. *J Biol Chem* 272:9809–9817
- Nagiec MM, Young CL, Zaworski PG, Kobayashi SD (2003) Yeast sphingolipid bypass mutants as indicators of antifungal agents selectively targeting sphingolipid synthesis. *Biochem Biophys Res Commun* 307:369–374
- Neuwald AF (1997) An unexpected structural relationship between integral membrane phosphatases and soluble haloperoxidases. *Protein Sci* 6:1764–1767
- Pierce SK (2002) Lipid rafts and B-cell activation. *Nature Rev Immunol* 2:96–105
- Ralton JE, McConville MJ (1998) Delineation of three pathways of glycosylphosphatidylinositol biosynthesis in *Leishmania mexicana*. Precursors from different pathways are assembled on distinct pools of phosphatidylinositol and undergo fatty acid remodeling. *J Biol Chem* 273:4245–4257
- Sato K, Noda Y, Yoda K (2009) Kei1: a novel subunit of inositolphosphorylceramide synthase, essential for its enzyme activity and Golgi localization. *Mol Biol Cell* 20:4444–4457
- Smith WL, Merrill AH (2002) Sphingolipid metabolism and signaling. *J Biol Chem* 277:25841–25842
- Thompson W, MacDonald G (1975) Isolation and characterization of cytidine diphosphate diglyceride from beef liver. *J Biol Chem* 250:6779–6785

- Thompson W, MacDonald G (1976) Cytidine diphosphate diglyceride of bovine brain. Positional distribution of fatty acids and analysis of major molecular species. *Eur J Biochem* 65:107–111
- Wang W, Yang X, Tangchaiburana S, Ndeh R, Markham JE, Tsegaye Y, Dunn TM, Wang GL, Bellizzi M, Parsons JF, Morrissey D, Bravo JE, Lynch DV, Xiao S (2008) An inositolphosphorylceramide synthase is involved in regulation of plant programmed cell death associated with defense in *Arabidopsis*. *Plant Cell* 20:3163–3179
- Zhong W, Murphy DJ, Georgopapadakou NH (1999) Inhibition of yeast inositol phosphorylceramide synthase by aureobasidin A measured by a fluorometric assay. *FEBS Lett* 463:241–244